The Influence of Production Routes on the Behaviour of Stainless Steel Structural Members

A thesis submitted to the University of London for the degree of Doctor of Philosophy

By

Rachel Bethan Cruise

Department of Civil and Environmental Engineering
Imperial College London
London SW7 2AZ

March 2007

BLANK PAGE IN ORIGINAL

Abstract

Current structural design codes for stainless steel employ material strengths, or 0.2% proof stress values that are significantly lower than the 0.2% proof stress of material taken from stainless steel structural cross sections. This discrepancy is attributed to the ability of stainless steel to significantly cold work during plastic deformation, which occurs in sheet rolling and cross section forming processes. The resulting under-estimation of the material strength in stainless steel cross sections leads to overly conservative structural designs. As the comparative expense of stainless steel demands efficient design, this study proposes models to predict the strength enhancements offered by different cross section production routes to increase the efficiency of stainless steel structural design.

This research project includes a substantial experimental program that has produced 0.2% proof stress distributions from over 450 tensile coupon tests for a total of 19 cross sections formed via three standard production routes: press braking, cold rolling and hot rolling. To obtain 0.2% proof stress variations to a higher resolution, Vickers hardness values have been obtained and correlated with the 0.2% proof stress values. Significant strength increases in the flat regions of cold rolled box sections have been found and related to the strain history of the sheet material used in production and the strain caused during section forming. Existing models to predict further strength enhancements in the corner regions have been modified and the extension of the region of cold work associated with corner forming has been quantified, defining the material strength distributions for both press braked and cold rolled sections. In addition, geometric profiles of 31 complete section lengths have been measured and over 800 residual strain readings performed. Since production routes also influence the geometric imperfections and residual stress distributions, they must be quantified to accurately predict structural behaviour. Simple models have been proposed to predict global and local imperfections and membrane and bending residual stresses in the three types of sections.

Based on available test data, the proposed 0.2% proof stress distribution for press braked sections offers, on average, cross section resistances 1.4 times those predicted using the minimum 0.2% proof stress. The 0.2% proof stress distribution proposed for cold rolled sections provides cross section compression resistances, column buckling resistances and in-plane bending resistances, on average, 2.1, 1.5 and 1.9 times respectively the values obtained using the minimum specified material strength. This research therefore identifies large increases in efficiency for stainless steel structural design which, combined with low maintenance requirements greatly increases the competitiveness of specifying stainless steel structures.

Acknowledgements

'I am always doing that which I cannot do, in order that I may learn how to do it.'

Pablo Picasso

This thesis is dedicated to my father with all my love and respect.

Dr. Gardner, Lecturer in the Department of Civil and Environmental Engineering supervised this research and I am extremely grateful for the fantastic opportunity he gave me to work on this project and for all his kindness, guidance and help throughout its duration.

I would like to thank Cui Ping Sok, José Ministro dos Santos and Krishnanth Krishnan who greatly aided the life cycle costing study and Qiang Fu who tirelessly conducted the hardness tests.

Financial support for the project was given by the Engineering and Physical Sciences Research Council (EPSRC) and Outokumpu Research Foundation. The support from Outokumpu, in particular the enthusiasm and technical knowledge of Dr. David Dulieu contributed greatly to the research. In addition production information was obtained from a number of manufacturers; Ancon, Corus Research and Development, La Meusienne, Metsec, and Stala Tube. Their time and help was invaluable.

The experimental program was carried out in the Structures Laboratory at Imperial College London and would not have been possible without the support of the technicians. I am particularly grateful for the expertise and good advice of Ron Millward and Jim Wright, and the patient hard work of Alfredo Olivo, Trevor Stickland, and Alan Roberts.

Finally I would like to thank the staff and students at The Civil and Environmental Engineering Department, Imperial College London and The Bartlett School of Architecture, University College London and others, in particular: Professor David Nethercot, Professor David Lloyd Smith, Professor Stephen Gage, Dr Sunday Popo-Ola, Jason Treadway, Juan Sagaseta, Ken Chan, Miguel Jose, Arash Soleiman Fallah, Ka Ho Nip, Mahmud Ashraf, Kee Ng, Phil Ayres, Stewart Dodd, Abi Abdolwahabi, Mark Smout, James Burch, Christian Derix, Katie Lloyd Thomas, Clive Hargreaves and Fionnuala Ni Dhonnbhain, for their encouragement in linking the architectural and civil engineering disciplines.

Contents

Chapter 3 - Experimental overview

Chapter 4 - Geometric imperfections

Chapter 5 - Residual stresses

Chapter 6 - Material strength

Chapter 7 *- Design method*

Chapter 8 *- Life cycle costing*

Notation

a_n	*cosine (real) Fourier coefficient or amplitude*
A	*Additional costs*
A	*Area*
A_{eff}	*Effective cross section area*
A_g	*Gross cross sectional area*
[A]	*Design matrix*
b	*Flange width*
b_l	*Lip width*
b_n	*sine (imaginary) Fourier coefficient or amplitude*
$\bar{b}$	*Plate width*
B	*Experimentally defined constant*
B_c	*Experimentally defined constant*
{c}	*Least squared coefficients in vector form*
C	*Column position*
C	*Experimentally defined constant*
C_1	*Experimentally defined constant*
C_2	*Experimentally defined constant*
d	*Web width*
D	*Chord length*
D_n	*Revised chord length*

E	*End of life costs*
E	*Young's modulus (Initial tangent modulus)*
$E_{0.2}$	*Tangent modulus at 0.2% proof stress*
$f_C(x_m)$	*Average profile created from column C with imperfections from rig removed*
$f_{CR}(x_m)$	*Profile created from transducer located in column C and row R with imperfections from rig removed*
f_{ya}	*Increased average section strength*
f_{yb}	*Basic material strength*
F	*Indenter force*
g	*Diameter of gauge hole*
[G]	*Weighting matrix*
h	*Concavity and convexity of internal elements*
h'	*Out of squareness for outstand elements*
HV	*Vickers hardness value*
HV_{av}	*Average Vicker hardness value taken over width of corresponding tensile coupon*
i	*Experimentally defined constant*
I	*Initial material costs*
j	*Experimentally defined constant*
k	*Numerical constant*
k	*Experimentally defined constant*
k	*Thermal conductivity*
k	*Neutral axis offset factor*
k_σ	*Buckling coefficient*
K	*Constant*
$laser_C$	*Laser reading aligned to a column position C*
L	*Length*
LCC	*Life cycle cost*
L_{av}	*Average diagonal measurement of hardness indent*
L_f	*Final length*
L_i	*Initial length*
L_o	*Gauge length*
L_1	*Diagonal measurement of hardness indent*
L_2	*Diagonal measurement of hardness indent*
m	*Experimentally defined constant*
m	*Location of discrete data point*

M	*Number of discrete data points*
M	*Maintenance costs*
MA	*Moving average*
$M_{c,exp}$	*Experimental in-plane bending resistance*
$M_{c,Rd}$	*Design bending resistance*
n	*Fourier number*
n	*Ramberg-Osgood strain hardening factor between zero and $\varepsilon_{0.2}$ strain*
$n_{bestfit}$	*Bestfit Ramberg-Osgood strain hardening factor between zero and $\varepsilon_{0.2}$ strain - based on 0.05% and 0.2% proof stress*
$n_{0.01}$	*Ramberg-Osgood strain hardening factor between zero and $\varepsilon_{0.2}$ strain - based on 0.01% and 0.2% proof stress*
$n_{0.05}$	*Ramberg-Osgood strain hardening factor between zero and $\varepsilon_{0.2}$ strain - based on 0.05% and 0.2% proof stress*
$n_{0.1}$	*Ramberg-Osgood strain hardening factor between zero and $\varepsilon_{0.2}$ strain - based on 0.1% and 0.2% proof stress*
n'	*Ramberg-Osgood strain hardening factor for strains greater than $\varepsilon_{0.2}$*
$n'_{bestfit}$	*Bestfit Ramberg-Osgood strain hardening factor for strains greater than $\varepsilon_{0.2}$*
N	*Nyquist frequency*
N	*Distance over which defection is measured*
$N_{b,exp}$	*Experimental column buckling resistance*
$N_{b,Rd}$	*Design column buckling resistance*
$N_{c,exp}$	*Experimental cross section compression resistance*
N_{cr}	*Elastic critical buckling load*
$N_{c,Rd}$	*Design cross section compression resistance*
$offset_{CR}$	*Offset value for transducer located in column C and row R*
p	*Width of the tension zone measured from the weld*
p	*Constant*
p_1	*Constant*
P	*Thickness of pellet*
P_{CR}	*Profile created from transducers located in column C and row R*
[Q]	*Covariance matrix*
r	*Number of degrees of freedom*
r	*Discount rate (%)*
r	*Constant*
r_i	*Internal corner radius*
r_n	*Corner radius to neutral axis*

r_2	*Constant*
R	*Row position*
R	*Residual value*
R	*Radius of curvature*
R_f	*Final strip curvature*
R_i	*Internal circular tube radius*
R_i	*Initial strip curvature*
R_{i-f}	*Change in radius caused by release of bending residual stress*
R_n	*Radius to neutral axis for circular tube and strip curvature*
s	*Constant*
s_1	*Constant*
S_i	*Initial deflection of strip*
S_f	*Final deflection of strip*
S_o	*Coupon cross section area*
t	*Thickness*
t_i	*Intervening years (years)*
t_n	*Design life (years)*
t_f	*Flange thickness*
t_w	*Web thickness*
T_{CR}	*Transducer reading located in column C and row R*
V	*Width of press brake die*
{V}	*Modelling error*
{w}	*Vector notation of imperfection function*
x	*Position in section face*
x_m	*Location along specimen length*
x_1	*Location of initial data point*
$\bar{x}_m$	*Normalised location along specimen length*
y	*Distance from the neutral axis though material thickness*
y	*Distance from the weld*

α	*Internal angle of diamond indenter*
α	*Thermal expansion coefficient*
α	*Local imperfection coefficient as defined by Dawson and Walker (1972)*
β	*Local imperfection coefficient as defined by Dawson and Walker (1972)*
δ	*Offset of half sine wave series*
ε	*Material factor*
ε	*Strain*
ε_b	*Bending residual strain*
$\varepsilon_{bf,in}$	*Final internal strain reading with both strain gauges affixed*
$\varepsilon_{bf,out}$	*Final external strain reading with both strain gauges affixed*
$\varepsilon_{bi,in}$	*Initial internal strain reading with both strain gauges affixed*
$\varepsilon_{bi,out}$	*Initial external strain reading with both strain gauges affixed*
ε_c	*Strain experienced by corner*
ε_f	*Strain experienced by flat face*
$\varepsilon_{f,exp}$	*Strain at fracture*
$\varepsilon_{f,in}$	*Final internal strain reading*
$\varepsilon_{f,out}$	*Final external strain reading*
$\varepsilon_{i,in}$	*Initial internal strain reading*
$\varepsilon_{i,out}$	*Initial external strain reading*
ε_m	*Membrane residual strain*
ε_{max}	*Maximum corner strain*
ε_n	*Normalised strain*
$\varepsilon_{n1.0}$	*Normalised total strain at 1.0% proof stress*
ε_{psnd}	*Second plastic strain required to determine the strain hardening factor*
$\varepsilon_{p1.0}$	*Plastic strain at 1.0% proof stress*
ε_{pult}	*Plastic strain at ultimate stress*
$\varepsilon_{t0.2}$	*Total strain at 0.2% proof stress*
$\varepsilon_{t1.0}$	*Total strain at 1.0% proof stress*
ε_{tsnd}	*Total strain at second proof stress*
ε_{tult}	*Total strain at ultimate stress*
$\varepsilon_{ult,exp}$	*Experimental strain measured at ultimate stress*
$\dot{\varepsilon}_x$	*Strain rate*
ζ	*Number of cross section widths equal to half wavelength*
ηt	*Width of Heat Affect Zone either side of weld*
θ	*Angle of curvature*
θ_c	*Revised angle of curvature*

$\bar{\lambda}$	*Member slenderness*
$\bar{\lambda}_p$	*Plate slenderness*
$\bar{\lambda}_{p,max}$	*Maximum plate slenderness*
ρ	*Density*
σ	*Stress*
σ_{an}^2	*Variance of least squared coefficients*
σ_b	*Bending residual stress*
σ_{exp}	*Experimental stress*
σ_m	*Membrane residual stress*
σ_m^2	*Experimental variance in spectral coefficients*
σ_n	*Normalised stress*
σ_{ox}	*Static flow stress*
σ_{rc}	*Combined magnitude of residual stresses*
σ_{snd}	*Second proof stress required to determine the strain hardening factor*
σ_{ult}	*Ultimate stress*
$\sigma_{ultav,exp}$	*Average experimental ultimate proof stress taken from central 50% of flat faces in cold rolled sections*
$\sigma_{ult,c}$	*Corner ultimate stress*
$\sigma_{ult,exp}$	*Ultimate stress*
$\sigma_{ult,f}$	*Flat face ultimate stress*
$\sigma_{ult,min}$	*Minimum specified ultimate stress*
$\sigma_{ult,mill}$	*Mill certificate/ Inspection document ultimate stress*
$\sigma_{ult,y}$	*Virgin sheet ultimate stress*
σ_x	*Stress at a given strain for a particular strain rate*
$\sigma_x(y)$	*Membrane residual stress at position y*
σ_y	*Yield stress*
$\sigma_{y,c}$	*Corner yield stress*
$\sigma_{y,v}$	*Virgin sheet yield stress*
$\sigma_{0.01}$	*0.01% proof stress*
$\sigma_{0.05}$	*0.05% proof stress*
$\sigma_{0.1}$	*0.1% proof stress*
$\sigma_{0.5}$	*0.5% proof stress*
$\sigma_{0.2}$	*0.2% proof stress*
$\sigma_{0.2av,exp}$	*Average experimental 0.2% proof stress taken from central 50% of flat faces in cold rolled sections*

$\sigma_{0.2,mill}$	*Mill certificate/ inspection document 0.2% proof stress*
$\sigma_{0.2,min}$	*Minimum specified 0.2% proof stress*
$\sigma_{1.0}$	*1.0% proof stress*
$\sigma_{0.2,exp}$	*Experimental 0.2% proof stress*
$\bar{\sigma}$	*Estimated experimental error*
$\bar{\sigma}_{0.2av,exp}$	*Predicted average 0.2% proof stress of 0.2% proof stresses from the central 50% of flat faces in cold rolled sections*
$\bar{\sigma}_{0.2,c}$	*Predicted corner 0.2% proof stress*
$\bar{\sigma}_{0.2,cr,c}$	*Predicted cold rolled corner 0.2% proof stress - based on mill certificate/ inspection document data*
$\bar{\sigma}_{0.2,exp}$	*Predicted 0.2% proof stress from hardness values*
$\bar{\sigma}_{0.2,f}$	*Predicted cold rolled flat face 0.2% proof stress - based on mill certificate/ inspection document data*
$\bar{\sigma}_{0.2,pb,c}$	*Predicted press braked corner 0.2% proof stress - based on mill certificate/ inspection document data*
$\bar{\sigma}'_{0.2,cr,c}$	*Predicted cold rolled corner 0.2% proof stress - based on minimum specified data*
$\bar{\sigma}'_{0.2,f}$	*Predicted cold rolled flat face 0.2% proof stress - based on minimum specified data*
$\bar{\sigma}'_{0.2,pb,c}$	*Predicted press braked corner 0.2% proof stress - based on minimum specified data*
$\hat{\sigma}_0^2$	*Variance factor*
φ	*Half the internal angle of Whittemore gauge point*
ω_o	*Amplitude of local imperfections*
ω_1	*Amplitude of local imperfections in internal elements*
ω_2	*Amplitude of local imperfections in outstand elements*
Δ	*Gauge point offset*

List of figures

List of tables

Chapter 1

Introduction

1.1 Background

The development of commercially available stainless steel is seen as the answer to the technical objective of achieving a 'rust-less' steel. The resulting material not only offers practical advantages but also the aesthetic of a durable exposed metallic surface. This appearance has over the years made the use of stainless steel highly desirable for designers of many products, as the surface finish reflects the modern desire for durability, cleanliness and expression of materiality. An understanding of the resulting material properties of stainless steel has suggested its benefits in many applications such as medical and domestic utensils and appliances. This thesis focuses on its use in structural applications where the high material cost of stainless steel structures demands the efficient use of material properties in design for more extensive use to be economically viable and for the advantages of low corrosivity to be utilised. These benefits include the potential to minimise a structure's maintenance cost and environmental impact.

1.2 Development of stainless steel

The defining property of stainless steel to resist corrosion and some types of chemical erosion is due to the addition of at least 10.5% chromium as an alloying element, which was isolated as an element in 1797 by Louis Vauqulien. Experiments in using this alloying element for the production of new types of steel started during the nineteenth century. Steels with a low chromium content of around 0.6% were manufactured in the USA and the UK towards the end of the century but its addition was driven by the desire to find ways of improving the mechanical properties of steel. Recognition that chromium improved corrosion resistance is first recorded in 1872 with a patent application for a 'weather resistant' steel containing 30-35% chromium. Developments in the creation of steels with higher chromium content occurred simultaneously by metallurgists in a number of countries including Germany, USA and the UK. A detailed historical account of this era of exploration is given by Truman (1985).

Harry Brearley, working in the Brown-Firth laboratories in Sheffield in 1913, greatly advanced the production and investigation of the non erosive properties of stainless steels with a martensitic microstructure. Amongst his numerous observations he importantly noticed an increase in the forces needed to process stainless steel after plastic deformation had occurred, a phenomenon termed cold working. It was his vision for the applications for stainless steel which anticipated its commercial potential. In the USA Elwood Haynes also contributed to the development of martensitic stainless steel with both Haynes and Brearley applying for patents in the USA during the years 1913 - 1916. Edward Maurer and Benno Strauss working at Krupps factory in Germany made significant progress in producing stainless steel with an austenitic microstructure which is now commonly used in the construction industry. Maurer and Strauss applied successfully for patents in the UK and Germany in 1912 - 1913. Post-first world war industry fulfilled Brearley's aspirations for the application of this new alloy with many of the now standard grades being developed during the 1920s and 30s.

The development of this family of steels is on going with the introduction of duplex grades in the 1930s. The duplex grades are a mixture of the ferritic and austenitic microstructure and provide superior strength and corrosion resistance but at a cost premium. Other specialist grades have also been developed, whose material characteristics are tailored to particular applications.

1.3 The stainless steel industry

The commercial production of stainless steel relied not just on advances in metallurgy but also on the technology to produce and process large quantities of stainless steel. The process still used as the main production route for stainless steel is the Electric Arc Furnace, EAF, which began its development in 1890. This is a process where recycled metals (stainless steel or carbon steel) and alloying elements such as chromium, that are used to modify the grade of stainless steel, are melted down using an electric current passed through the mix by graphite electrodes. Production techniques became more economical with the introduction of argon-oxygen decarburisation to control the content of carbon in the melt in the 1970s. The development of specialised equipment to process stainless steel owing to the significant cold working properties noted by Brearley has also played its part in making mass production viable.

The future growth of the stainless steel industry depends on improving efficiency of use to encourage wider application, meeting the increasing demand and finding a sustainable balance with regard to the use of energy and raw materials. Metals have the advantage that they can be theoretically 100% recycled with no degradation of material properties, however the lag time between stainless steel production and its entry into the scrap market combined with the current growth of between 5 and 6% per annum in demand for stainless steel (Jonsson, 2000 and Erkkilä, 2004) meant that only 20% of the stainless steel produced in 2004 was made from scrap stainless steel with the remaining 80% produced from scrap carbon steel and virgin alloying elements. In 2001 the demand for stainless steel products across the world was the highest in Western Europe when the production of stainless in these countries exceeded the demand. European use of stainless steel has now been overtaken by the rapidly growing market in China where only around 50% of the products used by China are produced within that country (Erkkilä, 2004). The demand and supply of stainless steel products and stainless steel scrap is one factor that controls the market price of stainless steel. A second factor is the highly volatile cost of the virgin alloying elements used to make stainless steel, particularly Nickel, which is based on their availability as limited natural resources.

The industry has traditionally grouped the variety of stainless steel grades into four categories according to their microstructure: ferritic, martensitic, austentic and duplex. The chemical composition of grades within these four families is set out in the material standard for stainless steels EN 10088-1 (2005). Whilst there are a number of designation systems for the different grades of stainless, the European system is adopted throughout this thesis.

The most common types of stainless steel used for structural products are the austenitic and duplex. Due to the relatively small demand for stainless steel in construction compared to carbon steel there are no standardised products, however, most structural products available in carbon steel can be produced in stainless steel. There are three principal production routes for stainless steel structural sections: hot rolling, and two types of cold forming: cold rolling and press braking. Cold rolled products have the largest presence in the market.

1.4 Use in the construction industry

Despite similarities to carbon steel, stainless steel has a number of characteristic material properties in addition to its increased corrosion resistance that have implications for structural design. These include the non linearity of its stress-strain curve, an ability to be cold worked to a significant degree and good retention of material properties at high temperatures (Gardner, 2005).

Due to the high material cost of stainless steel, its use in the construction industry has traditionally been confined to applications where maintenances is not physically possible, such as cavity wall ties, cladding brackets and reinforcement bars. Structural applications are seen in offshore structures, plant equipment and bridges where the harsh environments and limited access demand durability. An example of use in a pedestrian bridge is shown in Figure 1.1, whilst on a much larger scale and currently under construction is the single span cable stayed Stone cutters bridge in Hong Kong which will have a span of 1 km and whose pylons and structural cladding are being made from stainless steel.

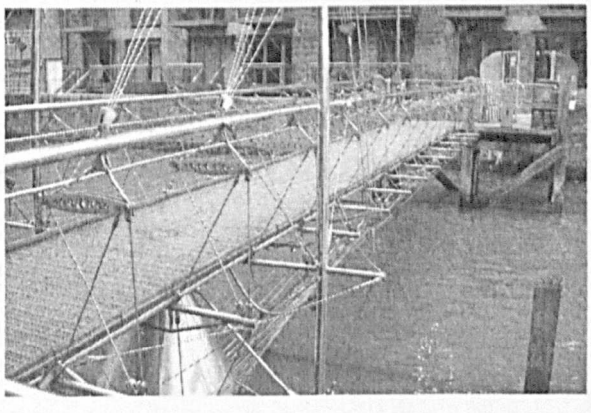

Figure 1.1: *Stainless steel bridge, St. Saviours Dock, Shad Thames, London*

Stainless steel has also found a market in prestige architectural and engineering projects where an exposed metallic surface has been key to achieving design objectives, such as the internal finishes and the cladding at the top of the Chrysler building, New York. This skyscraper shown in Figure 1.2 was designed by architect William van Alen in the art deco style and was completed in 1929. It is a testament to the durability and low maintenance of stainless steel as well as its ability to express opulent style.

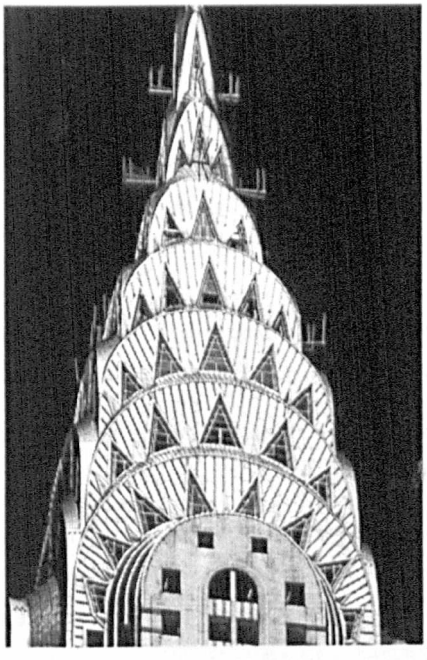

Figure 1.2: *The Chrysler building*

The wide range of surface finishes available in stainless steel gives the designer the opportunity to modulate how an architectural presence is felt. High shines allow the stainless steel to dissipate into reflections of the surrounding space, whilst less fine surfaces capture light and movement. The variety of surface finishes available for stainless steel products is partly set out in the material standard for stainless steel sheet products (EN 10088-2, 2005) summarised in Table 1.1 and show-cased by the architect Frank Gehry's portfolio of stainless steel clad buildings, two of which are shown in Figure 1.3.

Table 1.1: *A summary of standard surface finishes for stainless steel sheet*

Surface finish number	*Production route and appearance*
	Hot rolled sheet:
0	Hot band, plate products rolled to required thickness and annealed. Surface finish is black and scaled.
1	Hot rolled sheet, annealed, pickled and passivated to produced sheet with a dull rough surface. Used for industrial applications and to produce cold rolled sheet.
	Cold rolled sheet:
2D	Number 1 finish which is cold rolled, annealed, picked and passivated with a dull matt finish, used in industrial applications.
2B	2D sheet given a light skin pass by polished rollers to produce a semi-reflective finish.
2BA	Bright annealed finish achieved by feeding number 1 finish sheet through highly polished rollers and then annealing in an inert atmosphere.
3	Uni-directional finish used as intermediate surface for finishes of higher polish.
	Finer finishes (produced only on one side of the sheet product):
4	Finer unidirectional finish than number 3 finish. Used in environments were hardware is anticipated.
6	Non directional texture such as a satin finish.
7	Buffed finish which is highly reflective achieved with fine abrasives and buffing compounds.
8	Mirror finish, similar but finer polishing process to a number 7 finish.

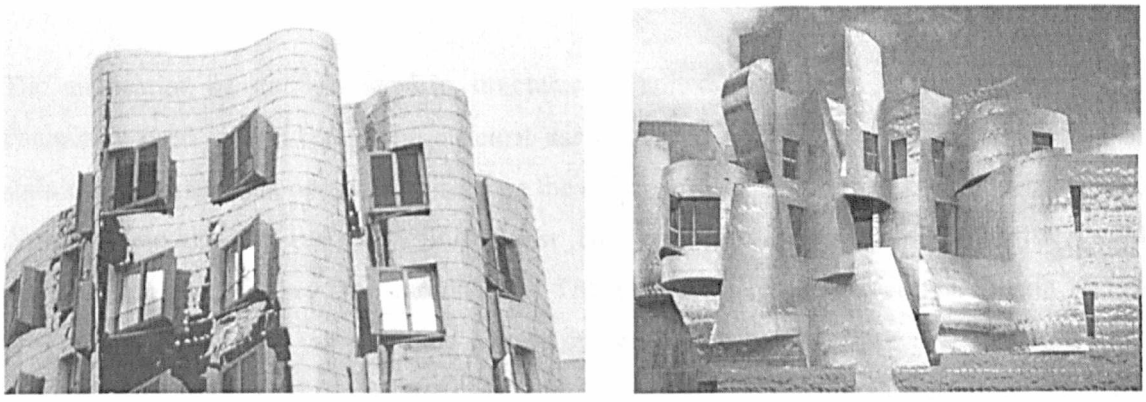

Figure 1.3: *Building B, Neuer Zollhofs, Dusseldorf, Germany with a number 8 finish cladding and the Teaching Museum, Minneapolis, Minnesota, U.S.A with a number 6 finish cladding*

After the industrial revolution in 1923 a Swiss architect Le Corbusier wrote in his famous text 'Vers Une Architecture' of the beauty of the new machines, as their functionality was directly expressed through their form. This radical proposition challenged the purely decorative aesthetics practised by past designers and was a point of departure suggesting that the expression of the internal workings of buildings could be used to provide visual impact. These ideas were put into practice in the 1960's by the High Tech architects such as Norman Foster and Richard Rodgers. Their use of external and internally exposed structures have heightened designers' interest in the industrial aesthetic that can be achieved by stainless steel structural components. Figure 1.4 shows the Sanamotalo building in Helsinki, a recent example of its use in structures, designed by Sarc Architects and completed in 1999, demonstrating the ability of stainless steel to be manufactured and fabricated as structural components to stunning effect.

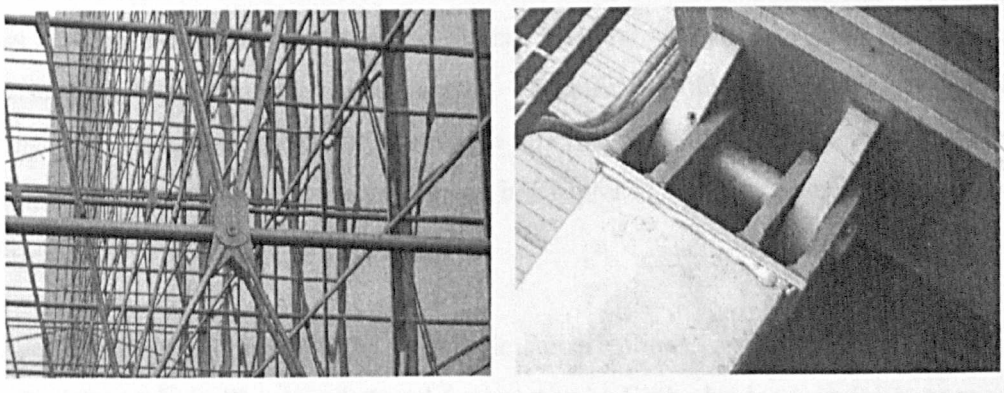

Figure 1.4: *Sanomatalo building, Helsinki*

1.5 Research objectives

The application of stainless steel in structures is limited by its high cost compared to the commonly used carbon steel. The efficient use of the significant cold working properties of stainless steel provides one way to increase the efficiency of the currently overtly conservative design predictions and reduce the initial cost. During plastic deformation stainless steel cold works to a greater degree than carbon steel. The aim of the research presented herein was to propose a methodology which would harness increases in material strength caused by plastic deformation experienced during the most common section production routes. In addition the research aimed to provide residual stress and imperfections distributions associated with each production route, as all three parameters are influenced by the production route and will influence the structural behaviour of stainless steel cross sections.

1.6 Outline of Thesis

This introductory chapter provides background information for the research and sets out the research objectives. The characteristic material properties of stainless steel are provided in Chapter 2, followed by a description of the principal production routes that are used to form stainless steel cross sections, a review of the development of design guidance and a summary of previous research projects which have focused on the structural behaviour of stainless steel.

An important part of the research project was an experimental program conducted to map the material properties around stainless steel cross sections from three principal production routes: press braked, cold rolled and hot rolled. The experimental program also mapped two other properties of cross sections that have been related to production processes for carbon steel sections and can have a detrimental effect on the structural behaviour of cross sections, namely geometric imperfections and residual stresses. The effect of these aspects must therefore be offset against the enhanced material strength offered by cold working stainless steel. An overview of the experimental program is given in Chapter 3. The experimental study considered sections made from austenitic grade 1.4301.

The thesis treats the three subjects: geometric imperfections, residual stresses and material properties separately in Chapters 4, 5 and 6 respectively. Each chapter contains a more specific literature review, details of the experiments conducted, data analysis, comparisons with existing

data and models and conclusions. Chapter 7 proposes a design method to incorporate more accurate material properties in structural design.

The economic viability of stainless steel structures is key to its future development. The high material costs can obscure the true economic value of specifying stainless steel, as savings over the lifetime of a structure due to minimised maintenance are not considered. A life cycle costing study was carried out in Chapter 8 to examine the effect of the long term benefits of structural stainless steel compared to carbon steel and aluminium structures. This study forms the basis for a discussion of cost savings given in the conclusions of the research.

The final chapter summaries the research project and looks at the implications for structural applications of stainless steel and the stainless steel industry as a whole, as well as identifying possible areas of future research.

Chapter 2

Literature review

2.1 Introduction

This chapter aims to establish the current research and industrial technology behind the structural behaviour of stainless steel and the structural sections production routes, whilst more detailed literature reviews are given in Chapters 4, 5 and 6 to provide specific background information to each research topic.

Underlying both the structural and manufacturing aspects examined in this thesis is the material behaviour of stainless steel, which is discussed as well as the development of material models for stainless steel. A general summary of the types of processes that are used in section production and industry standards that influence the manufactured product is given. The development of specific design rules for stainless steel structures is described together with the major research programs that have been carried out in this field.

2.2 Material properties

An understanding of the material behaviour of stainless steel is fundamental to the research project as it contributes not only to the prediction of the structural behaviour of members during loading but also because it is key to understanding the material properties observed after a particular strain path or thermal treatment has been implemented during a section forming process.

2.2.1 Stress-strain behaviour

Under an applied stress stainless steel exhibits non-linear material behaviour. This contrasts with behaviour of carbon steel which displays a clearly defined linear elastic region, a flat plastic plateau and a moderate degree of strain hardening at large strains (typically > 2%). The difference between the stress-strain curves is shown diagrammatically in Figure 2.1. The loading path of stainless steel is characteristically rounded at the transition between elastic and plastic behaviour, so convention defines the yield point as the 0.2 % proof stress $\sigma_{0.2}$, obtained at the point of the 0.2% plastic strain. Also due to the rounded nature of the stainless steel stress-strain curve the limit of proportionality is generally defined as the stress at 0.01% plastic strain $\sigma_{0.01}$. Beyond the elastic-plastic transition stainless steel displays considerable strain hardening which was observed by one of the key developers of stainless steel Brearley (Brearley, 1989).

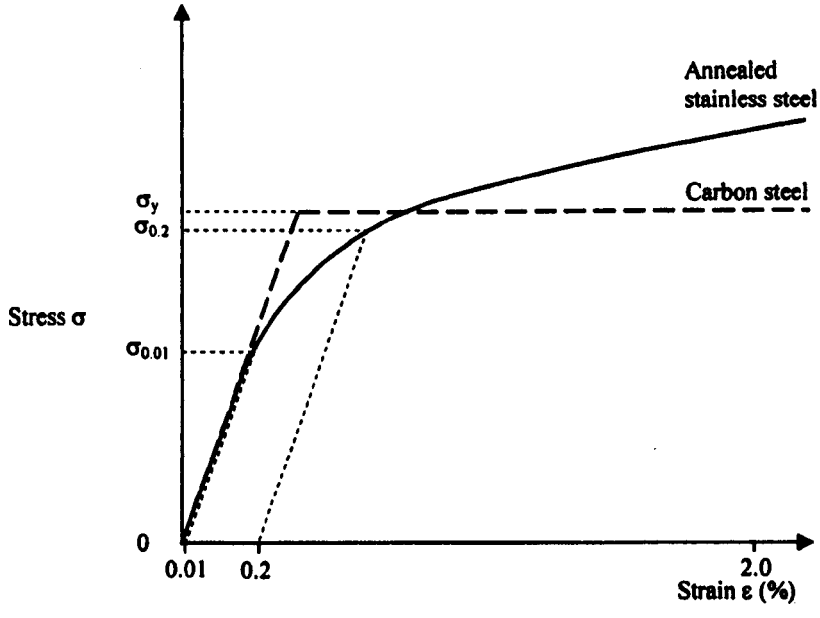

Figure 2.1: *Stainless steel and carbon steel material stress-strain behaviour*

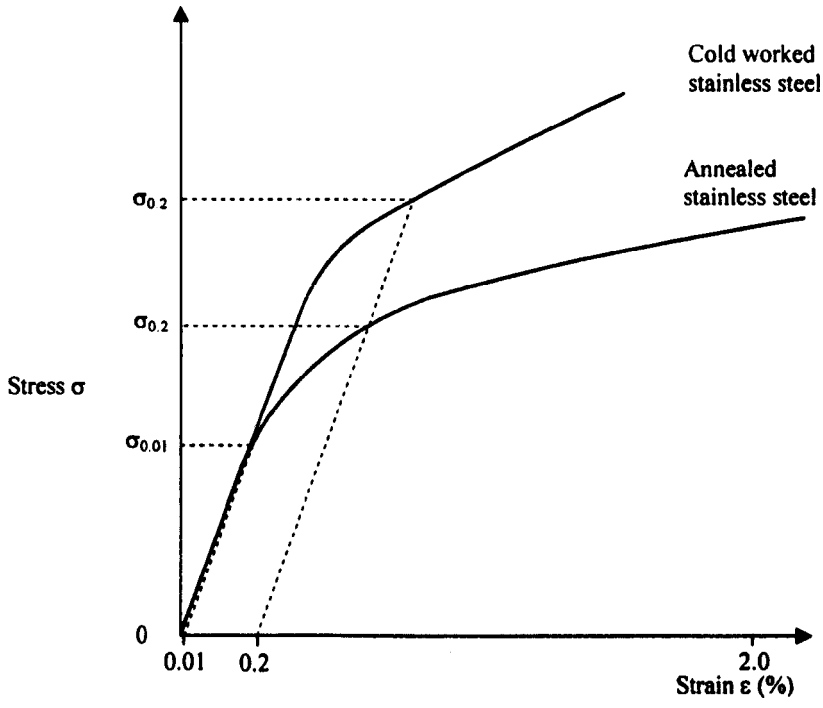

Figure 2.2: *Stainless steel material stress-strain behaviour*

2.2.1.1 Strain hardening

Straining of austenitic stainless steel, caused by an applied stress, occurs by the movement of dislocations in the metal lattice. During plastic deformation the number of dislocations present increases. Dislocations interact, impeding their ability to move through the lattice, reducing the strain observed for a particular increase in loading. In addition a strain induced martensite phase nucleates within the forming dislocation arrays. The martensite phase strengthens the austenitic phase and increases the strain hardening rate (Spencer et al., 2004). On removal and re-application of the applied stress this now strain hardened or cold worked material follows a new loading path, with a higher 0.2% proof stress and ultimate stress but which is less ductile. A diagrammatic comparison of a cold worked stainless steel and an annealed stainless steel is shown in Figure 2.2.

Strain hardening in materials occurs approximately below 0.4-0.5 of the melting point (Edwards and Endean, 1999), which is approximately 700°C for stainless steels. As the temperature increases dislocations can move at an increasing rate within the metal's lattice and so the amount by which they impede their own movement decreases. On annealing stainless steel above 700 °C re-crystallisation of the metal lattice occurs returning the material to a lower

dislocation density. In annealed material a lower yield point and ultimate stress but higher ductility is observed.

2.2.1.2 Anisotropy

Due to the ability of stainless steel to be cold worked the material properties depend on the strain history of the tested sample. The application of stresses that cause large deformations in a particular direction align the material grains with the direction of the deformation. On subsequent loading the amount of strain hardening observed in the transverse direction is higher than the strain hardening observed in the longitudinal direction. Directional deformation creates a pronounced anisotropic behaviour in stainless steel. These material properties are observed and discussed by Johnson and Winter (1966), and Wang et al. (1975).

2.2.1.3 Bauschinger effect

Another phenomenon that affects stainless steel and depends on the strain history of the sample is the Bauschinger effect. Loading of a stainless steel coupon beyond yield creates internal, or residual stresses, which means that on loading under compression material behaviour follows a different stress-strain path than that observed in tension where the 0.2% proof stress is higher than the yield point observed under compression. This difference in behaviour is also accentuated by cold working. Both tensile and compressive coupons were tested by Gardner (2002) and their behaviour compared. Overall the differences were small with the 0.2% proof stress being 5% lower and a 4% increase in the 1.0% proof stress.

2.2.1.4 Strain rates

The strength of stainless steel has been reported in the literature as strain rate dependant with an increase in strength observed at higher strain rates. Nordberg (2004), based on an experimental study for austenitic stainless steel grades 1.4301 and 1.4401, presents a model given in Equation 2.1 to predict the stress value σ_x for a given strain ε_x based on the strain rate $\dot{\varepsilon}_x$ and the static flow stress σ_{ox}. The static flow stress is defined as the stress observed at a strain rate of $10^{-3}s^{-1}$.

$$\sigma_x = \sigma_{ox} + 90 + (30 \log \dot{\varepsilon}_x) \tag{2.1}$$

The research shows that for a ten fold increase in strain rate an increase of approximately 50 N/mm^2 is predicted for the 0.2% proof stress of austenitic stainless steel. Dier (1991) found that on average a ten fold increase in strain rate causes a 4% increase in the 0.2% proof stress.

2.2.2 Thermal Behaviour

The thermal behaviour of stainless steel is also significantly different to that of carbon steel. The specific heat of stainless steel is approximately 500 J/kgK as compared to carbon steel which has a value of approximately 600J/kgK. The lower the specific heat of a material, the more rapidly it tends to heat up. For temperatures below about 1000°C, the thermal conductivity of stainless steel is lower than that of carbon steel; at low temperatures the difference is significant, whilst above about 700°C, the difference is small (Gardner, 2005 and Gardner and Ng, 2006). The coefficient of thermal expansion of stainless steel is up to approximately 50% larger than that of carbon steel, which may result in greater distortion of material during heat input.

At elevated temperatures, all metals lose strength and stiffness. A comparison of the strength and stiffness retention of carbon steel and stainless steel at elevated temperatures is made by Baddoo and Gardner (2000). Generally stainless steel offers superior retention of strength and stiffness at elevated temperature than carbon steel which is discussed in more detail by Gardner (2005).

2.3 Material models

2.3.1 Uniaxial constitutive models

To describe the uniaxial stress-strain behaviour of carbon steel, structural codes have adopted a bi-linear material model which defines a linear elastic region and a linear plastic plateau with the yield point at their intersection. This model is however inappropriate for the non linear behaviour of stainless steels. There have been several types of models suggested for the uniaxial stress-strain behaviour of non-linear materials.

Power models have been proposed by Swift and Luwik, which are described in Slater (1977). The power models have the disadvantage of limited accuracy in the elastic to yield region. Power polynomial expressions have been employed by Chryssanthopoulos and Low (2001) and Frye and Morris (Chen and Lui, 1991), though the high order of the polynomial required to give a good fit to experimental data creates numerous coefficients to define which have no relation to the physical properties of the stress-strain behaviour. The applicability of a material model for stainless steel structural design therefore depends not only on its accuracy within an appropriate strain range but also on the number of unknown parameters and the availability of the required material data for the marketed structural sections.

One model in particular has been used to approximate both the behaviour of aluminium and stainless steel due to its accuracy for strains lower than 0.2%. This model was proposed in 1943 by Ramberg and Osgood and it is shown in Equation 2.2. It can be used to model the behaviour of aluminium alloys, stainless steel and carbon steel. This expression sums the separate elastic and plastic components of strain to find the total strain, ε. The n parameter therefore controls the amount of plasticity or strain hardening modelled.

$$\varepsilon = \frac{\sigma}{E} + K\left(\frac{\sigma}{E}\right)^n \tag{2.2}$$

A modification to Equation 2.2 was made by Hill (1944) changing the constant K to a given value of plastic strain so that in the plastic component of the Ramberg-Osgood expression the Young's modulus is converted to the proof stress at the given value of plastic strain. The most common form of Hill's version of the Ramberg-Osgood expression is to use the 0.2% proof stress, $\sigma_{0.2}$ as shown in the following equation:

$$\varepsilon = \frac{\sigma}{E} + 0.002\left(\frac{\sigma}{\sigma_{0.2}}\right)^n \tag{2.3}$$

The expression uses three parameters: the modulus of elasticity E, the yield strength $\sigma_{0.2}$ and the n parameter to describe the non linear behaviour. Equation 2.3 has been found to give good approximations below the 0.2% proof stress but further modifications have been proposed to reduce the un-conservative predictions observed beyond this point.

Hill (1994) derived Equation 2.4 to determine the strain hardening parameter n by using the stress and plastic strain at two points. Typically one point taken is the 0.2% proof stress $\sigma_{0.2}$ and $\varepsilon_{0.2}$. The second stress-strain point is noted as σ_{snd} and ε_{psnd}.

$$n = \frac{\log\left(\frac{\varepsilon_{psnd}}{\varepsilon_{p0.2}}\right)}{\log\left(\frac{\sigma_{snd}}{\sigma_{0.2}}\right)} \tag{2.4}$$

To increase the accuracy of the model at higher strains Macdonald et al. (2000) proposes Equation 2.5, where i, j and k are experimentally defined variables and σ_{snd} is the stress at an offset strain. This equation is demonstrated to show a good approximation but only on limited tests that were restricted to one grade of stainless steel.

$$\varepsilon = \frac{\sigma}{E} + 0.002\left(\frac{\sigma}{\sigma_{snd}}\right)^{\left(i+j\left(\frac{\sigma}{\sigma_{snd}}\right)^{k}\right)} \tag{2.5}$$

An alternative compound expression was proposed by Mirambell and Real (2000) where Hill's expression was adopted up to the 0.2 % proof stress (Equation 2.6). The expression for strain above the 0.2% proof stress repeats the use of Equation 2.2 with a second Ramberg-Osgood expression that has its origins at $\sigma_{0.2}$ and $\varepsilon_{t0.2}$ and operates within a post-yield coordinate system defining a new strain hardening parameter, n'. This second Ramberg-Osgood expression requires replacing the elastic modulus, E with the tangent modulus at the 0.2 % proof stress, $E_{0.2}$ and the 0.2 % plastic strain 0.002 with the plastic strain component at the ultimate stress, ε_{pult}. This was then added to the total strain experienced prior to the 0.2 % proof stress, $\varepsilon_{t0.2}$ as shown in Equation 2.7.

$$\varepsilon = \frac{\sigma}{E} + 0.002\left(\frac{\sigma}{\sigma_{0.2}}\right)^{n} \qquad \sigma \leq \sigma_{0.2} \tag{2.6}$$

$$\varepsilon = \frac{(\sigma - \sigma_{0.2})}{E_{0.2}} + \varepsilon_{pult}\left(\frac{\sigma - \sigma_{0.2}}{\sigma_{ult} - \sigma_{0.2}}\right)^{n'} + \varepsilon_{t0.2} \qquad \sigma \geq \sigma_{0.2} \tag{2.7}$$

Simultaneously the same expression, with different notation was developed by Rasmussen (2003) to provide an accurate material model for a full stress-strain curve. In this study it is proposed that n can be calculated using natural logs and the 0.2% and the 0.01% proof stresses (Equation 2.8).

$$n = \frac{\ln(20)}{\ln\left(\frac{\sigma_{0.2}}{\sigma_{0.01}}\right)} \tag{2.8}$$

To obtain the second strain hardening parameter n' Rasmussen (2003) used an iterative method to fit the proposed model to experimental tensile coupon tests data. From these values an expression to predict the second strain hardening parameter was given:

$$n' = 1 + 3.5\frac{\sigma_{0.2}}{\sigma_{ult}} \tag{2.9}$$

In addition it was observed that as the compound Ramberg-Osgood model is expressed using the ultimate stress σ_{ult} it is not applicable to modelling compression tests since no ultimate stress can be determined as necking does not occur. Recognising these limitations expressions were proposed based on experimental data to give the ultimate stress and corresponding total strain values for cases where compression loading was considered.

An amendment to the compound Ramberg-Osgood equation was proposed by Gardner (2002) this was to modify the second post-yield Ramberg-Osgood expression. An additional factor was introduced to the plastic strain component to amend the curve described in Equation 2.7 so that it precisely intersects the point of ultimate strain and stress. Gardner then eliminates the need to define the ultimate stress by replacing the ultimate stress with the 1.0 % proof stress to give Equation 2.11. This final adjustment makes the expression suitable for behaviour in compression.

$$\varepsilon = \frac{\sigma}{E} + 0.002\left(\frac{\sigma}{\sigma_{0.2}}\right)^{n} \qquad \sigma \leq \sigma_{0.2} \tag{2.10}$$

$$\varepsilon = \frac{(\sigma - \sigma_{0.2})}{E} + \left(0.008 - \frac{\sigma_{1.0} - \sigma_{0.2}}{E_{0.2}}\right)\left(\frac{\sigma - \sigma_{0.2}}{\sigma_{1.0} - \sigma_{0.2}}\right)^{n'} + \varepsilon_{t0.2} \qquad \sigma \geq \sigma_{0.2} \tag{2.11}$$

If the logic of the post yield coordinate system, shown in Figure 2.3 is rigoursly adopted it is noted by Gardner and Ashraf (2006) that the plastic strain given as 0.008 in Equation 2.11 should in fact be replaced with the total strain and the resulting equation within the new coordinate system, is given in Equation 2.12.

$$\varepsilon = \frac{(\sigma - \sigma_{0.2})}{E} + \left(\varepsilon_{t1.0} - \varepsilon_{t0.2} - \frac{\sigma_{1.0} - \sigma_{0.2}}{E_{0.2}}\right)\left(\frac{\sigma - \sigma_{0.2}}{\sigma_{1.0} - \sigma_{0.2}}\right)^{n'} + \varepsilon_{t0.2} \tag{2.12}$$

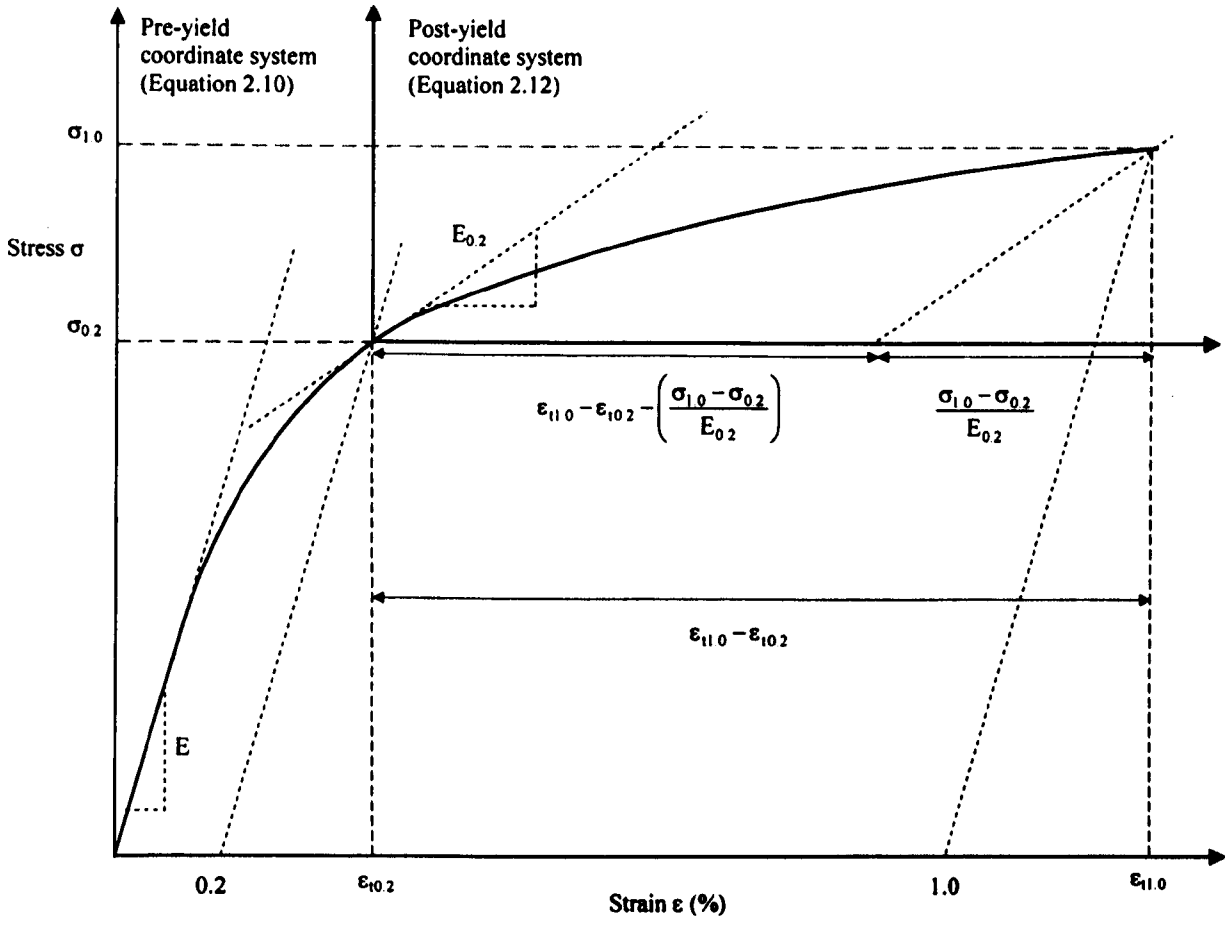

Figure 2.3: *The compound Ramberg-Osgood expression*

The n' parameter may therefore be determined by the expression given in Equation 2.13. The expression requires an additional proof stress σ_{snd} and corresponding strain ε_{tsnd} such as 0.5 % $\sigma_{0.5}$ as well as $\sigma_{1.0}$ and $\sigma_{0.2}$.

$$n' = \frac{\log\left(\frac{\left(\varepsilon_{tsnd} - \frac{\sigma_{snd} - \sigma_{0.2}}{E_{0.2}} - \varepsilon_{t0.2}\right)}{\varepsilon_{pl.0}}\right)}{\log\left(\frac{\sigma_{snd} - \sigma_{0.2}}{\sigma_{1.0} - \sigma_{0.2}}\right)} \qquad (2.13)$$

Expressions 2.10 and 2.12 are adopted in this study to model the material behaviour of tensile coupon tests.

One draw back of the Ramberg-Osgood expression is that it could not explicitly be solved for stress, however an inversion of the compound Ramberg-Osgood expression (Mirambell and Real, 2000) was proposed by Abdella (2006) which facilitated expressing the stress as a function of strain. The inversion was modified by Abdella (2007) to incorporate the modifications proposed by Gardner and Ashraf (2006) and showed its accuracy in modelling experimental data.

Expressed using normalised stress $\sigma_n=\sigma/\sigma_{0.2}$ and normalised strain $\varepsilon_n= \varepsilon/\varepsilon_{t0.2}$ Equation 2.14 describes the inversion below the 0.2% proof stress.

$$\sigma_n = \frac{r\varepsilon_n}{1+(r-1)(\varepsilon_n)^p} \qquad \varepsilon_{n\leq 1} \qquad (2.14)$$

Where r, r_2 and p are defined as follows:

$$p = r\frac{1-r_2}{r-1} \qquad (2.15)$$

$$r_2 = \frac{E_{0.2}\varepsilon_{t0.2}}{\sigma_{0.2}} \qquad (2.16)$$

$$r = \frac{E\varepsilon_{t0.2}}{\sigma_{0.2}} \qquad (2.17)$$

Equation 2.18 describes the inversion above the 0.2% proof stress.

$$\sigma_n = 1 + \frac{r_2(\varepsilon_n - 1)}{1+(s-1)\left(\frac{\varepsilon_n - 1}{\varepsilon_{n1.0} - 1}\right)^{p_1}} \qquad \varepsilon_{n>1} \qquad (2.18)$$

Where s, s_1 and p_1 and $\varepsilon_{n1.0}$ are defined as follows:

$$s = E_{0.2}\frac{\varepsilon_{t1.0}-\varepsilon_{t0.2}}{\sigma_{1.0}-\sigma_{0.2}} \qquad (2.19)$$

$$s_1 = E\frac{\varepsilon_{t1.0}-\varepsilon_{t0.2}}{\sigma_{1.0}-\sigma_{0.2}} \qquad (2.20)$$

$$p_1 = s\frac{1-s_1}{s-1} \tag{2.21}$$

$$\varepsilon_{n1.0} = \frac{\varepsilon_{t1.0}}{\varepsilon_{t2.0}} \tag{2.22}$$

In this form the ability of the Ramberg-Osgood expression to model nonlinear material behaviour and its applicability in structural engineering are greatly enhanced.

2.3.2 Biaxial constitutive models

Plastic deformation during section production is rarely caused by applied forces that act purely in axial tension or axial compression. Typically section forming is carried out by complex combinations of applied forces. Models of the observed plastic deformation require an approximation of these complex forces that are thought to be applied. The development of models that combine the stresses experienced by the material are the biaxial constitutive equations.

Out of the constitutive models that have been defined specifically for metals, the basic model developed by Richard von Mises in 1913 is the most commonly used for metal forming. This model is defined for an ideal plastic body where yield is assumed not to be initiated by hydrostatic stresses. The material is assumed to be isotropic (i.e. directional cold working is not accounted for), and that it does not exhibit the Bauschinger effect. The yield criterion illustrated in Figure 2.4 states how the combined stresses determine when the yielding stress is exceeded and when plastic deformation starts. This criterion defines a yield surface for combinations of stresses.

A more complex model suggested by Hill (1983) models strain hardening by proposing a single parameter, 'the effective strain' that is independent of the manner in which the stress is applied but dependant on the total amount of plastic deformation experienced. The von Mises–Hill theory was developed by Gozzi and Olsson (2003) specifically for modelling the anisotropic behaviour of duplex and cold worked stainless steel. The gradual yielding of stainless steel and the Bauschinger effect is allowed for by developing the single yield surface into two surfaces, one to define the elastic limit and the other a memory surface to record prior strain histories.

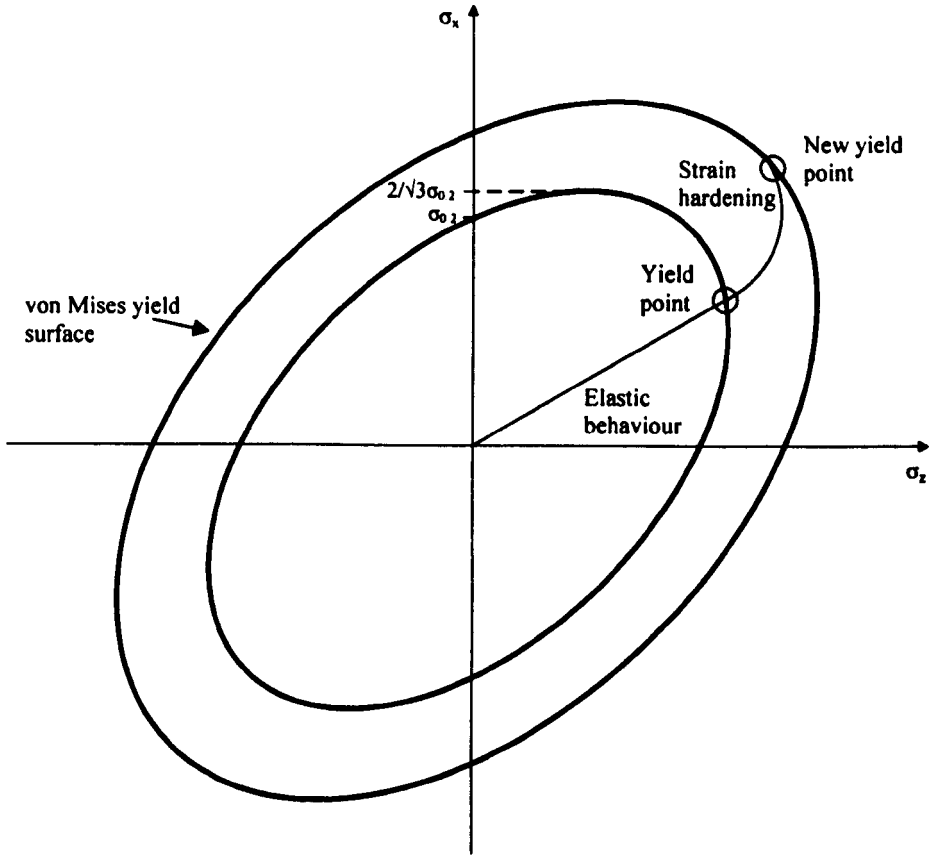

Figure 2.4: *von Mises yield surface with an isotropic hardening rule*

2.4 The production of stainless steel

2.4.1 Introduction

Due to the sensitivity of stainless steel to plastic deformation and thermal effects, a structural section production route has an important influence on the final material properties. In addition, the production routes influence the residual stresses and geometric imperfections found in the sections. An overview of stainless steel production through to the section forming processes is presented herein.

2.4.2 Production overview

Stainless steel is typically produced in an electric arc furnace (EAF) from a mixture of alloying elements and scrap carbon steel and/or stainless steel. Impurities such as silicon and sulphur are removed by combining them with oxygen, and argon is blown through the molten material to ensure consistency in the mix. This process is called argon oxygen decarburisation (AOD). The

molten stainless steel is then transferred into a continuous caster, where it passes through cooled moulds forming it into different shapes and sizes. Blooms, billets and slabs are produced from the continuous caster and are termed partial products. These partial products can then be used as the starting material for the manufacture of a number of final products. Reheated blooms and billets can be formed into hot rolled sections, whilst reheated slabs can be rolled into sheet material. However, it is more efficient to hot roll long products (e.g. hot rolled sections) and sheet material directly from the hot cast slabs on continuous production lines. The sheet material can then be formed unheated into cold formed sections. The two principal cold forming routes are press braking and cold rolling. A diagrammatic overview of the production route of structural sections is given in Figure 2.5 and the production of sheet material, press braking, cold rolling and hot rolling is detailed in the following section.

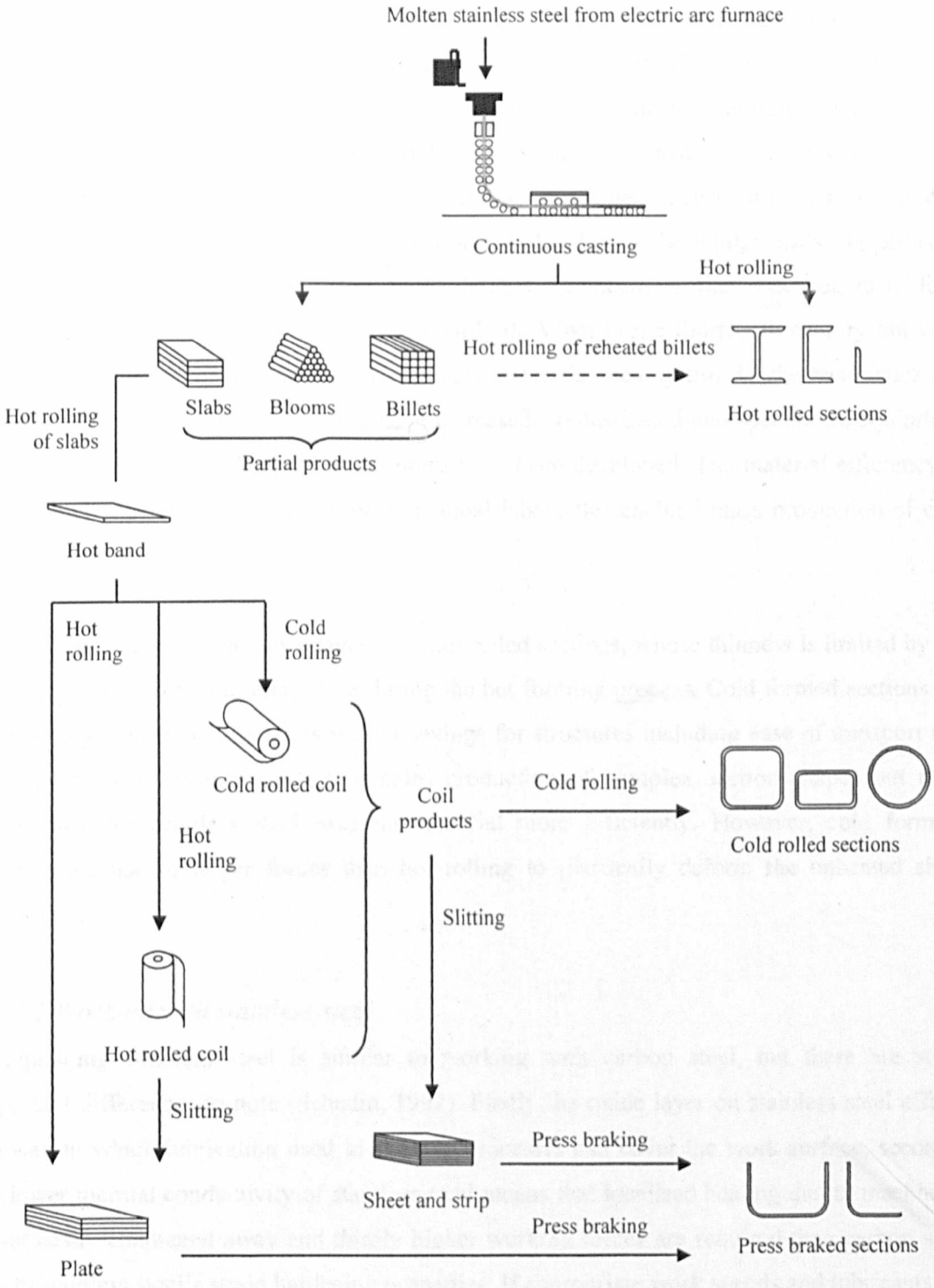

Figure 2.5: *An overview of structural section production*

2.4.3 Cold formed sections

The techniques for producing hot rolled sections were invented simultaneously with introduction of steel structures into the construction industry. The development of working with cold material to form sections was dependant on the invention of mechanised equipment to consistently produce thin sheet material that could be plastically deformed into sections. Forming the cold sheet material was initially carried out with manually operated equipment. Press braking sheet material is a one such forming technique which continues to be used to produce simple section shapes between a tool and die due to the equipment's versatility in producing different shapes and sizes. Early designs for machines that used rollers to form unheated sheet materials were made by Leonardo da Vinci in the fourteenth century but were for several centuries only used to roll very soft materials such as tin. As the techniques and understanding of this forming process have increased, sophisticated and specialised equipment that can manipulate a wide range of materials have been developed. The material efficiency of cold rolling and the ensuing reduction in manual labour has enabled mass production of cold formed sections.

Cold formed sections hold advantages over hot rolled sections, whose thinness is limited by the necessity of the section to retain heat during the hot forming process. Cold formed sections are increasingly slender which offers weight savings for structures including ease of transport and handling on site. This technology enables production of complex section shapes but most importantly for stainless steel uses the material more efficiently. However, cold forming requires the use of larger forces than hot rolling to plastically deform the unheated sheet material.

2.4.3.1 Working with stainless steel

Manipulating stainless steel is similar to working with carbon steel, but there are some important differences to note (Schedin, 1992). Firstly the oxide layer on stainless steel affects the way in which lubrication used in forming processes can cover the work surface, secondly the lower thermal conductivity of stainless steel means that localised heating due to machining is not easily conducted away and thirdly higher working forces are required than carbon steel due to stainless steel's strain hardening properties. If appropriate work speeds and lubricants are not used, all these factors increase the likelihood of galling to occur; where the work tool is not separated from the work piece by lubricant and the work piece or swaf from the work piece attaches itself to the tool.

2.4.3.2 Cold forming stainless steel

In cold formed sections it is the plastic deformation that occurs during production of the sheet material, from which sections are formed, and during the section forming process that is linked to the cold working of stainless steel (van den Berg and van der Merwe, 1992, Gardner, 2002 and Ashraf et al., 2005), the formation of residual stresses and the magnitude and distribution of geometric imperfections.

2.4.3.3 Sheet material

Sheet material may be produced either by hot rolling or cold rolling. Wide flat material formed from the continuous caster or from reheated slabs is called hot band, which can be further reduced whilst it is at high temperatures to produce hot rolled sheet. The minimum thickness of hot rolled sheet is limited by the fact that the sheet has to retain heat during the rolling process; typically the limit is 1.8-1.5 mm thick (Halmos, 2006). Alternatively, hot band can be cooled and rolled unheated to make cold rolled material which, whilst requiring higher forces to reduce the thickness enables thinner sheet material to be produced.

Hot rolled material is generally pickled and annealed before a final pass through temper mills. This pass compresses the surface layer of material to give the desired surface finish. Tests carried out by Johnson and Winter (1966) on annealed sheet indicate that this final pass is enough to induce anisotropy into stainless steel.

Cold rolling is performed in Sendzimir mills which were designed with multiple backing rolls to create large forces that would be transmitted to the work piece through a relatively small diameter work roll as shown in Figure 2.6. Work rolls in Sendzimir mills are not driven, instead the material is drawn through thereby causing the work piece to be held in tension during the reduction process. Different levels of cold work are achieved by varying the percentage reduction of the material thickness by sequential passes and sheet material can thereby be produced to different levels of cold working.

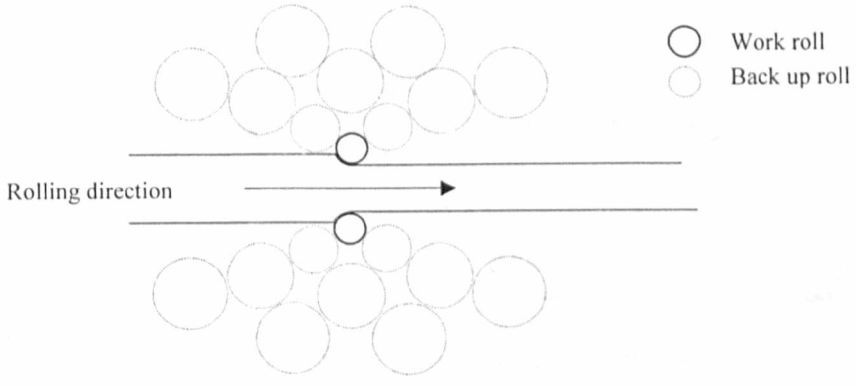

Figure 2.6: *A Sendzimir mill*

Sheet materials are typically wound into coils to facilitate compact storage and ease of transport as shown in Figure 2.7. There is a critical coil radius below which plastic deformation occurs during the coiling of sheet material (Quach, 2004), which depends on the thickness and material properties of the sheet. Whether values below this coil radius are obtained depends on the internal radius of the coil and the sheet's position in the roll. Prior to forming sections, the sheet material must be decoiled and levelled to ensure that no residual curvature exists in the material. This process is described in Figure 2.8.

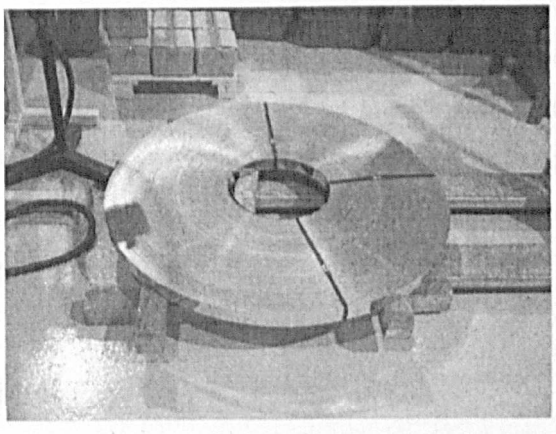

Figure 2.7: *Coiled strip*

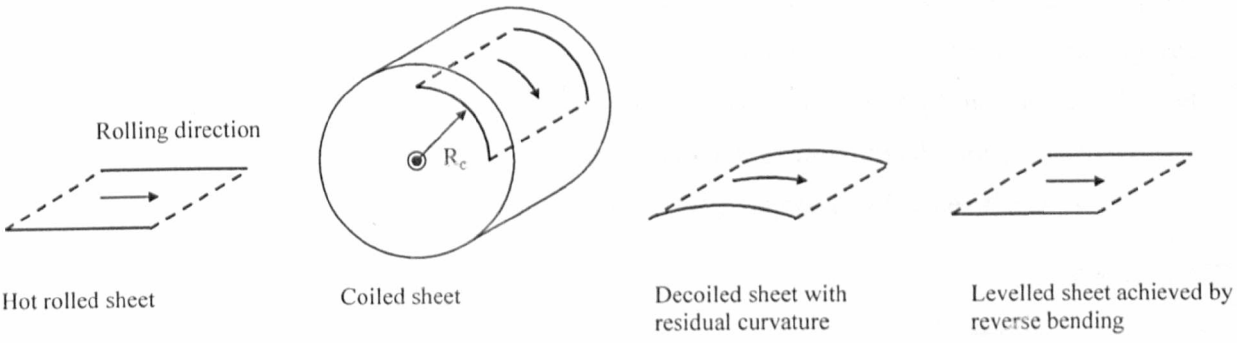

Figure 2.8: *Decoiling and levelling the sheet material*

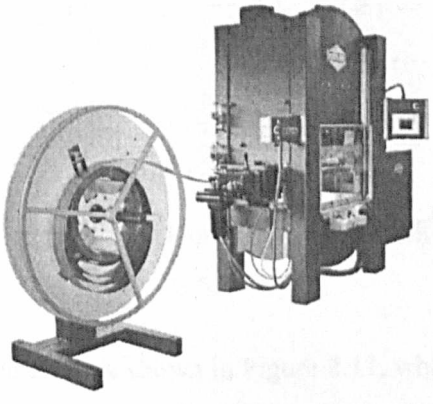

Figure 2.9: *Decoiler used to level the coiled material*

For cold rolled sections decoiling is carried out on an automatic decoiler (Figure 2.9) by the section manufacturer, whereas sheet and strip used for press braking sections is decoiled and slit into the required dimensions by the sheet manufacturer using similar equipment. It is critical for any residual curvature to be removed from sheet material which is to be press braked as press brakes can accommodate only small curvatures.

2.4.3.4 Press braked sections

Press braking is a process of cold forming sections from flat sheet by creating a simultaneous fold along the length of the sheet material with a tool that presses the material into a fixed die. This process is normally used to create open sections such as angles and channels, and tends to be used to produce small batches of bespoke or prototype sections. Owing to the physical

limitations of a press brake, the section lengths tend to be shorter than for cold rolled sections. The production of shorter members allows the length of the section to be taken transverse to the direction in which the sheet material has been rolled. The versatile process of air braking shown in Figure 2.10 uses a tool and die to produce a range of different angles. Spring back requires manufacturers to over bend the material so that the final recovered fold matches the desired angle. The final internal radius r_i and the internal angle θ of the formed corner is achieved by controlling the stoke depth and selecting the width of the die opening (termed the die V).

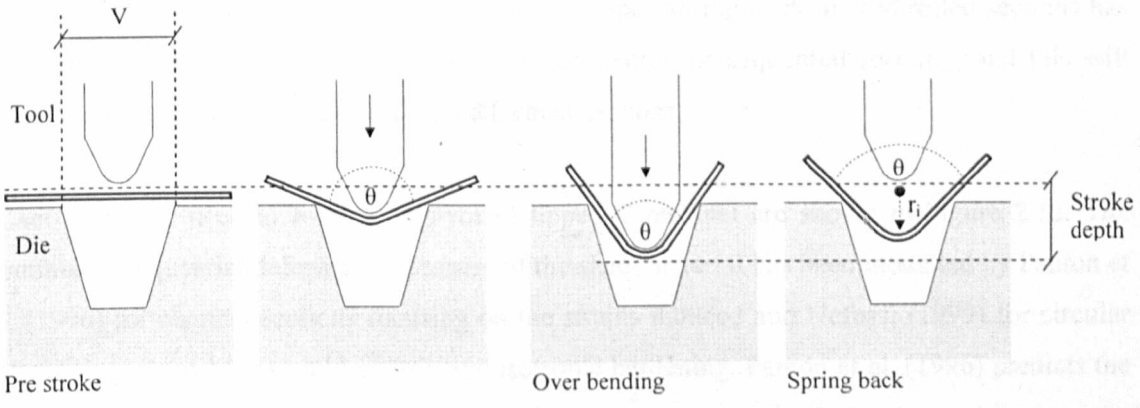

Figure 2.10: *The process of air braking*

A less common process is coin braking shown in Figure 2.11, where the tool and die fit into one another. Owing to larger radial forces employed in forming, this type of press braking causes smaller spring back to be experienced (Ingravsson 1979).

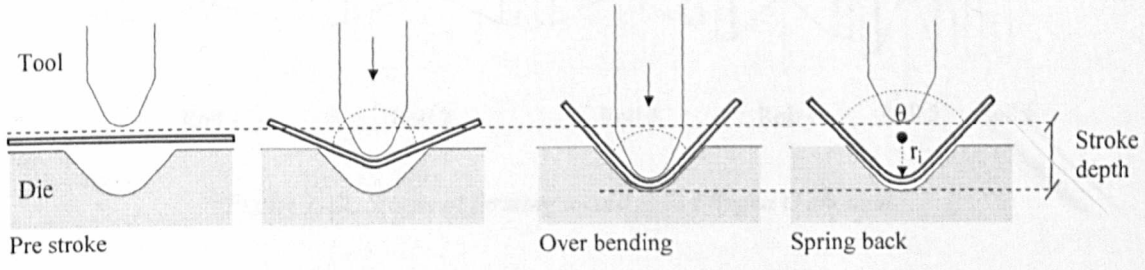

Figure 2.11: *The process of coin braking*

2.4.3.5 Cold rolled sections

Cold rolled sections represent the most widely used structural stainless steel product, where coiled sheet is passed through a series of shaped rollers to form both open and closed section types.

Cold rolling is an automated process generally used for the production of large volumes of the same cross section to a high tolerance. The sheet material is firstly taken from the coil and, in order to remove any residual curvature, is automatically levelled. The sheet material is drawn in its original rolling direction through a series of rollers (holding the material in longitudinal tension) that gradually form the required section shape. Spring back in cold rolled sections has to be more carefully controlled to allow the automation of sequential forming, and this will affect the residual stresses held within the formed sections.

A set of rollers used to form a cold rolled lipped C channel are shown in Figure 2.12. The continuous sequential deformation process of the sheet material has been modelled by Panton et al. (1996) for channel sections focusing on the strains induced and Nefussi (1999) for circular tubes using a von Mises yield criteria and isotropic hardening. Panton et al. (1996) predicts the longitudinal and shear stresses experienced in the forming process which may contribute to the section's membrane residual stress distribution.

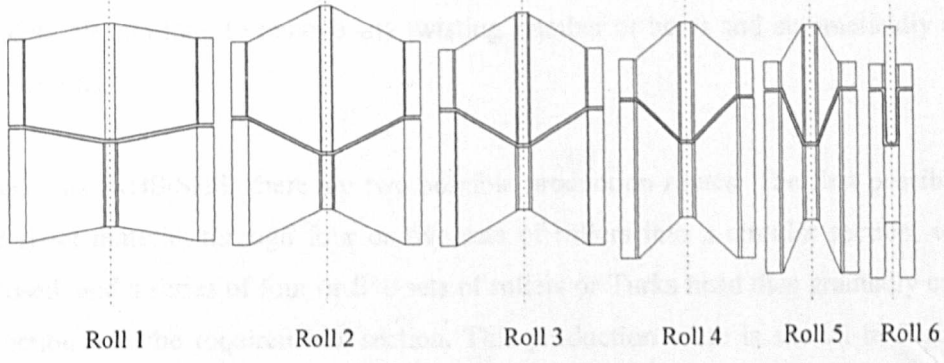

Figure 2.12: *Stages of forming a cold rolled lipped C channel*

Seam welding is commonly used in the production of cold rolled hollow sections; this creates high localised temperature gradients, potentially resulting in residual stresses and geometric imperfections due to uneven cooling rates and partial annealing of the section material.

There are a range of different seam welding processes that could be used by manufacturers. Tungsten Inert Gas Welding (TIG), Plasma Arc Welding (PAW), Submerged Arc Welding (SAW), Laser Beam Welding (LBW) and High Frequency Welding (HF). Heat dissipation from the fusion region into the section material causes a gradation of microstructure and hence material properties in the regions adjacent to the weld line. This region is known as the HAZ or the heat affected zone. Each of the potential processes vary in their range of heat input and therefore the size of the HAZ created will also vary.

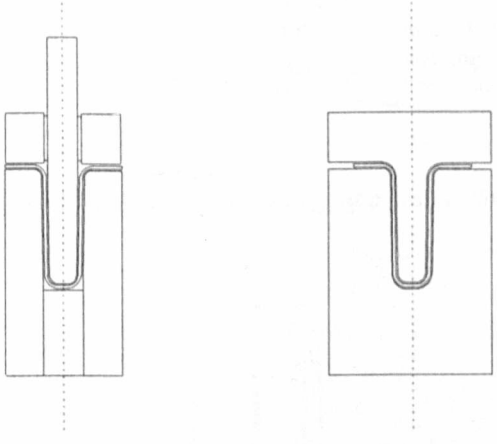

Figure 2.13: *Straightening dies for a lipped C channel*

Once formed, sections are most commonly forced through a straightening block (Figure 2.13) approximately 50 mm long to remove any twisting, camber or bows and automatically cut into individual lengths.

For box sections (RHS/SHS) there are two possible production routes. The first possible route forms the sheet material through four or five sets of rollers into a circular section, which is welded closed, and a series of four or five sets of rollers or Turks head dies gradually crush the circular section into the required box section. This production route is shown in Figure 2.14 with the rollers used to form the circular section illustrated in Figure 2.15 and the Turks head die shown in Figure 2.16.

The second production route forms the flat material by introducing fold into the sheet in the manner shown for a lipped C channel in Figure 2.12. This is an uncommon production route because initially the predominate cold rolled hollow section was the circular hollow section and when demand for hollow box sections increased the production route for circular hollow sections was adapted to produce them. The production of box sections from flat material holds

advantages for the manufacturer as more than one box size can be produced with the same size rolls. This means that less time is required to change rollers between batch sizes and so batches can be smaller and also less expensive. The work piece being formed is also less stiff in comparison to a circular tube so less force is required for section forming. For this reason this section shaping route allows for easier forming of thicker sections.

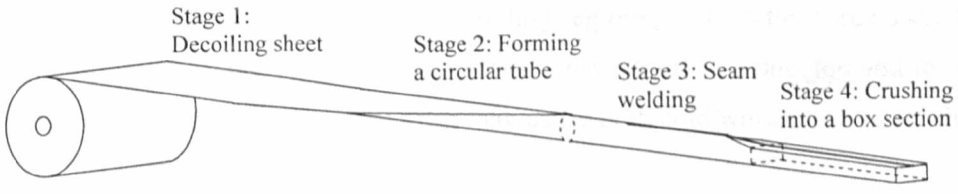

Figure 2.14: *Diagram of forming of a box section*

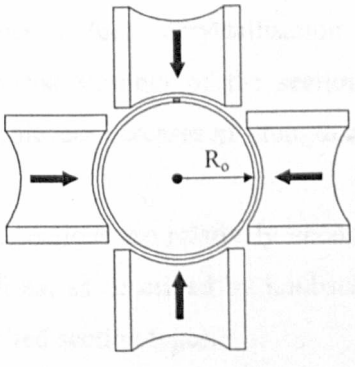

Figure 2.15: *Rollers forming a circular tube (Stage 2)*

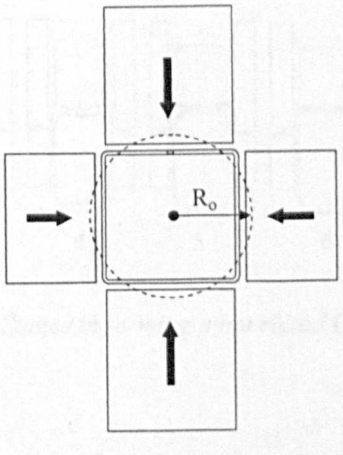

Figure 2.16: *Turks head crushing the circular tube into a box section (Stage 4)*

2.4.4 Hot rolled sections

Hot rolled sections are formed either directly from the continuous caster or from slabs that have been reheated in furnaces to about 1000-1200°C. The rolling process gradually forms the cross section shape by passing the work piece through a series of sequential forming rollers, an example of which is shown in Figure 2.17. Once formed, the members are left to cool on roller tables. Differential cooling rates due to variation in material thickness leads to the formation of residual stresses, where the faster cooling regions of the section, such as the flange tips are left in residual compression and the thicker, slower cooling regions, such as the corners are left in residual tension. A final rolling operation is sometimes performed to straighten and to reduce the geometric imperfections in the member - this may cause both cold working and modification to the residual stress pattern.

Cooling rates during forming may also influence the material strength of a section as faster cooling regions may warm work. Warm working like cold working causes increases in material strength, however the plastic deformation occurs at temperatures higher than room temperature but lower than temperatures which induce recrystallisation. Subsequent annealing of the sections may again alter the material strength of the sections but unless a full anneal or recystallisation of the material is achieved increases in strength may be retained.

Hot rolled structural stainless steel sections are relatively uncommon. However, such sections have been introduced in South Africa, as described by Laubscher and van der Merwe (2003), and are available elsewhere for limited section types.

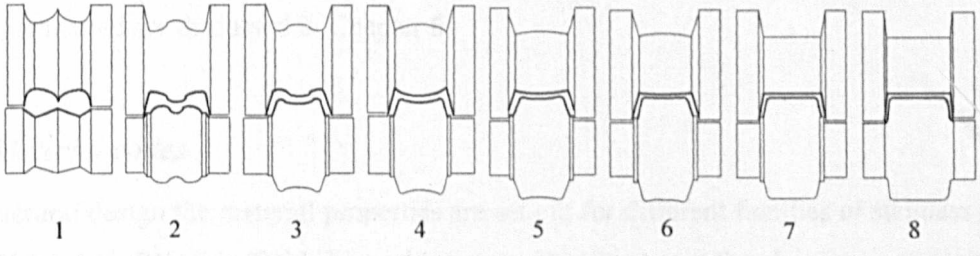

Figure 2.17: *Stages in forming a hot rolled C channel*

2.5 Design standards

2.5.1 Quality standards

Material properties of structural sections from any production route must be regulated by the supplier, and to ensure quality products, standards require the supplier to present the customer with an inspection document or mill certificate detailing the material properties of purchased sections. EN 10204 (2004) sets out the different types of inspection document. The following two types of inspection document are relevant for structural sections:

- Type 2.2: Material data are provided from non specific tests, where the data given could be from any products that have been formed from the same production route as the purchased goods.
- Type 3.1: Material data are provided from specific tests which must be carried out on the specific products supplied or test units of which the products are a part.

Inspection documents for structural sections reflect their specific production route. The manufacturer's material tests on hot rolled sections are specific tests on material extracted from within the cross sections resulting in a type 3.1 inspection document. For cold formed sections, the material tests are performed on the sheet material before it is formed into structural cross-sections. These tests are classed as non specific material tests and a type 2.2 inspection document is provided. For cold formed sections it is therefore the case that any strength enhancements that occur during the forming of the sheet material into sections is not accounted for in the 0.2% proof strength given in inspection documents or mill certificates.

The standards to which tensile tests are carried out by the manufacturers including the strain rate implemented are discussed in Chapter 6.

2.5.2 Material codes

For structural design the material properties are set out for different families of stainless steel in EN 10088 1-3 (2005). It is divided into three parts. Part 1 sets out the chemical composition for a range of ferrtic, martensitic and austenitic stainless steel grades. Part 2 gives the delivery conditions for sheet, plate and strip, which includes mechanical properties and the tests that are required to be carried out on the products. Similar information is set out in Part 3 for bars, rods and hot rolled sections.

In structural applications the most commonly used stainless steel grade is 1.4301. The material properties for the flat sheet and for the hot rolled sections from EN 10088-2 (2005) and EN 10088-3 (2005) respectively are given in Table 2.1. The data presented is taken from tensile coupon tests performed in accordance with EN 10002-1 (2001) over a proportional gauge length (discussed further in Chapter 6).

Table 2.1: *Material properties given for stainless steel 1.4301, taken from EN 10088 1-3 (2005)*

	Maximum thickness (mm)	*0.2% Proof stress (N/mm^2)*	*1.0% Proof stress (N/mm^2)*	*Tensile Strength (N/mm^2)*	*Elongation at fracture (transverse) A_{80} < 3 mm %*	*Elongation at fracture (transverse) $A \geq 3$ mm %*
Cold rolled strip (EN 10088-2, 2005)	8	230	260	540 - 750	45	45
Hot rolled strip (EN 10088-2, 2005)	13.5	210	250	520 - 720	45	45
Hot rolled plate (EN 10088-2, 2005)	75	210	250	520 - 720	45	45
Hot rolled sections (EN 10088-3, 2005)	160	190	225	500 - 700	35	-
Hot rolled sections (EN 10088-3, 2005	250	190	225	500 - 700	-	-

It is stated in EN 10088-3 (2005) that for hot rolled sections less than 35 mm thick, and that have had a final cold deformation, the ultimate strength can be increased by 200 N/mm^2 and the elongation decreased to 20%.

For sheet material the given values are based on tensile coupons tests carried out transverse to the rolling direction. For cold rolled sections these values are likely to be non-conservative for structural members where sheet material is formed with the axial direction aligned to the rolling direction of the sheet. The code therefore stipulates that for sheet less than 300 mm wide, the yield strength is reduced by 15 N/mm^2.

In addition to this material data, cold rolled sheet materials are divided into different tensile strength levels for different degrees of cold working as shown in Table 2.2. Due to the limitations of EN 1993-1-4 (2006), the Eurocode for the stainless steel structural design only cold worked levels CP350 or C700 can be used. To use higher yield strength values for cold worked material, samples of the members to be used are required to be tested.

Table 2.2: *Levels of cold work set out in EN 10088-2 (2005) and EN 1993-1-4 (2006)*

0.2% proof stress level	*0.2% proof stress, $\sigma_{0.2}$ (N/mm^2)*	*Tensile strength level*	*Tensile strength, σ_{ult} (N/mm^2)*
CP350	350-500	C700	700
CP500	500-700	C850	850
CP700	700-900	C1000	1000
CP900	900-1100	-	-
CP1100	1100-1300	-	-

2.5.3 Structural design and research programs

One of the first research programs on structural stainless steel was performed in America by Hammer and Peterson (1955). Johnston and Winter (1966) carried out a research program at Cornell University which initiated the first specific design rules for stainless steel structures; this was produced in America in 1968 by the American Iron and Steel Institute.

The limited test data available for structural stainless steel, due to its relatively recent introduction into the construction industry, has meant that experimental programs have often been carried out in order to inform design guidance.

In the U.K., prior to 1992, there was no design guidance for stainless steel structural design. Two advisory guides were produced on the use of stainless steel. The first: 'The structural design of stainless steel' was published by the Steel Construction Institute (SCI) in 1992 and the second: 'Design manual for structural stainless steel' by Euro-Inox and SCI was published in 1994. They were both based on the same research program carried out in 1988 and overseen by the SCI. Australia, New Zealand, South Africa and Japan have also developed specific stainless steel structural design codes and these are discussed in detail by Baddoo (2003). The Australian and New Zealand design code was published in (2001) and its development has been described by Rasmussen (2000).

The 'Concise guide to the structural design of stainless steel' (Burgan, 1992) was written to compliment the then current steel codes BS 5950-1 (1990). This document acts as a member design guide for engineers and it covers both austenitic and duplex grades. The basic Ramberg-Osgood equation is utilised to describe the nonlinear behaviour, with the strain hardening parameter n defined in the code's table 4.1. Values for n are given for both the longitudinal or

transverse directions in relation to the rolling direction. This enables the anisotropic behaviour of cold rolled stainless steel to be taken into account. This nonlinear model is however only incorporated into the deflection calculations. Ultimate limit state resistance formulae assume a similar form to those used for carbon steel where discrete section classes are presented. 'The structural design of stainless steel' (Euro Inox, 1994) provides similar advice. A second edition of 'The structural design of stainless steel' was published in 2002 (Euro Inox, 2002) to provide guidelines for circular hollow sections and a new section on fire resistant design. The third edition (Euro Inox, 2006) includes information on the cold working of stainless steel and life cycle costing.

The European pre-standard ENV 1993-1-4 (1996), was published in 1996. It was based on the second edition of the Euro Inox guide. Annex C presents the compound Ramberg-Osgood approximation, as proposed by Mirambell and Real (2000), to model the nonlinear behaviour which is again only incorporated into the deflection calculations. This code has now been published as a full European standard EN 1993-1-4 (2006).

To date, there have been several substantial test programs to determine the behaviour of structural stainless steel sections which are reviewed in Chapters 6 and 7. Based on test results EN 1993-1-4: (2006) is viewed as being overly conservative, a subject discussed by Sedlacek and Stangenberg (2000) and Burgan et al. (2000), and there have been new approaches to stainless steel structural design proposed to increase design efficiency (Gardner, 2002 and Ashraf, 2006).

Chapter 3

Experimental overview

3.1 Introduction

The experimental program conducted as part of this research is divided into three clearly defined investigations; the measurement of geometric imperfections, analysis of residual stresses and mapping of material properties, which are discussed separately in Chapters 4, 5 and 6 respectively. Experiments were principally carried out in the Civil and Environmental Engineering Department Structures Laboratory at Imperial College London with machining carried out by the Faculty Workshop, Imperial College London and hardness tests performed in the Materials Laboratories, Imperial College London.

The three investigations were carried out sequentially on the same specimens in order that the data obtained from the residual stresses and material properties would relate directly to one another. Specimens used in test program were formed by three production routes: hot rolling, press braking and cold rolling. Details of the production routes used to create the specimens and the naming conventions used in the thesis are set out in this chapter.

Initial geometric imperfections were measured on 31 lengths of structural cross sections; 4 hot rolled angle sections, 20 press braked angle and 7 cold rolled square and rectangular hollow sections (SHS and RHS). This part of the test program is described in Chapter 4.

Residual stress analysis using the sectioning technique was performed on 17 of the aforementioned specimens and an additional section from a previous experimental program (Gardner, 2002). The 18 specimens comprised: 3 hot rolled angle sections, 8 press braked angle sections and 7 cold rolled box sections (SHS and RHS). The analysis of magnitude and distribution of longitudinal membrane and bending residual stresses around the cross sections is presented in Chapter 5.

Tensile coupon tests were carried out on the resulting sectioned coupons from all of the sections used in the residual stress analysis and an additional section to map the distribution of material properties around the cross sections. The stress-strain curves from the tensile tests were used to quantify the amount of cold working occurring during the three considered forming processes. Hardness tests were carried out on 5 cold rolled box sections and 4 press braked angles to obtain a more detailed map of material variation. Chapter 6 presents this part of the experimental program. The specimens and the tests performed on them are summarised in Table 3.1.

3.2 Identification convention

Throughout this thesis, a specimen reference system has been adopted. The first two letters define the forming process: PB for press braked, CR for cold rolled and HR for hot rolled. When multiple specimens of nominally similar sections exist a specimen number is added, for example, PB1. The two cross section dimensions, b and d, and the thickness t, follow and finally the internal corner radii r_i, if specified is given in brackets. For fabricated sections, which are not included in the experimental program but are introduced from published residual stress data in Chapter 5, the same format is adopted however, whereby F is used to identify the production route and the thicknesses of both the web and flange are indicated sequentially.

Sectioning of each cross section produced a set of tensile coupons taken from the flat faces and corners of the sections. The faces of the sections are identified as shown in Figure 3.1. The flat coupons released are identified using the system given in Figure 3.2 where the first letter indicates the face from which the coupon has been cut and the number indicates its position in the face. The numbering starts from sections' corners and increases in the manner shown in

Figure 3.2. The corner coupons are identified as Cr and in the case of cold rolled box sections they are numbered sequentially.

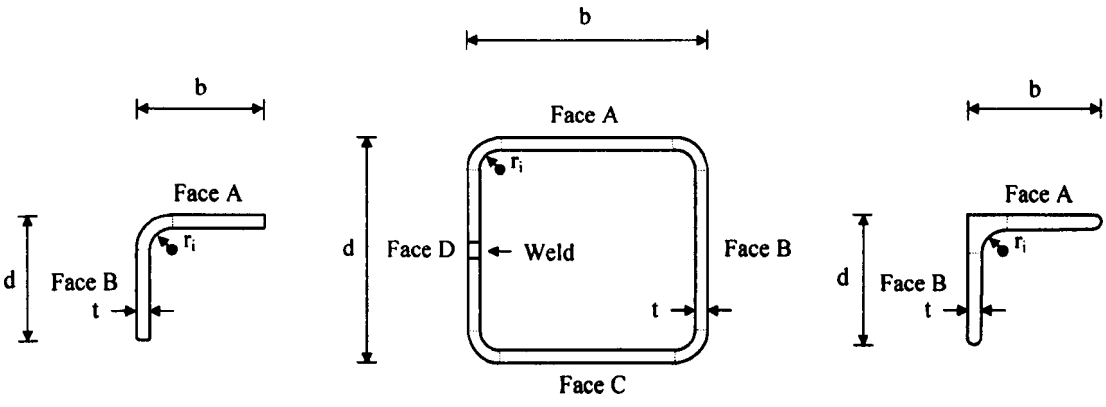

(a) Press braked angle *(b) Cold rolled box section* *(c) Hot rolled angle*

Figure 3.1: *Identification of faces in specimens*

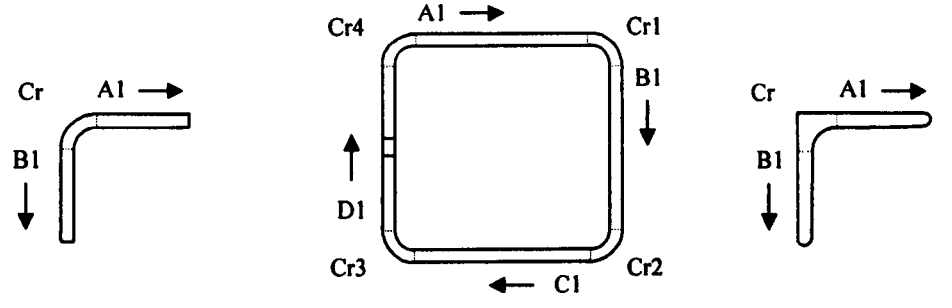

(a) Press braked angle *(b) Cold rolled box section* *(c) Hot rolled angle*

Figure 3.2: *Identification of coupons in specimens*

Table 3.1: *Test program*

Press braked equal angles	*Imperfection measurements (Chapter 4)*	*Residual stress analysis (Chapter 5)*	*Tensile coupon tests (Chapter 6)*	*Hardness tests (Chapter 6)*
PB1 50×50×2 (r_i=1.7)	+			
PB2 50×50×2 (r_i=1.7)	+			
PB3 50×50×2 (r_i=1.7)	+			
PB1 50×50×2 (r_i=3.2)	+			
PB2 50×50×2 (r_i=3.2)	+	+	+	
PB 50×50×2 (r_i=3.5)	+	+	+	+
PB 50×50×2 (r_i=4.5)	+	+	+	
PB 50×50×2 (r_i=7.5)	+	+	+	
PB1 50×50×3 (r_i=3.2)	+			
PB2 50×50×3 (r_i=3.2)	+	+	+	+
PB 50×50×3 (r_i=3.5)	+			
PB 50×50×3 (r_i=4.5)	+			
PB 50×50×3 (r_i=7.5)	+			
PB 50×50×4 (r_i=3.5)	+	+	+	+
PB 50×50×4 (r_i=4.5)	+			
PB 50×50×4 (r_i=7.5)	+			
PB 50×50×5 (r_i=3.5)	+	+	+	+
PB 50×50×5 (r_i=4.5)	+	+	+	
PB 50×50×5 (r_i=7.5)	+			
PB 50×50×6 (r_i=7.5)	+			
Cold rolled SHS/RHS				
CR 100×50×2	+	+	+	+
CR 100×100×2	+	+	+	
CR 100×50×3	+	+	+	+
CR 100×100×3	+	+	+	+
CR 100×50×4	+	+	+	+
CR 100×100×4	+	+	+	+
CR 150×150×4		+	+	
CR 100×50×6	+			
Hot rolled equal angles				
HR 50×50×3	+	+	+	
HR 50×50×5	+	+	+	
HR 50×50×6	+		+	
HR 50×50×10	+	+	+	

Table 3.2: *Press braked specimens' production information*

Specimen identification	*Section Manufacturer*	*Inspection document type*	*L(m)*	*Material formed*	*Press brake die 'V' (mm)*
PB1 50×50×2 (r_i=1.7)	Corus R&D	3.1[a]	2.0	Cold rolled coil sheet (2B)	12
PB2 50×50×2 (r_i=1.7)	Corus R&D	3.1[a]	2.0	Cold rolled coil sheet (2B)	12
PB3 50×50×2 (r_i=1.7)	Corus R&D	3.1[a]	2.0	Cold rolled coil sheet (2B)	24
PB1 50×50×2 (r_i=3.2)	Corus R&D	3.1[a]	2.0	Cold rolled coil sheet (2B)	24
PB2 50×50×2 (r_i=3.2)	Corus R&D	3.1[a]	2.0	Cold rolled coil sheet (2B)	24
PB 50×50×2 (r_i=3.5)	Ancon	3.1[a]	2.5	Cold rolled coil sheet (2B)	25
PB 50×50×2 (r_i=4.5)	Ancon	3.1[a]	2.5	Cold rolled coil sheet (2B)	30
PB 50×50×2 (r_i=7.5)	Ancon	3.1[a]	2.5	Cold rolled coil sheet (2B)	50
PB1 50×50×3 (r_i=3.2)	Corus R&D	3.1[a]	2.0	Cold rolled coil sheet (2B)	24
PB2 50×50×3 (r_i=3.2)	Corus R&D	3.1[a]	2.0	Cold rolled coil sheet (2B)	24
PB 50×50×3 (r_i=3.5)	Ancon	3.1[a]	2.5	Hot rolled coil plate (1D)	25
PB 50×50×3 (r_i=4.5)	Ancon	3.1[a]	2.5	Hot rolled coil plate (1D)	30
PB 50×50×3 (r_i=7.5)	Ancon	3.1[a]	2.5	Hot rolled coil plate (1D)	50
PB 50×50×4 (r_i=3.5)	Ancon	3.1[a]	2.5	Hot rolled coil plate (1D)	25
PB 50×50×4 (r_i=4.5)	Ancon	3.1[a]	2.5	Hot rolled coil plate (1D)	30
PB 50×50×4 (r_i=7.5)	Ancon	3.1[a]	2.5	Hot rolled coil plate (1D)	50

[a] Inspection document provided by Outokumpu, the sheet material manufacturer. No separate mill certificate was issued from the section manufacturers

Table 3.2 (continued): *Press braked specimens' production information*

Specimen identification	*Section Manufacturer*	*Inspection document type*	*L(m)*	*Material formed*	*Press brake die angle*
PB 50×50×5 (r_i=3.5)	Ancon	3.1[a]	2.5	Hot rolled coil plate (1D)	25°
PB 50×50×5 (r_i=4.5)	Ancon	3.1[a]	2.5	Hot rolled coil plate (1D)	30°
PB 50×50×5 (r_i=7.5)	Ancon	3.1[a]	2.5	Hot rolled coil plate (1D)	50°
PB 50×50×6 (r_i=7.5)	Ancon	3.1[a]	2.5	Hot rolled coil plate (1D)	50°

[a] Inspection document provided by Outokumpu, the sheet material manufacturer. No separate mill certificate was issued from the section manufacturers

Table 3.3: *Cold rolled specimens' production information*

Specimen identification	*Section Manufacturer*	*Inspection document type*	*L(m)*	*Material formed*	*Finishing processes*
CR 100×50×2	La Meusienne	2.2	6	-	-
CR 100×100×2	La Meusienne	2.2	6	-	-
CR 100×50×3	La Meusienne	2.2	6	-	-
CR 100×100×3	La Meusienne	2.2	6	-	-
CR 100×50×4	Marcegaglia	2.2	6	-	-
CR 100×100×4	Stala Tube	2.2	6	Coil sheet	Unpolished
CR 150×150×4[a]	Stala Tube	2.2	6	Coil sheet	Unpolished
CR 100×100×6	Stala Tube	2.2	6	Coil sheet	Unpolished

[a] Specimen obtained from previous experimental program (Gardner, 2002)

Table 3.4: *Hot rolled specimens' production information*

Specimen identification	*Section Manufacturer*	*Inspection document type*	*L(m)*	*Material formed*	*Finishing processes*
HR 50×50×3	Roldan	3.1	6	Billets from continuous caster	Annealed and pickled
HR 50×50×5	Viraj	3.1	6	Billets from continuous caster	Annealed and pickled
HR 50×50×6	Roldan	3.1	6	Billets from continuous caster	Annealed and pickled
HR 50×50×10	Roldan	3.1	6	Billets from continuous caster	Annealed and pickled

Table 3.5: *The material properties and chemical composition given in inspection documents/ mill certificates for the press braked specimens*

Specimen identification	*Inspection document material data*					*Inspection document chemical composition*										
	$\sigma_{0.2}$ (N/mm^2)	$\sigma_{1.0}$ (N/mm^2)	σ_{ult} (N/mm^2)	ε_f (%)	*HV*	*C*	*N*	*Si*	*P*	*S*	*Cr*	*Mn*	*Co*	*Cu*	*Ni*	*Nb*
PB1 50×50×2 (r_i=1.7)	317	346.5	625	50[a]	164	0.030	0.045	0.370	0.028	0.003	18.30	1.770	0.130	-	8.200	-
PB2 50×50×2 (r_i=1.7)	317	346.5	625	50[a]	164	0.030	0.045	0.370	0.028	0.003	18.30	1.770	0.130	-	8.200	-
PB3 50×50×2 (r_i=1.7)	317	346.5	625	50[a]	164	0.030	0.045	0.370	0.028	0.003	18.30	1.770	0.130	-	8.200	-
PB1 50×50×2 (r_i=3.2)	317	346.5	625	50[a]	164	0.030	0.045	0.370	0.028	0.003	18.30	1.770	0.130	-	8.200	-
PB2 50×50×2 (r_i=3.2)	317	346.5	625	50[a]	164	0.030	0.045	0.370	0.028	0.003	18.30	1.770	0.130	-	8.200	-
PB 50×50×2 (r_i=3.5)	304.5	331	626	51[a]	167	0.024	0.046	0.450	0.027	0.002	18.10	1.790	-	-	8.300	-
PB 50×50×2 (r_i=4.5)	304.5	331	626	51[a]	167	0.024	0.046	0.450	0.027	0.002	18.10	1.790	-	-	8.300	-
PB 50×50×2 (r_i=7.5)	304.5	331	626	51[a]	167	0.024	0.046	0.450	0.027	0.002	18.10	1.790	-	-	8.300	-
PB1 50×50×3 (r_i=3.2)	327	357.5	628.5	50[a]	173	0.020	0.058	0.420	0.029	0.001	18.30	1.770	0.070	-	8.200	-
PB2 50×50×3 (r_i=3.2)	327	357.5	628.5	50[a]	173	0.020	0.058	0.420	0.029	0.001	18.30	1.770	0.070	-	8.200	-
PB 50×50×3 (r_i=3.5)	287.5	336.5	604.5	54[b]	160	0.020	0.052	0.440	0.024	0.005	18.20	1.790	0.160	0.410	8.300	0.000
PB 50×50×3 (r_i=4.5)	287.5	336.5	604.5	54[b]	160	0.020	0.052	0.440	0.024	0.005	18.20	1.790	0.160	0.410	8.300	0.000
PB 50×50×3 (r_i=7.5)	287.5	336.5	604.5	54[b]	160	0.020	0.052	0.440	0.024	0.005	18.20	1.790	0.160	0.410	8.300	0.000
PB 50×50×4 (r_i=3.5)	317	367.5	634	52[b]	176	0.019	0.078	0.340	0.026	0.001	18.30	1.720	0.140	0.340	8.070	0.002
PB 50×50×4 (r_i=4.5)	317	367.5	634	52[b]	176	0.019	0.078	0.340	0.026	0.001	18.30	1.720	0.140	0.340	8.070	0.002
PB 50×50×4 (r_i=7.5)	317	367.5	634	52[b]	176	0.019	0.078	0.340	0.026	0.001	18.30	1.720	0.140	0.340	8.070	0.002

[a] Test pieces with a gauge length of 50 mm with a width of 12.5 mm.
[b] Test pieces with a gauge length of $5.65\sqrt{S_o}$ where S_o is the cross section area of the coupon.

Table 3.5 (continued): *The material properties and chemical composition given in inspection documents/ mill certificates for the press braked specimens*

Specimen identification	*Inspection document material data*					*Inspection document chemical composition*										
	$\sigma_{0.2}$ (N/mm^2)	$\sigma_{1.0}$ (N/mm^2)	σ_{ult} (N/mm^2)	ε_f (%)	*HV*	*C*	*N*	*Si*	*P*	*S*	*Cr*	*Mn*	*Co*	*Cu*	*Ni*	*Nb*
PB 50×50×5 (r_i=3.5)	311	362	632	51[b]	176	0.016	0.072	0.310	0.023	0.001	18.19	1.660	0.080	0.210	8.12	0.003
PB 50×50×5 (r_i=4.5)	311	362	632	51[b]	176	0.016	0.072	0.310	0.023	0.001	18.19	1.660	0.080	0.210	8.12	0.003
PB 50×50×5 (r_i=7.5)	311	362	632	51[b]	176	0.016	0.072	0.310	0.023	0.001	18.19	1.660	0.080	0.210	8.12	0.003
PB 50×50×6 (r_i=7.5)	318.5	367.5	626	51[b]	184	0.019	0.070	0.320	0.025	0.001	18.38	1.670	0.100	0.270	8.180	0.004

[a] Test pieces with a gauge length of 50 mm with a width of 12.5 mm.
[b] Test pieces with a gauge length of $5.65\sqrt{S_o}$ where S_o is the cross section area of the coupon.

Table 3.6: *The material properties and chemical composition given in inspection documents/ mill certificates for the cold rolled specimens*

Specimen identification	*Inspection document material data*					*Inspection document chemical composition*										
	$\sigma_{0.2}$ (N/mm^2)	$\sigma_{1.0}$ (N/mm^2)	σ_{ult} (N/mm^2)	ε_f (%)	*HV*	*C*	*N*	*Si*	*P*	*S*	*Ti*	*Cr*	*Mn*	*Co*	*Cu*	*Ni*
CR 100×50×2	485	510	685[a]	43	188	0.027	0.064	0.480	0.028	0.005	-	18.10	1.490	-	-	8.070
CR 100×100×2	485	510	685[a]	43	188	0.024	0.072	0.440	0.024	0.004	0.002	18.05	1.480	-	-	8.030
CR 100×50×3	485	510	685[a]	43	188	0.025	0.069	0.540	0.023	0.004	-	18.12	1.540	-	-	8.110
CR 100×100×3	485	510	685[a]	43	188	0.025	0.069	0.540	0.023	0.004		18.12	1.540			8.110
CR 100×50×4	288	324	625[a]	51	-	0.049	-	0.490	0.030	0.004	-	18.28	1.130	-	-	8.040
CR 100×100×4	337	374	626[b]	53	-	0.026	0.072	0.376	0.034	0.004	-	18.36	1.801	-	-	8.160
CR 150×150×4	304	349	613[b]	54	176	0.032	0.065	0.420	0.027	0.001	-	18.10	1.500	-	-	8.700
CR 100×50×6	324	364	631[b]	54	-	0.025	0.074	0.353	0.031	0.007	-	18.24	1.880	-	-	8.122

[a] Test pieces with a gauge length of $5.65\sqrt{S_o}$ where S_o is the cross section area of the coupon.
[b] Test pieces with a gauge length of 5 mm.

Table 3.7: *The material properties and chemical composition given in inspection documents/ mill certificates for the hot rolled specimens*

Specimen identification	*Inspection document material data*					*Inspection document chemical composition*										
	$\sigma_{0.2}$ (N/mm^2)	$\sigma_{1.0}$ (N/mm^2)	σ_{ult} (N/mm^2)	ε_f (%)	*HV*	*C*	*N*	*Si*	*P*	*S*	*Ti*	*Cr*	*Mn*	*Cu*	*Ni*	*Mo*
HR 50×50×3	439	483	671	47[a]	217	0.017	0.073	0.170	0.032	0.006	0.007	18.01	1.331	0.098	8.664	0.082
HR 50×50×5	306	-	651	49[a]	200	0.026	0.073	0.480	0.036	0.014	-	18.40	1.800	0.460	8.100	0.350
HR 50×50×6	439	483	672	44[a]	222	0.022	0.068	0.398	0.030	0.004	0.004	18.67	1.391	0.478	8.680	0.383
HR 50×50×10	478	521	671	47[a]	226	0.024	0.075	0.291	0.028	0.003	0.004	18.43	1.486	0.484	8.801	0.229

[a] Test pieces with a gauge length of $5.65\sqrt{S_o}$ where S_o is the cross section area of the coupon.

3.3 Specimens

The mode of production and therefore origin of the specimens is important to the research program. The production details of the sections are presented in Table 3.2 - 3.4 and the material properties and chemical properties provided for the specimens by the manufactures' inspection documents are given in Tables 3.5 - 3.7.

3.3.1 Press braked sections

Press braked angles were air braked by two companies, both sourcing the sheet material from Outokumpu which was guillotined to size. As the sheet material was sourced directly by the section manufacturers Type 3.1 inspection documents or mill certificates of the sheet material properties were provided by Outokumpu. Normal practice is that the material data given by the sheet material producers is re-issued by the section manufacturer in a Type 2.2 mill certificate. From the mill certificates for press braked sections it can be seen that cold rolled sheet has been used for sections less than 3 mm thick, whilst thicker sections have been made from hot rolled sheet. Three section sizes of different thickness and corner radii were produced by Corus Research and Development and 13 further sizes were provided by Ancon. All available production details, including the width of the press brakes die V, are provided in Table 3.2 and the press brake employed by Corus R&D is shown in Figure 3.3.

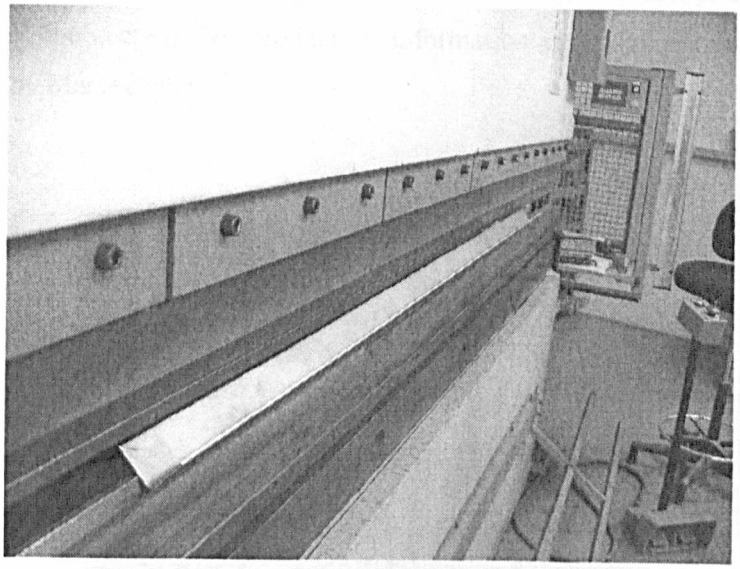

Figure 3.3: *Press brake and formed angle at Corus Research and Development*

3.3.2 Cold rolled sections

The cold rolled box sections were sourced from a stainless steel stockist, Perchcourt. The box sections were therefore produced by a range of manufacturers detailed in Table 3.3.

Correspondence with La Meusienne, part of the Arcelor group, who manufactured four of the seven cold rolled box sections, confirmed that the sections followed the production route described in Section 2.4.3.5. The sections are first formed by five shaping rolls into a circular shape. This circle is then aligned through a die to the welding torch. The speed and type of welding of depends on the section thickness and face dimensions. Two types of welding processes are used: High Frequency welding (HF) and Tungsten Inert Gas welding (TIG). For a section thickness of less than 2 mm and face dimensions (b or d) of less than 50 mm HF is used. For larger sizes TIG welding is employed. The speed of both welding processes is determined by the thickness of the section material. Once the hollow circular tube is complete, the section is polished for aesthetic reasons and four rollers crush the circular tube into the specified box section. The sections are then given an identification mark and cut into lengths. The sheet material used by La Meusienne is cold rolled below a thickness of 2 mm and hot rolled for thicker material. A sequence of rollers used to cold roll open sections is shown in Figure 3.4.

Three of the specimens were manufactured by Stala Tube. Information given on the Stala Tube website states the there are nine section forming lines which form sections via a circular hollow section and two production lines that form sections directly from the flat material. The production sequence is similar to that described by La Meusienne but TIG or Plasma welding is employed to close the section. No production information could be obtained regarding the section produced by Marcegaglia.

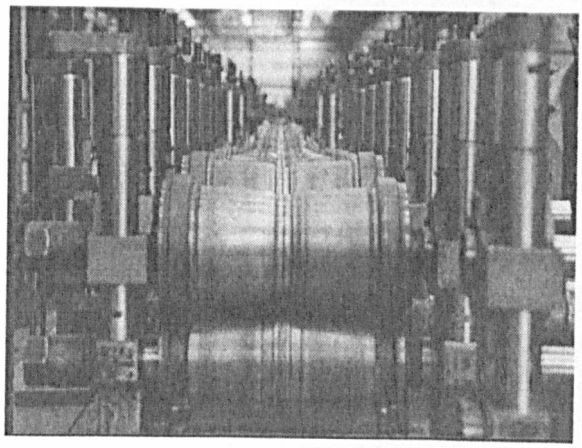

Figure 3.4: *Cold rolling mill at Metsec*

3.3.3 Hot rolled sections

The hot rolled sections were purchased from stockists: Aalco who sourced them from two manufacturers: Roldan, a company in South Africa, and Viraj, an Indian company. The sections produced by Rodan and Viraj are hot rolled from heated billets, straightened, annealed and pickled.

3.4 Conclusions

This section has set out the experimental program as an overview for the following three chapters. An identification system has been introduced for the specimens that will be continuously referenced in the thesis. All the available information on the origin of the specimens tested in the experimental program and the known details of their production routes have also been documented.

Chapter 4

Geometric imperfections

4.1 Introduction

The manufacture of structural members is carried out to specified tolerances. However, within these controlled geometric limits, imperfections exist that are directly attributable to the manner in which the sections were produced. Both the magnitude and distribution of these imperfections have an important influence on the load carrying capacity of structural members. Additional geometric imperfections or damage may also arise due to handling, storage and erection. These types of localised non-periodic imperfections (such as dents) are not well identified by the spectral analysis techniques implemented herein. Studies of the influence of localised imperfections on the structural performance of tubular members have been described by Pacheco and Durkin (1988) and Hambly and Calladine (1996).

The current study presents experimental results of detailed imperfection measurements made on austenitic stainless steel angles and hollow sections produced from three different production routes: hot rolling and two types of cold forming - press braking and cold rolling, which are described in Chapter 3. A total of twenty press braked angles, seven cold rolled box (RHS and

SHS) sections and four hot rolled angles, were examined. An imperfection rig was constructed that allowed samples of up to 5.7 m in length to be measured. Results of this part of the experimental program have been used to define suitable imperfections for inclusion in numerical models and for the development of structural design guidance. Simple predictive models are proposed and the results of the study are published in Cruise and Gardner (2006).

For structural stainless steel members there is a limited amount of published imperfection data. Measurements of local imperfections taken from short cold rolled stainless steel stub columns and global imperfections taken from long column samples were reported by Gardner and Nethercot (2004). As part of structural testing programmes on stainless steel members, Liu and Young (2003), Rasmussen and Hancock (1993a) and Talja and Salmi (1995) also presented global imperfection measurements.

Cases where detailed imperfection analyses and modelling has been carried out are typically for structural components that are known to be sensitive to the existence of initial imperfections. One such area is in shell structures where the ability to characterise initial imperfections has a very direct effect on the accuracy of predicting the load carrying capacity. To this end imperfection data banks were set up to collate the experimental data; this development is detailed by Singer and Abramovich (1995). The majority of measurements published and analysis techniques developed have been for carbon steel structural sections.

Spectral analysis has been performed in previous research on imperfection measurements for two reasons, firstly to identify periodic patterns in the profiles and secondly in order to generate representative imperfection profiles that can be used in finite element models. Use of the classic Fourier transform fits a series of cosine and sine functions to a given profile. This technique is based on the Fourier theorem (Bracewell, 1986) and has been employed, for example, by Berry et al. (2000) for the analysis of imperfections in carbon steel cylinders and Teng et al. (2005) used a two dimensional Fourier analysis on carbon steel silos. Schafer and Peköz (1998) also used the Fourier transform for the analysis of imperfection data from cold formed carbon steel lipped channel sections and proposed a probabilistic method to generate artificial imperfection profiles from experimental spectra for application in finite element models. Probabilistic methods of introducing imperfections have been implemented by Dubina and Ungureanu (2002) in finite element simulations of carbon steel channel and hat sections and used by Chryssanthopoulos and Poggi (1995) to map imperfections in other types of components such as composite panels.

An alternative to modelling an imperfection profile as a classic Fourier series, is to use the least squared method to fit a series of half sine waves. This technique allows direct correlation with global buckling modes and has been successfully employed by Bernard et al. (1999) and Wheeler and Pircher (2002). The technique had previously been used to identify chemical elements within pulse height spectra (Trombka and Schmadebeck, 1970 and Haaland and Thomas, 1988). Chryssanthopoulos et al. (1991), Lechner and Pircher (2005) and Hearn and Metcalfe (1995) discuss the Fourier and least squared methods for fitting alternative functions.

Sensitivity to imperfections in structural members depends upon material properties, loading arrangement and the local and global geometric proportions (slenderness) of the cross section and member. Typically global imperfections are considered as a fixed proportion of the member length L, whilst local imperfections are related to the thickness or local slenderness of the section. Finite element models presented by Chou et al. (2000), Kaitila (2002), and Gardner and Nethercot (2004) demonstrate an established method of including imperfections by introducing global and local eigenmodes of representative amplitudes.

Both the classical Fourier transform and the least squared technique are employed in the present study to model imperfection data collected through an experimental programme. The resulting spectral peaks are used to develop simple models for global and local imperfections amplitudes.

4.2 Modelling precedents

Extensive research has been carried out on the influence of imperfections on cold formed carbon steel structural members. A number of predictive models have been developed to estimate the magnitude of the local imperfections ω_0, such as those presented by Dawson and Walker (1972). Within their paper three models were considered. Firstly a simple model which relates the imperfection amplitude to the section's thickness t is given in Equation 4.1.

$$\omega_0 = 0.2t \tag{4.1}$$

Two more sophisticated expressions were proposed (Equations 4.2 and 4.3) both of which include the ratio of yield strength σ_y to elastic critical buckling stress σ_{cr}, representing the slenderness of the plate. The value of the coefficients α and β were derived from experimental data.

$$\frac{\omega_o}{t} = \alpha\left(\frac{\sigma_y}{\sigma_{cr}}\right) \tag{4.2}$$

$$\frac{\omega_o}{t} = \beta\left(\frac{\sigma_y}{\sigma_{cr}}\right)^{0.5} \tag{4.3}$$

Gardner and Nethercot (2004) determined values for the α and β coefficients for cold rolled stainless steel hollow sections based on imperfection measurements of short samples. Values of $\alpha = 0.023$ and $\beta = 7.3\times10^{-6}$ were proposed. As described in Chapter 2, the yield strength σ_y is conventionally taken as the 0.2% proof strength $\sigma_{0.2}$ due to the rounded nature of the stainless steel stress-strain curve. Equation 4.2 was found to best represent the experimental data.

Schafer and Peköz (1998) proposed expressions for local imperfections which differentiated between internal elements ω_1 and outstand elements ω_2 in cold formed sections. For internal elements, Equation 4.4 (based on plate width d) and Equation 4.5 (based on plate thickness t) were proposed.

$$\omega_1 = 0.006d \tag{4.4}$$

$$\omega_1 = 6te^{-2t} \tag{4.5}$$

For outstand elements, Equation 4.6 was proposed to estimate the local imperfection ω_2

$$\omega_2 \approx t \tag{4.6}$$

Geometric tolerances for structural sections are controlled by a number of standards. The European Standard EN 10162 (2003) defines the tolerances for cold rolled hollow sections. Global imperfections are defined as 'the deviation from straight', For square hollow sections a tolerance of 0.002 L, where L is the length of the member, is specified. Concavity and convexity of internal elements, h (Figure 4.1a) should not exceed 0.008d or 0.008b, where d and b are the plate widths, and should be less than an absolute value of 0.5 mm.

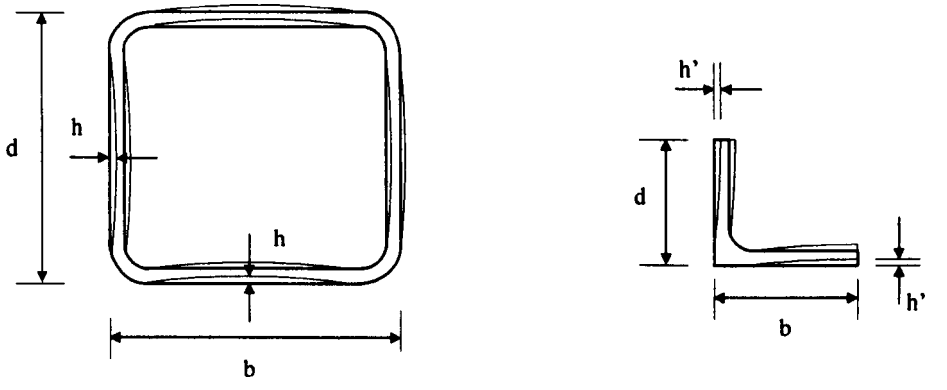

Figure 4.1: *(a) Convexity and concavity of box sections h, (b) Deviation from square of angle flanges, h'*

Tolerances for hot rolled angles are set out in EN 10056-2 (1993). EN 10056-2 is principally for hot rolled carbon steel angles, and in fact states that it is not applicable for stainless steel sections. However, Annex C of EN 10088-3 (2005), the material code for stainless steels refers explicitly to EN 10056-2 (1993) as the only relevant code and as the standard used by manufacturers. For equal angles, of flange width less than 150 mm, the specified tolerance on deviation from straight is 0.004 L, whilst on out of squareness h' (Figure 4.1b) an absolute tolerance of 1 mm is specified. EN 10162 (2003) explicitly states that it does not cover press braked sections, and no other suitable Standard has been determined.

4.3 Imperfection measurements

4.3.1 Specimens

Geometric imperfections were measured on 31 austenitic stainless steel sections from three different production routes: press braking, cold rolling and hot rolling. The measured dimensions of the specimens used are listed in Table 4.1, and further detail on the specimens is given in Chapter 3. The tolerance to which sections can be manufactured contributes to the observed imperfections. The geometric imperfections can therefore be controlled by the forming processes whether involving plastic deformation or shaping while molten. Thermal expansion and contraction can also induce imperfections during seam welding in closed sections or during the cooling of hot rolled sections.

Table 4.1: *Measured dimensions of specimens*

Press braked equal angles	t *(mm)*	r_i *(mm)*	L *(m)*
PB1 50×50×2 (r_i=1.7)	1.99	2.35	2.0
PB2 50×50×2 (r_i=1.7)	2.00	2.25	2.0
PB3 50×50×2 (r_i=1.7)	2.00	2.25	2.0
PB1 50×50×2 (r_i=3.2)	1.99	2.35	2.0
PB2 50×50×2 (r_i=3.2)	2.02	4.50	2.0
PB 50×50×2 (r_i=3.5)	1.95	4.33	2.5
PB 50×50×2 (r_i=4.5)	1.98	5.50	2.5
PB 50×50×2 (r_i=7.5)	1.98	8.00	2.5
PB1 50×50×3 (r_i=3.2)	2.98	4.50	2.0
PB2 50×50×3 (r_i=3.2)	2.99	4.50	2.0
PB 50×50×3 (r_i=3.5)	2.98	3.50	2.5
PB 50×50×3 (r_i=4.5)	2.97	4.67	2.5
PB 50×50×3 (r_i=7.5)	2.98	7.50	2.5
PB 50×50×4 (r_i=3.5)	3.92	3.42	2.5
PB 50×50×4 (r_i=4.5)	3.92	4.25	2.5
PB 50×50×4 (r_i=7.5)	3.92	7.58	2.5
PB 50×50×5 (r_i=3.5)	4.93	3.17	2.5
PB 50×50×5 (r_i=4.5)	4.89	4.33	2.5
PB 50×50×5 (r_i=7.5)	4.90	7.50	2.5
PB 50×50×6 (r_i=7.5)	6.03	7.50	2.5
Cold rolled SHS/RHS			
CR 100×50×2	1.98	2.31[a]	5.7
CR 100×100×2	1.96	2.94[a]	5.7
CR 100×50×3	2.86	3.56[a]	5.7
CR 100×100×3	2.43	4.25[a]	5.7
CR 100×50×4	3.98	1.93[a]	5.7
CR 100×100×4	3.81	3.59[a]	5.7
CR 100×50×6	5.93	4.75[a]	5.7
Hot rolled equal angles			
HR 50×50×3	3.00	5.00	5.7
HR 50×50×5	4.95	4.50	5.7
HR 50×50×6	6.35	4.75	5.7
HR 50×50×10	9.69	4.50	5.7

[a] *r_i for cold rolled sections is given as an average value*

4.3.2 Experimental technique

Imperfection measurements are commonly taken on short sample lengths due to the size restrictions imposed by measurement equipment. For example imperfection measurements reported on carbon steel structural sections have been taken with coordinate measuring machines, as the general technique adopted by the manufacturers. A more readily available alternative uses a mill bed to lay the sample on and a differential transformer is moved along the surface of a sample, taking measurements at intervals. This technique was adopted by Schafer and Peköz (1998). Both techniques use a flat surface as a reference plane from which measurements are taken.

Spectral imperfection analyses carried out on carbon sections have indicated that the significant peaks tend to occur at the lower frequency values (Wheeler and Pircher, 2003). Measurements taken over longer samples therefore allow more detailed information on the low frequency wavelengths, which relate to the global imperfections present in structural members.

To measure imperfections in samples over longer lengths, a technique of overlapping measurements was employed in order to identify and remove the imperfections in the test setup itself, so that the true surface profile of the sample could be mapped. Similar techniques have been successfully used to measure imperfections in steel silos (Ding et al., 1996), and large cylinders (Wheeler and Pircher, 2002).

The experimental setup employed in the present study comprised a carriage holding an array of three by five spring-loaded linear voltage displacement transducers located on two vertical guiding rails. The carriage was driven along the guide rails at a constant speed by a pulley hoist. The specimen lengths measured up to 5.7 m and were hung adjacent to the guide rails, as shown in Figure 4.2.

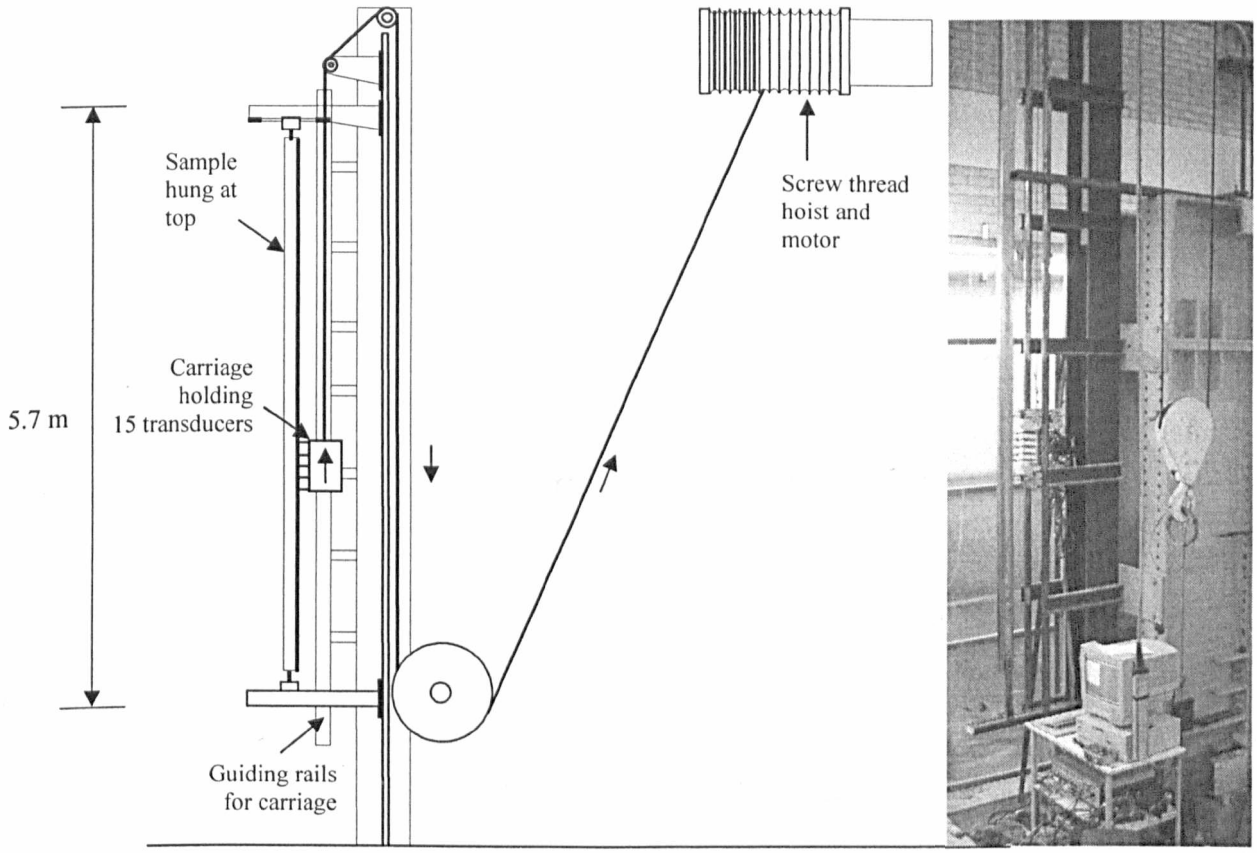

Figure 4.2: *Arrangement of the imperfection rig*

Data were recorded at one second intervals. This equated to measurements taken at 6.7 mm intervals along the length of the sample. The fifteen transducers were arranged in five rows and three columns, as shown in Figure 4.3. This enabled five overlapping measurements to be made at three locations on the faces of the cross sections. The numbering system shown in Figure 4.3 identifies the column C and row R of each transducer respectively. The transducers operated to an accuracy of ±0.01 mm. The data were recorded using the Dalite software package and processed in MatLab.

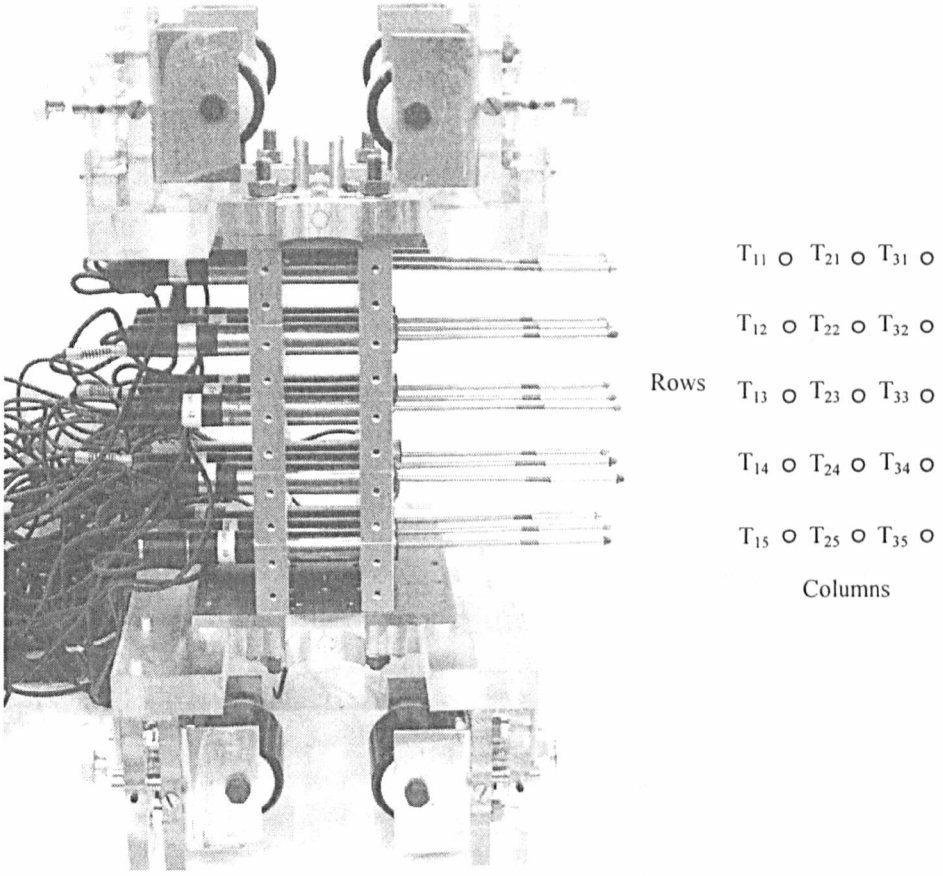

Figure 4.3: *Carriage and transducer arrangement*

The overall geometric shape of the two guiding rails was measured using an optical theodolite. The measurements showed that the guiding rails were within 1 mm of being absolutely straight. These global deviations of the imperfection rig were directly subtracted from the imperfection profile of the specimens. Local imperfections in the rig were removed using overlapping readings, as discussed in the following section. Nylon plastic tips of 10 mm diameter were affixed to the transducers to minimise friction with the specimens, and to ensure contact was maintained when taking edge readings on specimens that were imperfect perpendicular to the measurement direction. The transducers were spring loaded to maintain contact with the sample. The resulting lateral force from the springs caused the sample to deflect. In order to eliminate this deflection, the readings from the transducers were combined with measurements taken with a class IEC 825 laser, which had the accuracy quoted by the manufacturers of ±0.125 mm. This accuracy was however stated for use on a white surface. The metallic shine of the samples

affected the accuracy of the laser and a reduced accuracy of ±0.3 mm was estimated. Readings were taken in the three positions measured by the three columns of transducers. For the different types of sections the location of the three sets of readings on each face varied. The positions of the readings taken are shown in Figure 4.4.

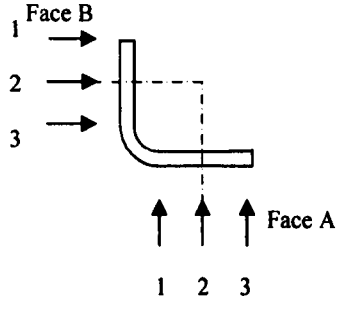

(b) Press braked angles

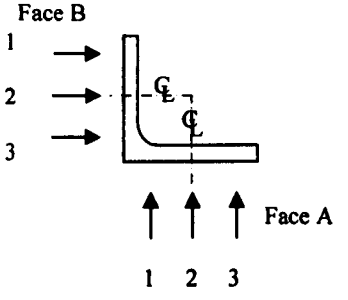

(a) Hot rolled angles

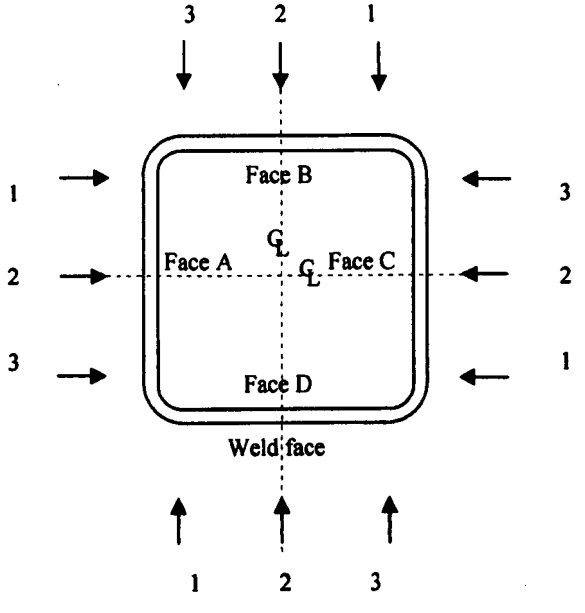

(c) Cold rolled square and rectangular sections

Figure 4.4: *Location of imperfection measurements for the different types of sections*

4.3.3 Data processing

In order to compile a profile of accuracy of ±0.01 mm and remove the deflection caused by the spring loaded transducers, the measurements taken by the laser and the transducer were combined. The global shape of the profile was taken from the laser reading and smaller

imperfections were taken from the more sensitive transducer readings. An example of a set of recorded data is shown in Figure 4.5. In order to compile a profile for each of the three locations the following procedure was employed.

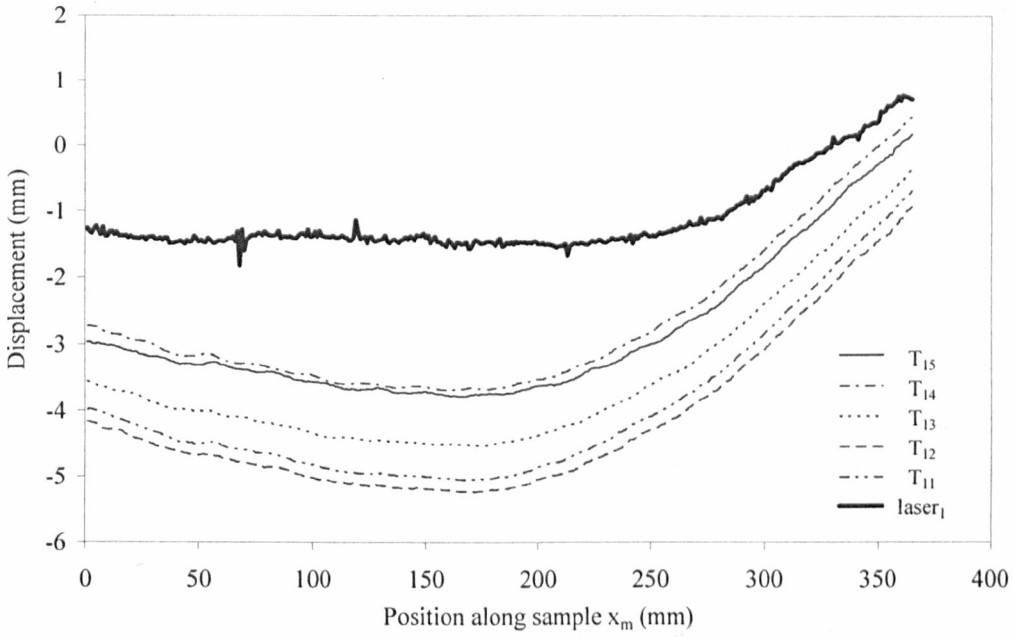

Figure 4.5: *Individual readings for transducers in column 1 (T_{11} to T_{15}) and the corresponding laser reading $laser_1$*

A moving average (MA ($laser_C$)) of 30 data points was determined to isolate the global shape of the imperfection data from the noise generated below the level of accuracy of the laser. To combine the transducer measurements with this global shape, moving averages were taken for each transducer reading (MA (T_{CR})), again removing any variations below 0.3 mm. Subtracting the reduced transducer reading from the complete transducer reading yielded the transducer measurements below the level of accuracy of the laser (T_{CR} - MA(T_{CR})). Finally, superimposing the global imperfection shape from the laser and these finer measurements from the transducers gave five profiles for each measurement location, without the deflection caused by the lateral force of the transducers. A graphical example of this process is shown in Figure 4.6.

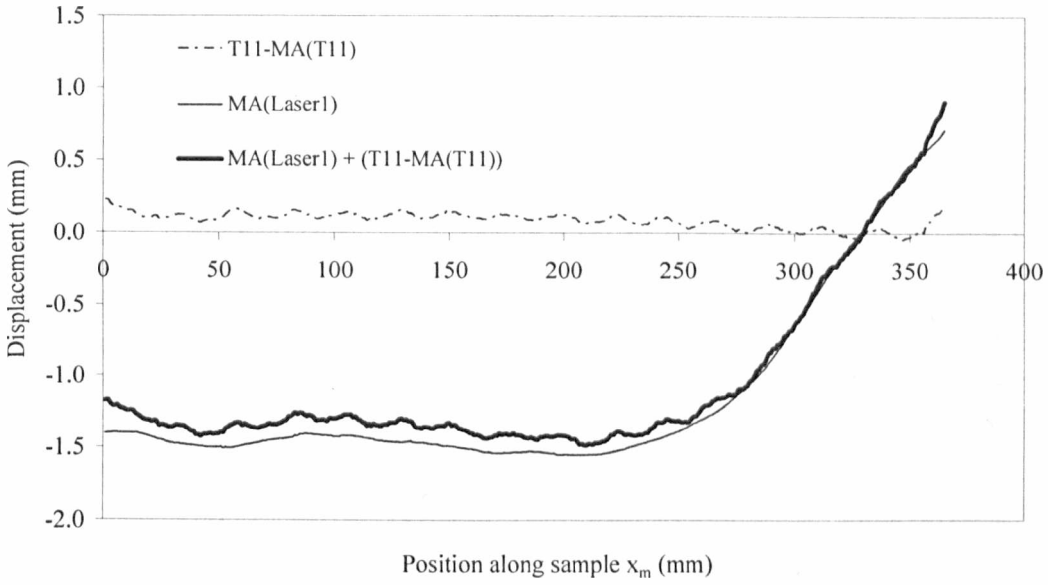

Figure 4.6: *Moving average of the laser reading MA(laser$_1$), the reduced transducer reading T_{11}-MA(T_{11}) and the combined profile MA(laser$_1$) + (T_{11}-MA(T_{11}))*

Each displacement profile P_{CR} (where C and R denote the column and row, respectively of the transducer) was related to the others by offsetting them according to readings taken at constant displacement, as given by Equation 4.7.

$$P_{CR} = MA(laser_C) + (T_{CR} - MA(T_{CR})) - offset_{CR} \tag{4.7}$$

The five overlapping measurements for each location were used to remove the local imperfections in the rig itself from the measured readings. Figure 4.7 illustrates that the five transducers in a column sequentially measure the same point whilst obtaining a different reading caused by the imperfect guiding rails. Due to the orientation of the carriage, the rig imperfections were expected to be the same for transducers in the same row. Profile differences determined by subtracting the individual transducers readings from an average of the transducer readings in the same column (Equation 4.8 and 4.9) showed excellent correlation as illustrated in Figure 4.8.

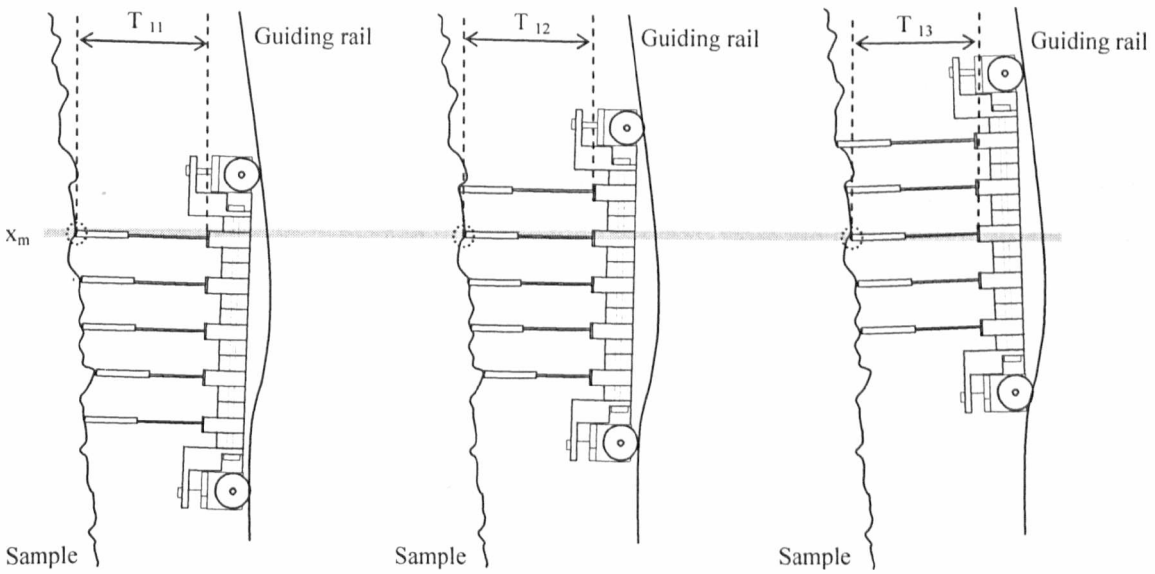

Figure 4.7: *Creation of profile differences due to the imperfections of the guiding rail*

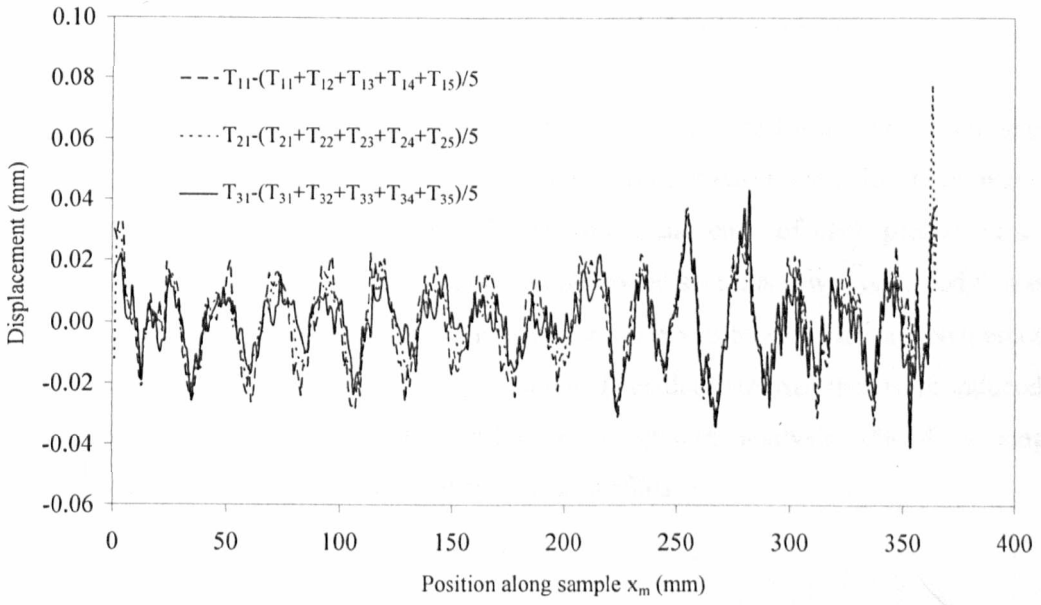

Figure 4.8: *Correlation between profile differences found for the first row of transducers (T_{11} to T_{31})*

$$P_{1R} - \left((P_{11} + P_{12} + P_{13} + P_{14} + P_{15})/5\right) \approx P_{2R} - \left((P_{21} + P_{22} + P_{23} + P_{24} + P_{25})/5\right) \tag{4.8}$$

$$P_{1R} - \left((P_{11} + P_{12} + P_{13} + P_{14} + P_{15})/5\right) \approx P_{3R} - \left((P_{31} + P_{32} + P_{33} + P_{34} + P_{35})/5\right) \tag{4.9}$$

Making the assumption, that, due to the length of the trolley compared to the magnitude of the rig imperfections, the change in angle between the carriage and the global shape of the guide rails is small, a small angle approximation is made and the identified profile differences are defined as the local imperfections of the rig. Since rig imperfections that move the transducers towards the sample will cause a decrease in any transducer reading and imperfections that move the transducer away from the sample will give the reverse effect, the average profile differences from the three transducers in each row were then removed from the individual profiles P_{CR}. This process is described by Equation 4.10 to give the corrected profiles $f_{CR}(x_m)$, where x_m is the location x along the specimen length at discrete data point m.

$$f_{CR}(x_m) = P_{CR} - \begin{pmatrix} (P_{1R} - ((P_{11} + P_{12} + P_{13} + P_{14} + P_{15})/5)) + (P_{2R} - ((P_{21} + P_{22} + P_{23} + P_{24} + P_{25})/5)) \\ + (P_{3R} - ((P_{31} + P_{32} + P_{33} + P_{34} + P_{35})/5))/3 \end{pmatrix} \quad (4.10)$$

These corrected profiles were averaged to provide a single profile for each of the three measurement locations on the specimen faces (Equation 4.11).

$$f_C(x_m) = (f_{C1}(x_m) + f_{C2}(x_m) + f_{C3}(x_m) + f_{C4}(x_m) + f_{C5}(x_m))/5 \quad (4.11)$$

The profiles were related to a common datum; resulting profiles for a press braked sample are shown in Figure 4.9. The profiles for each of the three measurement locations may also be considered as unrelated to one another by assuming the ends of each profile exist at zero displacement as shown in Figure 4.10. For the cold rolled sections it was observed that each end of the centre profile flared outwards. This was also observed by Gardner and Nethercot (2004) and is believed to be due to the release of bending residual stresses that were induced during production. In order for these not to influence the spectral analysis, 1% of the length was removed at either end of the cold rolled specimen profiles.

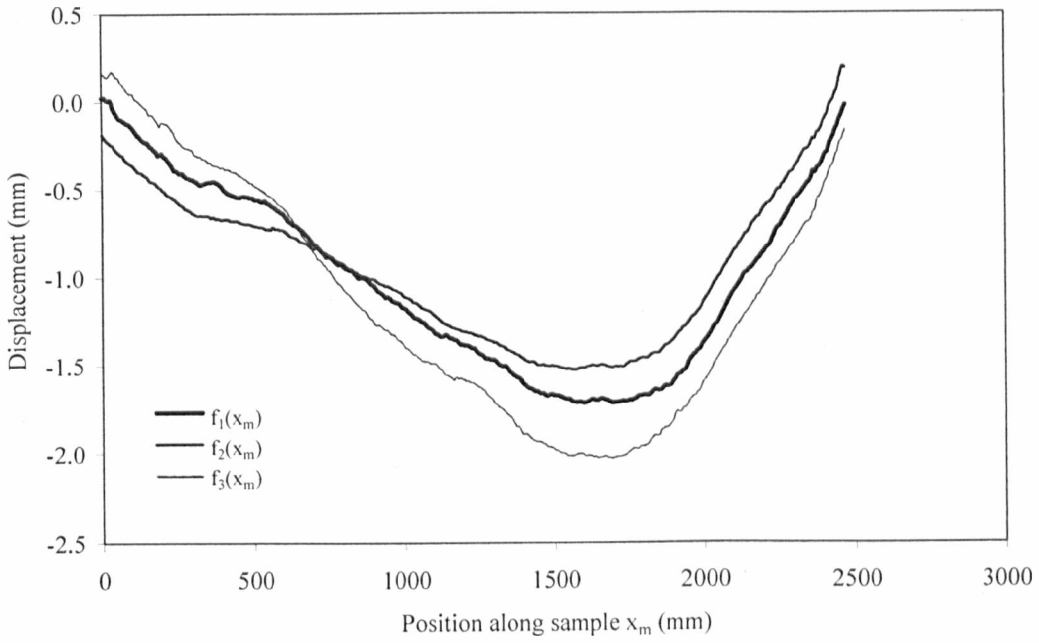

Figure 4.9: *Related profiles $f_1(x_m)$, $f_2(x_m)$, and $f_3(x_m)$ which are located at the corner, centre and edge of the outstand flange of a press braked angle section*

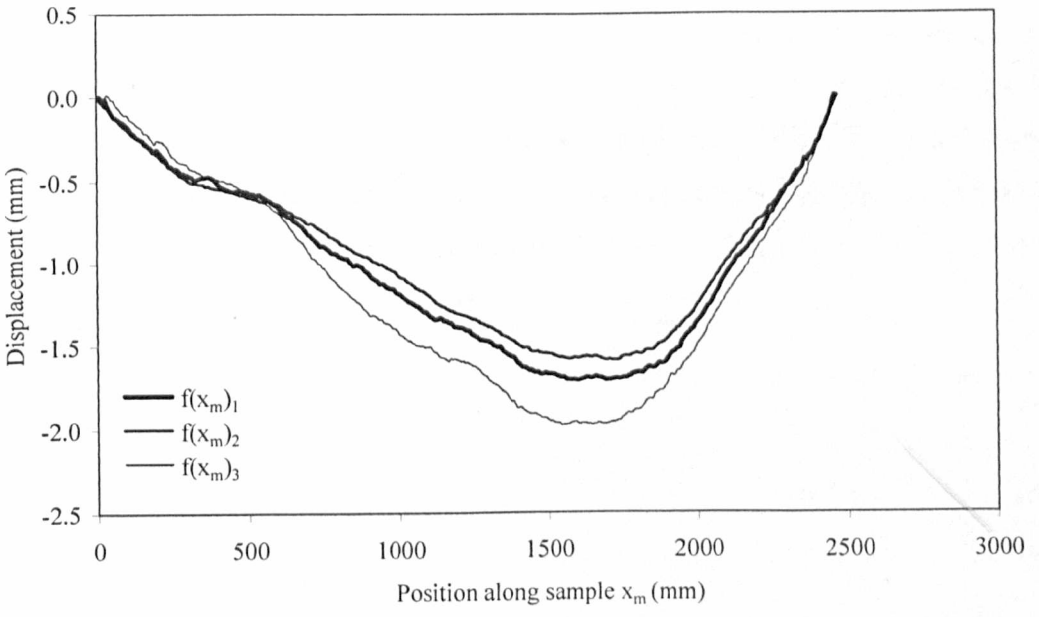

Figure 4.10: *Unrelated profiles $f_1(x_m)$, $f_2(x_m)$, and $f_3(x_m)$ which are located at the corner, centre and edge of the outstand flange of a press braked angle section*

4.3.4 Data analysis

This section sets out two principal techniques of obtaining spectral information from the collected imperfection measurements: the classic Fourier transform and the least squared method for half sine waves. Both techniques were used to analyse the related and the unrelated imperfection data.

The Fourier theorem states that the sum of odd and even functions in an infinite series can precisely model any continuous function. Therefore an imperfection function $f_C(x)$, where as $\bar{x}$, a position along the sample normalised against the sample length, can be expressed as the sum of cosine and sine functions of different frequencies as given by Equation 4.12.

$$f_c(\bar{x}) = \sum_{n=0}^{\infty} a_n \cos(n2\pi\bar{x}) + \sum_{n=0}^{\infty} b_n \sin(n2\pi\bar{x}) \qquad (4.12)$$

The frequency of each sinusoidal function is represented by an integer value n, which is the number of wavelengths within the imperfection function. The coefficients or amplitudes of the cosine and sine functions are a_n and b_n respectively.

In practical situations with a discrete set of data the frequency spectrum is limited by the Nyquist frequency N which is half the number of discrete data points. For the discrete case, the inverse of the Fourier transform still produces an exact model of the imperfection function because the highest frequency that can be detected (the Nyquist frequency N) is determined by the intervals at which the readings are taken. The modulus of the real coefficients and the imaginary coefficients are plotted separately in Figures 4.11 and 4.12 respectively. Figure 4.13 shows the combined spectral coefficients.

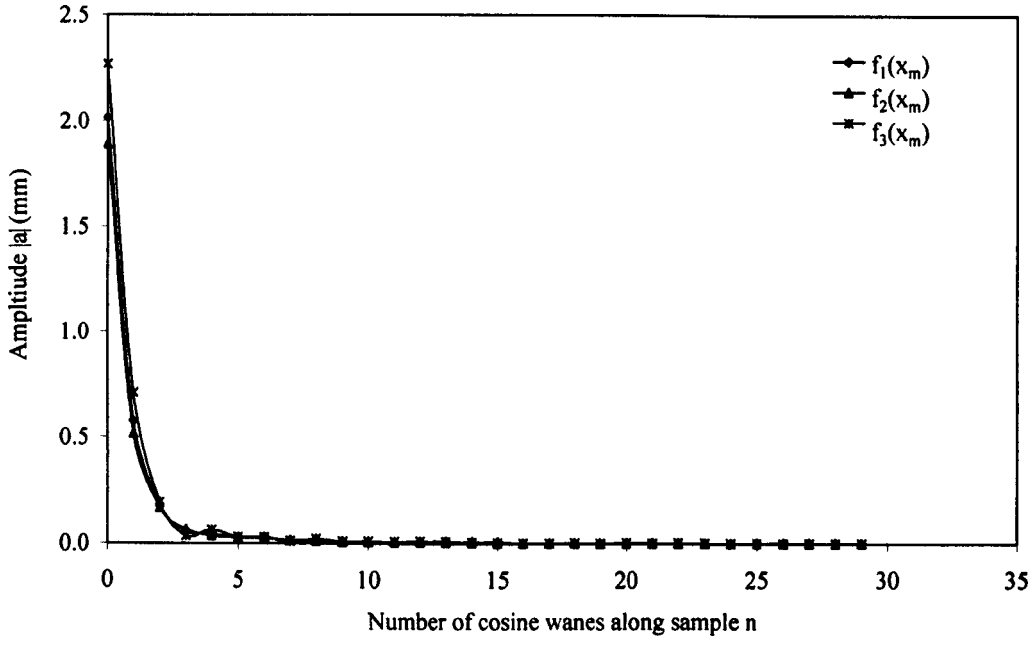

Figure 4.11: *Real (cosine) coefficients for $f_1(x_m)$, $f_2(x_m)$, and $f_3(x_m)$ which are located at the corner, centre and edge of the outstand flange of a press braked angle section*

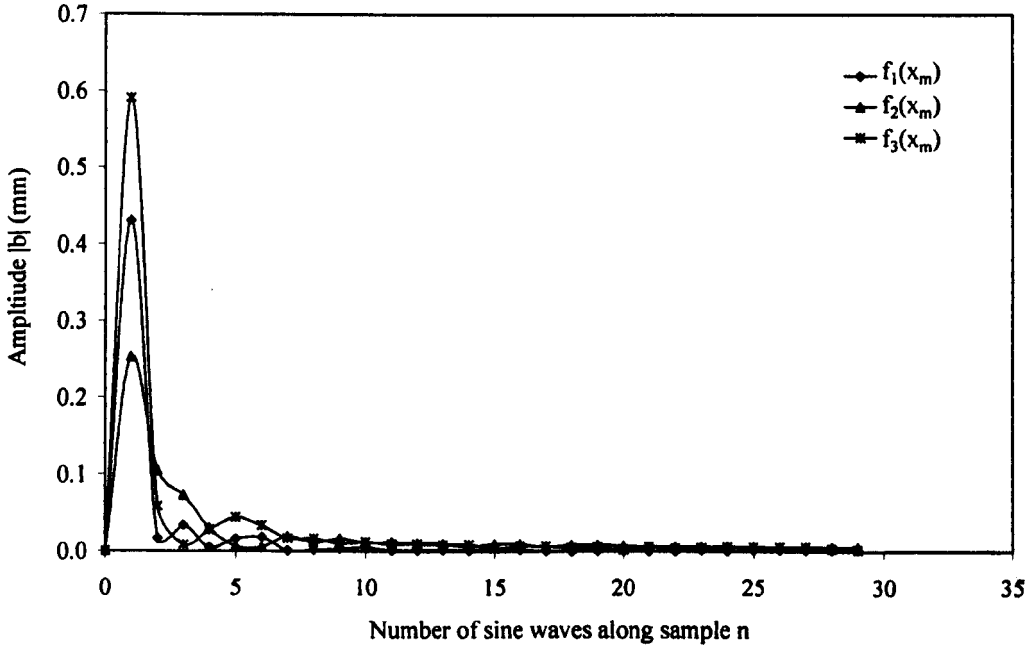

Figure 4.12: *Imaginary (sine) coefficients for $f_1(x_m)$, $f_2(x_m)$, and $f_3(x_m)$ which are located at the corner, centre and edge of the outstand flange of a press braked angle section*

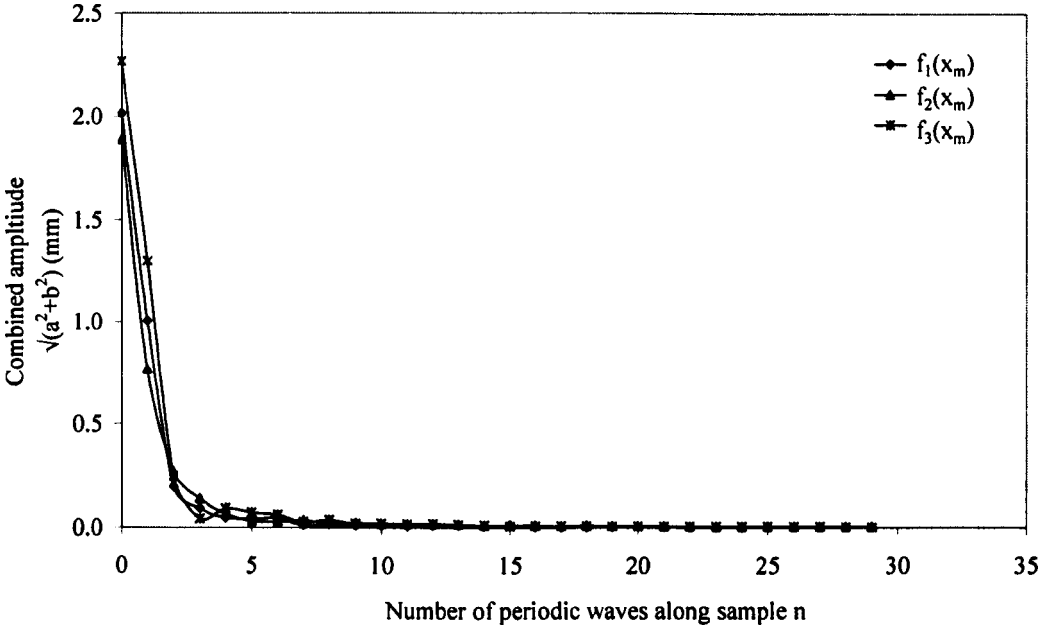

Figure 4.13: *Combined imaginary and real coefficients for $f_1(x_m)$, $f_2(x_m)$, and $f_3(x_m)$ which are located at the corner, centre and edge of the outstand flange of a press braked angle section*

The least squared approach models the imperfection function as the sum of a linear function and a series of (n = 1 to n = N) half sine functions as stated by Equation 4.13. This approach is summarised below and has been discussed in more detail by Bernard et al. (1999). Equation 4.13 is presented in terms of a normalised longitudinal position $\bar{x}_m$, given in Equation 4.14, where x_m is the location x along the specimen length for the discrete data point m, x_1 is the location of the initial data point, δ is an offset value and L is the specimen length. Since the half sine functions are not independent, the modelling function $f_C'(\bar{x}_m)$ will not be exact and will always exhibit a difference from the experimental imperfection function $f_C(\bar{x}_m)$. A process of minimising the resultant modelling error {V} of the spectral peaks is carried out by varying the offset value δ of the half sine series from the origin of the data.

$$f_C'(\bar{x}_m) = c_1 + c_2\bar{x}_m + \sum_{n=1}^{N} c_{n+2} n \sin\pi\bar{x}_m \tag{4.13}$$

$$\bar{x}_m = \left(\frac{x_m - x_1 - \delta}{L}\right) \tag{4.14}$$

Converting the notation to matrices, the design matrix [A] contains the function series and {w} contains the imperfection readings w_1 to w_M, as shown in Equations 4.15 and 4.16, where M is

the number of discrete data points. The spectral coefficients are given as $\{c\}$, defined in Equation 4.17, and the error between the experimental imperfection function and the modelling function is given as a vector $\{V\}$, which is defined in Equation 4.18.

$$[A] = \begin{bmatrix} 1 & \bar{x}_1 & \sin\pi\bar{x}_1 & \cdots & N\sin\pi\bar{x}_1 \\ 1 & \bar{x}_2 & \sin\pi\bar{x}_2 & \cdots & N\sin\pi\bar{x}_2 \\ \vdots & \vdots & \vdots & \vdots & \vdots \\ 1 & \bar{x}_M & \sin\pi\bar{x}_M & \cdots & N\sin\pi\bar{x}_M \end{bmatrix} \tag{4.15}$$

$$\{w\} = \begin{Bmatrix} w_1 \\ \vdots \\ w_M \end{Bmatrix} \tag{4.16}$$

$$\{c\} = \begin{Bmatrix} c_1 \\ c_2 \\ \vdots \\ c_{N+2} \end{Bmatrix} \tag{4.17}$$

$$\{V\} = \{w\} - [A]\{c\} \tag{4.18}$$

In order to estimate the variance in the spectral coefficients, the experimental error or the variance of each individual measurement is introduced in a weighting matrix [G] (Equation 4.19). Since the experimental error of each data point taken by the transducers was estimated as ±0.01 mm, σ_1^2 to σ_M^2 have been taken as the same value.

$$[G] = \begin{bmatrix} \frac{1}{\sigma_1^2} & & & \\ & \frac{1}{\sigma_2^2} & & \\ & & \ddots & \\ & & & \frac{1}{\sigma_M^2} \end{bmatrix} \tag{4.19}$$

The vector $\{c\}$ containing the least squared spectral coefficients is calculated from Equation 4.20:

$$\{c\} = ([A]^T[G][A])^{-1}[A]^T[G]\{w\} \tag{4.20}$$

The variance σ_{an}^2 associated with the each spectral coefficient in {c} can be calculated from Equation 4.21, where $\hat{\sigma}_0^2$ is the variance factor (Equation 4.23) and Q_{ii} are the diagonal values of the covariance matrix [Q] (Equation 4.22). Employing a normal distribution with a confidence level of 99.5%, the confidence levels for the peaks are found by multiplying σ_{an}^2 by 2.58. This confidence level defines a magnitude of the spectral peaks below which it is uncertain whether the peaks relate to the data or have been generated by experimental and modelling errors.

$$\sigma_{an}^2 = \hat{\sigma}_0^2 Q_{ii} \tag{4.21}$$

$$[Q] = ([A]^T[G][A])^{-1} \tag{4.22}$$

The ratio of the square of the modelling error to the experimental error of each data point is termed the variance factor $\hat{\sigma}_0^2$ which is calculated by Equation 4.23. Using a chi squared distribution with r degrees of freedom when the variance factor equals one i.e. when the modelling error equals the experimental error, the model is said to be a good fit to the experimental data. The number of degrees of freedom r is expressed by Equation 4.24.

$$\hat{\sigma}_0^2 = \frac{\{V\}^T[G]\{V\}}{r} \tag{4.23}$$

$$r = M - (N + 2) \tag{4.24}$$

In cases where the variance factor is not equal to unity, the assumed experimental error can be revised until the variance factor does equal unity, providing an estimated experimental error $\overline{\sigma}$. To find the best fit, the lowest value of the variance factor was sought whilst varying the offset value δ. Due to the asymmetrical nature of the half sine wave function the offset value δ was varied from –1 to 1. A common minimum variance factor was found for the three profiles taken from each section face. The offset values were found to occur repeatedly around values -1, 0 and 1 due to the significance of the first half sine wave in the imperfection profiles.

With the introduction of the offset into the analysis both the related and unrelated profiles can become discontinuous functions if the offset is not equal to -1 or 1. Profile functions with discontinuities caused large alternating positive and negative least squared coefficients and high variance values to be observed. These high variance values are also seen in the Gibbs phenomenon, discussed by Bracewell (1986). The Gibbs phenomenon is observed as ringing close to discontinuities in a function and it is caused by forming the profile from a truncated Fourier series thereby removing large amplitude high frequency terms that are required to fully describe the profile discontinuity. In order to remove the profile discontinuity and thereby reduce the variance of the imperfection data a method of tapering was employed. Priestley (1992) discusses typical tapering functions that can be employed. A hermite interpolation curve, described in Prenter (1975), was employed to generate five data points before the beginning of the profile and five data points afterwards, to taper the function and ensure the continuity between the beginning and the end of the imperfection function. An example of a least squared spectrum for three corresponding profiles is shown in Figure 4.14. The prediction error sum of squares or PRESS (Lechner and Pircher, 2005) was determined for least squared half sine wave coefficients to determine the significance of the individual component coefficients.

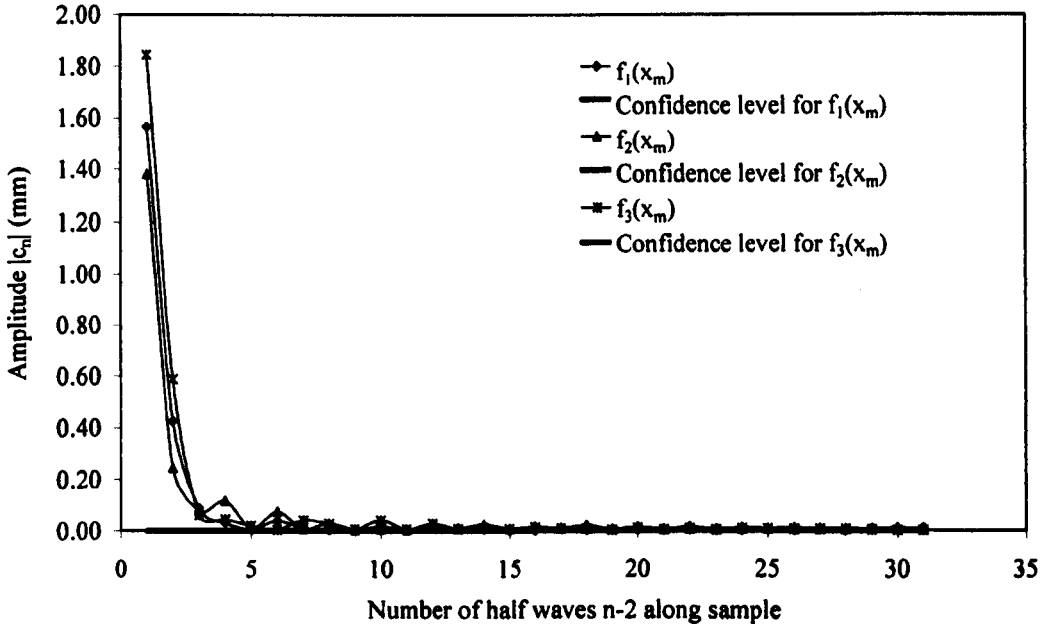

Figure 4.14: *Least squared coefficients and their confidence levels*

4.4 Results

Results from the Fourier and least squared spectral analyses are presented in Tables 4.2-4.4. The most significant peaks, according to the PRESS analysis for the least squared spectra was the first term of each series, with few exceptions. Figures 4.15 and 4.16 show the correlation between the modulus of the first real (cosine) coefficient a_0 (which is identical to the first combined coefficient) of the Fourier transform and the modulus of the first half sine wave amplitude c_3 from the least squared technique. Both relate to an overall bow in the specimens and are of a similar form to the buckled shape of an elastic pin-ended column.

Table 4.2: *Imperfection data for press braked samples*

Specimen identification	*L (mm)*	$\|a_0\|$ *(mm)*	$\|c_3\|$ *(mm)*	$2.54\sigma_{a3}^2$ *(mm)*	*δ/L*	$\overline{\sigma}$ *(mm)*	ω_o *(ζ=1) (mm)*	ω_o *(ζ=10) (mm)*
PB1 50×50×2 (r_i=1.7)								
Face A	1986	0.11	0.04	1.93×10^{-5}	-0.0008	4.61×10^{-3}	0.03	0.60
Face B	1993	0.55	0.42	8.92×10^{-5}	-0.0032	2.93×10^{-3}	0.04	0.25
PB2 50×50×2 (r_i=1.7)								
Face A	1993	0.08	0.03	1.11×10^{-3}	0.0056	4.03×10^{-3}	0.04	0.77
Face B	1980	0.12	0.00	1.54×10^{-5}	0.9988	3.73×10^{-3}	0.05	0.23
PB3 50×50×2 (r_i=1.7)								
Face A	1993	0.11	0.06	1.50×10^{-5}	0.0004	4.33×10^{-3}	0.02	0.75
Face B	1986	0.38	0.17	5.06×10^{-5}	0.9976	4.33×10^{-3}	0.03	0.24
PB1 50×50×2 (r_i=3.2)								
Face A	1986	0.50	0.38	2.03×10^{-5}	0.9984	3.78×10^{-3}	0.03	0.17
Face B	1993	0.49	0.35	5.69×10^{-5}	-0.9968	3.14×10^{-3}	0.03	0.14
PB2 50×50×2 (r_i=3.2)								
Face A	1980	2.07	1.55	4.95×10^{-3}	0.0064	5.70×10^{-3}	0.03	0.14
Face B	1993	2.39	1.76	3.36×10^{-5}	-0.9988	5.50×10^{-3}	0.02	0.14
PB 50×50×2 (r_i=3.5)								
Face A	2468	2.03	1.56	1.31×10^{-5}	-0.0012	3.15×10^{-3}	0.03	0.16
Face B	2475	0.06	0.13	3.39×10^{-3}	0.0056	3.59×10^{-3}	0.03	0.20
PB 50×50×2 (r_i=4.5)								
Face A	2481	3.34	2.50	5.80×10^{-5}	0.0016	5.52×10^{-3}	0.03	0.11
Face B	2475	2.89	2.30	2.19×10^{-5}	-0.0012	4.08×10^{-3}	0.02	0.14
PB 50×50×2 (r_i=7.5)								
Face A	2481	0.07	0.50	1.15×10^{-4}	0.9992	1.08×10^{-2}	0.03	0.23
Face B	2488	1.75	1.54	2.72×10^{-5}	-0.0004	5.77×10^{-3}	0.01	0.38
PB1 50×50×3 (r_i=3.2)								
Face A	1993	1.51	1.17	2.06×10^{-3}	0.0056	5.50×10^{-3}	0.06	0.25
Face B	1993	1.17	0.93	2.45×10^{-3}	-0.9944	6.00×10^{-3}	0.06	0.08
PB2 50×50×3 (r_i=3.2)								
Face A	1986	1.15	0.91	1.90×10^{-3}	0.9992	4.58×10^{-3}	0.02	0.12
Face B	1986	1.80	1.37	7.30×10^{-3}	-0.0008	2.84×10^{-3}	0.02	0.13
PB 50×50×3 (r_i=3.5)								
Face A	2475	2.82	2.22	2.01×10^{-5}	0.9980	2.65×10^{-3}	0.02	0.18
Face B	2475	4.00	3.07	4.22×10^{-5}	-0.0012	5.67×10^{-3}	0.02	0.14

Table 4.2 (continued): *Data for press braked samples*

Specimen identification	*L (mm)*	$\|a_0\|$ *(mm)*	$\|c_3\|$ *(mm)*	$2.54\sigma_{a3}^2$ *(mm)*	δ/L	$\overline{\sigma}$ *(mm)*	ω_o *(ζ=1) (mm)*	ω_o *(ζ=10) (mm)*
PB 50×50×3 (r_i=4.5)								
Face A	2481	1.98	1.54	1.24×10^{-5}	0.9984	2.56×10^{-3}	0.01	0.12
Face B	2475	2.44	1.86	7.91×10^{-6}	-0.0008	2.83×10^{-3}	0.00	0.18
PB 50×50×3 (r_i=7.5)								
Face A	2488	1.79	1.31	4.74×10^{-5}	0.9984	4.99×10^{-3}	0.03	0.49
Face B	2481	1.67	1.22	4.72×10^{-4}	-0.0036	4.83×10^{-3}	0.03	0.34
PB 50x50x4 (r_i=3.5)								
Face A	2475	3.22	2.50	4.28×10^{-6}	0.0000	2.37×10^{-3}	0.03	0.28
Face B	2481	3.06	2.38	1.75×10^{-5}	0.9980	2.46×10^{-3}	0.04	0.30
PB 50x50x4 (r_i=4.5)								
Face A	2481	4.47	3.46	8.65×10^{-5}	0.9972	3.42×10^{-3}	0.02	0.25
Face B	2481	2.99	2.32	6.94×10^{-6}	0.0004	2.91×10^{-3}	0.02	0.08
PB 50x50x4 (r_i=7.5)								
Face A	2475	4.12	3.26	2.16×10^{-5}	-0.0012	4.06×10^{-3}	0.02	0.24
Face B	2481	3.35	2.62	6.80×10^{-4}	0.0044	3.46×10^{-3}	0.02	0.10
PB 50x50x5 (r_i=3.5)								
Face A	2488	4.21	3.22	5.71×10^{-4}	-0.0036	5.32×10^{-3}	0.03	0.13
Face B	2488	4.69	3.43	1.35×10^{-2}	0.0064	4.14×10^{-3}	0.04	0.39
PB 50x50x5 (r_i=4.5)								
Face A	2495	4.48	3.41	1.41×10^{-3}	-0.0044	4.91×10^{-3}	0.02	0.19
Face B	2495	4.92	3.88	1.07×10^{-4}	-0.0032	2.93×10^{-3}	0.04	0.23
PB 50x50x5 (r_i=7.5)								
Face A	2488	5.67	4.33	1.76×10^{-4}	0.9968	3.81×10^{-3}	0.05	0.15
Face B	2488	4.36	3.41	1.03×10^{-5}	-0.0008	3.23×10^{-3}	0.02	0.12
PB 50x50x6 (r_i=7.5)								
Face A	2495	6.86	5.24	4.34×10^{-5}	0.9992	6.62×10^{-3}	0.05	0.25
Face B	2481	7.98	6.30	1.18×10^{-4}	-0.0020	6.38×10^{-3}	0.03	0.19

Table 4.3: *Imperfection data for cold rolled samples*

Specimen identification	*L (mm)*	$\|a_0\|$ *(mm)*	$\|c_3\|$ *(mm)*	$2.54\sigma_{a3}^2$ *(mm)*	*δ/L*	$\overline{\sigma}$ *(mm)*	ω_o *(ζ=1) (mm)*	ω_o *(ζ=10) (mm)*
CR 100×50×2								
Face A	5681	0.72	0.57	1.59×10^{-2}	0.9968	2.96×10^{-3}	0.02	0.30
Face B	5688	0.66	0.43	5.98×10^{-4}	-0.9980	3.29×10^{-3}	0.02	0.17
Face C	5695	3.76	3.00	1.31×10^{-5}	0.0004	3.56×10^{-3}	0.03	0.32
Face D	5681	4.13	3.30	6.35×10^{-5}	-0.0012	3.25×10^{-3}	0.03	0.14
CR 100×100×2								
Face A	5681	1.06	0.28	3.84×10^{-2}	0.0032	4.65×10^{-3}	0.07	0.54
Face B	5675	3.45	2.62	1.72×10^{-5}	-0.0004	4.08×10^{-3}	0.02	0.27
Face C	5675	4.97	3.85	6.56×10^{-4}	0.0020	3.46×10^{-3}	0.03	0.22
Face D	5675	6.35	5.00	4.10×10^{-5}	0.0008	4.31×10^{-3}	0.03	0.23
CR 100×50×3								
Face A	5695	0.72	0.57	1.59×10^{-2}	0.9968	2.96×10^{-3}	0.02	0.30
Face B	5695	0.66	0.43	5.98×10^{-4}	-0.9980	3.29×10^{-3}	0.03	0.17
Face C	5695	3.76	3.00	1.31×10^{-5}	0.0004	3.56×10^{-3}	0.03	0.32
Face D	5695	4.13	3.30	6.35×10^{-5}	-0.0012	3.25×10^{-3}	0.03	0.14
CR 100×100×3								
Face A	5681	1.07	0.95	8.20×10^{-5}	0.0012	3.69×10^{-3}	0.04	0.31
Face B	5688	1.47	1.06	4.43×10^{-4}	-0.0016	4.97×10^{-3}	0.05	0.36
Face C	5681	1.84	1.49	4.00×10^{-5}	-0.9992	4.24×10^{-3}	0.04	0.31
Face D	5681	4.56	3.66	1.78×10^{-4}	-0.9984	3.16×10^{-3}	0.04	0.36
CR 100×50×4								
Face A	5681	0.29	0.75	1.67×10^{-1}	-0.9964	5.41×10^{-3}	0.07	0.45
Face B	5695	1.61	1.18	7.93×10^{-4}	-0.0016	6.62×10^{-3}	0.04	0.09
Face C	5688	4.90	3.88	6.05×10^{-5}	0.0012	3.17×10^{-3}	0.02	0.28
Face D	5675	4.75	3.77	1.20×10^{-5}	1.0000	3.97×10^{-3}	0.02	0.07
CR 100×100×4								
Face A	5681	1.22	1.05	6.88×10^{-4}	-0.0024	1.98×10^{-3}	0.02	0.41
Face B	5681	1.30	1.16	3.04×10^{-3}	0.0024	4.17×10^{-3}	0.03	0.22
Face C	5675	2.08	1.66	3.52×10^{-6}	0.9996	1.85×10^{-3}	0.01	0.34
Face D	5688	2.54	2.08	3.38×10^{-5}	-0.0012	2.37×10^{-3}	0.02	0.30
CR 100×50×6								
Face A	5681	3.38	2.73	5.33×10^{-5}	-0.9988	2.98×10^{-3}	0.02	0.18
Face B	5681	0.58	0.37	4.97×10^{-6}	1.0000	2.55×10^{-3}	0.02	0.10
Face C	5681	1.33	1.09	3.85×10^{-6}	-0.9996	1.93×10^{-3}	0.01	0.25
Face D	5681	3.87	3.07	3.21×10^{-5}	0.0008	3.80×10^{-3}	0.01	0.14

Table 4.4: *Imperfection data for hot rolled samples*

Specimen identification	*L (mm)*	$\lvert a_0 \rvert$ *(mm)*	$\lvert c_3 \rvert$ *(mm)*	$2.54\sigma_{a3}^2$ *(mm)*	δ/L	$\overline{\sigma}$ *(mm)*	ω_o *(ζ=1) (mm)*	ω_o *(ζ=10) (mm)*
HR 50×50×3								
Face A	5580	4.23	3.14	3.35×10^{-6}	-0.9996	1.80×10^{-3}	0.01	0.13
Face B	5593	7.41	5.38	7.57×10^{-5}	-0.0008	5.80×10^{-3}	0.01	0.13
HR 50×50×5								
Face A	5593	5.34	4.14	2.16×10^{-5}	0.0004	4.57×10^{-3}	0.05	0.42
Face B	5588	1.02	0.87	8.84×10^{-6}	-0.0004	2.92×10^{-3}	0.03	0.27
HR 50×50×6								
Face A	5593	1.87	1.30	8.87×10^{-6}	-0.9996	2.92×10^{-3}	0.01	0.13
Face B	5580	5.55	4.49	2.73×10^{-5}	-0.0008	3.49×10^{-3}	0.02	0.20
HR 50×50×10								
Face A	5593	19.27	15.03	2.06×10^{-4}	0.9992	9.56×10^{-3}	0.03	0.23
Face B	5600	22.90	17.56	4.64×10^{-5}	-0.0004	6.68×10^{-3}	0.02	0.16

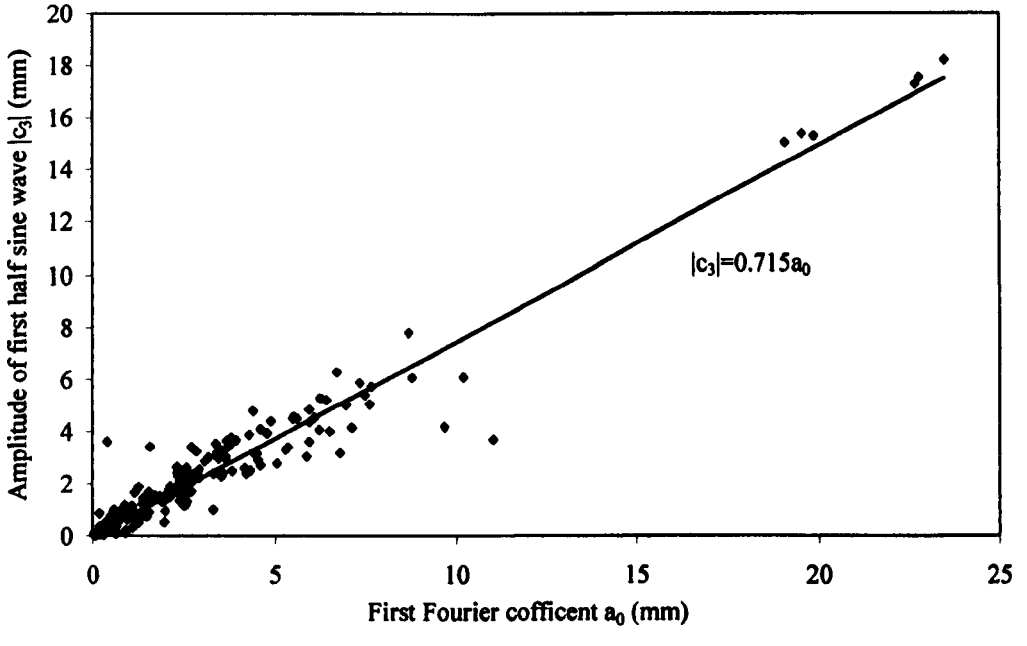

Figure 4.15: *Relationship between the first Fourier coefficient, a_o and the amplitude of the first half sine wave, c_3 for the related data*

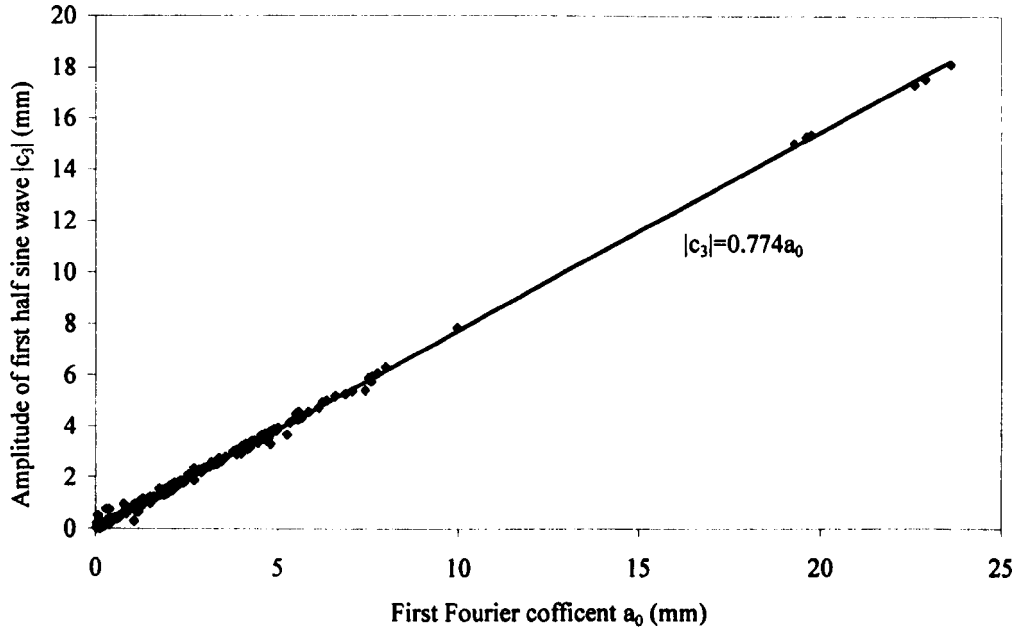

Figure 4.16: *Relationship between the first Fourier coefficient, a_o and the amplitude of the first half sine wave, c_3 for the unrelated data*

By equating the area under a half sine wave with an amplitude of c_3 to the areas under a full cosine curve of amplitude a_0 it can be shown that there is a linear dependency, as stated by Equation 4.25. This linear relationship is reflected in Figures 4.15 and 4.16 by considering the slope of the linear regression curve. The unrelated data (where the three profiles on each face are analysed independently) shows an excellent correlation, whilst the increased scatter for the related profiles shows the effect of considering the imperfection profiles with respect to a common (surface) datum. It is therefore proposed that the first Fourier coefficient from a Fourier transform can be approximated to the amplitude of the half sine wave with the amplitude c_3 through Equation 4.25 and this gives a good estimation of the global imperfection.

$$c_3 = \frac{\pi a_0}{4} \approx 0.785 a_0 \tag{4.25}$$

The least squared method of fitting a series of half sine waves to the imperfection function produces a function that is a very good fit to the experimental data, resulting in low covariance factors for the spectral peaks. The estimated experimental error is consistently lower than the actual experimental error, suggesting that the measurements were more accurate than predicted.

The modulus of the coefficient of the first half sine waves normalised against the specimen lengths L are plotted against their section thickness in Figures 4.17 to 4.19.

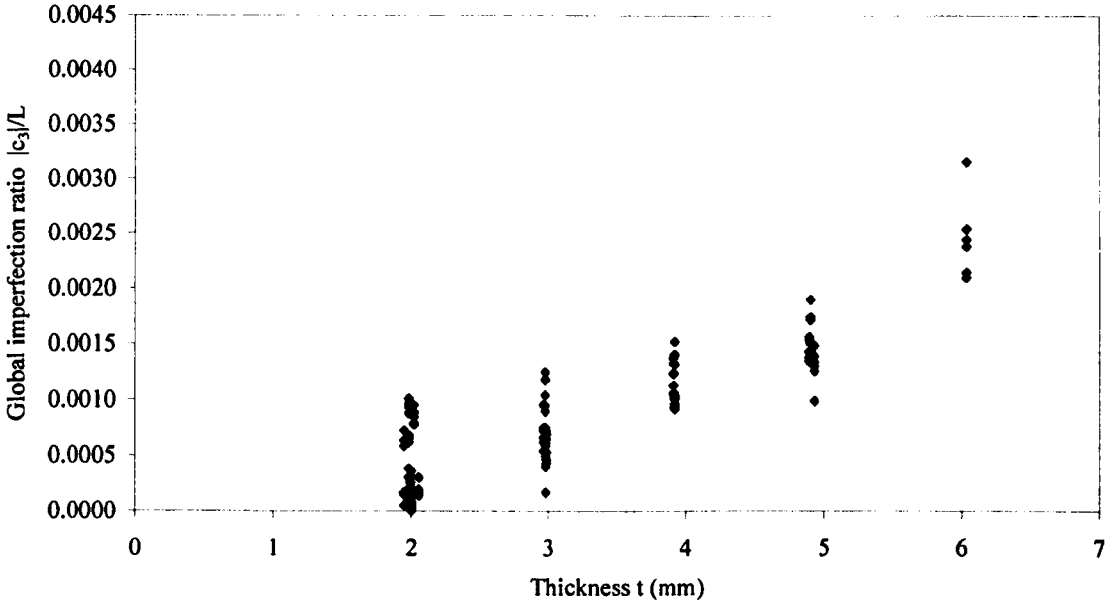

Figure 4.17: *Relationship between the normalised first half sine wave amplitude and the thickness of the section for press braked sections (unrelated data)*

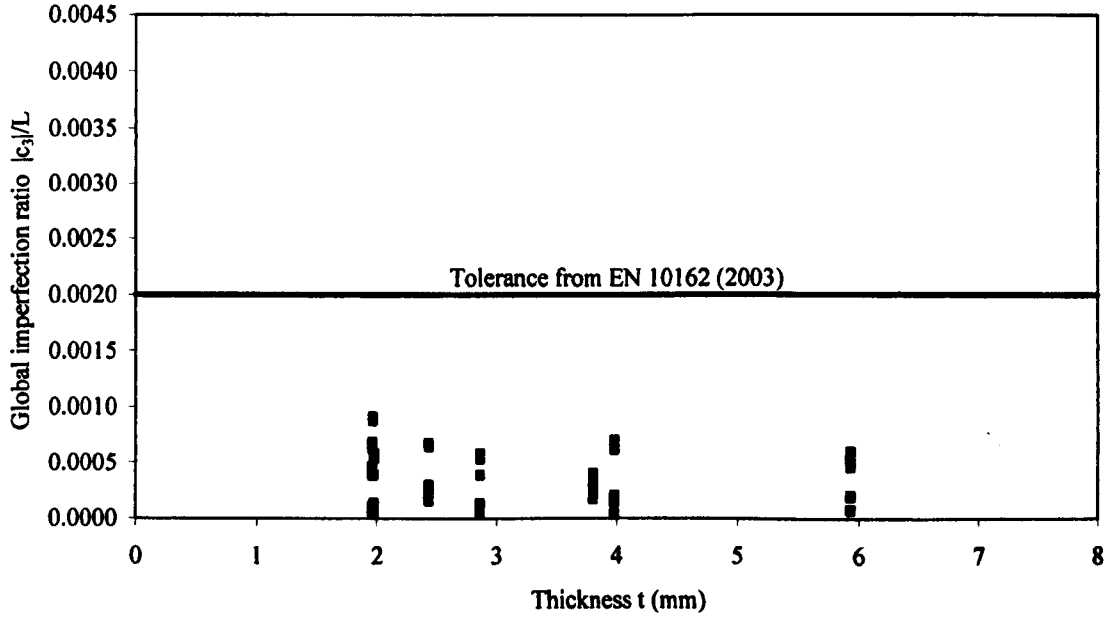

Figure 4.18: *Relationship between the first half sine wave amplitude and the thickness of the section for cold rolled sections (unrelated data)*

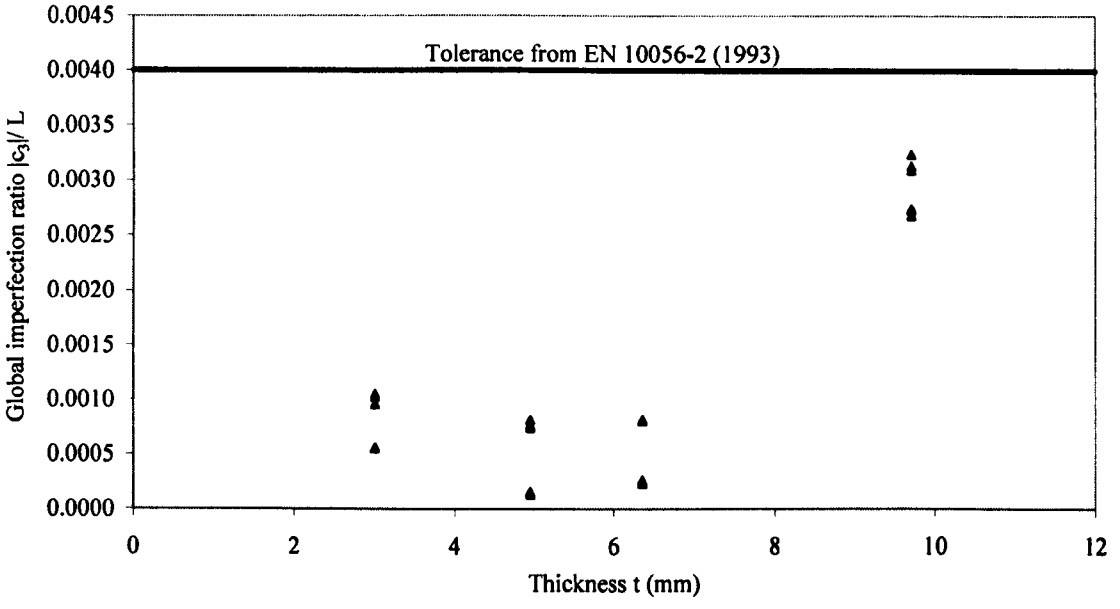

Figure 4.19: *Relationship between the first half sine wave amplitude and the thickness of the section for hot rolled sections (unrelated data)*

For the press braked sections a clear trend of normalised global imperfections increasing with thickness is observed. A similar trend is observed for the hot rolled sections, although more data would be required to confirm this relationship. The data presented does not however reveal any relationship that might exist between the global imperfection and the cross section slenderness, as the width of section is constant for both press braked and hot rolled sections. The global imperfections for the cold rolled sections showed no trend with thickness. Therefore, a half sine wave of amplitude c_3, presented as a proportion of the member length L and determined from mean values, is proposed for representing global geometric imperfections for the three different forming processes (Equations 4.26 to 4.28). Figures 4.18 to 4.19 show that the global imperfections for cold rolled sections and hot rolled sections fall within their respective codes acceptable tolerances.

Press braked sections $$\frac{c_3}{L} \approx 0.00084 \quad (4.26)$$

Cold rolled sections $$\frac{c_3}{L} \approx 0.00035 \quad (4.27)$$

Hot rolled sections $$\frac{c_3}{L} \approx 0.0012 \quad (4.28)$$

The amplitudes of the local imperfections have been investigated by considering profile data taken along the flange tip for the angle sections and along the centreline of the faces of the box sections. In order to determine representative amplitudes for local imperfections, the spectral peaks below a specified frequency were assumed to relate to global imperfections and were removed. This frequency was defined in reference to a multiple ζ of the cross section width; ζ = 1 represents a half wavelength equal to the cross section width, whilst ζ = 10 represents a half wavelength of ten times the cross section width. The remaining series was reformed as a profile of local imperfections and the maximum deviation from straightness ω_0 was obtained. Values of this representative local imperfection are shown in the Tables 4.2 to 4.4, for the two cases of ζ = 1 and ζ = 10.

Figures 4.20 to 4.22 plot the representative local imperfection amplitudes for ζ = 1 and ζ = 10 against the corresponding 0.2% proof stress (equivalent yield stress) to critical stress ratio ($\sigma_{0.2}/\sigma_{cr}$). A linear regression line passing through the origin has been determined for both sets of data to obtain values for α, as defined by the Dawson and Walker model of Equation 4.2. It can be seen in Figure 4.23 that α increases as ζ increases, which would be expected due to the inclusion of more low frequencies terms in the local imperfection profile which tend to be of larger amplitudes. Figure 4.23 also shows the relative variation of α between the three production routes.

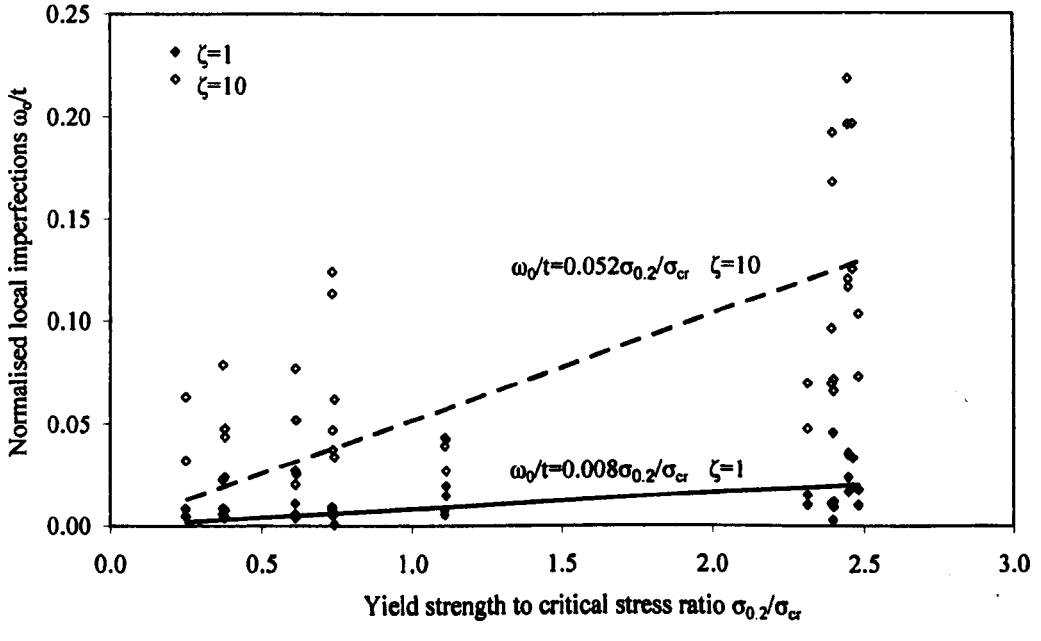

Figure 4.20: *Press braked local imperfections normalised by thickness plotted against yield strength to critical stress ratio to determine α*

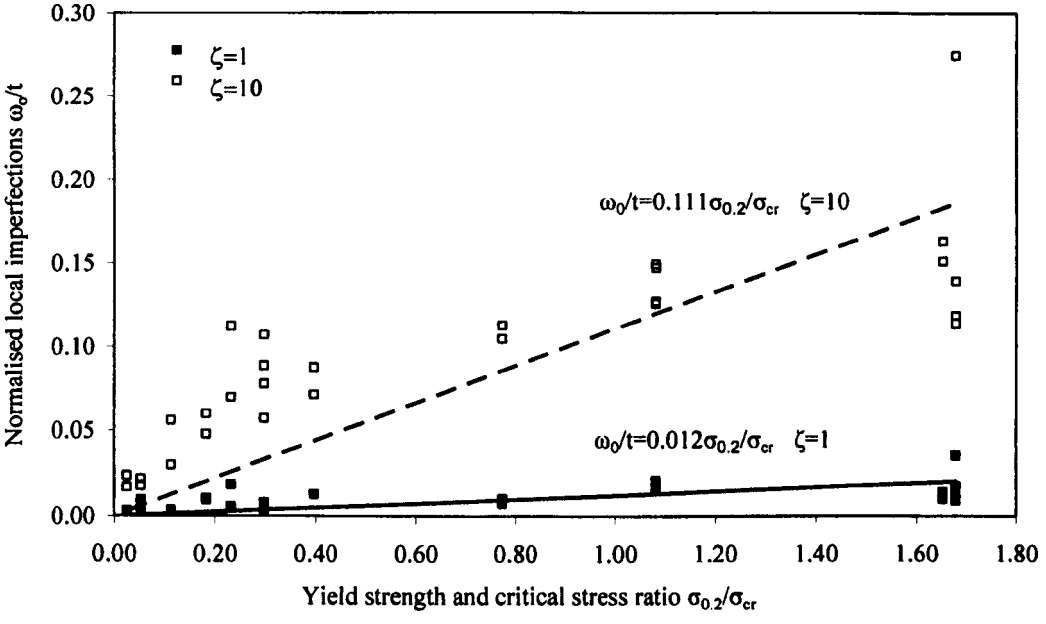

Figure 4.21: *Cold rolled local imperfections normalised by thickness plotted against yield strength to critical stress ratio to determine α*

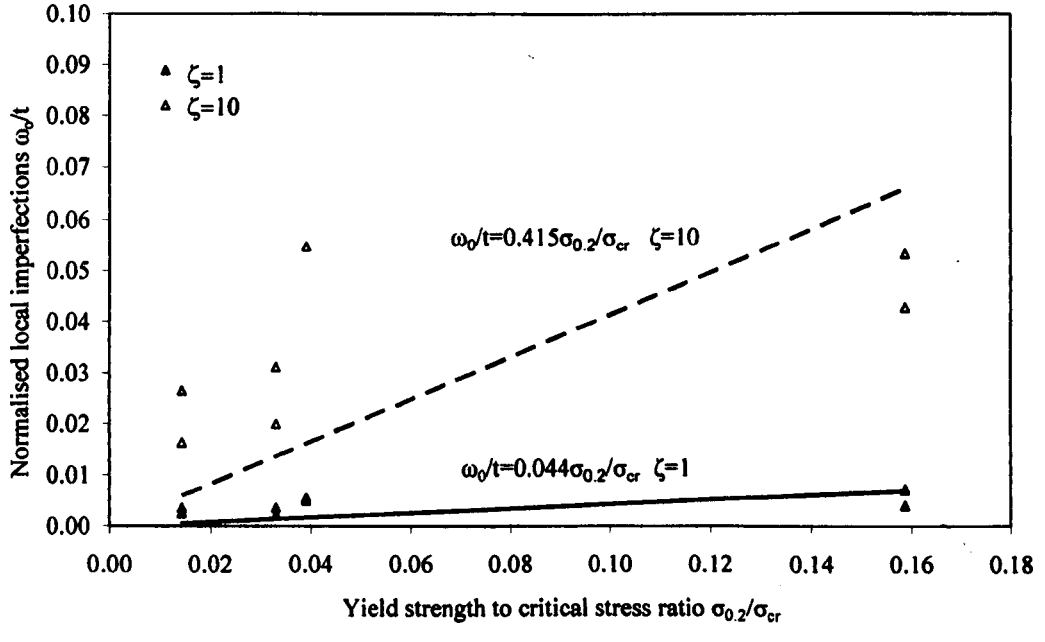

Figure 4.22: *Hot rolled local imperfections normalised by thickness plotted against yield strength to critical stress ratio to determine α*

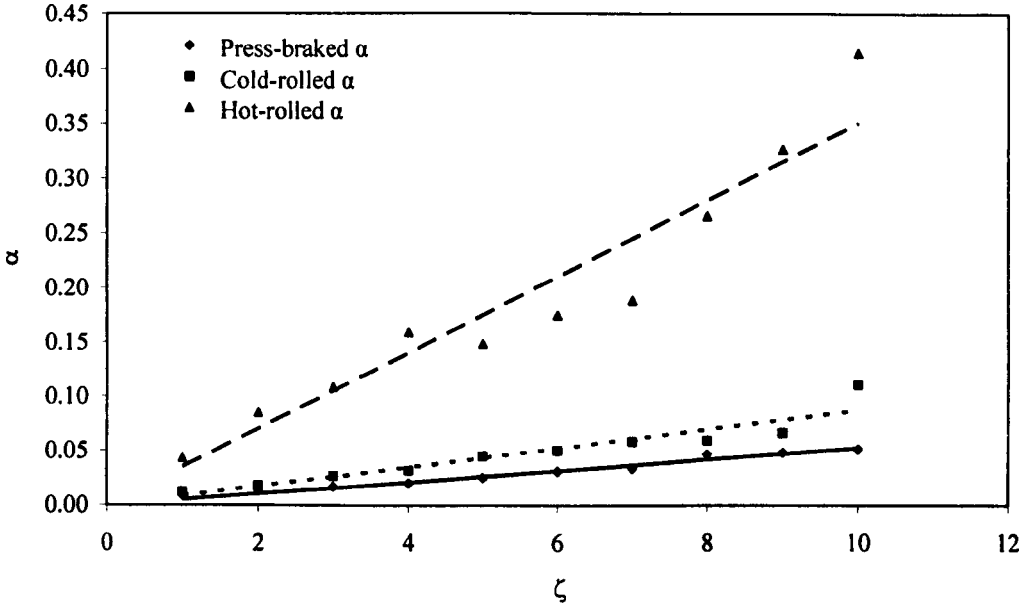

Figure 4.23: *Variation of α with ζ for the three different section types*

For the box sections, where the boundary conditions of the individual plate elements may be closely approximated as simply-supported, the half wavelength based on the elastic buckling mode (for practical aspect ratios) is equal to the plate width. This indicates that $\zeta = 1$ would provide the most suitable basis for determining local imperfection amplitudes. However, for outstand elements (one longitudinal edge simply-supported and one free), the half wavelength of the elastic buckling modes is equal to the length of the plate, though the failure mode localises due to post-buckling behaviour and plasticity. It is therefore less straightforward to determine the most suitable value for ζ. It is reasonable to assume that the imperfection amplitudes corresponding to $\zeta = 1$ represent lower bound values whilst those corresponding to $\zeta = 10$ represent upper bound values. A summary of the proposed values of α to be used in Equation 4.2 for the prediction of local imperfection amplitudes in structural stainless steel members is given in Table 4.5.

Table 4.5: *Upper and lower limits for values of α*

	α (ζ=1)	*α (ζ=10)*
Press braked equal angles	0.008	0.052
Cold rolled box sections	0.012	0.111
Hot rolled equal angles	0.044	0.415

4.5 Conclusions

This part of the experimental study has examined the magnitude and distribution of production related imperfections. An accurate method of measuring imperfections over long specimen lengths has been developed and implemented. Two analysis techniques, the classic Fourier transform and the least squared method fitting a series of half sine waves, have been employed to investigate the periodicity in the imperfections, from which the amplitudes of the global and local imperfections have been extracted. Simple predictive tools for both local and global imperfections have been developed to enable representative geometric imperfections for the three production processes (press braking, cold rolling and hot rolling) which could be incorporated into numerical models and design methods.

Chapter 5

Residual stresses

5.1 Introduction

Stresses that exist in structural sections in their unloaded state are termed residual stresses; these have been extensively quantified for carbon steel sections. The general influence of residual stresses on structural members is to cause premature yielding, leading to loss of stiffness and a reduction in load-carrying capacity. These stresses are self-equilibrating and are typically induced in structural components through plastic deformation and differential cooling during manufacture.

Both the magnitude and distribution of residual stresses in structural sections are greatly dependant on the production process. In hot rolled sections and welded sections, residual stresses are primarily induced through uneven cooling, whilst for cold formed sections, residual stresses are induced principally through plastic deformation. Plastic deformation may occur during the coiling and uncoiling of the sheet material, during cutting operations, and during forming of the section (whether press braked or cold rolled).

Extensive research into the effect of residual stresses has been carried out for carbon steel sections. For example, the influence of residual stresses on the behaviour of fabricated carbon steel sections has been discussed by Huber and Beedle (1954), Fukumoto and Itoh (1981) and Chernenko and Kennedy (1991), whilst hot rolled sections have been discussed by Nethercot (1974), Fukumoto and Itoh (1980) and Madugula et al. (1997). A summary of the formation and influence of residual stresses in hot rolled and fabricated sections has been reported by Lay and Ward (1969). Residual stresses in both press braked and cold rolled sections have been discussed by Weng and Peköz (1990) and Schafer and Peköz (1998). Residual stresses in cold rolled sections have been investigated by Chen and Ross (1977) and Kato and Aoki (1978), and in press braked sections by Weng and White (1990). The rigour with which these stresses have been quantified for carbon steel sections from different production routes reflects their potential influence on structural performance.The effect of residual stresses on the behaviour of structural stainless steel members has received less scrutiny, though Coetzee et al. (1990) have considered their influence on cold formed stainless steel sections and Bredenkamp et al. (1992) on welded stainless steel I sections.

With increased interest in the use of stainless steel in construction it is important to quantify the residual stresses that exist within structural members. It cannot simply be assumed that residual stresses in stainless steel sections are of the same magnitude or distribution as those in carbon steel sections, due to the different physical and thermal properties that stainless steel exhibits. Differences that may influence the formation of residual stresses include higher thermal expansion and lower thermal conductivity than carbon steel, and a rounded stress-strain curve with significant strain hardening; these properties are discussed in more detail in Chapter 2.

The sectioning technique was employed to quantify the longitudinal residual stress distributions in a range of structural stainless steel sections. Three hot rolled angles, eight press braked angles and seven cold rolled box sections were examined and the details of the specimens are given in Chapter 3. Measurements were taken with electrical strain gauges and, for one section, also with a mechanical strain gauge; an appraisal of the applicability of both of these techniques is made herein. Tensile coupons tests were performed on the released strips of material to obtain the corresponding material stress-strain relationship. The experimental technique, results and analysis are also presented in Cruise and Gardner (submitted).

Following a survey of existing residual stress data from carbon steel and stainless steel sections, together with proposed models for the prediction of residual stresses in carbon steel structural sections, the data presented herein have been combined with existing data and used to develop

residual stress models specifically for press braked, cold rolled, fabricated and hot rolled stainless steel sections (Gardner and Cruise, submitted).

5.2 Literature review

This section provides a summary of experimental techniques available for residual stress analysis and presents the common approach used to convert the measured strains into residual stress values.

Owing to the sensitivity of stainless steel to plastic deformation and thermal effects the influence production processes have over the residual stress distribution are examined for four types of sections: press braked, cold rolled, hot rolled and fabricated. A review of existing residual stress data is given and studies incorporating residual stress measurements in structural stainless steel sections are also introduced. This includes experimental data, analytical and numerical investigations, and proposed models for the prediction of the magnitude and distribution of residual stresses in sheet material and cold formed, fabricated and hot rolled sections.

5.2.1 Experimental techniques

There are three recognised types of residual stress that equilibrate over different scales. Type I residual stresses act and equilibrate over the macro scale. It is the type I stresses which, when present along the length of a member, have the greatest effect on the structural behaviour. Types II and III residual stresses act over the micro-scale and are related to more local stress disturbances caused between and within the metal grain structure. Further detail on these distinctions and the origin of residual stresses are given in Withers and Bhadeshia (2001b).

Techniques to measure type I residual stresses may be classified as either destructive or non-destructive. Non-destructive methods include X-ray, neutron or electron diffraction, ultrasonic methods and magnetic methods. The results of ultrasonic and magnetic techniques can however be sensitive to large grain structures, which have been observed in stainless steels. X-ray, neutron and electron diffraction techniques have been developed primarily to measure microscopic residual stresses and are limited by the depth to which measurements can be taken, though neutron and X-ray diffraction can be employed to measure type I residual stresses for engineering applications (Webster and Wimpory, 2001). Destructive methods rely on the measurement of deformations due to the release of residual stresses upon removal of material

from the specimen. One such method is the hole drilling method where rosette strain gauges are placed on the sample and a hole drilled through the centre. The strain released around the hole is recorded as the depth of the drilled hole is increased. This technique is useful in measuring through thickness type I residual stresses that are in a particular location, for example in the vicinity of welds. Hole drilling has the benefit that, depending on the size and type of component, it may be considered only partially destructive. Sectioning is the principal destructive technique used to measure residual stresses in structural members. This method has been used extensively to analyse residual stresses in structural carbon steel (Estuar and Tall, 1963), aluminium (Mazzolani, 1995), and stainless steel (Lagerqvist and Olsson, 2001) and Young and Lui, 2005) sections. A comprehensive description of the different techniques for measuring residual stresses has been presented in Withers and Bhadeshia (2001a).

5.2.2 Modelling residual stress

For the purposes of structural design, residual stresses which occur along the length of the member are the most influential on structural behaviour. Therefore, although significant residual stresses can exist in other directions, particularly in the circumferential direction (Chen and Ross, 1977), longitudinal strains on the internal and external surfaces of the section are most commonly measured and converted into stresses.

In general, the strips of material released by the sectioning process may exhibit both axial deformation and curvature, corresponding to membrane and bending (through thickness) residual stresses, respectively. Membrane residual stresses σ_m generally dominate in hot rolled and fabricated sections whereas bending residual stresses σ_b are generally dominant in cold formed sections. These two residual stress components are illustrated in Figure 5.1, where the bending stresses are assumed to be linearly varying through the thickness. From this assumption it follows that the combined membrane and bending residual stress pattern σ_{rc} is always a linear relationship (Schafer and Peköz, 1998). For thick plates, where it is possible to measure residual stresses at incremental depths through the material thickness, this assumption has been shown to be inaccurate by Weng and White (1990) and Brozzetti et al. (1971). For thinner material it is physically difficult to measure these through thickness changes, though analytical and finite element studies have also predicted a non-linear through thickness variation of residual stresses (Ingvarsson, 1975, Quach et al., 2006).

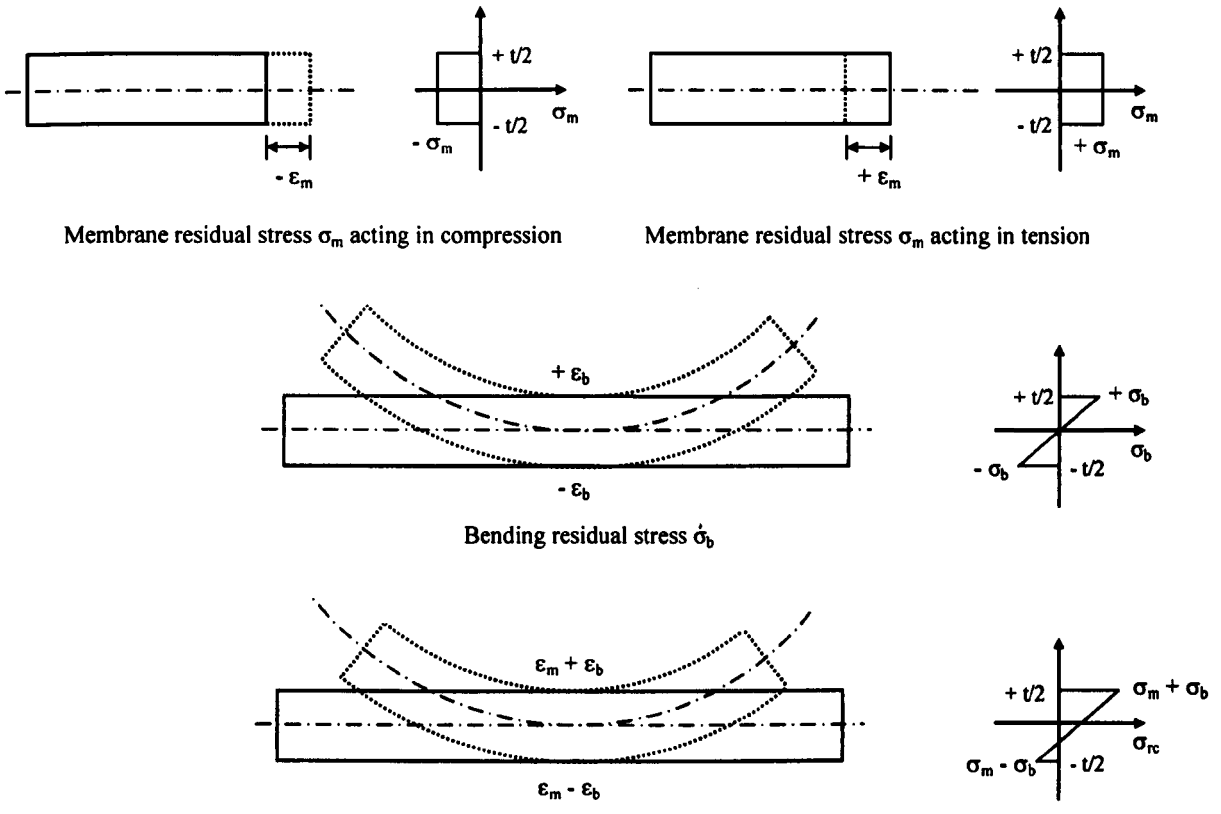

Membrane residual stress σ_m acting in compression

Membrane residual stress σ_m acting in tension

Bending residual stress σ_b

Combined bending and membrane residual stresses σ_{rc}

Figure 5.1: *Modelling of residual stresses with a membrane and a bending stress component*

5.2.3 Residual stresses in sheet materials

Both press braked and cold rolled sections are produced from sheet material. Extant residual stresses in the sheet material have the potential to contribute to the residual stress distributions observed in cold formed sections. Different strain paths are observed in processes used for sheet production which may influence the residual stress distribution in sheet materials, such as hot rolling to produce hot band, or hot rolling and subsequently cold rolling to produce cold rolled sheet. The coiling of the sheet for easy storage and transportation, as well as uncoiling and levelling of the sheet prior to section production could also potentially influence the sheets residual stress distribution.

Wang et al. (2002) employed neutron diffraction to investigate residual stresses in thin cold rolled stainless steel sheet and to determine the influence of annealing the material. Measurements revealed highly directional intergranular residual stresses after the rolling process. Annealing to 500°C was found to significantly reduce this degree of alignment.

Quach et al. (2004) carried out an analytical study, validated against a finite element study, to predict the residual stresses induced by the coiling and uncoiling of carbon steel material; an extension to this study was carried out by Quach (2005) for stainless steel sheet material. It was assumed that annealing occurred prior to coiling and therefore there were no residual stresses present in the sheet material before this coiling began. It was found, using the von Mises yield criteria and the Prandtl-Reuss plastic flow rule, that the created through thickness variation of residual stresses is non linear and that longitudinal residual stresses up to 25% greater than the original material yield strength may result. Residual stresses greater than the yield strength of the uncoiled material can be attributed to strain hardening of the outer fibres of the material during coiling and uncoiling, resulting in enhanced material strength in these locations. In addition, longitudinal stresses greater than the uniaxial yield stress are possible with the von Mises yield criterion in the presence of simultaneous transverse stresses. Residual stresses caused by the coiling processes are dependant on the curvature of the coil, which in turn is dependant on the thickness of the material, the inner diameter of the coil and the position from which the sheet material is taken from the coil. A range of inner coil diameters (200 to 700 mm) were considered in the study and it was proposed that this range could account for the variation of residual stresses observed along the lengths of cold rolled sections and between nominally similar sections.

5.2.4 Residual stresses in press braked sections

The simplicity of the forming process employed in press braking causes localised plastic deformation thereby suggesting that the residual stress distribution in the unformed part of the section be governed by the residual stresses in the sheet material. Spring back of the section after forming releases some elastic stresses that otherwise would contribute to the residual stresses remaining in the component. Residual stress data from the experimental program are examined herein and form the basis for the proposed residual stress models.

An investigation on the influence of residual stress on the structural behaviour of stainless steel press braked lipped channel sections was presented by Coetzee et al. (1990), however no experimental data was presented. The remainder of this sub-section presents experimental data and predictive residual stress models for press braked carbon steel sections. An experimental and analytical study of press braked sections was carried out by Ingvarsson (1975), where the experimental results revealed high corner bending residual stresses of approximately $0.5\sigma_y$ (determined on the assumption of a linearly varying through thickness stress distribution) where σ_y is the material yield stress. The existence of non linear, through thickness, longitudinal residual stresses in both press braked and cold rolled carbon steel sections was attributed to the

transverse strains associated with the corner forming process in conjunction with the Poisson effect. Weng and Peköz (1990) observed combined bending and membrane residual stresses in press braked sections in the range of $0.25\text{-}0.70\sigma_y$, of which the bending residual stresses represented a considerable proportion. Relatively uniform combined residual stresses were reported along the section faces, with increased values in the corner regions. The membrane residual stresses in the corner regions were reported to be low, showing that the increase in residual stresses in the corners was primarily due to an increase in bending residual stresses, related to the high localised plastic deformation. Based on a number of experimental studies of residual stresses in press braked carbon steel sections, Schafer and Peköz (1998) proposed the predictive model of Figure 5.2. The model contained only bending residual stresses since the membrane residual stresses were found to be of low magnitude (generally less than $0.06\sigma_y$).

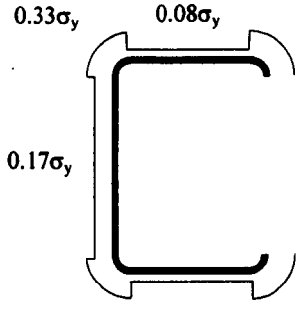

Figure 5.2: *Predictive model for bending residual stresses in press braked carbon steel sections proposed by Schafer and Peköz (1998)*

Quach et al. (2006) used finite element modelling to superimpose the residual stresses caused by cold forming of structural sections onto those obtained by modelling the coiling and uncoiling of the sheet material previously presented by Quach et al. (2004). The results were validated against an experimental study carried out by Weng and White (1990). The findings were similar to those of Ingvarsson (1975), predicting non linear through thickness residual stress distributions. Residual stresses obtained in the corner regions of the sections were found to be greater than the uniaxial yield strength of the material.

5.2.5 Residual stresses in cold rolled sections

During the forming of cold rolled box sections considerable plastic deformation is thought to occur throughout the section but to a more significant degree in the corners regions. It is this forming process combined with the extant sheet material residual stresses distribution that produces the residual stresses observed in the manufactured sections.

Residual stress measurements in cold rolled stainless steel box sections (SHS and RHS) have been reported by the Centre for Advanced Structural Engineering (1990), Clarin (2003), Young and Lui (2005) and in the current study. The Centre for Advanced Structural Engineering (1990) took residual stress measurements on two grade 1.4306 stainless steel hollow sections - one CHS and one SHS. As for the press braked sections, the membrane residual stress in the cold rolled CHS and SHS were found to be negligible compared to the bending stresses, and both residual stress components were higher in the SHS than in the CHS. Similarly large bending residual stresses were reported in a high strength stainless steel cold rolled box section by Young and Liu (2005). Clarin (2003) presented residual stress measurements from a cold formed stainless steel RHS produced from cold worked sheet material (grade 1.4306). These experimental results again revealed the presence of large bending residual stresses ($0.3\text{-}0.9\sigma_{0.2}$), and lower membrane residual stresses (less than $0.25\sigma_{0.2}$).

The remainder of this sub-section reviews previous residual stress studies on cold rolled carbon steel sections. Schafer and Peköz (1998) proposed a model (Figure 5.3) for the prediction of bending residual stresses in cold rolled carbon steel lipped channel sections. Higher bending residual stresses were proposed for the web than for the flanges, supported by the experimental data of Weng and Peköz (1990). Membrane residual stresses were reported to be less than $0.08\sigma_y$, with the highest values in the corner regions of the sections (Schafer and Peköz, 1998). Based on the results of Weng and Peköz (1990) and their own experimental data from two sizes of cold rolled lipped channels, Abdel-Rahman and Sivakumaran (1997) proposed that the bending residual stresses in all flat regions could be modelled as $0.18\sigma_y$ (despite an observed variation with face width) and those of the corner regions could be approximated as $0.40\sigma_y$.

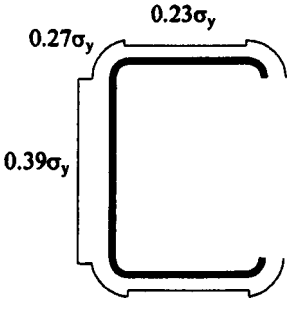

Figure 5.3: *Predictive model for bending residual stresses in cold rolled carbon steel sections proposed by Schafer and Peköz (1998)*

5.2.6 Residual stresses in fabricated sections

As fabricated sections are built up by the welding together of plate material, only membrane residual stresses are considered in welded sections, since the bending residual stresses are generally negligible. It may be observed from existing measurements that membrane residual stresses measured in welded I sections are significantly larger than those in cold formed sections. The membrane residual stresses depend upon the manner in which the plate material is cut and the welding techniques employed. Cutting options include flame, laser or saw cutting. Saw cutting may induce work hardening, whilst the flame and laser cutting can cause differential heating and cooling, leaving plate edges in residual tension. The welding process itself causes temperature gradients around the heat affected zone (HAZ) with hotter material at the weld being left in residual tension, whilst the faster cooling surrounding material is left in residual compression, as detailed by Lay and Ward (1969).

Stainless steel possesses different physical and thermal properties to carbon steel, both of which influence the formation of residual stresses as detailed in Chapter 2. The stress-strain behaviour of stainless steel is fundamentally different from that of carbon steel, being of a rounded nature with no sharply defined yield point. Austenitic stainless steel has a coefficient of thermal expansion of approximately 17×10^{-6}/ °C compared to 12×10^{-6}/ °C for carbon steel, and a room temperature thermal conductivity of 16.2 W/m °C compared to 52 W/m °C for carbon steel. The lower thermal conductivity tends to lead to higher thermal gradients in stainless steel, whilst the higher thermal expansion results in greater thermal stress and distortions. There have been two studies on fabricated stainless steel I beams (Lagerqvist and Olsson, 2001; Bredenkamp et al., 1992), though no predictive models have been proposed. Lagerqvist and Olsson (2001) examined residual stresses in austenitic (grade 1.4301) and duplex (austenitic-ferritic) stainless steel welded I sections, whilst Bredenkamp et al. (1992) sectioned four I beams fabricated from guillotined plates of ferritic stainless steel. The residual stress patterns for the ferritic sections were found to be similar to those shown in Figure 5.4(a) for carbon steel – this would be expected since ferritic stainless steels possess physical and thermal properties that are more comparable to those of carbon steel. The magnitude of the residual stresses was observed to increase with the thickness of material; this is attributed to the greater heat input required to form welds in thick material.

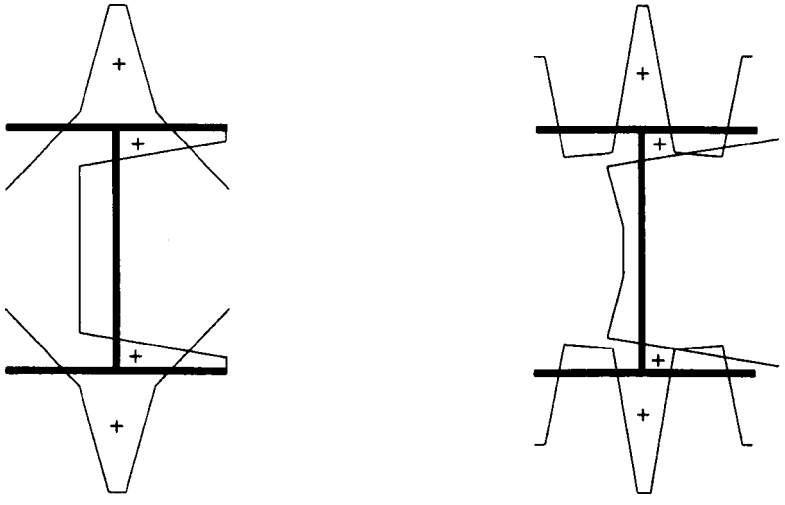

(a) Welded and mill cut plates *(b) Welded and oxygen cut plates*

Figure 5.4: *Two indicative residual stress distributions for welded I sections (Chernenko and Kennedy, 1991)*

Experience gained from residual stress studies of welded carbon steel sections are summarised below. Membrane residual stress models for both mill cut and flame cut fabricated carbon steel I sections were reviewed in detail by Chernenko and Kennedy (1991) and indicative distributions of those discussed are shown in Figure 5.4(a) and 5.4(b).

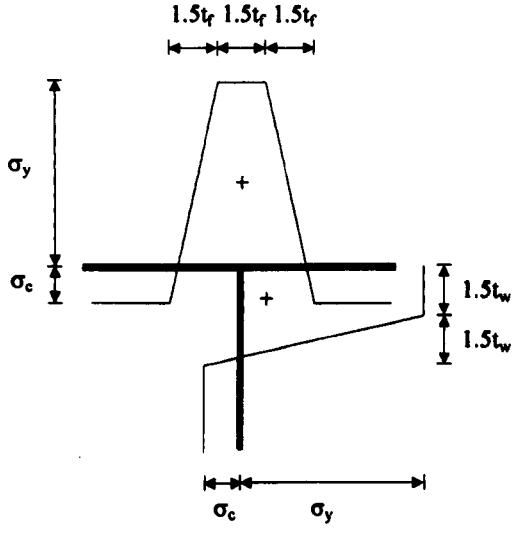

Figure 5.5: *Model of membrane stresses in a welded carbon steel I sections presented in the Swedish design rules BSK 99 (1999)*

Figure 5.5 shows the weld induced residual stress model proposed in the Swedish design code BSK 99 (1999). In this model, t_f and t_w are the thicknesses of the flanges and web respectively, and the magnitude of the compressive stress σ_c is defined to achieve equilibrium in the section. Fukumoto and Itoh (1981) compared residual stresses in fabricated and hot rolled carbon steel I beams and observed that there was more variation in the residual stresses measured in welded sections than in hot rolled I sections. The membrane residual stress magnitudes in the weld region were close to the yield strength of the material, whilst the compressive residual stresses in the web were approximately $0.4\text{-}0.6\sigma_y$; lower residual stresses were observed in the flanges. Dwight and Moxham (1969) and Masubuchi (1980) have also proposed predictive models for weld induced residual stresses in carbon steel sections. Dwight and Moxham (1969) proposed that the membrane residual stresses in the weld and heat affected zone (HAZ) can be considered to be equal to the yield strength of the material, where the width ηt of the HAZ either side of the weld could be approximated from Equation 5.1.

$$\eta t = \frac{CA}{\sigma_y \Sigma t} \tag{5.1}$$

in which t is the material thickness, Σt is the sum of the thicknesses of material to be welded, A is the cross sectional area of the added weld material and C is a constant defined by experimental data.

Masubuchi (1980) proposed that membrane residual stresses σ_x can be modelled as a function of distance y from the weld, as given by Equation 5.2.

$$\sigma_x(y) = \sigma_{max}\left(1-\left(\frac{y}{p}\right)^2\right)e^{-\frac{1}{2}\left(\frac{y}{p}\right)^2} \tag{5.2}$$

where σ_{max} is the maximum tensile residual stress measured at the weld, which is commonly taken as the yield strength of the material, y is the distance from the weld and p is the width of the tension zone created by the weld.

5.2.7 Residual stresses in hot rolled sections

As for fabricated sections, bending residual stresses in hot rolled sections are generally low, so typically only membrane residual stresses are examined. Residual stresses in hot rolled sections are attributed to differential cooling due to variation in thickness around the sections, as well as

any straightening process that might be employed once the section has cooled. The formation of residual stresses in hot rolled sections has been described in detail by Lay and Ward (1969). Residual stress data for three hot rolled stainless steel angle sections were measured as part of the experimental program, where both membrane and bending residual stresses were of low magnitude, generally less than $0.2\sigma_{0.2}$.

Residual stresses in hot rolled carbon steel I sections have been examined by Chernenko and Kennedy (1991), and as summarised by Nethercot (1974), a number of other researchers. These studies have resulted in the proposal of predictive models, which vary in complexity and differ in their predictions for the magnitude and distribution of residual stresses. Madugula et al. (1997) carried out residual stress measurements on 42 hot rolled carbon steel angles, but the results showed considerable variation and as a result no predictive models were proposed. Variations in residual stresses in hot rolled sections are generally attributed to differences in the hot rolling and straightening processes.

5.3 Experimental Program

An experimental program was carried out at Imperial College London to quantify the distributions of residual stresses in three different types of structural stainless steel sections: press braked angles, cold rolled box sections and hot rolled angles. More detailed information on the specimens is given in Chapter 3.

5.3.1 Specimen preparation

The specimens were set out as shown in Figure 5.6, with sufficient material either side of the central portions (Portions A and B) to ensure a representative initial residual stress distribution. The first central portion A was divided into a series of flat and corner strips; each corner region was assumed to be the arc of a quarter circle. Central portion B was included to allow spare corner strips to be produced. Typical strip divisions for the three cross section types are shown in Figure 5.16, 5.25, and 5.33.

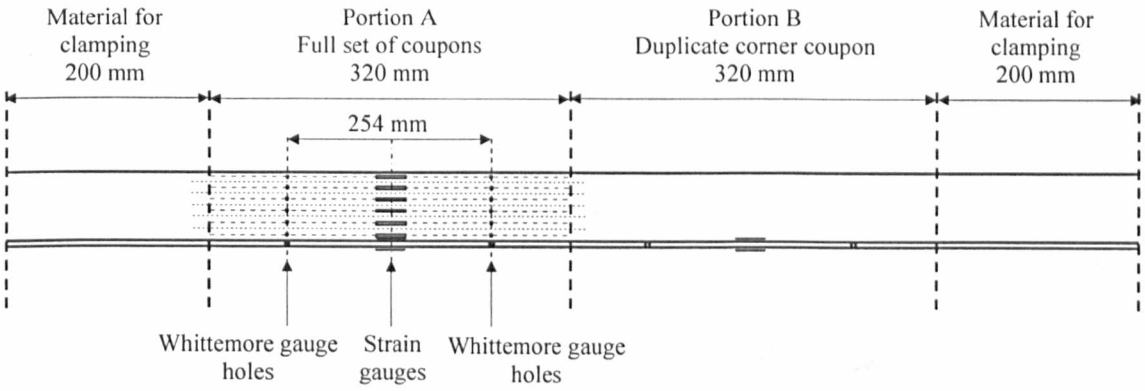

Figure 5.6: *Specimen setting out (angle section)*

The strains released during the cutting process were generally measured using electrical strain gauges, though mechanical curvature measurements were also made, and for one section, a mechanical strain gauge was also employed. The reasons for this will be discussed in the following section. Initial readings prior to the sectioning process and final readings after sectioning were taken for all released strips. Sectioning was performed on an automated milling machine using a 100 mm diameter, 1.2 mm thick, high speed steel circular blade with 36 teeth, as shown in Figure 5.7. The speed of cutting and feed speed of the mill bed were carefully controlled to ensure that no galling occurred. A set of released strips from a cold rolled box section are shown in Figure 5.8.

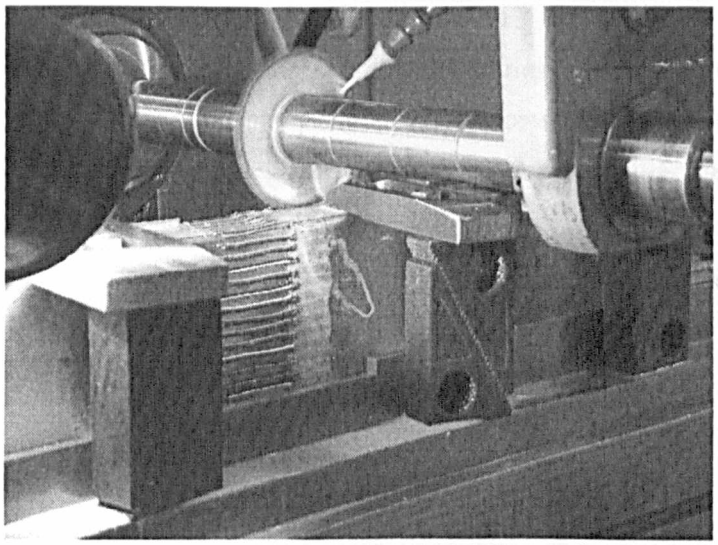

Figure 5.7: *Sectioning of a cold rolled box specimen*

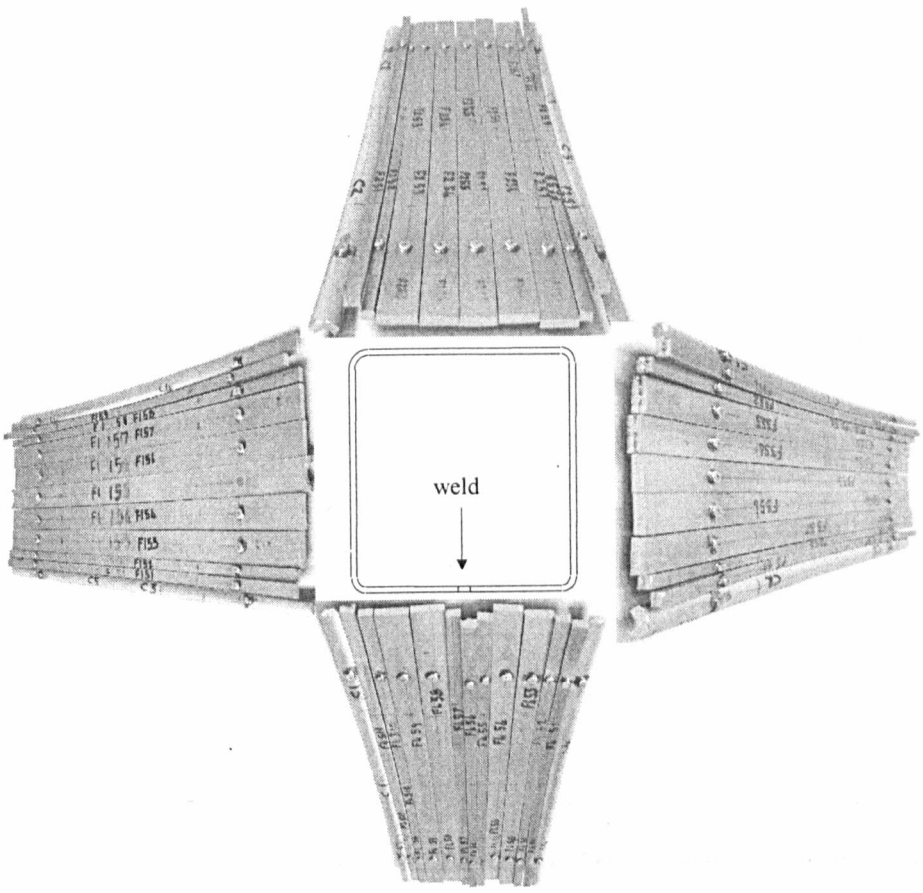

Figure 5.8: *A sectioned cold rolled box specimen*

5.3.2 Mechanical strain readings

For the first cold rolled box section, released residual strains were measured by mechanical means, following the procedure recommended in Galambos (1998). Membrane strains were measured using a mechanical strain gauge (or Whittemore gauge) (Figure 5.9a), whilst bending strains were measured with a curvature dial (Figure 5.9b).

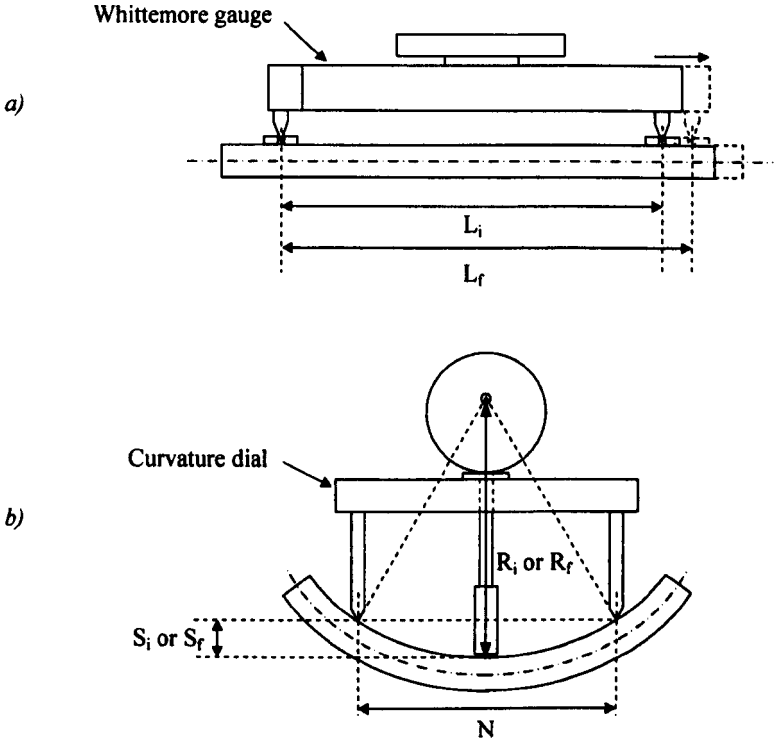

Figure 5.9: *The geometrical deformation measured by a) Whittemore gauge and b) Curvature dial*

To locate the Whittemore gauge on the specimens, pairs of pellets with pre-drilled gauge holes were adhered to the surface; this was done as an alternative to drilling holes into the specimen as proposed in Galambos (1998). The distance between the pellets was set to correspond to the middle of the range over which the Whittemore stain gauge operated, which was 254 mm. With the length of the strips being 350 mm, there was sufficient material either side of the pellets to eliminate possible disturbance to the residual stress patterns at the section ends. Initial readings using both the Whittemore gauge and the curvature dial were taken for each strip prior to sectioning; a mean value was determined from three readings. Measurements were also taken using the Whittemore gauge and the curvature dial from the released strips after sectioning had taken place. Similarly, mean values from three measurements were determined.

5.3.2.1 Bending residual stresses

Bending residual stresses σ_b were initially determined by assuming a linearly varying through thickness stress distribution, by means of Equation 5.3. A rectangular stress block distribution was also considered.

$$\sigma_b = \frac{Ey}{R_{i-f}} \tag{5.3}$$

where E is the Young's modulus, R_{i-f} is the change in radius of curvature and y is the distance from the neutral axis, taken as t/2 (where t is the material thickness) to determine the surface stresses. The asymmetry of the corner strips meant that the inner and outer surface stresses were not equal. The change in radius of curvature R_{i-f} of the strips was calculated from Equation 5.4. It was assumed that the curvature was constant along the length of the strips (which was confirmed with curvature dial measurements).

$$R_{i-f} = \frac{(S_f - S_i)}{2} + \frac{N^2}{8(S_f - S_i)} \tag{5.4}$$

where N is the length over which the deflection is measured (N = 100 mm), S_i is the initial deflection of the strip and S_f is the final deflection of strip (see Figure 5.9b).

5.3.2.2 Membrane residual stresses

The calculation of the membrane residual stress is more complex, as the measurements made by the Whittemore gauge must be corrected to remove the effects of strip curvature caused by the existence of bending residual stresses. Expressions to calculate membrane residual stresses from Whittemore gauge and curvature dial measurements have been proposed by Galambos (1998) and Sherman (1969). Both Galambos (1998) and Sherman (1969) approximate the curvature of the released strips as parabolic, though this is found herein to be inappropriate in the presence of large bending residual stresses, which are particularly prominent in cold rolled sections. An alternative circular approximation is therefore proposed, whereby the released strip is assumed to be a circular arc and the Whittemore gauge length (measured between gauge points at A and B in Figure 5.10) is assumed to be a chord of length D. The relationship between angle of curvature θ and chord length D, is expressed in Equation 5.5 and illustrated in Figure 5.10.

$$\sin\theta = \frac{D}{2R} \tag{5.5}$$

where R is the radius of curvature measured from the centre of curvature to the surface of the gauge hole pellets.

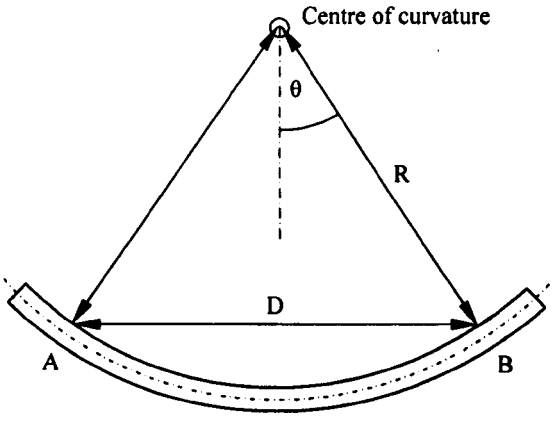

Figure 5.10: *Definition of angle of curvature θ*

There are three corrections required to convert the measurements taken from the Whittemore gauge and curvature dial to membrane residual stresses acting along the neutral axis of the strip Galambos (1998). In the context of the circular approximation, these are described in the following sub-sections.

5.3.2.2.1 The gauge hole correction

The Whittemore gauge has two conical points to enable it to be positioned in the gauge holes on the strip. Owing to the curvature of the strips, the centrelines of the conical points do not pass through the centreline of the gauge hole, but are offset by a distance Δ, as shown in Figure 5.11.

Assuming that the conical point remains in complete contact with the outer circumference of the gauge hole and that the strip is of constant curvature, the offset Δ can be determined from Equation 5.6.

$$\Delta = \left(\frac{g}{2}\right)\sin\theta\tan\phi \tag{5.6}$$

where g is the diameter of the gauge hole, θ is the angle of curvature, and ϕ is half the internal angle of the conical point. The new gauge length D_c can be used to calculate a revised angle of curvature θ_c from Equation 5.5.

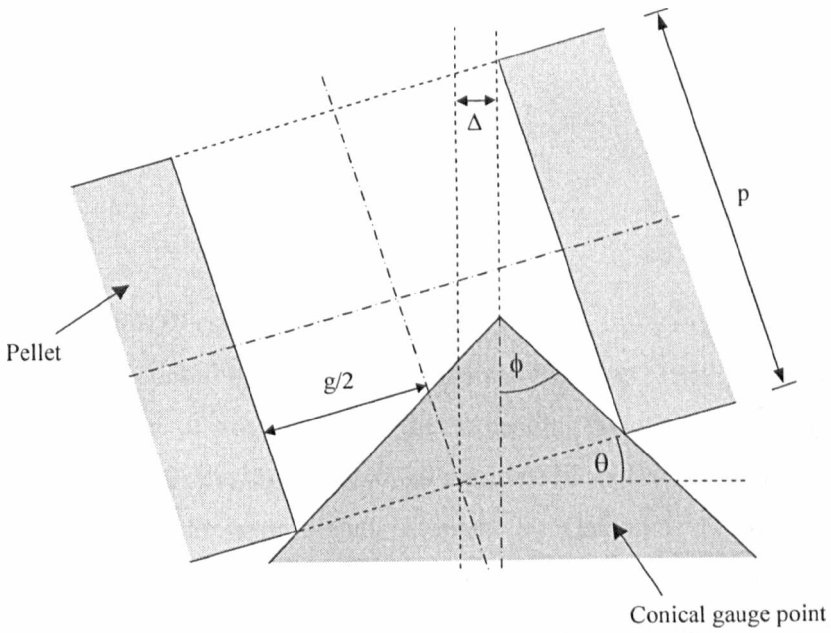

Figure 5.11: *The gauge hole correction*

5.3.2.2.2 The surface to neutral axis correction

Calculations so far have used the radius of curvature R from the centre of curvature to the surface of the gauge hole pellets. In order to remove the influence of bending residual stresses from the membrane stress calculation, the radius of curvature of the strips measured to the neutral axis R_n is required. For a strip of rectangular cross section, this simply requires the addition or subtraction of (t/2 + p) where t is the strip thickness and p is the pellet thickness from the radius of curvature R measured to the surface of the pellets. The corresponding chord length D_n can be obtained using Equation 5.5.

5.3.2.2.3 The chord to arc correction

The final correction is to convert the chord length D_n into the arc length L. Using the radius of curvature of the strips measured to the neutral axis R_n and the revised angle of curvature θ_c, the length along the arc can be calculated using Equation 5.7.

$$L = R_n \theta_c \tag{5.7}$$

By performing this process for both the initial and final state of the strips, the initial and final arc lengths L_i and L_f may be determined, and hence the membrane residual strain ε_m may be

calculated through Equation 5.8. Assuming an elastic material response, the residual stress may then be calculated by means of the Young's modulus.

$$\varepsilon_m = \frac{L_f - L_i}{L_i} \tag{5.8}$$

5.3.2.3 Discussion of corrections

The corrections proposed by Galambos (1998) and Sherman (1969) were developed principally to remove the effects of strip curvature (due to bending residual stresses) during the calculation of membrane residual stresses in hot rolled sections. In such sections, bending residual stresses are low and hence the approximations made by Galambos (1998) and Sherman (1969) (including representation of the curved strips as a parabola and small angle assumptions) induce only minimal errors. However, for cold formed sections, bending residual stresses are far more significant, and adoption of the Galambos or Sherman approximations leads to calculated membrane residual stresses displaying large discrepancies from those determined using the circular approximation described above. Deviation in calculated membrane residual stresses using the Galambos and Sherman approximations from the circular approximation is indicated in Figure 5.12 for a strip thickness of 4 mm; the results show that as the radius of curvature reduces, the deviation increases. It is later demonstrated, by comparison of residual stresses determined by mechanical means with those determined by electrical strain gauges, that the circular approximation remains accurate, even in the presence of the high curvatures associated with cold formed sections.

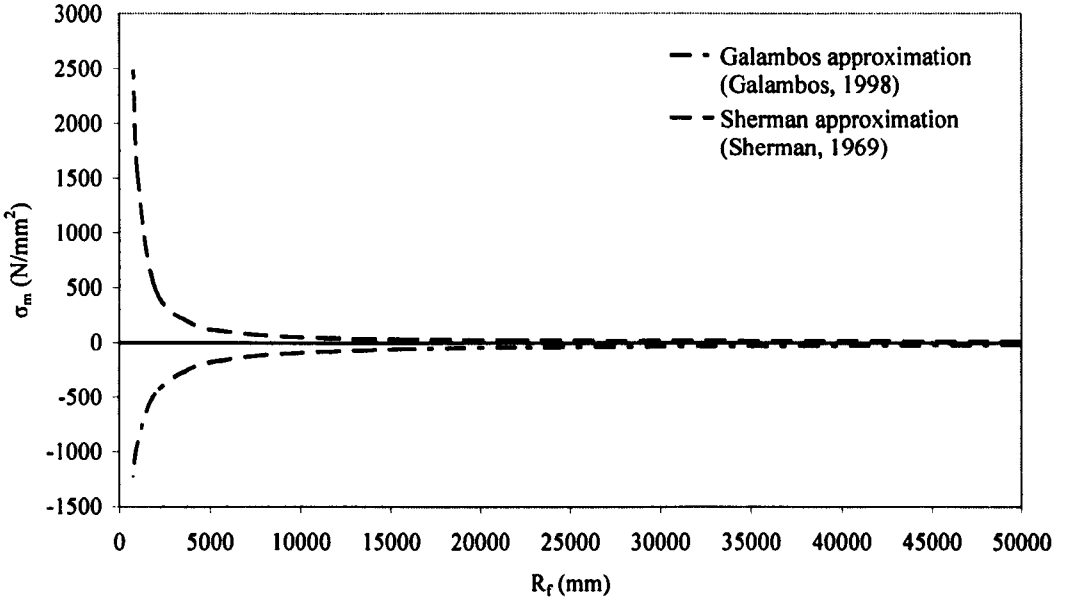

Figure 5.12: *Deviation of calculated membrane residual stresses of Galambos (1998) and Sherman (1969) from the circular approximation for varying radius of curvature*

5.3.3 Electrical strain readings

Electrical strain gauges were selected in preference to the mechanical strain gauge for the residual strain measurements of the remaining 17 cross sections. Curvature dial readings were still taken to verify the results of the electrical strain gauges. The electrical strain gauge width was 2 mm and the length was 20 mm. Narrow strain gauges were selected to enable fine divisions of the sections to be made (Figure 5.13). The strain gauges were affixed to the surface of the sections with a cyanoacrylate adhesive and were covered with an epoxy coating to prevent damage during the sectioning process. The strain gauges were read by a quarter bridge strain box and logged using Dalite software. For each set of readings, the strain box was zeroed against a high precision 120 Ω resistor with a temperature variation coefficient very close to that of the strain gauges to ensure any temperature effects on the resistance were accounted for. Different techniques were used to determine residual stresses in the angles and box sections due to the difficulties of affixing strain gauges to the inner surfaces of the box sections, as described in the following sub-sections.

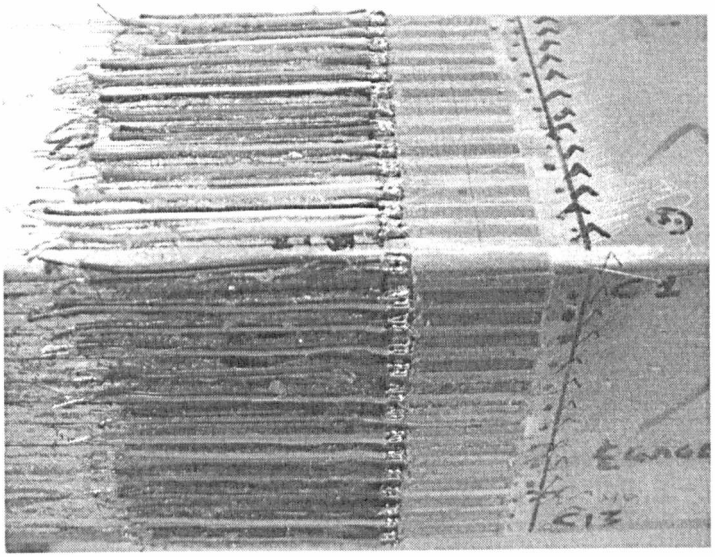

Figure 5.13: *Strain gauges affixed to cold rolled box specimen prior to sectioning*

5.3.3.1 Angle sections

Strain gauges were adhered to both the inner and outer surfaces of the hot rolled and press braked angle sections and readings were taken prior to ($\varepsilon_{i,in}$ and $\varepsilon_{i,out}$) and after ($\varepsilon_{f,in}$ and $\varepsilon_{f,out}$) sectioning. On the assumption that the residual strain distribution can be modelled as linearly varying through the material thickness, Equations 5.9 and 5.10 may be used to calculate both membrane and bending residual strains, where a positive value indicates a tensile residual strain and a negative value indicates a compressive residual strain.

$$\varepsilon_m = -\left(\frac{(\varepsilon_{f,out} - \varepsilon_{i,out}) + (\varepsilon_{f,in} - \varepsilon_{i,in})}{2}\right) \tag{5.9}$$

$$\varepsilon_b = \pm\left(\frac{(\varepsilon_{f,out} - \varepsilon_{i,out}) - (\varepsilon_{f,in} - \varepsilon_{i,in})}{2}\right) \tag{5.10}$$

5.3.3.2 Box sections

Due to physical constraints, it was not possible to mount strain gauges on the inner surface of the cold rolled box sections; strain gauges were therefore only mounted on the outer surface prior to sectioning. Hence, a different procedure was developed to establish residual stresses,

whereby the second set of strain gauges was attached to the strips after sectioning, to what was the inner surface of sections. The residual stresses were subsequently found by reintroducing the bending residual stresses through deforming the strips back to a flat configuration. This was achieved by holding the strips on a mill plate with two clamps, which were gradually adjusted until the strip was returned to a flat condition. Bending residual stresses determined by this means from the electrical strain gauges were compared with values obtained from the curvature dial; Figure 5.14 shows excellent correlation between the two approaches, suggesting that the circular approximation described earlier is a reasonable one to employ. The membrane residual strains were obtained by subtracting the bending strains from total strain readings taken on the outer strain gauges. Figure 5.15 illustrates this procedure, and Equations 5.11 and 5.12 express the membrane residual strains and bending residual strains in terms of the measured strains. The letter 'b' in the strain subscripts indicate measurements that were taken when both the inner and outer strain gauges were attached (see Figure 5.15).

$$\varepsilon_m = -(\varepsilon_{f,out} - \varepsilon_{i,out}) - (\varepsilon_{bf,out} - \varepsilon_{bi,out}) \tag{5.11}$$

$$\varepsilon_b = \pm\left(\frac{(\varepsilon_{bf,out} - \varepsilon_{bi,out}) - (\varepsilon_{bf,in} - \varepsilon_{bi,in})}{2}\right) \tag{5.12}$$

The results obtained are presented and discussed in the following section.

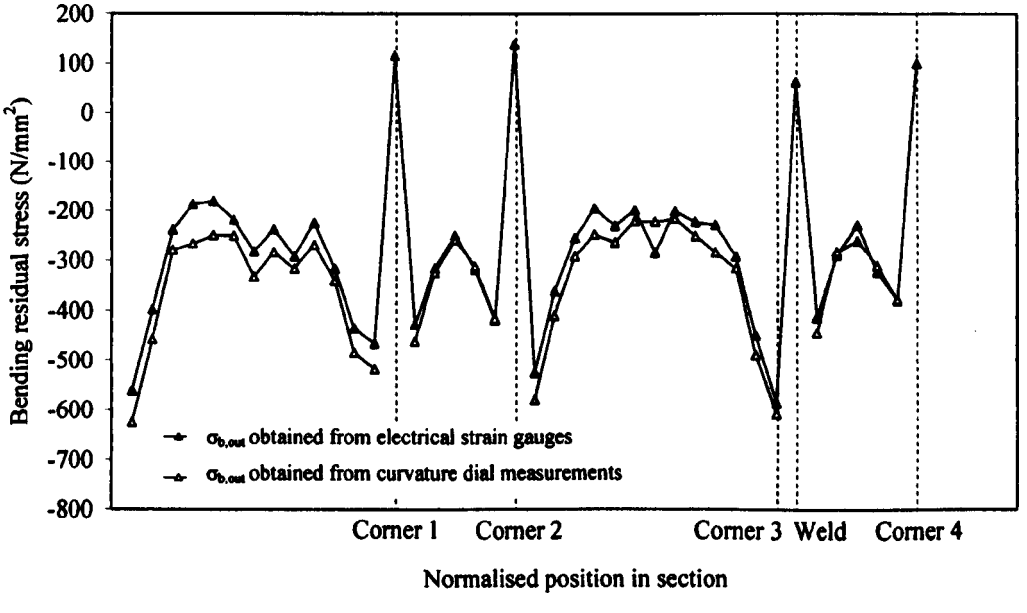

Figure 5.14: *Correlation between bending residual stress from mechanical and electrical strain gauges for CR 100×50×4 (No curvature dial readings were taken for the corner strips)*

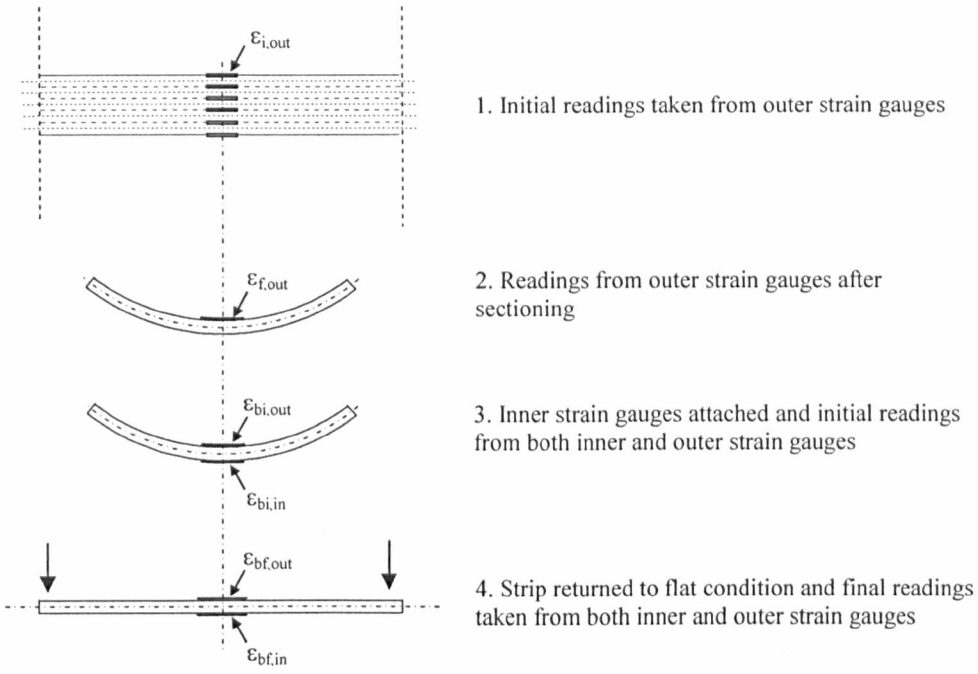

Figure 5.15: *Residual strain measurements for cold rolled box sections*

5.4 Results

5.4.1 Introduction

Residual stresses have been analysed in a total of 18 stainless steel cross sections. The results are presented and analysed in this section. Graphical results for all tested sections are presented in Figures 5.17 to 5.24 (for the press braked sections), Figures 5.26 to 5.32 (for the cold rolled sections) and Figures 5.34 to 5.36 (for the hot rolled sections). Tabulated results for three sections: one press braked angle (PB 50×50×2 (r_i = 4.5)), one cold rolled rectangular hollow section (CR 100×50×4) and one hot rolled angle (HR 50×50×3) are also given in this section. The complete tabulated set of residual stress data is given in Appendix A.

In order to evaluate the magnitude of the bending residual stresses, the initial through thickness stress distribution needs to be assumed (in the absence of measurements). Two possible initial stress distributions were considered – firstly, stresses were considered to vary linearly through the thickness, as commonly assumed for cold formed carbon steel sections (Weng and Peköz, 1990 and Schafer and Peköz, 1998) and secondly a rectangular stress block distribution was assumed, which is more representative of the distributions obtained experimentally (in thick

plates) by Weng and White (1990) and analytically and numerically in cold formed sections by Ingvarsson (1975) and Quach et al. (2006). For a rectangular cross section (as is the case for all the flat strips taken from cold rolled sections considered herein), surface bending residual stresses calculated on the basis of a linearly varying through thickness stress distribution will be some 50% higher than those calculated on the basis of rectangular stress blocks – this follows from the fact that rectangular sections have a shape factor of 1.5 in bending. In this study, bending residual stresses in the hot rolled sections were calculated on the basis of a linearly varying through thickness distribution. For cold formed sections however (both press braked and cold rolled), bending residual stresses were calculated on the assumption of rectangular stress blocks, a distribution associated with the large plastic bending deformations that occur during the production process.

5.4.2 Press braked sections

Figures 5.17 to 5.24 show the complete set of bending and membrane residual stress values for the eight stainless steel press braked sections. Table 5.1 presents the numerical data from sectioned strips obtained at different locations around the press braked section PB 50×50×2 (r_i = 4.5). The location of the strips within the cross section is shown in Figure 5.16.

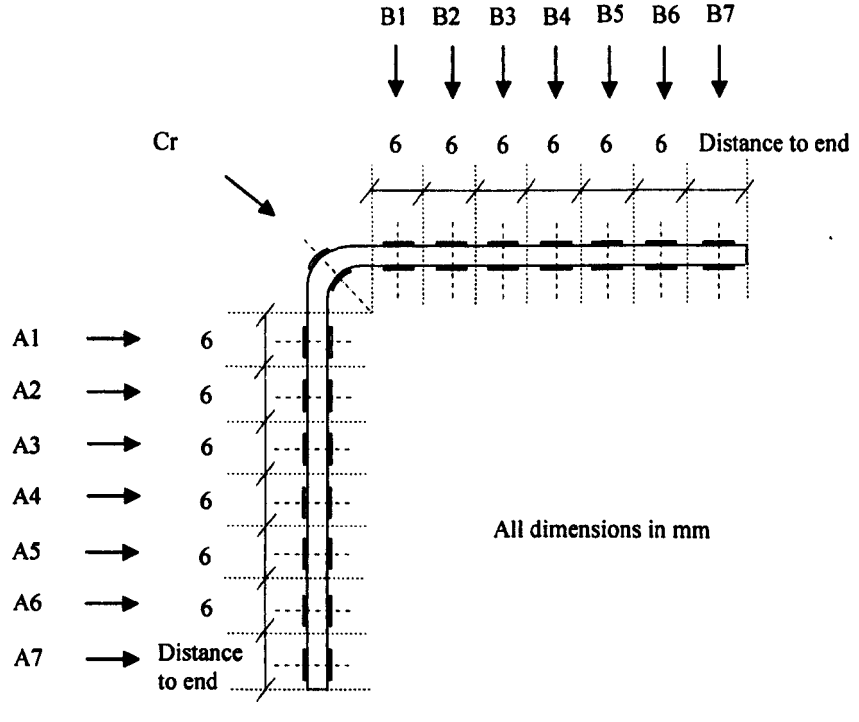

Figure 5.16: *Setting out of press braked section PB 50×50×2 (r_i=4.5)*

Table 5.1: *Residual stress distribution for PB 50×50×2 (r_i=4.5)*

PB 50×50×2 (r_i=4.5)	*Section position (mm)*	*Width (mm)*	σ_m *(N/mm²)*	σ_b *(N/mm²)*	σ_{rc} *(N/mm²)*	$\sigma_m/\sigma_{0.2}$	$\sigma_b/\sigma_{0.2}$	$\sigma_{rc}/\sigma_{0.2}$
A7	44.7	5.46	24	-10	34	0.07	-0.03	0.10
A6	38.2	4.63	8	-14	22	0.03	-0.04	0.08
A5	32.3	4.76	-8	-9	17	-0.03	-0.03	0.06
A4	26.4	4.71	-10	-11	21	-0.04	-0.03	0.07
A3	20.4	4.76	-9	-7	15	-0.03	-0.02	0.05
A2	14.5	4.76	-11	-10	21	-0.04	-0.03	0.07
A1	8.3	5.19	-4	-23	27	-0.01	-0.07	0.08
Cr (r_i=5.5)	0.0		19	-67	85	0.05	-0.21	0.25
B1	8.3	5.15	2	-29	31	0.01	-0.09	0.10
B2	14.4	4.70	12	-7	20	0.04	-0.02	0.07
B3	20.3	4.79	10	-8	18	0.04	-0.02	0.07
B4	26.3	4.72	12	-8	20	0.04	-0.03	0.07
B5	32.2	4.76	11	-10	21	0.03	-0.03	0.06
B6	38.2	4.82	2	-6	8	0.01	-0.02	0.03
B7	45.1	5.95	-11	-5	16	-0.04	-0.01	0.05

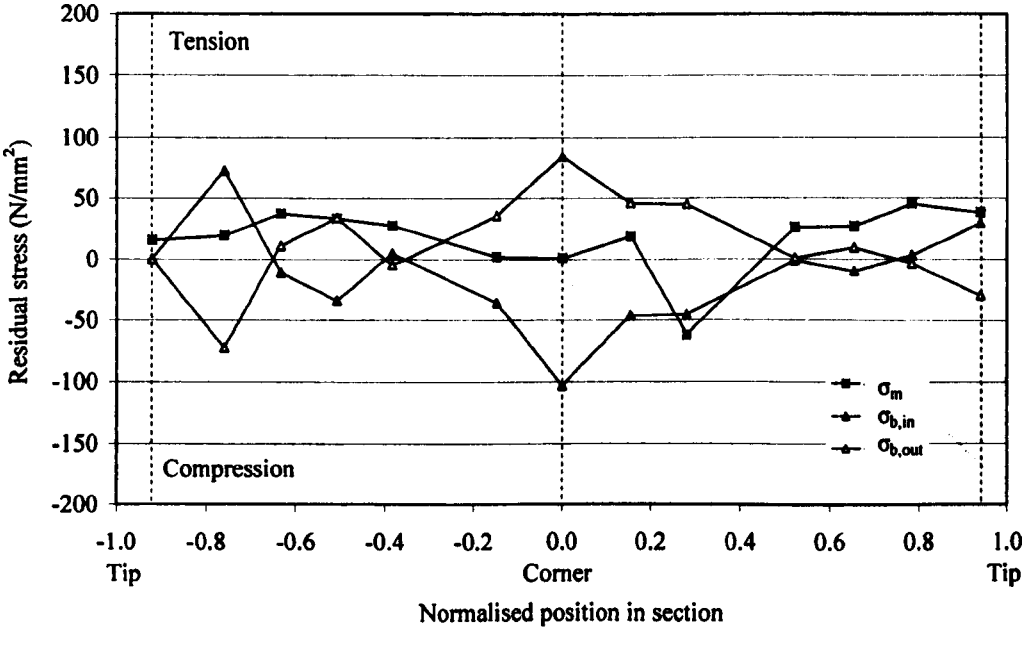

Figure 5.17: *Membrane and bending stresses distributions around PB2 50×50×2 (r_i=3.2) (Average material 0.2% proof strength from the flat regions was 289 N/mm². Material 0.2% proof strength from the corner strip was 362 N/mm²)*

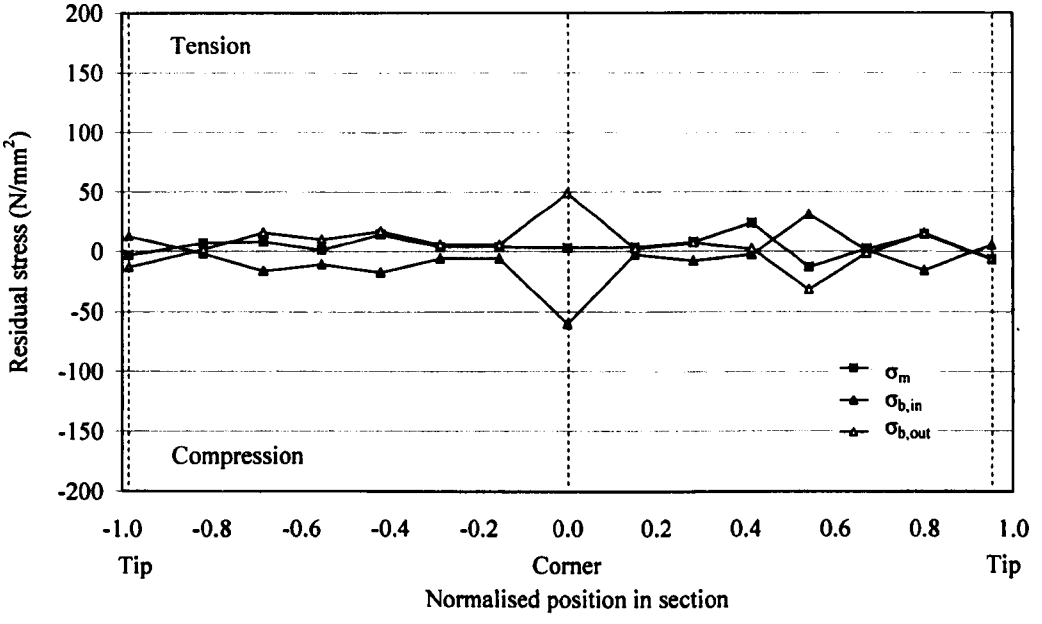

Figure 5.18: *Membrane and bending stresses distributions around PB 50×50×2 (r_i=3.5) (Average material 0.2% proof strength from the flat regions was 320 N/mm². Material 0.2% proof strength from the corner strip was 408 N/mm²)*

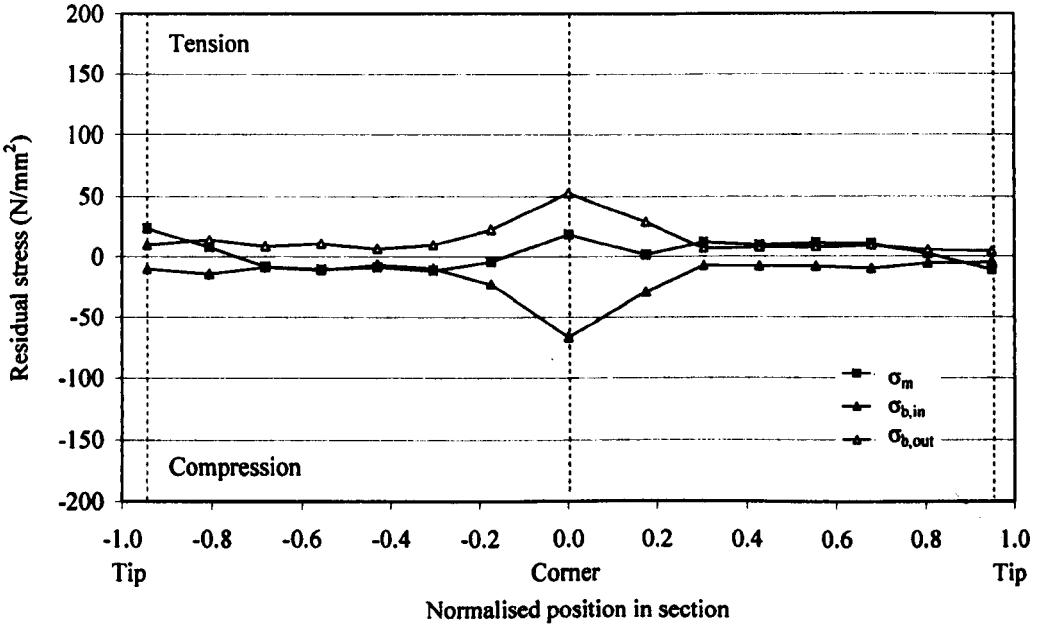

Figure 5.19: *Membrane and bending stresses distributions around PB 50×50×2 (r_i=4.5) (Average material 0.2% proof strength from the flat regions was 298 N/mm². Material 0.2% proof strength from the corner strip was 346 N/mm²)*

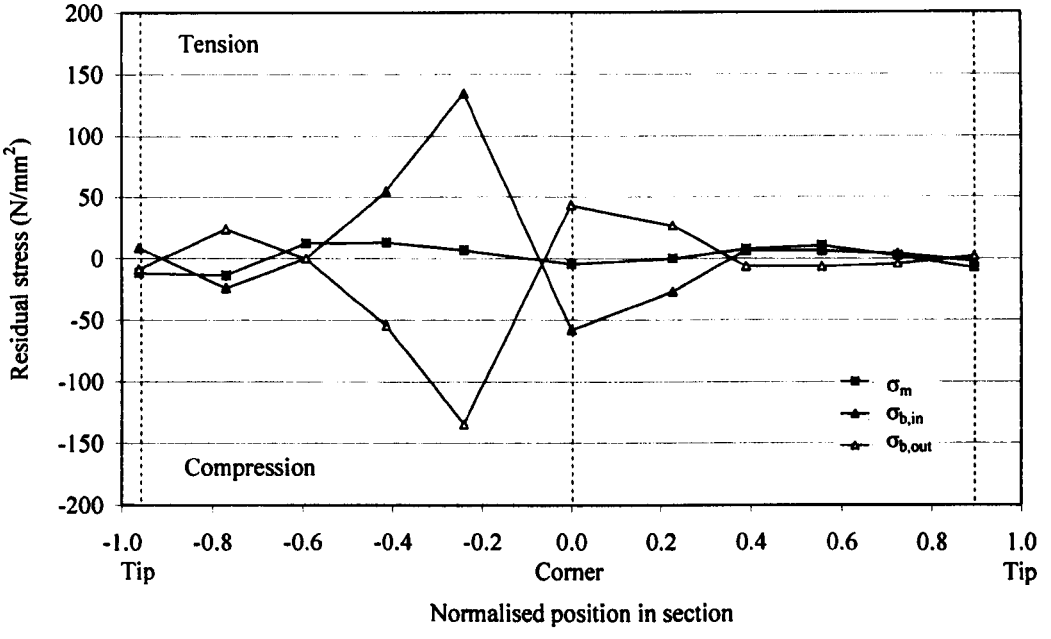

Figure 5.20: *Membrane and bending stresses distributions around PB 50×50×2 (r_i=7.5) (Average material 0.2% proof strength from the flat regions was 292 N/mm². Material 0.2% proof strength from the corner strip was 336 N/mm²)*

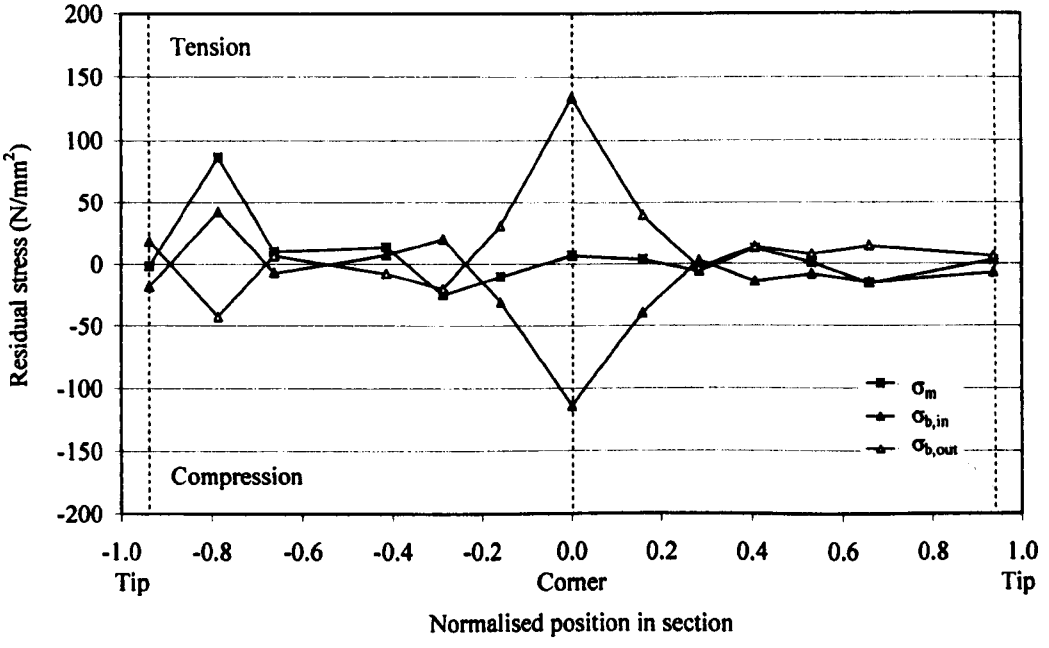

Figure 5.21: *Membrane and bending stresses distributions around PB2 50×50×3 (r_i=3.2) (Average material 0.2% proof strength from the flat regions was 333 N/mm². Material 0.2% proof strength from the corner strip was 605 N/mm²)*

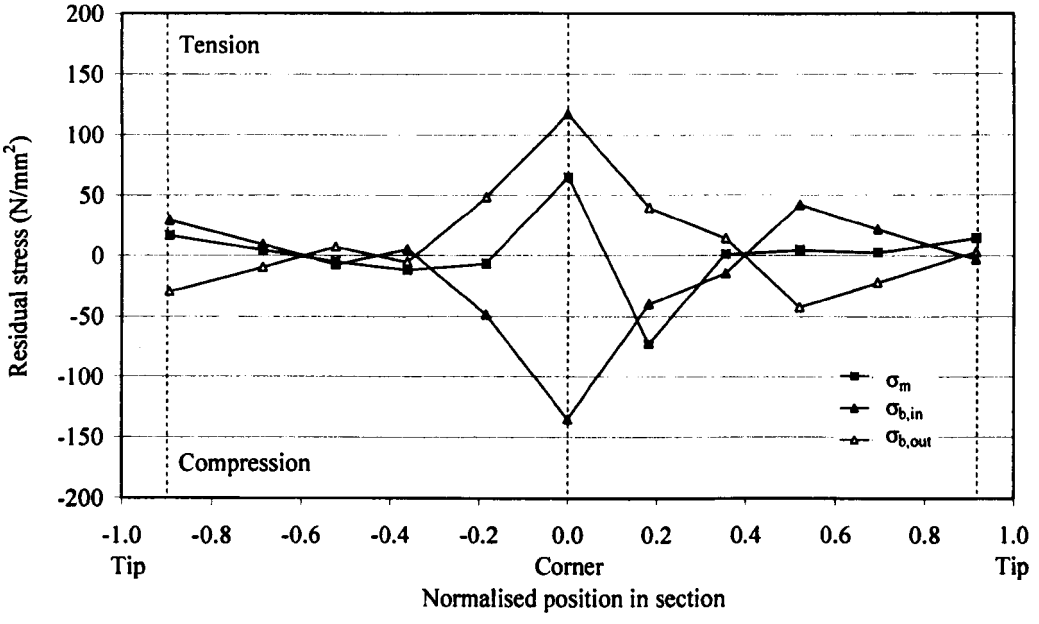

Figure 5.22: *Membrane and bending stresses distributions around PB 50×50×4 (r_i=3.5) (Average material 0.2% proof strength from the flat regions was 328 N/mm². Material 0.2% proof strength from the corner strip was 479 N/mm²)*

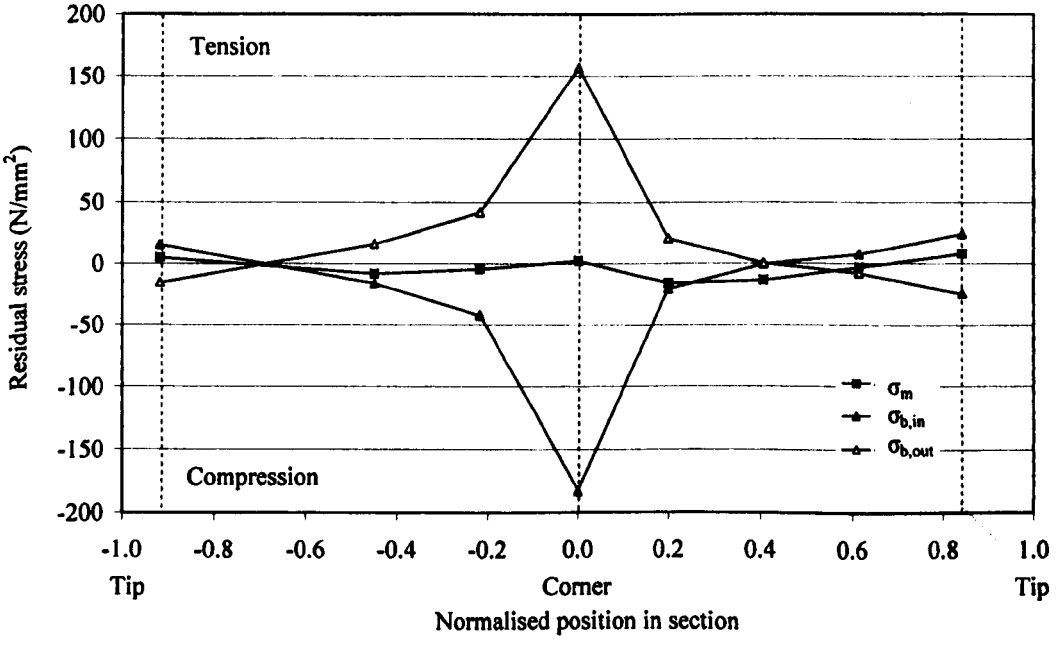

Figure 5.23: *Membrane and bending stresses distributions around PB 50×50×5 (r_i=3.5) (Average material 0.2% proof strength from the flat regions was 314 N/mm². Material 0.2% proof strength from the corner strip was 497 N/mm²)*

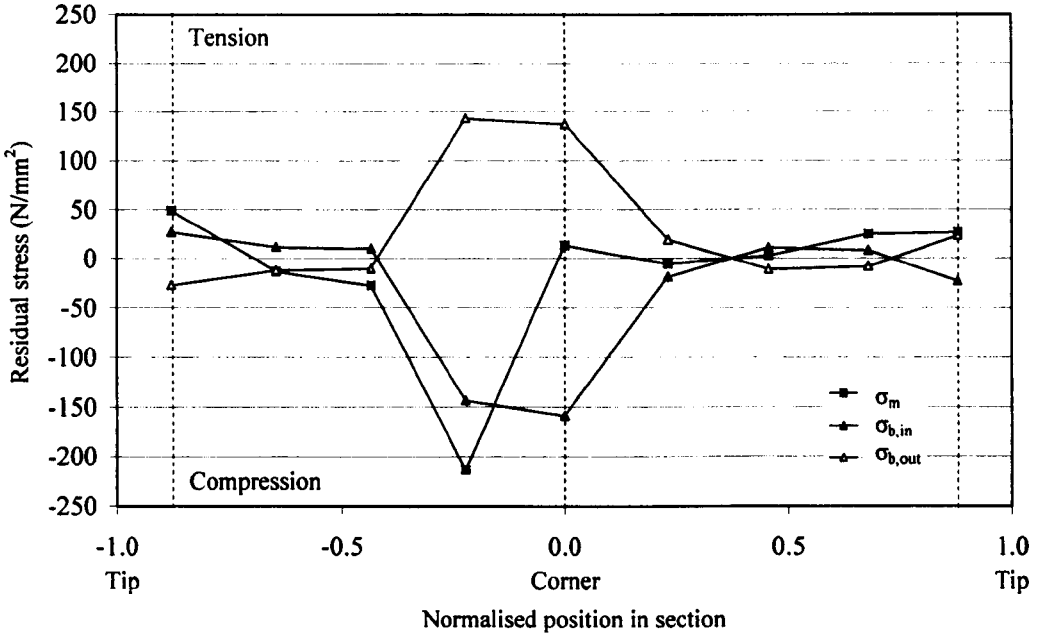

Figure 5.24: *Membrane and bending stresses distributions around PB 50×50×5 (r_i=4.5) (Average material 0.2% proof strength from the flat regions was 302 N/mm². Material 0.2% proof strength from the corner strip was 632 N/mm²)*

The membrane and bending residual stresses for the unformed flat regions of the press braked sections are generally low, typically below 10% of the material 0.2% proof strength. As explained in section 5.4.1, the bending residual stresses in the press braked sections were calculated on the basis of a rectangular stress block distribution. In the corner regions, however, where large plastic deformation occurs, higher bending residual stresses may be seen. The corner bending residual stresses typically reach about 30% of the corner material 0.2% proof strength, which itself has been enhanced beyond the strength of the flat material due to cold work during production.

5.4.3 Cold rolled sections

The residual stress maps for the seven cold rolled stainless steel box sections are shown in Figures 5.26 to 5.32. The numerical data and setting out diagram for the cold rolled section CR 100×50×4 are given in Table 5.2 and Figure 5.25 respectively. The results reveal slightly higher membrane residual stresses than those observed in the hot rolled and press braked sections, and considerably higher bending residual stresses. As for the press braked sections, the bending residual stresses in the cold rolled box sections were calculated on the assumption of a rectangular stress block distribution. The bending residual stresses typically range between

about 30% and 70% of the material 0.2% proof stress. The results are discussed further in the following section.

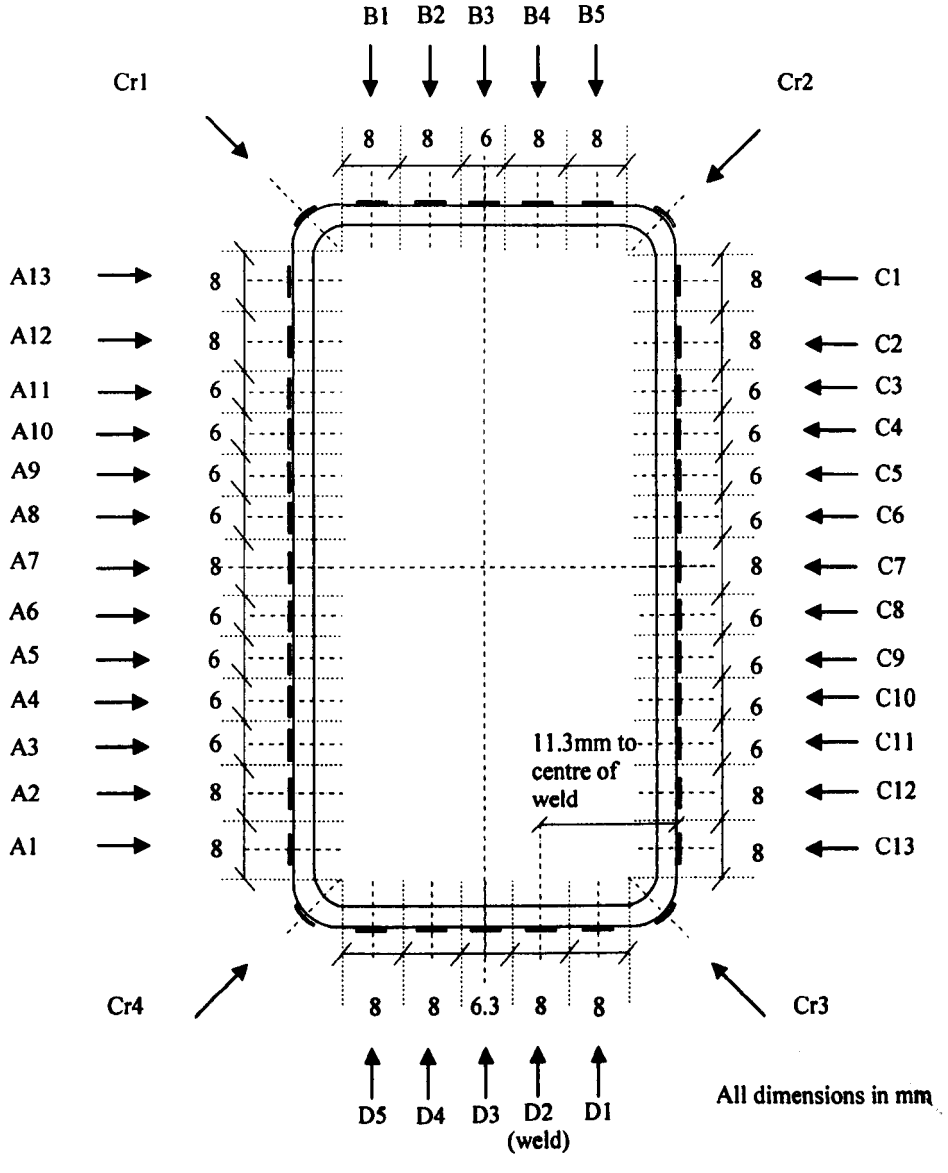

Figure 5.25: *Setting out of cold rolled section CR 100×50×4*

Table 5.2: *Residual stress distribution for CR 100×50×4*

CR 100×50×4	*Section position (mm)*	*Width (mm)*	σ_m *(N/mm²)*	σ_b *(N/mm²)*	σ_{rc} *(N/mm²)*	$\sigma_m/\sigma_{0.2}$	$\sigma_b/\sigma_{0.2}$	$\sigma_{rc}/\sigma_{0.2}$
A1	7.5	7.11	13	-561	574	0.02	-0.85	0.87
A2	15.5	6.60	96	-398	493	0.16	-0.68	0.85
A3	22.7	5.27	21	-239	259	0.04	-0.41	0.45
A4	28.8	4.63	-4	-187	191	-0.01	-0.35	0.35
A5	34.7	4.73	-34	-181	215	-0.06	-0.32	0.38
A6	40.8	4.93	-35	-218	253	-0.07	-0.42	0.49
A7	47.9	6.92	-54	-282	336	-0.10	-0.51	0.61
A8	55.0	4.89	-90	-237	327	-0.18	-0.46	0.64
A9	61.1	4.88	-103	-292	395	-0.19	-0.55	0.74
A10	67.1	4.69	-83	-225	308	-0.14	-0.39	0.54
A11	73.1	4.91	-6	-316	322	-0.01	-0.54	0.55
A12	80.0	6.66	89	-436	525	0.14	-0.70	0.84
A13	87.7	6.36	53	-466	519	0.07	-0.60	0.67
Cr1 (r_i=2.3)	0.0		106	-177	282	0.15	-0.25	0.40
B1	7.6	7.34	165	-428	593	0.24	-0.61	0.85
B2	15.8	6.64	233	-316	548	0.37	-0.50	0.87
B3	23.0	5.27	282	-250	532	0.46	-0.41	0.87
B4	30.3	6.92	281	-318	599	0.44	-0.49	0.93
B5	38.7	7.61	240	-419	658	0.36	-0.63	0.99
Cr2 (r_i =1.3)	0.0		100	-234	333	0.14	-0.33	0.48
C1	5.6	6.85	42	-526	567	0.06	-0.77	0.83
C2	13.8	7.07	84	-362	446	0.14	-0.60	0.74
C3	21.0	4.99	54	-255	309	0.09	-0.45	0.54
C4	27.1	4.76	-8	-195	203	-0.01	-0.36	0.38
C5	33.3	5.41	22	-231	253	0.04	-0.44	0.48
C6	40.1	5.80	13	-200	213	0.02	-0.38	0.40
C7	47.0	5.50	30	-285	315	0.06	-0.55	0.61
C8	53.3	4.73	30	-202	232	0.06	-0.39	0.45
C9	59.4	5.05	22	-224	246	0.04	-0.41	0.45
C10	65.8	5.38	47	-229	276	0.09	-0.42	0.51
C11	72.2	5.00	82	-293	375	0.14	-0.49	0.63
C12	78.9	5.93	399	-450	849	0.67	-0.75	1.42
C13	86.3	6.61	56	-585	641	0.08	-0.83	0.91
Cr3 (r_i =2.3)	0.0		59	-95	154	0.09	-0.15	0.24
D1	8.7	9.48	76	-414	490	0.11	-0.60	0.71
D2 (weld)	17.5	5.69	192	-290	481	0.32	-0.48	0.80
D3	24.1	5.22	410	-230	639	0.64	-0.36	0.99
D4	31.2	6.53	251	-322	574	0.43	-0.56	0.99
D5	39.4	7.46	223	-380	603	0.32	-0.54	0.85
Cr4 (r_i =2.3)	0.0		75	-159	234	0.09	-0.19	0.28

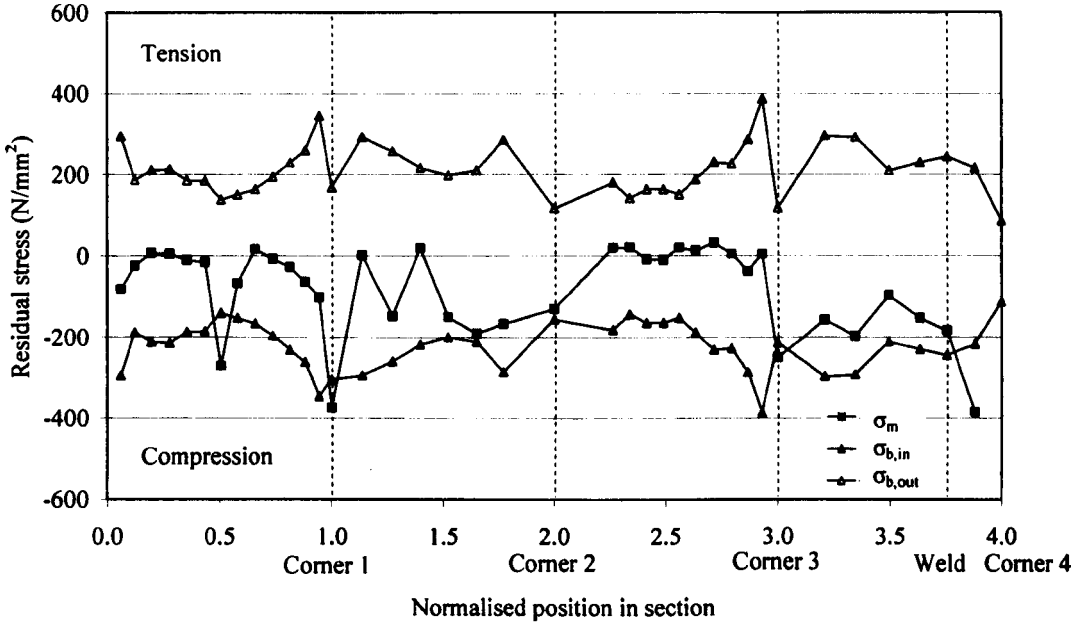

Figure 5.26: *Membrane and bending stresses distributions around CR 100×50×2 (Average material 0.2% proof strength from the flat regions was 488 N/mm². Average material 0.2% proof strength from the corner strips was 615 N/mm²)*

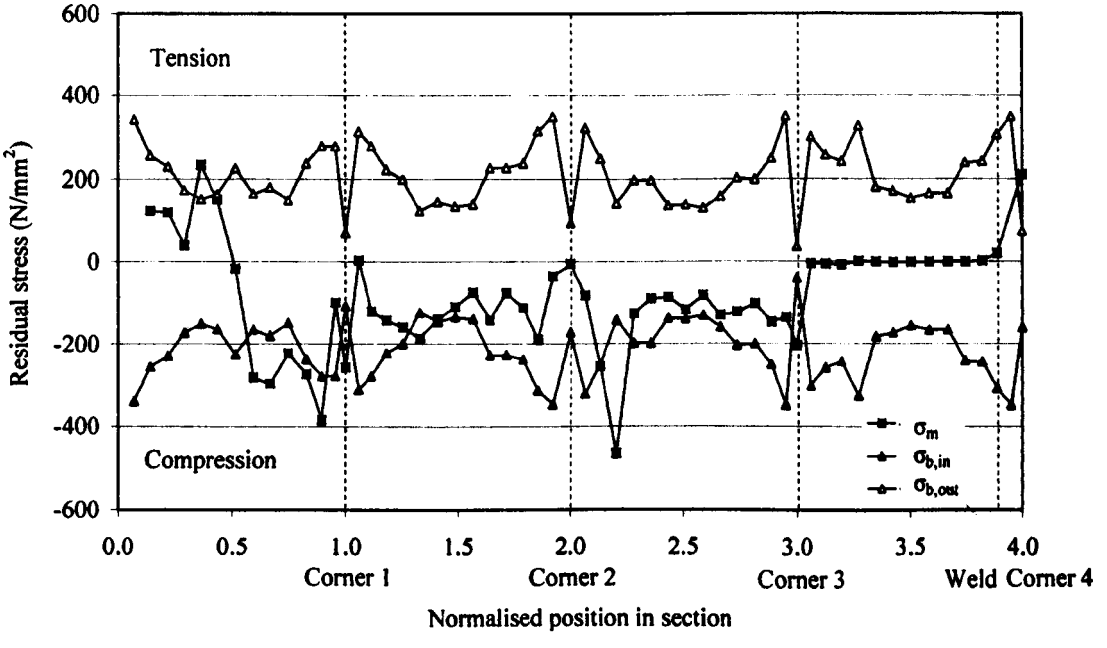

Figure 5.27: *Membrane and bending stresses distributions around CR 100×100×2 (Average material 0.2% proof strength from the flat regions was 481 N/mm². Average material 0.2% proof strength from the corner strips was 573 N/mm²)*

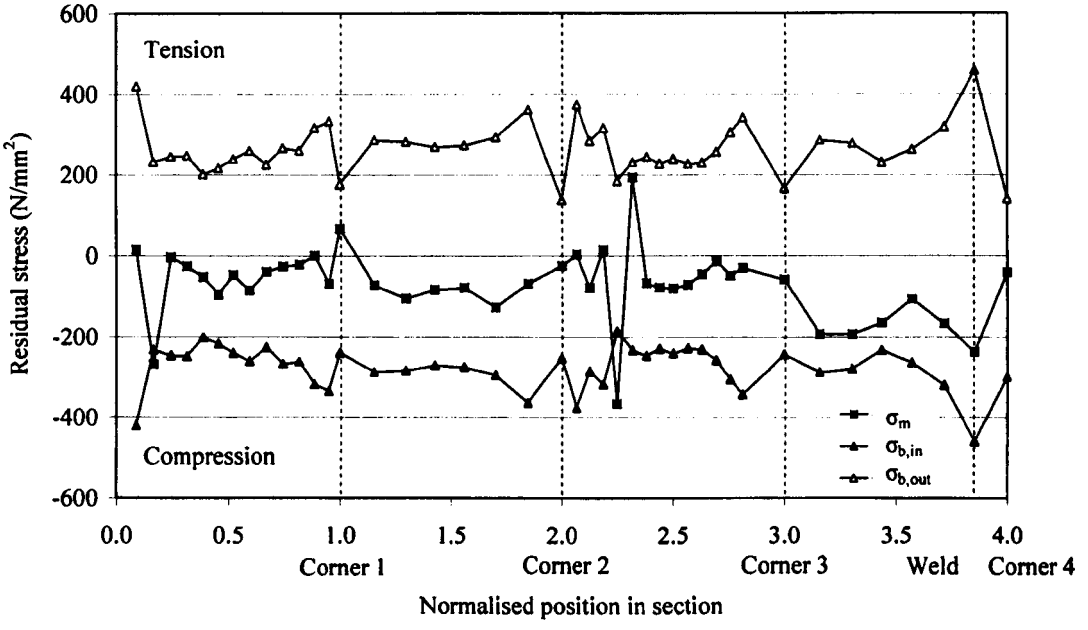

Figure 5.28: *Membrane and bending stresses distributions around CR 100×50×3 (Average material 0.2% proof strength from the flat regions was 521 N/mm². Average material 0.2% proof strength from the corner strips was 602 N/mm²)*

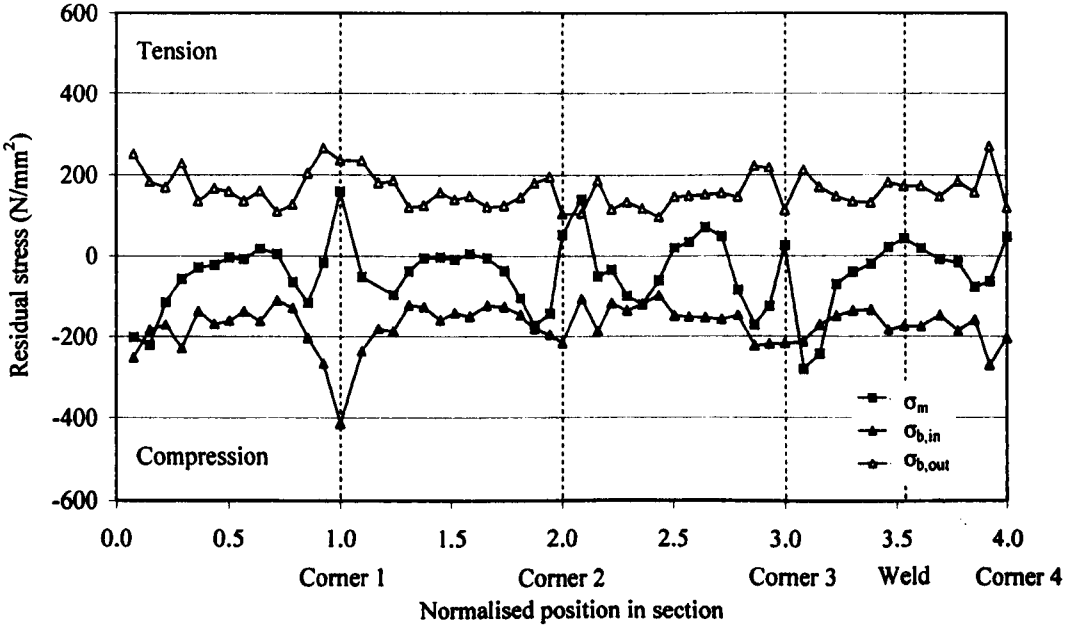

Figure 5.29: *Membrane and bending stresses distributions around CR 100×100×3 (Average material 0.2% proof strength from the flat regions was 506 N/mm². Average material 0.2% proof strength from the corner strips was 534 N/mm²)*

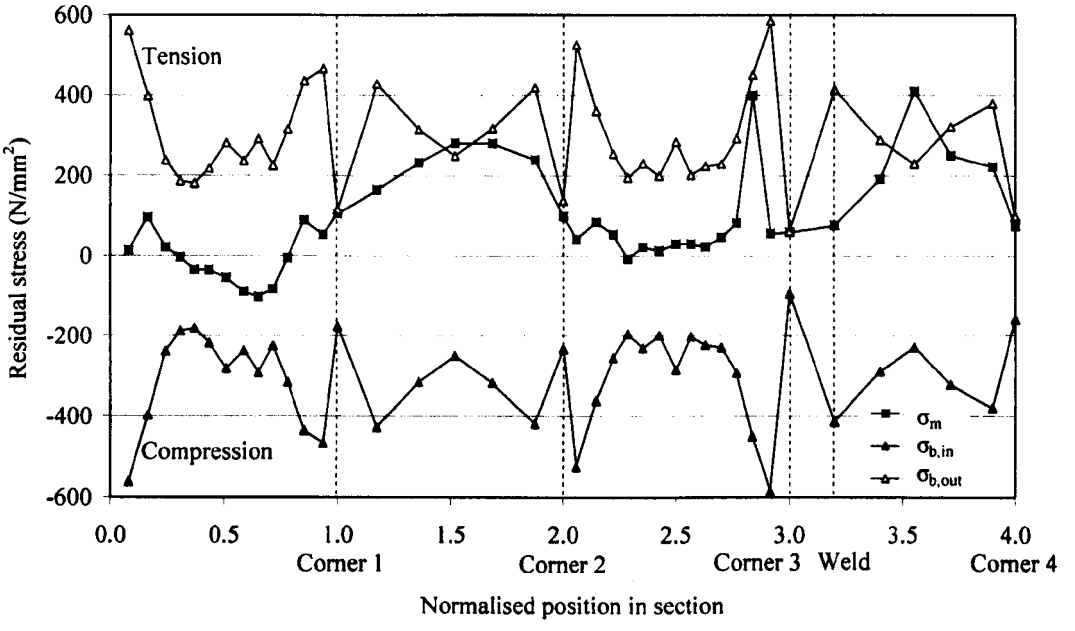

Figure 5.30: *Membrane and bending stresses distributions around CR 100×50×4 (Average material 0.2% proof strength from the flat regions was 599 N/mm². Average material 0.2% proof strength from the corner strips was 717 N/mm²)*

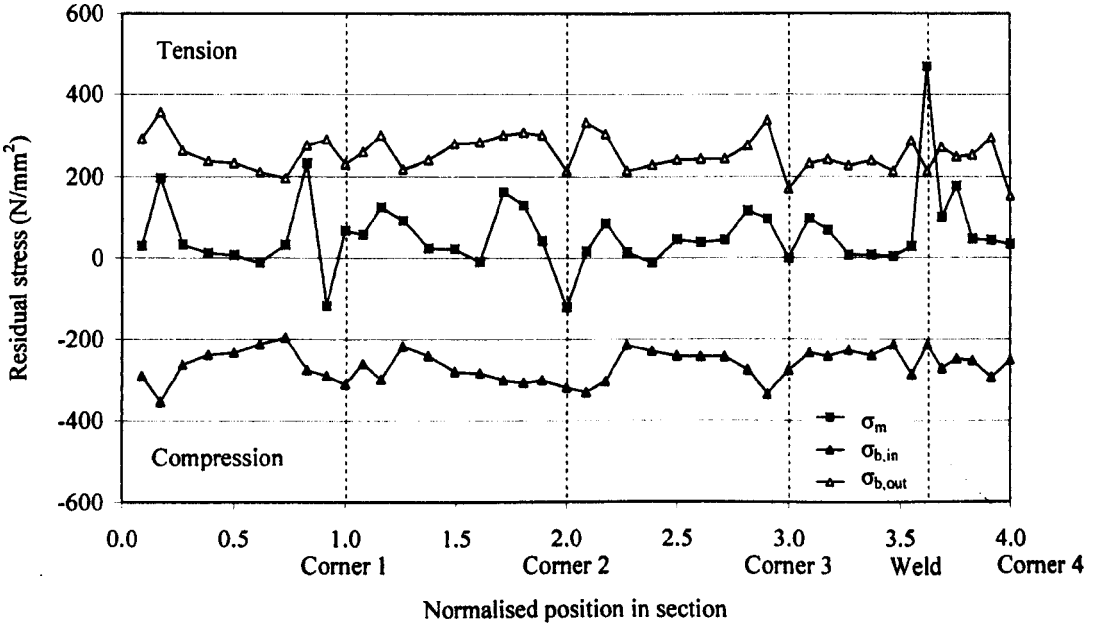

Figure 5.31: *Membrane and bending stresses distributions around CR 100×100×4 (Average material 0.2% proof strength from the flat regions was 452 N/mm². Average material 0.2% proof strength from the corner strips was 536 N/mm²)*

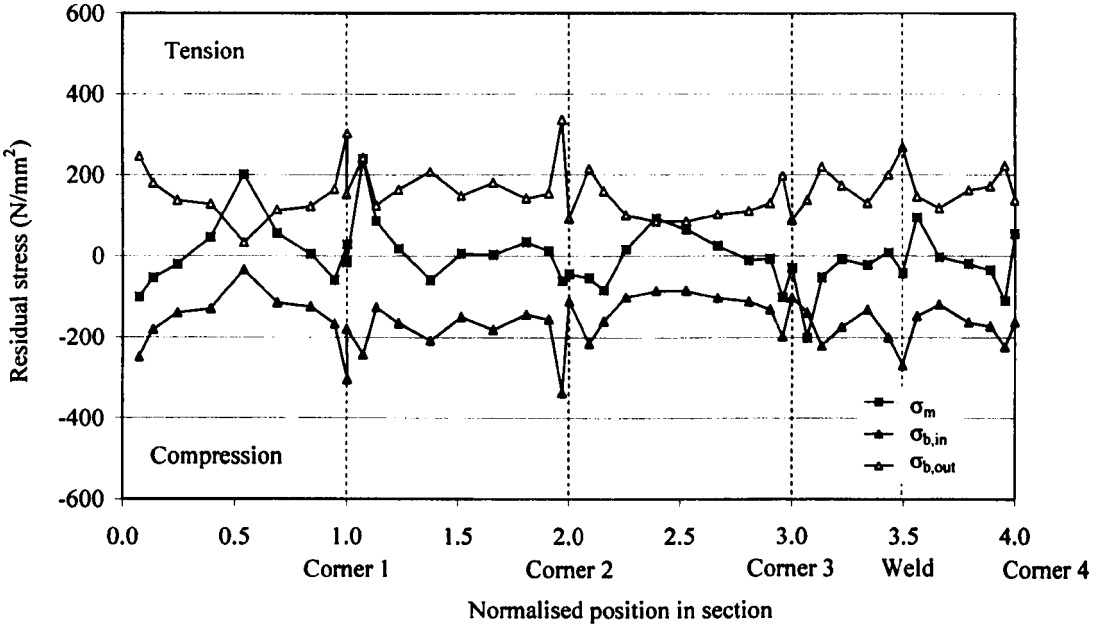

Figure 5.32: *Membrane and bending stresses distributions around CR 150×150×4 (Average material 0.2% proof strength from the flat regions was 362 N/mm². Average material 0.2% proof strength from the corner strips was 550 N/mm²)*

5.4.4 Hot rolled sections

The residual stress results for the three hot rolled angles are presented in Figures 5.34, 5.35 and 5.36. Table 5.3 presents the numerical data from sectioned strips obtained at different locations around the cross section for specimen HR 50×50×3. The location of the strips within the cross section is given in Figure 5.33.

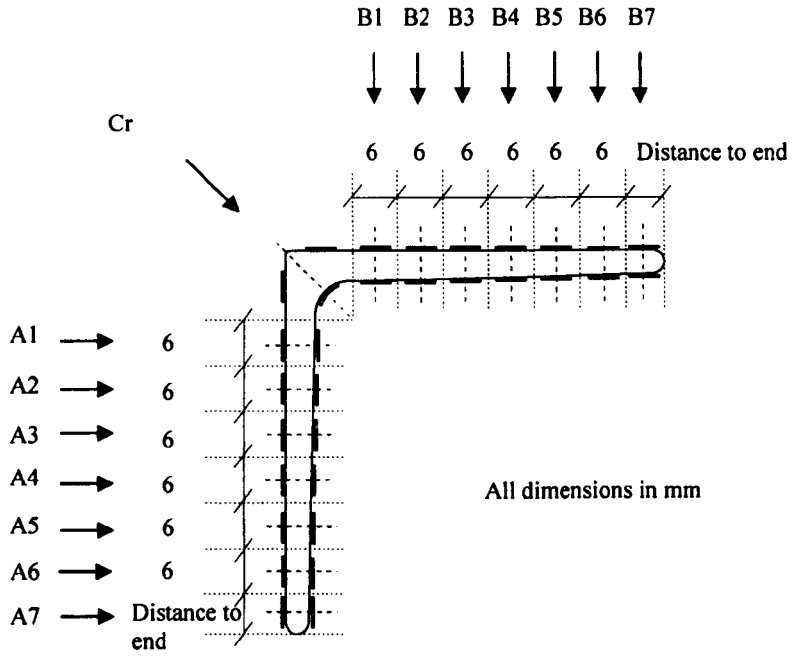

Figure 5.33: *Setting out of hot rolled section HR 50×50×3*

Table 5.3: *Residual stress values for HR 50×50×3*

HR 50×50×3	*Section position (mm)*	*Width (mm)*	σ_m *(N/mm²)*	σ_b *(N/mm²)*	σ_{rc} *(N/mm²)*	$\sigma_m/\sigma_{0.2}$	$\sigma_b/\sigma_{0.2}$	$\sigma_{rc}/\sigma_{0.2}$
A7	38.4	3.36	-32	-36	68	-0.08	-0.09	0.16
A6	33.2	3.36	-27	4	31	-0.07	0.01	0.08
A5	28.3	3.44	-21	-26	47	-0.06	-0.07	0.13
A4	23.3	3.51	-26	-42	68	-0.07	-0.12	0.19
A3	18.3	3.52	-1	-67	68	0.00	-0.20	0.20
A2	13.3	3.50	24	-18	42	0.07	-0.05	0.13
A1	8.3	3.49	-5	-50	55	-0.01	-0.14	0.15
Cr (r_i =5.0)	0.0		-31	-107	138	-0.11	-0.37	0.48
B1	8.4	3.56	-29	-60	89	-0.08	-0.17	0.25
B2	13.4	3.60	17	-22	39	0.05	-0.07	0.12
B3	18.5	3.62	7	-34	41	0.02	-0.10	0.12
B4	23.7	3.60	-19	-28	46	-0.05	-0.08	0.13
B5	28.7	3.54	92	119	211	0.27	0.34	0.61
B6	33.8	3.56	2	22	23	0.00	0.06	0.07
B7	39.2	3.58	-20	-4	24	-0.05	-0.01	0.06

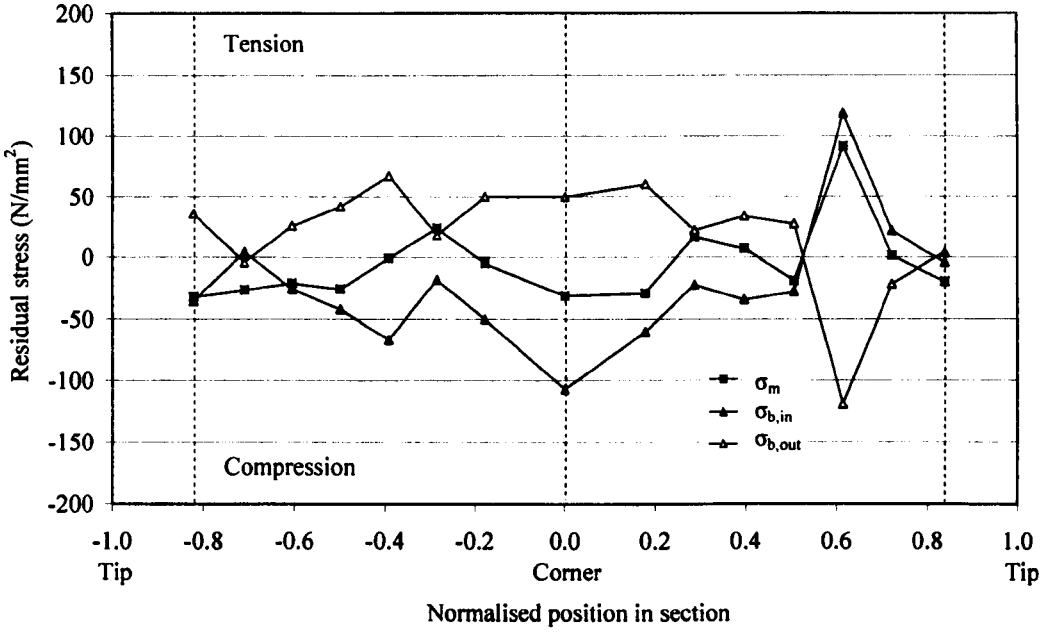

Figure 5.34: *Membrane and bending stress distributions around HR 50×50×3 (Average material 0.2% proof strength from the flat regions was 362 N/mm². Material 0.2% proof strength from the corner strip was 289 N/mm²)*

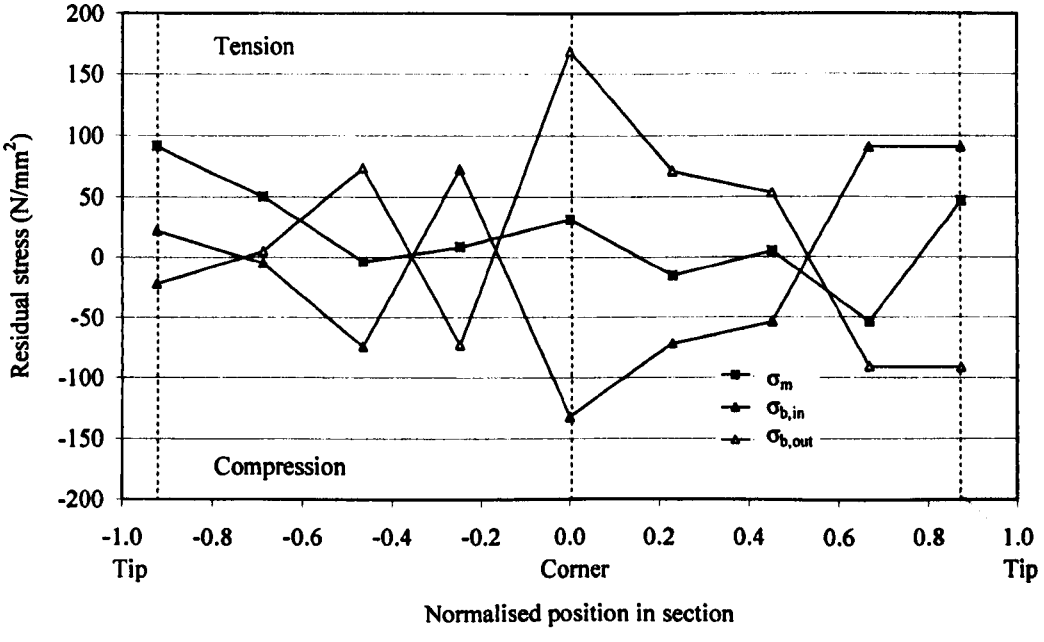

Figure 5.35: *Membrane and bending stresses distributions around HR 50×50×5 (Average material 0.2% proof strength from the flat regions was 510 N/mm². Material 0.2% proof strength from the corner strip was 528 N/mm²)*

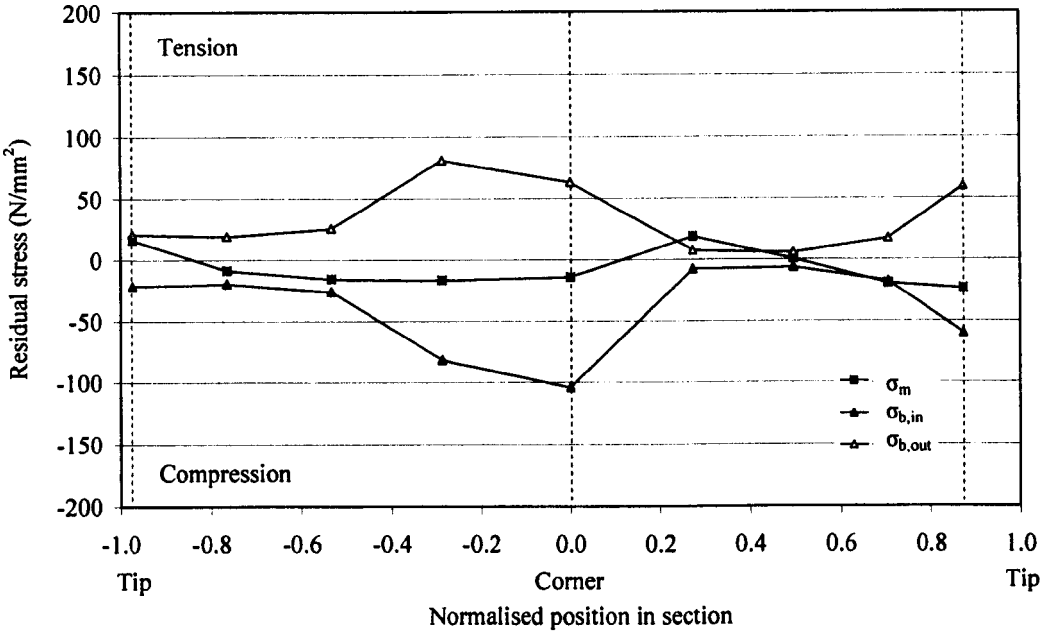

Figure 5.36: *Membrane and bending stresses distributions around HR 50×50×10 (Average material 0.2% proof strength from the flat regions was 396 N/mm². Material 0.2% proof strength from the corner strip was 353 N/mm²)*

For the hot rolled stainless steel angles, both the bending and membrane residual stresses may be seen to be relatively low. Bending residual stresses were calculated on the assumption of a linearly varying through thickness distribution. The results show that membrane residual stresses were typically below 10% of the material 0.2% proof stress, whilst bending residual stresses, were of slightly higher magnitude and typically below about 20% of the material 0.2% proof stress.

5.4.5 Discussion

The residual stresses observed in both the hot rolled and press braked stainless steel angles are generally of relatively low magnitude, typically below 20% of the material 0.2% proof strength. In the corner regions of press braked sections, where large plastic deformation occurs during production, higher bending residual stresses, typically around 30% of the enhanced corner material 0.2% proof strength, are observed.

For the cold rolled stainless steel box sections, the observed residual stresses are high, particularly the bending residual stresses. The calculated bending residual stresses for all seven box sections have been normalised by the material 0.01% proof stress (the approximate elastic

limit) and the 0.2% proof stress (the equivalent yield stress) of the corresponding strips and plotted in Figures 5.37 and 5.38, respectively. The 0.01% proof stress used was calculated from the compound Ramberg-Osgood material model (Equation 2.10) based on the data from each tensile coupon test. This ensured that fluctuations at early stages of each tensile coupon test did not affect the values given. The results show that whilst the residual stresses are generally below the material 0.2% proof stress, the 0.01% proof stress is often exceeded, implying that the residual stresses may be inelastic. If this were to be the case, calculation of the residual stresses from the measured residual strains on the assumption of elastic material behaviour would overestimate their magnitude. The residual stresses are, however, believed to be largely elastic, on the basis that the released strips exhibited the same residual strains upon deforming them back to their initial (flat) configuration and subsequently re-releasing. Two explanations for the appearance of residual stresses greater than the material 0.01% proof stress, but still remaining elastic are offered. The first relates to the strain hardening of the sheet material during the coiling and uncoiling process where the outer fibres of the sheet receive the greatest cold work. This results in material stratification through the thickness with higher strength material at the extreme fibres, from where the greatest contributions to residual curvature emanate. However, calculated residual stresses have simply been normalised by the average material strength of the strip obtained from a tensile coupon test. The detailed through thickness strength distribution has not been measured directly, but indicative results supporting the above assertions have been obtained from hardness tests. The second explanation relates to presence of transverse residual stresses, in addition to the measured longitudinal residual stresses. According to the von Mises yield criterion, if the residual stress condition is purely uniaxial, stresses are limited to the yield stress in order to remain elastic. However with a two-dimensional stress system, the plane stress condition predicts that a maximum longitudinal stress of $2/\sqrt{3}\ \sigma_y$ can be obtained in the presence of transverse stress before yielding occurs (Hill, 1983).

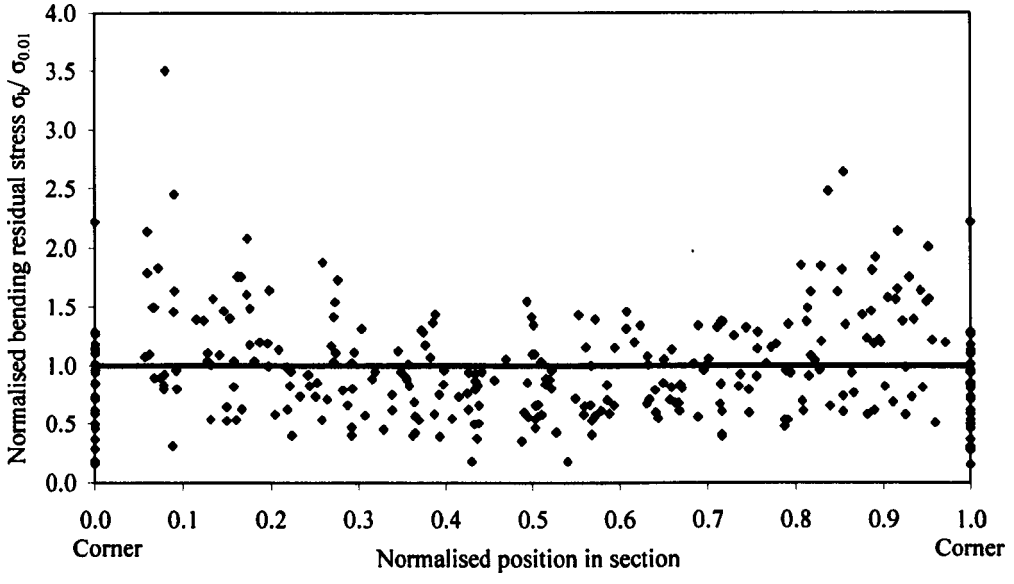

Figure 5.37: *Bending residual stresses from cold rolled box sections normalised by material 0.01% proof strength*

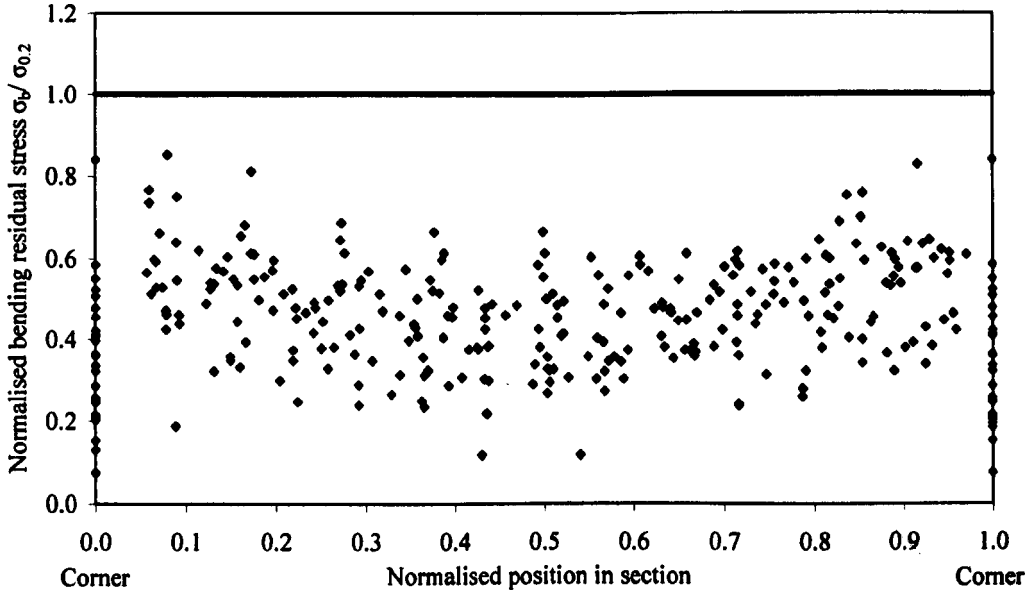

Figure 5.38: *Bending residual stresses from cold rolled box sections normalised by material 0.2% proof strength*

5.5 Proposed predictive models

5.5.1 Introduction

The experimental data from the current experimental program have been combined with existing data to propose or modify membrane and bending residual stress models for four different types of stainless steel sections - press braked, cold rolled, fabricated and hot rolled. Throughout this section, the bending σ_b and membrane σ_m residual stresses have been normalised by the material strength (taken as the 0.2% proof stress $\sigma_{0.2}$) and the position in the section face has been normalised by the distance along the section face's neutral axis, between the mid point of both corner radii.

5.5.2 Press braked sections

All available residual stress data from the current experimental program has been calculated using a rectangular stress block through thickness distribution for stainless steel press braked sections. The normalised membrane and bending residual stresses obtained are shown in Figures 5.39 and 5.41, and the magnitude of the normalised bending and membrane residual stresses are shown in Figures 5.40 and 5.42. Based on the 200 readings that were taken, the overall mean residual stress values for the flat faces and corners, together with the mean ± 1.64 standard deviations (representing the 95% characteristic values based on a normal distribution) are indicated in Figures 5.39 to 5.42. Table 5.4 summarises the numerical values of the normalised residual stresses from each individual tested press braked section, whilst Table 5.5 presents the mean and standard deviation of the magnitude of the normalised residual stresses.

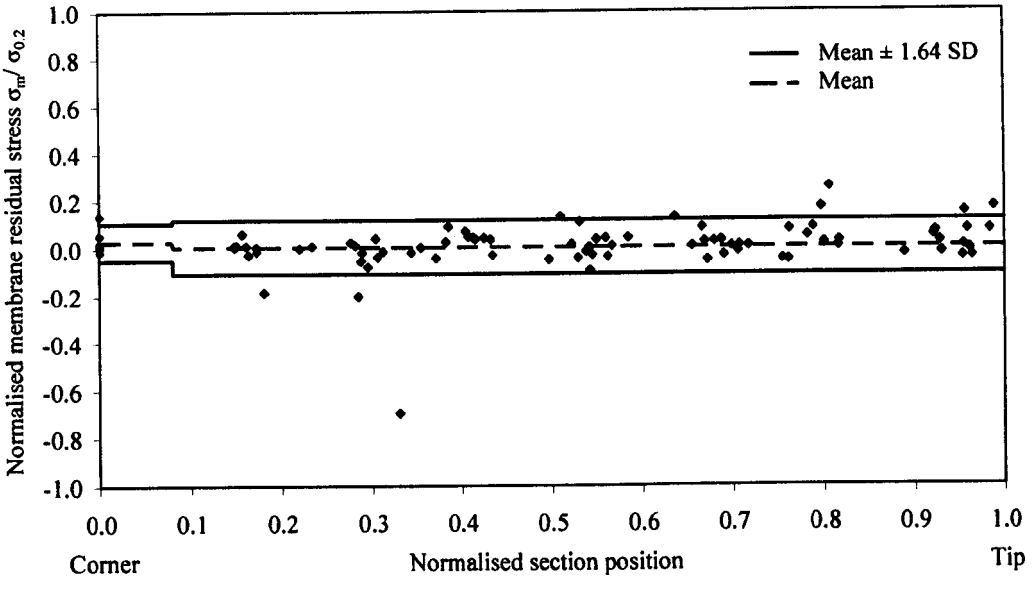

Figure 5.39: *Normalised membrane residual stress for press braked angles*

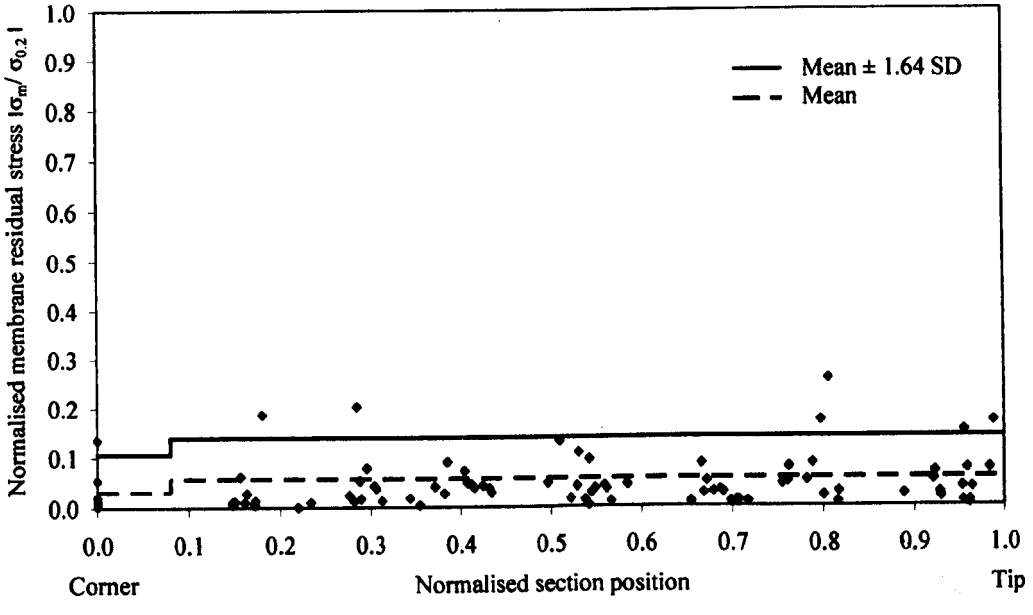

Figure 5.40: *The magnitude of the normalised membrane residual stress for press braked angles*

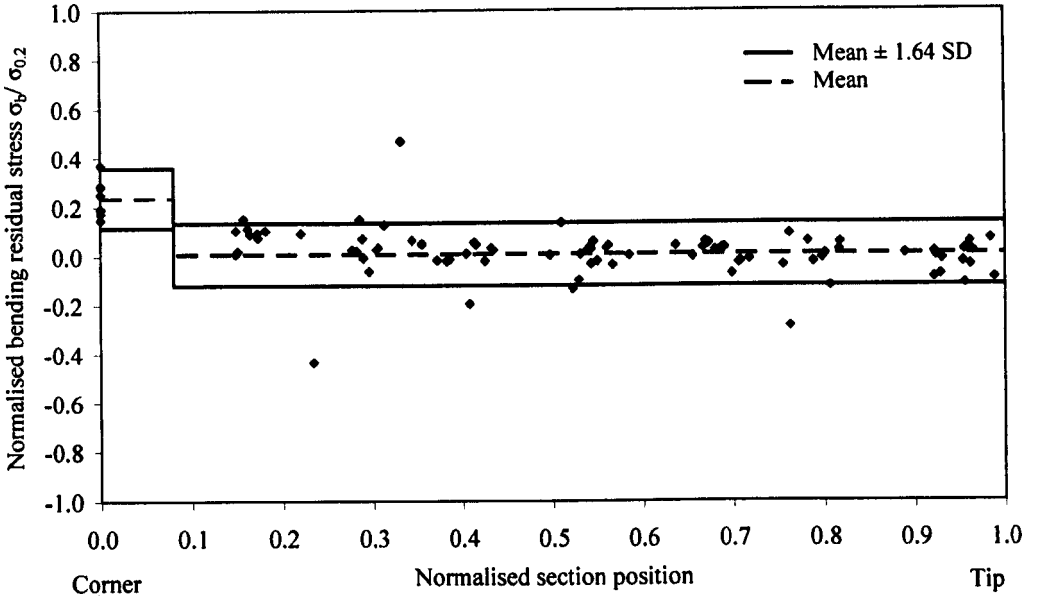

Figure 5.41: *Normalised bending residual stress for press braked angles (assuming a rectangular block variation through thickness)*

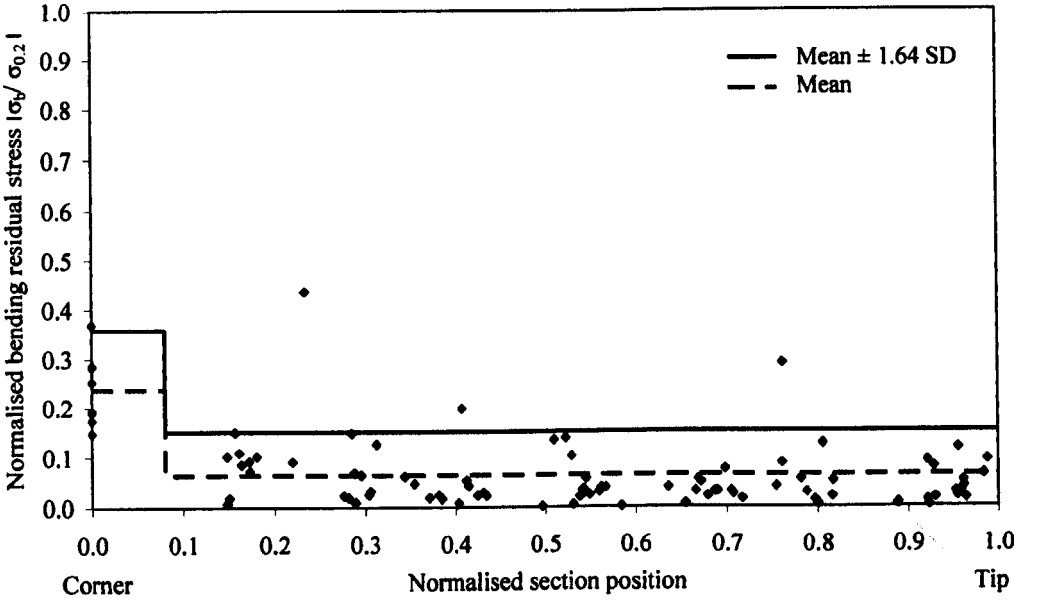

Figure 5.42: *The magnitude of the normalised bending residual stress for press braked angles (assuming a rectangular block variation through thickness)*

Table 5.4: *Weighted mean normalised membrane and bending residual stresses for press braked angles*

Specimen identification	*Flat faces*				*Corner regions*			
	$\sigma_m/\sigma_{0.2}$		$\sigma_b/\sigma_{0.2}$		$\sigma_m/\sigma_{0.2}$		$\sigma_b/\sigma_{0.2}$	
	Mean	*SD*	*Mean*	*SD*	*Mean*	*SD*	*Mean*	*SD*
PB2 50×50×2 (r_i=3.2)	0.08	0.07	0.01	0.10	-	-	-	-
PB 50×50×2 (r_i=3.5)	0.01	0.03	0.01	0.04	-	-	-	-
PB 50×50×2 (r_i=4.5)	0.01	0.03	0.04	0.02	-	-	-	-
PB 50×50×2 (r_i=7.5)	0.01	0.03	-0.05	0.14	-	-	-	-
PB2 50×50×3 (r_i=3.2)	0.02	0.06	0.02	0.05	-	-	-	-
PB 50×50×4 (r_i=3.5)	-0.01	0.06	-0.02	0.06	-	-	-	-
PB 50×50×5 (r_i=3.5)	-0.01	0.02	0.01	0.06	-	-	-	-
PB 50×50×5 (r_i=4.5)	-0.06	0.23	0.04	0.16	-	-	-	-
Mean	0.02	0.07	0.01	0.08	0.03	0.05	0.24	0.07

Table 5.5: *Weighted mean of the magnitude of normalised membrane and bending residual stresses for press braked angles*

Specimen identification	*Flat faces*				*Corner regions*			
	$\lvert\sigma_m/\sigma_{0.2}\rvert$		$\lvert\sigma_b/\sigma_{0.2}\rvert$		$\lvert\sigma_m/\sigma_{0.2}\rvert$		$\lvert\sigma_b/\sigma_{0.2}\rvert$	
	Mean	*SD*	*Mean*	*SD*	*Mean*	*SD*	*Mean*	*SD*
PB2 50×50×2 (r_i=3.2)	0.11	0.04	0.08	0.03	-	-	-	-
PB 50×50×2 (r_i=3.5)	0.02	0.02	0.03	0.02	-	-	-	-
PB 50×50×2 (r_i=4.5)	0.03	0.02	0.04	0.02	-	-	-	-
PB 50×50×2 (r_i=7.5)	0.03	0.01	0.09	0.12	-	-	-	-
PB2 50×50×3 (r_i=3.2)	0.04	0.05	0.05	0.03	-	-	-	-
PB 50×50×4 (r_i=3.5)	0.05	0.05	0.06	0.04	-	-	-	-
PB 50×50×5 (r_i=3.5)	0.03	0.01	0.06	0.03	-	-	-	-
PB 50×50×5 (r_i=4.5)	0.15	0.20	0.10	0.13	-	-	-	-
Mean	0.06	0.05	0.06	0.05	0.03	0.05	0.24	0.07

Both membrane and bending residual stresses may be seen to be low compared to the material 0.2% proof strength. The results of Table 5.4 also show that the sum of the mean normalised membrane residual stresses of the flat and corner regions is approximately zero, indicating that the requirement for longitudinal equilibrium is met, though no clear pattern of tensile and compressive regions emerges from Figure 5.39. The mean magnitude of the membrane residual stresses for the corners given in Table 5.5 is similar to that given by Schafer and Peköz (1998) in carbon steel press braked sections ($0.07\sigma_{0.2}$). The sum of the mean normalised bending residual stresses in the flat regions is also close to zero, though this is not a requirement for equilibrium, since equilibrium is achieved by variation through the material thickness. A consistent increase in the bending residual stresses can be seen in the corner regions of the angle sections where high localised plastic deformation is known to occur during the forming process. Figure 5.43 shows how the magnitude of the bending residual stresses in the press braked sections varies with the material 0.2% proof strength. The graph generally shows higher bending residual stresses with increasing material strength, indicating that their presence is linked with plastic deformation and cold work.

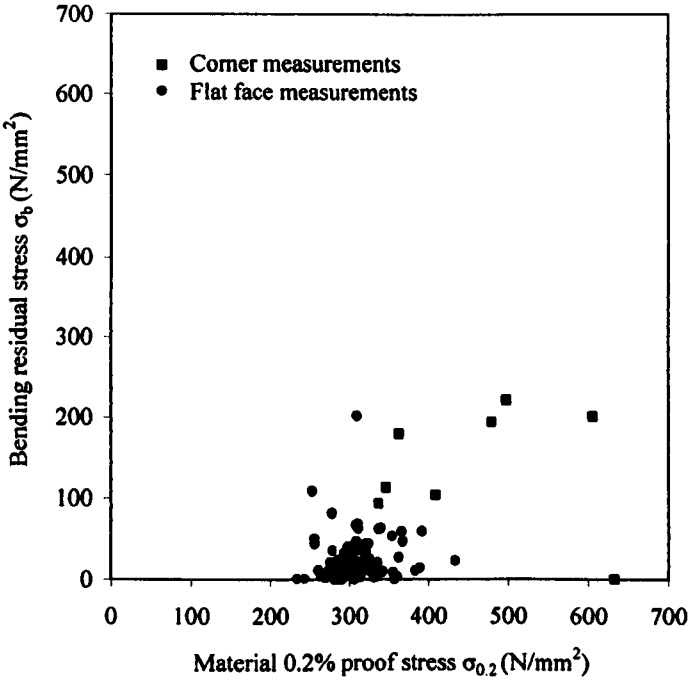

Figure 5.43: *Magnitude of bending residual stresses against material strength for press braked angles*

Based on characteristic values of residual stress magnitudes (Mean + 1.64 standard deviations) observed in press braked stainless steel angles, the following proposals are made: Membrane residual stress magnitudes may be taken as $0.14\sigma_{0.2}$ in the flat regions and $0.11\sigma_{0.2}$ in the corner regions (but no distribution is recommended), and bending residual stresses may be taken $0.15\sigma_{0.2}$ in the flat regions and $0.36\sigma_{0.2}$ in the corner regions, based on a rectangular stress block distribution (Fig. 5.44). The recommendations for bending residual stresses in the corner regions are similar in magnitude to those made by Schafer and Peköz (1998) for press braked carbon steel lipped channels.

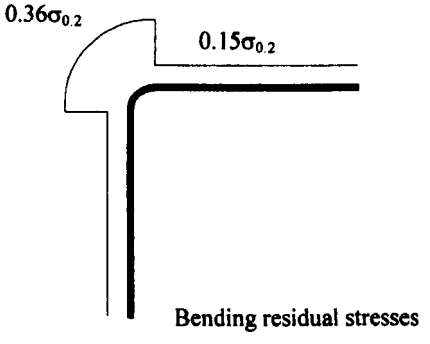

Figure 5.44: *Proposed bending residual stresses model for press braked sections (assuming a rectangular block through thickness distribution)*

5.5.3 Cold rolled sections

All available experimental residual stress data from cold rolled stainless steel box sections (the Centre for Advanced Structural Engineering, 1990; Clarin, 2003; Young and Liu, 2005 and the current experimental program) have been collated, and are shown in Figures 5.45 to 5.48 and Tables 5.6 and 5.7. The mean magnitudes of normalised membrane residual stresses are presented in Table 5.7 for the corner and flat regions. Corner residual stress values are similar to those presented herein for press braked sections, whereas the residual stresses for the flat regions are significantly higher.

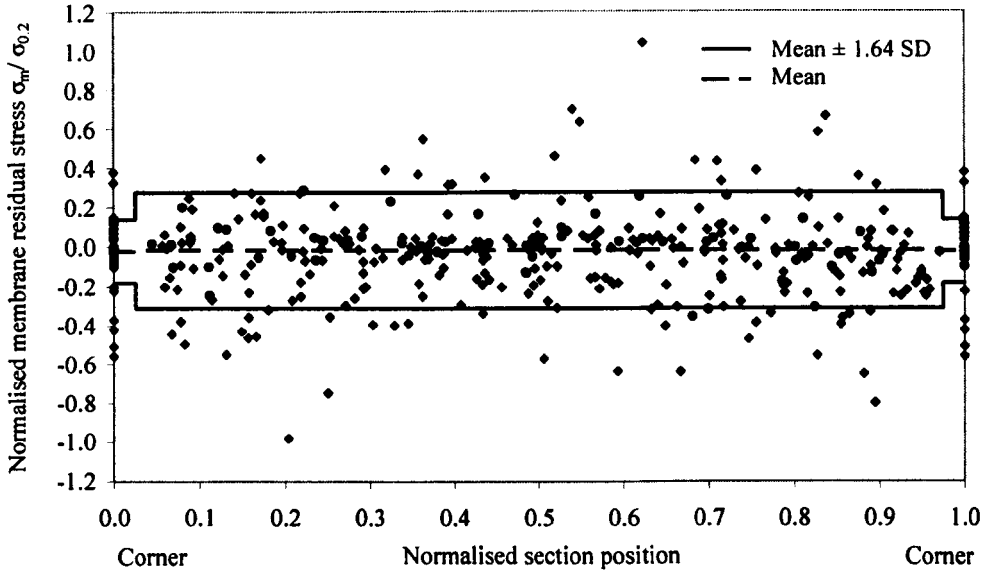

Figure 5.45: *Normalised membrane residual stress for cold rolled boxes*

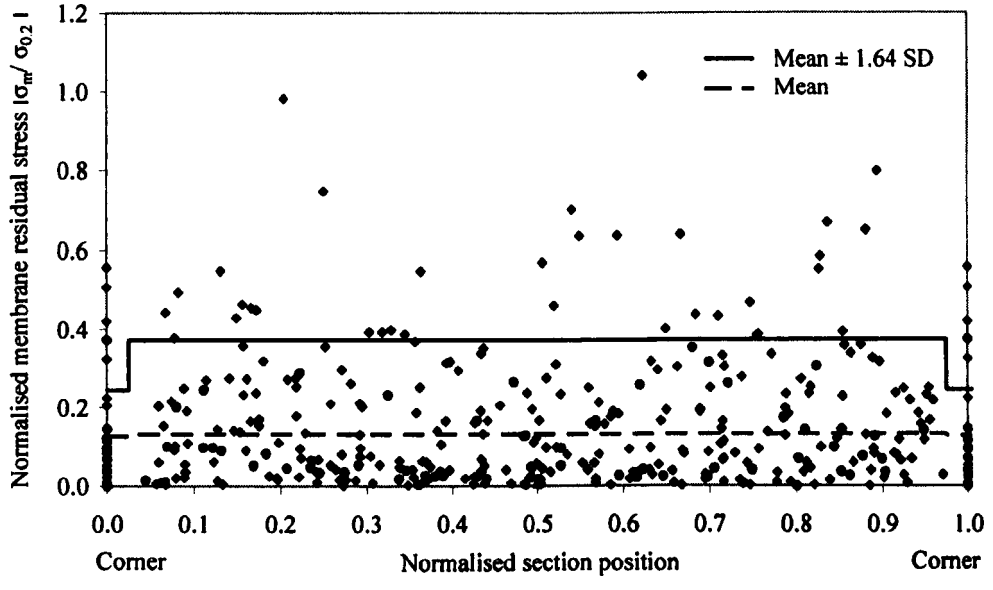

Figure 5.46: *The magnitude of the normalised membrane residual stress for cold rolled boxes*

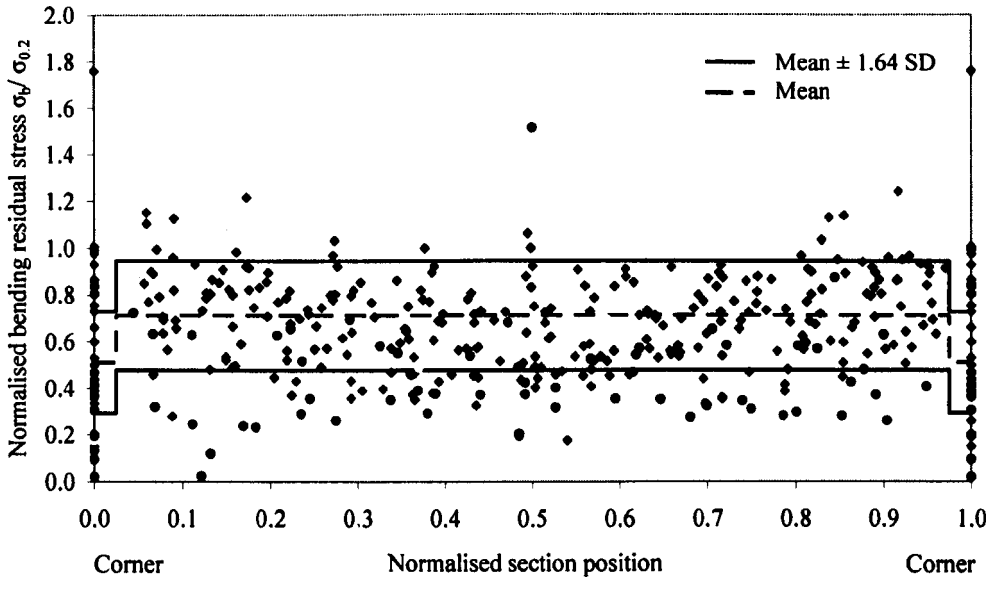

Figure 5.47: *Normalised bending residual stress for cold rolled boxes (assuming a rectangular block variation through thickness)*

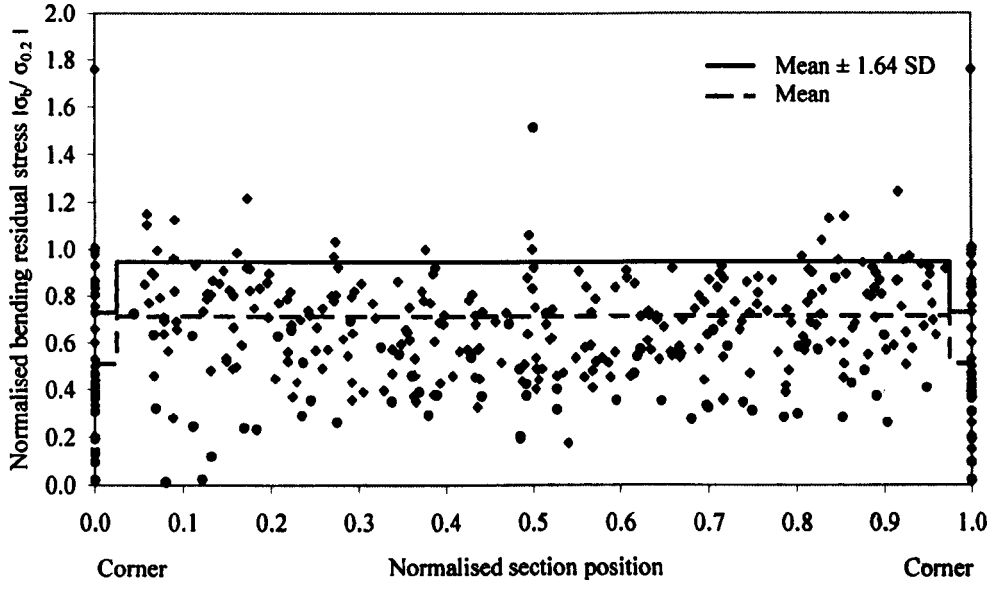

Figure 5.48: *The magnitude of the normalised bending residual stress for cold rolled boxes (assuming a rectangular block variation through thickness)*

The normalised bending residual stresses in the cold rolled box sections show a consistent tendency of tension on the outside and compression on the inside of the section. The mean of the normalised bending residual stresses is very high in the flat regions of the section and generally lower in the corner regions (though the material strength in the corner region is higher). A similar pattern was observed by Schafer and Peköz (1998) where the bending residual stresses in the webs of cold rolled carbon steel channels were greater than those in the corners, though Abdel-Rahman and Sivakumaran (1997) reported the reverse. The magnitudes of bending residual stresses in the corner regions are slightly higher than those predicted for carbon steel sections by Schafer and Peköz (1998) and Abdel-Rahman and Sivakumaran (1997).

Figure 5.49 shows how the magnitude of the bending residual stresses in the cold rolled sections varies with the material 0.2% proof strength. The graph shows a strong trend, more so than for the press braked sections (Figure 5.43), that bending residual stresses are linked to increasing material strength associated with greater plastic deformation. This finding was predicted analytically by Ingvarsson (1975) for carbon steel sections.

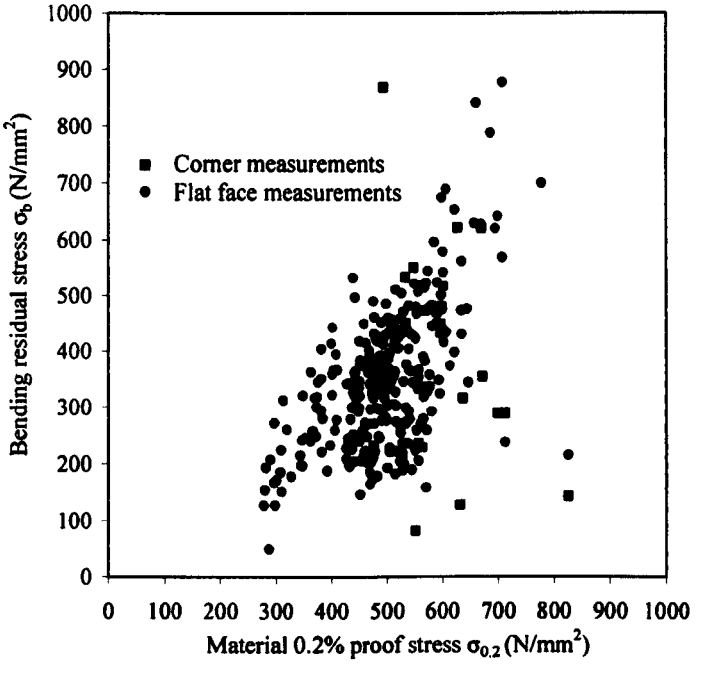

Figure 5.49: *Magnitude of bending residual stresses plotted against material strength for cold rolled boxes*

Table 5.6: *Weighted mean normalised membrane and bending residual stresses for cold rolled boxes*

Specimen identification	*Flats faces*				*Corner regions*			
	$\sigma_m/\sigma_{0.2}$		$\sigma_b/\sigma_{0.2}$		$\sigma_m/\sigma_{0.2}$		$\sigma_b/\sigma_{0.2}$	
	Mean	*SD*	*Mean*	*SD*	*Mean*	*SD*	*Mean*	*SD*
CR 120×80×3[a]	0.11	0.17	0.40	0.06	0.01	0.10	0.20	0.02
CR 200×110×4[b]	-0.05	0.12	0.24	0.10	0.05	0.10	0.09	0.07
CR 200×110×4[b]	0.00	0.11	0.19	0.06	0.02	0.03	0.05	0.06
CR 80×80×3[c]	0.01	-	1.01	-	0.01	-	0.06	-
CR 100×50×2[d]	-0.13	0.19	0.52	0.13	-0.41	0.11	0.32	0.09
CR 100×100×2[d]	-0.18	0.28	0.45	0.11	-0.09	0.32	0.22	0.07
CR 100×50×3[d]	-0.15	0.19	0.53	0.07	-0.03	0.06	0.43	0.03
CR 100×100×3[d]	-0.10	0.15	0.33	0.08	0.15	0.10	0.51	0.18
CR 100×50×4[d]	0.15	0.20	0.54	0.14	0.12	0.02	0.21	0.07
CR 100×100×4[d]	0.13	0.17	0.58	0.07	-0.01	0.11	0.54	0.03
CR 150×150×4[d]	0.04	0.22	0.43	0.14	-0.06	0.02	0.24	0.04
Mean	-0.01	0.18	0.47	0.09	-0.02	0.10	0.26	0.07

[a] Clarin (2003); [b] Young and Liu (2005); [c] The Centre for Advanced Structural Engineering (1990); [d] Cruise and Gardner (submitted)

Table 5.7: *Weighted mean of the magnitude of normalised membrane and bending residual stresses for cold rolled boxes*

Specimen identification	*Flat faces*				*Corner regions*			
	$\lvert\sigma_m/\sigma_{0.2}\rvert$		$\lvert\sigma_b/\sigma_{0.2}\rvert$		$\lvert\sigma_m/\sigma_{0.2}\rvert$		$\lvert\sigma_b/\sigma_{0.2}\rvert$	
	Mean	*SD*	*Mean*	*SD*	*Mean*	*SD*	*Mean*	*SD*
CR 120×80×3[a]	0.15	0.11	0.40	0.06	0.08	0.04	0.20	0.02
CR 200×110×4[b]	0.08	0.09	0.24	0.10	0.07	0.07	0.09	0.07
CR 200×110×4[b]	0.07	0.08	0.19	0.06	0.02	0.03	0.05	0.06
CR 80×80×3[c]	0.01	-	1.01	-	0.01	-	0.06	-
CR 100×50×2[d]	0.16	0.18	0.52	0.13	0.41	0.11	0.32	0.09
CR 100×100×2[d]	0.22	0.22	0.45	0.11	0.28	0.21	0.22	0.07
CR 100×50×3[d]	0.18	0.16	0.53	0.07	0.08	0.02	0.43	0.03
CR 100×100×3[d]	0.13	0.12	0.33	0.08	0.15	0.10	0.51	0.18
CR 100×50×4[d]	0.18	0.17	0.54	0.14	0.12	0.02	0.21	0.07
CR 100×100×4[d]	0.14	0.15	0.58	0.07	0.10	0.07	0.54	0.03
CR 150×150×4[d]	0.14	0.17	0.43	0.14	0.06	0.02	0.24	0.04
Mean	0.13	0.15	0.47	0.09	0.12	0.07	0.26	0.07

[a] Clarin (2003); [b] Young and Liu (2005); [c] The Centre for Advanced Structural Engineering (1990); [d] Cruise and Gardner (submitted)

A simple model for bending residual stresses assuming a rectangular stress block distribution is given in Figure 5.50 and is based on characteristic values of residual stress magnitudes (Mean + 1.64 standard deviations). The magnitude of membrane residual stresses can be taken as $0.37\sigma_{0.2}$ in the flat region and $0.24\sigma_{0.2}$ in the corner regions but no distribution is proposed.

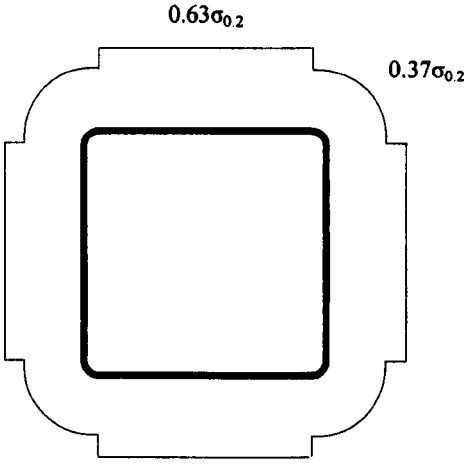

Figure 5.50: *Proposed bending residual stress model for cold rolled boxes (assuming a rectangular block variation through thickness)*

5.5.4 Fabricated sections

Residual stress data for fabricated stainless steel I sections have been reported by Lagerqvist and Olsson (2001) and Bredenkamp et al. (1992). In the case of Bredenkamp et al. (1992) numerical data has been extracted from published graphs for four ferritic (grade 1.4512) I sections: F 140×70×4.5×3.5, F 300×160×10×6, F 250×140×8×6 and F 180×90×6×4.5. Lagerqvist and Olsson (2001) analysed two I sections - F 120×300×12×4.01 (austenitic grade 1.4301) and F 50×50×13×3.99 (austenitic-ferritic grade 1.4462). The residual stress data are shown in Tables 5.8 and 5.9.

Table 5.8: *Weighted mean normalised membrane and bending residual stresses for fabricated I sections*

Specimen identification	*Flat faces*			
	$\sigma_m/\sigma_{0.2}$		$\sigma_b/\sigma_{0.2}$	
	Mean	*SD*	*Mean*	*SD*
F 120×300×12×4.01[a]	-0.09	0.34	0.01	0.16
F 50×50×13×3.99[b]	0.00	0.25	-0.03	0.14
F 140×70×4.5×3.5[c]	-0.01	0.15	-	-
F 300×160×10×6[c]	-0.06	0.23	-	-
F 250×140×8×6[c]	-0.05	0.19	-	-
F 180×90×6×4.5[c]	-0.04	0.22	-	-
Mean	-0.04	0.23	-0.01	0.15

[a] Austenitic (1.4301): Lagerqvist and Olsson (2001)
[b] Austenitic-ferritic (1.4462): Lagerqvist and Olsson (2001)
[c] Ferritic (1.4512): Bredenkamp et al. (1992)

Table 5.9: *Weighted mean of the magnitude of normalised membrane and bending residual stresses for fabricated I sections*

Specimen identification	*Flat faces*			
	$\lvert\sigma_m/\sigma_{0.2}\rvert$		$\lvert\sigma_b/\sigma_{0.2}\rvert$	
	Mean	*SD*	*Mean*	*SD*
F 120×300×12×4.01[a]	0.30	0.24	0.08	0.13
F 50×50×13×3.99[b]	0.19	0.14	0.10	0.10
F 140×70×4.5×3.5[c]	0.11	0.10	-	-
F 300×160×10×6[c]	0.18	0.16	-	-
F 250×140×8×6[c]	0.17	0.11	-	-
F 180×90×6×4.5[c]	0.18	0.13	-	-
Mean	0.19	0.15	0.09	0.12

[a] Austenitic (1.4301): Lagerqvist and Olsson (2001)
[b] Austenitic-ferritic (1.4462) : Lagerqvist and Olsson (2001)
[c] Ferritic (1.4512): Bredenkamp et al. (1992)

The membrane residual stresses shown in Figures 5.51, 5.52, 5.55 and 5.56 exhibit the anticipated pattern of tensile residual stresses in the weld region, and equilibrating compressive residual stresses, of lower magnitude, in the other parts of the section. Bending residual stresses (calculated assuming a linear through thickness distribution) may also be observed in Figures 5.53 and 5.54. The distributions suggest that the asymmetry at the web-to-flange joint (the weld being on one side of the flange only) has created a tensile residual stress on the internal face of

the flange and an opposing compressive stress on inner face for the surrounding material. This phenomenon has been observed and discussed in detail by Weisman (1976).

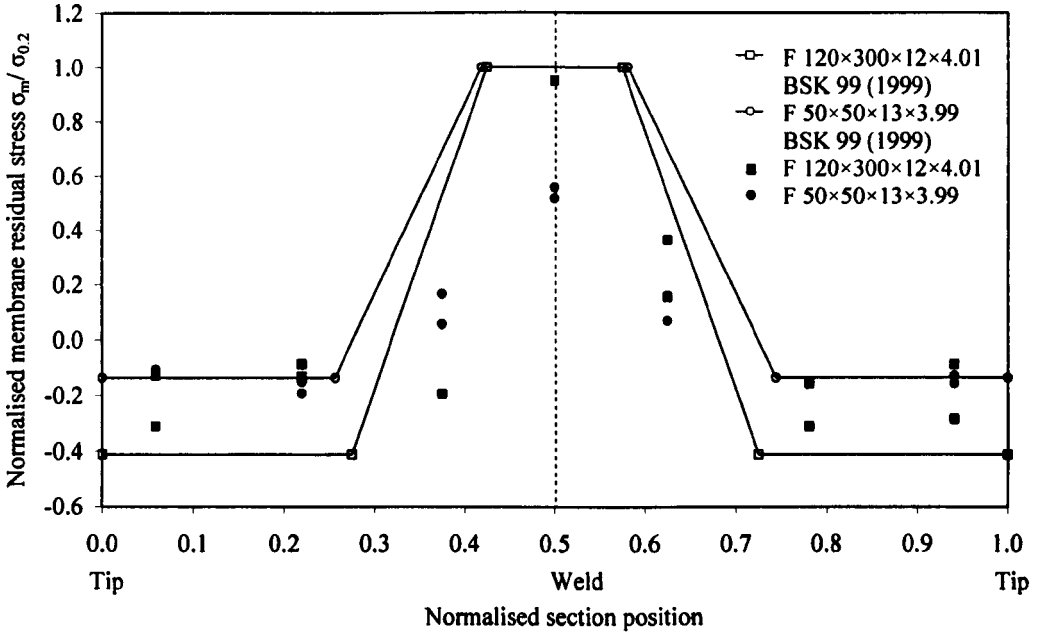

Figure 5.51: *Normalised membrane residual stress for the flanges of austenitic and austenitic-ferritic fabricated sections tested by Lagerqvist and Olsson (2001)*

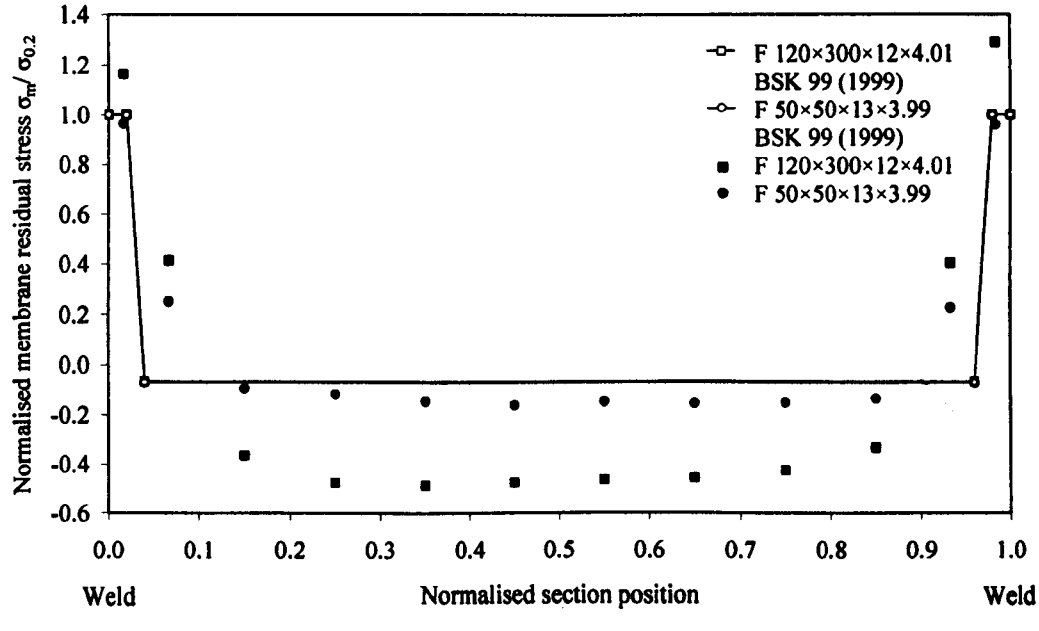

Figure 5.52: *Normalised membrane residual stress for the webs of austenitic and austenitic-ferritic fabricated sections tested by Lagerqvist and Olsson (2001)*

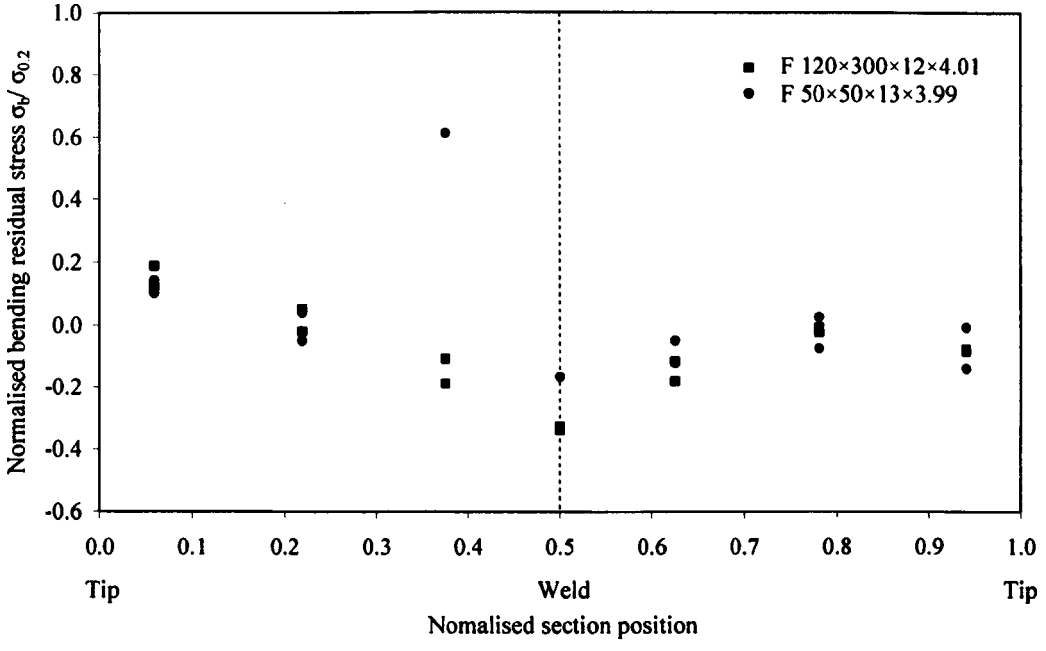

Figure 5.53: *Normalised bending residual stress for the flanges of austenitic and austenitic-ferritic fabricated sections tested by Lagerqvist and Olsson (2001) (assuming linear variation through thickness)*

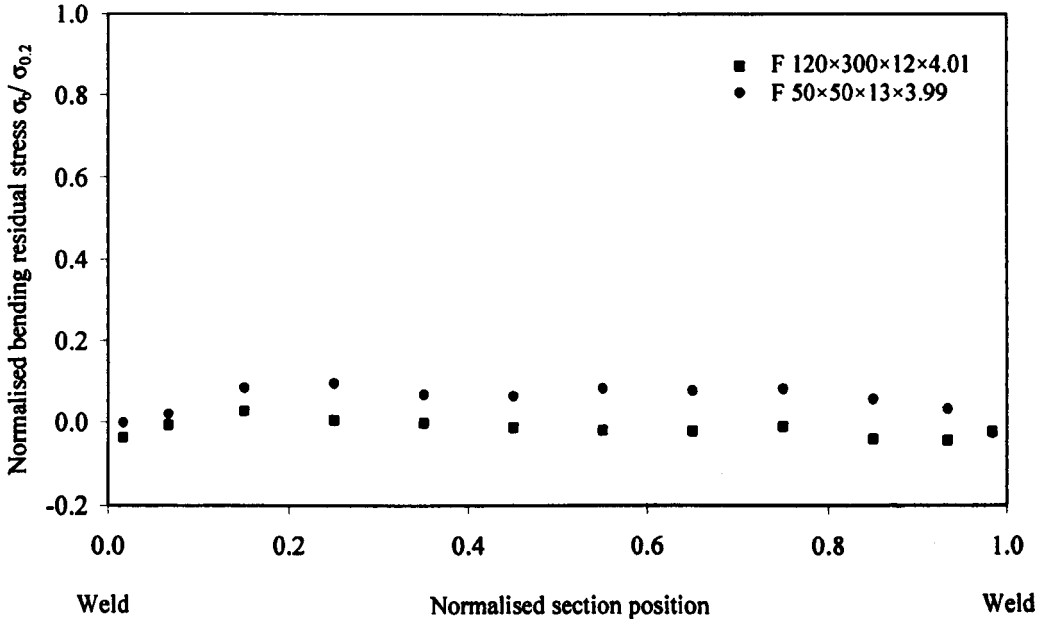

Figure 5.54: *Normalised bending residual stress for the webs of austenitic and austenitic-ferritic fabricated sections tested by Lagerqvist and Olsson (2001) (assuming linear variation through thickness)*

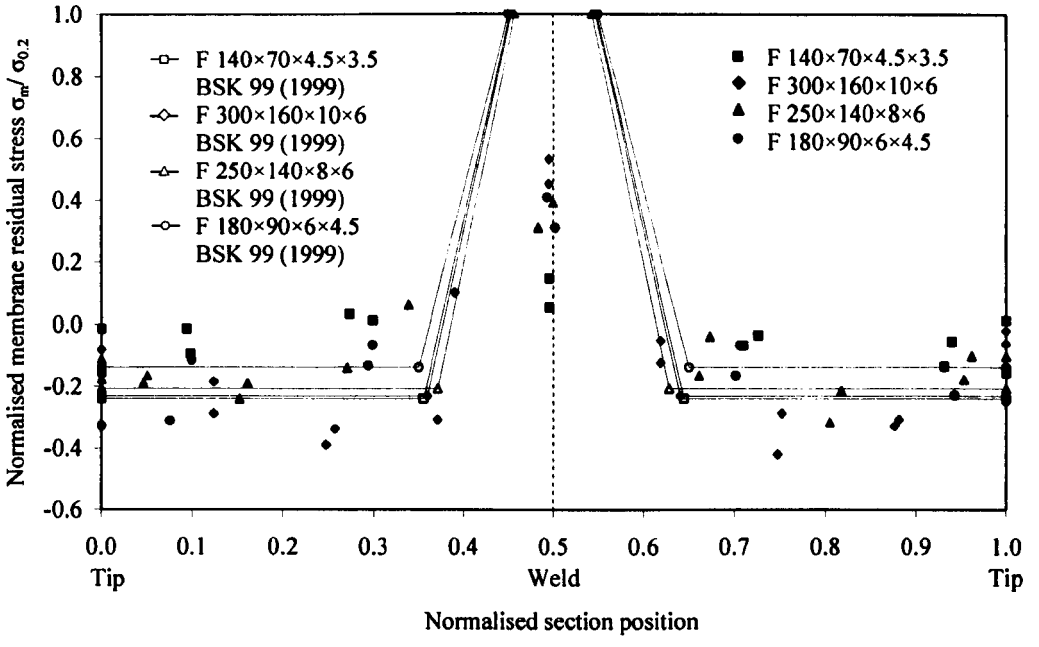

Figure 5.55: *Normalised membrane residual stress for the flanges of ferritic fabricated sections tested by Bredenkamp et al. (1992)*

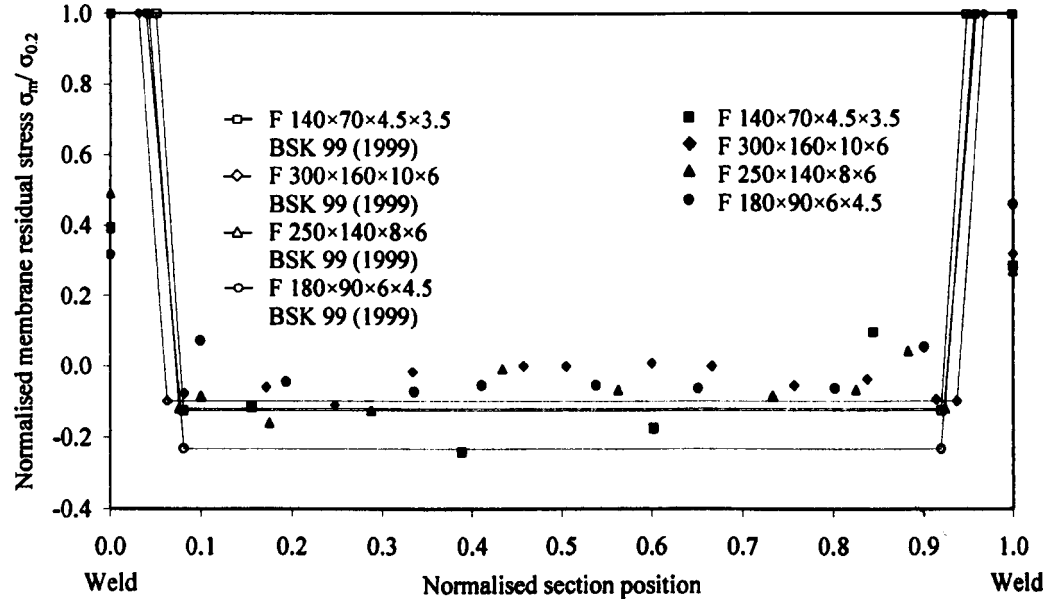

Figure 5.56: *Normalised membrane residual stress for the webs of ferritic fabricated sections tested by Bredenkamp et al. (1992)*

Comparing the membrane residual stresses in Figures 5.51, 5.52, 5.55 and 5.56 with the BSK 99 (1999) model (which varies between sections due to its dependence on the material and geometric properties), a reasonable agreement is shown. However, it may be observed that the tensile residual stresses in the web of the austenitic section are of larger magnitude than the model and have a larger region of influence for both the austenitic and austenitic-ferritic sections. This may be attributed to the higher thermal expansion of the material. For the ferritic sections, the tensile peaks in the weld regions may be seen to be significantly lower than the material yield strength.

For austenitic and austenitic-ferritic stainless steel sections it is proposed to modify the model given in the Swedish design code BSK 99 (1999) by increasing the magnitude of the tensile regions to $1.3\sigma_{0.2}$ and increasing the regions of tension in the web to $3t_w$ as shown in Figure 5.57. For ferritic sections, given the similarity in microstructure with carbon steel and the acceptable agreement with the BSK 99 model shown in Figure 5.55 and 5.56, it is proposed to adopt the existing model.

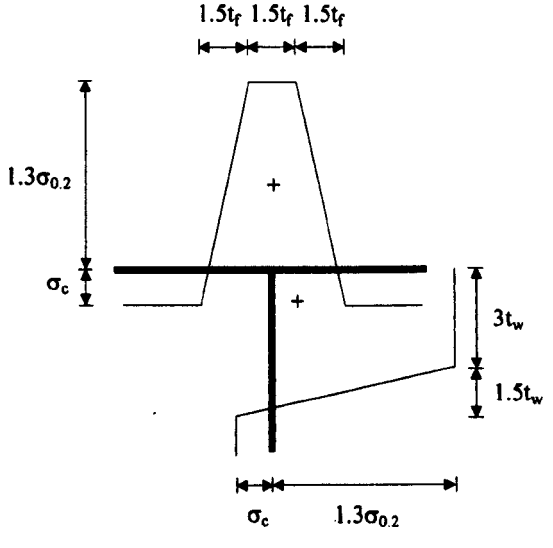

Figure 5.57: *Proposed membrane residual stress model for austenitic and austenitic-ferritic stainless steel fabricated I sections*

5.5.5 Hot rolled sections

The majority of residual stress models developed for hot rolled sections have been for I sections. However, no data for hot rolled stainless steel I sections are available, and data only exists for hot rolled stainless steel angles from the current experimental program. The residual

stress patterns for the webs and flanges of I sections tend to describe a region close to the web-to-flange junction in high residual tension, with the remainder of the section in residual compression. This pattern exists following hot rolling due to the differential cooling around the section which arises from the variation in thickness (or surface area to volume ratio). The cooling rate at the web-to-flange junction is slower than surrounding regions due to its lower surface area to volume ratio.

The residual stress data for three stainless steel hot rolled angles (Cruise and Gardner, submitted) are plotted in Figures 5.58 to 5.61 and tabulated in Tables 5.10 and 5.11. Both the membrane and bending residual stresses may be seen to be of relatively low magnitude.

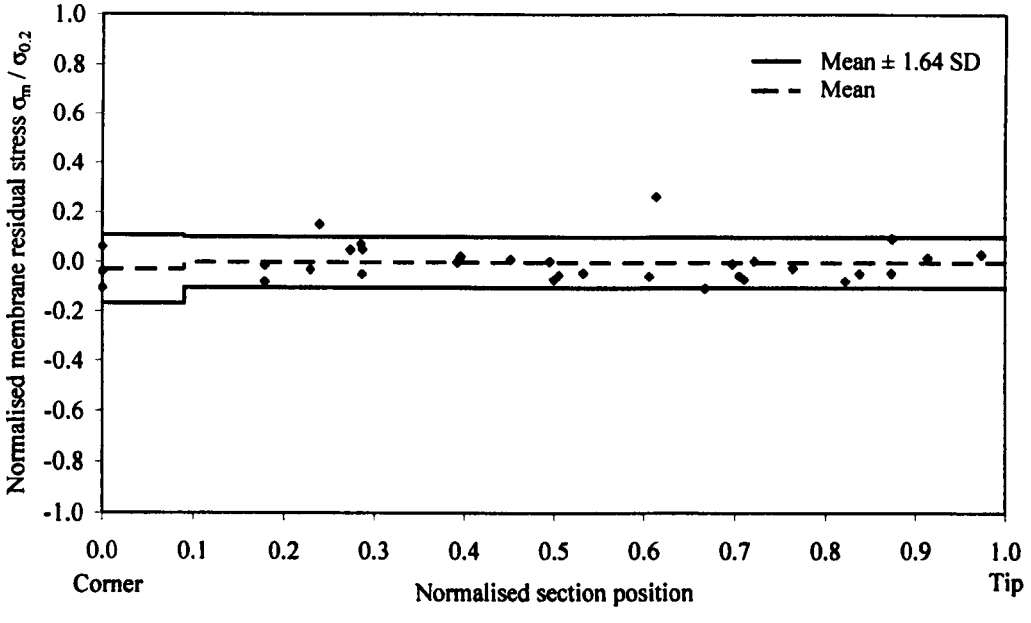

Figure 5.58: *Normalised membrane residual stress for hot rolled angles*

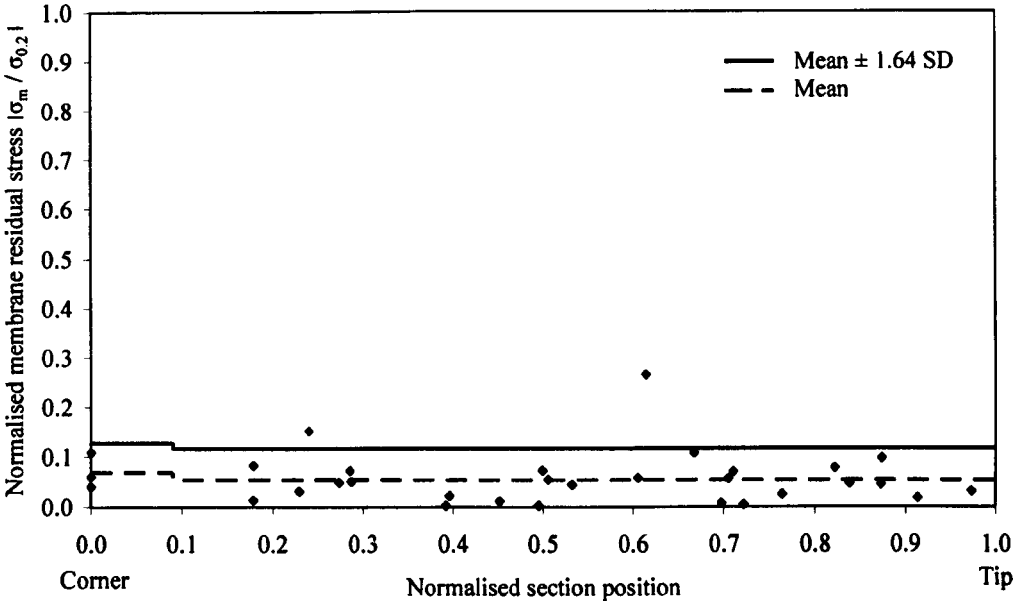

Figure 5.59: *The magnitude of the normalised membrane residual stress for hot rolled angles*

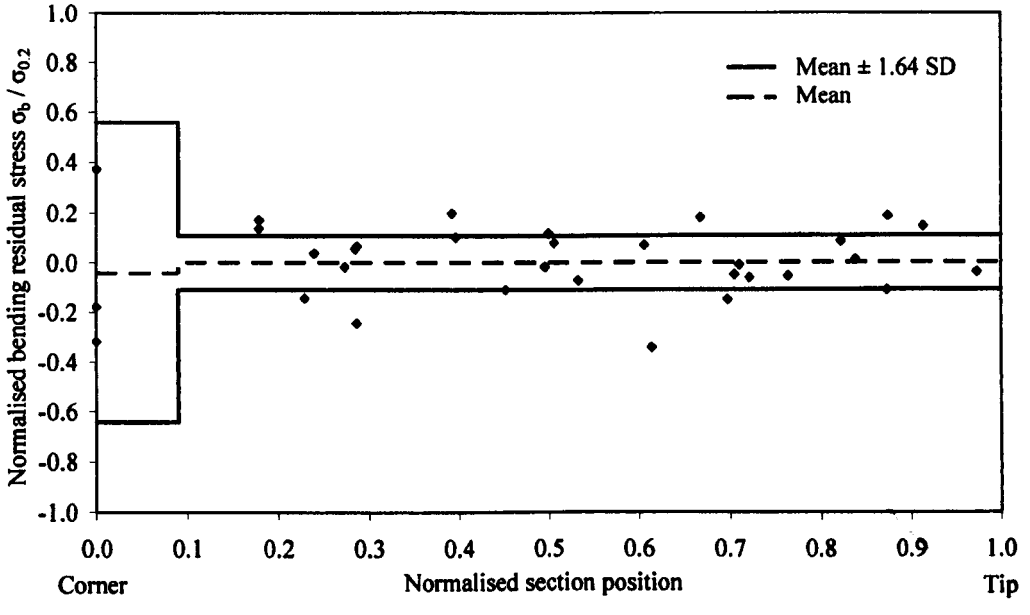

Figure 5.60: *Normalised bending residual stress for hot rolled angles (assuming a linear through thickness variation)*

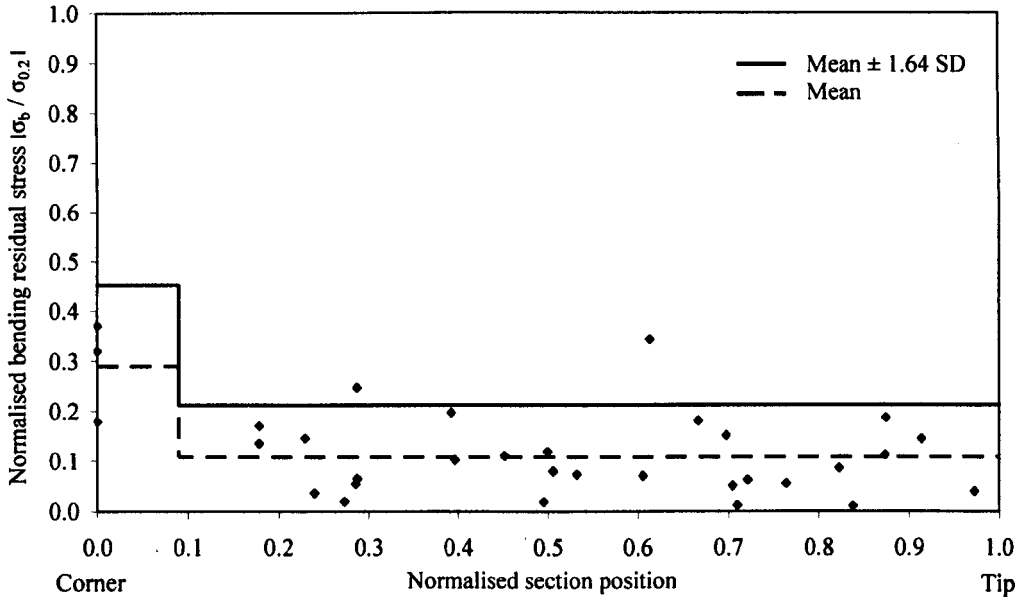

Figure 5.61: *The magnitude of the normalised bending residual stress for hot rolled angles (assuming a linear through thickness variation)*

Table 5.10: *Weighted mean normalised membrane and bending residual stresses for hot rolled angles*

Specimen identification	*Flat faces*				*Corner regions*			
	$\sigma_m / \sigma_{0.2}$		$\sigma_b / \sigma_{0.2}$		$\sigma_m / \sigma_{0.2}$		$\sigma_b / \sigma_{0.2}$	
	Mean	*SD*	*Mean*	*SD*	*Mean*	*SD*	*Mean*	*SD*
HR 50×50×3	0.00	0.08	0.05	0.12	-	-	-	-
HR 50×50×5	0.02	0.07	0.03	0.13	-	-	-	-
HR 50×50×10	-0.02	0.04	-0.08	0.07	-	-	-	-
Mean	0.00	0.06	0.00	0.11	-0.03	0.08	-0.04	0.36

Table 5.11: *Weighted mean of the magnitude of normalised membrane and bending residual stresses for hot rolled angles*

Specimen identification	*Flat faces*				*Corner regions*			
	$\lvert\sigma_m / \sigma_{0.2}\rvert$		$\lvert\sigma_b / \sigma_{0.2}\rvert$		$\lvert\sigma_m / \sigma_{0.2}\rvert$		$\lvert\sigma_b / \sigma_{0.2}\rvert$	
	Mean	*SD*	*Mean*	*SD*	*Mean*	*SD*	*Mean*	*SD*
HR 50×50×3	0.06	0.06	0.11	0.08	-	-	-	-
HR 50×50×5	0.06	0.04	0.14	0.04	-	-	-	-
HR 50×50×10	0.04	0.02	0.08	0.07	-	-	-	-
Mean	0.05	0.04	0.11	0.06	0.07	0.04	0.29	0.10

The membrane residual stress values from the flat regions of the stainless steel angle sections are of comparable magnitude and similar scatter to those presented for carbon steel sections by Madugula et al. (1997). Given the variation of patterns observed between sections, a simple model for bending residual stresses assuming a linear through thickness variation is proposed in Figure 5.62 using the characteristic magnitude of the bending residual stresses from Figure 5.61 (Mean + 1.64 standard deviations). For the membrane residual stresses, no clear pattern emerges from Figure 5.58, but characteristic membrane residual stress magnitudes (Figure 5.59) of $0.12\sigma_{0.2}$ for the flat regions and $0.13\sigma_{0.2}$ for the corners may be adopted.

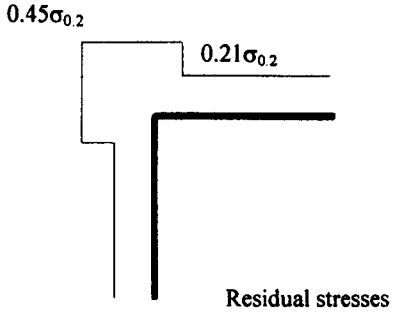

Figure 5.62: *Proposed bending residual stresses model for hot rolled angles (assuming a linear through thickness variation)*

5.6 Conclusions

Stainless steel exhibits differing physical and thermal properties from carbon steel, both of which influence the formation of residual stresses, and it cannot simply be assumed that residual stress models for carbon steel are also appropriate for stainless steel. Comprehensive residual stress distributions have been obtained for a total of eighteen stainless steel structural sections from three different production routes. Three hot rolled angles, eight press braked angles and seven cold rolled box sections were analysed using the sectioning method, with a total of over 800 readings taken. Existing data on residual stresses in stainless steel sections has been examined together with that generated from the current experimental program. The collated residual stress data have been used to develop models for predicting the magnitude and distribution of residual stresses in press braked, cold rolled, hot rolled and fabricated stainless steel structural sections.

The principal means of determining residual stresses was through the use of electrical strain gauges, though a mechanical (Whittemore) gauge and curvature dial was also employed. The calculation of the membrane residual stresses based on measurements made by the Whittemore gauge must be corrected to remove the effects of strip curvature caused by the existence of bending residual stresses. Existing methods developed for hot rolled sections, where bending residual stresses are low, assume strip curvature to be parabolic and make small angle approximations. When applied to cold formed sections, where bending residual stresses are high, large discrepancies from the circular approximation recommended herein were observed.

The two types of cold formed sections (press braked and cold rolled) generally showed low membrane residual stresses, but high bending residual stresses. These bending residual stresses are principally associated with the plastic deformation that occurs in section production, which also causes significant cold working. For the press braked sections, the membrane and bending residual stresses in the unformed flat regions were generally low, typically below 10% of the material 0.2% proof strength. In the corner regions, however, where large plastic deformation occurs, higher bending residual stresses were observed. The corner bending residual stresses typically reached about 30% of the corner material 0.2% proof strength, which itself has been enhanced beyond the strength of the flat material due to cold work during production. Based on characteristic values of residual stress magnitudes (Mean + 1.64 standard deviations) observed in press braked stainless steel angles, it is proposed that membrane residual stress magnitudes may be taken as $0.14\sigma_{0.2}$ in the flat regions and $0.11\sigma_{0.2}$ in the corner regions (but no distribution is recommended), and bending residual stresses may be taken $0.15\sigma_{0.2}$ in the flat regions and $0.36\sigma_{0.2}$ in the corner regions, based on a rectangular stress block distribution.

For the cold rolled sections, the results reveal slightly higher membrane residual stresses than those observed in the hot rolled and press braked sections, and considerably higher bending residual stresses. The bending residual stresses typically ranged between about 30% and 70% of the material 0.2% proof stress. Again based on characteristic values, the magnitude of membrane residual stresses can be taken as $0.37\sigma_{0.2}$ in the flat region and $0.24\sigma_{0.2}$ in the corner regions but no distribution is proposed. Bending residual stresses may be taken as $0.63\sigma_{0.2}$ in the flat regions and $0.37\sigma_{0.2}$ in the corner regions, based on a rectangular stress block distribution.

In the hot rolled sections, the results showed that membrane residual stresses were relatively low and were typically below 10% of the material 0.2% proof stress, whilst bending residual stresses were of slightly higher magnitude, though typically below about 20% of the material

0.2% proof stress. The membrane residual stress values from the flat regions of the stainless steel angle sections were found to be of comparable magnitude and similar scatter to existing carbon steel data. Simple predictive models for the hot rolled sections were proposed, but the limited data set and relatively high scatter dictates a degree of uncertainty. For the fabricated stainless steel sections, residual stress results from the ferritic sections were similar to those predicted by the BSK 99 model for carbon steel; this would be anticipated due to the similar micro-structure, and it was proposed simply to adopt the existing model unchanged.

Fabricated austenitic and austenitic-ferritic sections showed higher thermally induced residual stresses in the weld regions, as well as larger areas of influence than in residual stress models developed for carbon steel; this is principally due to the higher rate of thermal expansion and has been reflected by appropriate modification to the existing BSK 99 model.

Chapter 6

Material strength

6.1 Introduction

This chapter focuses on mapping the variation of material properties around stainless steel cross sections. The variation observed is caused during section forming processes due to the sensitivity of stainless steel to cold working. The change in material strength or 0.2% proof stress that occurs during section forming in any location within a stainless steel cross section is dependant on the amount of plastic deformation and heat treatment experienced by the material in that location. Strength enhancements induced during section forming offer higher design strength for structural sections that are not currently harnessed.

As part of the experimental program strips previously cut for residual stress analysis from press braked, cold rolled and hot rolled cross sections have been tested in tension, to obtain the stress-strain behaviour of the strips, and therefore the variation of material properties around the sections. The experimental techniques implemented, the resulting data and the analysis methods employed are presented herein.

Due to physical restraints in size of the tensile coupons, the resolution to which the material properties could be determined was limited. In order to map the material properties in the corner regions for the cold formed sections to a higher resolution, Vickers microhardness tests were performed at smaller intervals in the sections than were possible for the tensile coupons. A relationship has then been determined between the 0.2% proof stress and the hardness values. This relationship has been used to predict the variation of the 0.2% proof stress particularly in the corner regions of cold formed sections, where considerable increases in the 0.2% proof stress have been previously noted.

Structural engineering experimental programs commonly include tensile coupon tests to provide basic data for subsequent member tests and finite element simulations of structural components. The tensile coupon data from all the available published test programs on press braked and cold rolled sections has been collated and its origin discussed. No published data was available for hot rolled sections.

Combining the data from the current experimental program and all available published data, the variation observed in material strength in cold formed sections can be mapped. The large forming strains used to create corners in both the press braked and cold rolled sections give significant increases in material strength. Previous research reviewed in this chapter has quantified the strain and resulting strength increases in the corner regions of cold formed sections. Modifications are proposed to the current strength enhancement models. Using the hardness values to predict the 0.2% proof stress the extent of the region adjacent to the section corners that also experiences cold work due to the forming of the corner regions is established for both press braked sections and cold rolled sections. Models have also been developed to predict the substantial strength enhancements observed in the flat faces of cold rolled sections.

A methodology to establish the 0.2% proof stress for structural design of hot rolled sections, press braked sections and cold rolled sections is proposed that allows for the strength enhancements which occur during production.

6.2 Published tensile coupon data

6.2.1 Introduction

Material properties of structural sections are often obtained as part of an experimental program by carrying out longitudinal tensile coupon tests. Whilst the number of test programs that have focused on stainless steel sections is significantly lower than carbon steel, published results from a number of important research programs provide material data from various locations around cross sections which have been fabricated by different production routes. This section provides the details associated with all the available test programs that have published material data taken from structural stainless steel sections. In some cases, as the section location from which the coupons were taken was not reported the data could not be included in this study.

6.2.2 Press braked sections

Tensile coupon tests carried out on material taken from press braked sections are limited to a few studies, but the simplicity of the forming process has allowed for detailed investigations into the material strength enhancements in corner forming. Such test programs where the samples are manufactured specifically for the study sometimes do not have inspection documents or mill certificates provided with the sections. Test data carried out on the unformed sheet material is often produced as part of the experimental program instead.

In a similar manner to the experimental program presented herein research carried out in the Rand Afrikaans University by Coetzee et al. (1990), divided three complete press braked lipped C channels into sets of strips. Strips from three sections were tested as tensile coupons in accordance with ASTM tensile testing standards A370-77 (1981). The coupons tested mapped the variation of material properties around the cross sections including in the corner regions. Further strips from the same sections were also tested in compression. The three sections were made from austenitic stainless steel grades 1.4301 and 1.4401 and a ferritic grade 1.4003.

Korvink et al. (1995) carried out material tests but only on the unformed plate material of press braked lipped C channels of stainless steel grade 1.4301 and 1.4016. Both longitudinal and transverse coupons were tested in compression and tension showing the enhanced asymmetry and anisotropy due to cold rolling of the unformed plate material.

Through tensile testing of stainless steel press braked corners van den Berg and van der Merwe (1992) established experimentally the importance of the ratio of the internal radius r_i to the

material thickness t in predicting the observed strength enhancements. Press braked corners of different r_i/t ratios were tested to show the increased cold working associated with decreasing r_i/t ratios. The corners specimens were cut from 2 mm thick sheet to include material of a width equal to the material thickness beyond the curved region of the corner and were made in four stainless steel grades: 1.4301 and 1.4512 (austenitic grades) and 1.4016 and 1.4003 (ferritic grades). Ten coupons for each grade were prepared according to A370-77 (1981). It was commented that the grips in the tensile coupon testing machine crushed the ends of the coupons during loading.

Corner material was also taken from press braked lipped C channels and tested both in tension and compression by Lecce and Rasmussen (2004). The channels were made from austenitic grade 1.4301 and ferritic grade 1.4003 and 1.4016 sheet material. Ferritic grade 1.4016 corner coupons were only tested in tension. The material properties published are an average of two tensile coupon tests and as reported by van den Berg and van der Merwe (1992), the end of the corner coupons are noted to crush in the tensile coupon testing machine grips during the testing.

A test program was conducted at the University of Tokyo by Kuwamura (2003) on press braked open and hollow sections of grades 1.4301 and 1.4318. However the section location from which the tensile coupons were obtained was not specified.

6.2.3 Cold rolled sections

A number of test programs have been carried out on hollow cold rolled stainless steel sections. Most test programs have tested specimens made from the most common structural grade of austenitic stainless steel 1.4301, however some experimental programs have focused on the relatively new grades of high strength and duplex stainless steel grades. The mill certificates obtained with specimens used in experimental tests are commonly published with the experimental data.

Rasmussen and Hancock (1993a and 1993b) at the University of Sydney carried out an experimental program on grade 1.4306 cold rolled sections. Longitudinal coupons were taken from the flat faces and the corners of a cold rolled square hollow section, as well as from a circular hollow section. Tests were conducted both in tension and in compression. The dimensions of the circular hollow section were close to the dimensions of a circular tube that would have been crushed to form the square hollow section. The strain rates employed in the tests were lower than 15 με/s for strains below 20 000 με and for strains above this limit a strain rate of approximately 500 με/s was used in compliance with the Australian tensile testing

standard AS 1391 (1974). Flat coupons were taken at two locations in the square hollow section; both set out from a corner coupon. The centre of the first coupon was 26 mm away from a corner on the face opposite the weld and the centre of the second coupon was 35 mm away from the same corner on the adjacent section face. The corner coupons were released from the section by cutting at 135° to the faces of the section thereby creating a corner coupon with bevelled edges and not an exact quarter arc. The results show that the 0.2% proof stress $\sigma_{0.2,exp}$ in the square hollow sections is a little higher than in the circular hollow sections, suggesting that additional forming in a process such as crushing may have occurred during the production of the box section. The corner regions in the box section show additional increases in strength.

The University of Oulu produced a report (Hyttinen, 1994) on the structural behaviour of stainless steel square hollow sections for austenitic (1.4301) and two ferritic grades of stainless steel (1.4512 and 1.4003). The square hollow sections were documented to have been formed from annealed sheet material by crushing a circular tube. The report notes that Eurocode 3 part 1.4 (currently EN 1993-1-4, 2006) uses the annealed material properties for structural design over looking the strength enhancements caused by cold working during the cold forming of the sections. Flat coupons were taken from the centre of the section faces as well as corner coupons and tested in tension in compliance with ASTM E 8-93 (1993). As with tensile corner coupons carried out by the University of Sydney, the corners were cut at 135° resulting in bevelled edges. In order for the corner coupons to be gripped in the tensile coupon testing machine the ends were flattened which may have introduced a loading eccentricity and caused cold work in the coupon material held by the grips. For strains lower than 20 000 με a strain rate of less than 50 με/s was employed and for strains above this limit a strain rate of 500 με/s was implemented. The strain hardening observed in the austenitic sections showed higher strength enhancements than the ferritic grades, which tend to have material properties more similar to carbon steel. The strength increases reported were above two times the current minimum 0.2% proof stress used in design $\sigma_{0.2,min}$ for the flat coupons from the austenitic grades and over three times for the corner regions. For the ferritic sections the increases in the flat coupons were just below twice the current minimum 0.2% proof stress used in design $\sigma_{0.2,min}$ and ranged from two to two and a half times the minimum 0.2% proof stress $\sigma_{0.2,min}$ for the higher strength corner coupons. The coupon data was used to show that material properties obtained from full cross section tensile tests compared well with the average weighted material properties of the flat faces of the sections. In addition the higher 0.2% proof stress values in the corner regions were shown to only have a small influence on the overall cross section behaviour due to their comparatively small cross sectional area. Hyttinen (1994) recommends that material tests provided in sections' mill certificates should be carried out on the formed sections, not the unformed sheet material.

The resulting strength of sections could then be classified into levels of work hardening such as those given for flat products in structural design standards (Table 2.2).

A research program carried out in the technical research centre of Finland to inform the development of Eurocode 3 Annex S: Designing of steel structures: The use of stainless steels (1993), which is now the present EN 1993-1-4 (2006) was carried out by Talja & Salmi (1995). The research included both tensile and compression tests using coupons cut from austenitic grade 1.4301 rectangular hollow sections of three different nominal dimensions. The three types of sections tested were produced by the two different cold rolling production routes discussed in Chapter 2. Five 60×60×5 sections tested were made by forming a circular tube which was seam welded and then crushed into a rectangular hollow section. Six further sections, three of dimensions 150×100×3 and three sections of dimensions 150×100×6 were formed by folding flat sheet and then seam welding. Longitudinal coupons were taken from two locations in each of the sections, from the centre of the section face opposite the weld (in the flange) and the centre of a face 90° to the weld. The coupons were tested in tension in compliance with EN 10002-1 (1990). Strain rates employed were 43.2 με/s up to 2% strain and beyond this point the strain rate was increased to 1445 με/s. The 0.2% proof stress from the flat faces of the 60×60×5 sections formed via a circular tube were approximately twice the mill certificate values. In contrast the 0.2% proof stress $\sigma_{0.2,exp}$ from the flat faces of the sections formed by sequential folding were generally close to the mill certificate 0.2% proof stress $\sigma_{0.2,mill}$. Compression tests were also made on the same sections.

More recently, research at the technical research centre of Finland (Ala-Outinen, 2005) has included a study of the behaviour of grade 1.4301 stainless steel structural members in fire. As part of the experimental program tensile coupons taken from the web and flange of two cold rolled square hollow sections were conducted at normal temperatures. The tests were conducted in accordance with EN 10002-1 (1990). The internal radii of the corners of these sections were not reported and therefore the data published cannot be included in some parts of the data analysis.

Macdonald et al. (2000) carried out coupon tests on material from the webs of cold rolled lipped C channels, however the location in the section where the coupons were taken from was not reported. Full section tensile tests were also conducted on the same specimens and higher 0.2% proof stresses for the full section tests were noted in comparison with the 0.2% proof stresses obtained from the tensile coupon tests. This was attributed to the influence of cold worked corners on the full section behaviour.

As part of a large experimental program carried out at Imperial College London comprising stub columns, bending and flexural buckling tests, Gardner (2002) carried out 54 tensile coupon tests on material taken from the centre of the flat faces in 15 grade 1.4301 cold rolled square and rectangular hollow sections, as well as 5 coupons cut from the section corners. The tests were carried out in accordance with ASTM 370-87a (1987). A curvature was found in all coupons released from the cold rolled sections indicating the presence of bending residual stresses in the complete section. During tensile testing these bending stresses were reintroduced into the coupons as the applied load straightened the coupons. Corner coupons were tested in pairs to ensure that the tensile loading was applied concentrically. The resulting material properties showed an increased 0.2% proof stress in the corner coupons over those taken from corresponding flat faces. The coupons taken from the flat faces generally gave 0.2% proof stresses $\sigma_{0.2,exp}$ that were higher than the mill certificate 0.2% proof stress $\sigma_{0.2,mill}$.

A study carried out by Gardner et al. (2006) on high strength stainless steel cross sections included tensile coupon tests on material taken from four different sized cold rolled square and rectangular sections made from cold worked C850 sheet material (see Table 2.2). Tensile coupons were also taken from nominally similar sections made from annealed sheet material of austenitic grade 1.4318, which is approximately equivalent to the cold worked tensile strength level C700 (see Table 2.2). For each section, coupons were taken from the centre of the sections web and flange and tested in compliance with EN 10002-1 (1990). The reported data is an average of three nominally similar tests. The test program also included stub column tests, flexural buckling tests, bending tests and web crippling tests.

A number of recent experimental programs have been reported by the University of Hong Kong. Young and Lui (2005) carried out tests on high strength and duplex stainless steel square and rectangular hollow sections and Zhou and Young (2005) reported tests carried out on austenitic (1.4301), high strength and duplex sections. For this test program material data from mill certificates was not available. Whilst the data is presented herein, due to the lack of mill certificate data, this experimental data cannot be included in some analyses and modelling. Young and Lui (2005) performed coupon tests that conformed to the Australian coupon testing standard AS 1391 (1991). From each of five sections (three duplex and two high strength) one flat coupon was taken from the centre of a section face 90° to the weld face and one corner coupon was taken. Two further sections, one high strength and one duplex were cut into strips to obtain a series of tensile coupons in order to map the distribution of material properties around half sections. Static values of the 0.2% proof stress $\sigma_{0.2,exp}$ and the ultimate strength $\sigma_{ult,exp}$ were obtained by holding the loading constant for 1.5 minutes close to these respective

points. This allowed for redistribution of the imposed load and caused the measured load to drop slightly. Results showed higher strength in the corner regions due to high plastic deformation causing cold working. Zhou and Young (2005) reported data from tensile coupons taken from the centre of the webs of box sections which had been cold rolled via a circular tube. The tests were conducted in accordance with the American standard ASTM E 8M-07 (1997) and the Australian standard AS 1391 (1991). As in Young and Lui (2005) static values of the 0.2% proof stress $\sigma_{0.2,exp}$ and the ultimate stress $\sigma_{ult,exp}$ were obtained. The results reported included data from Young and Lui (2005) but with a further 8 coupon tests.

6.2.4 Hot rolled sections

No published material data on stainless steel hot rolled sections was available.

6.3 Tensile coupon tests

6.3.1 Introduction

Tensile coupon tests were carried out in accordance with EN 10002-1 (2001) to determine the stress-strain behaviour of material around cross sections formed by the three studied production routes: press braking, cold rolling and hot rolling.

6.3.2 Coupons

Strips previously sectioned from austenitic stainless steel sections for residual stress measurements were employed as parallel sided tensile coupons as described in the American tensile testing standard A370 87a (1987). The location of the coupons for all sections are given in Appendix A. The width of the coupons was, where possible, a multiple of the nominal thickness of the material, with a finer resolution in the corner regions.

In many cases the linear electrical post-yield strain gauges affixed to the centre of the internal and external surfaces of the strips, that had been used to measure the residual stress distribution, were also used to measure the strain during the tensile loading. In the cases where the strain gauges were damaged, the coupon was cleaned and the damaged strain gauges carefully replaced with new ones.

Two types of tensile coupons were generated, firstly flat coupons (Figure 6.1) taken from the faces of the sections and secondly corner coupons. To obtain the cross section area S_o of the flat coupons vernier callipers were employed to take three measurements along the width and three

measurements along the thickness of the coupon. Average width and thickness values were multiplied together to give the cross section area. For the corner coupons it was not accurate enough to approximate the cross section area to be a quarter arc of a measured thickness due to geometric deviations in these regions. Therefore slivers were cut from both ends of the coupons and these were scanned into a computer. The image of both cross sections was imported into Auto Cad and the perimeters were drawn round. The area of each cross section was calculated from the scanned image and scaled against the known area of a square which was also scanned in. An average of the two cross section areas was taken. The length of each coupon, which was cut to an approximate length of 320 mm, was also more accurately determined.

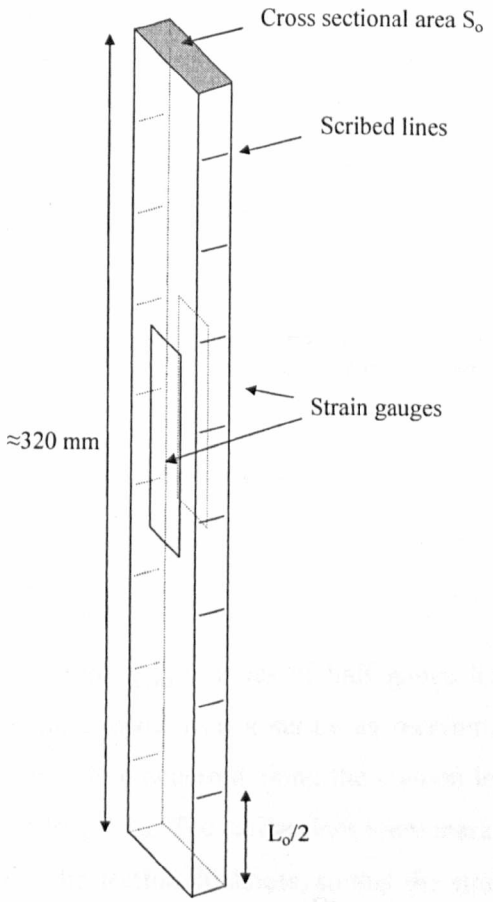

Figure 6.1: *Flat tensile coupon*

6.3.3 Strain at ultimate stress

The post yield strain gauges employed were specified to reach the largest available strain of 20%. This strain limit meant that the gauges could not record the strain at ultimate stress $\varepsilon_{ult,exp}$. To establish this value a less accurate method had to be adopted. A linear voltage displacement

transducer was attached to the loading ram of the tensile coupon testing machine which measured the overall extension of the coupon which occurred during loading. From this measurement a displacement reading could be obtained that corresponded to the ultimate stress $\sigma_{ult,exp}$. To establish the original length of the coupon over which this extension had occurred, the distance from the ends of the coupons, where no straining had occurred was subtracted from the measured original full length of each coupon. The region that had experienced no strain was determined from markings made on the tensile coupons by the jaws of the tensile coupon testing machine. From the spacing between these marks shown in Figure 6.2, made at approximately 1 mm intervals, the distance from the end of the coupon to the position where the marks started to stretch and separate could be observed and this was defined as the region of the coupon where no strain was experienced.

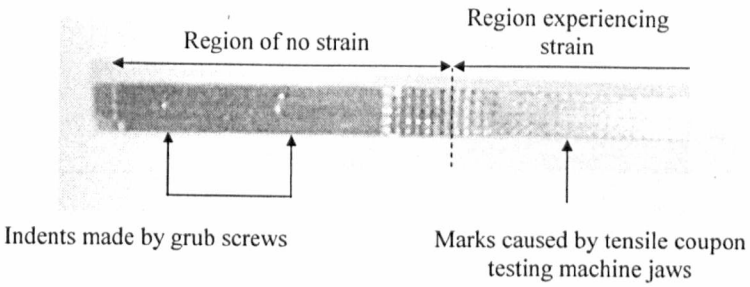

Figure 6.2: *End of test coupon*

6.3.4 Strain at fracture

In order to obtain the strain at fracture $\varepsilon_{f,exp}$ a series of half gauge lengths $L_o/2$ were finely marked along the full length of the coupon with a scribe as recommended by EN 10002-1 (2001). This ensured that wherever failure occurred along the coupon length the fracture point was always located within a gauge length L_o. The scribe lines were marked on the both sides of the coupon, which corresponded to the section thickness, so that the strain gauge placed on the internal and external face did not affect the spacing and measurement of the gauge length as shown in Figure 6.1. The tensile tests performed were proportional tests defined in EN 10002-1 (2001), where the gauge length L_o is related to the cross sectional area S_o through Equation 6.1.

$$L_o = k\sqrt{S_o} \tag{6.1}$$

The constant k is defined as 5.65 with the provision that the resulting gauge length L_o must be greater than 20 mm. For coupons where the cross section did not allow the expression to conform to this limit k was taken as 11.3.

Post failure the two halves of coupon were carefully matched back together as shown in Figure 6.3. The final gauge length was measured between scribe marks, which were chosen so that the fracture point fell as far as possible from either scribe mark. This ensured that the necking observed at the point of fracture did not distort the final gauge length reading. The gauge length measurement was carried out on both sides of the coupon and an average taken. If failure occurred in the grips of the tensile coupon machine strain at fracture was not noted as the friction of the grips would influence the strain experienced in this region of the coupon.

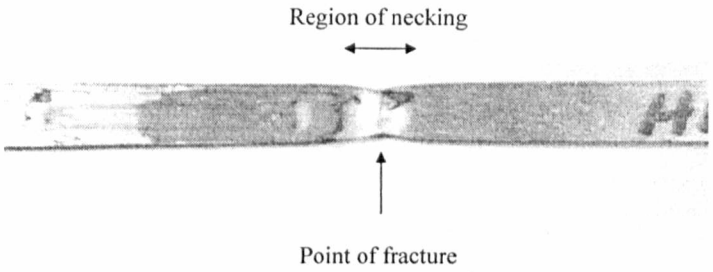

Figure 6.3: *Reassembled tensile coupon showing the necking around the fracture point*

6.3.5 Test rig

Coupons prepared in the manner described above were often as narrow as the strain gauges would permit to enable the finest resolution of material properties to be obtained. To prevent any slippage of the coupons in the jaws of the tensile coupon testing machine and to avoid drilling holes through such thin material, a pair of clamps was designed, one of which is shown in Figure 6.4. Both ends of the coupon were gripped by a pair of grub screws within each clamp to hold the coupon above and below the jaws of the tensile machine until the jaws had fully gripped the coupon. The clamps could therefore hold coupons of different thicknesses. No slippage of the grub screws was observed by looking at the indents made in the coupon by the grub screws after each test. An example of the indents is shown in Figure 6.2.

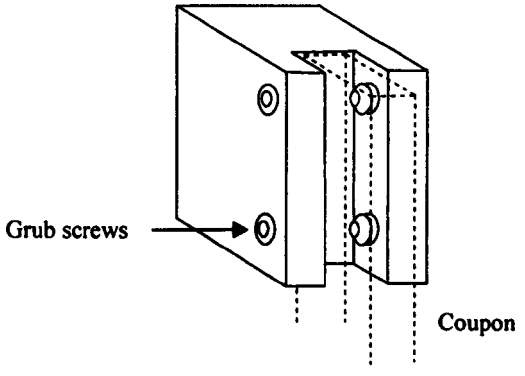

Figure 6.4: *Tensile coupon clamp*

Owing to the residual stresses released while sectioning, the press braked angles and to a greater degree cold rolled box sections, exhibited a large curvature in the strips. This curvature was not removed prior to testing to avoid causing cold working during flattening and hence altering the coupons material properties. The curved coupon was fitted into the jaws of the tensile coupon testing machine and the loading during the start of the tensile test drew the coupon straight. It should be noted that this process causes the influence of the bending residual stresses observed in the coupons to be incorporated in the resulting stress-strain data.

The tensile coupon machine used was principally an Amsler 100kN hydraulic testing machine, but for samples whose failure load was anticipated to be higher than 100kN, an Amsler 350 kN hydraulic testing machine shown in Figure 6.5 was employed. In either case flat grips were used to hold the flat coupons and for corner coupons, grips with a suitable groove to hold the coupon was used to reduce the risk of the coupon ends being crushed.

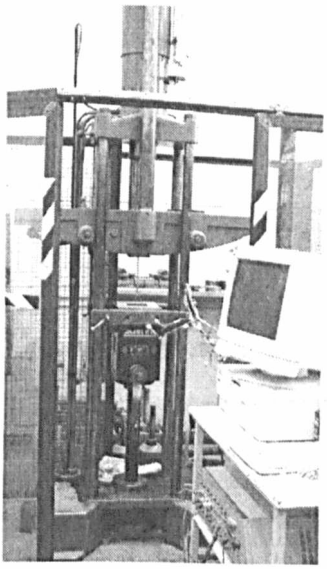

Figure 6.5: *350kN Amsler tensile testing machine*

Data from a calibrated loading transducer in the tensile testing machine, linear voltage displacement transducer and strain gauges were transferred to a Datascan data logger and recorded by Dalite software once every second.

6.3.6 Strain rates

Both tensile testing machines were load controlled. For every test the loading rate was held constant just above the lower limit of 6 MPa per second given in EN 10002-1 (2001). Resulting strain rates were approximately ten times lower than the maximum limit of 2500με/s. Due to this low strain rate a lower static yield point was not observed when the load was held at a constant value. The low strain rate also meant that the 0.2% proof stresses obtained would be conservative compared to 0.2% proof stresses obtained with higher strains rates, which may have been employed to obtain material data given in the mill certificates.

6.3.7 Data analysis

From the resulting stress-strain data for each tensile coupon a number of values were extracted. Firstly the best-fit Young's modulus was obtained. By a process of iteration a series of proof stresses and the corresponding strains were also defined. Proof stresses were determined at 0.01% plastic strain $\sigma_{0.01,exp,}$ 0.05% plastic strain $\sigma_{0.05,exp}$, 0.1% plastic strain $\sigma_{0.1,exp}$, 0.2% plastic strain $\sigma_{0.2,exp}$, 0.5% plastic strain $\sigma_{0.5,exp}$, 1.0% plastic strain $\sigma_{1.0,exp}$ and 2.0% plastic strain $\sigma_{2.0,exp}$. At the 0.2% proof stress the tangent $E_{0.2}$ was also determined. In addition, values were obtained

for the ultimate stress $\sigma_{ult,exp}$ and corresponding strain $\varepsilon_{ult,exp}$, as well as the strain at fracture $\varepsilon_{f,exp}$ as described in sections 6.3.3 and 6.3.4 respectively. An example stress-strain curve is shown in Figure 6.6 where the Young's modulus, 0.2% proof stress and the fitted compound Ramberg-Osgood expression are also shown.

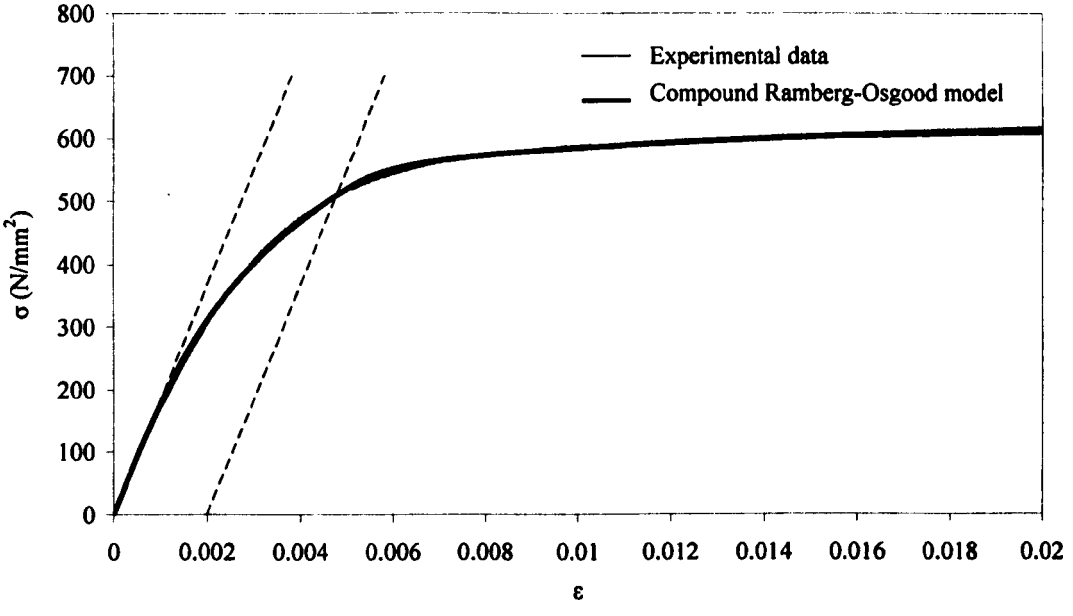

Figure 6.6: *Stress-strain data for a tensile coupon together with the fitted compound Ramberg-Osgood model*

A program written in MatLab calculated the strain hardening parameter n defined for the basic Ramsberg-Ogood model which is given in Chapter 2 by Equation 2.4. Three values for the strain hardening parameter were obtained using Equation 2.4 as $n_{0.01}$, $n_{0.05}$ and $n_{0.1}$ respectively where the proof stresses 0.01% proof stress $\sigma_{0.01,exp}$ 0.05% proof stress $\sigma_{0.05,exp}$ and 0.1% proof stress $\sigma_{0.1,exp}$ were alternately taken as the second proof stress σ_{snd}. For the compound Ramberg-Osgood expression the n' strain hardening parameter is defined by Equation 2.13 taking σ_{snd} and ε_{snd} as the 1.0% proof stress $\sigma_{1.0,exp}$ and the corresponding strain, as adopted by Gardner and Ashraf (2006). The program also obtained best fit values for both strain hardening parameters n and n'.

6.3.8 Results

The resulting material properties extracted from the data are tabulated in their entirety in Appendix A. The data for three example sections; a press braked angle, cold rolled box and hot

rolled angle are presented within this section as well as the complete set of data provided graphically.

PB 50×50×2 (r_i=4.5) is chosen as the exemplar press braked angle section and its setting out diagram is given in Figure 6.7. The material properties for PB 50×50×2 (r_i=4.5) are presented in Table 6.1. Table 6.2 gives the strain hardening parameters n and n', as described in section 6.3.7, as well as the ratio of the measured 0.2% proof stress $\sigma_{0.2,exp}$ to 0.2% proof stress given by the mill certificates $\sigma_{0.2,mill}$, and the ratio of the measured 0.2% proof stress $\sigma_{0.2,exp}$ to the 0.2% proof stress given in the minimum specifications EN 10088-2 (2005) $\sigma_{0.2,min}$. Figures 6.8-6.15 plot the 0.2% proof stress $\sigma_{0.2,exp}$ and the ultimate stress $\sigma_{ult,exp}$ for the eight press braked sections, indicating the mill certificate 0.2% proof stress $\sigma_{0.2,mill}$ and minimum 0.2% proof stress $\sigma_{0.2,min}$ specified. Generally, the 0.2% proof stress $\sigma_{0.2,exp}$ observed is close to the corresponding values given in the mill certificate $\sigma_{0.2,mill}$, with the exception of the corners where an increase in strength is observed. The ultimate strength $\sigma_{ult,exp}$ shows less susceptibility to variation in the corner regions although it is seen to increase in some samples such as PB 50×50×5 (r_i=3.5) which has a small r_i/t ratio. This increase is less than that observed for the 0.2% proof stress. There appears to be a variation in the 0.2 % proof stress $\sigma_{0.2,exp}$ at the tips of the flanges which may be due to the techniques employed to cut the material prior to forming, causing cold working or annealing. The measured 0.2% proof stress $\sigma_{0.2,exp}$ is consistently higher than the minimum specified 0.2% proof stress $\sigma_{0.2,min}$. A measure of ductility is given as the strain at fracture ε_f in Table 6.1 where the cold work observed in the corner regions can also be seen to cause a reduction in ductility.

To illustrate the seven cold rolled box sections tested, the setting out of coupons for CR 100×50×4 is shown in Figure 6.16 and the material properties and strain hardening parameters for this section are given in Tables 6.3 and 6.4 respectively. The full set of material properties are plotted in the same manner as the press braked sections in Figures 6.17-6.23. The 0.2% proof stress $\sigma_{0.2,exp}$, as in the press braked sections, increases in the corner regions with a corresponding but smaller increase in the ultimate stress $\sigma_{ult,exp}$. For sections CR 100×50×2, CR 100×100×2, CR 100×50×3, CR 100×100×3 and CR 150×150×4 the 0.2% proof stress measured $\sigma_{0.2,exp}$ in the centre of the box faces tends to be close to or slightly lower than the mill certificate value $\sigma_{0.2,mill}$. The strength values that are lower than the mill certificate may be explained by the lower strain rate employed during the experimental program than that used to obtain the data given in the mill certificate. For stockier sections CR 100×50×4 and CR 100×100×4, increases in the 0.2% proof stress from the mill certificate values may be observed in the centre of the section faces. The mill certificate 0.2% proof stress for the 2 mm and 3 mm thick sections is

considerably above the minimum specified value. For the 4 mm sections the mill certificate is closer to the minimum specified. This is thought to be the case because sheet thickness of up to and including 3 mm are typically produced by cold rolling rather than hot rolling which causes greater increases in strength. As with the press braked sections, the measured 0.2% proof stress $\sigma_{0.2,exp}$ is consistently higher than the minimum specified 0.2% proof stress $\sigma_{0.2,min}$ by significant amounts for most sections except CR 100×50×4. Table 6.3 also shows the depreciation of ductility corresponding to the increase of the 0.2% proof stress.

Four sets of coupons from hot rolled angles were tested and the section HR 50×50×3 has been chosen as the exemplar section. The setting out for HR 50×50×3 is given in Figure 6.24. The material properties and strain hardening parameters are tabulated in Tables 6.5 and 6.6 respectively. For the three sections manufactured by Roldan HR 50×50×3, 50×50×6 and 50×50×10, the 0.2% proof stress $\sigma_{0.2,exp}$ shown in Figures 6.25, 6.26 and 6.28 is, on average, below the mill certificate 0.2 % proof stress $\sigma_{0.2,mill}$ but is constantly considerably above the minimum specified value $\sigma_{0.2,min}$. This large difference between experimental data and the minimum specified value, could be due to warm working of the stainless steel, which occurs as the molten material cools during section forming, increasing the 0.2% proof stress in a similar way to cold working. At the tips of these three sections, an increase in the measured 0.2% proof stress $\sigma_{0.2,exp}$ is observed, perhaps due to faster cooling in these regions, which are the thinnest in the section; this area may have been warm worked to a comparatively higher level. The reason that the mill certificate 0.2% proof stresses $\sigma_{0.2,mill}$ are high in comparison to most of the measured values in these sections except in the tip regions may be because the material taken from the section to provide the mill certificate 0.2% proof stress $\sigma_{0.2,mill}$ has been taken from this region. The ductility measured as the strain at fracture is considerably higher in all four hot rolled sections than in the cold formed sections. The fourth hot rolled section HR 50×50×3 manufactured by Viraj has 0.2% proof stress values $\sigma_{0.2,exp}$ shown in Figure 6.27 that are all well above the mill certificate value which suggests this manufacturer obtains their material properties given in the mill certificates in a different manner than Roldan. Whilst the increases in the hot rolled sections are significant, it is proposed that the 0.2% proof stress from the mill certificate could be taken in structural design. Further investigation would be required to determine how the strength enhancements are induced.

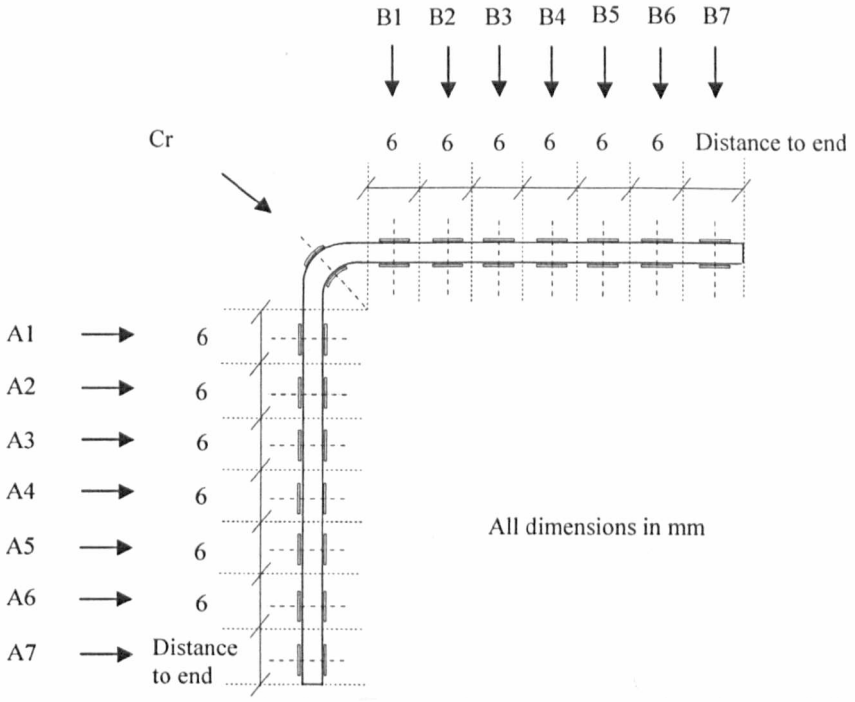

Figure 6.7: *Setting out of press braked section PB 50×50×2 (r_i=4.5)*

Table 6.1: *Material properties distribution for PB 50×50×2 (r_i=4.5)*

PB 50×50×2 (r_i=4.5)	*Section position (mm)*	*Width (mm)*	*E (N/mm²)*	*$\sigma_{0.01,exp}$ (N/mm²)*	*$\sigma_{0.2,exp}$ (N/mm²)*	*$\sigma_{1.0,exp}$ (N/mm²)*	*$\sigma_{ult,exp}$ (N/mm²)*	*$\varepsilon_{f,exp}$*
A7	44.7	5.46	199000	166	322	393	645	0.43
A6	38.2	4.63	218500	106	275	345	627	0.50
A5	32.3	4.76	204000	112	284	339	635	0.49
A4	26.4	4.71	191400	137	289	352	631	0.48
A3	20.4	4.76	212700	144	296	358	643	0.54
A2	14.5	4.76	180500	201	304	361	657	0.57
A1	8.3	5.19	186000	180	320	381	655	0.51
Cr (r_i=5.5)	0.0		181500	155	346	418	641	0.39
B1	8.3	5.15	192900	165	321	382	645	0.46
B2	14.4	4.70	181400	192	293	351	649	0.52
B3	20.3	4.79	187100	163	273	336	624	0.48
B4	26.3	4.72	183000	199	279	344	636	0.46
B5	32.2	4.76	200700	214	335	376	651	0.56
B6	38.2	4.82	203400	139	279	347	638	0.47
B7	45.1	5.95	214200	132	302	357	639	0.43

Table 6.2: *Proof stress ratios and Ramberg-Osgood strain parameters for PB 50×50×2 (r_i=4.5)*

PB 50×50×2 (r_i=4.5)	*Section position (mm)*	*Width (mm)*	$\sigma_{0.2,exp}/\sigma_{0.2,mill}$	$\sigma_{0.2,exp}/\sigma_{0.2,min}$	$n_{0.01}$	$n_{0.05}$	$n_{0.1}$	$n_{bestfit}$	n'	$n'_{bestfit}$
A7	44.7	5.46	1.06	1.40	4.5	5.5	5.9	6.81	3.6	3.6
A6	38.2	4.63	0.90	1.20	3.2	5.3	4.3	5.79	3.9	3.9
A5	32.3	4.76	0.93	1.24	3.2	5.9	6.8	6.13	3.6	3.6
A4	26.4	4.71	0.95	1.25	4.0	6.0	12.2	7.57	2.4	2.4
A3	20.4	4.76	0.97	1.28	4.2	7.5	7.4	6.40	2.8	2.8
A2	14.5	4.76	1.00	1.32	7.2	7.1	6.7	8.44	2.6	2.6
A1	8.3	5.19	1.05	1.39	5.2	5.8	6.3	6.01	1.5	1.5
Cr (r_i=5.5)	0.0		1.14	1.50	3.7	4.2	4.5	4.60	2.8	2.8
B1	8.3	5.15	1.05	1.39	4.5	5.8	7.2	5.76	2.6	2.6
B2	14.4	4.70	0.96	1.27	7.1	5.9	6.0	8.94	6.7	6.7
B3	20.3	4.79	0.90	1.19	5.8	5.4	9.9	7.71	4.3	4.3
B4	26.3	4.72	0.92	1.21	8.9	10.4	13.4	9.37	4.4	4.4
B5	32.2	4.76	1.10	1.46	-	-	-	6.7	-	0.9
B6	38.2	4.82	0.92	1.21	4.3	5.7	7.0	5.65	2.5	2.5
B7	45.1	5.95	0.99	1.31	3.6	4.9	5.6	5.14	2.5	2.5

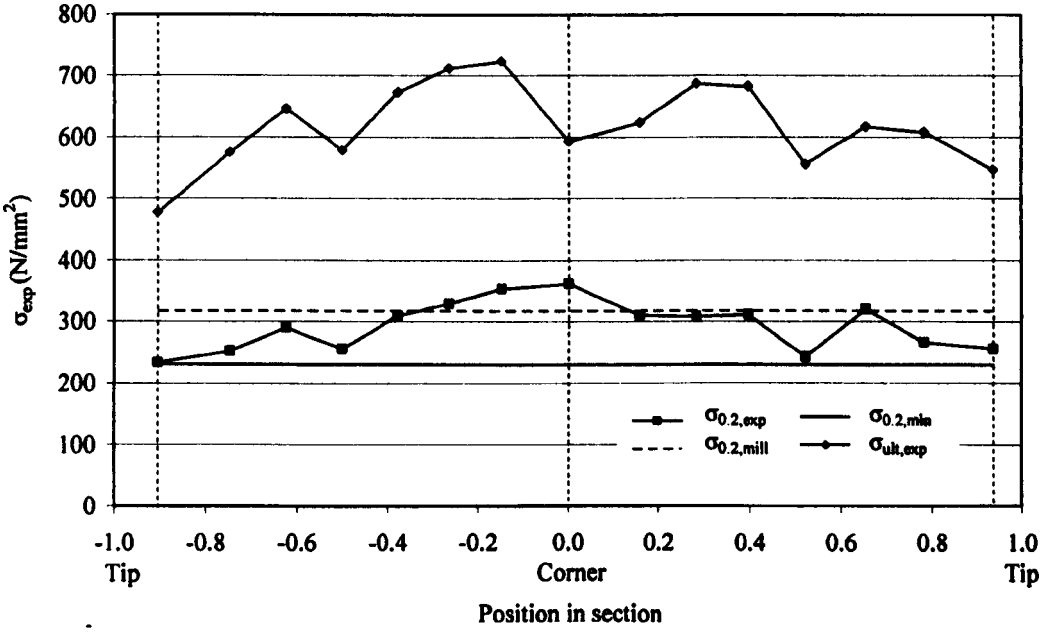

Figure 6.8: *0.2% proof stress $\sigma_{0.2,exp}$ and ultimate stress $\sigma_{ult,exp}$ around PB2 50×50×2 (r_i=3.2) ($\sigma_{0.2,mill}$ = 317 N/mm² and $\sigma_{0.2,min}$ = 230 N/mm²)*

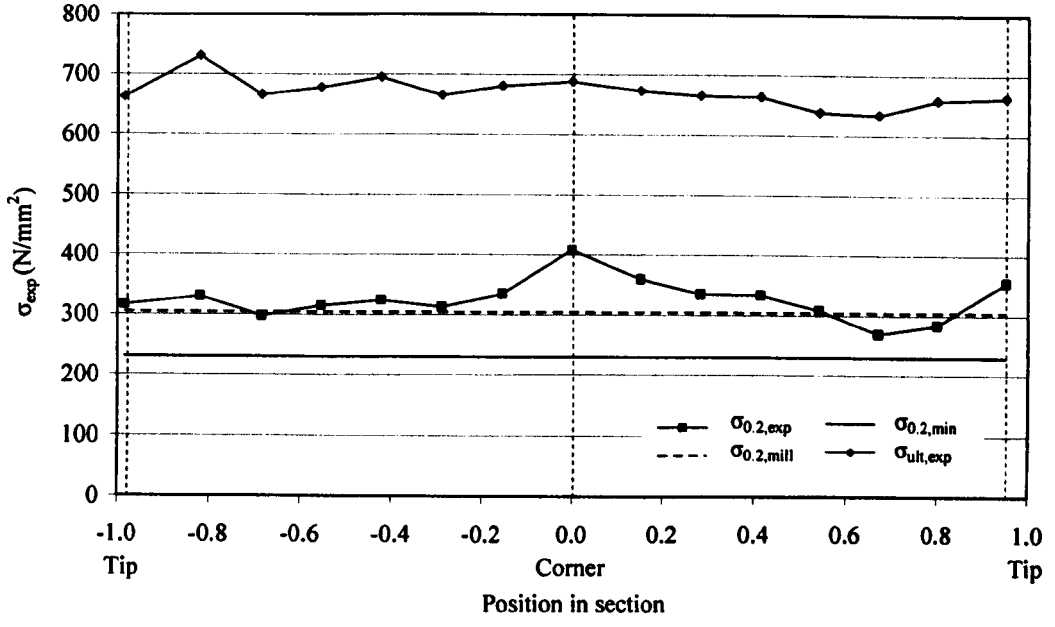

Figure 6.9: *0.2% proof stress $\sigma_{0.2,exp}$ and ultimate stress $\sigma_{ult,exp}$ around PB 50×50×2 (r_i=3.5) ($\sigma_{0.2,mill}$ = 305 N/mm² and $\sigma_{0.2,min}$ = 230 N/mm²)*

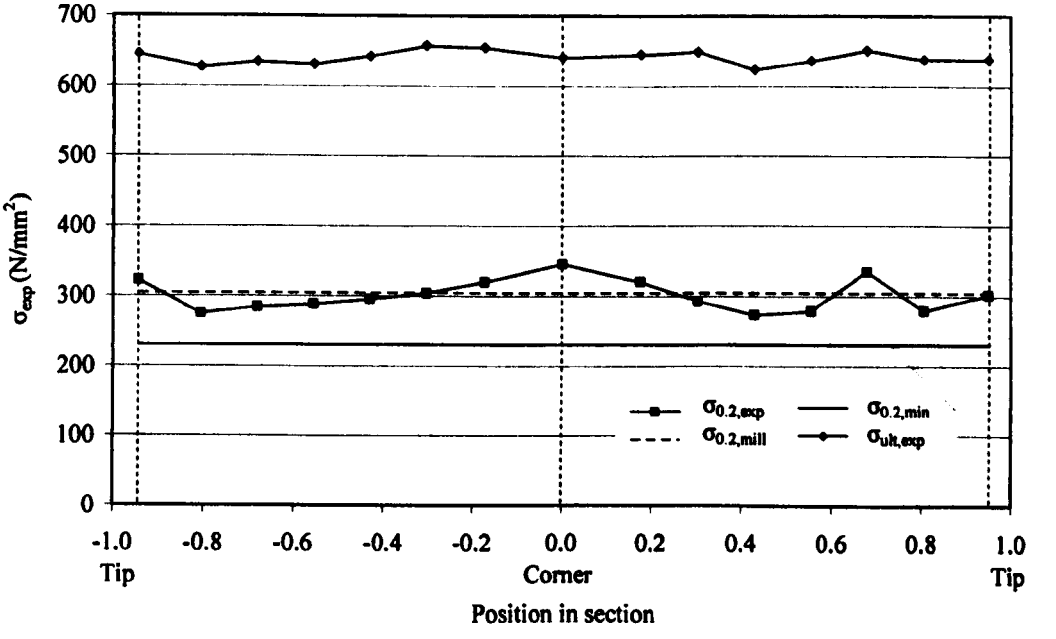

Figure 6.10: *0.2% proof stress $\sigma_{0.2,exp}$ and ultimate stress $\sigma_{ult,exp}$ around PB 50×50×2 (r_i=4.5) ($\sigma_{0.2,mill}$ = 305 N/mm² and $\sigma_{0.2,min}$ = 230 N/mm²)*

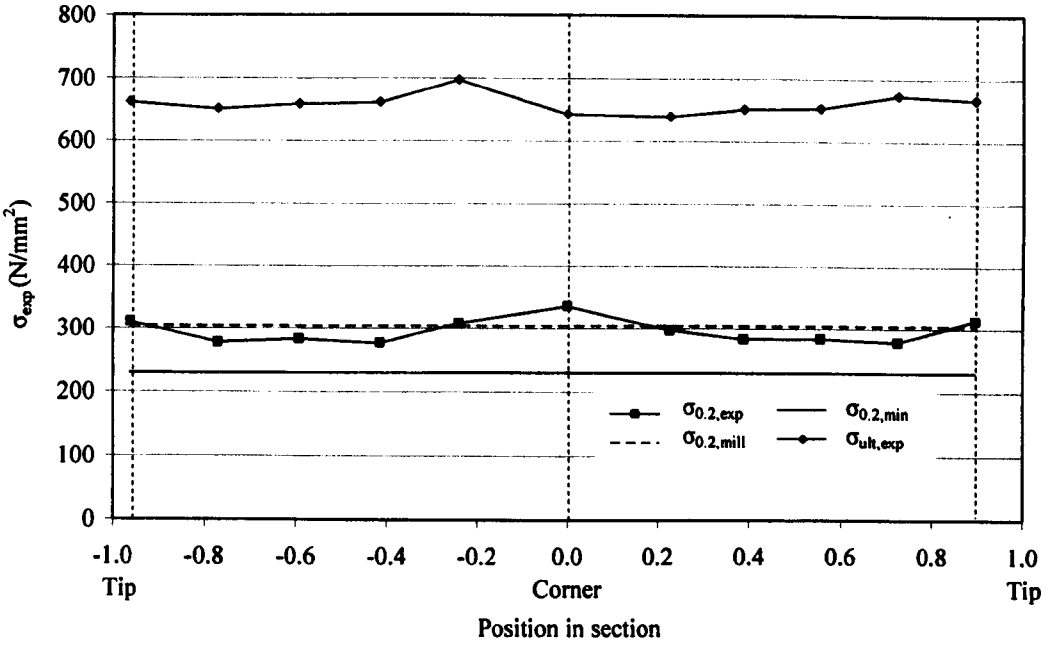

Figure 6.11: *0.2% proof stress $\sigma_{0.2,exp}$ and ultimate stress $\sigma_{ult,exp}$ around PB 50×50×2 (r_i=7.5) ($\sigma_{0.2,mill}$ = 305 N/mm² and $\sigma_{0.2,min}$ = 230 N/mm²)*

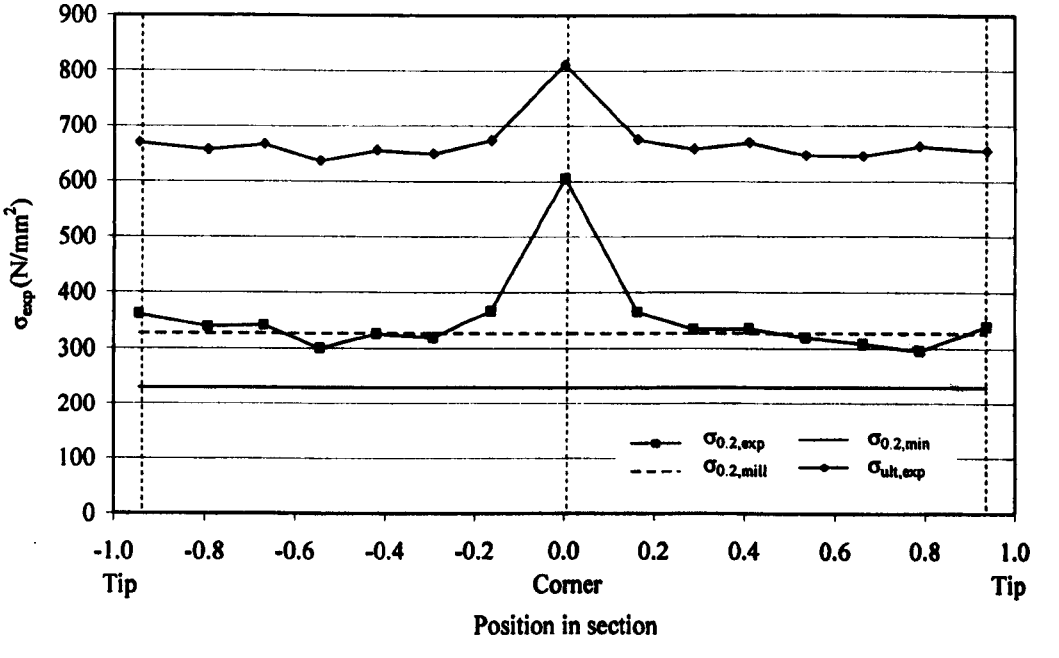

Figure 6.12: *0.2% proof stress $\sigma_{0.2,exp}$ and ultimate stress $\sigma_{ult,exp}$ around PB2 50×50×3 (r_i=3.2) ($\sigma_{0.2,mill}$ = 327 N/mm² and $\sigma_{0.2,min}$ = 230 N/mm²)*

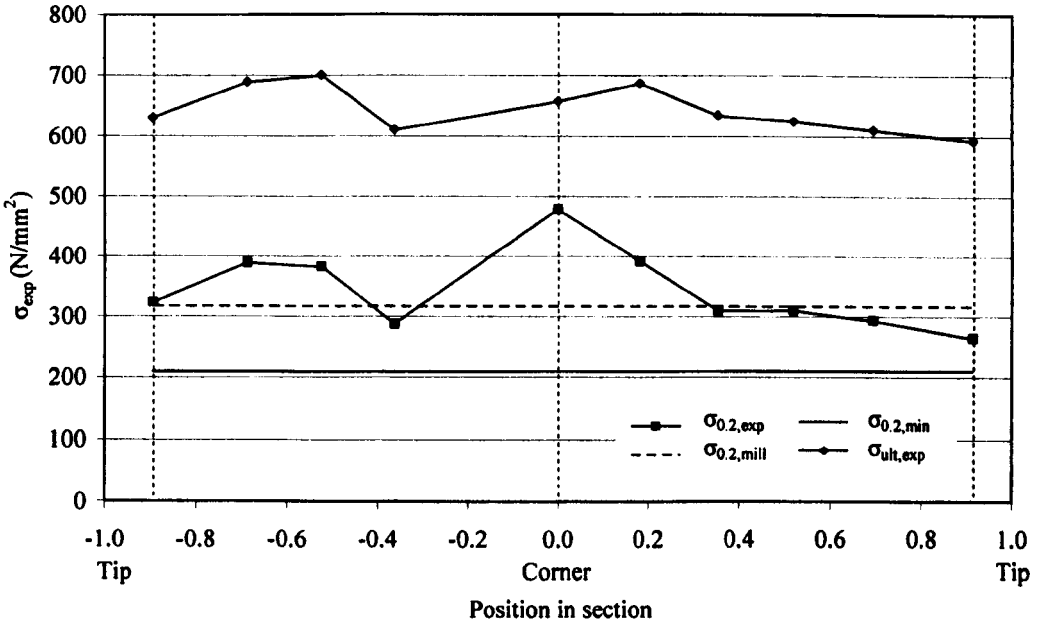

Figure 6.13: *0.2% proof stress $\sigma_{0.2,exp}$ and ultimate stress $\sigma_{ult,exp}$ around PB 50×50×4 (r_i=3.5) ($\sigma_{0.2,mill}$ = 317 N/mm² and $\sigma_{0.2,min}$ = 210 N/mm²)*

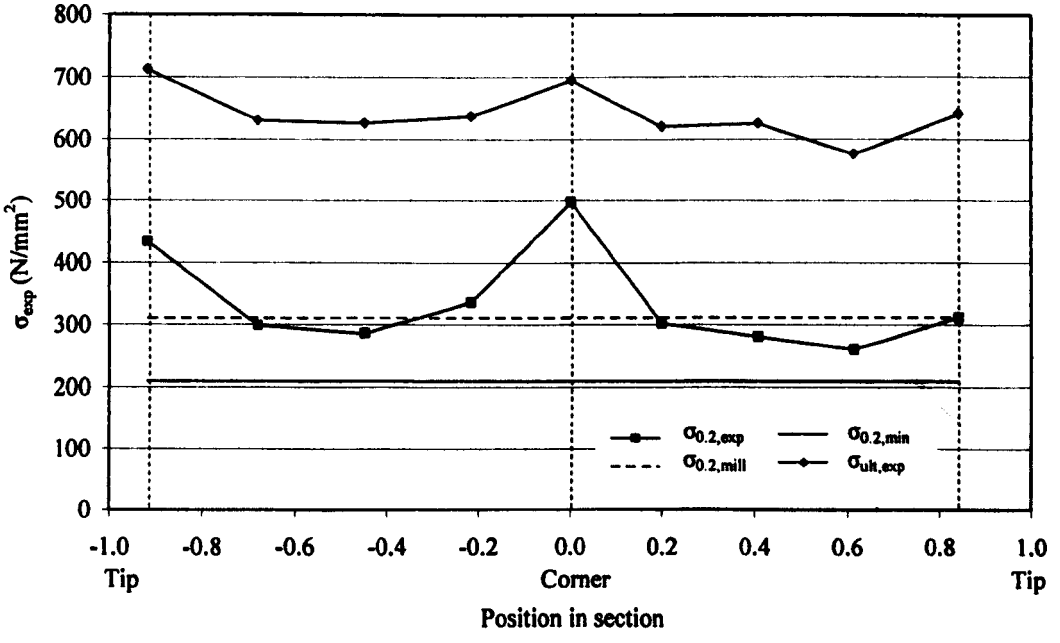

Figure 6.14: *0.2% proof stress $\sigma_{0.2,exp}$ and ultimate stress $\sigma_{ult,exp}$ around PB 50×50×5 (r_i=3.5) ($\sigma_{0.2,mill}$ = 311 N/mm² and $\sigma_{0.2,min}$ = 210 N/mm²)*

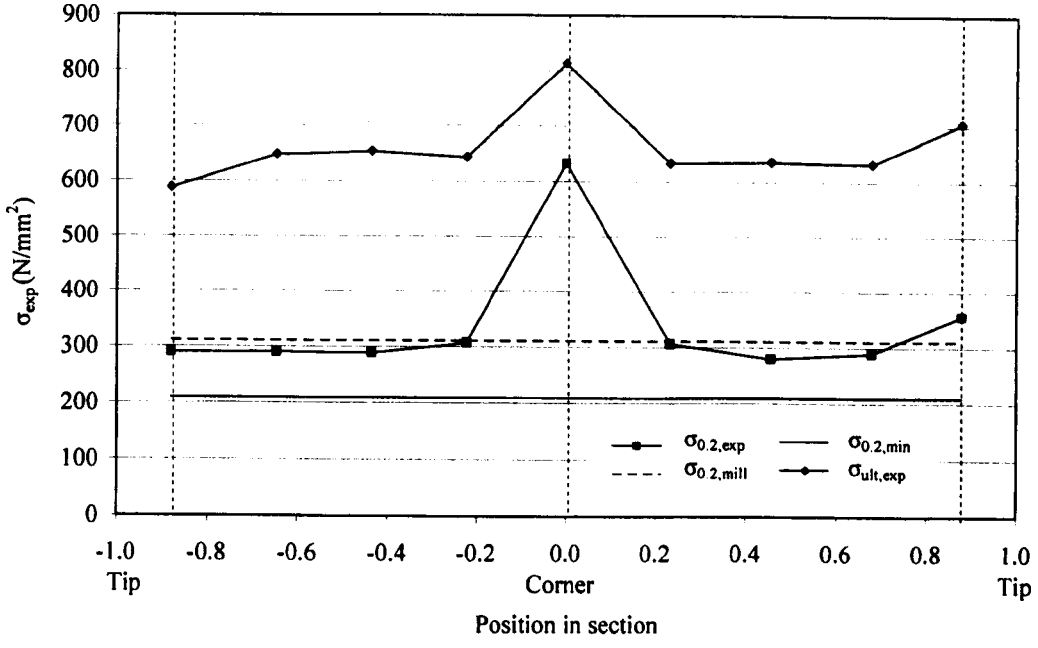

Figure 6.15: *0.2% proof stress $\sigma_{0.2,exp}$ and ultimate stress $\sigma_{ult,exp}$ around PB 50×50×5 (r_i=4.5) ($\sigma_{0.2,mill}$ = 311 N/mm^2 and $\sigma_{0.2,min}$ = 210 N/mm^2)*

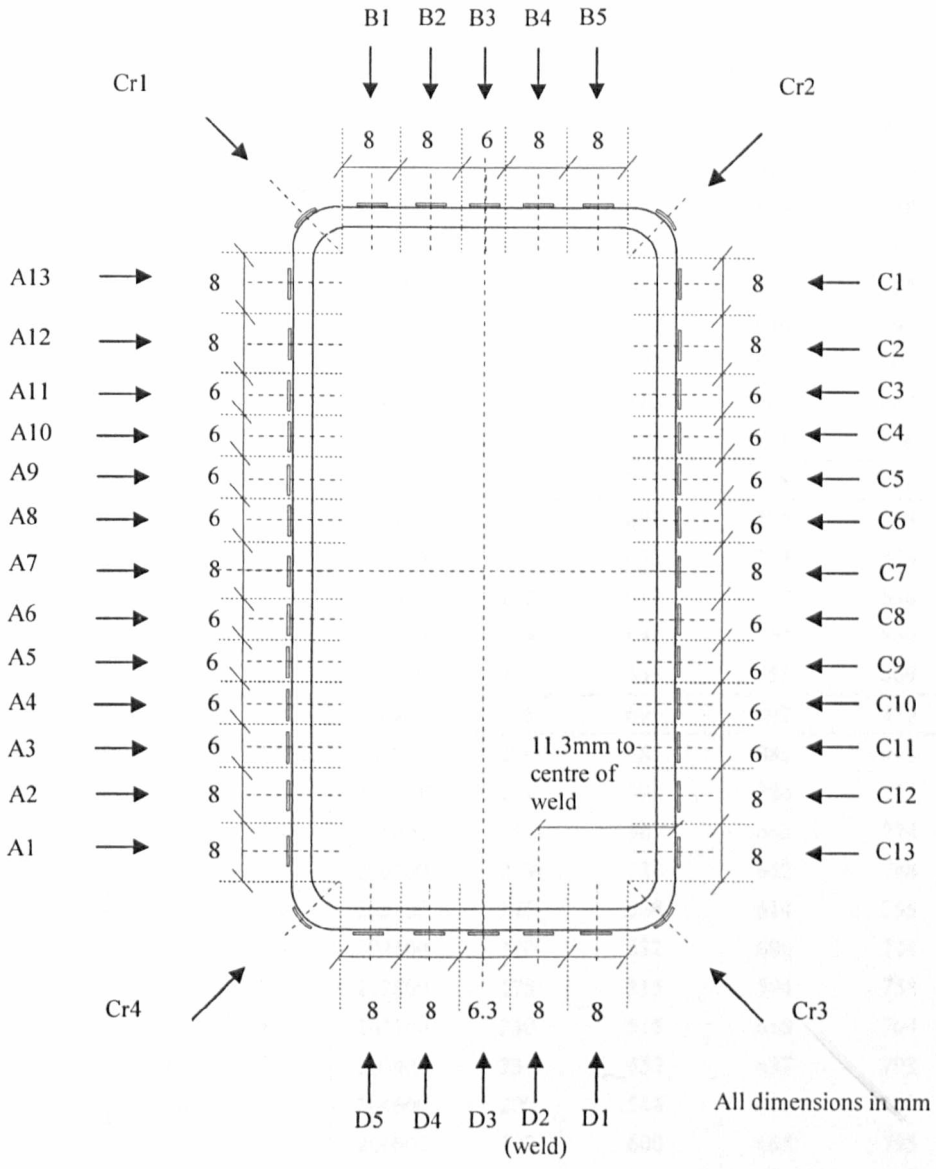

Figure 6.16: *Setting out of cold rolled section CR 100×50×4*

Table 6.3: *Material properties distribution for CR 100×50×4*

CR 100×50×4	*Section position (mm)*	*Width (mm)*	*E* (N/mm^2)	$\sigma_{0.01,exp}$ (N/mm^2)	$\sigma_{0.2,exp}$ (N/mm^2)	$\sigma_{1.0,exp}$ (N/mm^2)	$\sigma_{ult,exp}$ (N/mm^2)	$\varepsilon_{f,exp}$
A1	7.5	7.11	191500	148	660	894	913	0.32
A2	15.5	6.60	199500	176	583	721	808	0.53
A3	22.7	5.27	208500	163	575	673	787	0.54
A4	28.8	4.63	189500	267	540	631	707	0.53
A5	34.7	4.73	210000	264	560	658	803	0.53
A6	40.8	4.93	203400	227	514	617	760	0.57
A7	47.9	6.92	215200	205	550	639	788	0.65
A8	55.0	4.89	202400	262	511	592	769	0.73
A9	61.1	4.88	202200	245	535	613	785	0.57
A10	67.1	4.69	190700	355	576	646	795	0.52
A11	73.1	4.91	203900	239	588	694	806	0.55
A12	80.0	6.66	211700	203	622	786	862	0.53
A13	87.7	6.36	218300	323	778	951	966	0.48
Cr1 (r_i=2.3)	0.0		214300	283	712	838	902	0.38
B1	7.6	7.34	200100	207	699	886	903	0.38
B2	15.8	6.64	207300	227	632	753	843	0.48
B3	23.0	5.27	220900	182	612	727	838	0.55
B4	30.3	6.92	210300	219	642	758	859	0.52
B5	38.7	7.61	200200	267	668	851	869	0.47
Cr2 (r_i =1.3)	0.0		216400	416	699	802	879	0.49
C1	5.6	6.85	187900	296	685	885	900	0.34
C2	13.8	7.07	2048900	224	599	726	824	0.46
C3	21.0	4.99	205800	257	567	662	774	0.51
C4	27.1	4.76	206500	249	538	652	788	0.51
C5	33.3	5.41	203100	247	528	614	755	0.53
C6	40.1	5.80	202500	320	532	606	744	0.63
C7	47.0	5.50	212800	175	515	594	758	0.59
C8	53.3	4.73	203100	250	515	610	764	0.60
C9	59.4	5.05	203400	234	552	637	793	0.58
C10	65.8	5.38	204600	200	544	626	755	0.57
C11	72.2	5.00	206600	192	600	685	795	0.51
C12	78.9	5.93	208600	110	598	737	815	0.48
C13	86.3	6.61	199400	289	707	916	934	0.35
Cr3 (r_i =2.3)	0.0		216800	302	632	727	837	0.45
D1	8.7	9.48	203800	193	694	880	891	0.36
D2 (weld)	17.5	5.69	216500	253	605	718	803	0.68
D3	24.1	5.22	212600	249	644	738	839	0.55
D4	31.2	6.53	201000	214	579	686	767	0.49
D5	39.4	7.46	209900	307	707	891	918	0.41
Cr4 (r_i =2.3)	0.0		204600	575	826	889	904	0.49

Table 6.4: *Proof stress ratios and Ramberg-Osgood strain parameters for CR 100×100×4*

CR 100×50×4	*Section position (mm)*	*Width (mm)*	$\sigma_{0.2,exp}/\sigma_{0.2,mill}$	$\sigma_{0.2,exp}/\sigma_{0.2,min}$	$n_{0.01}$	$n_{0.05}$	$n_{0.1}$	$n_{bestfit}$	n'	$n'_{bestfit}$
A1	7.5	7.11	2.3	3.1	2.0	2.1	2.3	2.3	3.7	3.7
A2	15.5	6.60	2.0	2.8	2.5	3.2	3.8	3.8	4.5	4.6
A3	22.7	5.27	2.0	2.7	2.4	4.5	4.4	5.1	4.4	4.4
A4	28.8	4.63	1.9	2.6	4.3	6.3	7.3	7.3	4.6	4.6
A5	34.7	4.73	1.9	2.7	4.0	7.2	6.9	6.9	4.7	4.7
A6	40.8	4.93	1.8	2.4	3.7	4.7	5.9	6.4	4.4	4.4
A7	47.9	6.92	1.9	2.6	3.0	4.1	5.8	5.8	3.9	4.0
A8	55.0	4.89	1.8	2.4	4.5	5.5	5.4	6.1	3.8	3.8
A9	61.1	4.88	1.9	2.5	3.8	5.0	5.0	5.7	3.8	3.9
A10	67.1	4.69	2.0	2.7	6.2	4.8	5.8	7.5	4.4	4.4
A11	73.1	4.91	2.0	2.8	3.3	4.0	4.1	4.3	4.4	4.4
A12	80.0	6.66	2.2	3.0	2.7	2.8	4.0	3.5	3.9	3.9
A13	87.7	6.36	2.7	3.7	3.4	3.6	3.7	4.1	24.4	24.4
Cr1 (r_i=2.3)	0.0		2.5	3.4	3.2	4.1	5.7	6.0	3.6	3.6
B1	7.6	7.34	2.4	3.3	2.5	3.0	3.8	3.8	4.3	4.3
B2	15.8	6.64	2.2	3.0	2.9	4.1	5.7	5.7	3.9	3.9
B3	23.0	5.27	2.1	2.9	2.5	3.7	5.5	4.6	4.5	4.5
B4	30.3	6.92	2.2	3.1	2.8	4.9	4.9	4.9	3.7	3.7
B5	38.7	7.61	2.3	3.2	3.3	3.6	4.0	4.1	4.3	4.3
Cr2 (r_i=1.3)	0.0		2.4	3.3	5.8	5.1	5.2	7.2	6.0	6.0
C1	5.6	6.85	2.4	3.3	3.6	3.1	3.9	4.5	5.8	5.8
C2	13.8	7.07	2.1	2.9	3.0	3.2	3.9	3.9	4.0	4.0
C3	21.0	4.99	2.0	2.7	3.8	3.8	4.5	4.9	3.3	3.3
C4	27.1	4.76	1.9	2.6	3.9	5.2	6.0	6.7	5.3	5.3
C5	33.3	5.41	1.8	2.5	3.9	4.3	4.1	5.0	3.5	3.5
C6	40.1	5.80	1.8	2.5	5.9	4.9	7.2	7.5	3.4	3.4
C7	47.0	5.50	1.8	2.5	2.8	4.8	5.7	5.2	4.4	4.4
C8	53.3	4.73	1.8	2.5	4.1	7.4	5.8	9.5	8.7	8.7
C9	59.4	5.05	1.9	2.6	3.5	6.4	8.0	8.0	4.2	4.2
C10	65.8	5.38	1.9	2.6	3.0	3.7	3.7	4.1	2.7	2.7
C11	72.2	5.00	2.1	2.9	2.6	3.8	5.8	4.8	3.9	3.9
C12	78.9	5.93	2.1	2.8	1.8	2.6	3.2	3.2	4.2	4.2
C13	86.3	6.61	2.5	3.4	3.4	3.2	2.9	3.6	4.9	4.9
Cr3 (r_i=2.3)	0.0		2.2	3.0	4.1	5.0	5.1	6.3	5.7	5.7
D1	8.7	9.48	2.4	3.3	2.3	3.3	3.2	3.5	4.5	4.5
D2 (weld)	17.5	5.69	2.1	2.9	3.4	5.7	3.8	5.8	4.5	4.5
D3	24.1	5.22	2.2	3.1	3.1	5.0	4.8	5.2	3.5	3.6
D4	31.2	6.53	2.0	2.8	3.0	3.7	3.7	4.1	3.5	3.5
D5	39.4	7.46	2.5	3.4	3.6	3.8	3.8	4.2	4.7	4.7
Cr4 (r_i=2.3)	0.0		2.9	3.9	8.2	7.6	8.7	11.2	1.0	1.0

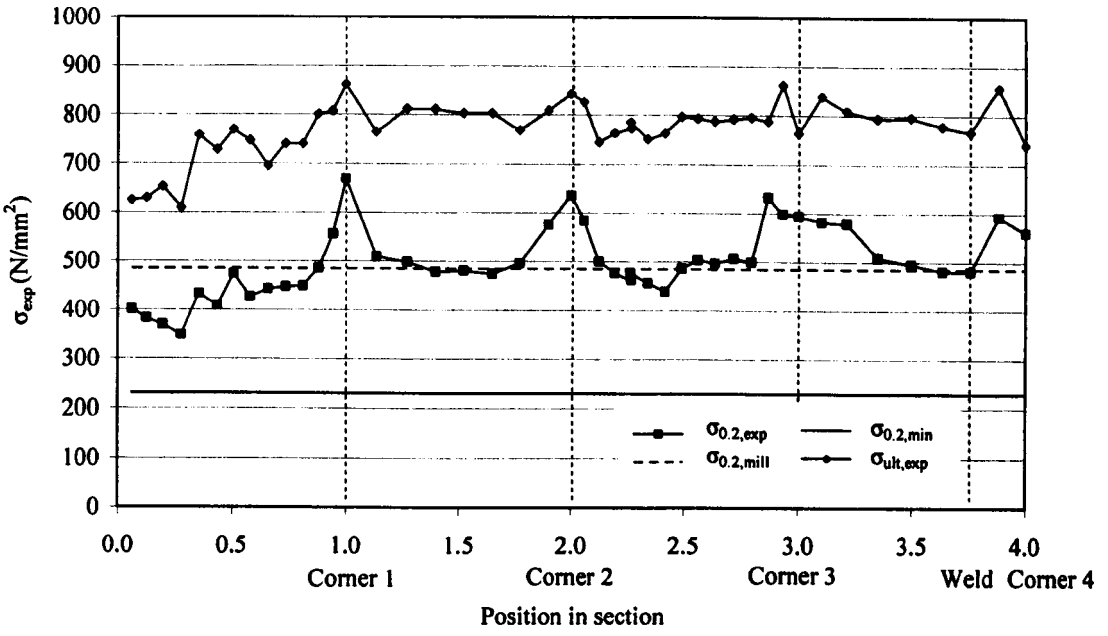

Figure 6.17: *0.2% proof stress $\sigma_{0.2,exp}$ and ultimate stress $\sigma_{ult,exp}$ around CR 100×50×2 ($\sigma_{0.2,mill}$ = 485 N/mm^2 and $\sigma_{0.2,min}$ = 230 N/mm^2)*

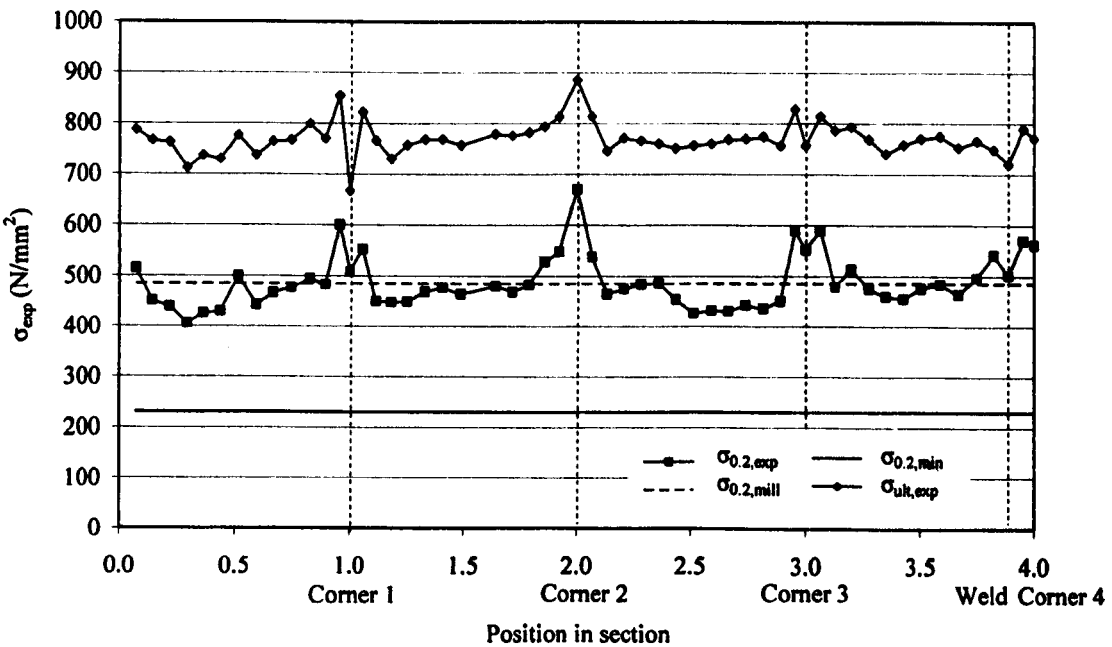

Figure 6.18: *0.2% proof stress $\sigma_{0.2,exp}$ and ultimate stress $\sigma_{ult,exp}$ around CR 100×100×2 ($\sigma_{0.2,mill}$ = 485 N/mm^2 and $\sigma_{0.2,min}$ = 230 N/mm^2)*

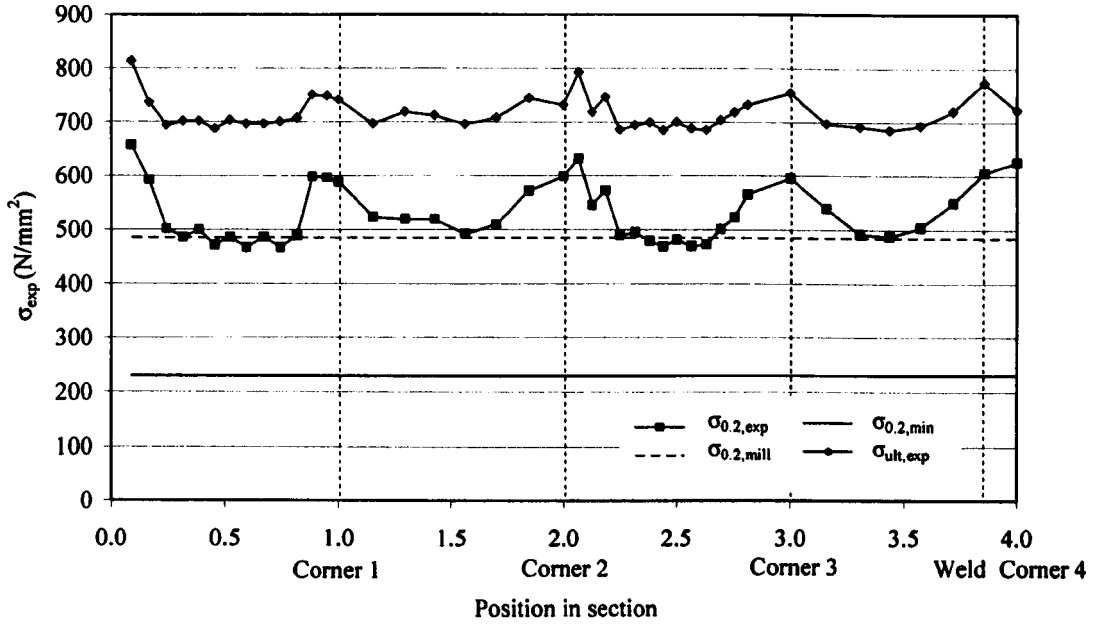

Figure 6.19: *0.2% proof stress $\sigma_{0.2,exp}$ and ultimate stress $\sigma_{ult,exp}$ around CR 100×50×3 ($\sigma_{0.2,mill}$ = 485 N/mm^2 and $\sigma_{0.2,min}$ = 230 N/mm^2)*

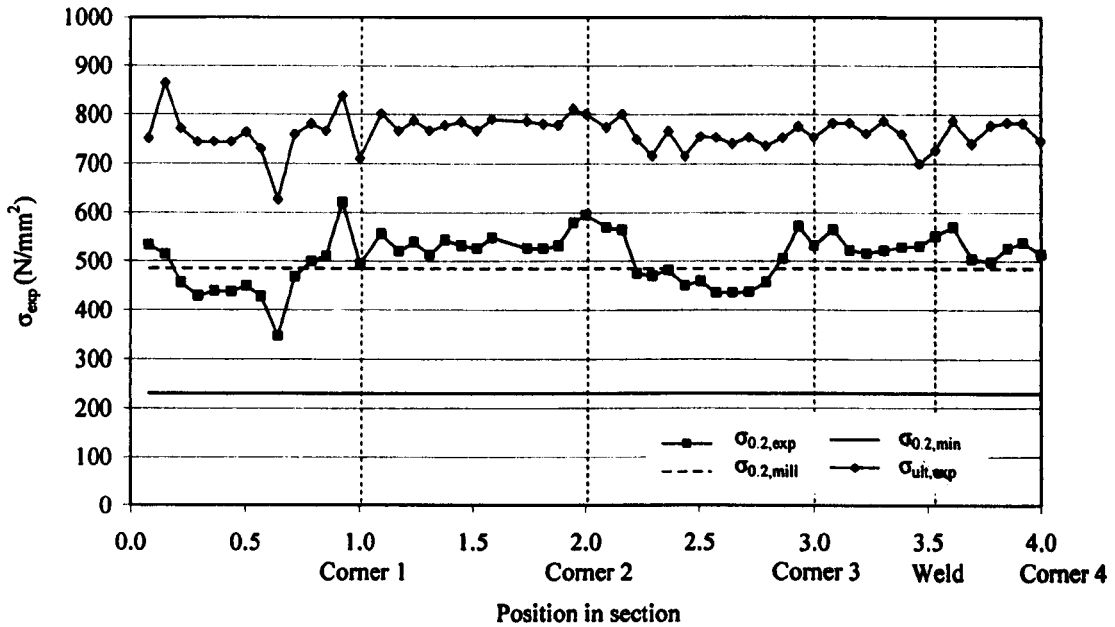

Figure 6.20: *0.2% proof stress $\sigma_{0.2,exp}$ and ultimate stress $\sigma_{ult,exp}$ around CR 100×100×3 ($\sigma_{0.2,mill}$ = 485 N/mm^2 and $\sigma_{0.2,min}$ = 230 N/mm^2)*

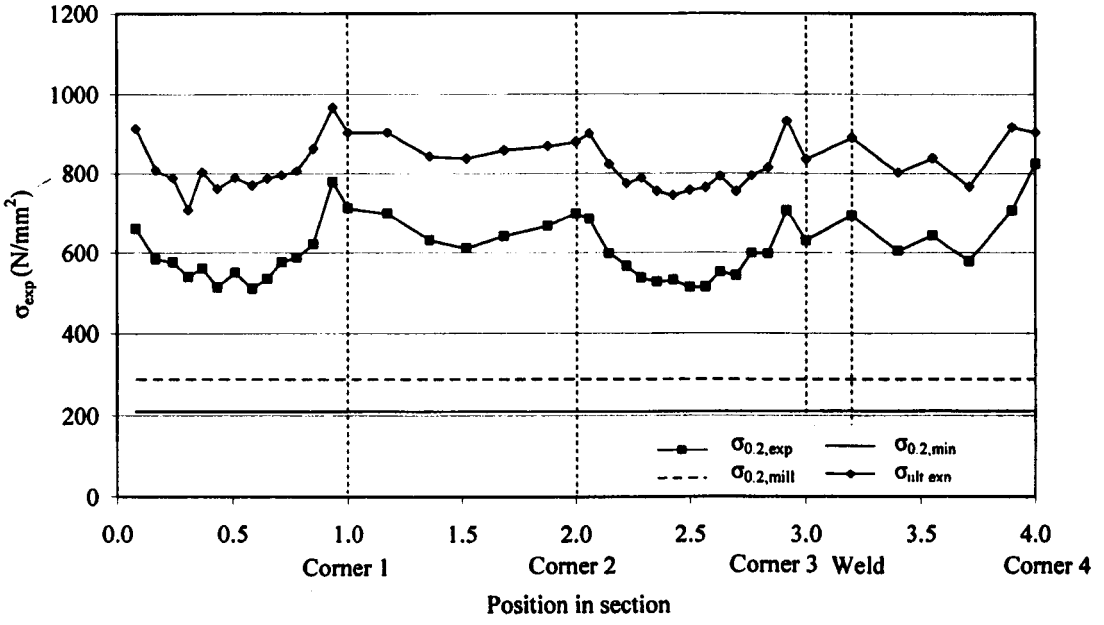

Figure 6.21: *0.2% proof stress $\sigma_{0.2,exp}$ and ultimate stress $\sigma_{ult,exp}$ around CR 100×50×4 ($\sigma_{0.2,mill}$ = 288N/mm^2 and $\sigma_{0.2,min}$ = 210 N/mm^2)*

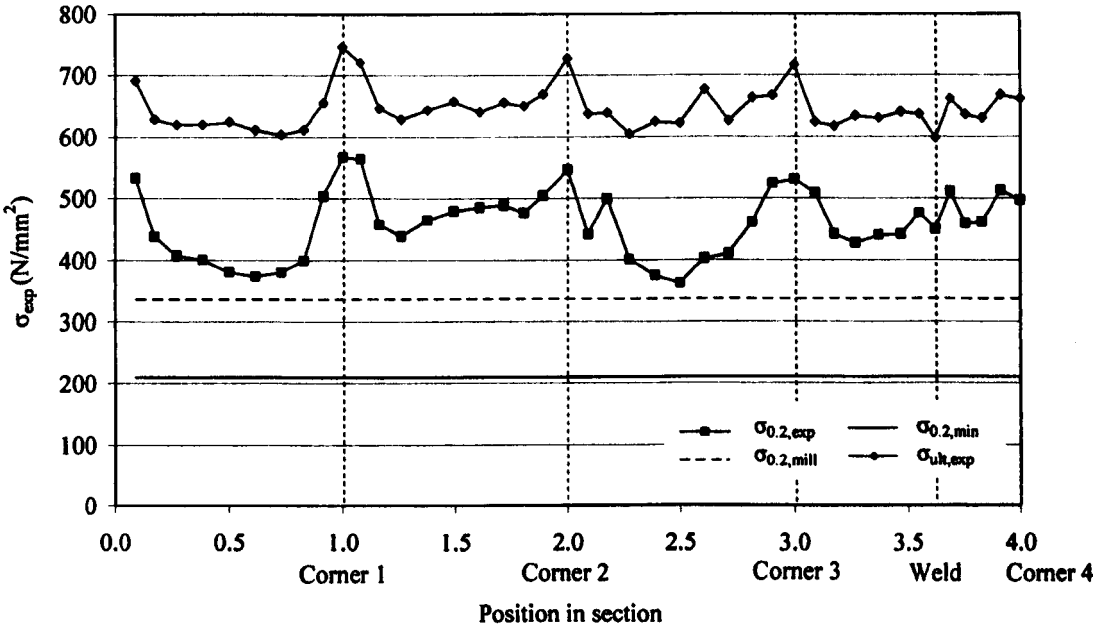

Figure 6.22: *0.2% proof stress $\sigma_{0.2,exp}$ and ultimate stress $\sigma_{ult,exp}$ around CR 100×100×4 ($\sigma_{0.2,mill}$ = 337 N/mm^2 and $\sigma_{0.2,min}$ = 210 N/mm^2)*

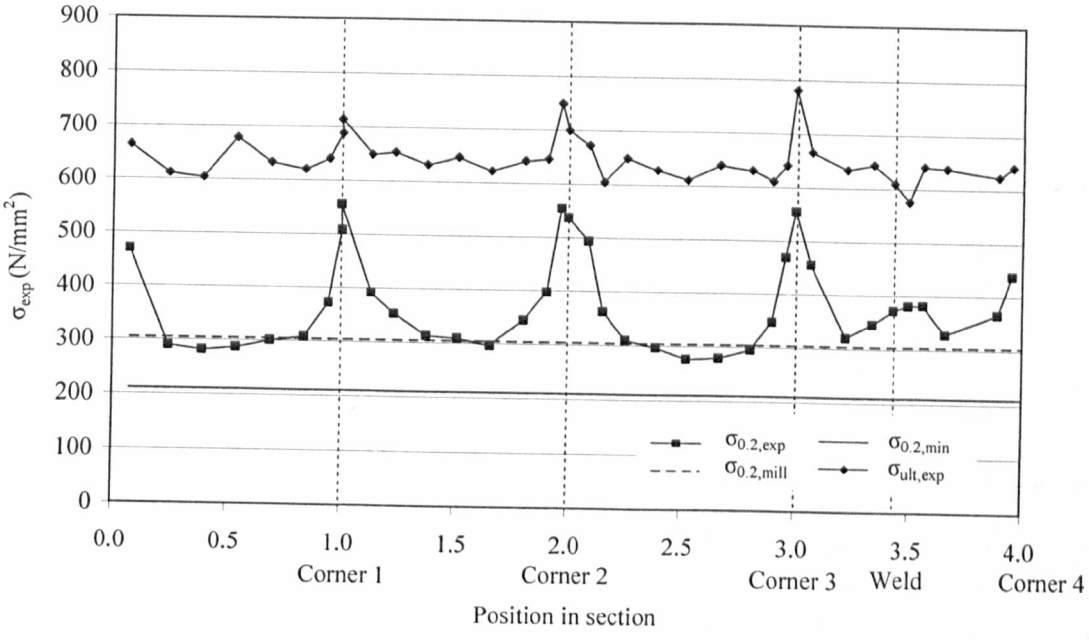

Figure 6.23: *0.2% proof stress $\sigma_{0.2,exp}$ and ultimate stress $\sigma_{ult,exp}$ around CR 150×150×4 ($\sigma_{0.2,mill}$ = 304 N/mm^2 and $\sigma_{0.2,min}$ = 210 N/mm^2)*

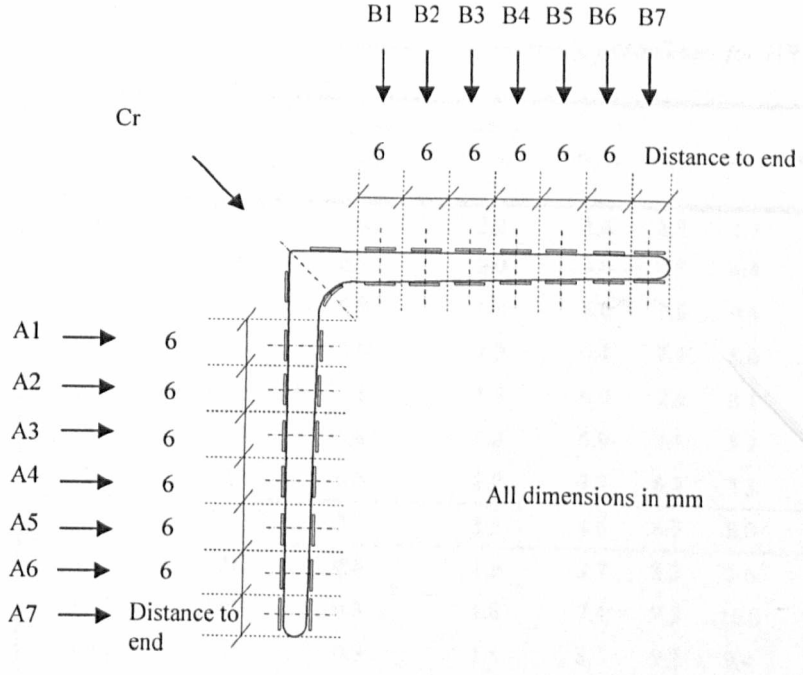

Figure 6.24: *Setting out of cold rolled section HR 50×50×3*

Table 6.5: *Material properties distribution for HR 50×50×3*

HR 50×50×3	*Section position (mm)*	*Width (mm)*	E (N/mm^2)	$\sigma_{0.01,exp}$ (N/mm^2)	$\sigma_{0.2,exp}$ (N/mm^2)	$\sigma_{1.0,exp}$ (N/mm^2)	$\sigma_{ult,exp}$ (N/mm^2)	$\varepsilon_{f,exp}$
A7	38.4	3.36	199100	181	419	494	794	0.64
A6	33.2	3.36	183800	164	381	450	725	0.70
A5	28.3	3.44	189900	202	366	428	709	0.88
A4	23.3	3.51	190700	217	356	422	707	0.73
A3	18.3	3.52	187900	221	340	408	691	0.80
A2	13.3	3.50	194300	200	334	402	690	0.77
A1	8.3	3.49	206100	166	371	439	713	0.68
Cr (r_i=5.0)	0.0		180400	150	289	338	588	0.70
B1	8.4	3.56	204200	157	353	415	702	0.89
B2	13.4	3.60	186800	227	339	400	694	0.82
B3	18.5	3.62	187600	234	335	395	697	0.82
B4	23.7	3.60	186100	245	348	407	702	0.82
B5	28.7	3.54	185200	237	346	401	698	0.82
B6	33.8	3.56	195100	171	346	402	675	0.82
B7	39.2	3.58	205300	235	427	495	826	0.64

Table 6.6: *Proof stress ratios and Ramberg-Osgood strain parameters for HR 50×50×3*

HR 50×50×3	*Section position (mm)*	*Width (mm)*	$\sigma_{0.2,exp}/\sigma_{0.2,mill}$	$\sigma_{0.2,exp}/\sigma_{0.2,min}$	$n_{0.01}$	$n_{0.05}$	$n_{0.1}$	$n_{bestfit}$	n'	$n'_{bestfit}$
A7	38.4	3.36	1.0	2.2	3.6	3.8	4.5	3.9	2.7	2.7
A6	33.2	3.36	0.9	2.0	3.6	3.7	4.4	3.9	2.7	2.7
A5	28.3	3.44	0.8	1.9	5.0	7.8	9.4	7.8	2.2	2.2
A4	23.3	3.51	0.8	1.9	6.1	7.7	8.6	7.8	2.3	2.3
A3	18.3	3.52	0.8	1.8	6.9	7.8	8.1	7.6	2.4	2.4
A2	13.3	3.50	0.8	1.8	5.9	7.5	8.2	7.3	2.4	2.4
A1	8.3	3.49	0.8	2.0	3.7	6.2	7.3	5.7	2.3	2.3
Cr (r_i=5.0)	0.0		0.7	1.5	4.6	6.7	8.0	6.7	2.0	2.0
B1	8.4	3.56	0.8	1.9	3.7	6.3	7.6	6.0	2.1	2.1
B2	13.4	3.60	0.8	1.8	7.4	9.3	10.0	9.1	2.3	2.3
B3	18.5	3.62	0.8	1.8	8.3	9.2	9.4	9.2	2.8	2.8
B4	23.7	3.60	0.8	1.8	8.5	9.3	10.0	10.0	2.3	2.3
B5	28.7	3.54	0.8	1.8	7.9	9.0	9.1	9.2	2.2	2.2
B6	33.8	3.56	0.8	1.8	4.3	6.5	10.8	6.6	1.7	1.7
B7	39.2	3.58	1.0	2.2	5.0	6.0	6.7	6.3	2.0	2.0

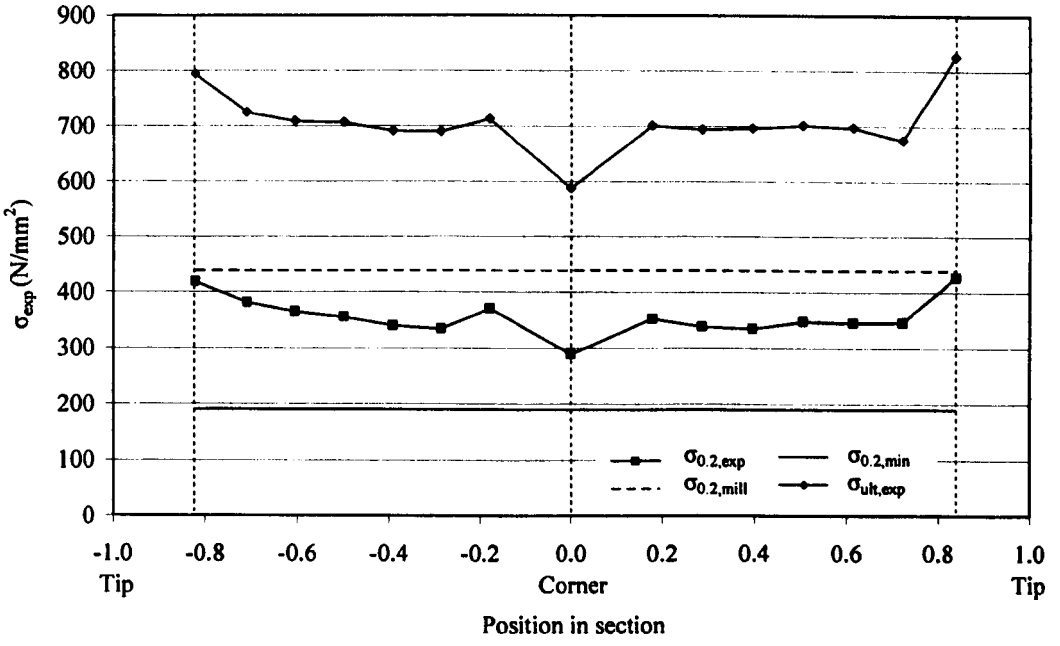

Figure 6.25: *0.2% proof stress $\sigma_{0.2,exp}$ and ultimate stress $\sigma_{ult,exp}$ around HR 50×50×3 ($\sigma_{0.2,mill}$ = 439 N/mm² and $\sigma_{0.2,min}$ = 190 N/mm²)*

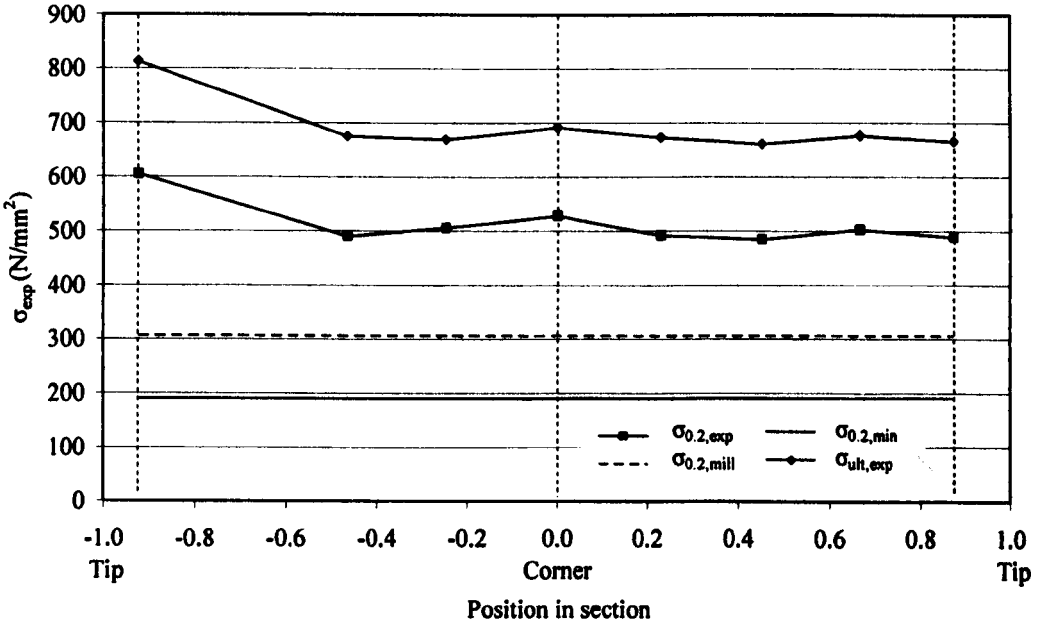

Figure 6.26: *0.2% proof stress $\sigma_{0.2,exp}$ and ultimate stress $\sigma_{ult,exp}$ around HR 50×50×5 ($\sigma_{0.2,mill}$ = 306 N/mm² and $\sigma_{0.2,min}$ = 190 N/mm²)*

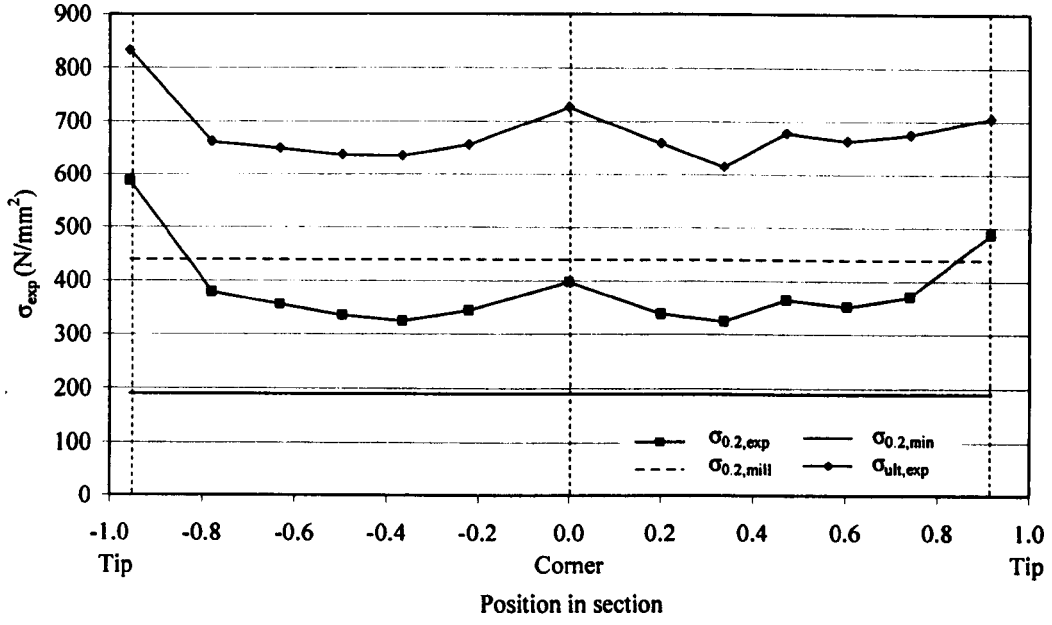

Figure 6.27: *0.2% proof stress $\sigma_{0.2,exp}$ and ultimate stress $\sigma_{ult,exp}$ around HR 50×50×6 ($\sigma_{0.2,mill}$ = 439 N/mm^2 and $\sigma_{0.2,min}$ = 190 N/mm^2)*

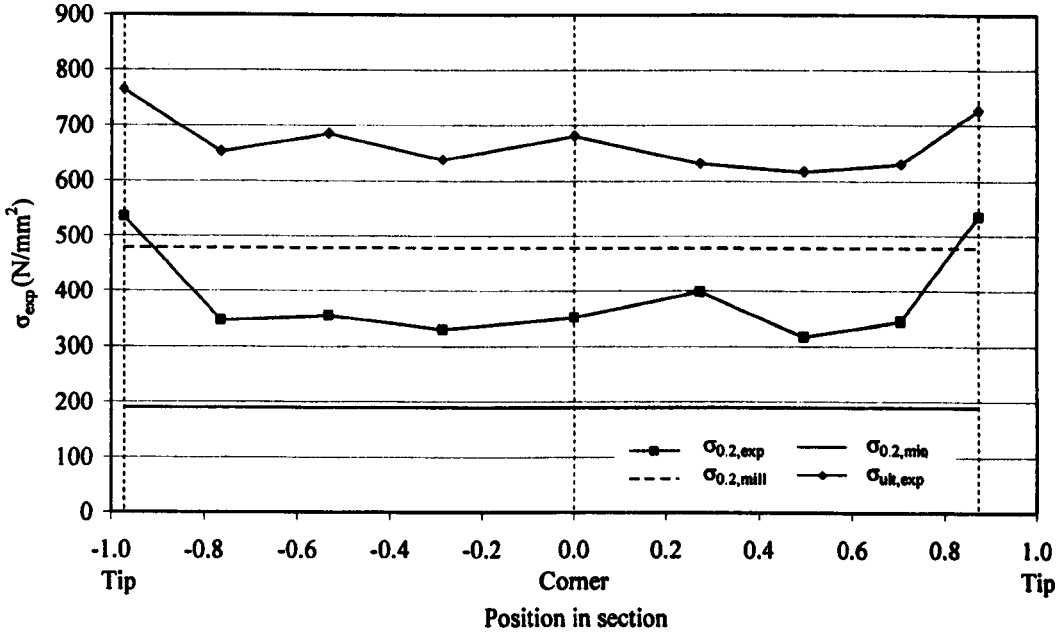

Figure 6.28: *0.2% proof stress $\sigma_{0.2,exp}$ and ultimate stress $\sigma_{ult,exp}$ around HR 50×50×10 ($\sigma_{0.2,mill}$ = 478 N/mm^2 and $\sigma_{0.2,min}$ = 190 N/mm^2)*

6.4 Hardness tests

6.4.1 Introduction

Hardness measurements have frequently been used in the manufacturing industry to give an estimate of the yield strength in metals. Since the area of specimen required to perform a hardness test is often very small compared to the specimen size, a finer resolution of measurements than was possible from tensile coupon tests can therefore be attained. The relationship between hardness and strength in stainless steel requires a more thorough investigation, which is not within the scope of this research. This section however details hardness measurements made on two types of cold formed sections: four press braked angles and five cold rolled box sections, specifically to identify the extent of cold working beyond the corner regions of both types of sections.

6.4.2 Literature review

The use of hardness tests to predict material strength has developed as, depending on the size of the component, hardness tests can be considered non-destructive compared to performing tensile coupon tests. Other advantages are that hardness tests are quick and require only small test pieces and minimal preparation. Relationships between hardness and material yield strength, and hardness and ultimate strength have been established for many metals. A relationship for carbon steel is presented in the American Society for Metals, Metals Handbook Vol. 11 (ASM, 1976).

There are three principal methods for measuring hardness, the Brinell, Rockwell and Vickers test. The Vickers microhardness tests employed in this study use a pyramidal indenter to create diamond shaped indents in the sample surfaces as is shown in Figures 6.31-6.33. The force, F with which indents are made and the area of the indent A can be used to calculate the Vickers hardness value, HV which is proportional to the pressure (F/A) applied to the test piece. Equation 6.2 defines the Vicker hardness where k is a constant of proportionality. The area of indent A is defined by Equation 6.3, where l_{av} is the average length of the indent's diagonals, l_1 and l_2 in millimetres and α is the internal angle of the indenter.

$$HV = k\frac{F}{A} = 0.102\left(\frac{2F\sin\left(\frac{\alpha}{2}\right)}{l_{av}^{\,2}}\right) \qquad (6.2)$$

$$A = \frac{l_{av}^{\ 2}}{2\sin\left(\frac{\alpha}{2}\right)} \tag{6.3}$$

An analytical relationship between hardness and yield strength for all metals was established by Tabor (1951), where a linear correlation between the pressure caused by the indenter and the yield strength of the test piece is established. Hardness and material strength relationships have also been developed for specific metals, such as different phase structures of carbon steel (Umemoto et al., 2001), die cast magnesium alloys (Cáceres et al., 2005) and reinforced aluminium alloys (Kozola and Shen, 2003).

Macdonald et al. (1998) used the Vickers hardness tests and Tabor's conversion expression to determine the extent of cold work in press braked carbon steel sections with internal angles of 90° and 135°. The highest hardness values were obtained in the quarter arc corners and the values decreased in the adjacent section face over 2-3 mm. It was commented that a degree of scatter was observed and that predictions of the yield strength were not very accurate. Whilst a hardness value may not be a precise indicator of the yield strength, the relationship gives a qualitative indication of the variation of yield strength in the sections tested. The measurements made by Macdonald et al. (1998) were taken along the mid thickness of the sections, in addition some measurements were made across the thickness of the material, where higher hardness values were observed on the extreme fibres of the section material thickness.

6.4.3 Experimental testing

Vickers hardness tests were carried out on nine cold formed stainless steel samples in order to establish a relationship between hardness values and 0.2% proof stress, to predict the variation of material strength in the corners regions of the sections.

6.4.3.1 Sample preparation

30 mm long samples were cut from each of the nine specimens as shown in Figure 6.29. The samples were cut a distance away from either end of the specimens to ensure the samples were representative of the majority of the whole specimen. For each sample the section faces were milled to be parallel to each other and then polished to obtain a good surface finish on which to perform the hardness tests. The polishing was carried out on rotating plates saturated with water and covered with wet micro grit sand paper of increasing fineness (P600 to P1200).

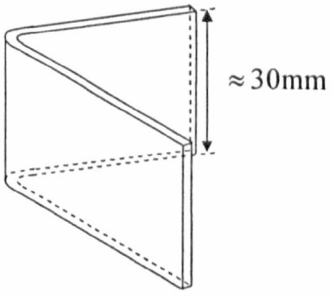

Figure 6.29: *Press braked sample*

Owing to size of the micro-hardness clamping bed the cold rolled box samples were cut into four pieces for the 100×50 sections and six pieces for the 100×100 sections (see Figure 6.30). The 50×50 press braked angles had to be mounted on the testing bed with their flanges held at 45° so that the samples did not have to be cut into smaller pieces or re-clamped between individual hardness measurements.

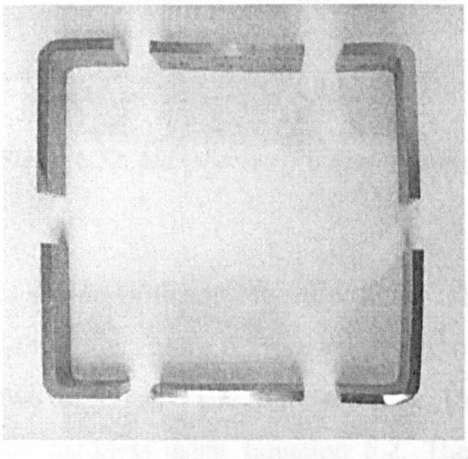

Figure 6.30: *Cold rolled samples*

6.4.3.2 Hardness testing

Vickers microhardness tests were carried out in accordance with EN ISO 6507-1 (2005) at different positions along the section at the mid thickness of the cold formed stainless steel specimens. The microhardness testing machine used a pyramidal indenter with an internal angle α of 136° which was set up to strike the specimen with a force of 500g N (Figure 6.31). The

resulting indent created in the specimen during the test is viewed on plan (Figure 6.32) as a diamond shape.

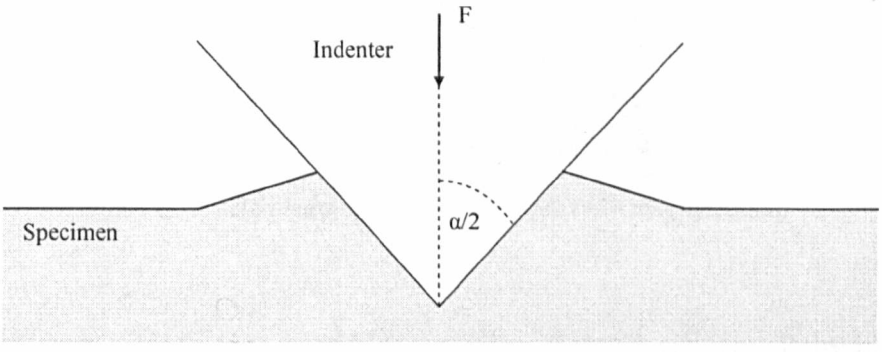

Figure 6.31: *Microhardness indenter (in section)*

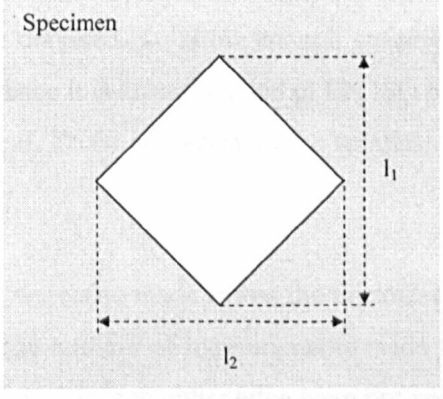

Figure 6.32: *Microhardness indent (in plan)*

The indent was photographed at a magnification factor of 40 by the camera in the micro testing machine, such as the image shown in Figure 6.33, and relayed to a computer where software automatically measured the two diagonals l_1 and l_2 of the indent. The average of l_1 and l_2, l_{av} was used to calculate the Vickers hardness using Equation 6.2. The microhardness testing bed clamped the samples securely and screw threads allowed the precise repositioning for the next hardness test without having to re-clamping the sample.

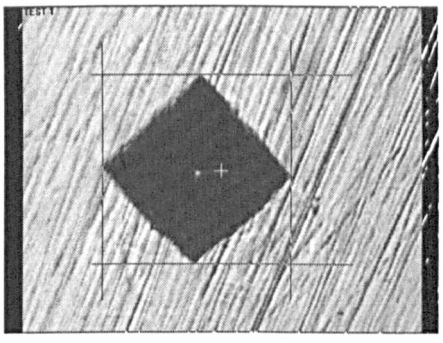

Figure 6.33: *Microhardness indent in sample (40× magnification)*

Measurements were made to correspond to the positions of tensile coupons discussed in Section 6.3, in order to establish a relationship between the Vickers hardness value HV and the 0.2% proof stress $\sigma_{0.2,exp}$. In the corner regions the resolution to which the measurements were made was as fine as possible so that a qualitative pattern for the variation of the 0.2% proof stress $\sigma_{0.2,exp}$ in this region could be obtained. To allow enough spacing between adjacent indents in order to eliminate any interference it is recommended in EN ISO 6507-1 (2005) that the spacing is 3 times the size of the indent. To be conservative the smallest interval between indents was adopted as 1.5 mm.

Some hardness measurements were also made across the thickness of the section to observe any through thickness variation. The number of measurements made through the section thickness was limited as measurements very close to either edge were not possible.

6.4.4 Results

The complete set of hardness values from measurements made on the nine samples are given in Appendix A whilst two sets of data, one for the press braked angle PB 50×50×2 (r_i=3.5) and one for the cold rolled box section CR 100×50×4 are presented in Tables 6.7 and 6.8-6.11 respectively. The hardness data from all sections are related to the positions of the tensile coupons, shown for each example section in Tables 6.7-6.11 by the coupon identity codes. An average hardness value HV_{av} was obtained for each corresponding tensile coupon. Plotting this average hardness HV_{av} against the 0.2% proof stress $\sigma_{0.2,exp}$ obtained from the tensile coupon test, a proportional relationship as described by Tabor (1951), can be defined as shown in Figure 6.34 and given by Equation 6.4.

$$\bar{\sigma}_{0.2,exp} = 2.01 HV_{av} \tag{6.4}$$

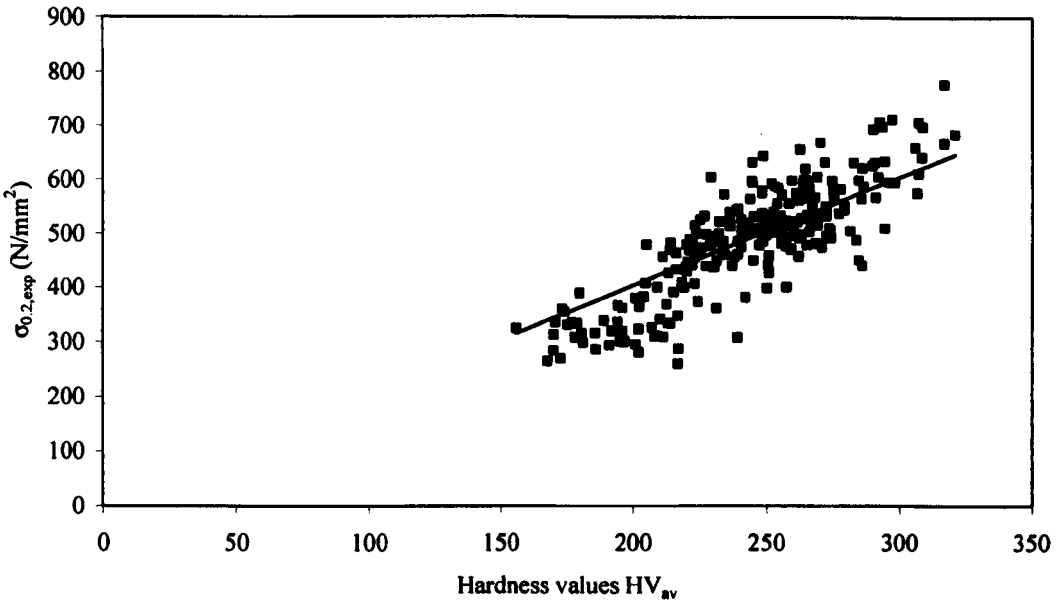

Figure 6.34: *Correlation of 0.2% proof stress $\sigma_{0.2,exp}$ with corresponding average hardness value HV_{av}*

Using this expression, a predicted value of the 0.2% proof stress $\overline{\sigma}_{0.2,exp}$ can be obtained for the individual hardness values HV. The scatter observed in the correlation shown in Figure 6.34 may be due to an observed variation of hardness through the thickness of the section material. Both Figures 6.35 and 6.36 show the significance of this variation by plotting the predicted 0.2% proof stress $\overline{\sigma}_{0.2,exp}$ over the normalised section thickness position for different section thicknesses. The measurements presented in Figures 6.35 were taken from material in the face of a cold rolled section and the measurements shown in Figure 6.35 were taken from corner material in a cold rolled section. An increase in the predicted 0.2% proof stress towards the outer fibres from values at the centre of the material thickness can be seen (as noted by Macdonald et al., 1998). This increase can be greater than 100 N/mm^2 and so any movement away from the mid thickness occurring during testing would greatly contribute to the scatter of the hardness values. A further reason for the scatter may be due to the anisotropic material properties of the section material sometimes causing significant differences to exist between the length of the indent's diagonals l_1 and l_2.

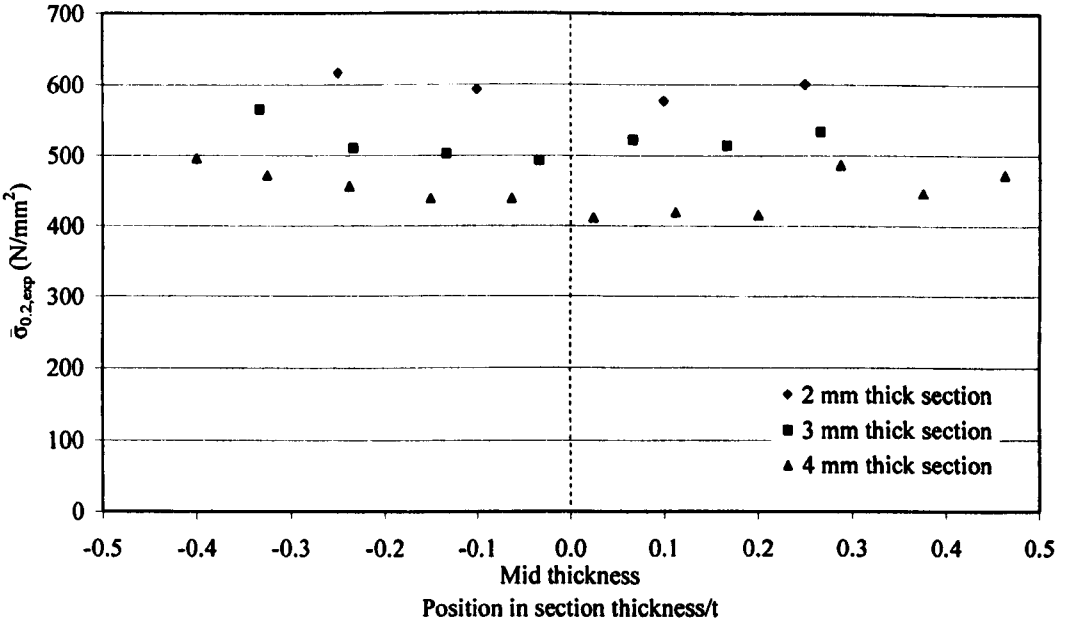

Figure 6.35: *The variation of the predicted 0.2% proof stress $\bar{\sigma}_{0.2,exp}$ through the section thickness for material in a cold rolled box face*

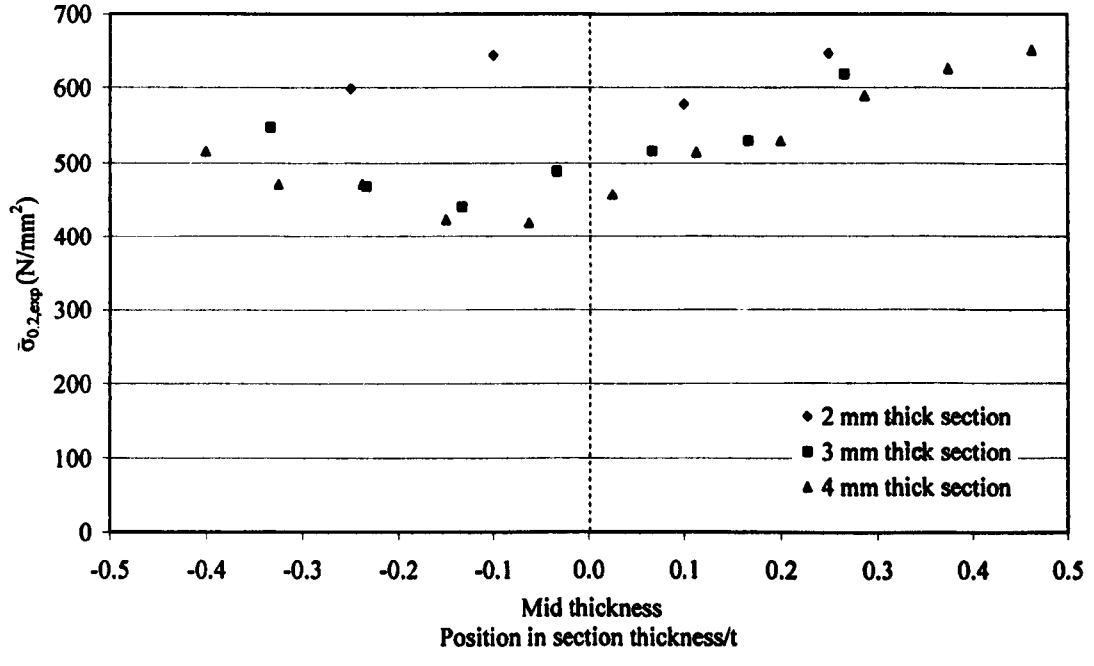

Figure 6.36: *The variation of the predicted 0.2% proof stress $\bar{\sigma}_{0.2,exp}$ through the section thickness for material in a cold rolled box corner*

Tables 6.7 and 6.8-6.11 show the predicted 0.2% proof stress value $\overline{\sigma}_{0.2,exp}$ for locations around the press braked angle PB 50×50×2 (r_i=3.5) and the cold rolled box section CR 100×50×4 respectively, and Figures 6.37-6.45 show the predicted 0.2% proof stress $\overline{\sigma}_{0.2,exp}$ plotted against the normalised section position for all the tested press braked and cold rolled samples. The corresponding measured 0.2% proof stress obtained from tensile coupons are plotted on the same axis as a line indicating the normalised width of the coupons and therefore the region over which the measured 0.2% proof stress $\sigma_{0.2,exp}$ were obtained. In general, whilst the predicted values $\overline{\sigma}_{0.2,exp}$ are not precise, the variation corresponds well to that observed in the measured 0.2% proof stress $\sigma_{0.2,exp}$.

Table 6.7: *Hardness values HV and predicted 0.2% proof stress* $\overline{\sigma}_{0.2,exp}$ *for PB 50×50×2* (r_i=3.5)

PB 50×50×2 (r_i=3.5)	*Section position (mm)*	*HV*	$\overline{\sigma}_{0.2,exp}$ *(N/mm²)*
A7	0.92	186	375
A6	0.80	175	354
A5	0.67	181	366
A4	0.55	181	365
A3	0.42	156	315
A2	0.29	167	337
	0.22	174	351
A1	0.19	166	336
	0.16	172	347
	0.13	177	357
	0.09	194	392
Cr	0.06	227	459
	0.03	213	429
	0.00	210	424
	0.03	188	380
	0.06	180	363
	0.09	203	410
B1	0.12	178	359
	0.15	177	357
	0.18	166	336
B2	0.22	162	326
	0.28	180	364
B3	0.40	179	362
B4	0.52	178	360
B5	0.65	173	349
B6	0.77	170	344
B7	0.86	174	352

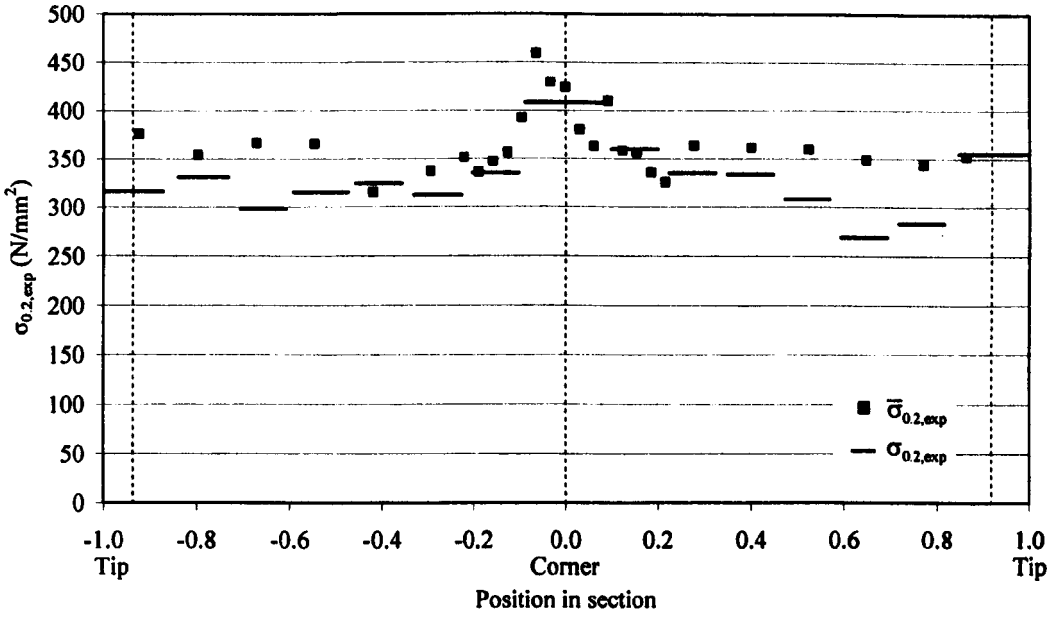

Figure 6.37 *Predicted 0.2% proof stress $\bar{\sigma}_{0.2,exp}$ and measured 0.2% proof stress $\sigma_{0.2,exp}$ around PB 50×50×2 (r_i=3.5)*

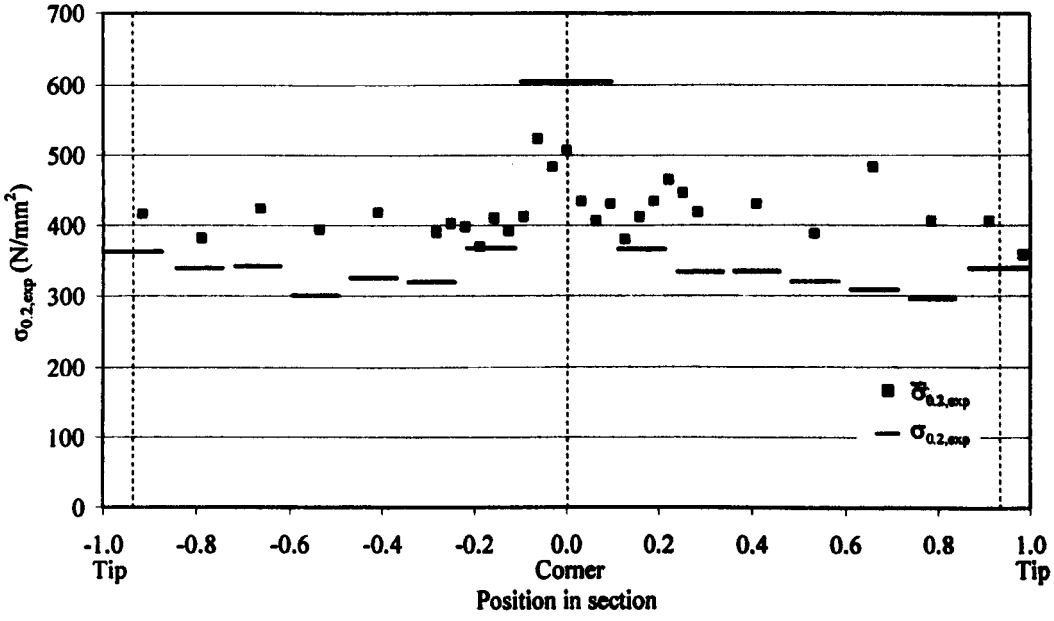

Figure 6.38: *Predicted 0.2% proof stress $\bar{\sigma}_{0.2,exp}$ and measured 0.2% proof stress $\sigma_{0.2,exp}$ around PB2 50×50×3 (r_i=3.2)*

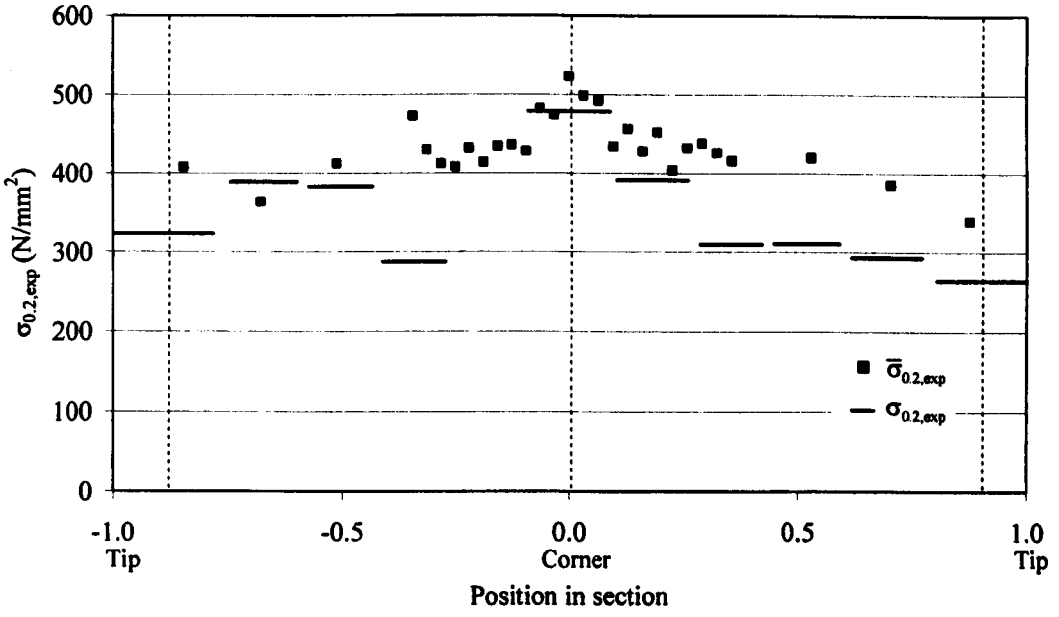

Figure 6.39 *Predicted 0.2% proof stress* $\bar{\sigma}_{0.2,exp}$ *and measured 0.2% proof stress* $\sigma_{0.2,exp}$ *around PB 50×50×4* (r_i*=3.5)*

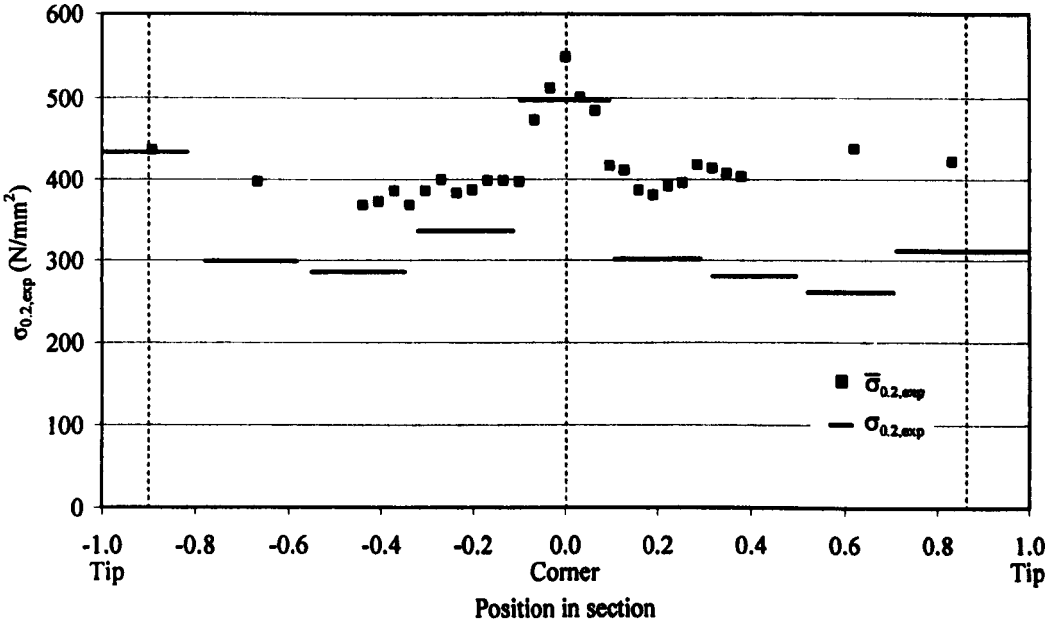

Figure 6.40: *Predicted 0.2% proof stress* $\bar{\sigma}_{0.2,exp}$ *and measured 0.2% proof stress* $\sigma_{0.2,exp}$ *around PB 50×50×5* (r_i*=3.5)*

Table 6.8: *Hardness values HV and predicted 0.2% proof stress* $\overline{\sigma}_{0.2,exp}$ *for CR 100×50×4 Face A*

CR 100×50×4	*Section position (mm)*	*HV*	$\overline{\sigma}_{0.2,exp}$ *(N/mm²)*
Cr4	0.00	255	516
	0.02	295	595
	0.03	328	663
A1	0.05	336	679
	0.06	316	639
	0.08	298	602
	0.10	296	597
	0.11	282	570
A2	0.13	275	555
	0.14	269	543
	0.16	254	512
A3	0.23	248	501
A4	0.30	253	510
A5	0.36	267	539
A6	0.43	250	505
A7	0.50	274	553
	0.50	270	545
A8	0.57	294	594
A9	0.64	265	535
A10	0.70	261	527
A11	0.77	253	511
A12	0.84	283	572
	0.86	282	570
	0.87	279	564
	0.89	299	604
A13	0.90	316	638
	0.92	321	648
	0.94	324	654
	0.95	323	652
Cr1	0.97	336	679
	0.98	314	634
	1.00	268	541

Table 6.9: *Hardness values HV and predicted 0.2% proof stress* $\overline{\sigma}_{0.2,exp}$ *for CR 100×50×4 Face B*

CR 100×50×4	*Section position (mm)*	*HV*	$\overline{\sigma}_{0.2,exp}$ *(N/mm²)*
Cr1	0.00	268	541
	0.03	275	556
	0.07	321	648
B1	0.10	348	703
	0.14	316	638
	0.17	311	628
	0.20	311	628
	0.24	256	517
	0.27	287	580
B2	0.31	267	539
	0.34	298	602
B3	0.50	306	618
	0.50	308	621
B5	0.66	281	568
	0.69	306	619
	0.73	325	657
	0.76	319	644
B6	0.80	289	583
	0.83	314	634
	0.86	332	671
	0.90	318	641
	0.93	331	668
Cr2	0.97	314	634
	1.00	296	597

Table 6.10: *Hardness values HV and predicted 0.2% proof stress* $\overline{\sigma}_{0.2,exp}$ *for CR 100×50×4 Face C*

CR 100×50×4	*Section position (mm)*	*HV*	$\overline{\sigma}_{0.2,exp}$ *(N/mm²)*
Cr2	0.00	296	597
	0.02	268	541
C1	0.03	327	660
	0.05	318	641
	0.06	335	676
	0.08	315	636
	0.10	309	624
C2	0.11	311	629
	0.13	280	566
	0.14	266	537
	0.16	280	566
C3	0.23	268	541
C4	0.30	277	559
C5	0.36	269	543
C6	0.42	270	545
C7	0.50	274	553
	0.50	259	523
C8	0.58	269	543
C9	0.64	267	539
C10	0.70	279	564
C11	0.77	264	533
C12	0.84	269	543
	0.86	280	566
C13	0.87	284	574
	0.89	289	583
	0.90	311	629
	0.92	318	641
	0.94	332	671
	0.95	331	668
	0.97	339	685
Cr3	0.98	315	636
	1.00	265	535

Table 6.11: *Hardness values HV and predicted 0.2% proof stress* $\overline{\sigma}_{0.2,exp}$ *for CR 100×50×4 Face D*

CR 100×50×4	*Section position (mm)*	*HV*	$\overline{\sigma}_{0.2,exp}$ *(N/mm²)*
Cr3	0.00	265	535
	0.03	289	583
	0.07	319	644
D1	0.10	319	644
	0.14	306	619
	0.17	293	592
	0.20	297	600
	0.24	277	560
	0.27	279	564
	0.31	257	520
D2	0.34	269	543
D3	0.50	250	505
	0.50	247	499
D5	0.66	245	494
	0.69	263	531
	0.73	268	541
	0.76	279	564
D6	0.80	275	555
	0.83	281	568
	0.86	314	634
	0.90	289	583
	0.93	348	702
	0.97	247	499
Cr4	1.00	255	516

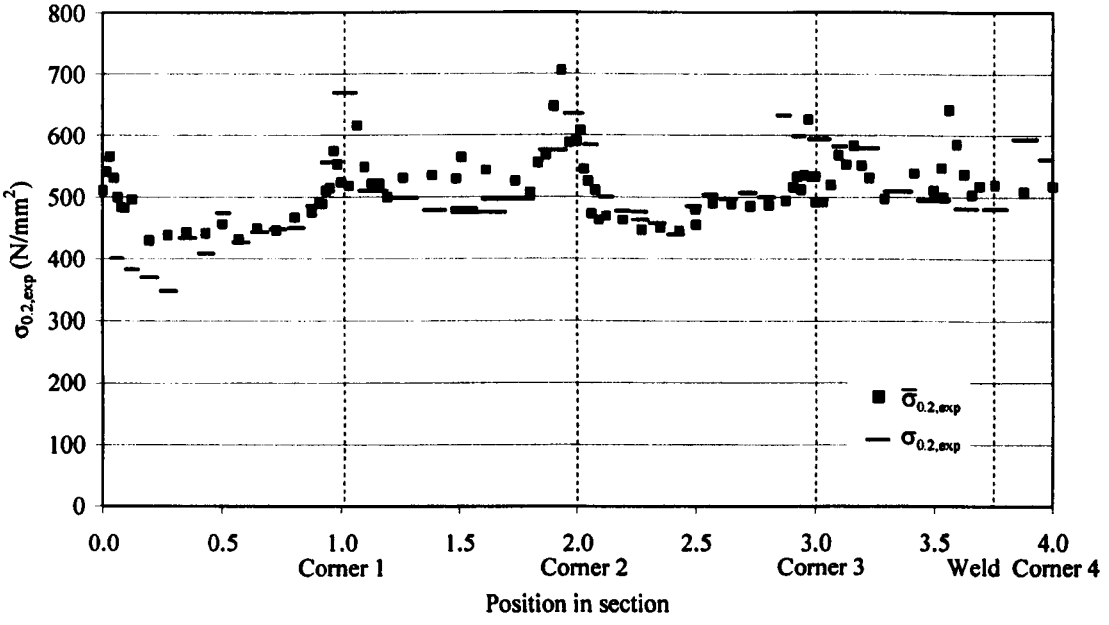

Figure 6.41: *Predicted 0.2% proof stress $\overline{\sigma}_{0.2,exp}$ and measured 0.2% proof stress $\sigma_{0.2,exp}$ around CR 100×50×2*

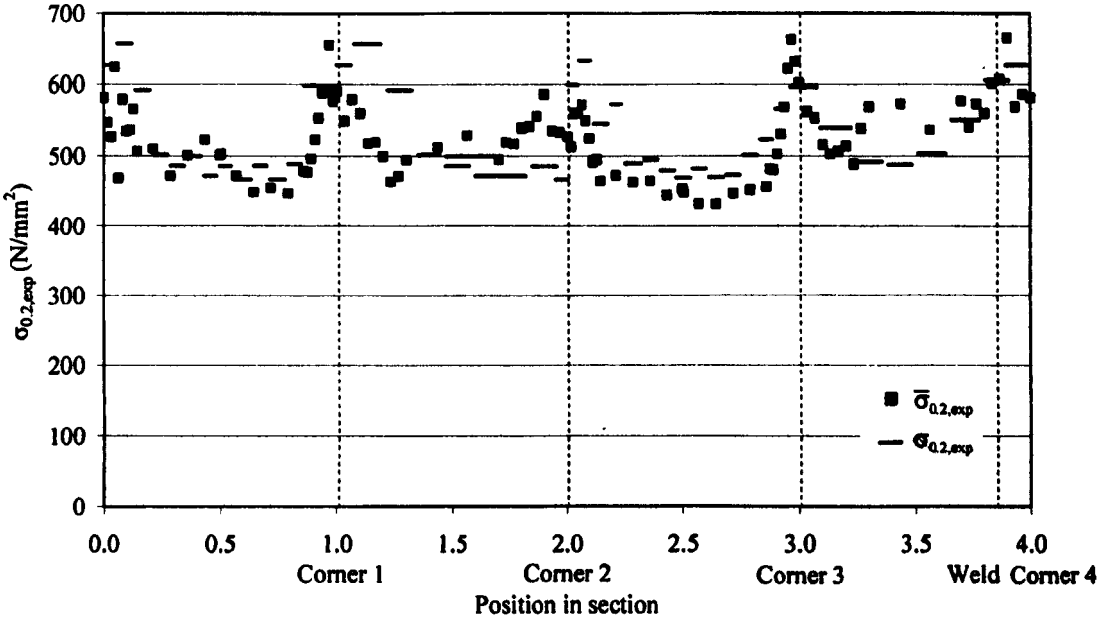

Figure 6.42: *Predicted 0.2% proof stress $\overline{\sigma}_{0.2,exp}$ and measured 0.2% proof stress $\sigma_{0.2,exp}$ around CR 100×50×3*

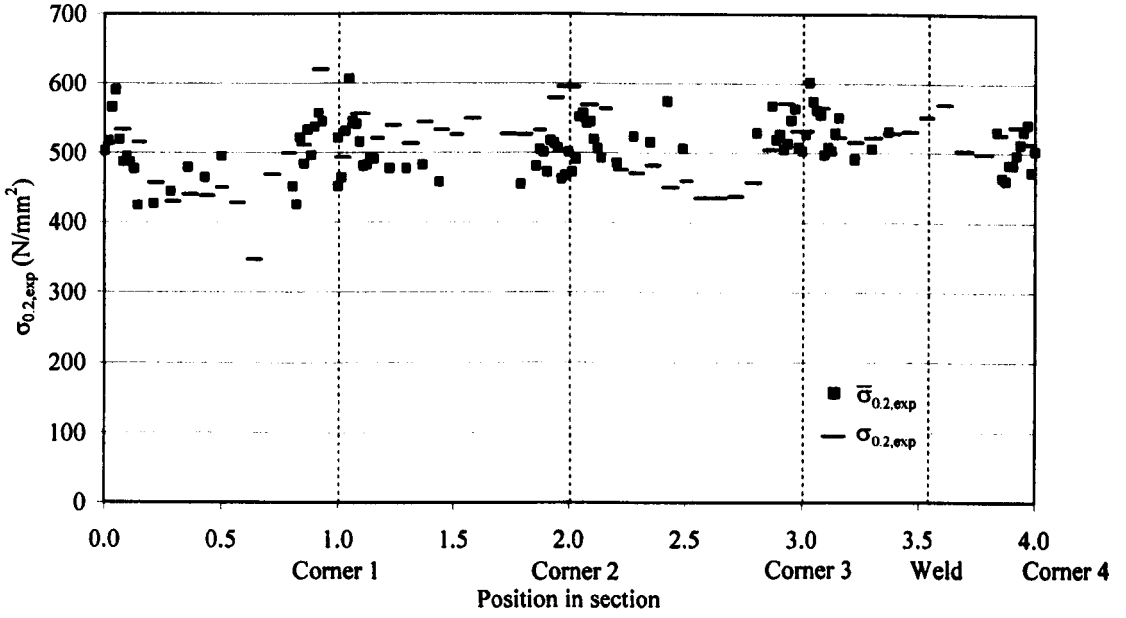

Figure 6.43: *Predicted 0.2% proof stress* $\bar{\sigma}_{0.2,exp}$ *and measured 0.2% proof stress* $\sigma_{0.2,exp}$ *around CR 100×100×3*

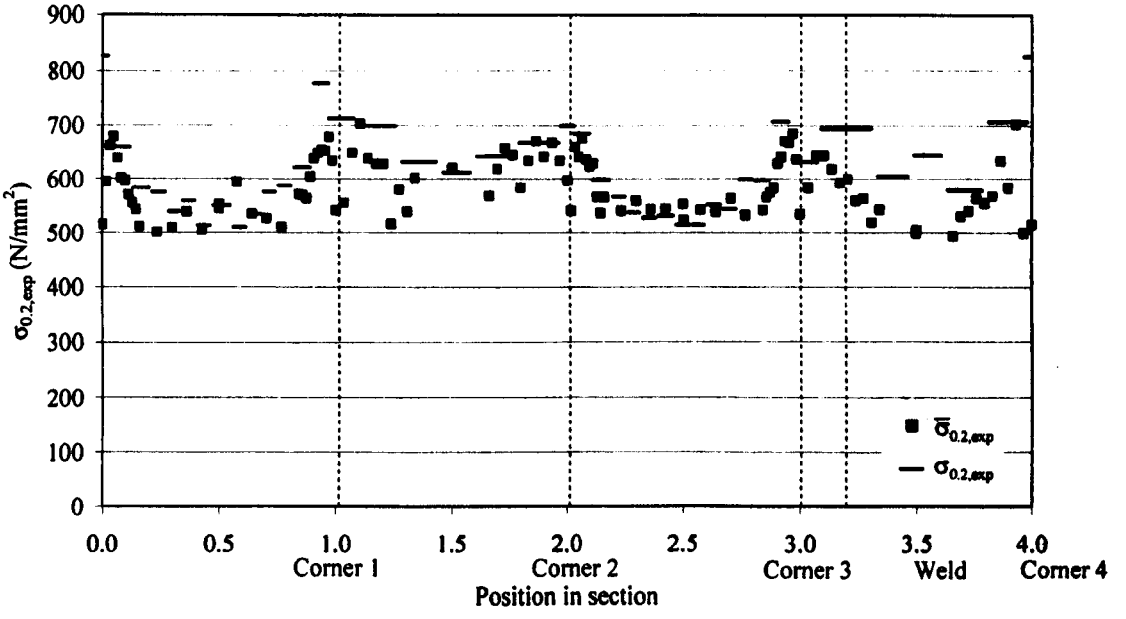

Figure 6.44: *Predicted 0.2% proof stress* $\bar{\sigma}_{0.2,exp}$ *and measured 0.2% proof stress* $\sigma_{0.2,exp}$ *around CR 100×50×4*

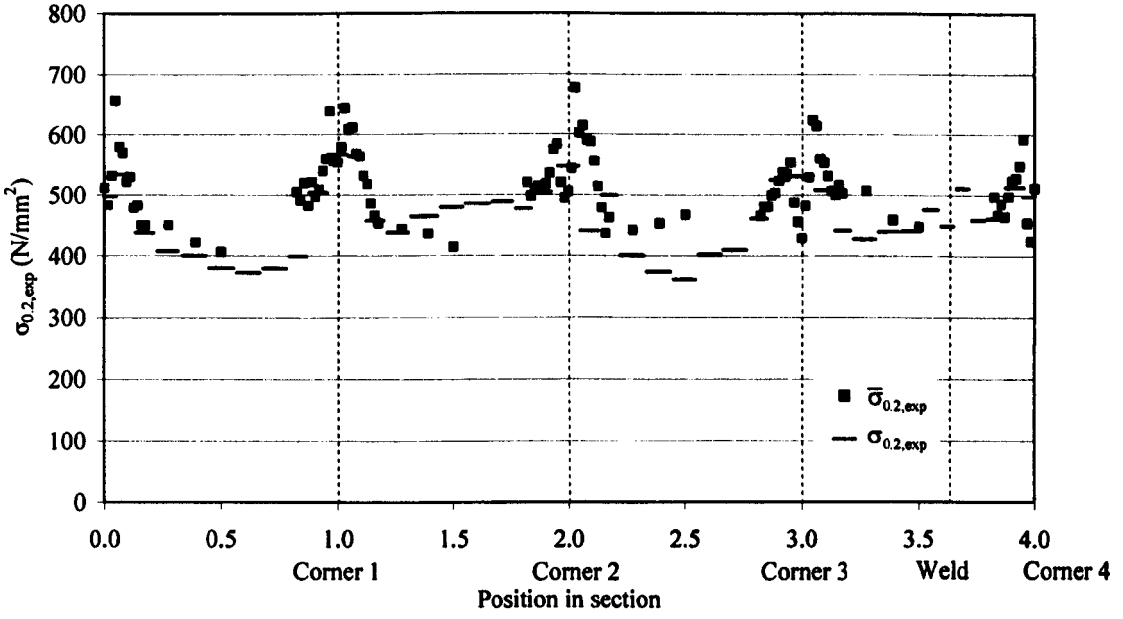

Figure 6.45: *Predicted 0.2% proof stress $\bar{\sigma}_{0.2,exp}$ and measured 0.2% proof stress $\sigma_{0.2,exp}$ around CR 100×100×4*

6.5 Corner forming

6.5.1 Introduction

Previous research into the influence of the forming processes on material strength has focused on quantifying the large plastic strains caused by forming the corner regions and harnessing the resulting significant strength increases. These strength enhancements are particularly advantageous when the structural members are in bending, since the higher strength material is generally furthest from the neutral axis of the section.

The different methods of forming corners may create different strain patterns. For example, compared to air braking coin braking employs radial pressure on the sheet material to cause plastic deformation (Ingvarsson, 1979). However, existing strength enhancement models tend to provide universal models.

6.5.2 Strain in corner forming

Geometrically modelling the formation of a corner as the creation of a quarter arc from a flat sheet by bending alone leads to a maximum strain being created in the internal and external

extreme fibres ε_c stated by Equation 6.5 and illustrated in Figure 6.46. r_n is the radius to the neutral axis of the corner, which can be expressed as $r_n=r_i+t/2$, where r_i is the internal radius of the corner and t is the material thickness.

$$\varepsilon_c = \frac{r_n - r_i}{r_n} = \frac{r_i + \frac{t}{2} - r_i}{r_i + \frac{t}{2}} = \frac{t}{2\left(r_i + \frac{t}{2}\right)} = \frac{1}{2\frac{r_i}{t} + 1} \tag{6.5}$$

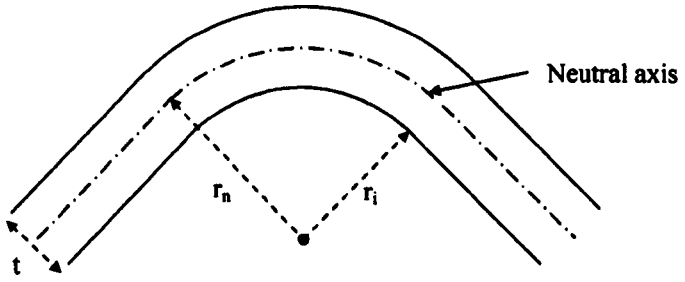

Figure 6.46: *Corner model assuming pure bending*

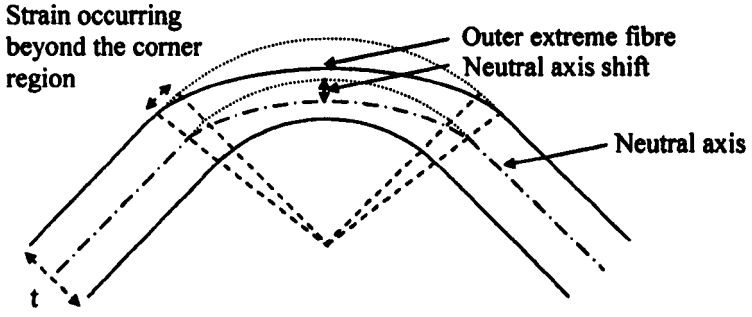

Figure 6.47: *Observed corner with a neutral axis shift*

During the formation of a corner, the material at the outer radius thins whereas the internal radius thickens. Karren (1967) and Weng and White (1990) experimentally showed that the formation of a radius therefore shifts the neutral axis from the mid thickness of the material towards the internal radius. Both experimental programs applied a grid of dots to the material prior to bending so that changes in strain could be measured; Weng and White (1990) also used post yield strain gauges. Weng and White's (1990) tests were carried out on air braked sections

and the specimens used by Karren were formed by: roll forming, air braking and coin braking. Figure 6.47 shows the geometrical difference between an assumed pure bending condition and the observed neutral axis shift. The reduction in thickness observed by Karren (1967) was between 0% to 3%, with the largest reduction caused by the smallest r_i/t ratio.

Roll forming software discussed by Halmos (2006) is used to predict the required size of blank sheet and the subsequent forming stages for a cross section. The software models the repositioned neutral axis assuming it is just confined to the corner radius as shown in Figure 6.48. k, shown in Figure 6.48, is the fraction of the material thickness that the repositionned neutral axis is from the internal radius. The expression used to define k given in Equation 6.6 is based on the internal radius to the sheet thickness ratio (r_i/t), the yield strength σ_y and ultimate strength σ_{ult} of the formed sheet material in ksi. Plotting the graph of k against the r_i/t ratio for a carbon steel of yield strength σ_y 275 N/mm^2 and ultimate strength σ_{ult} 430 N/mm^2 in Figure 6.49 it can be seen that the neutral axis approaches the mid thickness as k reaches 0.5 and the r_i/t ratio increases. When the r_i/t ratio is above ten, the neutral axis does not shift signifcantly from the mid thickness of the section so k can be approximated to be 0.5.

$$k = 0.567\frac{\frac{r_i}{t}+0.25}{1.2\frac{r_i}{t}+1}\left(1+\frac{\sigma_y^{2.5}}{250\sigma_{ult}^{1.41}}\right) \tag{6.6}$$

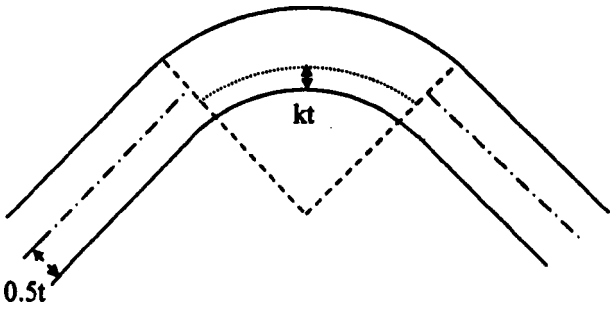

Figure 6.48: *Corner model with a neutral axis shift*

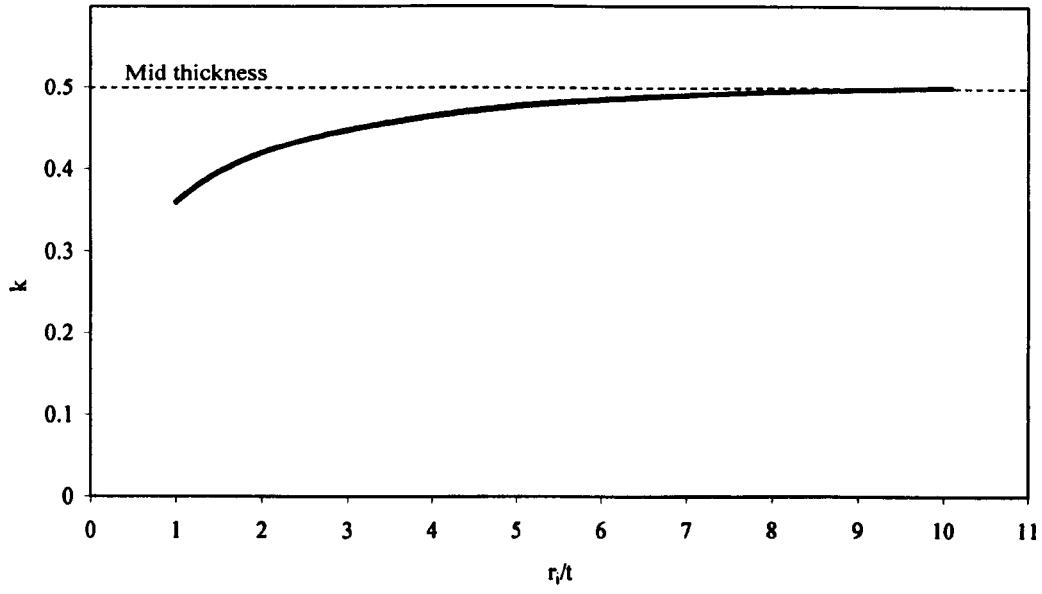

Figure 6.49: *Variation of k with internal radius to thickness ratio*

An empircal relationship given in Equation 6.7 was developed by Cook (1966) to determine the maximum strain ε_{max} in corner forming.

$$\varepsilon_{max} = \frac{1}{1.8\frac{r_i}{t} + 0.82} \tag{6.7}$$

An alternative expression (Equation 6.8) was given by Johnson and Mellor (1980) which is used for plates which have a width greater than ten times the thickness of the plate material and a corner angle greater than 70°. In both expressions the neutral axis is assummed to be offset towards the internal radius by around 5% of the material thickness.

$$\varepsilon_{max} = \frac{1}{1.8\frac{r_i}{t} + 1.00} \tag{6.8}$$

Figure 6.50 shows the maximum strains in the extreme fibres predicted by Cook (1966), Johnson and Mellor (1980) and the pure bending model (given in Equation 6.5) for different r_i/t ratios. The strain for all three models converge with no significant difference once the r_i/t ratio is above 4.

Equation 6.7 given by Cook (1966) is found to best fit the test results of Weng and White (1990) for corners of angle 90°. Whilst the current research focuses on corners of 90°, Weng and White (1990) measured strains on three different corner angles 90°, 120° and 150° and it is commented that the maximum strain would also depend the angle of the corner formed.

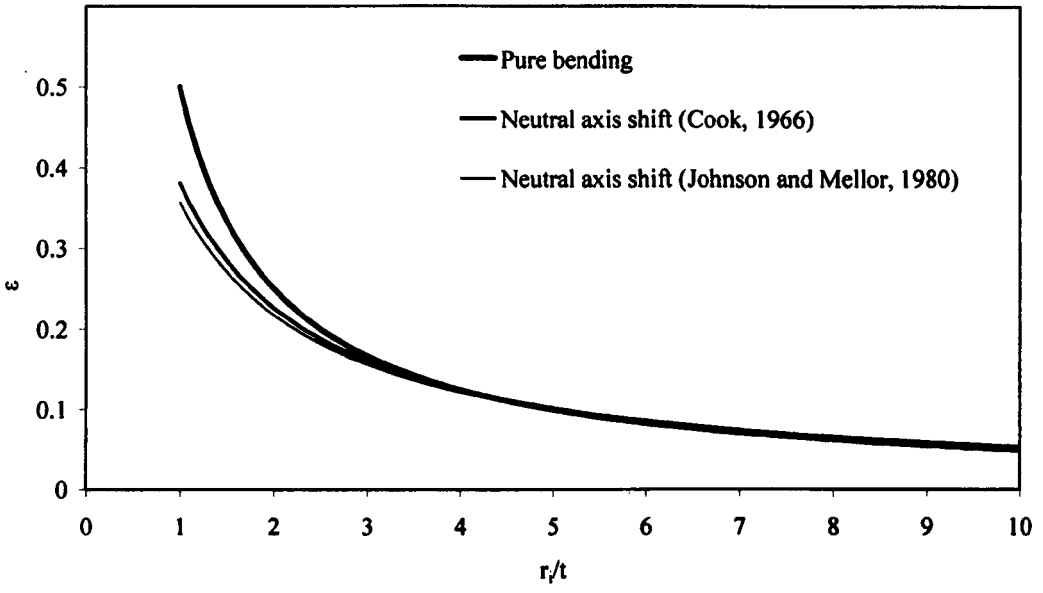

Figure 6.50: *Comparison of strain predicted by two empirical models with the pure bending model*

6.5.3 Extent of strain in corner forming

The shift of the neutral axis in the corner region is thought in reality to cause a gradual transition, shown in Figure 6.47, between the position of the neutral axis in the corner radius (modelled as a quarter arc) and the neutral axis at the mid thickness of the unformed regions in the section. Strain is therefore also experienced in the unformed section material in regions adjacent to the corner radius. Weng and White (1990) plot the change in strain against distance from the centre of the corner for the internal and external radius for air braked 1 inch thick carbon steel plates, showing the region of influence of corner forming to be approximately three times the material thickness beyond the external radius and about two and a half times the material thickness from the internal radius.

6.5.4 Strength enhancement in corner forming

Models for predicting increases in material strength were initially developed for carbon steel. EN 1993-1-3 (2006) allows such corner strength enhancements to be included for a fully effective section either by determining the strength increase from the basic material strength f_{yb} by experimentation or by using the expression given in Equation 6.9 to calculate an increased average section strength f_{ya}. Equation 6.10 gives a restriction to its application to ensure sufficient ductility.

$$f_{ya} = f_{yb} + (f_u - f_{yb})\frac{knt^2}{A_g} \tag{6.9}$$

Where:

$$f_{ya} \leq \frac{(f_u + f_{yb})}{2} \tag{6.10}$$

where: A_g is the gross-sectional area

k is a numerical coefficient that depends on the type of forming as follows:

7 for cold rolling

5 for other forming methods

n is the number of 90° bends in the cross- section with a internal radius of $r_i \leq 5t$ (fractions of 90° should be counted as fractions of n)

t is the design core thickness of the steel material before cold forming, exclusive of metal and organic coatings.

Karren (1967) developed two analytical models for predicting the strength increase caused during the corner forming process. Firstly a model assuming corners are formed through pure bending is given and secondly a model was proposed assuming that in addition to bending a uniform radial pressure is also experienced during forming. Comparing these models with tensile coupon data from coin braked, air braked, and cold rolled carbon steel samples the second relationship given in Equation 6.11, between the corner yield strength $\sigma_{y,c}$, the internal corner radius r_i of the bend created, and the thickness of the material t gave the best correlation with experimental results suggesting that radial pressures are experienced during all three corner forming processes.

$$\sigma_{y,c} = \frac{kB}{(r_i/t)^m} \tag{6.11}$$

The constant B in Equation 6.11 is modified to B_c to include the yield strength $\sigma_{y,v}$ of the unprocessed material in Equation 6.12. This equation is used as a design equation for cold formed sections.

$$\sigma_{y,c} = \frac{B_c \sigma_{y,v}}{(r_i/t)^m} \tag{6.12}$$

Van den Berg and van der Merwe (1992) used Karren's expression to predict the corner yield strength in stainless steel press braked samples and it was found that the expression gives a good approximation for different grades of stainless steel, although it was commented that further experimentation would be needed to confirm this for more strain hardened material. Van den Berg and van der Merwe (1992) proposed Equations 6.13 and 6.14 to define constants B_c and m, for use in Equation 6.12, where $\sigma_{ult,v}$ and $\sigma_{0.2,v}$ are the ultimate and 0.2% proof stress respectively of the unformed or virgin sheet material.

$$B_c = 3.289\frac{\sigma_{ult,v}}{\sigma_{0.2,v}} - 0.861\left(\frac{\sigma_{ult,v}}{\sigma_{0.2,v}}\right)^2 - 1.240 \tag{6.13}$$

$$m = 0.060\frac{\sigma_{ult,v}}{\sigma_{0.2,v}} + 0.031 \tag{6.14}$$

Based on tests using cold rolled box sections Gardner (2002) proposes a simpler relationship between the material properties of the formed corners versus the material properties of the flat section faces. Equation 6.15 gives a relationship between the ultimate strength $\sigma_{ult,f}$ of the flat material and the 0.2% proof stress, $\sigma_{0.2,c}$ of the corner regions.

$$\sigma_{0.2,cr,c} = 0.85\sigma_{ult,f} \tag{6.15}$$

By updating this analysis to include additional data from austenitic grade 1.4301 sections, Ashraf (2006) modified the coefficient used in Equation 6.15 from 0.85 to 0.82. Ashraf et al. (2005) proposed an alternative method to predict the 0.2% proof stress of the corners in both types of cold formed sections $\sigma_{0.2,c}$ (press braking and cold rolling). Two relationships were obtained from corner test data taken from cold formed sections. The first, Equation 6.16, used the 0.2% proof stress of the unprocessed material $\sigma_{0.2,v}$ and the internal radius and thickness ratio, r_i/t to predict the 0.2% proof stress of the corners in cold formed sections $\sigma_{0.2,c}$.

$$\sigma_{0.2,c} = \frac{1.881\sigma_{0.2,v}}{\left(\frac{r_i}{t}\right)^{0.194}} \tag{6.16}$$

The second expression, Equation 6.17 includes the ultimate stress of the unprocessed material $\sigma_{ult,v}$ and the internal radius and thickness ratio r_i/t.

$$\frac{\sigma_{0.2,c}}{\sigma_{ult,v}} = \frac{C_1}{\left(\frac{r_i}{t}\right)^{C_2}} \tag{6.17}$$

The values of C_1 and C_2 are defined in Equations 6.18 and 6.19 respectively.

$$C_1 = -0.382\left(\frac{\sigma_{ult,v}}{\sigma_{0.2,v}}\right) + 1.711 \tag{6.18}$$

$$C_2 = -0.176\left(\frac{\sigma_{ult,v}}{\sigma_{0.2,v}}\right) - 0.1496 \tag{6.19}$$

A third expression, Equation 6.20 was proposed by Ashraf et al. (2005) to predict the ultimate strength of the corners, $\sigma_{ult,c}$ using the 0.2% proof stress of the corner material, $\sigma_{0.2,c}$ and the 0.2% proof stress, $\sigma_{0.2,v}$ and the ultimate stress, $\sigma_{ult,v}$ of the unprocessed material.

$$\sigma_{u,c} = 0.75\sigma_{0.2,c}\left(\frac{\sigma_{ult,v}}{\sigma_{0.2,v}}\right) \tag{6.20}$$

6.5.5 Region of stress enhancement in corner forming

The shift in the neutral axis from the mid thickness of the section material in the corner radius gradually reduces moving away from the corner radius into the unformed sheet material. A corresponding strength increase in the material adjacent to the corner radius has been observed by experimental programs which have proposed the extent of this region, shown in Figure 6.51.

From Karren's test results on air braked, coin braked and cold rolled carbon steel corners it was proposed that the cold working due to press braking extends beyond the corner radius by about one to two times the material thickness. It is also noted that corners formed by press braking and cold rolling may experience different forming forces and so therefore cannot be assumed to exhibit identical regions that are influenced by cold work.

Abdel-Rahman and Sivakumaran (1997) found that cold working occurred in carbon steel sections in the region $\pi r_i /2$ beyond the corner radius. This increase in material strength was noted to be lower than the increase observed in the corners themselves.

The extent of cold working from the corner regions was investigated in stainless steel sections by Gardner and Nethercot (2004) where FE models of cold rolled stub columns were compared against experimental data. The FE models simulated the region of increase in strength due to corner forming firstly by assuming that the region of strength enhancement extended the material thickness t beyond the corner and secondly by assuming that the region extended 2t beyond the corner. It was shown that the FE stub column models with the enhanced corner properties extended 2t beyond the corner gave a better correlation with the experimental results.

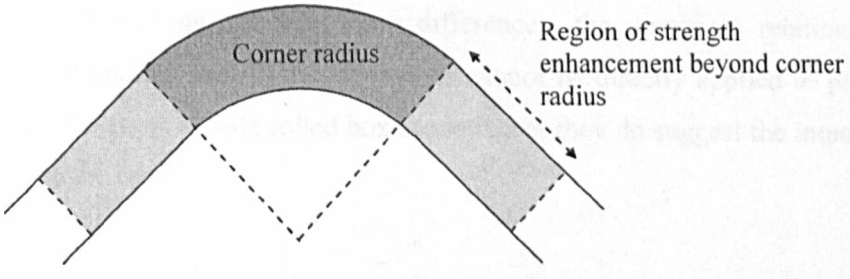

Figure 6.51: *Extent of strength enhancement beyond corner*

6.6 Modelling strength enhancements

6.6.1 Face forming

6.6.1.1 Introduction

The material in the flat face of sections constitutes the majority of the cross sectional area and therefore any strength increases to these regions will contribute substantially to the overall resistance of the section.

6.6.1.2 Face forming strain models

The flat faces of press braked sections do not undergo a shape change during forming and therefore no strength enhancements due to cold work are induced. During the formation of the flat faces in cold rolled box sections, as described in Chapter 2 a circular tube is initially created. In forming the radius of a circular tube, the strain is geometrically equivalent to (and one forming stage towards) creating a corner in a section (Figure 6.52). The strain expression in the subsequent crushing stage constitutes the reverse of corner forming. Despite the similarity between the two forming processes, the radius of the circular tube is of the order of ten times that of the corner region, and it can therefore be assumed that the neutral axis shift is less significant than in corner forming. Due to these differences, the empirical relationships developed to predict strength increases in corner regions cannot be directly applied to predict strength increases in the flat faces of cold rolled box sections, but they do suggest the important parameters that influence the case.

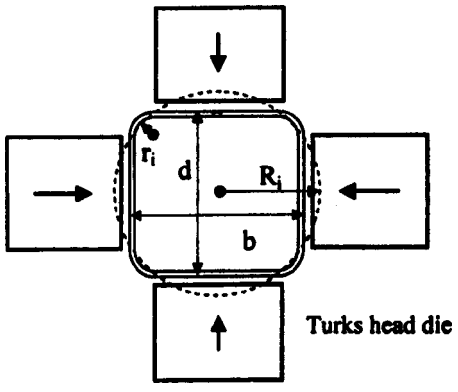

Figure 6.52: *Crushing a box section*

The radius of the circular tube R_i produced prior to crushing can be calculated using Equation 6.21 in terms of the thickness t, internal corner radius r_i and box dimensions b and d. Since the magnitude of R_i/t ratios are typically greater than 10, it has been assumed that the neutral axis remains at the mid thickness of the formed material. The corner radii are modelled as identical quarter arcs and the shift of the neutral axis for these corner regions is assumed to be negligible compared to the overall strain caused by forming the box section. Carrying forward these assumptions, the strain ε_f in forming one flat face from a circular tube, i.e. the region between the corners radii, is identical to the expression given in Equation 6.5, and can be written as Equation 6.22, replacing r_i for R_i and r_n with R_n. Since forming a circular tube from flat sheet and forming a box section's flat face from a circular tube cause the stainless steel sheet to experience the same magnitude of strain, the strain of just the last case has been considered.

$$R_i = \frac{b + d + (\pi - 4)r_i - 4t}{\pi} \tag{6.21}$$

$$\varepsilon_f = \frac{R_n - R_i}{R_n} = \frac{R_i + \frac{t}{2} - R_i}{R_i + \frac{t}{2}} = \frac{t}{2\left(R_i + \frac{t}{2}\right)} = \frac{1}{2\frac{R_i}{t} + 1} \tag{6.22}$$

The combination of Equation 6.21 and Equation 6.22 can be simplified to Equation 6.23. This simplification removes the necessity of knowing the corner radii (which is often not given in manufacturers' specifications) and introduces only small errors for practical section sizes.

$$\varepsilon_f = \frac{\pi t}{2(b + d)} \quad . \tag{6.23}$$

6.6.1.3 Face forming strength enhancement models

Data from tensile coupon tests performed as part of this research program have been combined with those from other research programs (Coetzee et al., 1990; Gardner, 2002; Gardner et al., 2006; Hyttinen, 1994; Talja and Salmi, 1995; Rasmussen and Hancock, 1993a; Ala-Outinen, 2005) and plotted in Figures 6.53 to 6.56. Figures 6.53 and 6.55 show the measured 0.2% proof stress $\sigma_{0.2,exp}$ normalised by values taken from the corresponding mill certifcate $\sigma_{0.2,mill}$ and plotted against the position along the section face normalised by the distance along the neutral axis between the centre points of the adjacent corner radii.

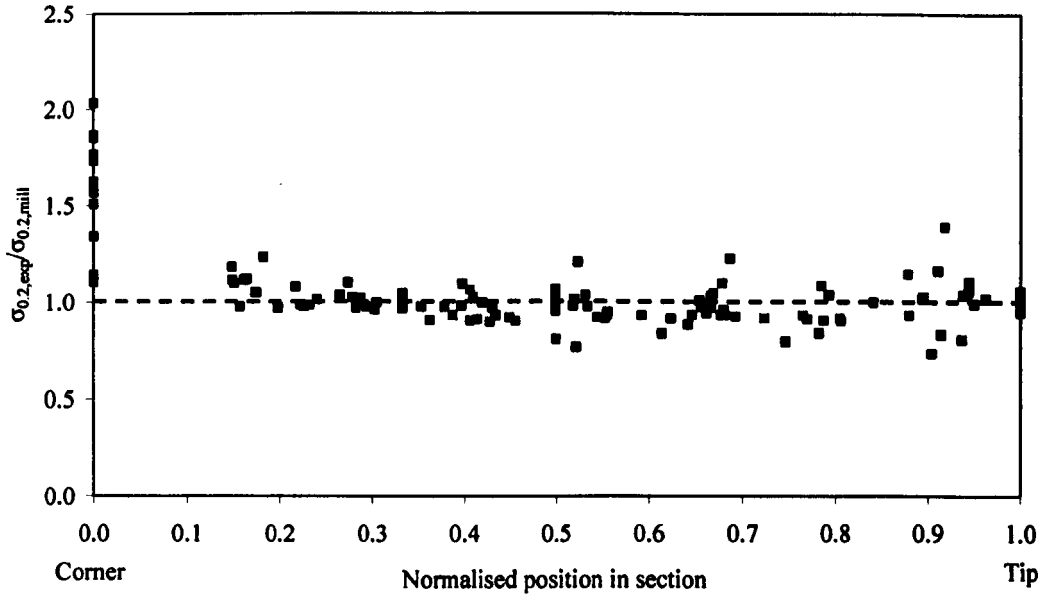

Figure 6.53: *0.2% proof stress $\sigma_{0.2,exp}$ normalised by the mill certificate value $\sigma_{0.2,mill}$ for section faces of press braked angles*

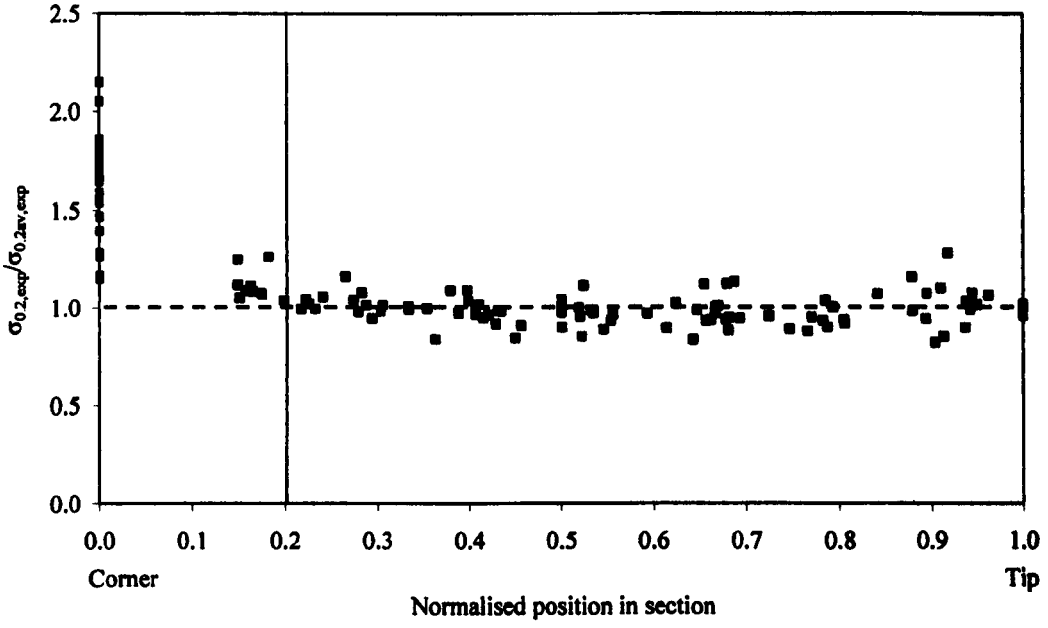

Figure 6.54: *0.2% proof stress $\sigma_{0.2,exp}$ normalised by average face data for section faces of press braked angles $\sigma_{0.2av,exp}$*

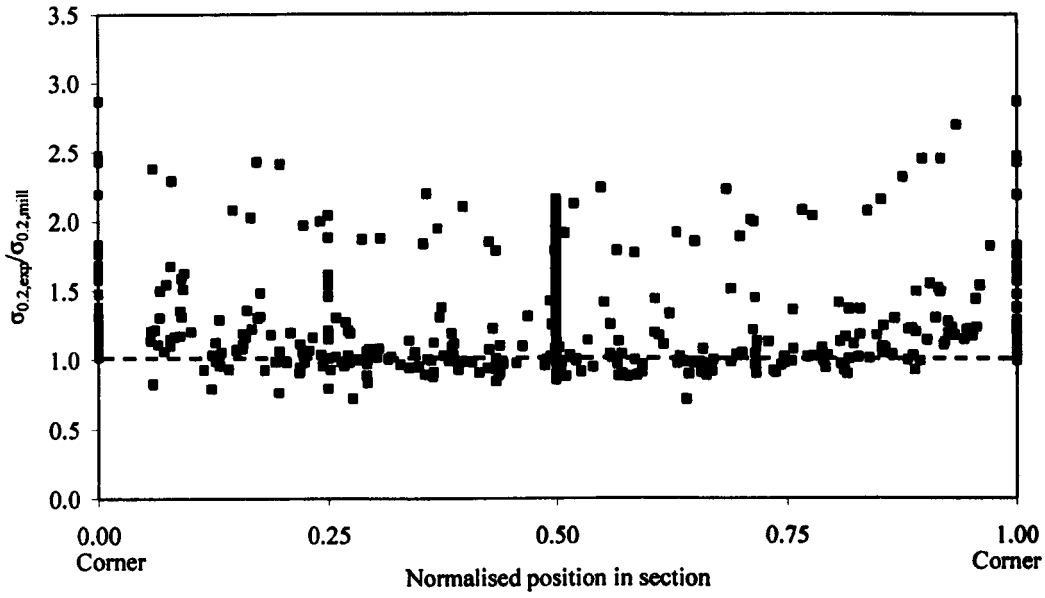

Figure 6.55: *0.2% proof stress $\sigma_{0.2,exp}$ normalised by the mill certificate value $\sigma_{0.2,mill}$ for section faces of cold rolled boxes*

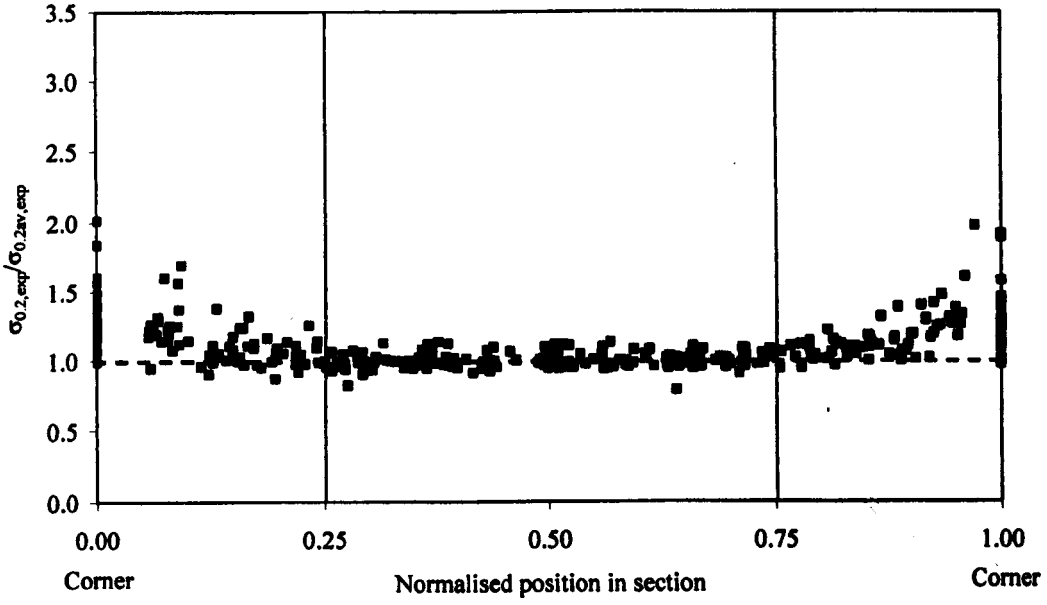

Figure 6.56: *0.2% proof stress $\sigma_{0.2,exp}$ normalised by average central 50% face data $\sigma_{0.2av,exp}$ for section faces of cold rolled boxes*

Figure 6.53 shows a clear increase in material strength in the corner radii of the press braked sections. In the flat regions of the section, the measured material strength accords well with the 0.2% proof stresses presented in the corresponding mill certifcate $\sigma_{0.2,mill}$, indicating that no strength enhancements have occurred during press braking. Figure 6.55 shows the distibution of material properties in the faces of cold rolled sections from the collated tensile coupon data. Substantial strength increases are again noted in the corner radii. However, in addition to this, strength increases up to 2.3 times the mill certifcate values $\sigma_{0.2,mill}$, may also been seen in the flat regions of the sections. This enhancement in material strength in the faces of the sections may be attributed to cold working that occurs during the tube forming and face crushing processes.

Figure 6.54 shows the 0.2% proof stresses $\sigma_{0.2,exp}$ for press braked angles normalised by the weighted average of the 0.2% proof stress values from the face of the section $\sigma_{0.2av,exp}$ (i.e. omitting the corner data). This average strength is close to strength values given in the mill certifcates $\sigma_{0.2,mill}$, confirming that no cold working has occurred in the section faces. Figure 6.56 shows the 0.2% proof stresses for the cold rolled box sections normalised by the weighted average of 0.2% proof stress values from the central 50% of each respective section face. The central 50% of the section has been identified as a region essentially uninfluenced by the cold working induced by corner forming (see Figure 6.56). Taking the available tensile coupon data for this portion of the section, the strength enhancements due to the face forming process can be isolated. In order to make a fair comparison between sections where different numbers of coupons in this region were avaliable a weighted average of the coupon data per section is used in the following analysis and presented in Table 6.12.

Table 6.12: *Weighted average coupon data and predicted strength enhancements in cold rolled box flat faces*

Source	*Section*	$\pi t/2(b+d)$	$\sigma_{0.2,mill}$ *(N/mm²)*	$\sigma_{ult,mill}$ *(N/mm²)*	$\sigma_{0.2av,exp}$ *(N/mm²)*	$\sigma_{ultav,exp}$ *(N/mm²)*	$\overline{\sigma}_{0.2,f}$ *(N/mm²)*	$\overline{\sigma}_{ult,f}$ *(N/mm²)*
Ala-Outinen (2005)	CR 200×200×5	0.010	289	621	363	654	285	644
	CR 200×200×5	0.008	336	645	314	623	321	665
Cruise (2007)	CR 100×50×2	0.022	485	685	469	772	572	736
	CR 100×100×2	0.015	485	685	460	760	522	722
	CR 100×50×3	0.030	485	685	486	696	645	755
	CR 100×100×3	0.019	485	685	486	750	548	729
	CR 100×50×4	0.041	288	625	557	784	441	713
	CR 100×100×4	0.030	337	626	431	635	446	690
	CR 150×150×4	0.020	304	618	310	632	351	661

Table 6.12 (continued): *Weighted average coupon data and predicted strength enhancements in cold rolled box flat faces*

Source	*Section*	$\pi t/2(b+d)$	$\sigma_{0.2,mill}$ (N/mm^2)	$\sigma_{ult,mill}$ (N/mm^2)	$\sigma_{0.2av,exp}$ (N/mm^2)	$\sigma_{ultav,exp}$ (N/mm^2)	$\overline{\sigma}_{0.2,f}$ (N/mm^2)	$\overline{\sigma}_{ult,f}$ (N/mm^2)
Gardner (2002)	CR 60×40×4	0.051	279	615	535	739	478	723
	CR 80×80×4	0.037	291	628	475	726	424	708
	CR 100×50×2	0.019	319	634	404	714	363	676
	CR 100×100×2	0.015	275	623	375	667	293	656
	CR 100×50×3	0.030	485	685	463	704	643	755
	CR 100×100×3	0.022	286	634	378	688	341	682
	CR 100×50×4	0.039	258	596	490	704	386	676
	CR 100×100×4	0.030	299	620	459	713	396	683
	CR 100×50×6	0.063	318	612	592	746	629	750
	CR 100×100×6	0.046	279	605	478	704	455	702
	CR 100×100×8*	0.062	295	620	318	657	576	757
	CR 120×80×3	0.023	485	685	426	744	580	738
	CR 120×80×6	0.046	289	616	506	711	470	714
	CR 150×100×4	0.024	289	600	306	662	352	649
	CR 150×150×4	0.020	304	613	302	656	349	655
Gardner et al. (2006)	CR 80×80×3	0.030	361	755	520	835	479	832
	CR 100×100×3	0.02	361	755	481	806	440	817
	CR 120×80×3	0.024	361	755	540	841	440	817
	CR 140×60×3	0.024	361	755	556	847	441	817
	CR 80×80×3	0.030	645	990	713	1048	856	1090
	CR 100×100×3	0.024	645	990	608	943	787	1070
	CR 120×80×3	0.024	645	990	658	970	785	1070
	CR 140×60×3	0.024	645	990	652	997	787	1070
Hyttinen (1994)	CR 30×30×3	0.053	313	637	503	741	555	756
	CR 40×40×2	0.039	321	637	455	716	481	723
	CR 60×60×5	0.062	297	631	557	788	582	771
	CR 30×30×3	0.053	257	437	498	513	452	518
	CR 40×40×2	0.039	302	428	462	486	448	484
	CR 30×30×3	0.055	343	502	536	576	616	598
	CR 40×40×2	0.041	385	540	511	541	584	615
Rasmussen and Hancock (1993a)	CR 80×80×3	0.029	297	614	408	695	390	675
Talja and Salmi (1995)	CR 60×60×5	0.064	284	604	572	755	565	742
	CR 60×60×5	0.064	284	604	560	756	566	742
	CR 60×60×5	0.062	284	604	565	747	557	738
	CR 60×60×5	0.064	284	604	530	669	570	744
	CR 60×60×5	0.062	284	604	544	760	555	738

* section omiited from analysis

The ratios of $\sigma_{0.2av,exp}/\sigma_{0.2,mill}$ and $\sigma_{ultav,exp}/\sigma_{ult,mill}$ indicate the increase of the 0.2% proof stress and ultimate stress respectively due to the forming process. A linear relationship between these two parameters is described by the experimental data where, during cold working a small increase of the ultimate stress relates to a more significant increase in the 0.2% proof stress. The best fit model is shown in Figure 6.57 and expressed in Equation 6.24,

$$\left(\frac{\sigma_{ultav,exp}}{\sigma_{ult,mill}}\right) = 0.19\left(\frac{\sigma_{0.2av,exp}}{\sigma_{0.2,mill}}\right) + 0.85 \tag{6.24}$$

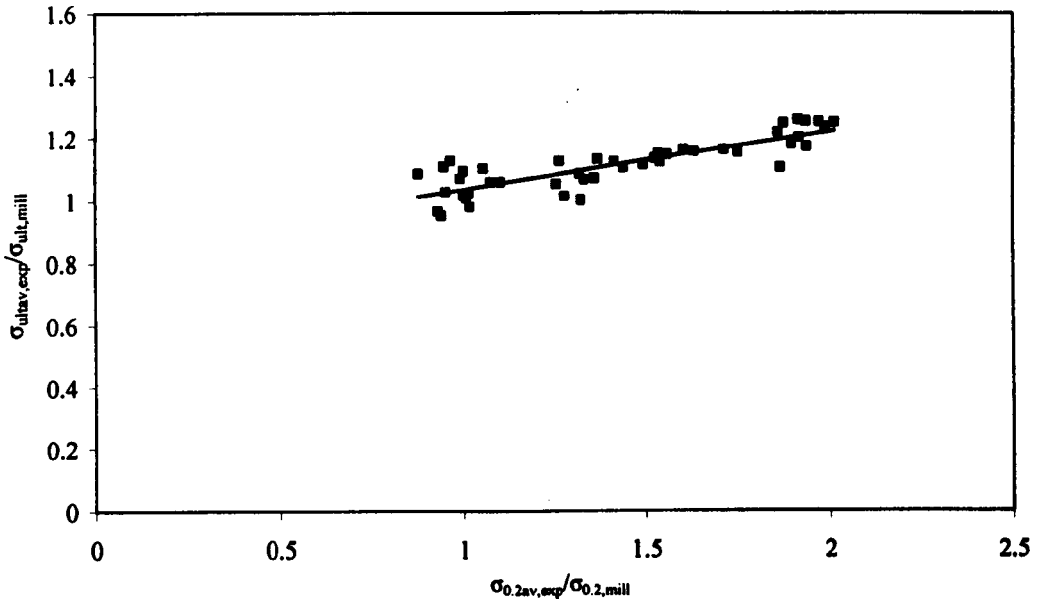

Figure 6.57: *Normalised ultimate stress $\sigma_{ultav,exp}/\sigma_{ult,mill}$ versus normalised 0.2% proof stress $\sigma_{0.2av,exp}/\sigma_{0.2,mill}$*

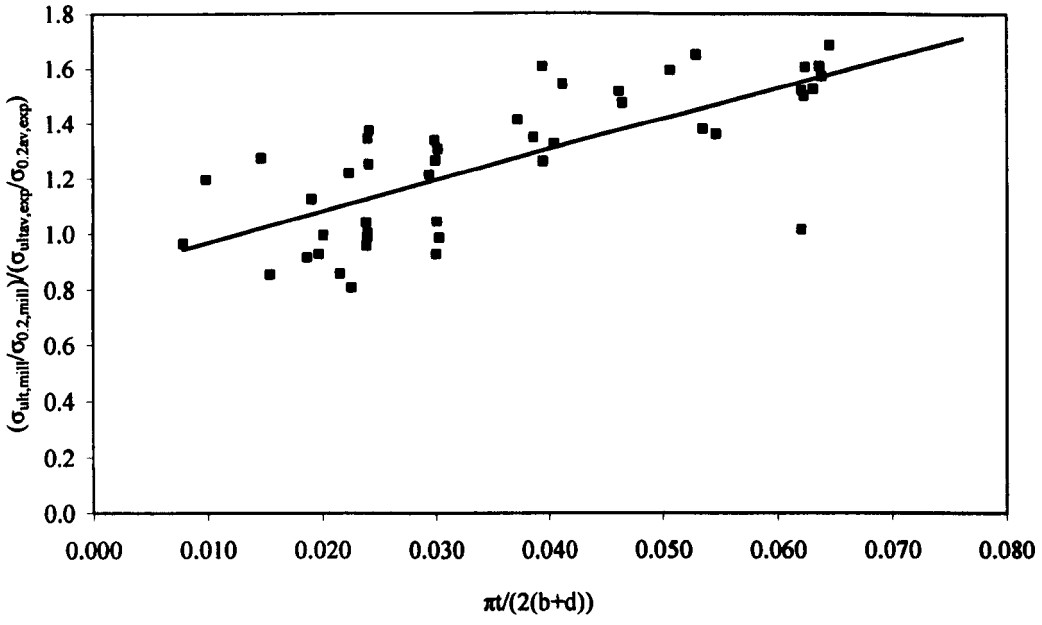

Figure 6.58 *Increase of cold working parameter* $(\sigma_{ult,mill}/\sigma_{0.2,mill})/(\sigma_{ultav,exp}/\sigma_{0.2av,exp})$ *with section face forming strain* $\pi t/(2(b+d))$ *including section CR 100×100×8 (Gardner,2002)*

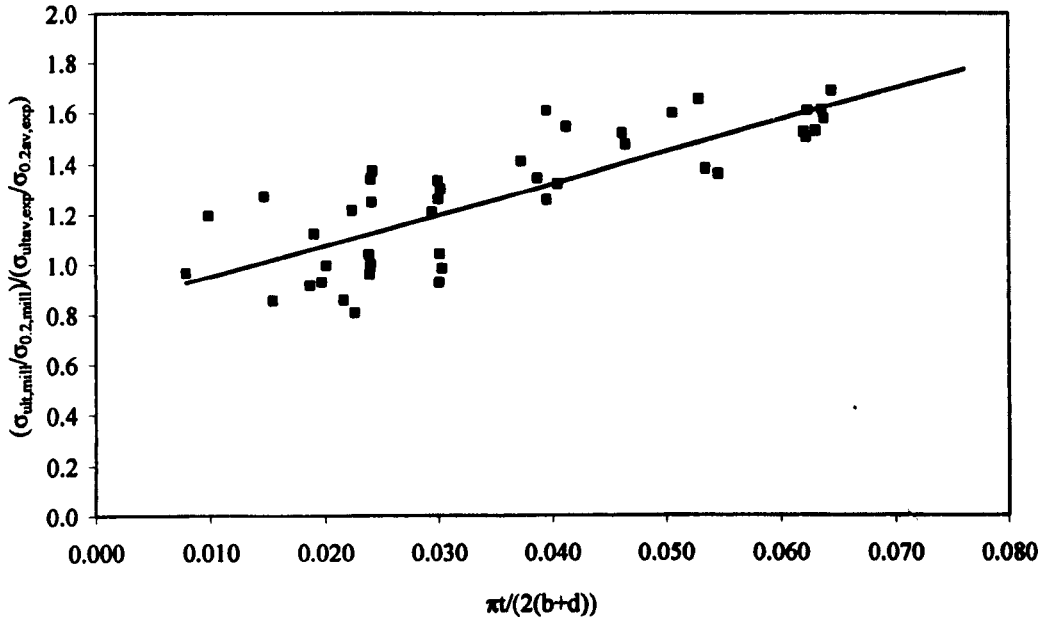

Figure 6.59: *Increase of cold working parameter* $(\sigma_{ult,mill}/\sigma_{0.2,mill})/(\sigma_{ultav,exp}/\sigma_{0.2av,exp})$ *with section face forming strain* $\pi t/(2(b+d))$ *for sections less than 8 mm thick*

Cold working thereby brings the 0.2% proof stress closer to the ultimate stress. As a measure of the level of cold work that has been carried out during the forming of the section faces, the parmeter $(\sigma_{ult,mill}/\sigma_{0.2,mill})/(\sigma_{ultav,exp}/\sigma_{0.2av,exp})$ has been taken. The larger the value of this parameter the greater the level of cold work that the section has undergone. Plotting this parameter against the simplified strain parameter (Figure 6.58) an outlier data point is observed for section CR 100×100×8 (Gardner, 2002). The reason for the low strain hardening seen in this section compared to the forming strain experienced may in part be due to the section forming route not being the one assumed. Due to the large difference between the data from this section and the data from others it has been removed from the data set yielding a best fit linear relationship for sections of thickness less than 8 mm as given by Equation 6.25 (see Figure 6.59).

$$\frac{\left(\frac{\sigma_{ult,mill}}{\sigma_{0.2,mill}}\right)}{\left(\frac{\sigma_{ultav,exp}}{\sigma_{0.2av,exp}}\right)} = 12.41\left(\frac{\pi t}{2(b+d)}\right) + 0.83 \tag{6.25}$$

The two relationships given in Equations 6.24 and 6.25 can be combined in the following manner (Equations 6.26-30) and used to predict the 0.2% proof stress $\overline{\sigma}_{0.2,f}$ of the central 50% of the faces in cold rolled box sections, resulting in Equation 6.31.

$$\frac{1}{\left(\frac{\sigma_{ult,exp}}{\sigma_{ult,mill}}\right)}\frac{\sigma_{0.2av,exp}}{\sigma_{0.2av,mill}} = 12.41\left(\frac{\pi t}{2(b+d)}\right) + 0.83 \tag{6.26}$$

$$\frac{1}{\left(0.19\frac{\sigma_{0.2,exp}}{\sigma_{0.2,mill}} + 0.85\right)}\frac{\sigma_{0.2av,exp}}{\sigma_{0.2av,mill}} = 12.41\left(\frac{\pi t}{2(b+d)}\right) + 0.83 \tag{6.27}$$

$$\frac{1}{\left(0.19 + 0.85\frac{\sigma_{0.2av,mill}}{\sigma_{0.2av,exp}}\right)} = 12.41\left(\frac{\pi t}{2(b+d)}\right) + 0.83 \tag{6.28}$$

$$0.19 + 0.85\frac{\sigma_{0.2,mill}}{\sigma_{0.2av,exp}} = \frac{1}{12.41\left(\frac{\pi t}{2(b+d)}\right) + 0.83} \tag{6.29}$$

$$\sigma_{0.2av,exp} = \frac{0.85\sigma_{0.2,mill}}{-0.19 + \frac{1}{12.41\left(\frac{\pi t}{2(b+d)}\right) + 0.83}} \tag{6.30}$$

$$\overline{\sigma}_{0.2,f} = \frac{0.85\sigma_{0.2,mill}}{-0.19 + \frac{1}{12.41\left(\frac{\pi t}{2(b+d)}\right) + 0.83}} \qquad t < 8 \text{ mm} \tag{6.31}$$

Equation 6.31 includes the 0.2% proof stress given in mill certifcates $\sigma_{0.2,mill}$ and geometrical parameters equivalent to an R_i/t ratio and, in this way it is comparable to the expression proposed to predict strength increases in the corner regions. Substituting the calculated 0.2% proof stress $\overline{\sigma}_{0.2,f}$ into the relationship described in Equation 6.24, the corresponding ultimate stress $\overline{\sigma}_{ult,f}$ can be determined giving Equation 6.32. Figures 6.60 and 6.61 show the correlation between the predicted values of 0.2% proof stress (Equation 6.31) and ultimate stress (Equation 6.32) respectively with the experimental data. The correlation between predicted and measured values is good for the 0.2% proof stress with Equation 6.31 giving a coefficent of determination R^2 of 0.64, but due to the relative insensitivity of the ultimate stress to cold working, the correlation between the predicted and measured ultimate stress shows less scatter where the best fit Equation 6.32 has an R^2 value of 0.71.

$$\overline{\sigma}_{ult,f} = \sigma_{ult,mill}\left(0.19\left(\frac{\overline{\sigma}_{0.2,f}}{\sigma_{0.2,mill}}\right) + 0.85\right) \qquad t < 8 \text{ mm} \tag{6.32}$$

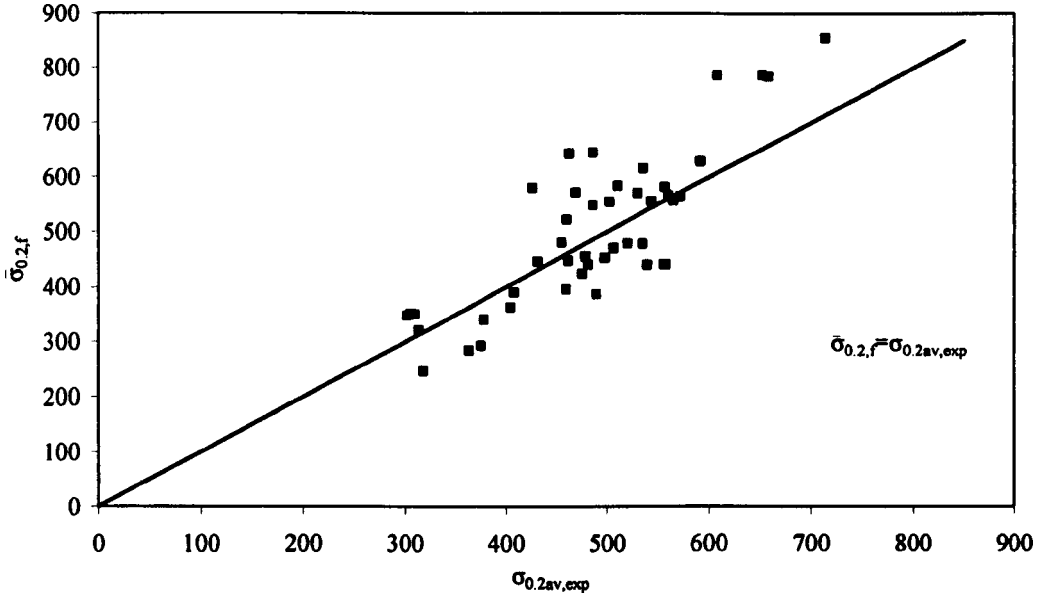

Figure 6.60: *Correlation between predicted and experimental 0.2% proof stress ($\bar{\sigma}_{0.2,f}$ and $\sigma_{0.2av,exp}$)*

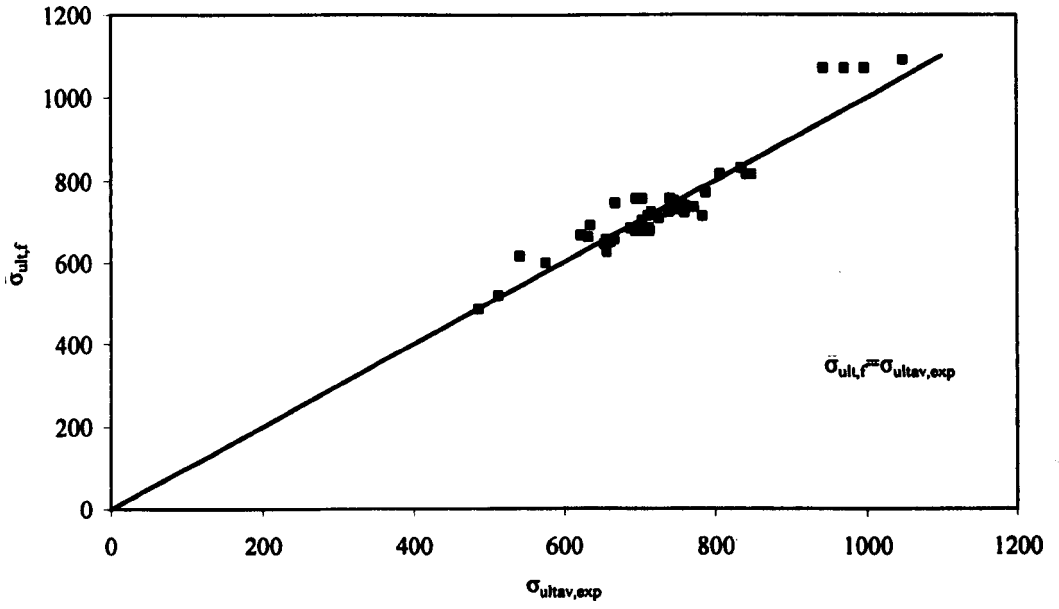

Figure 6.61: *Correlation between predicted and experimental ultimate stress ($\bar{\sigma}_{ult,f}$ and $\sigma_{ultav,exp}$)*

6.6.2 Extent of the corner regions

The regions of the faces of press braked sections and cold rolled sections where the cold work induced by corner forming does not influence the material properties, in particular the 0.2% proof stress, have been determined in the previous section. For a press braked angle this region is defined as starting at 20% of the section length measured (along the neutral axis) from the center of the corner radius and ending at the tip of the flange. For a cold rolled box section this region is defined as the central 50% of the flat section faces. These regions are shown in Figures 6.54 and 6.56 respectively.

Using the hardness measurements to predict the 0.2% proof stress $\overline{\sigma}_{0.2,exp}$ to a higher resolution the extent and variation within the corner regions can be investigated. The variation of 0.2% proof stress through the corner and section face can be observed in Figure 6.62 for press braked angles, where the predicted 0.2% proof stress is normalised over the weighted average of the predicted material strength from the section faces $\overline{\sigma}_{0.2av,exp}$ (i.e. neglecting data taken within the corner radius). In Figure 6.63, the predicted 0.2% proof stress $\overline{\sigma}_{0.2,exp}$ is normalised over the weighted average of the central 50% of predicted material strength for cold rolled box sections $\overline{\sigma}_{0.2av,exp}$. It can be seen in both cases that the regions where no cold working due to corner forming is observed correspond well to those determined with the tensile coupon test data.

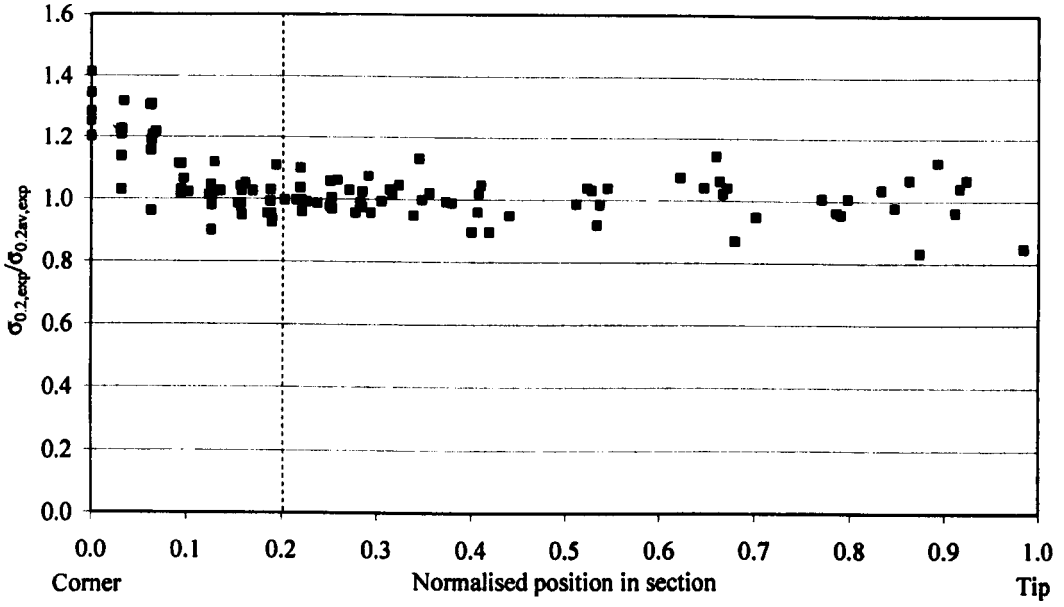

Figure 6.62: *Normalised predicted 0.2% proof stress in a press braked angle face*

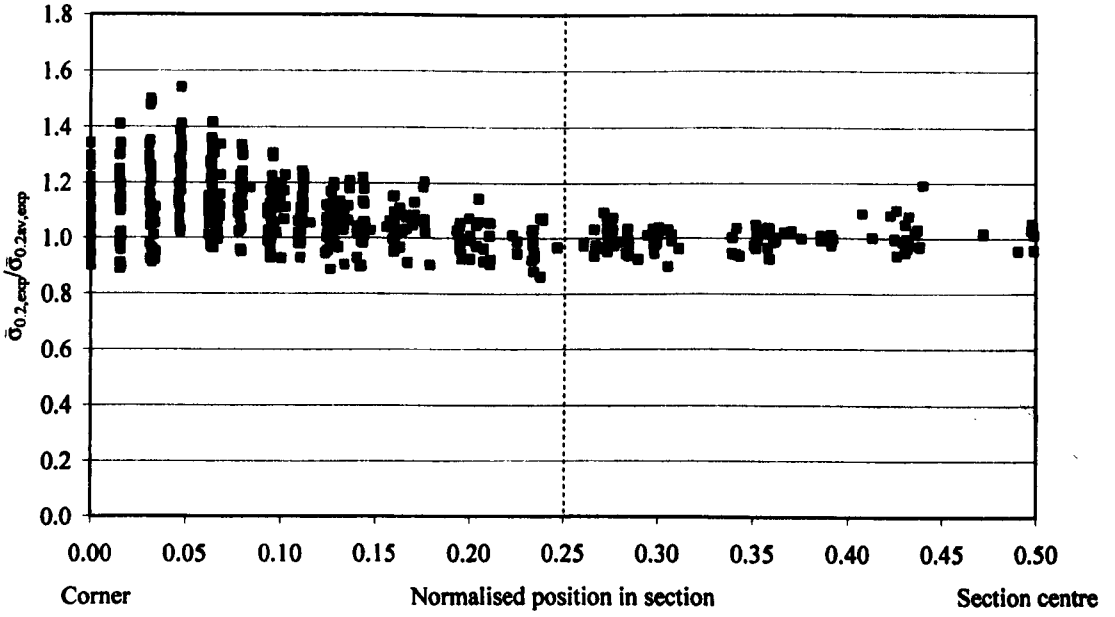

Figure 6.63: *Normalised predicted 0.2% proof stress in half a cold rolled box section face*

In Figures 6.64 and 6.65 the origin has been redefined for the data sets as the boundary between the corner radius (defined as a quarter arc) and the flat faces. In this manner the extent of the

cold work beyond this quarter arc region is easier to observe. Discussing both Figures 6.62 and 6.64, the predicted 0.2% proof stress in press braked sections can be seen to peak at the centre of the corner indicating that this region experiences the largest amount of plastic deformation. This point corresponds approximately with the location of the tool of the press brake as it strikes the sheet material to form the corner. The predicted 0.2% proof stress $\overline{\sigma}_{0.2,exp}$ deteriorates approximately linearly from this peak value, reaching the predicted 0.2% proof stress of the unformed sheet material close to the junction of the corner radius and flat face. Comparing this variation with that shown for cold rolled sections in Figures 6.63 and 6.65 significant differences are seen. The peak value shown in Figure 6.65 is not at the centre of the corner but at the junction of the corner radius and the face suggesting that this region is in fact where the largest plastic deformation occurs and is caused whilst the Turk head rollers crush the circular tube into a box section. The predicted 0.2% proof stress $\overline{\sigma}_{0.2,exp}$ then decreases towards the centre of the corner to values similar to those observed in the face of the box section. Moving away from the corner radius into the flat section face, the proof stress again falls approximately linearly over 18% of the length of the section (measured along the neutral axis between the centre of the corner radii) to values observed in the central 50% of the box section face. The extent of the cold working observed beyond the cold rolled corner radii is therefore larger than in press braked sections.

The average of the material strength distribution $\overline{\sigma}_{0.2,exp}$ predicted from the hardness values should estimate the 0.2% proof stress $\sigma_{0.2,exp}$ obtained from the corresponding corner tensile coupons for press braked and cold rolled sections. Generally, the 0.2% proof stress for corner coupons from cold rolled sections and press braked sections is higher than 0.2% proof stresses $\sigma_{0.2,exp}$ obtained from the flat section faces, however in some cases lower 0.2% proof stresses from the cold rolled corner coupons have been obtained than those obtained from flat coupons adjacent to the corners. This can be clearly observed for Corners 1 and 3 in section CR 150×150×4 (Figure 6.18). It is also worth noting that according to the predicted 0.2% proof stress distribution $\overline{\sigma}_{0.2,exp}$ as tensile corner coupons are cut from cold rolled sections along the junction of the corner and the flat face the highest strength material is likely to be removed in the thickness of the cut, lowering the tensile coupons' 0.2% proof stress. It is therefore also significant that corner coupons tested by Rasmussen (1993a) and Hyttinen (1994) were cut with bevelled corner edges. This is not an issue for press braked sections where the peak strength value is located in the centre of the corner coupon. The cold rolled corner predicted 0.2% proof stress distribution may be one reason for the high scatter observed in cold rolled corner 0.2% proof stresses.

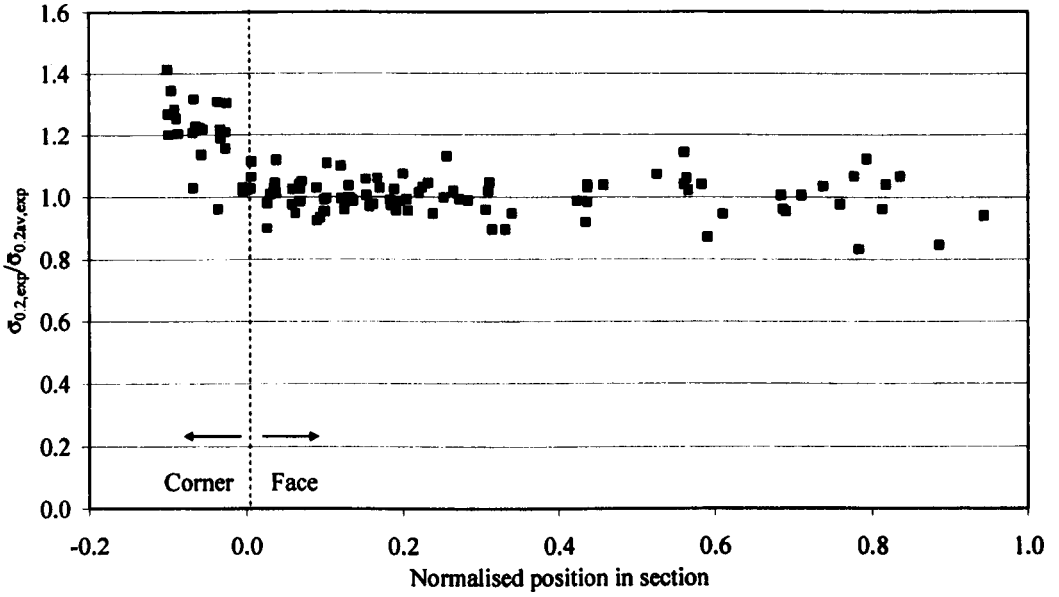

Figure 6.64: *Normalised predicted 0.2% proof stress in a press braked angle face*

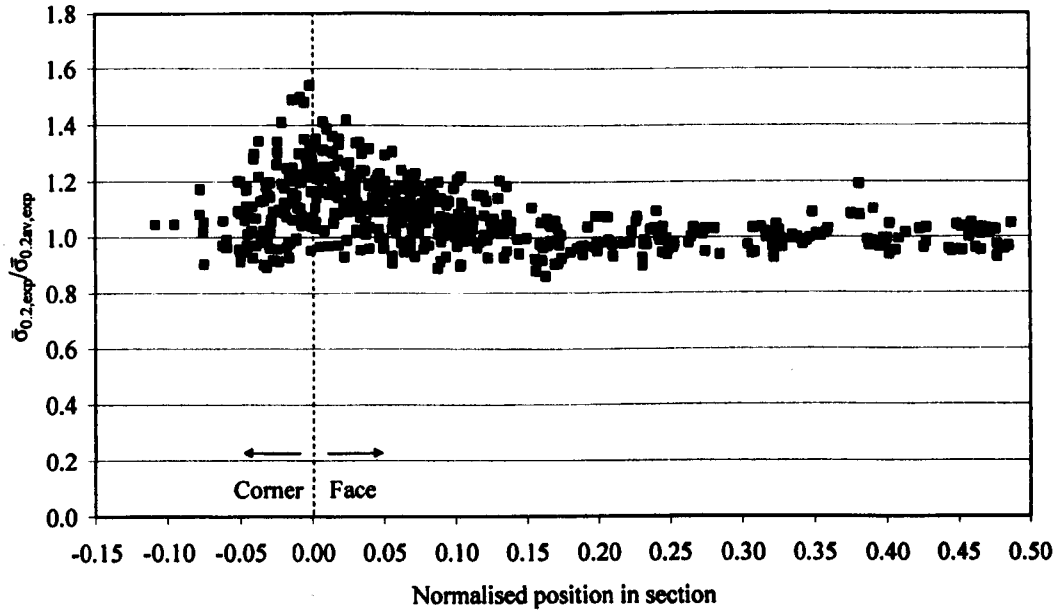

Figure 6.65: *Normalised predicted 0.2% proof stress in half a cold rolled box section face*

In order to compare the extent of the cold worked region beyond the corner radii with the values given in the current literature the section position of the normalised predicted 0.2% proof stresses data sets has been normalised over the section thickness t in Figures 6.66 and 6.67 and the internal corner radii r_i in Figures 6.68 and 6.69 for press braked angles and cold rolled box sections respectively. Figures 6.64 to 6.69 all set the origin of the data to the junction of the corner and the section face.

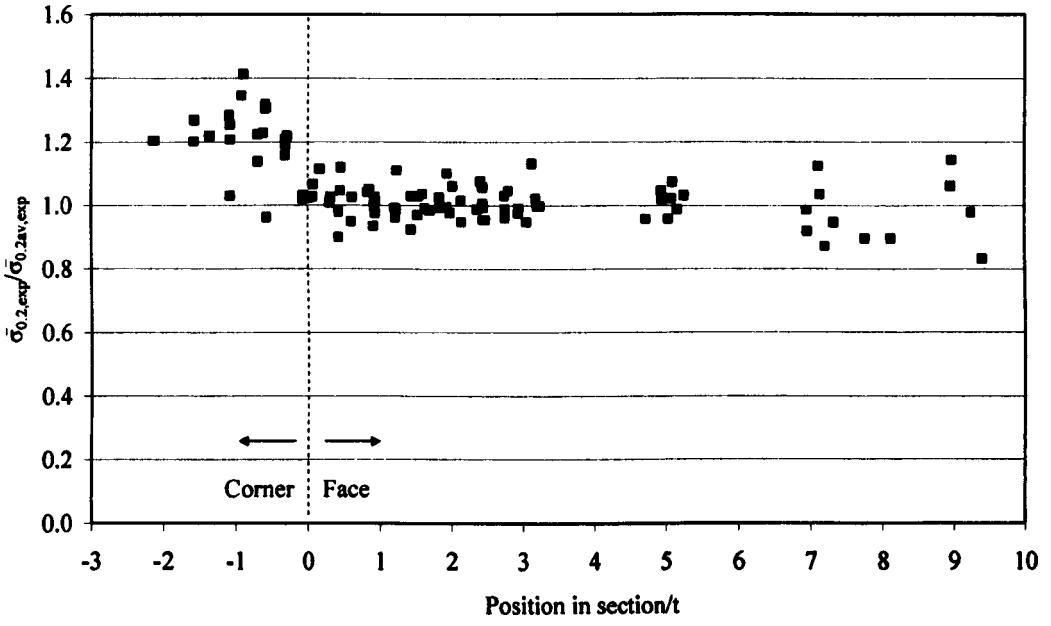

Figure 6.66: *Normalised predicted 0.2% proof stress for press braked angles at a section position normalised by thickness t*

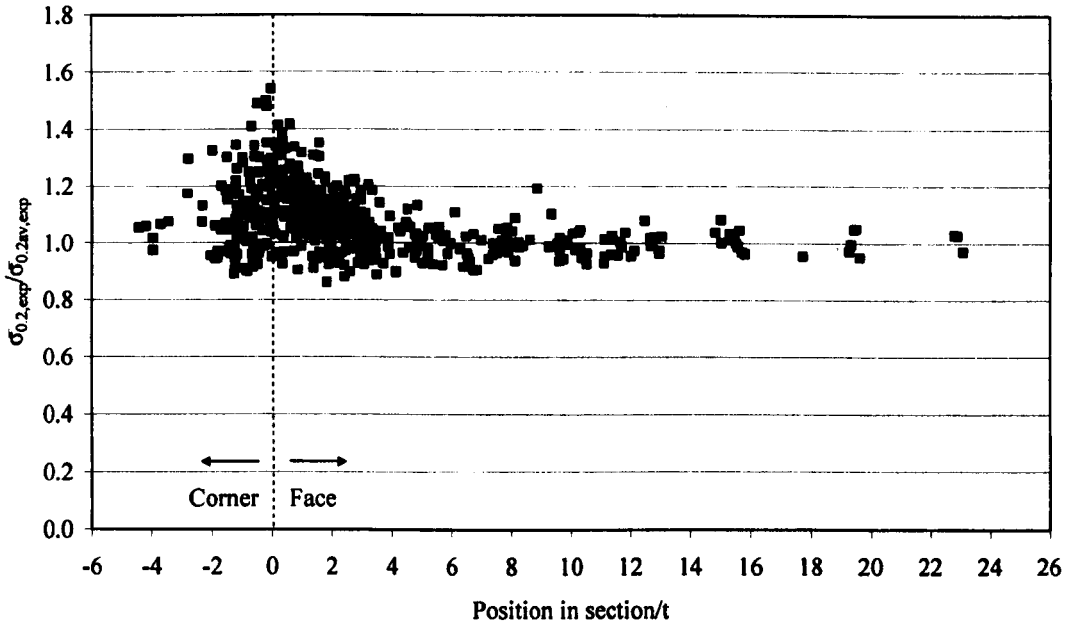

Figure 6.67: *Normalised predicted 0.2% proof stress for cold rolled boxes at a section position normalised by thickness t*

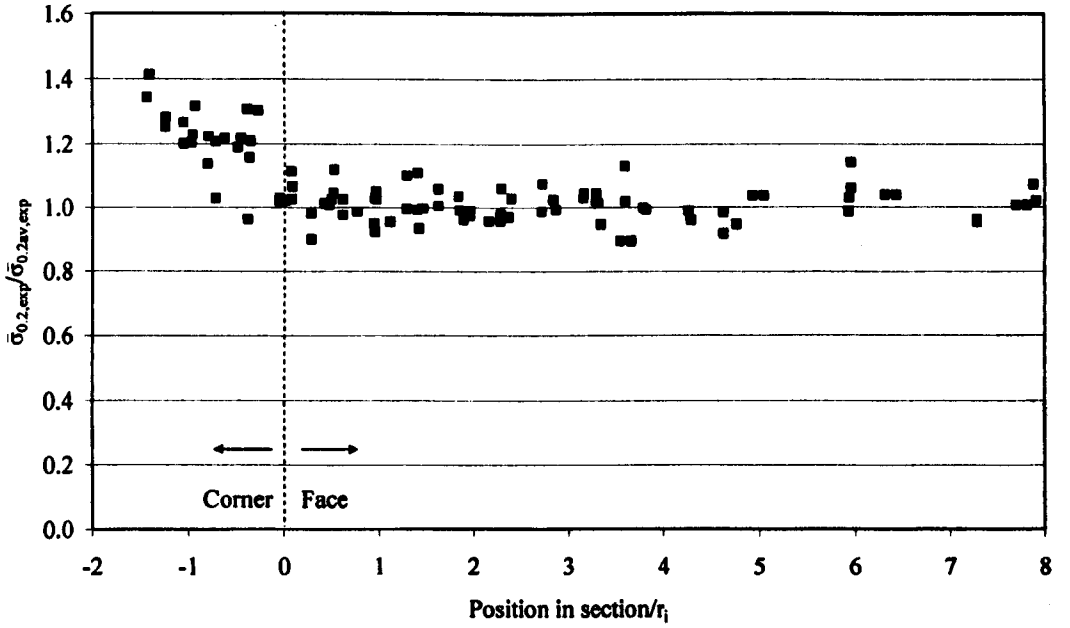

Figure 6.68: *Normalised predicted 0.2% proof stress for press braked angles at a section position normalised by the internal corner radius r_i*

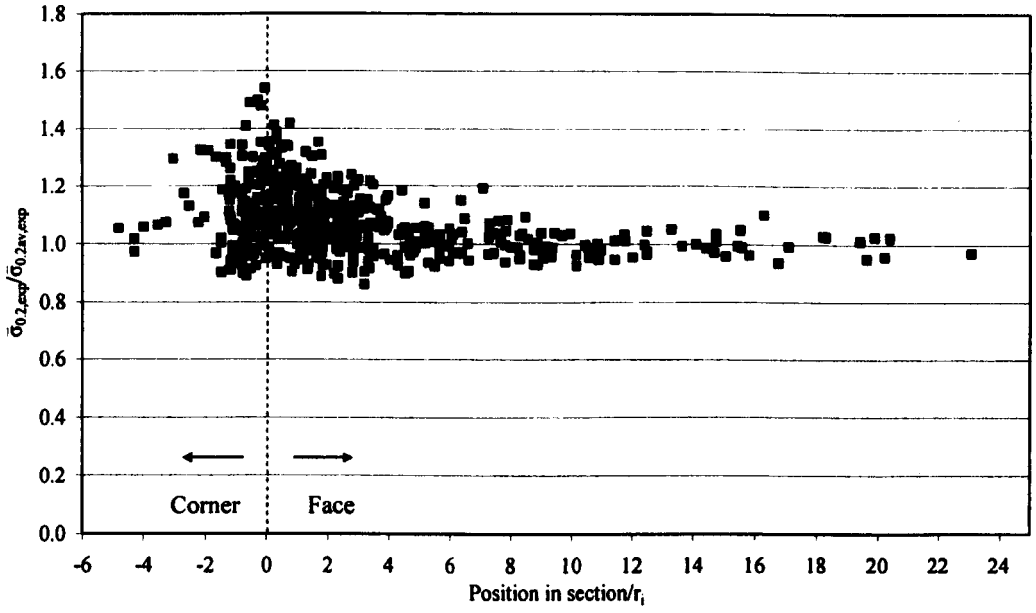

Figure 6.69: *Normalised predicted 0.2% proof stress for cold rolled boxes at a section position normalised by the internal corner radius r_i*

It can be conservatively estimated, despite the scatter in data, that cold working in press braked sections does not extend beyond the corner radius. This extension is less than predicted by other studies (Karren, 1967). From Figures 6.67 and 6.69 the extent of cold work beyond the corner in cold rolled box sections may be seen. The 0.2% proof stress decreases from its peak at the junction of the corner and the flat face approximately linearly over four times the section thickness 4t or four times the corners internal radius $4r_i$. An equivalent distribution would be to take the 0.2% proof stress of the corner $\sigma_{0.2,c}$ as extending without depreciation $2r_i$ or 2t beyond the corner radius, which corresponds well with the deductions of Gardner and Nethercot (2004).

6.6.3 Modelling strength enhancements in the corner region

Prediction of the corner material properties of cold formed stainless steel sections has been considered in previous research programs, as described in section 6.5.4. There have been three proposed models: Equations 6.15, 6.16 and 6.17-19. Based on all avaliable published corner test data for both press braked sections and cold rolled sections, including data from this current experimental program, these existing models have been reviewed.

Cold rolled data has been compiled from Gardner (2002), Gardner et al., (2006), Hyttinen, (1994), Rasmussen and Hancock, (1993a) and Talja and Salmi, (1995). Press braked data has been sourced from Coetzee et al. (1990), Lecce and Rasmussen (2004) and van den Berg and van der Merwe (1992). The cold rolled corner data and the press braked corner data are presented separately in Tables 6.13 and 6.14 respectively.

Table 6.13: *Predictive models for cold rolled corner 0.2% proof stress values*

Source	*Grade*	*r/t*	$\sigma_{0.2,cr,c}$	*Equation 6.35*		*Equation 6.33*		*Equation 6.17-6.19*	
				$\overline{\sigma}_{0.2,c,cr}$	$\overline{\sigma}_{0.2,c,cr} / \sigma_{0.2,exp}$	$\overline{\sigma}_{0.2,c,cr}$	$\overline{\sigma}_{0.2,c,cr} / \sigma_{0.2,exp}$	$\overline{\sigma}_{0.2,c,cr}$	$\overline{\sigma}_{0.2,c,cr} / \sigma_{0.2,exp}$
Cruise (2007)	1.4301	1.25	562	611	1.09	789	1.40	785	1.40
		1.32	669	611	0.91	784	1.17	781	1.17
		1.00	635	611	0.96	811	1.28	802	1.26
		1.25	594	611	1.03	789	1.33	785	1.32
		1.92	561	600	1.07	747	1.33	752	1.34
		1.41	508	600	1.18	777	1.53	776	1.53
		1.53	671	600	0.89	769	1.15	769	1.15
		1.21	551	600	1.09	792	1.44	787	1.43
		1.69	627	627	1.00	759	1.21	762	1.22
		1.07	588	627	1.07	805	1.37	797	1.36
		1.43	599	627	1.05	776	1.30	775	1.29
		1.07	596	627	1.05	805	1.35	797	1.34
		1.32	514	605	1.18	783	1.53	781	1.52
		1.89	493	605	1.23	749	1.52	754	1.53
		1.70	595	605	1.02	759	1.28	761	1.28
		1.60	532	605	1.14	764	1.44	766	1.44
		0.56	826	592	0.72	518	0.63	630	0.76
		0.56	712	592	0.83	518	0.73	630	0.88
		0.31	699	592	0.85	558	0.80	723	1.03
		0.56	632	592	0.94	518	0.82	630	1.00
		1.04	497	573	1.15	560	1.13	622	1.25
		0.75	567	573	1.01	584	1.03	659	1.16
		0.91	547	573	1.05	570	1.04	637	1.16
		1.04	531	573	1.08	560	1.05	622	1.17
		1.45	556	548	0.99	485	0.87	535	0.96
		2.35	537	548	1.02	457	0.85	484	0.90
		1.14	556	548	0.99	500	0.90	562	1.01

Table 6.13 (continued): *Predictive models for cold rolled corner 0.2% proof stress values*

Source	*Grade*	*r/t*	$\sigma_{0.2,cr,c}$	*Equation 6.35*		*Equation 6.33*		*Equation 6.17-6.19*	
				$\overline{\sigma}_{0.2,c,cr}$	$\overline{\sigma}_{0.2,c,cr}$ / $\sigma_{0.2,exp}$	$\overline{\sigma}_{0.2,c,cr}$	$\overline{\sigma}_{0.2,c,cr}$ / $\sigma_{0.2,exp}$	$\overline{\sigma}_{0.2,c,cr}$	$\overline{\sigma}_{0.2,c,cr}$ / $\sigma_{0.2,exp}$
Gardner (2002)	1.4301	1.20	594	587	0.99	476	0.80	534	0.90
		0.68	587	544	0.93	483	0.82	580	0.99
		1.60	563	543	0.97	471	0.84	515	0.91
		1.46	572	539	0.94	461	0.81	508	0.89
		0.92	631	623	0.99	538	0.85	607	0.96
Gardner et al. (2006)	1.4318 (C700)	1.38	638	691	1.08	579	0.91	640	1.00
		1.40	586	691	1.18	578	0.99	639	1.09
	1.4318 (C850)	0.74	865	905	1.05	1063	1.23	1107	1.28
		0.91	774	905	1.17	1035	1.34	1078	1.39
Hyttinen (1994)	1.4301	0.47	669	627	0.94	576	0.86	696	1.04
		0.49	684	600	0.88	587	0.86	699	1.02
		1.12	673	640	0.95	490	0.73	554	0.82
		1.12	663	640	0.97	490	0.74	554	0.84
		1.12	703	640	0.91	490	0.70	554	0.79
	1.4512	0.48	521	430	0.82	472	0.91	518	0.99
		0.52	500	402	0.80	700	1.40	677	1.35
	1.4003	0.43	526	496	0.94	638	1.21	634	1.20
		0.45	558	510	0.91	712	1.28	686	1.23
Rasmussen and Hancock (1993a)	1.4306	0.83	580	560	0.97	508	0.88	588	1.01
				Mean	1.00	Mean	1.08	Mean	1.14
				COV	0.11	COV	0.25	COV	0.19

Table 6.14: *Predictive models for press braked corner 0.2% proof stress values*

Source	*Grade*	*r/t*	$\sigma_{0.2,pb,c}$	*Equation 6.33*		*Equation 6.17-6.19*	
				$\overline{\sigma}_{0.2,pb,c}$	$\overline{\sigma}_{0.2,pb,c} / \sigma_{0.2,exp}$	$\overline{\sigma}_{0.2,pb,c}$	$\overline{\sigma}_{0.2,pb,c} / \sigma_{0.2,exp}$
Coetzee et al. (1990)	1.4301	1.28	520	480	0.92	531	1.02
		2.24	464	447	0.96	460	0.99
		2.23	471	447	0.95	460	0.98
		1.15	552	486	0.88	546	0.99
	1.4401	1.42	486	443	0.91	487	1.00
		2.04	445	423	0.95	445	1.00
		2.13	444	421	0.95	441	0.99
		1.37	487	445	0.91	492	1.01
	1.4003	1.35	519	482	0.93	499	0.96
		2.20	486	453	0.93	471	0.97
		2.25	482	452	0.94	469	0.97
		1.38	528	481	0.91	498	0.94
Cruise (2007)	1.4301	2.26	362	479	1.32	510	1.41
		1.50	605	520	0.86	569	0.94
		2.17	408	462	1.13	492	1.20
		2.81	346	447	1.29	465	1.35
		4.07	336	427	1.27	430	1.28
		0.86	479	540	1.13	619	1.29
		0.64	497	550	1.11	648	1.30
		0.88	632	529	0.84	607	0.96
Lecce and Rasmussen (2004)	1.4301	2.04	570	384	0.67	353	0.62
		2.04	570	384	0.67	353	0.62
	1.4016	2.41	444	436	0.98	453	1.02
		2.23	460	440	0.96	457	0.99
	1.4003	1.98	540	519	0.96	525	0.97
		1.98	547	519	0.95	525	0.96
van den Berg and van der Merwe (1992)	1.4301	1.99	452	453	1.00	476	1.05
		2.22	425	446	1.05	463	1.09
		3.40	407	423	1.04	416	1.02
		3.43	397	423	1.07	415	1.05
		4.43	398	409	1.03	389	0.98
		4.47	374	409	1.09	388	1.04
		5.75	362	396	1.09	364	1.01
		5.85	358	395	1.10	363	1.01
		6.63	366	389	1.06	352	0.96

Table 6.14 (continued): *Predictive models for press braked corner 0.2% proof stress values*

Source	*Grade*	*r/t*	$\sigma_{0.2,pb,c}$	*Equation 6.33*		*Equation 6.17-6.19*	
				$\overline{\sigma}_{0.2,pb,c}$	$\overline{\sigma}_{0.2,pb,c} / \sigma_{0.2,exp}$	$\overline{\sigma}_{0.2,pb,c}$	$\overline{\sigma}_{0.2,pb,c} / \sigma_{0.2,exp}$
van den Berg and van der Merwe (1992)	1.4512	1.80	370	348	0.94	373	1.01
		1.87	374	346	0.93	370	0.99
		3.00	365	326	0.89	343	0.94
		3.26	353	323	0.91	339	0.96
		4.20	350	313	0.89	325	0.93
		4.31	334	312	0.93	324	0.97
		5.36	328	303	0.92	313	0.95
		5.97	317	299	0.94	307	0.97
		6.24	322	297	0.92	305	0.95
		7.09	305	293	0.96	299	0.98
	1.4016	1.94	471	468	0.99	497	1.06
		2.39	488	456	0.93	482	0.99
		3.12	458	441	0.96	463	1.01
		4.32	451	423	0.94	441	0.98
		4.61	442	420	0.95	437	0.99
		5.30	435	412	0.95	428	0.98
		6.09	415	405	0.98	419	1.01
		6.54	418	402	0.96	414	0.99
		7.27	407	396	0.97	408	1.00
	1.4003	1.61	423	436	1.03	455	1.08
		2.25	450	418	0.93	436	0.97
		3.08	437	402	0.92	419	0.96
		3.16	420	400	0.95	417	0.99
		4.09	409	387	0.95	404	0.99
		4.33	392	385	0.98	401	1.02
		5.10	371	377	1.02	393	1.06
		5.64	379	372	0.98	388	1.02
		6.25	396	367	0.93	383	0.97
		6.70	371	364	0.98	379	1.02
				Mean	0.97	Mean	1.01
				COV	0.11	COV	0.12

Equations 6.17-6.19, proposed by Ashraf (2006), based on both the press braked and cold rolled data, have been used to predict the corner 0.2% proof stress for the currently available data set. A simple power rule (Equation 6.16), also proposed by Ashraf (2006), has been refitted to the press braked and cold rolled data yielding a modified expression which is given in Equation 6.33 and shown in Figure 6.70. The mean of the predicted corner 0.2% proof stress normalised over the test value and the corresponding coefficient of variation for cold rolled and press braked sections are shown in Tables 6.13 and 6.14 respectively.

$$\sigma_{0.2,c} = \frac{1.673\sigma_{0.2,mill}}{\left(\frac{r_i}{t}\right)^{0.126}} \tag{6.33}$$

The expression to predict the 0.2% proof stress for cold rolled corners proposed by Gardner (2002) and modified by Ashraf (2006) (Equation 6.15) is also refitted to the available data. The relationship obtained between the corner 0.2% proof stress $\sigma_{0.2,c,exp}$ and the ultimate stress of the central 50% of the cold rolled flat faces $\sigma_{u,av,exp}$ is given in Equation 6.34 where the best fit coefficient is found to be 0.83. However, using Equations 6.31 and 6.32 to predict the ultimate stress values for material in the flat faces of cold rolled sections $\overline{\sigma}_{ult,f}$ the 0.2% proof stress of the corner regions can be defined in terms of the mill certificate 0.2% proof stress $\sigma_{0.2,mill}$ and the section geometry (Equation 6.35). Predictions of the 0.2% proof stress of the corner region using Equation 6.35 yields a mean of the ratio of the predicted 0.2% proof stress of the corner regions to the test values closest to unity, showing that it is the closest predictor of the test values for cold rolled sections. The corresponding coefficient of variation is also the smallest out of the three possible models. This expression does not contain the internal radius to thickness parameter r_i/t that represents the strain involved in corner forming, however the expression still accurately predicts the corner 0.2% proof stress because the r_i/t ratios in cold rolled sections do not vary a considerable amount and the ultimate stress of the flat material used in the expression is not very sensitive to the amount of strain hardening experienced. Equation 6.35 is therefore proposed to predict the corner strength of cold rolled box sections $\overline{\sigma}_{0.2,cr,c}$.

$$\overline{\sigma}_{0.2,cr,c} = 0.83\sigma_{ult,av,exp} \tag{6.34}$$

$$\overline{\sigma}_{0.2,cr,c} = 0.83\overline{\sigma}_{ult,f} \tag{6.35}$$

The r_i/t ratios for cold rolled sections vary from 0.31 to 2.35, whereas for press braked sections the r_i/t ratios range from to 0.41 to 7.27. Figure 6.70 shows the relative ranges of the r_i/t ratios for press braked and cold rolled sections and the modified power rule (Equation 6.33).

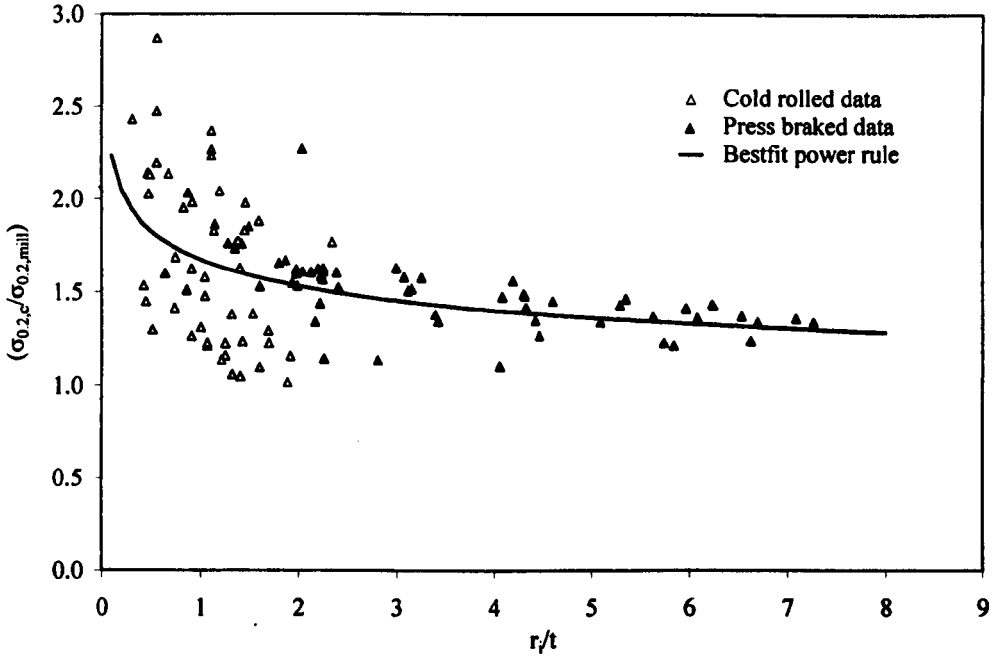

Figure 6.70: *Modified simple power expression to predict corner 0.2% proof stress indicating press braked and cold rolled test data*

For predicting the 0.2% proof stress of the press braked corner regions, both models give an average predicted to test 0.2% proof stress ratio close to unity and similar coefficients of variation. Whilst a relationship based purely on the press braked section data might give a slightly better predictive model with less scatter, there are few available small r_i/t press braked corner data and including the cold rolled corner data helps describe this region of the relationship. The modified power model given by Equations 6.33 is the simplest to use and Equation 6.36 is therefore proposed to predict the 0.2% proof stress of the press braked corner regions $\overline{\sigma}_{0.2,pb,c}$.

$$\overline{\sigma}_{0.2,pb,c} = \frac{1.673\sigma_{0.2,mill}}{\left(\frac{r_i}{t}\right)^{0.126}} \tag{6.36}$$

6.7 Material models

Based on the tensile coupon data, 0.2% proof stress distributions are proposed for press braked, hot rolled and cold rolled sections as illustrated in Figures 6.71-6.73 respectively.

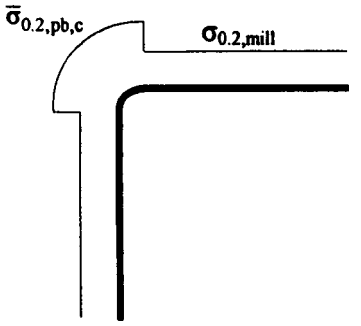

Figure 6.71: *The proposed 0.2% proof stress distribution for press braked angles, where $\overline{\sigma}_{0.2,pb,c}$ is defined by Equation 6.36*

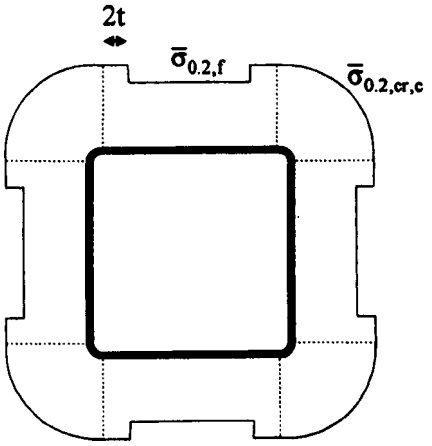

Figure 6.72: *The proposed 0.2% proof stress distribution for cold rolled box sections < 8 mm thick (formed via a circular tube), where $\overline{\sigma}_{0.2,cr,c}$ is defined by Equation 6.35 and $\overline{\sigma}_{0.2,f}$ is defined by Equation 6.31*

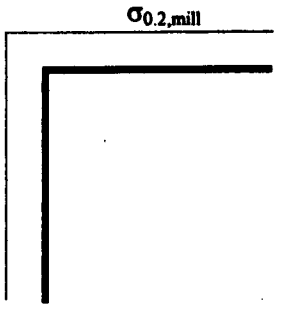

Figure 6.73: *The proposed 0.2% proof stress distribution for hot rolled angles*

6.8 Conclusions

This chapter has described the influence of section forming routes on the distribution of the 0.2% proof stress (yield strength) around stainless steel structural sections. Through tensile coupon tests carried out on the material removed from varying locations around press braked, cold rolled and hot rolled sections, methods to predict the strength enhancements have been proposed.

The hot rolled angles generally exhibited significantly higher strengths than the minimum specifications. This is thought to be related to warm working of the partially cooled material during the forming process. The measured strength values were typically slightly lower than the mill certificate value, which may be due to the higher strain rates generally employed by manufacturers or related to the location of the coupon taken by the manufacturer from within the cross section. For hot rolled sections, material properties can be quantified using the 0.2% proof stress obtained from manufacturers' values.

The press braked angles showed 0.2% proof stress values close to those provided by the manufacturer, but considerably higher than the minimum specifications; some localised increases in strength and reductions in ductility were observed in the section corners. By estimating the 0.2% proof stress from hardness measurements the cold work caused by corner forming was found not to extend beyond the defined quarter arc corner.

In contrast, the cold rolled sections showed a substantial strength increase in the flat portions of the cross sections beyond both the minimum specified values and the sheet values given by the manufacturers, with yet further increases in the corner regions. The extent of cold working caused by corner forming was found to decrease from a peak value of the predicted 0.2% proof stress observed at the corner and flat section face junction over approximately four times the thickness. Models to predict the strength enhancements in the section faces of cold rolled sections have been proposed, as well as modification of models that predict the strength enhancements in the corner regions of both press braked and cold rolled sections, thereby defining the complete distribution of material properties in both press braked and cold rolled sections.

Chapter 7

Design method

7.1 Introduction

The strength enhancements modelled in Chapter 6 offer increased material efficiency if employed in structural design. This chapter adopts different 0.2% proof stress distributions including a uniform minimum specified 0.2% proof stress given in EN 10088-2 (2005) and the proposed 0.2% proof stress distribution given in Chapter 6, in combination with the current stainless steel structural design codes (EN 1993-1-4, 2006) to predict cross section, and member resistance in compression and bending. Effective section properties have been calculated for Class 4 sections. The presented study thereby quantifies the increase in design efficiency offered by employing the proposed material models. The comparisons have been carried out on all available sections tested as part of published experimental programs. The available data comprises stub column test data for press braked angles, channels and lipped channel sections as well as stub column, column and beam test data for cold rolled box sections.

The presented design method does not explicitly include the modelled geometric imperfections and residual stress distributions detailed in chapters 4 and 5. Nominal residual stresses and

geometric imperfections are however included in this study through buckling curves given in EN 1993-1-4 (2006).

7.2 Press braked member resistance

7.2.1 Background

From the test programs that have been carried out on stainless steel structural cross sections, only a few have been performed on press braked sections (Kuwamura, 2003 and Rhodes et al., 2000). Rhodes et al. (2000) performed a total of seventy seven concentrically and eccentrically loaded column tests on stainless steel (grade 1.4301) press braked lipped channels. The material properties from the tested sections' mill certificates were not reported. However Rhodes et al. (2000) supplied the 0.2% proof stress of tensile coupons performed on material taken from the web of the formed section. Due to the small size of the sections tested it cannot be assumed that the material properties of the coupons are equivalent to mill certificate values, as it is not certain that these coupons were taken from a region where no cold work had occurred during press braking. The column tests were therefore not included in this study.

A test program performed at the University of Tokyo on press braked sections was reported by Kuwamura (2003) who carried out a series of stub column tests on twelve equal angles, eleven channels and twelve lipped channels. The sections were made from two austenitic grades of stainless steel, 1.4301 and 1.4318. The details of the angles, channels and lipped channels are given in Tables 7.1, 7.2 and 7.3 respectively.

7.2.2 Predictive study

The stub column resistance has been predicted for press braked sections using four scenarios of different 0.2% proof stress distributions to determine the cross section resistance $N_{c,Rd}$. The effects of distortional buckling have been ignored for the lipped channel sections and only local buckling considered as their influence on the cross section resistance is thought to be small. Scenario A considers the full section to have a 0.2% proof stress equal to the minimum specified 0.2% proof stress $\sigma_{0.2,min}$ as given in EN 10088-2 (2005). Scenario B considers the full cross section to have a uniform distribution of the 0.2% proof stress given in the mill certificate $\sigma_{0.2,mill}$. Scenario C supposes that no mill certificate data is available, with the flat faces having the minimum specified 0.2% proof stress $\sigma_{0.2,min}$, and the minimum 0.2% proof stress is also used to replace the 0.2% proof stress from the mill certificate in Equation 6.36 to predict an enhanced corner strength $\overline{\sigma}'_{0.2,pb,c}$. The weighted average of this stratified distribution is used in

design. As a final scenario, supposing that mill certificate data are available, Scenario D implements the proposed model of a stratified material distribution given in Chapter 6 where the weighted average of the proposed 0.2% proof stress distribution is used in design. In the proposed model, the flat regions of the press braked sections are considered to have the 0.2% proof stress given in the mill certificate $\sigma_{0.2,mill}$ and the 0.2% proof stress of the corner region $\overline{\sigma}_{0.2,pb,c}$ is predicted by implementing Equation 6.36 using, as stated, the 0.2% proof stress from the mill certificate $\sigma_{0.2,mill}$. These four scenarios are illustrated in Figure 7.1 for a press braked angle.

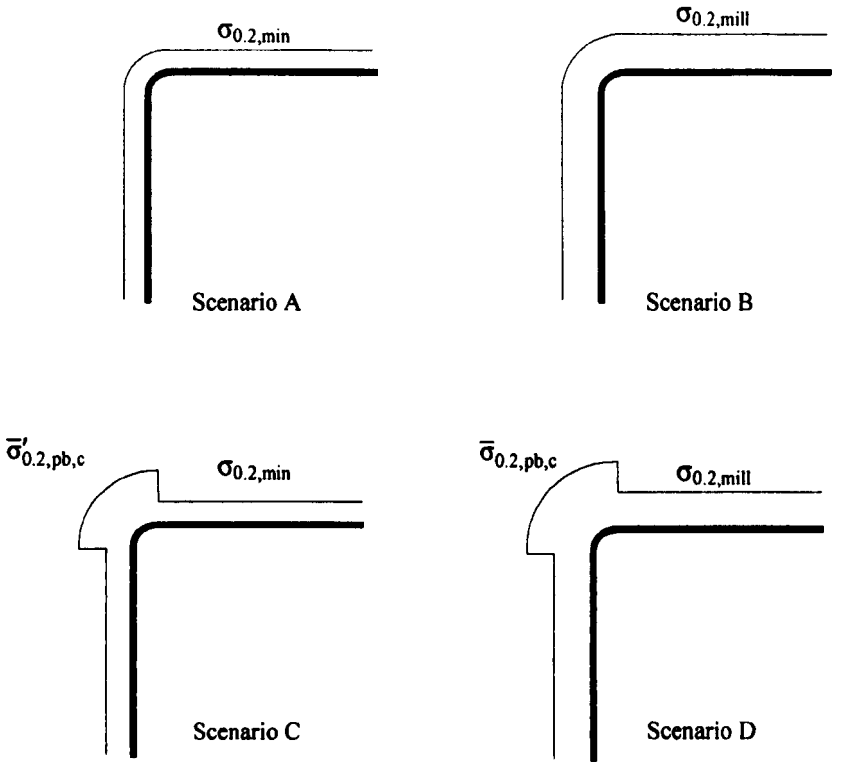

Figure 7.1: *Four considered scenarios for the material stratification of press braked sections*

Table 7.1: *Predicted cross section resistance for press braked equal angle stub column data*

Section properties					*Scenario A*		*Scenario B*		*Scenario C*		*Scenario D*	
Source	*L (mm)*	*d (mm)*	*r_i (mm)*	*t (mm)*	$\bar{\lambda}_{p,max}$	$N_{c,Rd}/N_{c,exp}$	$\bar{\lambda}_{p,max}$	$N_{c,Rd}/N_{c,exp}$	$\bar{\lambda}_{p,max}$	$N_{c,Rd}/N_{c,exp}$	$\bar{\lambda}_{p,max}$	$N_{c,Rd}/N_{c,exp}$
Kuwamura (2003) Grade: 1.4301	75.0	24.90	3.08	2.92	0.46	0.54	0.51	0.66	0.49	0.59	0.54	0.72
	90.0	30.00	4.07	2.93	0.56	0.62	0.61	0.75	0.58	0.68	0.64	0.82
	120.0	40.05	4.07	2.93	0.74	0.71	0.82	0.81	0.77	0.74	0.85	0.86
	120.0	39.85	4.07	2.93	0.74	0.72	0.82	0.83	0.76	0.75	0.84	0.87
	150.0	50.00	4.07	2.93	0.93	0.77	1.02	0.88	0.95	0.80	1.05	0.91
	180.0	59.00	3.07	2.93	1.10	0.81	1.21	0.92	1.12	0.83	1.23	0.94
Kuwamura (2003) Grade: 1.4318	75.0	25.30	3.03	2.97	0.59	0.60	0.71	0.83	0.62	0.66	0.75	0.89
	90.0	30.00	4.03	2.97	0.70	0.61	0.85	0.81	0.73	0.65	0.88	0.87
	120.0	40.00	2.98	3.02	0.92	0.61	1.11	0.79	0.95	0.63	1.14	0.82
	120.0	40.05	3.98	3.02	0.92	0.66	1.11	0.85	0.95	0.69	1.15	0.90
	150.0	50.05	2.99	3.01	1.15	0.66	1.39	0.84	1.18	0.68	1.43	0.87
	180.0	60.00	3.97	3.03	1.38	0.73	1.66	0.92	1.41	0.75	1.69	0.95
					Mean	0.67	Mean	0.82	Mean	0.70	Mean	0.87
					COV	0.12	COV.	0.09	COV	0.10	COV	0.07

Table 7.2: *Predicted cross section resistance for press braked channel stub column data*

Section properties						*Scenario A*		*Scenario B*		*Scenario C*		*Scenario D*	
Source	*L (mm)*	*d (mm)*	*b (mm)*	r_i *(mm)*	*t (mm)*	$\bar{\lambda}_{p,max}$	$N_{c,Rd}/N_{c,exp}$	$\bar{\lambda}_{p,max}$	$N_{c,Rd}/N_{c,exp}$	$\bar{\lambda}_{p,max}$	$N_{c,Rd}/N_{c,exp}$	$\bar{\lambda}_{p,max}$	$N_{c,Rd}/N_{c,exp}$
Kuwamura (2003) Grade: 1.4301	150.0	49.75	24.83	4.07	2.93	0.47	0.56	0.52	0.68	0.50	0.63	0.55	0.77
	240.0	80.30	39.58	4.08	2.92	0.76	0.72	0.83	0.85	0.78	0.76	0.86	0.90
	300.0	100.45	49.98	3.07	2.93	0.95	0.79	1.05	0.91	0.97	0.82	1.07	0.94
	300.0	101.10	49.6	3.07	2.93	0.95	0.82	1.04	0.94	0.97	0.85	1.07	0.97
	450.0	150.40	49.68	3.08	2.92	0.95	0.79	1.05	0.90	0.97	0.81	1.07	0.92
	150.0	50.25	49.48	4.08	2.92	0.95	0.65	1.04	0.76	0.98	0.69	1.08	0.81
Kuwamura (2003) Grade: 1.4318	150.0	50.25	25.03	3.98	3.02	0.59	0.51	0.71	0.72	0.62	0.57	0.75	0.80
	240.5	80.05	39.98	2.98	3.02	0.94	0.63	1.13	0.83	0.96	0.66	1.16	0.91
	300.0	100.45	50.05	3.48	3.02	1.17	0.69	1.41	0.88	1.20	0.75	1.45	0.98
	300.0	100.45	50.05	2.99	3.01	1.18	0.69	1.42	0.88	1.20	0.76	1.45	0.99
	450.5	150.50	50.00	3.98	3.02	1.17	0.75	1.41	0.95	1.20	0.85	1.44	1.08
						Mean	0.69	Mean	0.85	Mean	0.74	Mean	0.92
						COV	0.14	COV	0.10	COV	0.13	COV	0.10

Table 7.3: *Predicted cross section resistance for press braked lipped channel stub column data*

Section properties							*Scenario A*		*Scenario B*		*Scenario C*		*Scenario D*	
Source	L *(mm)*	d *(mm)*	b *(mm)*	b_l *(mm)*	r_i *(mm)*	t *(mm)*	$\bar{\lambda}_{p,max}$	$N_{c,Rd}/N_{c,exp}$	$\bar{\lambda}_{p,max}$	$N_{c,Rd}/N_{c,exp}$	$\bar{\lambda}_{p,max}$	$N_{c,Rd}/N_{c,exp}$	$\bar{\lambda}_{p,max}$	$N_{c,Rd}/N_{c,exp}$
Kuwamura (2003) 1.4301	300.0	100.20	50.35	19.80	3.07	2.93	0.56	0.61	0.61	0.83	0.58	0.75	0.64	0.89
	450.0	150.40	50.30	19.85	3.07	2.93	0.87	0.70	0.96	0.93	0.90	0.84	1.00	0.99
	450.0	150.15	65.50	19.75	3.09	2.91	0.88	0.73	0.97	0.96	0.90	0.86	1.00	1.01
	600.0	200.30	74.80	25.25	3.09	2.91	1.20	0.77	1.32	1.01	1.23	0.89	1.35	1.05
	100.0	32.80	17.45	6.70	1.06	0.94	0.56	0.59	0.62	0.80	0.59	0.72	0.65	0.86
	150.0	50.20	17.25	6.95	0.55	0.95	0.92	0.73	1.01	0.93	0.94	0.83	1.04	0.97
	150.0	50.10	22.25	6.80	1.05	0.95	0.89	0.71	0.99	0.94	0.92	0.83	1.01	0.99
	200.0	67.70	25.30	8.20	1.06	0.94	1.25	0.74	1.38	0.97	1.28	0.85	1.41	1.01
Kuwamura (2003) 1.4318	300.0	100.05	49.85	20.00	2.98	3.02	0.89	0.54	0.82	0.87	0.70	0.67	0.85	0.93
	450.0	150.65	50.45	19.55	3.98	3.02	1.05	0.61	1.27	0.99	1.09	0.77	1.31	1.05
	450.0	150.40	64.80	19.95	2.99	3.01	1.24	0.67	1.29	1.05	1.10	0.80	1.33	1.10
	600.0	200.25	75.05	24.45	2.99	3.01	1.48	0.70	1.75	1.06	1.49	0.81	1.79	1.09
							Mean	0.67	Mean	0.94	Mean	0.80	Mean	1.00
							COV	0.11	COV	0.08	COV	0.08	COV	0.07

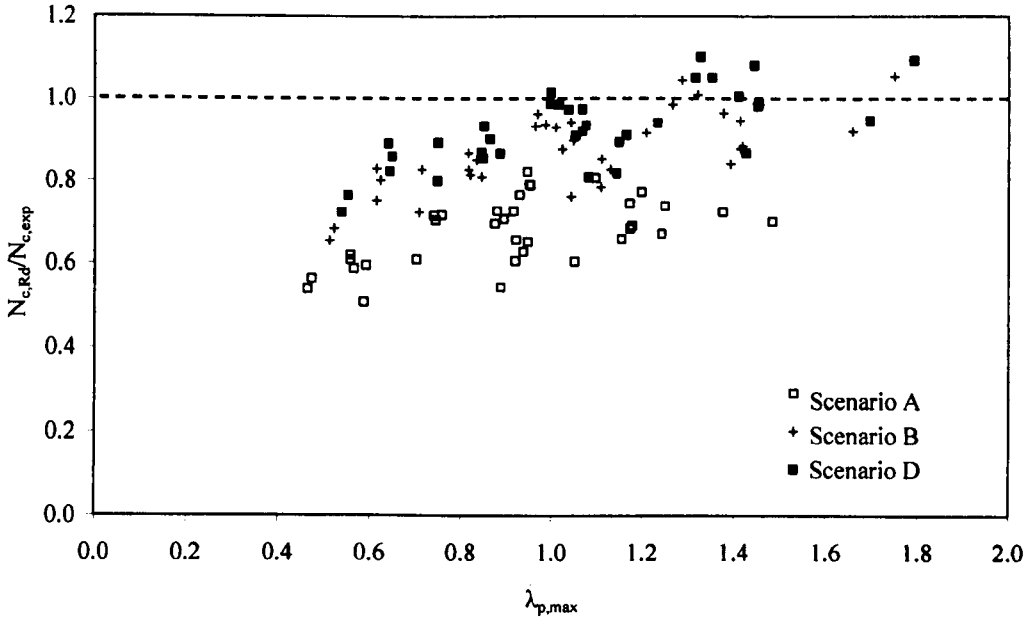

Figure 7.2: *The ratio of predicted cross section resistance to the test value plotted against the maximum plate slenderness for the material distributions considered in Scenarios A, B and D for press braked angles, channels and lipped channels*

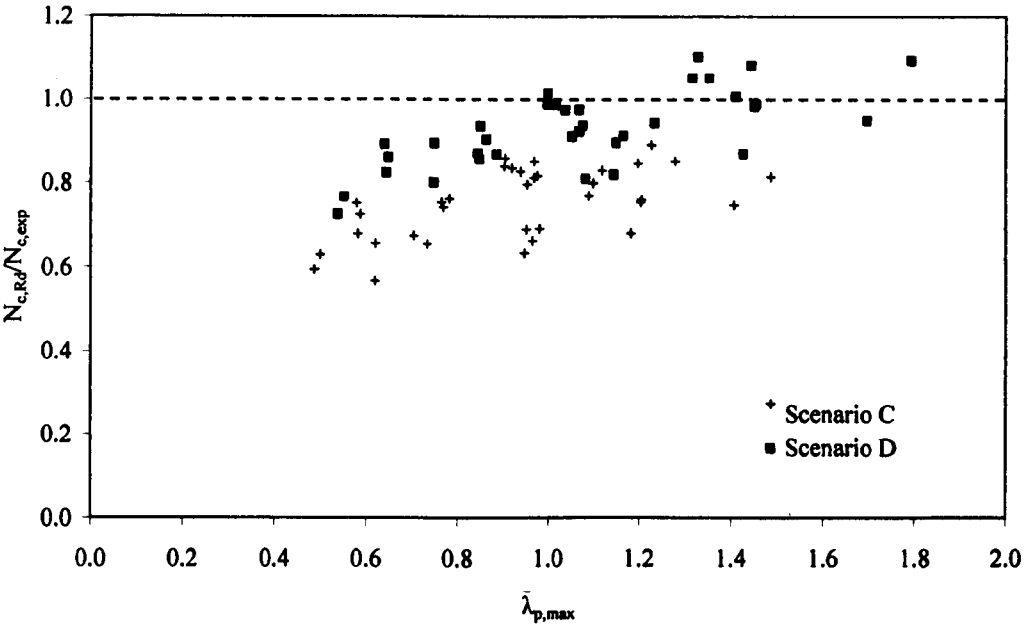

Figure 7.3: *The ratio of predicted cross section resistance to the test value plotted against the maximum plate slenderness for the material distributions considered in Scenarios C and D for press braked angles, channels and lipped channels*

7.2.3 Results

The ratio of the predicted cross section resistance $N_{c,Rd}$ of the four different 0.2% proof stress distributions and the cross section resistance obtained experimentally by Kuwamura (2003) $N_{c,exp}$ indicates how accurately the design code predicts the real behaviour of the sections. This ratio is given for all angle, channel and lipped channel sections in Tables 7.1-3 respectively as well as the maximum plate slenderness of the sections $\bar{\lambda}_{p,max}$. The plate slenderness $\bar{\lambda}_p$ is given in Equation 7.1, where $\bar{b}$ is the appropriate plate width, k_σ is the buckling factor and ε is the material factor.

$$\bar{\lambda}_p = \sqrt{\frac{\bar{b}/t}{28.4\varepsilon\sqrt{k_\sigma}}} \tag{7.1}$$

Tables 7.1-3 also detail the geometric dimensions of each specimen where L is the length of the stub column, r_i is the internal corner radius and t is the thickness of the section. d and b are the widths and breadths of the sections. For equal angles only d is specified, and for lipped channels the width of the lip is given as b_l. Figure 7.2 plots the ratio of the predicted over the test cross section resistance, against the maximum plate slenderness for Scenarios A, B and D. It can be seen both in the tabulated data and in Figure 7.2 that for Scenario A, where a uniform distribution of the minimum specified 0.2% proof stress $\sigma_{0.2,min}$ is employed, the average cross section resistance is predicted to be around 0.68 of the test value $N_{c,exp}$. In Scenario B, where a uniform distribution of the 0.2% proof stress given in the mill certificate $\sigma_{0.2,mill}$ is assumed in design, the average predicted cross section resistance $N_{c,Rd}$ increases substantially to 0.82-0.94 of the test value $N_{c,exp}$. Including the predicted corner strength $\bar{\sigma}_{0.2,pb,c,}$ and maintaining the mill certificate 0.2% proof stress $\sigma_{0.2,mill}$ in the section's flat faces, Scenario D gives an average increase of approximately 0.06 of the test value $N_{c,exp}$ in the cross section resistance compared to cross section resistances obtained by considering Scenario B and a reduction in the scatter of the predictions. Scenario D provides the best prediction of the cross section resistance obtained experimentally with an average increase of 1.4 times the cross section resistance determined with a uniform minimum specified 0.2% proof stress $\sigma_{0.2,min}$, for all considered section types.

Figure 7.3 shows a comparison between the predicted over test cross section resistance for Scenarios C and D. For Scenario C, where the minimum 0.2% proof stresses have replaced the mill certificate values in the proposed design model, cross section resistances are predicted to be on average 1.1 times higher than cross section resistances calculated assuming Scenario A, the minimum specified 0.2% proof stress. Whilst Scenario C gives lower predictions for the cross

section resistance than the proposed distribution (Scenario D), which is based on the mill certificate 0.2% proof stress, Scenario C does give values higher than the minimum specified 0.2% proof stress and could be used in design cases where the mill certificate data is unknown.

7.3 Cold rolled member resistance

7.3.1 Background

There have been many more test programs carried out on cold rolled sections than on press braked sections (Gardner, 2002, Rasmussen and Hancock, 1993a and 1993b, Real, 2001, Talja and Salmi, 1995, and Young and Lui, 2003). However, the 0.2% proof stress from the mill certificate $\sigma_{0.2,mill}$ is required in this study, which meant that not all test data could be included. Three test programs, Gardner (2002), Rasmussen and Hancock, (1993a and 1993b) and Talja and Salmi (1995) supplied mill certificate data for specimens which were tested as stub columns, columns and beams enabling a comparison between seven different scenarios for modelling the material strength of cold rolled box sections. As part of a previously reviewed experimental program (Chapter 6) Gardner (2002) performed 33 stub column tests, 22 pin ended column tests, (including buckling about the major and minor axes) and 9 simply supported beam tests. Talja and Salmi (1995) whose test program is also described in more detail in Chapter 6 performed stub column tests on 2 rectangular hollow sections and 1 square hollow section, as well as column tests and beam tests on 6 rectangular and 3 square hollow sections. The rectangular sections tested in this experimental program are known to have been formed by sequential folding of the sheet material through rollers. The strength enhancements proposed for sections formed via a circular tube should therefore not apply to these rectangular sections. They are however included in this study to see how the proposed material distributions would affect the prediction of the member resistance of box sections from different production routes compared to those from the considered forming path. The specimens of both test programs were made from the austenitic stainless steel grade 1.4301. Rasmussen and Hancock (1993a) performed a test program on one size of circular and one size of square hollow section made from grade 1.4306 stainless steel, reporting one stub column and six column tests (three concentrically loaded and three eccentrically loaded) for each section type. Rasmussen and Hancock (1993b) reported in-plane bending tests performed on the same sections. Only the data from the square hollow sections are included in this analysis.

7.3.2 Predictive study

Seven different 0.2% proof stress distributions were considered. They are illustrated as Scenarios A-G in Figure 7.4. Each of the seven different scenarios were employed in the design prediction of the stub column, column and beam resistances, the results of which are given in Tables 7.4-5, 7.6-7 and 7.8-9 respectively, where the data for square hollow sections and rectangular hollow sections have been tabulated separately.

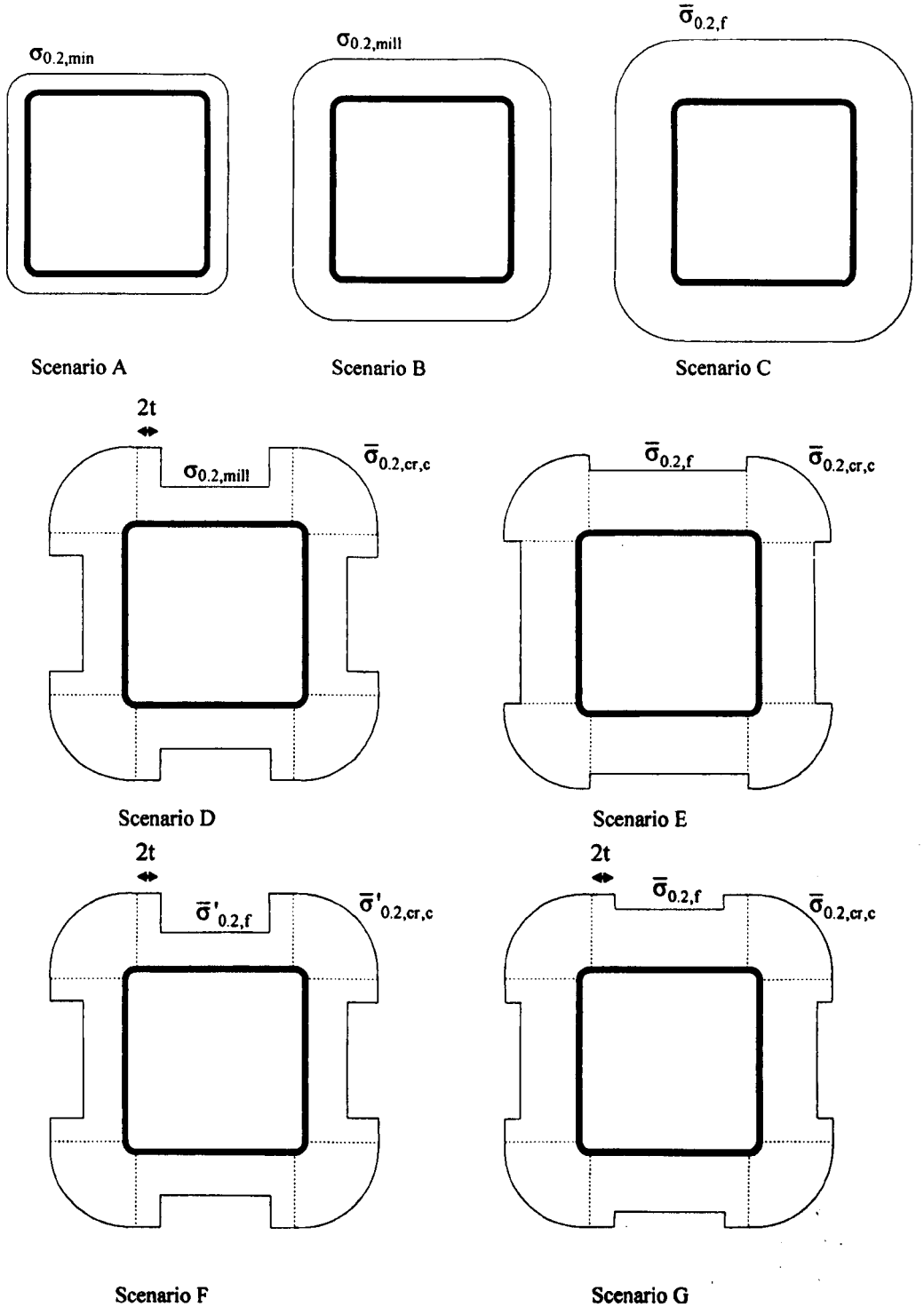

Figure 7.4: *Seven considered scenarios for the material stratification of cold rolled box sections*

Scenarios A-C consider a uniform distribution for the minimum specified 0.2% proof stress $\sigma_{0.2,min}$, the mill certificate 0.2% proof stress $\sigma_{0.2,mill}$, and the predicted 0.2% proof stress for sections flat face $\bar{\sigma}_{0.2,f}$, respectively. Scenario E considers the inclusion of the enhanced corner 0.2% proof stress $\bar{\sigma}_{0.2,cr,c}$ defined by Equation 6.35 within the quarter arc of the section corner combined with the predicted 0.2% proof stress $\bar{\sigma}_{0.2,f}$ taken for the sections' flat faces. Scenario D and G consider the inclusion of the enhanced corner 0.2% proof stress $\bar{\sigma}_{0.2,cr,c}$ for extended corner regions (2t beyond the corner to flat face junction). Scenario D adopts the 0.2% proof stress from the mill certificates $\sigma_{0.2,mill}$ for the sections' flat faces and Scenario G assumes the predicted 0.2% proof stress for this region $\bar{\sigma}_{0.2,f}$. Scenario F uses the proposed cold rolled 0.2% proof stress model (Equations 6.31 and 6.35) replacing the mill certificate 0.2% proof stress $\sigma_{0.2,mill}$ and ultimate stress $\sigma_{ult,mill}$ with minimum specified values $\sigma_{0.2,min}$ and $\sigma_{ult,min}$. The resulting 0.2% proof stress of the flat faces and corners is given as $\bar{\sigma}'_{0.2,f}$ and $\bar{\sigma}'_{0.2,cr,c,}$. A range of ultimate stress values are given in EN 10088-2 (2005) for each grade. In order to be conservative the minimum ultimate stress value has been used in the calculations. For the four stratified 0.2% proof stress distributions considered, Scenarios D-G, the weighted average of the distributions has been used in design.

7.3.3 Results

7.3.3.1 Stub columns

The predicted cross section resistances, $N_{c,Rd}$, normalised over the experimental values $N_{c,exp}$ obtained from rectangular and square hollow section stub column tests, are given in Tables 7.4 and 7.5 respectively, including the maximum plate slenderness of the cross section $\bar{\lambda}_{p,max}$ (Equation 7.1). These two parameters are plotted for square and rectangular hollow sections in Figures 7.5-7.7 for the seven different 0.2% proof stress distributions described previously. Figure 7.5 shows the three considered uniform distributions of the 0.2% proof stress (Scenarios A-C). In this graph it can be seen that the predicted cross section resistance closest to the test results has been obtained by employing the 0.2% proof stress distribution of Scenario C where the predicted 0.2% proof stress of the flat region $\bar{\sigma}_{0.2,f}$ is used. The cross section resistances predicted in this scenario for the square and rectangular hollow sections are, on average, 1.7 and 1.9 times those predicted using the minimum 0.2% proof stress value $\sigma_{0.2,min}$ (Scenario A). For both section types, when the cross section resistance is predicted using a uniform distribution of the mill certificate 0.2% proof stress $\sigma_{0.2,mill}$ (Scenario B), on average an

increase of 1.4 times the cross section resistance predicted with Scenario A is obtained. It can be clearly seen in Figure 7.5 that the stockier sections show a greater increase in cross section resistance between Scenario C and A because there are greater strength increases for stocky sections and the full cross section strength can be used in design.

The normalised cross section resistances predicted by Scenarios C, E and G are compared in Figure 7.6. The influence of including enhanced corner material properties $\bar{\sigma}_{0.2,cr,c}$ is compared with Scenario C where a uniform predicted 0.2% proof stress $\bar{\sigma}_{0.2,f}$ is considered with no corner enhancements. Scenario E assumes corner enhancements are located solely in the corner radius and Scenario G assumes extended corner enhancements. The comparison shows the small contribution that the corner enhancements make even for stocky sections. On average, for square and rectangular hollow sections respectively the increases of the cross section resistance from Scenario C to E are 0.03 and 0.02 of the test value and from Scenario E to G they are slightly higher at 0.05 and 0.13 of the test value.

Figure 7.7 compares the 0.2% proof stress distributions Scenario D, G and F which all consider distributions with extended enhanced corner 0.2% proof stresses. Scenario D employs the weighted average of the 0.2% proof stress from mill certificates for the sections' flat faces and the enhanced 0.2% proof stress for extended corners and predicts increases of 0.8 above the minimum specified distribution (Scenario A). Employing the weighted average of the proposed 0.2% proof stress distribution given in Scenario G for cross section design shows the closest prediction to the test results and a substantial average increase in cross section resistance for both square and rectangular hollow sections of 2.1 times values determined using the minimum specified 0.2% proof stress (Scenario A). If no mill certificate data is available, Scenario F is considered which replaces the mill certificate 0.2% proof stress and ultimate stress with the corresponding minimum specified values in the proposed 0.2% proof stress models. The average increases are 1.6 times the cross section resistance obtained through adopting the minimum specified values (Scenario A).

Table 7.4: *Predicted cross section resistance for cold rolled square hollow sections*

Section properties					*Scenario A*		*Scenario B*		*Scenario C*		*Scenario D*		*Scenario E*		*Scenario F*		*Scenario G*	
Source	*L (mm)*	*d (mm)*	*r_i (mm)*	*t (mm)*	$\bar{\lambda}_{p,max}$	$N_{c,Rd}/N_{c,exp}$	$\bar{\lambda}_{p,max}$	$N_{c,Rd}/N_{c,exp}$	$\bar{\lambda}_{p,max}$	$N_{c,Rd}/N_{c,exp}$	$\bar{\lambda}_{p,max}$	$N_{c,Rd}/N_{c,exp}$	$\bar{\lambda}_{p,max}$	$N_{c,Rd}/N_{c,exp}$	$\bar{\lambda}_{p,max}$	$N_{c,Rd}/N_{c,exp}$	$\bar{\lambda}_{p,max}$	$N_{c,Rd}/N_{c,exp}$
Gardner (2002)	400.2	79.9	4.6	3.68	0.30	0.31	0.36	0.43	0.43	0.62	0.41	0.58	0.44	0.65	0.40	0.54	0.46	0.70
	399.9	80.1	4.4	3.82	0.29	0.33	0.35	0.46	0.42	0.67	0.40	0.61	0.43	0.70	0.39	0.58	0.44	0.75
	399.4	80.1	4.4	3.83	0.29	0.33	0.35	0.46	0.42	0.67	0.40	0.62	0.43	0.71	0.39	0.58	0.44	0.76
	400.5	100.2	1.3	1.91	0.86	0.64	0.94	0.72	0.97	0.75	0.99	0.80	0.99	0.76	0.94	0.74	1.02	0.83
	400.2	99.9	1.3	1.91	0.86	0.67	0.94	0.75	0.97	0.79	0.99	0.84	0.99	0.80	0.93	0.78	1.02	0.87
	400.0	100.1	1.5	2.87	0.56	0.51	0.62	0.60	0.68	0.67	0.67	0.67	0.69	0.69	0.64	0.64	0.71	0.74
	399.8	100.1	1.5	2.84	0.56	0.49	0.63	0.58	0.68	0.65	0.67	0.65	0.69	0.66	0.65	0.62	0.72	0.71
	399.8	99.8	4.5	3.84	0.37	0.39	0.44	0.55	0.50	0.73	0.49	0.68	0.51	0.76	0.46	0.61	0.53	0.81
	400.4	99.7	4.5	3.83	0.37	0.39	0.44	0.55	0.50	0.73	0.49	0.68	0.52	0.76	0.46	0.61	0.53	0.81
	399.8	100.1	5.8	5.94	0.22	0.30	0.25	0.40	0.33	0.65	0.31	0.57	0.33	0.67	0.31	0.58	0.34	0.72
	399.6	100.2	5.8	5.92	0.22	0.30	0.26	0.40	0.33	0.65	0.31	0.57	0.33	0.67	0.31	0.58	0.34	0.72
	399.1	100.3	8.0	7.97	0.14	0.36	0.17	0.50	0.24	0.99	0.22	0.83	0.24	1.00	0.22	0.81	0.24	1.03
	400.0	100.1	8.0	7.97	0.14	0.32	0.17	0.46	0.24	0.89	0.22	0.75	0.24	0.91	0.22	0.73	0.24	0.93
	449.9	150.4	5.8	3.79	0.60	0.60	0.72	0.77	0.77	0.85	0.77	0.87	0.79	0.87	0.69	0.74	0.81	0.93
	450.7	150.2	6.0	3.74	0.60	0.59	0.73	0.77	0.78	0.84	0.78	0.87	0.79	0.87	0.70	0.74	0.82	0.93
Rasmussen and Hancock (1993a)	300	80.4	5.5	3	0.48	0.46	0.53	0.55	0.61	0.68	0.59	0.67	0.62	0.71	0.59	0.66	0.64	0.75
	298	79.7	5.5	3	0.48	0.47	0.52	0.56	0.60	0.59	0.59	0.68	0.62	0.73	0.59	0.68	0.64	0.77
Talja and Salmi (1995)	400.2	79.9	4.6	3.68	0.20	0.26	0.24	0.36	0.33	0.66	0.30	0.57	0.33	0.71	0.30	0.59	0.34	0.73
					Mean	0.43	Mean	0.55	Mean	0.73	Mean	0.69	Mean	0.76	Mean	0.65	Mean	0.81
					COV	0.30	COV	0.24	COV.	0.15	COV	0.15	COV	0.13	COV	0.13	COV	0.12

Table 7.5: *Predicted cross section resistance for cold rolled rectangular hollow sections*

Section properties						*Scenario A*		*Scenario B*		*Scenario C*		*Scenario D*		*Scenario E*		*Scenario F*		*Scenario G*	
Source	*L (mm)*	*d (mm)*	*b (mm)*	*r_i (mm)*	*t (mm)*	$\bar{\lambda}_{p,max}$	$N_{c,Rd}/N_{c,exp}$	$\bar{\lambda}_{p,max}$	$N_{c,Rd}/N_{c,exp}$	$\bar{\lambda}_{p,max}$	$N_{c,Rd}/N_{c,exp}$	$\bar{\lambda}_{p,max}$	$N_{c,Rd}/N_{c,exp}$	$\bar{\lambda}_{p,max}$	$N_{c,Rd}/N_{c,exp}$	$\bar{\lambda}_{p,max}$	$N_{c,Rd}/N_{c,exp}$	$\bar{\lambda}_{p,max}$	$N_{c,Rd}/N_{c,exp}$
Gardner (2002)	180.3	60.0	40.0	2.9	3.83	0.21	0.29	0.24	0.38	0.34	0.73	0.31	0.73	0.34	0.75	0.31	0.75	0.35	0.93
	179.6	60.0	40.0	2.9	3.82	0.21	0.28	0.24	0.38	0.34	0.72	0.31	0.72	0.34	0.74	0.31	0.74	0.35	0.92
	359.9	120.1	80.2	4.6	2.93	0.64	0.53	0.94	0.96	1.03	1.09	0.96	1.11	1.03	1.10	0.76	0.76	1.03	1.22
	360.0	120.0	80.2	4.6	2.91	0.65	0.53	0.94	0.96	1.03	1.09	0.97	1.11	1.03	1.10	0.77	0.76	1.04	1.22
	360.1	119.9	80.4	7.0	5.85	0.28	0.30	0.33	0.42	0.42	0.68	0.40	0.69	0.43	0.71	0.39	0.67	0.44	0.85
	360.1	120.0	80.3	7.0	5.85	0.28	0.30	0.33	0.42	0.42	0.67	0.40	0.68	0.43	0.70	0.39	0.66	0.44	0.85
	450.4	149.9	99.9	5.6	3.82	0.58	0.56	0.69	0.73	0.76	0.86	0.75	0.92	0.78	0.89	0.70	0.82	0.80	1.03
	450.0	149.9	99.9	5.6	3.83	0.58	0.56	0.68	0.73	0.76	0.86	0.75	0.92	0.78	0.90	0.70	0.83	0.80	1.03
	300.6	99.8	49.8	2.3	1.85	0.87	0.55	1.02	0.71	1.10	0.79	1.09	0.86	1.12	0.81	0.99	0.74	1.15	0.93
	299.8	99.8	50.0	2.3	1.84	0.87	0.55	1.03	0.71	1.10	0.79	1.10	0.86	1.12	0.81	1.00	0.74	1.15	0.93
	299.9	100.1	50.1	3.1	2.89	0.54	0.46	0.79	0.83	0.91	1.04	0.82	0.99	0.91	1.04	0.68	0.72	0.91	1.17
	300.0	100.1	50.0	3.1	2.89	0.54	0.45	0.79	0.82	0.91	1.02	0.82	0.97	0.91	1.02	0.68	0.70	0.91	1.15
	300.4	99.7	49.9	3.6	3.73	0.39	0.34	0.43	0.42	0.52	0.63	0.51	0.66	0.54	0.67	0.51	0.68	0.56	0.80
	300.6	99.8	49.8	3.6	3.68	0.39	0.34	0.43	0.42	0.53	0.62	0.51	0.64	0.54	0.65	0.52	0.66	0.57	0.78
	300.0	100.1	50.1	5.6	5.95	0.22	0.27	0.27	0.41	0.37	0.80	0.33	0.74	0.37	0.80	0.33	0.72	0.37	0.94
	300.1	100.0	50.1	5.5	5.96	0.22	0.27	0.27	0.41	0.37	0.80	0.33	0.74	0.37	0.80	0.33	0.72	0.37	0.94
Talja and Salmi (1995)	1048.0	150.6	100.6	3.0	2.89[a]	0.90	0.72	1.00	0.83	1.06	0.90	1.01	0.91	1.06	0.90	1.00	0.91	1.06	0.97
	1049.0	149.8	100.2	6.0	5.77[a]	0.39	0.43	0.46	0.62	0.56	0.88	0.47	0.70	0.55	0.86	1.00	0.82	0.53	0.90
						Mean	0.43	Mean	0.62	Mean	0.83	Mean	0.83	Mean	0.85	Mean	0.74	Mean	0.98
						COV	0.31	COV	0.34	COV	0.18	COV	0.15	COV	0.17	COV	0.09	COV	0.14

[a] Sections formed by gradually folding sheet material

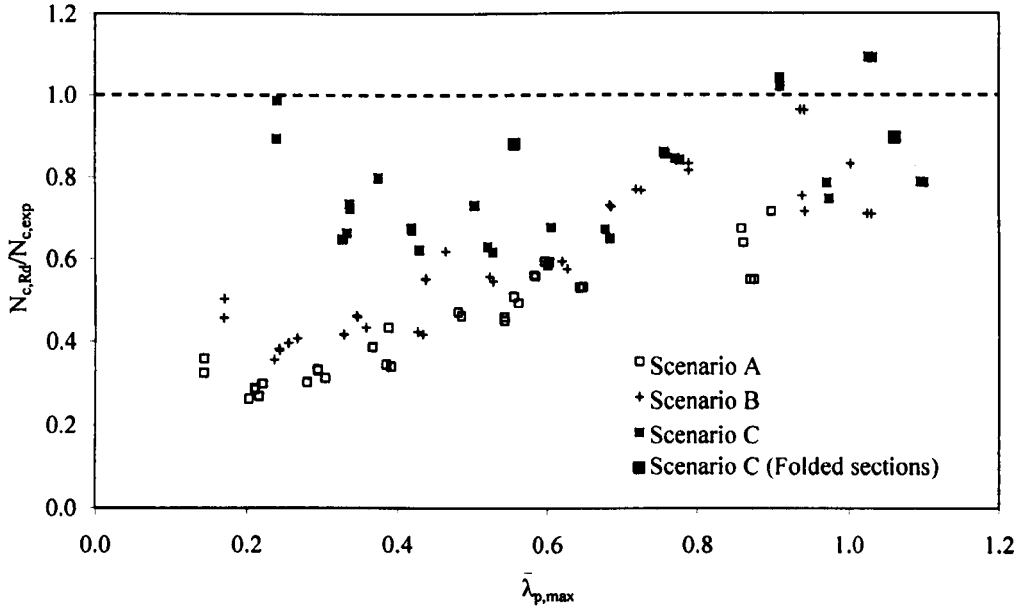

Figure 7.5: *The ratio of predicted cross section resistance to the test value plotted against slenderness for cold rolled box sections designed with uniform material distributions; minimum specified 0.2% proof stress (Scenario A), mill certificate 0.2% proof stress (Scenario B) and the predicted flat 0.2% proof stress of the cold rolled box sections (Scenario C)*

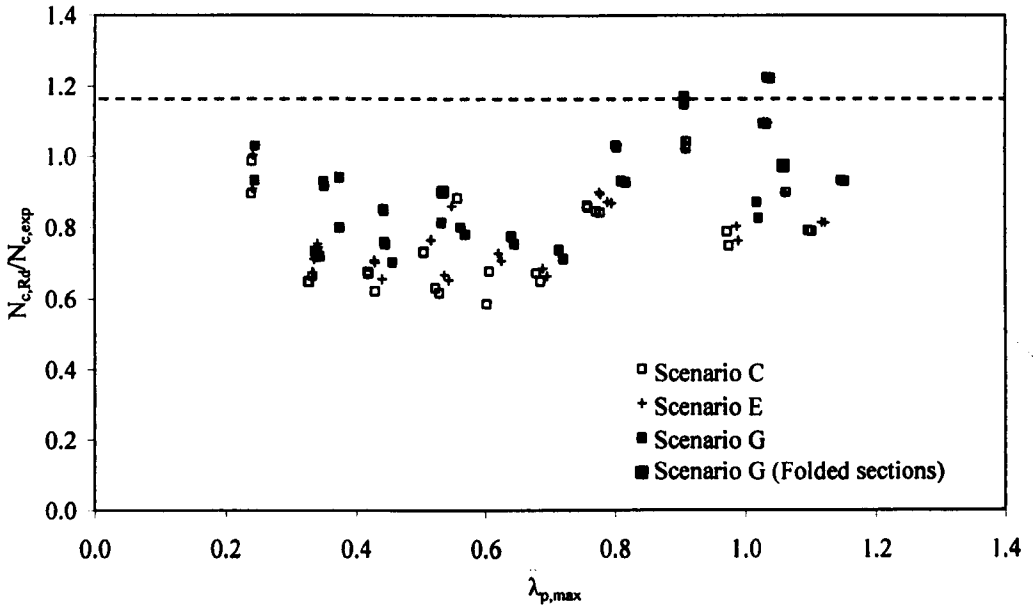

Figure 7.6: *The ratio of predicted cross section resistance to the test value plotted against slenderness for cold rolled box sections designed with the predicted flat 0.2% proof stress (Scenario C), predicted flat and enhanced corner 0.2% proof stress (Scenario E) and predicted flat and extended enhanced corner 0.2% proof stress (Scenario G)*

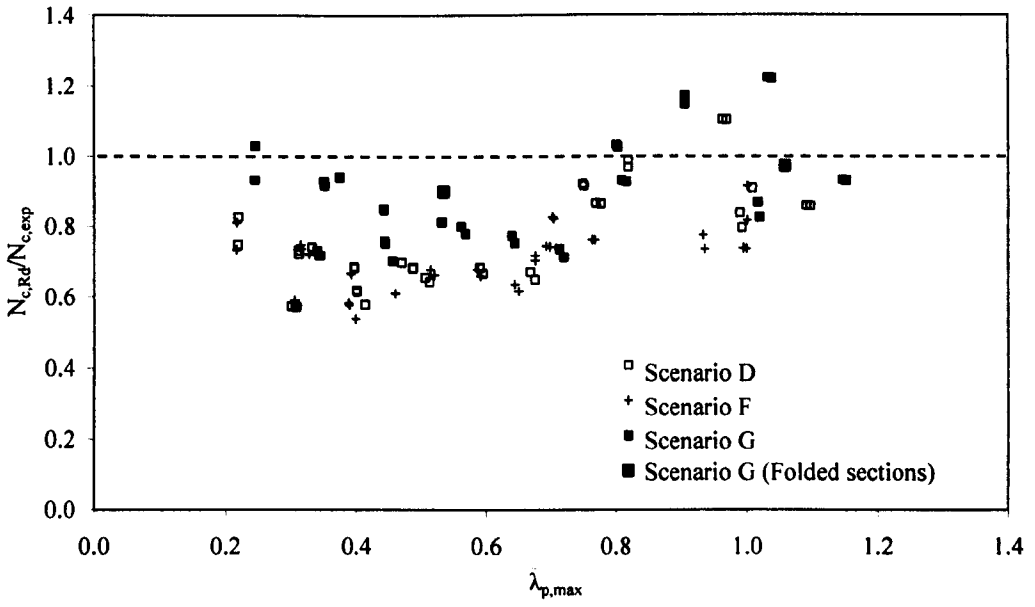

Figure 7.7: *The ratio of predicted cross section resistance to the test value plotted against slenderness for cold rolled box sections designed with the mill certificate and extended enhanced corner 0.2% proof stress (Scenario D), predicted flat and extended enhanced corner 0.2% proof stress based on minimum specified values (Scenario F) and predicted flat and extended enhanced corner 0.2% proof stress based on mill certificate values (Scenario G)*

7.3.3.2 Columns

Tables 7.6 and 7.7 show the predicted column buckling resistance $N_{b,Rd}$ normalised over the test values $N_{b,exp}$ for square and rectangular hollow sections respectively. The increases noted between adopting the minimum specified 0.2% proof stress distribution given in Scenario A and the alternative six Scenarios B-G are less than for the cross section resistances due to overall buckling dominating the column resistance of slender members. Figures 7.9-11 show the normalised predicted member resistance for both square and rectangular sections plotted against member slenderness $\bar{\lambda}$ which is given in Equation 7.2 for Class 1, 2 and 3 cross sections and Equation 7.3 for Class 4 cross sections. A and A_{eff} are the cross section area and effective cross section area respectively, $\sigma_{0.2}$ is the assumed weighted average 0.2% proof stress for Scenarios A-G and N_{cr} is the elastic critical buckling load.

$$\bar{\lambda} = \sqrt{\frac{A\sigma_{0.2}}{N_{cr}}} \qquad \text{for Class 1, 2 and 3 cross sections} \qquad (7.2)$$

$$\bar{\lambda} = \sqrt{\frac{A_{eff}\sigma_{0.2}}{N_{cr}}} \qquad \text{for Class 4 cross sections} \qquad (7.3)$$

The scenarios considered in Figure 7.8 are for an assumed uniform 0.2% proof stress distributions of the minimum specified values $\sigma_{0.2,min}$ (Scenario A), the mill certificate value $\sigma_{0.2,mill}$ (Scenario B) and the predicted 0.2% proof stress of the flat faces $\bar{\sigma}_{0.2,f}$ (Scenario C). Average increases of the column resistance of 0.4 of the test value for both square and rectangular hollow sections can be seen between Scenario A and Scenario C and a smaller average increase of 0.2 of the test value for both square and rectangular hollow sections between Scenario A and B. Figure 7.9 plots data for Scenario C, E and G whilst Figure 7.10 plots the data for Scenario D, F and G. Figure 7.9 shows the comparatively small increase due to including the corner strength enhancements (Scenario E) and extended corner strength enhancements (Scenario G), with the predicted 0.2% proof stress $\bar{\sigma}_{0.2,f}$ taken for the sections' flat faces.

The extended corner strength enhancements $\bar{\sigma}_{0.2,cr,c}$ together with the predicted flat 0.2% proof stress for the sections' flat regions $\bar{\sigma}_{0.2,f}$ given in Scenario G predicts the highest test column resistance being on average 1.5 times values obtained by assuming the uniform minimum specified 0.2% proof stress distribution (Scenario A) for all considered sections. Scenario F considers the proposed material model based on the minimum specified 0.2% proof stress and ultimate stress values yielding increases of 1.3 times the column resistance obtained by assuming the uniform minimum specified 0.2% proof stress distribution in Scenario A.

Table 7.6: *Predicted column resistance for cold rolled square hollow sections*

Section properties					*Scenario A*		*Scenario B*		*Scenario C*		*Scenario D*		*Scenario E*		*Scenario F*		*Scenario G*	
Source	*L (mm)*	*d (mm)*	*r_i (mm)*	*t (mm)*	$\bar{\lambda}$	$N_{b,Rd}/N_{b,exp}$	$\bar{\lambda}$	$N_{b,Rd}/N_{b,exp}$	$\bar{\lambda}$	$N_{b,Rd}/N_{b,exp}$	$\bar{\lambda}$	$N_{b,Rd}/N_{b,exp}$	$\bar{\lambda}$	$N_{b,Rd}/N_{b,exp}$	$\bar{\lambda}$	$N_{b,Rd}/N_{b,exp}$	$\bar{\lambda}$	$N_{b,Rd}/N_{b,exp}$
Gardner (2002)	1899.8	79.7	4.5	3.74	0.63	0.64	0.75	0.80	0.90	0.99	0.87	0.95	0.92	1.01	0.84	0.92	0.96	1.05
	2000.7	79.7	4.5	3.78	0.67	0.66	0.79	0.81	0.95	0.99	0.91	0.96	0.97	1.02	0.88	0.93	1.01	1.05
	2000.3	99.9	1.3	1.86	0.45	0.65	0.47	0.72	0.48	0.74	0.49	0.76	0.49	0.75	0.47	0.71	0.50	0.78
	2000.4	100.2	1.5	2.83	0.53	0.64	0.57	0.73	0.60	0.79	0.60	0.78	0.61	0.81	0.58	0.75	0.62	0.84
	2000.4	99.9	4.5	3.77	0.53	0.59	0.63	0.78	0.72	0.95	0.70	0.91	0.74	0.97	0.66	0.84	0.76	1.02
	1999.9	100.3	5.8	5.92	0.54	0.49	0.63	0.61	0.80	0.85	0.75	0.79	0.82	0.87	0.76	0.79	0.85	0.90
	1999.6	100.4	8.0	7.96	0.55	0.69	0.65	0.90	0.91	1.36	0.84	1.24	0.92	1.37	0.79	1.17	0.93	1.39
	1999.8	150.2	5.8	3.77	0.34	0.62	0.38	0.79	0.40	0.86	0.40	0.86	0.41	0.88	0.38	0.75	0.42	0.91
Rasmussen and Hancock (1993a)	1001	80.5	3.1	2.90	0.35	0.53	0.39	0.67	0.45	0.83	0.43	0.79	0.45	0.85	0.43	0.77	0.46	0.88
	2000	80.4	3.0	2.99	0.69	0.87	0.79	1.03	0.90	1.19	0.87	1.14	0.92	1.21	0.86	1.13	0.94	1.23
	3002	80.7	2.6	2.95	1.04	1.20	1.18	1.31	1.34	1.40	1.29	1.38	1.35	1.41	1.27	1.37	1.38	1.42
Talja and Salmi (1995)	1050.0	59.7	3.0	4.77	0.51	0.47	0.59	0.60	0.82	0.96	0.71	0.80	0.82	0.96	0.76	0.87	0.82	0.95
	1700.0	59.7	3.0	4.77	0.82	0.64	0.95	0.75	1.34	0.94	1.16	0.87	1.33	0.94	1.23	0.90	1.33	0.94
	2350.0	59.7	3.0	4.77	1.13	0.77	1.32	0.84	1.85	0.95	1.60	0.91	1.84	0.95	1.70	0.92	1.83	0.95
					Mean	0.68	Mean	0.81	Mean	0.99	Mean	0.94	Mean	1.00	Mean	0.92	Mean	1.02
					COV	0.27	COV	0.22	COV	0.20	COV	0.20	COV	0.20	COV	0.20	COV	0.19

Table 7.7: *Predicted column resistance for cold rolled rectangular hollow sections*

Section properties						*Scenario A*		*Scenario B*		*Scenario C*		*Scenario D*		*Scenario E*		*Scenario F*		*Scenario G*	
Source	*L (mm)*	*d (mm)*	*b (mm)*	r_i *(mm)*	*t (mm)*	$\bar{\lambda}$	$N_{b,Rd}/N_{b,exp}$	$\bar{\lambda}$	$N_{b,Rd}/N_{b,exp}$	$\bar{\lambda}$	$N_{b,Rd}/N_{b,exp}$	$\bar{\lambda}$	$N_{b,Rd}/N_{b,exp}$	$\bar{\lambda}$	$N_{b,Rd}/N_{b,exp}$	$\bar{\lambda}$	$N_{b,Rd}/N_{b,exp}$	$\bar{\lambda}$	$N_{b,Rd}/N_{b,exp}$
Gardner (2002)	2000.1	60.0	40.0	2.9	3.83	0.99	0.77	1.14	0.86	1.57	1.00	1.45	0.98	1.59	1.01	1.47	0.98	1.64	1.02
	2000.2	99.8	49.8	2.3	1.83	0.53	0.58	0.61	0.71	0.64	0.76	0.64	0.78	0.65	0.78	0.59	0.68	0.67	0.82
	2000.2	100.1	50.1	3.1	2.87	1.03	0.92	1.39	1.10	1.56	1.14	1.45	1.11	1.55	1.14	1.23	1.03	1.58	1.15
	2000.2	99.7	49.9	3.6	3.70	1.00	0.75	1.11	0.81	1.36	0.91	1.32	0.90	1.39	0.92	1.34	0.90	1.45	0.93
	2000.2	100.0	50.0	5.5	5.96	1.05	0.77	1.29	0.88	1.80	1.00	1.60	0.96	1.80	1.00	1.58	0.96	1.80	1.00
	1999.0	120.0	80.2	4.6	2.91	0.64	0.65	0.86	0.94	0.92	1.01	0.89	0.98	0.92	1.01	0.73	0.78	0.94	1.03
	2000.4	120.0	80.4	7.0	5.87	0.66	0.54	0.78	0.67	0.99	0.87	0.94	0.82	1.01	0.88	0.93	0.81	1.05	0.90
	1999.5	149.8	99.9	5.6	3.79	0.50	0.67	0.57	0.83	0.61	0.94	0.61	0.94	0.63	0.97	0.58	0.85	0.65	1.02
	1000.2	59.9	39.9	2.9	3.82	0.68	0.68	0.79	0.82	1.09	1.12	1.00	1.06	1.10	1.13	1.01	1.06	1.13	1.15
	1000.2	99.8	50.0	2.3	1.82	0.45	0.58	0.52	0.72	0.54	0.79	0.55	0.80	0.55	0.80	0.50	0.69	0.57	0.85
	1000.1	100.1	50.0	3.1	2.86	0.52	0.56	0.70	0.89	0.78	1.02	0.73	0.94	0.78	1.02	0.62	0.74	0.79	1.04
	999.6	99.7	50.3	3.6	3.73	0.50	0.48	0.55	0.57	0.67	0.77	0.65	0.74	0.69	0.80	0.66	0.75	0.72	0.85
	999.8	100.0	50.1	5.6	5.94	0.52	0.48	0.64	0.67	0.90	1.02	0.80	0.89	0.90	1.02	0.79	0.88	0.90	1.02
	1000.6	120.0	80.2	4.6	2.86	0.32	0.52	0.43	0.92	0.45	1.02	0.44	0.98	0.46	1.02	0.37	0.68	0.47	1.06
Talja and Salmi (1995)	2700.0	150.4	100.3	3.0	2.89[a]	0.47	0.75	0.48	0.80	0.50	0.85	0.52	0.91	0.53	0.93	0.50	0.84	0.54	0.96
	4350.0	150.4	100.3	3.0	2.89[a]	0.75	0.82	0.78	0.86	0.81	0.90	0.84	0.95	0.85	0.96	0.80	0.89	0.87	0.98
	6000.0	150.4	100.3	3.0	2.89[a]	1.04	0.81	1.07	0.83	1.12	0.85	1.16	0.88	1.17	0.88	1.11	0.85	1.20	0.89
	2700.0	149.8	100.2	5.0	5.85[a]	0.46	0.66	0.55	0.89	0.66	1.18	0.60	1.01	0.67	1.20	0.58	0.96	0.66	1.18
	4350.0	150.6	100.6	6.0	5.77[a]	0.74	0.89	0.88	1.10	1.06	1.29	0.96	1.19	1.08	1.31	0.92	1.15	1.06	1.29
	6000.0	150.6	100.6	6.0	5.77[a]	1.02	1.05	1.22	1.18	1.46	1.29	1.32	1.23	1.49	1.30	1.27	1.21	1.46	1.29
						Mean	0.70	Mean	0.85	Mean	0.99	Mean	0.95	Mean	1.00	Mean	0.89	Mean	1.02
						COV	0.22	COV	0.18	COV	0.16	COV	0.13	COV	0.15	COV	0.17	COV	0.13

[a] Sections formed by gradually folding sheet material

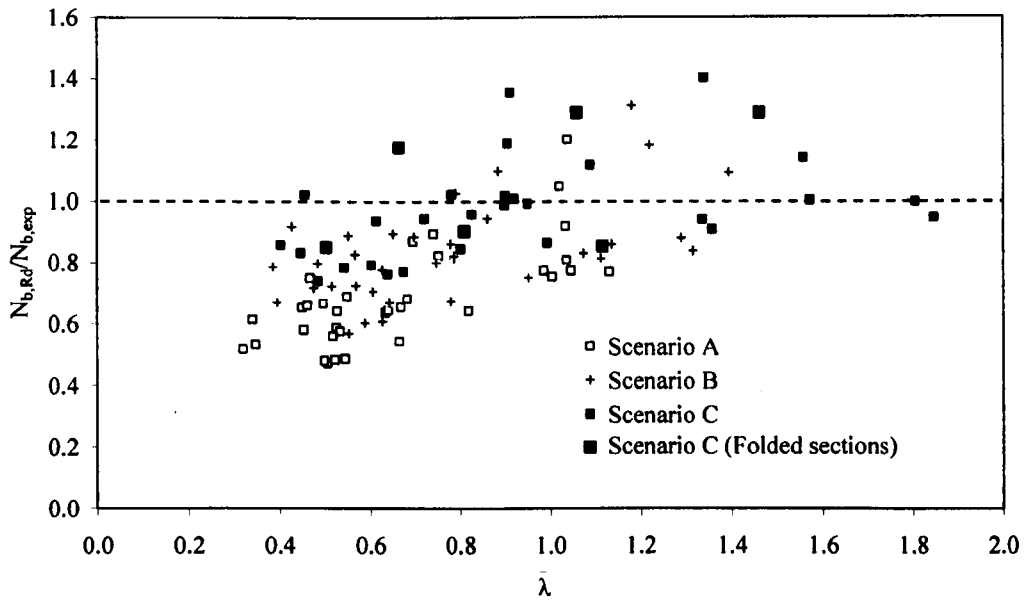

Figure 7.8: *The ratio of predicted column resistance to the test value plotted against slenderness for cold rolled box sections designed with uniform material distributions; minimum specified 0.2% proof stress (Scenario A), mill certificate 0.2% proof stress (Scenario B) and the predicted flat 0.2% proof stress of the cold rolled box sections (Scenario C)*

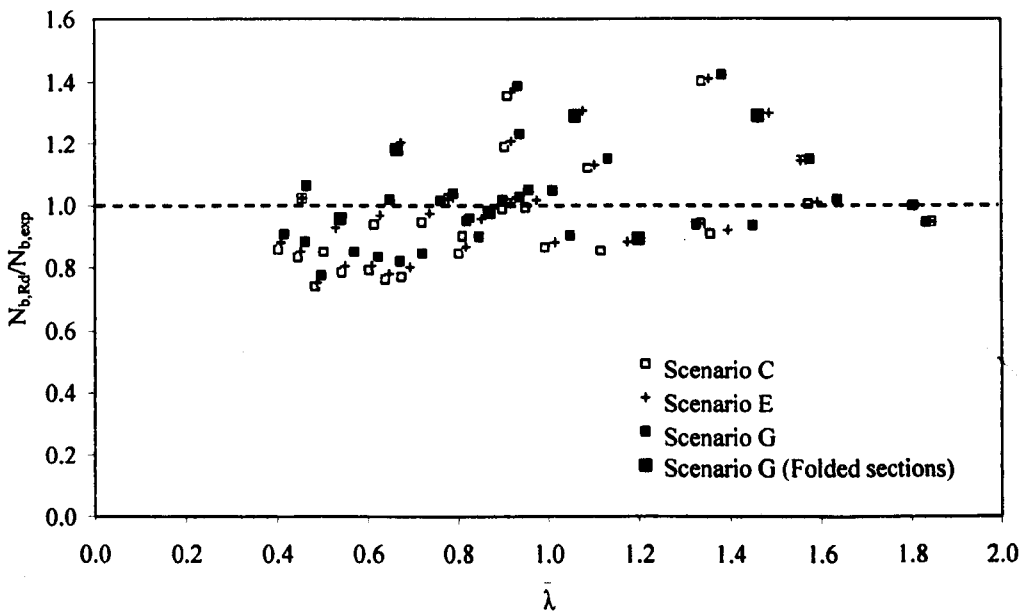

Figure 7.9: *The ratio of predicted column resistance to the test value plotted against slenderness for cold rolled box sections designed with the predicted flat 0.2% proof stress (Scenario C), predicted flat and enhanced corner 0.2% proof stress (Scenario E) and predicted flat and extended enhanced corner 0.2% proof stress (Scenario G)*

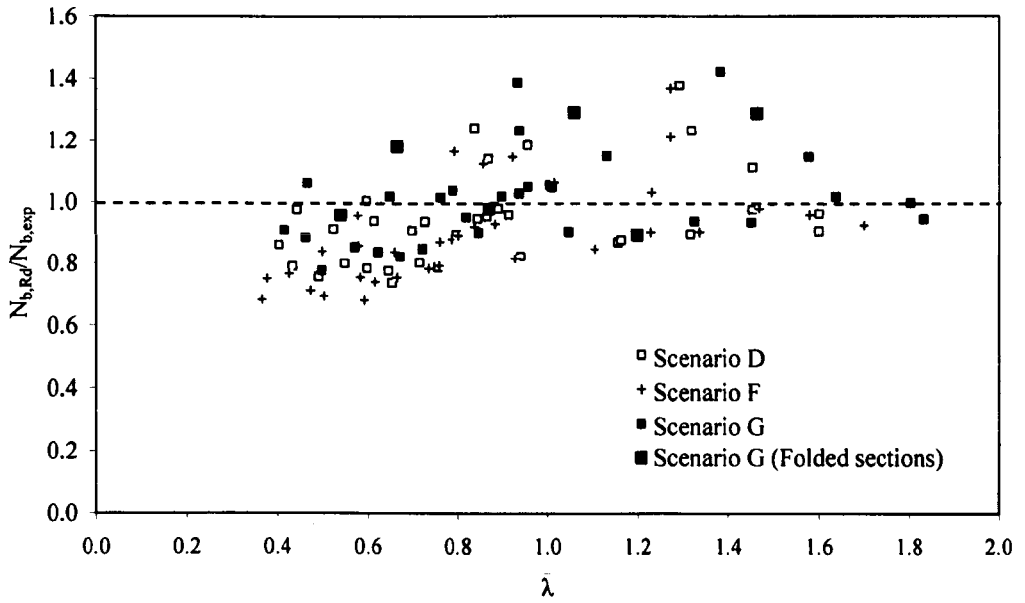

Figure 7.10: *The ratio of predicted column resistance to the test value plotted against slenderness for cold rolled box sections designed with the mill certificate and extended enhanced corner 0.2% proof stress (Scenario D), predicted flat and extended enhanced corner 0.2% proof stress based on minimum specified values (Scenario F) and predicted flat and extended enhanced corner 0.2% proof stress based on mill certificate values (Scenario G)*

7.3.3.3 Beams

The predicted bending resistance $M_{c,Rd}$ normalised over the experimentally obtained bending resistance $M_{c,exp}$ for square and rectangular hollow sections is given in Table 7.8 and 7.9 and this ratio obtained for Scenarios A-C is plotted against the maximum plate slenderness $\bar{\lambda}_{p,max}$ in Figure 7.11. Here the increase in 0.2% proof stress included in design by assuming a uniform distribution of the predicted 0.2% proof stress in the flat regions $\bar{\sigma}_{0.2,f}$ (Scenario C) is, on average, 1.7 times the bending resistance predicted for a uniform distribution of the minimum specified 0.2% proof stress $\sigma_{0.2,min}$ (Scenario A). If a uniform distribution of the 0.2% proof stress of the mill certificate $\sigma_{0.2,mill}$ is assumed (Scenario B), the increase in the predicted bending resistance is on average significantly less at 1.2 times the bending resistance predicted for Scenario A.

Figure 7.12 shows the influence of introducing enhanced material strength in the corners in Scenario E, and extended enhanced material strength in the corner regions in Scenario G, from the uniform distribution of predicted flat 0.2% proof stress given in Scenario C. On average, by

including the material enhancements in the extended corner region the predicted bending resistance increases by 0.06 of the test value $M_{c,exp}$ from values obtained by adopting Scenario C, which is larger than the average increase in the normalised bending moment predicted by just considering the material enhancements to be restricted to the corners with an average increase of 0.02 of the test value.

Implementing the weighted average 0.2% proof stress of Scenario G in design gives a predicted bending moment that is closest to the test value giving average increases of 1.9 times the bending moment predicted using the uniform minimum specified 0.2% proof stress $\sigma_{0.2,min}$ distribution (Scenario A). Assuming no mill certificate data is available and replacing the mill certificate 0.2% proof stress and ultimate stress in the proposed model with the minimum specified values, an average increase of 1.5 times the bending resistance predicted assuming the minimum values is achieved. Data for this model is shown in Figure 7.13.

Table 7.8: *Predicted bending moment for cold rolled square hollow sections*

Section properties					*Scenario A*		*Scenario B*		*Scenario C*		*Scenario D*		*Scenario E*		*Scenario F*		*Scenario G*	
Source	*L (mm)*	*D (mm)*	*r_i (mm)*	*t (mm)*	$\bar{\lambda}_{p,max}$	$M_{c,Rd}/M_{c,exp}$	$\bar{\lambda}_{p,max}$	$M_{c,Rd}/M_{c,exp}$	$\bar{\lambda}_{p,max}$	$M_{c,Rd}/M_{c,exp}$	$\bar{\lambda}_{p,max}$	$M_{c,Rd}/M_{c,exp}$	$\bar{\lambda}_{p,max}$	$M_{c,Rd}/M_{c,exp}$	$\bar{\lambda}_{p,max}$	$M_{c,Rd}/M_{c,exp}$	$\bar{\lambda}_{p,max}$	$M_{c,Rd}/M_{c,exp}$
Gardner (2002)	1290.0	79.7	4.4	3.75	0.29	0.36	0.34	0.50	0.41	0.73	0.39	0.67	0.42	0.76	0.38	0.63	0.43	0.82
	1148.0	99.9	1.3	1.84	0.89	0.54	0.98	0.62	1.01	0.65	1.03	0.67	1.02	0.67	0.96	0.61	1.05	0.70
	1299.0	100.2	1.5	2.84	0.56	0.45	0.63	0.54	0.69	0.62	0.68	0.61	0.70	0.64	0.65	0.57	0.72	0.67
	1300.0	99.8	4.5	3.79	0.37	0.41	0.44	0.58	0.51	0.69	0.49	0.65	0.52	0.72	0.47	0.66	0.54	0.77
	1299.4	100.5	8.0	7.92	0.15	0.35	0.17	0.49	0.24	0.96	0.22	0.81	0.24	0.98	0.22	0.81	0.25	1.01
Rasmussen and Hancock (1993b)	1000.0	80.0	3.0	2.98	0.41	0.40	0.47	0.52	0.54	0.55	0.52	0.52	0.55	0.57	0.51	0.50	0.56	0.60
Talja and Salmi (1995)	900.0	59.8	3.5	4.77	0.16	0.28	0.19	0.38	0.26	0.76	0.24	0.63	0.26	0.77	0.24	0.64	0.27	0.80
	900.0	59.4	3.0	4.89	0.16	0.32	0.18	0.44	0.26	0.88	0.23	0.72	0.26	0.89	0.24	0.74	0.26	0.92
	900.0	59.7	3.0	4.77	0.16	0.29	0.19	0.39	0.27	0.76	0.24	0.62	0.27	0.78	0.24	0.65	0.27	0.80
					Mean	0.38	Mean	0.50	Mean	0.73	Mean	0.65	Mean	0.75	Mean	0.64	Mean	0.79
					COV	0.22	COV	0.16	COV	0.17	COV	0.12	COV	0.17	COV	0.14	COV	0.16

Table 7.9: *Predicted bending moment for cold rolled rectangular hollow sections*

Section properties						*Scenario A*		*Scenario B*		*Scenario C*		*Scenario D*		*Scenario E*		*Scenario F*		*Scenario G*	
Source	*L (mm)*	*D (mm)*	*B (mm)*	r_i *(mm)*	*t (mm)*	$\bar{\lambda}_{p,max}$	$M_{c,Rd}/M_{c,exp}$	$\bar{\lambda}_{p,max}$	$M_{c,Rd}/M_{c,exp}$	$\bar{\lambda}_{p,max}$	$M_{c,Rd}/M_{c,exp}$	$\bar{\lambda}_{p,max}$	$M_{c,Rd}/M_{c,exp}$	$\bar{\lambda}_{p,max}$	$M_{c,Rd}/M_{c,exp}$	$\bar{\lambda}_{p,max}$	$M_{c,Rd}/M_{c,exp}$	$\bar{\lambda}_{p,max}$	$M_{c,Rd}/M_{c,exp}$
Gardner (2002)	1100.0	59.9	39.9	2.9	3.79	0.12	0.31	0.14	0.41	0.19	0.79	0.18	0.67	0.20	0.81	0.18	0.69	0.20	0.85
	1000.0	99.7	49.8	2.3	1.79	0.41	0.67	0.48	0.40	0.51	0.45	0.51	0.45	0.52	0.47	0.47	0.86	0.54	0.50
	1100.0	100.1	50.0	3.2	2.88	0.23	0.41	0.34	0.87	0.39	1.15	0.35	0.94	0.39	1.15	0.29	0.64	0.39	1.14
	1100.0	99.7	49.9	3.6	3.68	0.16	0.31	0.18	0.38	0.22	0.56	0.21	0.53	0.23	0.59	0.22	0.54	0.24	0.65
Talja and Salmi (1995)	4000.0	150.6	100.2	3.0	2.89[a]	0.54	0.66	0.60	0.63	0.64	0.70	0.64	0.71	0.65	0.72	0.60	0.64	0.67	0.76
	4000.0	150.4	100.3	3.0	2.89[a]	0.54	0.65	0.60	0.63	0.64	0.70	0.64	0.71	0.65	0.72	0.61	0.64	0.67	0.76
	4000.0	150.6	100.2	3.0	2.89[a]	0.54	0.66	0.60	0.63	0.64	0.70	0.64	0.71	0.65	0.72	0.60	0.64	0.67	0.76
	2200.0	149.9	100.2	4.5	5.85[a]	0.21	0.36	0.25	0.52	0.30	0.75	0.28	0.66	0.31	0.77	0.28	0.62	0.32	0.82
	2200.0	149.9	100.2	4.5	5.85[a]	0.21	0.36	0.25	0.52	0.30	0.75	0.28	0.66	0.31	0.77	0.28	0.62	0.32	0.82
	2200.0	149.8	100.1	4.5	5.85[a]	0.21	0.36	0.25	0.52	0.30	0.75	0.28	0.66	0.31	0.77	0.28	0.62	0.32	0.82
						Mean	0.48	Mean	0.55	Mean	0.73	Mean	0.67	Mean	0.75	Mean	0.65	Mean	0.79
						COV	0.34	COV	0.27	COV	0.25	COV	0.19	COV	0.23	COV	0.13	COV	0.21

[a]Sections formed by gradually folding sheet material

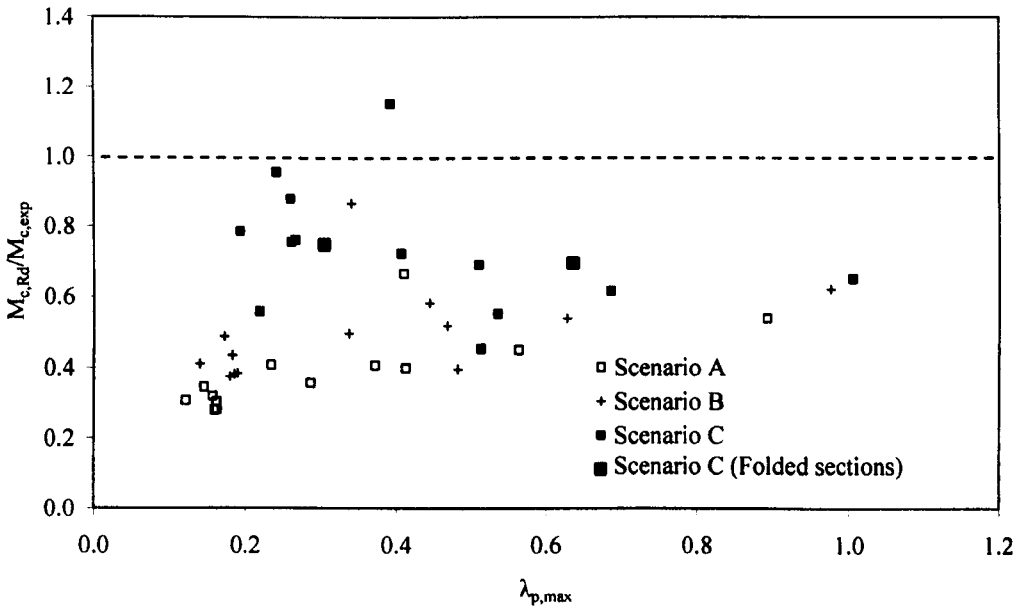

Figure 7.11: *The ratio of predicted bending moment to the test value plotted against slenderness for cold rolled box sections designed with uniform material distributions; minimum specified 0.2% proof stress (Scenario A), mill certificate 0.2% proof stress (Scenario B) and the predicted flat 0.2% proof stress of the cold rolled box sections (Scenario C)*

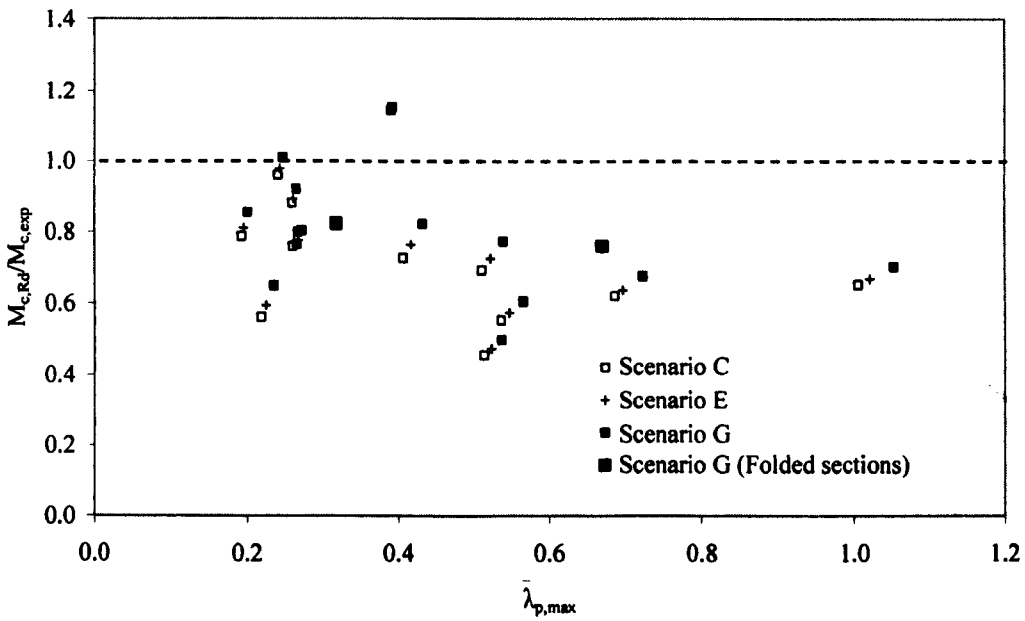

Figure 7.12: *The ratio of predicted bending resistance to the test value plotted against slenderness for cold rolled box sections designed with the predicted flat 0.2% proof stress (Scenario C), predicted flat and enhanced corner 0.2% proof stress (Scenario E) and predicted flat and extended enhanced corner 0.2% proof stress (Scenario G)*

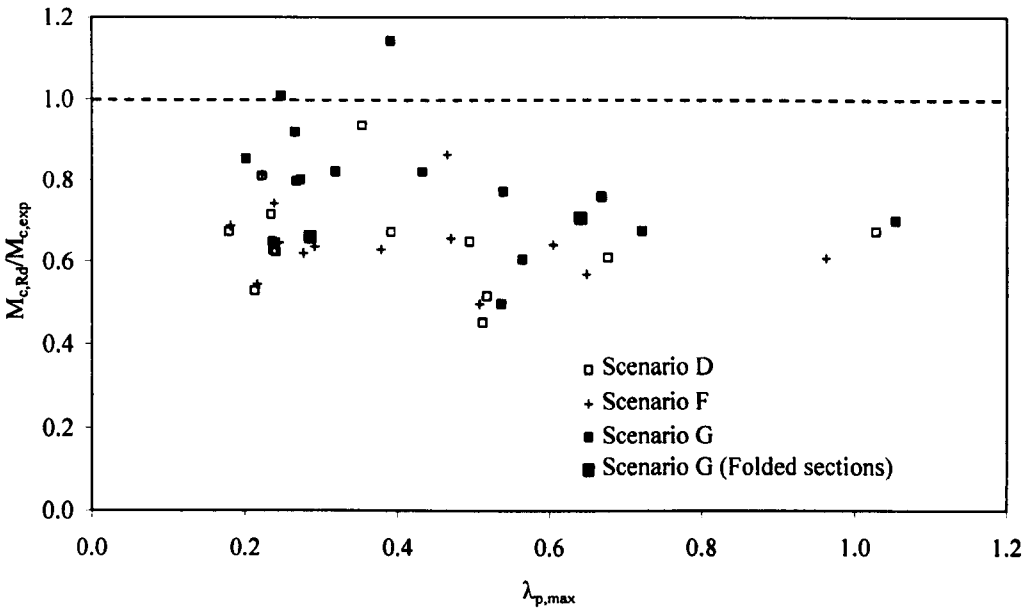

Figure 7.13: *The ratio of predicted bending resistance to the test value plotted against slenderness for cold rolled box sections designed with the mill certificate and extended enhanced corner 0.2% proof stress (Scenario D), predicted flat and extended enhanced corner 0.2% proof stress based on minimum specified values (Scenario F) and predicted flat and extended enhanced corner 0.2% proof stress based on mill certificate values (Scenario G)*

7.4 Conclusions

By implementing the current design code together with the proposed material distributions given in Chapter 6 to harness the increased material strength caused during the cold forming of sections, a comparison has been made between the predicted stub column, column buckling and bending resistances with those values obtained from published test results. This study quantifies the increase in resistance obtained by adopting the proposed 0.2% proof stress distributions for press braked sections and cold rolled box sections, rather than implementing the minimum 0.2% proof stress values recommended in EN 10088-2 (2005). Owing to the flat faces representing a large proportion of the cross section area, strength enhancements in the flat faces of the sections contribute most to the increase in member resistances with smaller increases caused by material strength enhancements in the corner regions.

In all cases the proposed 0.2% proof stress distributions given in Chapter 6 brought the average predicted member resistance closer to the test values. For press braked sections where only stub column data was available for comparison the proposed model showed an increase in cross section resistance of on average 1.4 times the cross section resistance calculated by assuming the recommended minimum 0.2% proof stress. This increase is due to the slightly higher 0.2% proof stress given in mill certificates than the minimum specified value and the inclusion of corner strength enhancements.

For cold rolled box sections where the forming route induces increases of the 0.2% proof stress in the flat regions as well as additional increases in the corner regions, employing the proposed 0.2% proof stress distribution revealed resistances to be substantially higher than those predicted with the minimum 0.2% proof stress recommended in EN 10088-2 (2005). On average, increases of 2.1 for stub columns, 1.5 for columns and 1.9 for beams have been determined. If the proposed 0.2% proof stress distribution based on mill certificate values was used in design, owing to the increased material efficiency, cost savings could be made that are equivalent to the increase in calculated member resistance, thereby almost halving the cost of designing in hollow structural stainless steel box sections. If no mill certificate data was available, through employing the proposed models by replacing the mill certificate values with the specified minimum 0.2% proof stress and ultimate stress, increases of 1.6 times the cross sections resistance, 1.3 times the column buckling resistance and 1.5 times the bending resistance obtained by adopting the minimum specified values are achieved.

The cold rolled rectangular hollow sections formed by gradually folding sheet material, whose test results were reported by Talja and Salmi (1995), have been highlighted in Figures 7.5-7.13 and are not seen to give unduly unconservative design predictions by adopting the 0.2% proof stress distribution proposed for box sections formed by crushing a circular tube. However the test results for these sections do not cover a large range of cross section or member slenderness values and so conservative predictions cannot be assumed to be obtained for all member sizes.

This more efficient design method highlights the importance of utilising the strength enhancements caused during the production of stainless steel structural members in order to accurately predict the behaviour of stainless steel structural cross sections and members.

Chapter 8

Life cycle costing

8.1 Introduction

8.1.1 Background

The elegance and functionality of metallic structures have long been a feature of the construction industry. Historically, the overriding factor in the selection of structural materials has been initial cost, leading to the dominance of structural carbon steel over other metallic materials. Familiarity and ease of design and construction using carbon steel, together with a comprehensive range of structural products, have also contributed. However, growing pressure on the construction industry to consider the longer term financial and environmental implications of projects is encouraging a more holistic approach. Thus, materials with higher initial costs, but which offer cost savings over the life cycle of a structure, are gaining increasing recognition. The life cycle costs of structures of two such metallic materials, stainless steel and aluminium alloy, are compared to those of carbon steel structures in the present study. Overviews of the structural use of aluminium alloys and stainless steel have been prepared by Mazzolani (2004) and Gardner (2005), respectively. The study presented in this chapter compliments the previous experimental analysis by considering the current cost implications of

specifying stainless steel, thereby emphasising the benefits of stainless steel and the importance of lowering the initial material costs to encourage wider application. Life cycle costing (LCC) is essentially an analytical tool to assess the long-term cost implications of a project, where future expenditures are converted to their present value through a discount rate. This tool will be formally defined in the draft International Standard, ISO 15686-5. The application of life cycle costing to construction projects has been advocated in 'Rethinking Construction' (DTLR, 1998).

This study focuses on the costs directly associated with the three considered structural metallic materials. Numerous cost comparisons have been made between carbon steel and reinforced concrete structures. The costs utilised in the study have been taken from the most up to date sources available; this includes using quotes from producers and values given in research documents which will be detailed for each particular structure considered. In order to show how the results of the analysis might change due to variations in the adopted values, sensitivity studies have been carried out.

Within this chapter LCC is performed for two different structural applications: a typical office building and a bridge. A third application, an offshore structure, is discussed. These applications differ in scale, life time expectancy, environmental corrosivity, maintenance requirements, cost of disrupted use and in the manner in which they are funded.

8.1.2 Life cycle costing

The life cycle costing calculations carried out in this study calculates a standard LCC value by implementing Equation 8.1. In Equation 8.1 the cost components, initial material costs (I) and the costs (A) associated with initial corrosion and fire protection are taken at their present values, whilst maintenance costs (M), end of life costs (E) and the residual value of the structure (R) are future costs that are discounted to their present value by means of the discount rate r. For this study, the discount rate has been taken as 3.5%, as recommended in the Green Book (HM Treasury, 2003). Whilst maintenance costs are discounted at the year t_i in which the maintenance is anticipated, end of life costs and the residual value of the structure are discounted over the total design life t_n (in years). The issues and costs included in each cost component are summarised below.

$$LCC = I + A + \sum_{0}^{t_n}\left(\frac{M}{(1+r)^{t_i}}\right) + \left(\frac{E}{(1+r)^{t_n}}\right) + \left(\frac{R}{(1+r)^{t_n}}\right) \quad (8.1)$$

where:

I - Initial material costs, including:
- Raw materials (alloying elements)
- Fabrication of members

A - Additional initial costs, including:
- Corrosion protection
- Fire protection

M - Maintenance and inspection, including:
- Material cost of repairs to corrosion and fire protection
- Disrupted use of structure

E - End of life costs, including:
- Demolition/ Deconstruction

R - Residual value of materials, including:
- Recycling

r - Discount value (%)

t_i - Intervening time (years)

t_n - Design life (years)

For any built scheme the actual lifetime of a structure relies on factors beyond the scope of this standard life cycle costing calculation. Two such factors are flexibility (generally defined as capacity for low cost alterations due to change of use) and adaptability (generally defined as capacity for higher cost structural changes or extensions), both of which determine the ability of a structure to fulfil its purpose despite changing demands (Kincaid, 2002). The importance of considering these aspects can be seen in numerous studies, such as those provided by Davis

Landgon and Everest et al. (2004) where the cost of structural grids of varying spans was presented. The study showed that although costs increase with larger spans, the greater flexibility that results is attractive to stakeholders and prospective tenants, leading to a property of higher value. A building with larger structural spans can also accommodate more internal change before it is regarded as obsolete or before it requires an expensive outfit or conversion. Whilst the current study presents a standard LCC analysis it is important to note that market forces and factors such as flexibility and adaptability may greatly influence the actual life cycle cost of a given scheme.

8.1.3 Linking life cycle costing with sustainability

With growing environmental concerns, sustainability is becoming an increasingly important issue in the construction industry. An LCC analysis does not directly consider the issue of sustainability; this is considered in a life cycle assessment (LCA). LCA has been defined by its own specific ISO standard, however additional independent tools such as BREEAM (BRE Environmental Assessment Methods) and CEEQUAL (the Civil Engineering Environmental Quality and Assessment Scheme) have been developed. However, the process that is initiated by performing an LCC encourages discussions and recording of information associated with the durability, performance and end of life use of proposed schemes and their components. This includes consideration of the required level of maintenance and the residual value of components. Minimising the need for maintenance and replacement of components and utilising the potential residual value of components clearly supports the sustainable ethos.

Direct links between sustainability and economic growth have been found by financial markets which now monitor the sustainable performance of companies. The London stock exchange has correlated the sustainability performance of the largest companies in the UK in the FTSE4Good Index, showing that the 50 most sustainable companies have out performed the FTSE 100 Index by 15% for five consecutive years up to 2004 (BSSA, 2004).

8.2 Material selection

8.2.1 Introduction

The life cycle performance of three metallic materials, namely carbon steel, aluminium alloy and stainless steel, employed in two structural applications – an office building and a bridge – has been analysed. Typical grades for structural use of each material have been selected (see Table 8.1). A range of contributory factors have been included in the analyses; these are

introduced in the following subsections. A summary of the key material properties of the specific grades of carbon steel, aluminium and stainless steel used in the study is given in Table 8.1.

Table 8.1: *Material properties of carbon steel, aluminium and stainless steel*

	Carbon steel	Aluminium alloy	Stainless steel
Grade	S275	EN AW 6061 T4	EN 1.4401
Material yield strength σ_y or $\sigma_{0.2}$ (N/mm^2)	275	110	220
Young's modulus E (N/mm^2)	210000	70000	200000
Strain at fracture A_o (%)	24	12	45
Density ρ (kg/m^3)	7850	2700	8000
Thermal expansion coefficient α (K^{-1})	12×10^{-6}	23.2×10^{-6}	16×10^{-6}
Thermal conductivity k (W/mK)	54	250	16
Total amount of material recycled (%)	60[a]	70[a]	70[a]

[a] Department of trade and industry, (2005)

8.2.2 Material cost

Structural material selection has traditionally been based on initial material cost, leading to the dominance of carbon steel over other metallic materials. The cost per tonne of aluminium alloy is approximately 1.5 times that of carbon steel (Dwight, 1999), whilst the cost per tonne of stainless steel is around four to six times that of carbon steel (Baddoo et al., 1997). These higher costs are partly due to the low volume of production of aluminium alloys and stainless steel in comparison to carbon steel, but are primarily linked to the cost of the base material and of the constituent alloying elements that give the different grades their particular properties. Stainless steel, production of which has increased at a rate of approximately 6% per year since 1960 (Jonsson, 2000), comprises at least 10.5% chromium and differing levels of nickel and molybdenum depending on the grade. The cost of these alloying elements can be highly variable, for example the world wide cost of nickel was seen to triple between 2001 and 2004 (ASSDA, 2006).

Clearly the cost of a structure is not only dependant upon the cost per tonne of the structural material, but also on the material density, strength, stiffness, efficiency of use and so on. Whilst stainless steel and carbon steel are of similar density, aluminium has a significantly lower density, approximately one third of the values of stainless steel and aluminium. However, as explained in the following sub section, aluminium also has a stiffness (Young's modulus) of only one third of that of carbon steel, generally necessitating the use of larger sections. Weight

savings, where they can be achieved, may also lead to reduced transportation, erection and foundation costs. Structural efficiency is partly due to the choice of structural form, to which similar principles apply for all three metallic materials, and partly due to the sophistication of the design codes. Again although similar principles apply in design, structural carbon steel codes are more developed than those for either aluminium or stainless steel because of the greater pool of available structural performance data and more expansive research capacity.

Based on quotations obtained in 2005 (Corus, 2005; AEi, 2005), the initial material costs per tonne for this study have been taken as £720 for carbon steel (grade S275), £1750 for aluminium alloy (grade EN AW 6061 T4) and £3060 for austenitic stainless steel (grade EN 1.4401). This gives an initial material cost ratio per tonne (carbon steel: aluminium alloy: stainless steel) of approximately 1.0: 2.5: 4.0. All subsequent cost ratios will be given in the order - carbon steel: aluminium alloy: stainless steel.

8.2.3 Strength, stiffness, ductility and fatigue resistance

Strength, stiffness, ductility and fatigue resistance are crucial properties for structural materials. In general, strength and stiffness are required to provide load carrying capacity and to control deflections, whilst ductility is important for avoiding brittle failures, allowing redistribution of stresses and for energy absorption. Fatigue resistance is important in applications where the structural material is subjected to cyclic loading, such as that due to traffic on a road bridge.

A wide range of strengths can be achieved for each of the considered metallic materials through variation in alloy content, level of cold work and heat treatment as seen for stainless steel in Chapter 6. For the present study, typical structural grades have been selected, the material strengths (yield strength, σ_y for carbon steel and 0.2% proof strength, $\sigma_{0.2}$ for aluminium and stainless steel) of which are compared in Table 8.1. Unlike strength, the stiffness of a metal cannot be significantly altered. The stiffness (Young's modulus) of carbon steel and stainless steel are similar (see Table 8.1), though the rounded stress-strain curve of stainless steel results in increased deflections. Aluminium, in contrast, has a much lower Young's modulus, approximately one third of that of carbon steel and stainless steel. Ductility, generally defined as strain at fracture varies considerably between the materials; as shown in Table 8.1, for the grades considered, carbon steel (S275) has a strain at fracture of about 24%, aluminium about 12% and stainless steel about 45%. The fatigue resistance of carbon steel and stainless steel is similar (Gardner, 2005), whereas the fatigue resistance of aluminium is about one-third that of carbon steel (Kissell and Ferry, 1995). The fatigue performance of aluminium also deteriorates rapidly at elevated temperatures and in corrosive environments. The inferior fatigue

performance of aluminium may be partly offset by the lower stress ranges that are likely to result from the use of larger aluminium sections (which will generally be required to account for the lower strength and stiffness).

8.2.4 Production and fabrication

The prevalence of carbon steel in the construction industry has led to the development of efficient production processes, a comprehensive range of structural products in standard section sizes and familiarity and efficiency in structural design, fabrication and construction. For both aluminium and stainless steel, there is generally less familiarity amongst structural engineers and fabricators, and reduced product availability and standardisation. With increasingly widespread usage, these shortcomings are being overcome.

Schedin (1992) describes particular aspects of fabrication of stainless steel that require specialist knowledge. More attention, for example, is required to control local distortions during welding since the coefficient of thermal expansion of stainless steel is between 30% and 50% greater than that of carbon steel (Baddoo et al., 1997). Welding aluminium on the other hand, encounters the possibility of localised deterioration of material properties, though specific aluminium alloys have been developed that retain their properties after welding (Mazzolani, 1995).

8.2.5 Corrosion resistance

Both aluminium and stainless steel react with oxygen to form a protective oxide layer (aluminium oxide and chromium oxide, respectively). This oxide layer adheres to the surface of the material and prevents the occurrence of further oxidation or corrosion. When damaged, provided oxygen is present, this oxide layer very rapidly reforms. Carbon steel also oxidises to form iron oxide. However, unlike aluminium and chromium oxide, iron oxide does not adhere to the material, but rather occupies a larger volume and becomes detached from the surface, exposing un-corroded material to further oxidation.

In certain conditions, both aluminium and stainless steel can be susceptible to corrosion. One such instance is where insufficient oxygen is present to regenerate the oxide layer (anaerobic corrosion). This occurs where the metallic surface is immersed in water. Other aggressive environments, where particular care needs to be taken to select appropriate material grades to avoid severe corrosion, include strongly acidic or alkaline conditions; sea water, for example, is a weak chloride solution. General guidance on the corrosion of aluminium has been presented

by Davis (1999), whilst information relating to the corrosion of stainless steel is also available (Sedriks, 1996).

In this study it has been assumed that no corrosion protection is required for either aluminium or stainless steel, whilst for carbon steel allowance for the initial cost of corrosion protection and subsequent maintenance thereof has been made. For the building, an allowance of £3.60/m^2 of surface area of structural steelwork has been made (Corus, 2002). For bridges, corrosion protection requirements are more onerous due to the more aggressive environment. For this study an allowance for a four-coat epoxy and polyurethane corrosion protection system of £25.00/m^2 of surface area of structural steelwork has been made, and a maintenance period of fifteen years has been assumed, based on the Highways Agency's minimum requirements for coating systems. Additional costs associated with maintenance of the corrosion protection, including access, surface preparation, worker health and waste disposal have also been included (Koch et al., 2002). Maintenance may also lead to traffic disruption, and an allowance of ten days of disruption for the steel bridge, five days for the aluminium bridge and 2.5 days for the stainless steel bridge has been made. The cost of disruption for a single carriageway was assumed to be £8000 per day (Wong, 2004); 10% of this cost accounts for traffic management schemes and 90% is to account for the cost of traffic disruption.

8.2.6 Fire resistance

At elevated temperatures, all metals lose strength and stiffness. A comparison of the strength and stiffness retention of carbon steel, aluminium and stainless steel at elevated temperatures is shown in Figures 8.1 and 8.2. In Figure 8.1, the strength reduction factor is defined as the elevated temperature yield strength normalised by the room temperature yield. In the case of stainless steel the strength reduction factor is initially greater than unity due to the strain hardening nature of the material and an allowance for higher deformation (and strain limits) in fire. In Figure 8.2, the stiffness reduction factor is defined as the elevated temperature Young's modulus normalised by the Young's modulus at room temperature. From Figures 8.1 and 8.2, it may be observed that generally stainless steel offers superior retention of strength and stiffness at elevated temperature than carbon steel, whilst aluminium alloys are considerably inferior.

In order to comply with building regulations (ODPM, 2000), which generally require 60 minutes of fire resistance to allow occupants to evacuate and fire fighters to operate, an allowance of £10.50/m^2 of surface area (Corus, 2002) has been made for the carbon steel building. To reflect the respective material performance at elevated temperature, the cost of fire protection for the aluminium building has been estimated as 1.5 times that for carbon steel,

whilst for stainless steel the cost of fire protection has been estimated as half that for carbon steel. No allowance for fire protection has been made for the bridge scenario. General guidance on the fire protection of structures of a range of materials is given by Buchanen (2001).

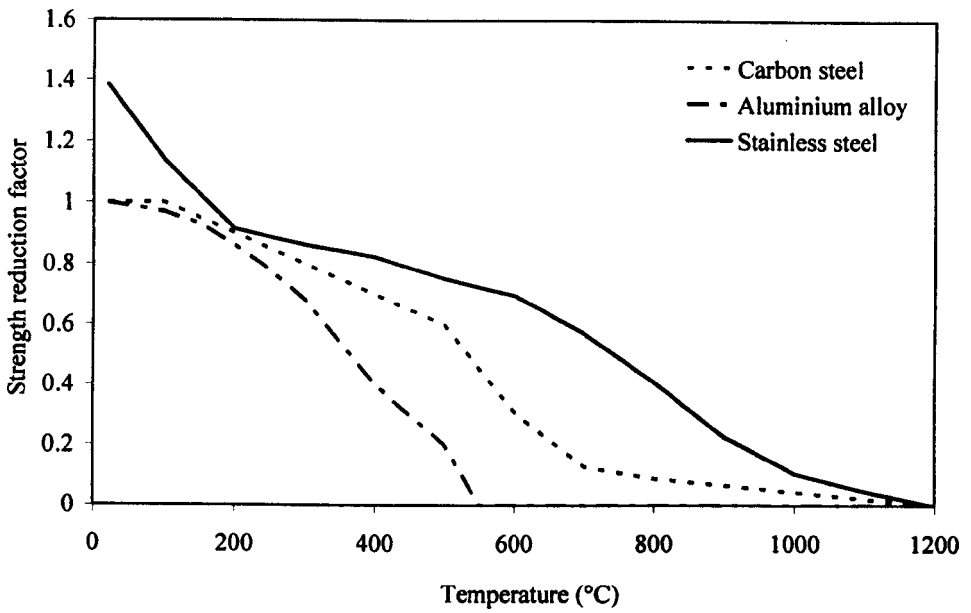

Figure 8.1: *Comparison of strength reduction factors at elevated temperature for carbon steel, aluminium alloy and stainless steel*

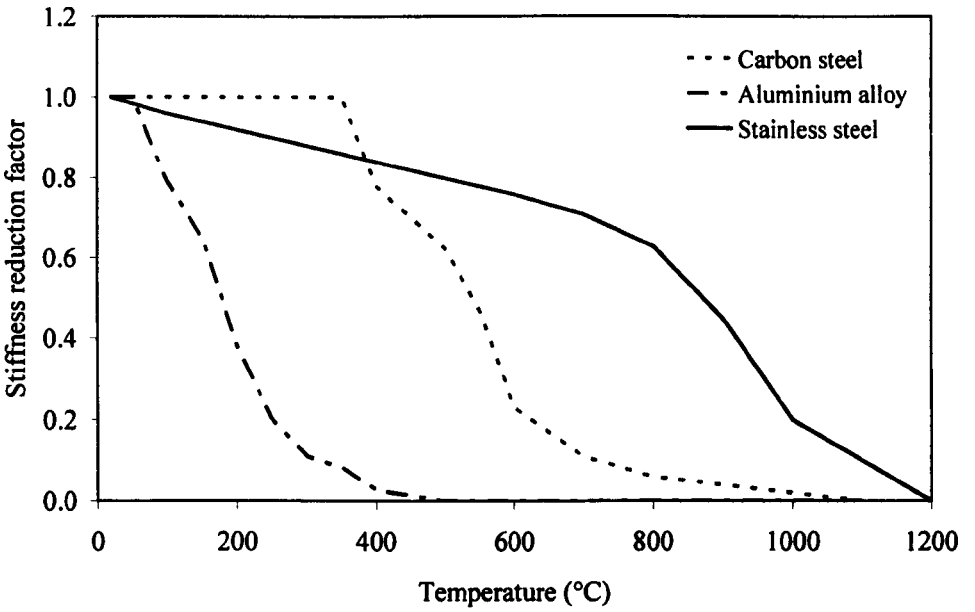

Figure 8.2: *Comparison of stiffness reduction factors at elevated temperature for carbon steel, aluminium alloy and stainless steel*

8.2.7 End of life costs and residual value

The residual value of a structure depends upon whether it is demolished, and if so whether the material can be recycled, or more carefully deconstructed to allow structural components to be reused. All three metals can be recycled without any loss of material properties but sometimes the material is difficult to recover. Table 8.1 sets out the overall percentage of each metal that is thought to be reclaimed from all industries and subsequently recycled (Department of Trade and Industry, 2005). The price of recycled scrap metal, as with the material cost, varies with the market demand. The values adopted herein are average values taken from European metal recycling (2004), the London metal exchange (2004), and quotes obtained from Metal world in 2004.

In the analysis of the building structure the cost of demolition and, as an alternative end of life scenario, deconstruction has been considered. Only the demolition scenario has been considered for the bridge structure. In a study reported by Geyer et al. (2002) it was stated that if a structure is demolished, 99% of the material from structural steel sections can be recovered at a cost of £50 per tonne. In the current study, a conservative estimate of 80% recovery was taken. Deconstruction (or dismantling) of a structure is a much more labour intensive operation and therefore incurs higher costs, taken as £100 per tonne (Geyer et al., 2002). Birat et al. (2002)

suggest that 90% of material can be recovered by deconstruction. The advantage of deconstruction is that damage of components is less likely and they may therefore be sold for reuse within the construction market rather than being recycled.

8.3 Life cycle costing

In this section, the life cycle costs of two structures (a typical office building and a bridge) of the three considered structural metallic materials are presented. The studies are based on current costs of the three structural materials (carbon steel, aluminium alloy and stainless steel) giving an initial ratio of the material cost per tonne of 1.0: 2.5: 4.0. The sources of costs used in the analysis have been detailed in the previous section. Based on the material costs per tonne, the material densities and an initial design of the primary members of the structures (to the current European structural design standards given in Table 8.2) ratios of the initial estimated costs of structural material for the building and the for the bridge were obtained. A brief description of the structures and discussion of the results of the life cycle costings are given in the following sub sections.

Table 8.2: *Data used for LCC study for three types of structures*

	Carbon steel	Aluminium alloy	Stainless steel
Structural code	EN 1993-1-1	ENV 1999-1-1	EN 1993-1-4
Office building			
Design life in years	50	50	50
Initial cost (£/tonne)	720	1750	3060
Corrosion protection (£/m^2)	3.60	-	-
Time interval for maintenance (years)	10	10	10
Fire protection (£/m^2)	10.50	15.75	5.25
Material recovery - Demolition (%)	80	80	80
Cost of Demolition (£/tonne)	50	50	50
Material recovery - Deconstruction (%)	90	90	90
Cost of Deconstruction (£/tonne)	100	100	100
Recovered value of scrap (£/tonne)	93	875	1080
Bridge			
Design life (years)	120	120	120
Initial cost (£/tonne)	720	1750	3060
Corrosion protection (£/m^2)	625	-	-
Time interval for maintenance (years)	15	15	15
Down time for maintenance (days)	10	2.5	5
Cost of traffic management system and disruption (£/day)	8000	8000	8000
Cost of maintenance (£/day)	7200	7200	7200
Decommissioning (£/tonne)	100	100	100
Recovered value of scrap (£/tonne)	93	875	1080

8.3.1 Office building

A typical, flat-roofed four-storey office building was chosen as the basis for the life cycle costing study. The overall dimensions of the structure were 48 m by 13.5 m on plan, and the inter-storey height was 2.7 m. The span of the primary beams was 6 m and the span of the secondary beams was 13.5 m. A design life of 50 years was assumed. Although it is likely that no significant maintenance would be required on protected internal steelwork, four scenarios (two of which make an allowance for inspection and maintenance of the corrosion protection at ten yearly intervals) were considered:

- Maintenance costs incurred every ten years and end of life demolition.
- No maintenance costs incurred and end of life demolition.
- Maintenance costs incurred every ten years and end of life deconstruction.

- No maintenance costs incurred and end of life deconstruction.

Results of the building study are presented in Table 8.3 with the costs shown as a ratio of the total material costs for the carbon steel structure. The initial material cost of the structures, taking due account of the material cost per tonne, the material densities and the structural properties, normalised to that of the carbon steel structure were found to be 1.00: 1.82: 4.87. Inclusion of the additional initial costs (corrosion protection and fire protection) gives initial cost ratios of 1.37: 2.36: 5.02. These ratios confirm that, on an initial cost basis, carbon steel represents the most economic solution. Assessing the maintenance and end of life costs of the building, it may be observed that the durability and residual value of both aluminium and stainless steel offer cost savings, but once discounted to their present value these savings are small, and on a life cycle costing basis, the carbon steel building remains the most economic solution for all four scenarios considered. Accumulation of normalised life cycle costs (including maintenance) with time for the three structural materials for the more likely scenario of demolition of the building is shown in Figure 8.3.

Table 8.3: *LCC results for the office building (costs normalised to initial material costs of carbon steel structure)*

Office building	Carbon steel	Aluminium alloy	Stainless steel
Normalised weight of structure	1.00	0.75	1.15
Initial costs			
Material cost	1.00	1.82	4.87
Corrosion protection cost	0.10	-	-
Fire protection cost	0.28	0.50	0.14
Total initial costs	1.37	2.32	5.02
Maintenance costs (discounted)			
Maintenance	0.22	0.13	0.13
Decommissioning cost (discounted)			
Demolition	0.01	0.01	0.01
Deconstruction	0.03	0.02	0.03
Residual value (discounted)			
Value recovered (Demolition)	0.02	0.13	0.25
Value recovered (Deconstruction)	0.02	0.15	0.28
Life cycle costs			
Total cost including maintenance (Demolition)	1.58	2.33	4.92
Total cost excluding maintenance (Demolition)	1.36	2.20	4.79
Total cost including maintenance (Deconstruction)	1.59	2.32	4.90
Total cost excluding maintenance (Deconstruction)	1.38	2.19	4.77

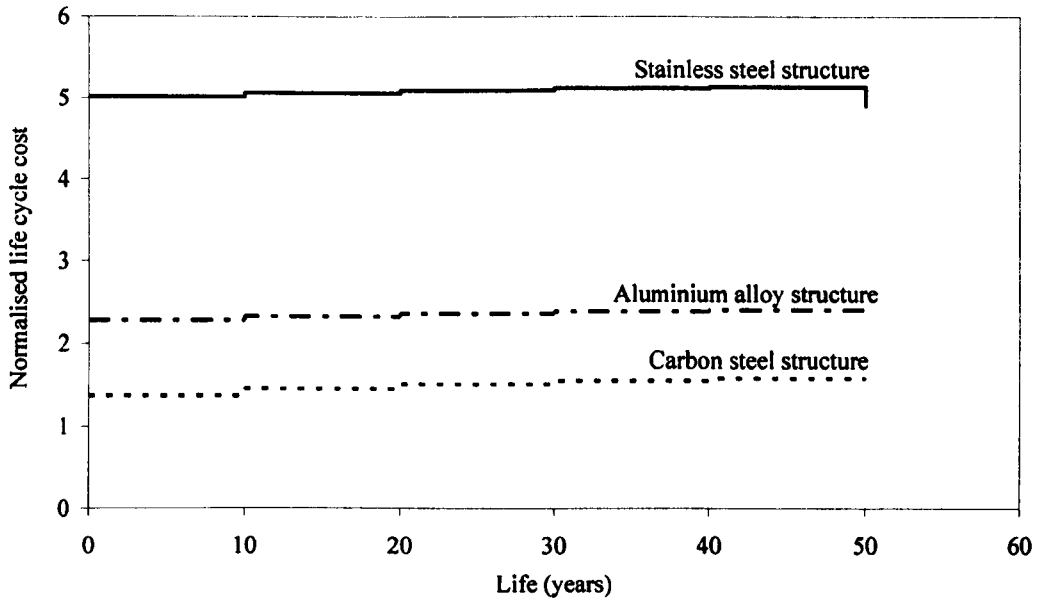

Figure 8.3: *Accumulation of cost for a building structure*

The results of the study on the building indicate that the higher initial material costs of the aluminium alloy and stainless steel are not offset by the lower corrosion protection costs, maintenance costs and decommissioning costs over the life cycle of the structure. This is likely to be true in all low maintenance applications. However, it may be appropriate to consider these materials in exposed areas of a building structure, where maintenance requirements will be greater and aesthetics may be enhanced.

8.3.2 Bridge

Modern bridges are designed with an envisaged life span of 120 years, which, coupled with the more exposed nature of the structural elements, means that maintenance costs are generally a far more significant portion of the total life cycle costs than for the case of buildings. It has been estimated, for example, that the total annual cost of highway bridge maintenance (to prevent corrosion) in the US is between £3.67 billion and £5.79 billion (Koch et al., 2002). The same study also highlighted that the ensuing traffic disruption is thought to cost ten times that of the corrosion protection in loss of productivity.

A typical plate girder highway bridge of 57.5 m span has been taken as the basis for the second life cycle costing study. Initial sizing of the primary members has been performed to current European design standards, but no consideration has been given to fatigue due to traffic loading.

Two scenarios have been considered – one including maintenance and the other excluding maintenance. Results of the life cycling costing study are shown in Table 8.4. The initial material cost ratio for the bridge structure was found to be 1.00: 1.73: 5.47 and the ratio of the material weight for each structure was 1.00: 0.71: 1.29. In research carried out by Moss and Saetre (1991) on offshore trusses, aluminium alloy structures were found to be 60-65% of the weight of those of carbon steel, whilst in a separate study carried out by Shuttleworth (1989) the weight for stainless steel structures was found to be 125 % of carbon steel structures. These values broadly support those found in this study. Accumulation of normalised life cycle costs (including maintenance) with time for the three structural materials for the bridge application is shown in Figure 8.4.

Table 8.4: *LCC results for the bridge structure (costs normalised to initial material costs of carbon steel structure)*

Bridge structure	Carbon steel	Aluminium alloy	Stainless steel
Normalised weight of structure	1.00	0.71	1.29
Initial costs			
Material cost	1.00	1.73	5.47
Corrosion protection cost	0.15	-	-
Total initial costs	1.15	1.73	5.47
Maintenance costs (discounted)			
Corrosion protection	5.33	-	-
Traffic management and disruption	0.84	0.42	0.21
Total maintenance costs	6.17	0.42	0.21
Decommissioning cost (discounted)			
Demolition	0.00	0.00	0.00
Residual value (discounted)			
Value recovered	0.00	0.01	0.03
Life cycle costs			
Total cost including maintenance	7.32	2.14	5.66
Total cost excluding maintenance	1.15	1.72	5.45

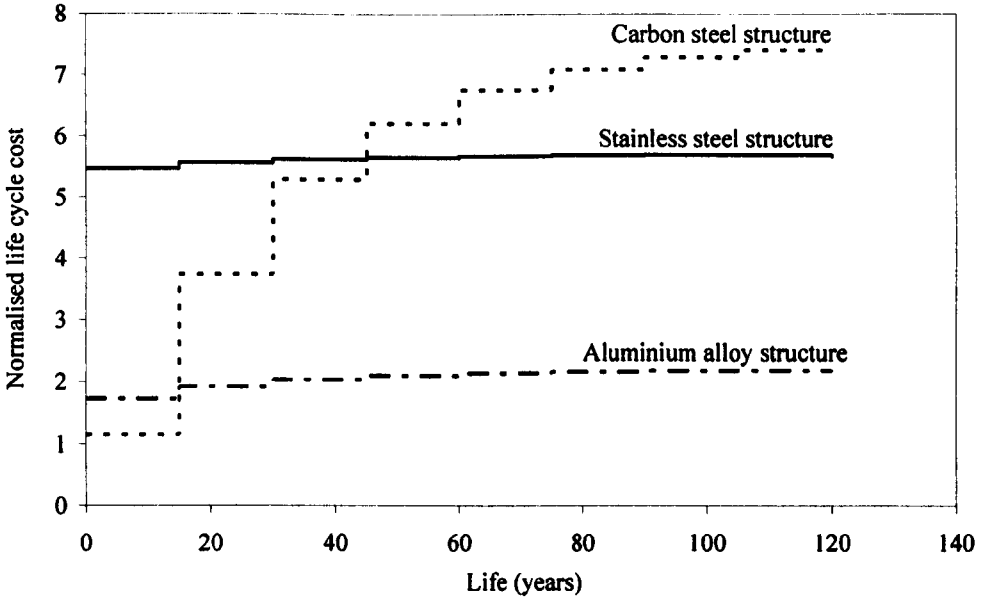

Figure 8.4: *Accumulation of cost for a bridge structure*

Considering the first scenario (which included maintenance), the life cycle cost ratio was found to be 7.32: 2.14: 5.66, with the aluminium alloy providing the most competitive solution, and carbon steel being the least competitive. Stainless steel offers the lowest maintenance costs and highest residual value, resulting in a more competitive life cycle solution than carbon steel, but its high initial cost makes it less competitive than aluminium. If all maintenance costs are ignored, the life cycle cost ratio becomes 1.15: 1.72: 5.45, but clearly the performance and life expectancy of the carbon steel structure will be comprised, and the no-maintenance scenario is unsustainable.

8.3.3 Potential use in offshore structures

The use of aluminium alloys and stainless steel in offshore structures such as the common topside and jacket structure of offshore oilrigs is a third potential application. Offshore applications for aluminium alloys have been previously discussed by Moss and Saetre (1991), and for stainless steel by Shuttleworth (1989).

In offshore applications, the corrosive environment is severe. A number of methods are employed to protect offshore carbon steel structures from corrosion, including protective coatings and cathodic protection. Over-sizing of structural members is also commonly carried out to allow for loss of material. The inherent corrosion resistance of aluminium and stainless steel would clearly be of benefit in offshore applications. However, given the harshness of the

environment, higher performance grades, (at greater expense) will generally be required. Stainless steel offers the additional advantages of superior fire resistance and impact resistance. Savings in maintenance costs may also be augmented by savings related to shorter periods of down time and minimising loss of production.

8.4 Sensitivity studies

Representative values for all contributory components of the described life cycle costing analyses have been obtained from a range of sources, as summarised in Table 8.2. However, there is clearly a degree of uncertainty, variability and fluctuation with market conditions associated with many of these values. A set of sensitivity studies has therefore been performed to assess the influence of the following variables on the calculated life cycle costs: material cost, design life, discount rate and duration of traffic disruption (in the case of the bridge). Throughout the sensitivity studies, all life cycle costs have been presented relative to the life cycle cost of the original corresponding carbon steel structure.

8.4.1 Influence of initial material costs

Initial material costs were varied between 0.2 and 2.4 times their assumed values of Table 8.2. Figure 8.5 and 8.6 shows the resulting variation in the life cycle costs for the building and bridge respectively, given relative to the life cycle cost of the original corresponding carbon steel structure. The influence of variation in initial material costs is most significant for the stainless steel structures since compared to the other metals considered, the initial material cost of stainless steel is a larger proportion of the LCC. For the bridge structure (Figure 8.6), variation of the initial material costs was found to have less impact on the total life cycle costs than seen in the building structure (Figure 8.5). This was due to the high maintenance costs associated with the bridge, which represented a large portion of the life cycle costs.

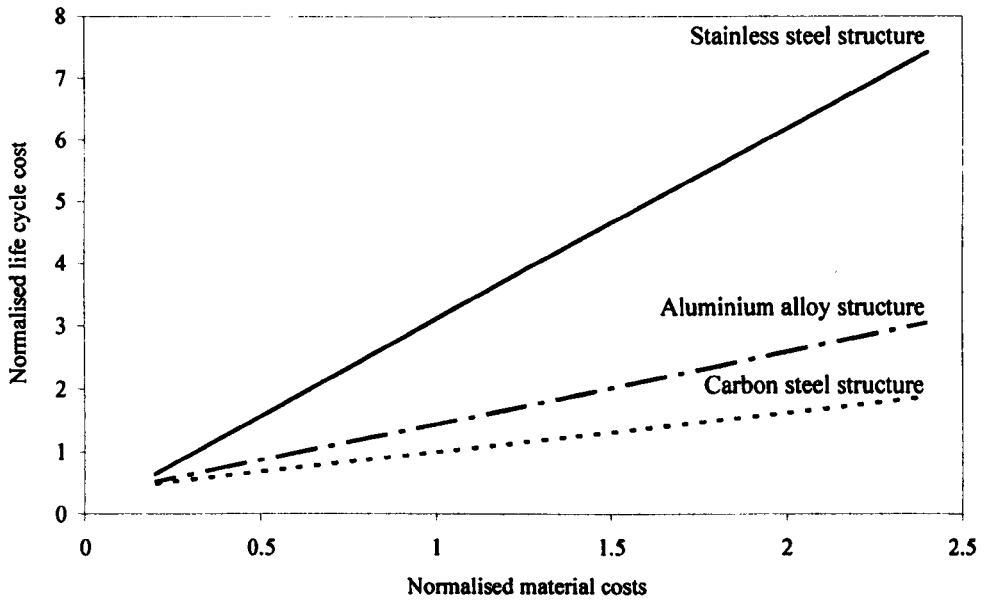

Figure 8.5: *Sensitivity of LCC for a building structure to variation in initial material costs*

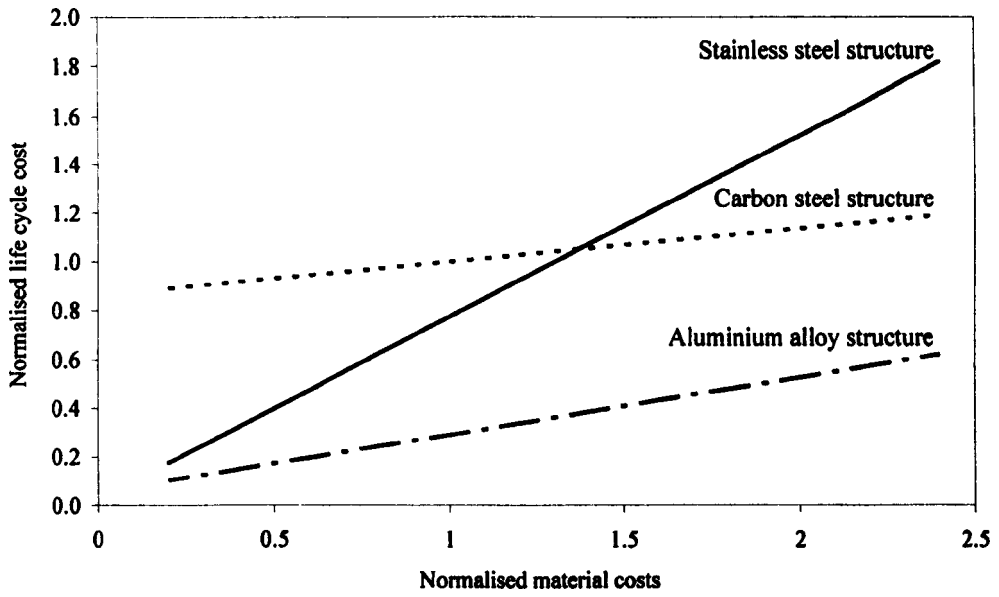

Figure 8.6: *Sensitivity of LCC for a bridge structure to variation in initial material costs*

8.4.2 Influence of design life

The sensitivity of the results of the study to variation in design life was found to be less than the sensitivity to variation in initial material costs. In the case of the both the building (Figure 8.7)

and the bridge (Figure 8.8), although variation in design life influences life cycle costs, the relative competitiveness of the three materials is essentially unaffected. The lower maintenance requirements associated with shorter design lives are most beneficial in the case of the carbon steel bridge, where the life cycle costs may be seen to reduce rapidly (Figure 8.8).

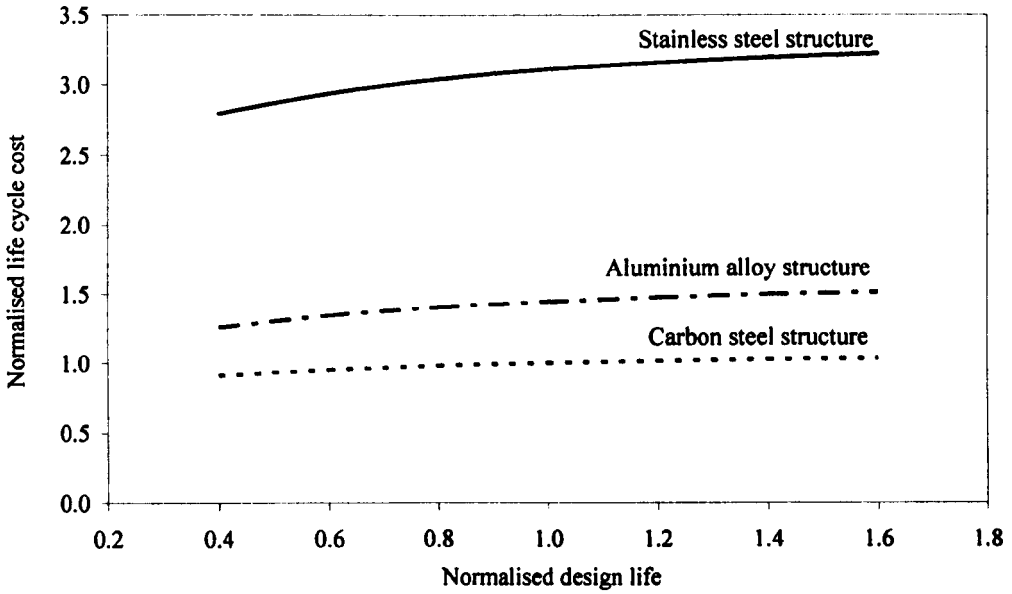

Figure 8.7: *Sensitivity of LCC for a building structure to variation in design life*

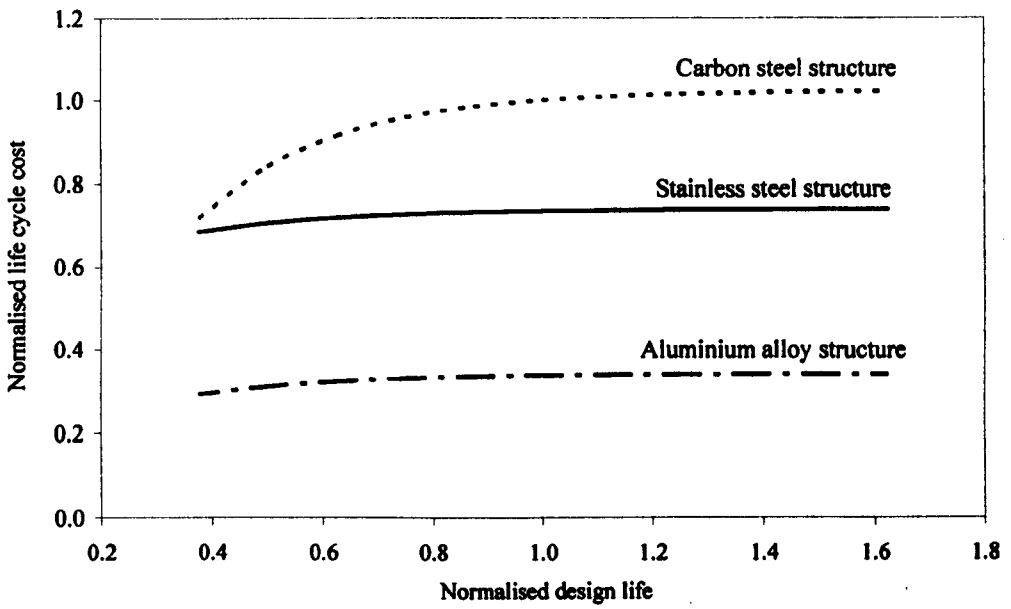

Figure 8.8: *Sensitivity of LCC for a bridge structure to variation in design life*

8.4.3 Influence of discount rate

The discount rate controls the present value of costs incurred over the life cycle of the structure. A lower discount rate increases the influence of costs associated with maintenance and end of life costs. With the initial costs making up a large portion of the life cycle costs, the building is relatively insensitive to variation in discount rate (see Figure 8.9). The reduction in life cycle cost that may be observed in Figure 8.9 for the aluminium and stainless steel building for low discount rates is due to the increased influence of the residual value of the structure. The aluminium and stainless steel bridge structures show little sensitivity to variation in discount rate, due to the low maintenance costs. Conversely, the carbon steel bridge shows a high level of sensitivity to discount rate (Figure 8.10).

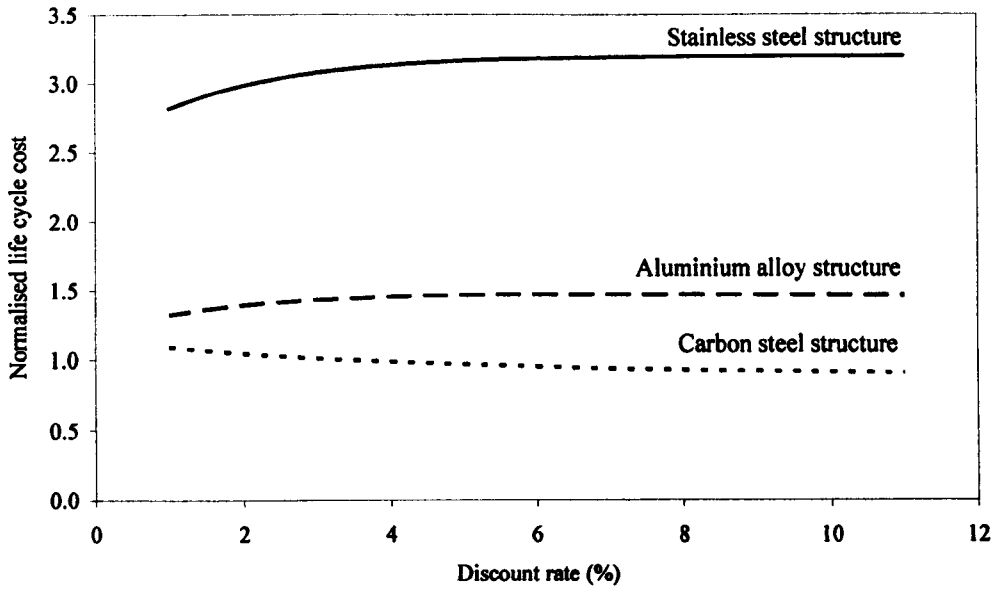

Figure 8.9: *Sensitivity of LCC for a building structure to variation in the discount rate*

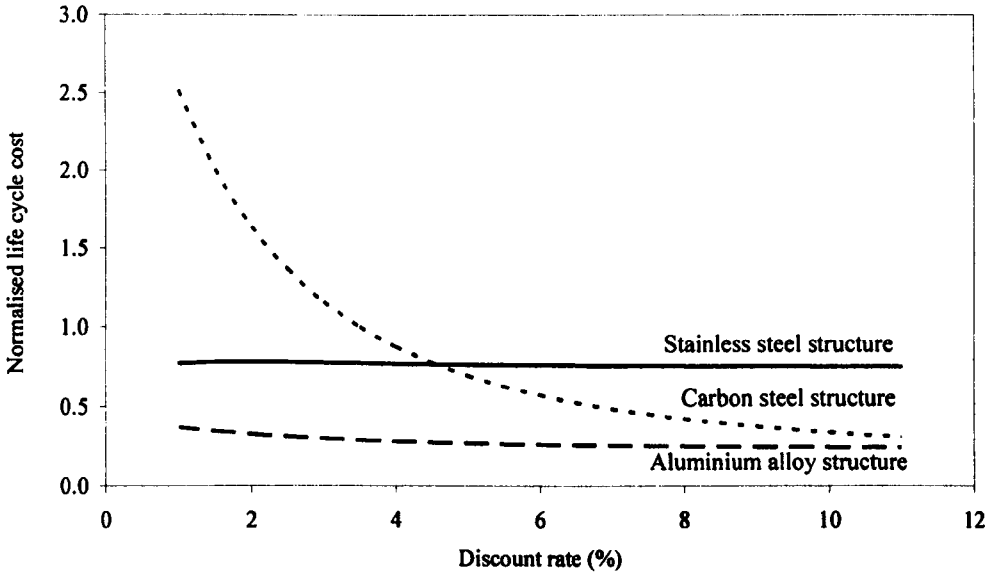

Figure 8.10: *Sensitivity of LCC for a bridge structure to variation in the discount rate*

8.4.4 Influence of duration of traffic disruption

Variation in the duration of assumed traffic disruption resulting from maintenance of the bridge structure does not greatly affect the economic outcome of the study. Figure 8.11 shows, as anticipated, that the carbon steel option is more sensitive to this variation due to the initially assumed longer maintenance periods.

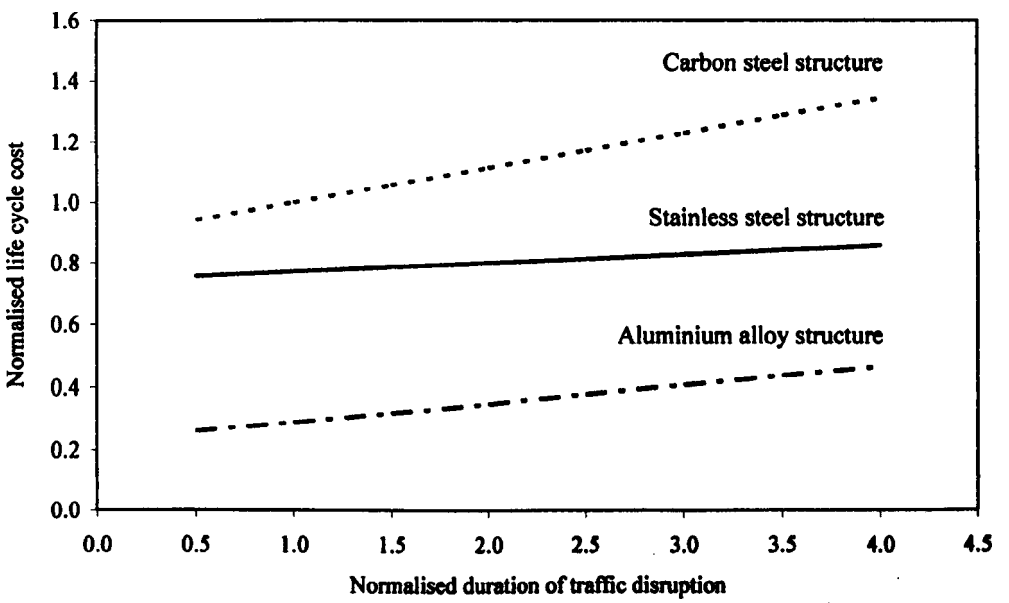

Figure 8.11: *Sensitivity of LCC to variation in duration of traffic disruption*

8.5 Conclusions

To date, carbon steel has dominated the metallic construction market owing to its relatively low initial material cost, good structural properties, a comprehensive product range and familiarity within the industry. This dominance is set to continue, but, growing pressure on the construction industry to consider the longer term financial and environmental implications of projects has led to materials with higher initial costs, but which offer cost savings over the life cycle of a structure, gaining increasing recognition. In this chapter, the life cycle performance of two such materials, stainless steel and aluminium alloy, employed in two structural applications – an office building and a bridge – has been analysed, and compared to that of carbon steel. The ratio of initial material cost per tonne was assumed to be 1.0: 2.5: 4.0 (carbon steel: aluminium alloy: stainless steel). Following a preliminary structural design to current European design standards taking due account of the material densities and structural properties (principally strength and stiffness), initial material cost ratios of 1.00: 1.82: 4.87 for the building and 1.00: 1.73: 5.47 for the bridge were obtained. Additional initial costs (corrosion protection and fire protection) altered these ratios to 1.37: 2.32: 5.02 for the building and 1.15: 1.73: 5.47 for the bridge (where ratios are relative to the initial material costs of the corresponding carbon steel structure). On an initial cost basis, carbon steel offers the most competitive solution for both the building and the bridge. However, considering the additional life cycle costs including maintenance costs, end of life costs and the residual value of the structure (appropriately discounted to present values), the situation changes. For the building, with only modest maintenance requirements, the life cycle cost ratio was found to be 1.58: 2.33: 4.92, but for the bridge, where maintenance requirements are significant, the life cycle cost ratio was found to be 7.32: 2.14: 5.66. Although there is clearly a degree of uncertainty and variability associated with the component costs of the life cycle analyses, the results indicate that carbon steel offers the most competitive life cycle solution for the office building, but delivers the most expensive life cycle solution for the bridge. Overall, it is concluded that on a whole-life basis aluminium alloy and stainless steel may offer more competitive solutions than carbon steel for bridges and exposed areas of building structures.

This study demonstrates the influence of initial material costs of stainless steel in applications such as the office building and therefore the importance of producing material efficient design guidance, including, for example, exploiting in design the ability of stainless steel to cold work. Combining the results of these studies for stainless steel with the potential cost savings through

material efficiency demonstrated in Chapter 7, the application of stainless steel in structures becomes significantly more economical.

Chapter 9

Conclusions

9.1 Project summary

The minimum specified material strength defined as the 0.2% proof stress given in the current material standard can be significantly lower than the 0.2% proof stresses observed in coupon tests performed on material taken from formed structural sections. This conservatism in the material strength, when employed in structural design, considerably underestimates member resistances. The objective of this study is to address this loss of efficiency in predicting the behaviour of stainless steel structural sections through establishing a methodology to determine a more accurate material strength distribution.

The sensitivity of stainless steel's material properties, most importantly the 0.2% proof stress, to cold working caused by plastic deformation, required the study to include a thorough investigation into the different possible production routes of structural sections where different degrees of plastic deformation occur, as well as identifying the quality standards associated with product standardisation. It has been shown through this research program that the forming

routes of the structural cross sections and the previous strain history of the material influence the resulting section's 0.2% proof stress distribution.

In order to develop a methodology to predict the observed strength distributions, the presented research project comprised an experimental program which was primarily carried out to determine the 0.2% proof stress distribution for two types of cold formed sections: press braked angles and cold rolled box sections (square and rectangular hollow sections). Hot rolled stainless steel angles were simultaneously investigated as an alternative production process against which to compare the strength enhancements observed in cold forming.

The production routes of cross sections also influence the geometric tolerances of the formed sections and can induce residual stresses. Residual stresses and geometric imperfections both influence the structural behaviour of sections and so many detailed studies have been carried out on both imperfections and residual stresses distributions for carbon steel cross sections. It cannot be assumed that imperfections and residual stress distributions will be similar to those observed for carbon steel owing to differences in material and thermal behaviour between the two metals. The relatively recent introduction of stainless steel structural members means that there have been few geometric imperfection, residual stress and material strength data published. This research project therefore contributes a substantial amount of imperfection and residual stress data to the field and provides simple models for predicting global and local imperfections and bending and membrane residual stresses, as well as providing considerable material data on which a methodology to predict material distributions in stainless steel cross sections has been developed.

Geometric profiles were measured at different locations around 31 austenitic (grade 1.4301) cross sections including: 20 press braked angles, 7 cold rolled box sections and 4 hot rolled sections. A total of 228 profiles were generated. Measurements were made along the specimen lengths, as obtained from the manufacturers. The maximum lengths measured were close to six metres. In order to make accurate measurements over these lengths an experimental rig was designed and an analysis technique developed to remove the need for a physical flat datum against which geometric imperfections are traditionally measured. Two types of analysis have been implemented on the resulting imperfection data: a classic Fourier transform and a least square fit of a series of half sine waves. For specimens from the three considered production routes the spectral peak corresponding to an overall member bow in both types of analysis is found to have the most significant magnitude, with higher frequencies rapidly decreasing in magnitude. A relationship has been developed between the magnitude of the most significant

spectral peaks identified by the two analysis techniques employed. The global and local imperfections were extracted from the data for all three section types and the global tolerances were found to be within the section tolerances set out in the standards. Simple models for predicting global and local imperfections have been proposed.

The distribution of residual stresses have been mapped around the cross sections of 8 press braked angles, 7 cold rolled box sections and 3 hot rolled angles. The distributions were carefully determined by sectioning of the cross sections into strips thereby relaxing the residual stresses. The released strains during this stress relaxing process were measured on the internal and external surfaces of the sections providing over 900 individual strain readings. Techniques developed for the measurement of residual strains in carbon steel hot rolled sections have been modified in order to determine strains accurately in the presence of large bending residual stresses observed as the curvatures of strips released from cold formed sections. A method for determining both the membrane and bending strains of sections has also been developed where strain gauges could not be adhered to the internal surface of the sections prior to sectioning.

Analysis of measured residual strains has shown that the common assumption of a linearly varying through thickness bending residual stress can considerably over estimate the residual stresses calculated. An alternative rectangular stress block distribution has been proposed for cold formed sections to model the through thickness bending residual stress distributions. The through thickness residual stress distribution is thought to be greatly influenced by the sheet material used in press braked and cold rolled sections being coiled and decoiled for storage prior to forming. Bending residual stress models have been proposed for press braked, cold rolled and hot rolled sections, together with characteristic membrane residual stress values. Data from previous research has been used to propose models for membrane residual stresses in welded austenitic and duplex I sections.

The sectioned strips from the residual stress analysis were tested in tension to provide material data corresponding to the residual stress distributions around 8 press braked sections, 7 cold rolled sections and 4 hot rolled sections. In total, over 450 tensile coupons tests were performed. The material data obtained was modelled using a compound Ramberg-Osgood expression proposed in previous research programs specifically to describe the nonlinear stress-strain curve of stainless steel. The 0.2% proof stresses extracted were compared against the minimum specified 0.2% proof stress recommended in structural design standards and the 0.2% proof stress values given by the manufacturer in the sections' inspection document or mill certificate, which is commonly supplied for quality assurance with the purchase of the structural members.

Owing to the limited resolution of the 0.2% proof stress distribution obtained through tensile coupon tests, Vickers hardness tests were also performed. A correlation between the 0.2% proof stress and hardness values was established allowing the distribution of 0.2% proof stress in the corner regions of the section to be estimated, more accurately.

From the material data, methods are proposed by which the 0.2% proof stress distribution in press braked sections, cold rolled sections and hot rolled sections can be accurately predicted for structural design. The considerable strength enhancements observed in the flat regions of cold rolled box sections, formed by crushing a circular tube, are modelled. Modifications to existing models to predict the 0.2% proof stress in the corner regions of press braked and cold rolled sections are proposed and the extent of the enhanced material properties from corner forming has been determined, thereby defining the complete 0.2% proof stress distributions for both press braked and cold rolled sections. These material models have been used to predict the cross section compression resistance, column buckling resistance and beam in-plane bending resistance of sections collated from other experimental programs and they give, on average, significantly more accurate predictions. The 0.2% proof stress distribution proposed for press braked sections offer cross section resistances of, on average, 1.4 times the minimum specified 0.2% proof stress in design standards. For the more commonly specified cold rolled box sections, greater increases from the minimum recommended 0.2% proof stress exist in the flat regions than for the press braked sections and so more substantial increases are predicted for the cross section compression resistances, column buckling resistances and bending resistances. The average increases are respectively 2.1, 1.5 and 1.9 times those predicted using the minimum specified 0.2% proof stress recommended by the design standard. The proposed 0.2% proof stress distributions for the cold rolled sections would therefore approximately double the material strength that is utilised in structural design. This methodology represents substantial cost savings for stainless steel which could considerably widen its potential application.

Alternatively if during design no mill certificate data are available, by replacing the mill certificate 0.2% proof stress and ultimate stress with minimum specified values in the models proposed for cold rolled sections (Chapter 6), lower, but still valuable, increases of resistance are obtained. On average, 1.6, 1.3 and 1.5 times the values predicted using the minimum specified 0.2% proof stress are obtained for the cross section compression resistance, column buckling resistance and bending resistance respectively.

In the closing chapter a life cycle costing comparison has been presented which recognises the longer term economic benefits of specifying stainless steel by considering its lower maintenance

requirements. Combined with the proposed increase in material efficiency, stainless steel can now be seen as an increasingly competitive alternative to other metallic structural materials.

9.2 Recommendations

This research has shown the significance of the structural engineer being able to determine the production route of stainless steel structural sections. It is therefore important that clarity in the origins of sections is offered to engineers so that appropriate section specification can be performed. Information regarding production routes and the manner in which compliance with material standards is achieved is currently only obtained solely at the discretion of the manufacturer and therefore this part of the research conclusions aims to identify several changes to the design and specification system that could aid achieving efficient structural design. Achieving efficient design in stainless steel and developing the market for its structural application holds advantages for both stainless steel manufacturers and designers. At a very basic level it is important that the production route of a manufactured section can be identified by the engineer as either press braked, cold rolled or hot rolled so that the different types of products can be specified with confidence.

For hot rolled sections it is observed that the 0.2% proof stress is considerably higher than the minimum recommended design 0.2% proof stress, and this is thought to be due to warm working of the stainless steel as the stainless steel cools during the forming process. The material tests which are carried out to inform the inspection documents or mill certificates are taken from nominally similar formed sections and are therefore a good indication of the 0.2% proof stress of a section for design.

Both cold formed section types included in the study are formed from sheet stainless steel, from which the 0.2% proof stress values given in inspection documents or mill certificates have been obtained. Increases in 0.2% proof stress from the 0.2% proof stress of the sheet material, due to the forming process of press braked angle sections, are localised in the corner regions. Hardness tests indicate that these strength enhancements reside only within the corner radius, with the peak strength at the centre of the corner, where the tool strikes the sheet material during forming. To predict these strength enhancements they have been related to the radius to thickness ratio. As press braked sections are produced to order and due to the manual nature of the production route, the specification of these parameters by the design engineer is realistic. The unformed material in the flat section of the angles corresponds well to the 0.2% proof stress

values obtained in the mill certificate. Therefore, the 0.2% proof stress from the mill certificate is proposed to be used for the flat section faces in design, assuming this information is available during the design stage.

Cold rolled box sections produced by crushing a circular tube show significant strength enhancements in the flat section faces. It is therefore important to identify them from cold rolled sections formed by rolling paths where the material in the flat faces is not plastically deformed, although these are thought to be rare. It has been proposed to model the enhanced material strength of the flat faces by an expression that uses the mill certificate proof stress and the geometric dimensions of the cross section. The corner strength enhancements are predicted using the ultimate strength of the flat section faces. The need to know the corner radii of these sections is omitted as it is not often given as part of the product description from the manufacturer and as sections are produced as standard stock it is not so easily specified and obtained. The hardness tests showed that the distribution of 0.2% proof stress in the cold rolled corners is different from press braked sections, with the peak material strength occurring at the junction of the corner and the flat face, and the extent of the strength enhancements is up to four times the section thickness beyond the corner radius.

The industry procedure for obtaining 0.2% proof stress values from the sheet material prior to the forming process means that any increase in strength due to plastic deformation occurring during section forming is not quantified by the manufacturer. Monitoring the real 0.2% proof stress distributions in cross sections by the manufacturers would allow the cold working ability of stainless steel to be used in the manufacturers' design process, enabling innovation in the forming route adopted as well as in the final shape of cross section.

Finally rather than implementing the proposed 0.2% proof stress distributions the ideal solution would be for cold formed sections (as with hot rolled sections) to have their mill certificate material properties determined by tensile tests performed on longitudinal tensile coupons taken from specific locations in the cross section such as the centre of the flat faces and the corners. This would enable a manufacturer to market sections of a particular strength distribution without having to disclose their manufacturing details, which in turn would enable a simpler structural design process that did not depend on obtaining appropriate 0.2% proof stress values in mill certificates.

9.3 Future work

During the progress of this study, further areas of research that would be interesting and beneficial to explore have presented themselves. This final section describes potential future areas of exploration.

9.3.1 Through thickness residual stress distribution

The experimental analysis of residual stresses in stainless steel cross sections has shown that the though thickness variation cannot be assumed to be linear for cold formed sections. This finding is supported by analytical modelling of the coiling and uncoiling process of sheet material. Further experimental work could be undertaken to determine the through thickness residual stress distributions in the sheet material, as well as in the cold formed sections. A possible technique that could be employed would be neutron diffraction. By establishing a model by which this through thickness distribution could be predicted, the strain measured by the sectioning technique presented herein could be more accurately converted to a residual stress value and importantly a maximum through thickness residual stress could be determined. Existing analytical and finite element modelling of the coiling and uncoiling process may be validated from the experimental results and extended to predict residual stresses caused in cold rolled box sections during the forming of the circular tube and subsequent crushing. This study would help complete the understanding of the origin of the high bending residual stresses observed particularly in cold rolled sections.

9.3.2 Stub column tests

To investigate the combined effect of the geometric imperfections, residual stress distribution and variation of 0.2% proof stress around cross sections from the different production routes, stub column tests should be carried out on the remainder of the specimens tested herein. The test data from this program is important in order to determine if provisions for geometric imperfections and residual stresses in the current design code are appropriate and if not establish appropriate modifications for their inclusion. The data from stub column tests would therefore demonstrate to what degree the proposed increases in material strength are offset by any negative influence of residual stresses and geometric imperfections. Finite element models that are validated with the resulting test data could also be used to determine the relative importance and the accuracy of proposed models for geometric imperfections, residual stress and 0.2% proof stress distributions.

9.3.3 Hardness testing

Further work relating the correlation of hardness and material strength to theoretical models should be attempted and measurements made to establish the variability of the hardness measurements performed. In addition future work could focus on determining any annealing in the weld regions of closed sections as well as the through thickness variation of material strength.

9.3.4 Life cycle costing and section reuse

The life cycle cost studies could be extended by looking at the use of stainless steel in offshore structures where durability, fatigue resistance and maintaining strength and stiffness at high temperatures would be important factors in design.

Due to stainless steel's durability, a structural section is likely to perform its function longer than the desired design life of the structure. It would therefore be interesting to consider the economic issues, environmental advantages and the practical feasibility of section reuse as an alternative to recycling stainless steel sections. Owing to the sensitivity of stainless steel to variations in material strength, due to plastic deformation and heat treatment, careful thought would be required to recertify second hand stainless steel sections where previous welded joints may significantly alter the local material properties of the cross sections.

References

Abdella, K. (2006). Inversion of a full-range stress-strain relation for stainless steel alloys. *International Journal of Non-Linear Mechanics,* **41:3,** 456 - 463.

Abdella, K. (2007). An explicit stress formulation for stainless steel applicable in tension and compression. *Journal of Constructional Steel Research,* **63:3,** 326 - 331.

Abdel-Rahman, N. and Sivakumaran, K. S. (1997). Material properties models for analysis of cold-formed members. *Journal of Structural Engineering,* ASCE. **123:9,** 1135 - 1143.

AEi Corporation Ltd. See http://www.aei.com.sg.

Ala-Outinen, T. (2005). Members with Class 4 cross-sections in fire: Work package 3. ECSC project 'Stainless steel in fire (SSIF)', Contract No. RFS-CR-04048, VTT, (Confidential).

Ashraf, M. (2006). Structural stainless steel design: Resistance based on deformation capacity. PhD. Thesis, Structures section, Department of Civil and Environmental Engineering, Imperial College London, UK.

Ashraf, M., Gardner, L. and Nethercot, D. A. (2005). Strength of the corner regions of stainless steel cross sections. *Journal of Constructional Steel Research,* **61:1,** 37 - 52.

ASM, (1976). Metals Handbook, Volume 11: Nondestructive inspection and quality control. 8th edition, American Society for Metals.

ASSDA (Australian Stainless Steel Development Association). See http://www.assda.asn.au.

ASTM A370-87a (1987). American Society for Testing and Materials, Standard methods and definitions for mechanical testing of steel products. Annual book of ASTM Standards.

ASTM E 8-93 (1993). Standard test methods for tension testing of metallic materials. Annual Book of ASTM Standards.

ASTM E 8M-07 (1997). Standard test methods for tension testing of metallic materials. Annual Book of ASTM Standards.

AS 1391 (1974). Methods for tensile testing of metals, Standards Association of Australia, Sydney.

AS 1391 (1991). Methods for tensile testing of metals, Standards Association of Australia, Sydney.

Australian and New Zealand design code, (2001). Cold-formed stainless steel structures. Australian/ New Zealand Standard, AS/ NZS 4673:2001, Standards Australia, Sydney.

A370-77 (1981). American Society for Testing and Materials, Standard methods and definitions for mechanical testing of steel products. Annual book of ASTM Standards.

Baddoo, N. R. (2003). A comparison of structural stainless steel design standards. *Proceedings of the Stainless Steel Structures International Experts' Seminar,* Ascot, UK. 131 - 149.

Baddoo, N. R., Burgan, R. and Ogden, R. (1997). Architects' guide to stainless steel. The Steel Construction Institute, Ascot, UK.

Baddoo, N. R., and Gardner, L. (2000). WP5.2: Member behaviour at elevated temperatures. ECSC project - Development of the use of stainless steel in construction, Contact No. 7210 SA/842. The Steel Construction Institute, Ascot, UK.

Bernard, E. S., Coleman, R. and Bridge, R. Q. (1999). Measurement and assessment of geometric imperfections in thin walled panels. *Thin Walled Structures,* **33:2,** 103 - 126.

Berry, P. A., Rotter, J. M. and Bridge, R. Q. (2000). Compression tests on cylinders with circumferential weld depressions. *Journal of Engineering Mechanics,* ASCE, **126:4**, 405 - 413.

Birat, J. P., Dalsheimer, J., Gros, B. and Phelouzat, J. L. (2002). Waste recycling in the construction sector. International Iron and Steel Institute.

Bracewell, R. N. (1986). The Fourier Transform and its applications. 2nd edition, Mcgraw-Hill International Editions.

Brearley, H. (1989). Harry Brearley: Stainless pioneer. British Steel Stainless and The Kelham Island Industrial Museum, Sheffield (eds.), McCann-Erickson Central Solihull, West Midlands.

Bredenkamp, P. J., van den Berg, G. J. and van der Merwe, P. (1992). Residual stresses and the strength of stainless steel I-section columns. *Proceedings of the Structural Stability Research Council, Annual Technical Session,* Pittsburg, USA, 69 - 86.

Brozzetti, J., Alpsten, G. A. and Tall, L. (1971). Welding parameters, thick plates and column strength. *Welding Research Supplement,* **50:8**, 331 - 342.

BSK 99 (1999). Boverkets handbok om Stalkonstruktioner, Boverket, Karlskrona, Sweden. (In Swedish)

BSSA (British Stainless Steel Association) (2004). Stainless steel and sustainable construction. Special BSSA report, BSSA.

BS 5950-1 (1990). Structural use of steelwork in buildings - Part 1: Code of practice for design in simple and continuous: hot rolled sections. British Standards Institution.

Buchanen, A. H. (2001). Structural Design for Fire Safety, John Wiley & Sons Ltd., Chichester.

Burgan, B. A. (1992). Concise Guide to the Structural Design of Stainless. The Steel Construction Institute, Ascot, UK.

Burgan, B. A., Baddoo, N. R. and Gilsenan, K. A. (2000). Structural design of stainless steel members - comparison between Eurocode 3, Part 1.4 and test results. *Journal of Constructional Steel Research*, **54:1**, 51 - 73.

Cáceres, C. H., Griffiths, J. R., Pakdel, A. R., and Davidson, C. J. (2005). Microhardness mapping and the hardness-yield strength relationship in high-pressure diecast magnesium alloy AZ91. *Materials, Science and Engineering*, A402, 258 - 268.

Centre for Advanced Structural Engineering, (1990). Compression tests of stainless steel tubular columns. Investigation Report S770, University of Sydney, Sydney, Australia.

Chen, W. F. and Lui, E. M. (1991). Stability design of steel frames. CRC Press, Inc., 243 - 251.

Chen, W. F. and Ross, D. A. (1977). Tests of fabricated tubular columns. *Journal of the Structural Division,* ASCE, **103:3,** 619 - 634.

Chernenko, D. E. and Kennedy, D. J. L. (1991). An analysis of the performance of welded wide flange columns. *Canadian Journal of Civil Engineering,* **18:14,** 537 - 554.

Chou, S. M., Chai, G. B. and Ling, L. (2000). Finite element technique for design of stub columns. *Thin walled structures,* **37:2,** 97 - 112.

Chryssanthopoulos, M. K., Baker, M. J. and Dowling, P. J. (1991). Statistical analysis of imperfections in stiffened cylinders. *Journal of Structural Engineering,* ASCE, **117:7,** 1979 - 1997.

Chryssanthopoulos, M. K. and Low, Y. M. (2001). A method for predicting the flexural response of tubular members with non-linear stress-strain characteristics. *Journal of Constructional Steel Research,* **57:11,** 1197 - 1216.

Chryssanthopoulos, M. K and Poggi, C. (1995). Probabilistic imperfection sensitivity analysis of axially compressed composite cylinders. *Engineering structures,* **17:6,** 398 - 406.

Clarin, M. (2003). Measurement of longitudinal residual stresses in a cold formed rectangular hollow section, *Structural design of cold worked austenitic stainless steel, Internal report 2003-08-30,* Lulea University of Technology.

Coetzee, J. S., van den Berg, G. J. and van der Merwe, P. (1990). The effect of work hardening and residual stresses due to cold-work of forming on the strength of cold-formed stainless steel lipped channels. *Proceedings of the Tenth International Specialty Conference on Cold-Formed Steel Structures,* St. Louis, Missouri, U.S.A., 143 - 162.

Cook, N. H. (1966). Manufacturing analysis. Addison-Wesley Co.

Corus Construction Centre, (2002). Corrosion Protection of Steel Bridges. Corus, Scunthorpe. UK.

Corus Commercial and Industrial, (2004). Supporting the Commercial Decision - Comparing the cost of steel and concrete framing options for commercial buildings. Corus, Scunthorpe, UK.

Corus Construction and Industrial, (2005). Price list 5; Structural sections. 22nd edition, Corus, Scunthorpe, UK.

Cruise, R. B. and Gardner, L. (submitted). Residual stress analysis of structural stainless steel sections. *Journal of Constructional Steel Research.*

Cruise, R. B. and Gardner, L. (2006). Measurement and prediction of geometrical imperfections in stainless steel members. *Structural Engineering and Mechanics.* **24:1, 63 - 89.**

Davis, J. R. and Associates (eds.) (1999). Corrosion of aluminium and aluminium alloys. ASM International, Materials Park, Ohio, USA.

Davis Landgon and Everest, Davis Landgon and Mott Green and Wall, (2004). Office design - cost model. *Building Magazine,* 10th December.

Dawson, R. G. and Walker, A. C. (1972). Post-buckling of geometrically imperfect plates. *Journal of the Structural Division,* ASCE, **98:ST1, 75 - 94.**

Department of Trade and Industry. See http:// www.dti.gov.co.uk .

Dier, A., (1991). Design manual for structural stainless steel. Joint industry study, SCI Report, SCI-RT-256, Rev.0. The Steel Construction Institute, Ascot, UK.

Ding, X., Colman, R. and Rotter, J. M. (1996). Surface profiling system for measurement of engineering structures. *Journal of Surveying Engineering,* ASCE, **122:1**, 3 - 14.

DTLR, Department of Transport Local Government and the Regions, (Formerly Department of the Environment, Transport and the Regions) (1998). Rethinking Construction (Egan report). Office of the Deputy Prime Minister.

Dubina, D. and Ungureanu, U. (2002). Effect of imperfections on numerical simulation of instability behaviour of cold-formed steel members. *Thin Walled Structures*, **40:3**, 239 - 262.

Dwight, J. (1999). Aluminium design and construction, E&FN Spon, New York.

Dwight, J. B. and Moxham, K. E. (1969). Welded steel plates in compression. *The Structural Engineer,* **47:2**, 49 - 66.

Edwards, L. and Endean, M. (eds.) (1999). Manufacturing with Materials. Open University, Butterworth-Heinemann Ltd.

EN ISO 6507-1, (2005). Metallic materials - Vickers hardness test - Part 1: Test method. CEN.

ENV 1999-1-1, (1998). Eurocode 9: Design of aluminium structures–Part 1-1: General rules and rules for buildings. European standard. CEN.

EN 1993-1-1, (2005). Eurocode 3: Design of steel structures - Part 1.1: General rules and rules for buildings. European Standard, CEN.

EN 1993-1-3, (2006). Eurocode 3: Design of steel structures - Part 1.3: General rules. Supplementary rules for cold formed thin gauge members and sheeting. European Standard, CEN.

EN 1993-1-4, (1996). Eurocode 3: Design of steel structures - Part 1.4: General rules. Supplementary Rules for Stainless steels. European standard, CEN.

EN 1993-1-4, (2006). Eurocode 3: Design of steel structures - Part 1.4: General rules. Supplementary Rules for Stainless steels. European standard, CEN.

EN 10002-1 (1990). Metallic materials - Tensile testing, Part 1: Method of test. European Standard, CEN.

EN 10002-1 (2001). Metallic materials - Tensile testing, Part 1: Method of test. European Standard, CEN.

EN 10056-2 (1993). Specification for structural steel equal and unequal leg angles - Part 2: Tolerances on shape and dimensions. European Standard, CEN.

EN 10088-1 (2005). Stainless steels - Part 1: List of stainless steels. European Standard, CEN.

EN 10088-2 (2005). Stainless steels - Part 2: Technical delivery conditions for sheet/plate and strip of corrosion resisting steel for general purposes. European Standard, CEN.

EN 10088-3 (2005). Stainless steels - Part 3: Technical delivery conditions for semi-finished products, bars, rods and sections for general purpose. European Standard, CEN.

EN 10162 (2003). Cold rolled steel sections - Technical delivery conditions - Dimensions and cross-sectional tolerances. European Standard, CEN.

EN 10204 (2004). Metallic products - Types of inspection documents. European Standard, CEN.

Erkkilä, P. (2004). Trends and challenges in the stainless steel industry. Ironmaking and Steelmaking, **31:4**, 277 - 284.

Estuar, F. R. and Tall, L. (1963). Experimental investigation of welded built-up columns. *Welding Research Supplement,* **42:4**, 164 - 175.

Eurocode 3 - Annex S (Draft), (1993). Design of steel structures. The use of stainless steels. Document CEN/TC:250/SC3 N277E. London, Secretariat of CEN/TC250/SC3.

Euro Inox/ SCI, (1994). Design Manual for Structural Stainless Steel. NiDI, Toronto, Canada.

Euro-Inox/ SCI, (2002). Design Manual for Structural Stainless Steel. 2nd edition, NiDI, Toronto, Canada.

Euro-Inox/ SCI, (2006). Design Manual for Structural Stainless Steel. 3rd edition. NiDI, Toronto, Canada.

European metal recycling website. See http:// www.emrltd.com.

Fukumoto, Y. and Itoh, Y. (1980). Strength variation of laterally unsupported beams. *Journal of the Structural Division,* ASCE, **106:1**, 165 - 181.

Fukumoto, Y. and Itoh, Y. (1981). Statistical study of experiments on welded beams. *Journal of the Structural Division,* ASCE, **107:1**, 89 - 103.

Galambos, T. V. (1998). Guide to Stability Design Criteria for Metal Structures. 5th edition, John Wiley and Sons Inc, New York.

Gardner, L. (2002). A new approach to structural stainless steel design. PhD. Thesis, Structures section, Department of Civil and Environmental Engineering. Imperial College London, UK.

Gardner, L. (2005). The use of stainless steel in structures, *Progress in Structural Engineering and Materials*, **7:2**, 45 - 55.

Gardner, L. and Ashraf, M. (2006). Structural design for non-linear metallic materials, *Engineering Structures,* **28:6**, 926 - 934.

Gardner, L. and Cruise, R. B. (submitted). Modelling of residual stresses in structural stainless steel structural sections. *Journal of Structural Engineering,* ASCE.

Gardner, L. and Nethercot, D. A. (2001). Numerical modelling of cold-formed stainless steel sections. *Proceedings of the Ninth Nordic Steel Construction Conference*, Mäkeläinen, P., Kesti, J., Jutila, A. and Kautila, O. (eds.), Helsinki, Finland, 781 - 789.

Gardner, L. and Nethercot, D. A. (2004). Numerical modelling of stainless steel structural components - a consistent approach. *Journal of Structural Engineering*, ASCE, **130:10**, 1586 - 1601.

Gardner, L. and Ng, K. T. (2006). Temperature development in structural stainless steel sections exposed to fire, *Fire Safety Journal*, **41:3**, 185 - 203.

Gardner, L., Talja, A. and Baddoo. N. R. (2006). Structural design of high-strength austenitic stainless steel. *Thin-walled structures*, **44:5**, 517 - 528.

Geyer, R., Jackson, T. and Clift, R., (2002). Economic and environmental comparison between recycling and reuse of structural steel section. *10th LCA Studies Symposium and 2002 European meeting of International Society for Industrial Ecology.*

Gozzi, J. and Olsson, A. (2003). Stainless steel - Plasticity and constitutive modelling. *Proceedings of the Stainless Steel Structures International Experts' Seminar*, Ascot, UK. 115 - 122.

Haaland, D. M. and Thomas, E. V. (1988). Partial least-Squares methods for spectral analyses. Relationship to other quantitative calibration methods and the extraction of qualitative information. *Analytical Chemistry*, **60**, 1193 - 1202.

Halmos, G. T. (ed.) (2006), Roll forming handbook, Taylor & Francis.

Hambly, E. T. and Calladine, C. R. (1996). Buckling experiments on damaged cylindrical shells. *International Journal of Solids and Structures*, **33:24**, 3539 - 3548.

Hammer, E. W. Jr. and Peterson, R. E. (1955). Column curves for type 301 stainless steel. *Aeronautical Engineering Review*, **14:12**, 33 - 39 and 48.

Hearn, G. E. and Metcalfe, A. V. (1995). Spectral analysis in engineering concepts and cases. Arnold publishers.

Hill, H. N. (1944). Determination of stress-strain relations from the offset yield strength values, Technical Note No. 927, National Advisory Committee for Aeronautics, Washington D.C., USA.

Hill, R. (1983). The mathematical theory of plasticity. Carendon press, Oxford, UK.

HM Treasury, (2003). *The Green Book - Appraisal and evaluation in the central government,* TSO, London, UK.

Huber, A. W. and Beedle, L. S. (1954). Residual Stress and Compressive Strength of Steel. *Welding Research Supplement,* **33:12**, 589 - 614.

Hyttinen, V. (1994). Design of cold-formed stainless steel SHS beam-columns. Report 41: Laboratory of Structural Engineering, University of Oulu, Finland.

Ingvarsson, L. (1975). Cold-forming residual stresses. Effect on buckling. *Proceedings of the Third Speciality Conference on Cold-formed Steel Structures,* University of Missouri-Rolla, United States, 85-119.

Ingvarsson, L. (1979). Cold-forming residual stresses in thin-walled structures, *Proceedings of the First International Conference on Thin-Walled Structures,* University of Strathclyde, Glasgow, 575 - 587.

Johnson, A. L. and Winter, G. (1966). Behaviour of stainless steel columns and beams. *Journal of the Structural Division,* ASCE. **ST5**, 97 - 118.

Johnson, W. and Mellor, P. B. (1980). Engineering plasticity. Van Nostrand Reinhold, New York.

Jonsson, J. (2000). Stainless steel in a sustainable society- what we know and what we need to investigate. AvestaPolarit, Research and Development, Avesta.

Kaitila, O. (2002). Imperfection sensitivity analysis of lipped channel columns at high temperatures. *Journal of Constructional Steel research,* **58:3**, 333 - 351.

Karren, K. W. (1967). Corner properties of cold-formed steel shapes. *Journal of the Structural Division.* ASCE. **93(ST1)**, 401 - 432.

Kato, B. and Aoki, H. (1978). Residual stresses in cold-formed tubes. *Journal of Strain Analysis*, **13:4**, 193 - 204.

Kincaid, D. (2002). Adapting buildings for changing uses: guidelines for change of use refurbishment. Spon press, London.

Kissell, J. R. and Ferry, R. L. (1995). Aluminium Structures: A guide to their specifications and design. Wiley, New York, Chichester.

Koch, G. H., Broongers, M. P. O., Thompson, N. G., Virmani, Y. P. and Payer, J. H. (2002). Corrosion cost and preventative strategies in the United States. JA, FHWA-RD-01-156. Federal Highway Administration, McLean.

Korvink, S. A., van den Berg, G. J. and van der Merwe, P. (1995). Web Crippling of stainless steel cold-formed beams. *Journal of Constructional Steel Research*, **34:2-3**, 225 - 248.

Kozola, B. D. and Shen, Y. L. (2003). A mechanistic analysis of the correlation between overall strength and indentation hardness in discontinuously reinforced aluminium. *Journal of Materials Science*, **38:5**, 901 - 907.

Kuwamura, H. (2003). Local buckling of thin-walled stainless steel members. *Steel Structures*, **3**, 191 - 201.

Lagerqvist, O. and Olsson, A. (2001). Residual stresses in welded I-girders made of stainless steel and structural steel. *Proceedings of the Ninth Nordic Steel Construction Conference*, Mäkeläinen, P., Kesti, J., Jutila, A. and Kautila, O. (eds.), Helsinki, Finland, 737 - 744.

Laubscher, R. F. and van der Merwe, P. (2003). Structural design in hot rolled 3Cr12 sections, *Proceedings of the Stainless Steel Structures International Experts' Seminar*, The Steel Construction Institute, Ascot, UK. 93 - 100.

Lay, M. G., and Ward, R. (1969). Residual stresses in steel sections. *Journal of the Australian Institute of Steel Construction*, **3:3**, 2 - 21.

Lecce, M. and Rasmussen, K. J. R. (2004). Experimental investigation of distortional buckling of cold-formed stainless steel sections. *Proceedings of the 17th International Speciality Conference on Cold-formed Steel Structures,* Orlando, USA.

Lechner, B. and Pircher, M. (2005). Analysis of imperfection measurements of structural members. *Thin-Walled structures*, **43:3**, 351 - 374.

Liu, Y. and Young, B. (2003). Buckling of stainless steel square hollow section compression members, *Journal of Constructional Steel Research,* **59**, 165 - 177.

London metal exchange. See http:// www.lme.co.uk.

Macdonald, M., Rhodes, J. and Taylor, G. T. (1998). The effect of cold forming on the yield strength of thin gauge steel - hardness test approach. *Thin-Walled Structures,* **29:1-4**, 243 - 256.

Macdonald, M., Rhodes, J. and Taylor, G. T. (2000). Mechanical properties of stainless steel lipped channels. *Fifteenth International Conference on Cold-Formed Steel Structures.* St. Louis, Missouri, USA. 673 - 686.

Madugula, M. K. S., Haidur, R., Monforton, G. R. and Marshall, D. G. (1997). Additional residual stress and yield stress tests on hot-rolled angles. *Proceedings of the Structural Stability Research Council,* Annual Technical Session. Toronto, Canada, 55 - 68.

Masubuchi, K. (1980). Analysis of welded structures. Pergamon Press Ltd.

Mazzolani, F. M. (1995). Aluminium Alloy Structures. 2nd edition, E&FN Spon, Chapman and Hall.

Mazzolani, F. M. (2004) Competing issues for aluminium alloys in structural engineering. *Progress in Structural Engineering and Materials*, **6**, 185 - 196.

Metal world. See http://www.metalworld.com/specs.

Mirambell, E. and Real, E. (2000). On the calculation of deflections in structural stainless steel beams: an experimental and numerical investigation. *Journal of Constructional Steel Research,* **54:1**, 109 - 133.

Moss, P. K. and Saetre, I. (1991). Use of aluminium in offshore trussed structures. *Proceedings of 10th International Conference on Offshore Mechanics and Arctic Engineering,* American Society of Mechanical Engineering, Volume III Part A.

Nefussi, G., Proslier L. & Gilormini, P. (1999). Simulation of the cold-roll forming of circular tubes. *Journal of Material Processing Technology.* **95:1-3,** 126 - 221.

Nethercot, D. A. (1974). Residual stresses and their influence upon the lateral buckling of rolled steel beams, *The Structural Engineer,* **3:52,** 89 - 96.

Nordberg, H. (2004), Note on the sensitivity of stainless steels to strain rate. Research Report No. 04.0-1. AvestaPolarit, Research and Development, Avesta.

ODPM Building Regulations, (2000). Approved Document B. Office of the Deputy Prime Minister.

Pacheco, L. A. and Durkin, S. (1988). Denting and collapse of tubular members – a numerical and experimental study. *International Journal of Mechanical Sciences,* **50:5,** 317 - 331.

Panton, S. M., Zhu, S. D. & Duncan, J. L. (1994). Fundamental deformation types and sectional properties in roll forming. *International Journal of Mechanical Sciences.* **36:8,** 725 - 735.

Prenter, P. M. (1975). Splines and variational methods. John Wiley and Sons.

Priestly, M. B. (1992). Spectral analysis and time series. Academic press Ltd.

Quach, W. M. (2005). Residual stresses in cold formed steel sections and their effect on column behaviour. PhD Thesis, Department of Civil and Structural Engineering, The Hong Kong Polytechnic University.

Quach, W. M., Teng, J. G. and Chung, K. F. (2004). Residual stresses in steel sheets due to coiling and uncoiling: a closed form analytical solution. *Engineering structures,* **26:9,** 1249 - 1259.

Quach, W. M., Teng, J. G. and Chung, K. F. (2006). Finite element predictions of residual stresses in press-braked thin-walled steel sections. *Engineering structures,* **28:11,** 1609 - 1619.

Ramberg, W. and Osgood, W. R. (1943). Description of stress-strain curves by three parameters. Technical Note No. 902, National Advisory Committee for Aeronautics. Washington.

Rasmussen, K. J. R. (2000). The development of an Australian standard for stainless steel structures. *Proceedings of the Fifteenth International Speciality Conference on Cold-formed Steel Structures,* St. Louis Missouri, USA. 659 - 671.

Rasmussen, K. J. R. (2003). Full range stress-strain curves for stainless steel alloys. *Journal of Constructional Steel Research,* **59:1,** 47 - 61.

Rasmussen, K. J. R. and Hancock, G. J. (1993a). Design of cold-formed stainless steel tubular members, I: Columns. *Journal of Structural Engineering,* ASCE, **119:8,** 2349 - 2367.

Rasmussen, K. J. R. and Hancock, G. J. (1993b). Design of cold-formed stainless steel tubular members, II: Beams,. *Journal of Structural Engineering,* ASCE, **119:8,** 2368 - 2386.

Real, E. (2001). Aportaciones al estudio del comportamiento a flexion de estructuras de acero inoxiddable. Tesis Doctoral, Departamento de Ingeniería de la Construcción, Universitat Politècnica de Catalunya. UPC-ETSECCP, Barcelona, Mayo. (In Spanish).

Rhodes, J. Macdonald, M. and McNiff, W. (2000). Buckling of cold formed stainless steel columns under concentric and eccentric loading. *Fifteenth International Speciality Conference on Cold-Formed Steel Structures,* St. Louis, Missouri, USA. 687 - 699.

Schafer, B. W. and Peköz, T. (1998). Computational modelling of cold-formed steel: characterizing geometric imperfections and residual stresses. *Journal of Constructional Steel Research,* **47:3,** 193 - 210.

Schedin, E. (1992). Forming Properties of Stainless Steel Sheet. *International Conference on the Application of Stainless Steel,* Kista Stockholm, Sweden, 137 - 146.

Sedlacek, G. and Stangenberg, H. (1999). Numerical modelling of the behaviour of stainless steel members in tests. *Proceedings of the Fourth International Conference on Steel and Aluminium Structures,* Mäkeläinen, P. Hassinen, P., Espoo (eds.), Finland, 503 - 512.

Sedriks, A. J. (1996). *Corrosion of stainless steels.* 2nd edition, John Wiley & Sons.

Sherman, D. R. (1969). Residual stress measurement in tubular members. *Journal of the Structural Division,* ASCE, **95:4**, 635 - 648.

Shuttleworth, E. P. (1989). Structural applications to stainless steel offshore - Report to Nickel Development Institute. SCI-RT-030, The Steel Construction Institute, Ascot, UK.

Singer, J. and Abramovich, H. (1995). The development of shell imperfection measurement techniques. *Thin-walled structures*, **23:1-4**, 379 - 398.

Slater, R. A. C. (1977). Engineering Plasticity Theory and application to metal forming processes. The Macmillan Press Ltd.

Spencer, K., Embury, J. D., Conlon, K. T., Véron, M. and Bréchet, Y. (2004). Strengthening via the formation of strain-induced martensite in stainless steels. *Materials Science and Engineering* A, **387 - 389**, 873 - 881.

Tabor, D. (1951). The hardness of metals. Oxford University Press, UK.

Talja, A. and Salmi, P. (1995). Design of stainless steel RHS beams, columns and beam-columns. Research note: 1619, VTT Building Technology, Finland.

Teng, J. G., Lin, X., Rotter, J. M. and Ding, X. L. (2005). Analysis of geometric imperfections in full-scale welded steel silos, *Engineering structures,* **27:6**, 938 - 950.

Trombka, J. I. and Schmadebeck, R. L. (1970). A numerical least-squared technique for resolving complex pulse-height spectra. Blackburn, J.A (ed). Spectral methods and techniques, New York, Marcel Dekker.

Truman, J. (1985). The initiation and growth of high alloy (stainless) steel production. *Journal of the Metallurgy Society,* **19:1**, 116 - 125.

Umemoto, M., Liu, Z. G., Tsuchiya, K., Sugimoto, S., and Bepari, M. M. A. (2001). Relationship between hardness and tensile properties in various single structured steels. *Materials Science and Technology,* **17:5**, 505 - 511.

Van den Berg, G. J. and van der Merwe, P. (1992). Prediction of corner mechanical properties for stainless steels due to cold forming. *Proceedings of the 11th International Speciality Conference on Cold-Formed Steel Structures.* St. Louis, Missouri, USA. 571 - 586.

Wang, S .T., Errera, S. J. and Winter G., (1975). Behaviour of cold-rolled stainless steel members. *Journal of the Structural Division,* ASCE, **101(ST11)**, 2337 - 2357.

Wang, Y. D., Lin Peng, R., Wang, X. L. and McGreevy, R. L. (2002). Grain-orientation-dependant residual stress and the effect of annealing in cold-rolled stainless steel. *Acta Materialia*, **50:7**, 1717 - 1734.

Webster, G. A. and Wimpory, R. C. (2001). Non-destructive measurement of residual stress by neutron diffraction. *Journal of Material Processing Technology,* **117:3**, 395 - 399.

Weisman, C. (Ed.) (1976). American Welding Society Welding handbook, Vol. 1, Fundamentals of welding, 7th edition, Macmillan.

Weng, C. C. and Peköz, T. (1990). Residual stresses in cold formed sections. *Journal of Structural Engineering,* ASCE, **116:6**, 1611 - 1625.

Weng, C. C. and White, R. N. (1990). Residual stresses in cold-bent thick steel plates. *Journal of Structural Engineering*, ASCE, **116:1**, 24 - 39.

Wheeler, A. and Pircher, M. (2002). Measured imperfections in six thin walled steel tubes. Research Report CCTR:001, Centre of Construction Technology and Research, University of Western Sydney, Australia.

Wheeler, A. and Pircher, M. (2003). Measured imperfections in six thin walled steel tubes. *Journal of Constructional Steel Research,* **59:11**, 1385 - 1395.

Withers, P. J. and Bhadeshia, H. K. D. H. (2001a). Residual stress: Part 1 – Measurement techniques. *Materials Science and Technology*, **17:4**, 355 - 365.

Withers, P. J. and Bhadeshia, H. K. D. H. (2001b). Residual stress: Part 2 – Nature and Origins. *Materials Science and Technology*, **17:4**, 366 - 375.

Wong, S. M. (2004), Element and system risk considerations in bridge management. PhD Thesis, Transport section, Department of Civil and Environmental Engineering, Imperial College London, UK.

Young, B. and Liu, Y. (2003), Experimental investigation of cold-formed stainless steel columns, *Journal of Structural Engineering,* ASCE, **129:2**, 169 - 176.

Young, B. and Lui, W. M. (2005). Behavior of Cold-formed high strength stainless steel sections. *Journal of Structural Engineering,* ASCE. **131:11**, 1738 - 1745.

Zhou, F. and Young, B. (2005). Tests of cold-formed stainless steel tubular flexural members. *Thin-Walled Structures*, **43:9**, 1325 - 1337.

Appendix A

A.1 PB2 50×50×2 (r_i=3.2)

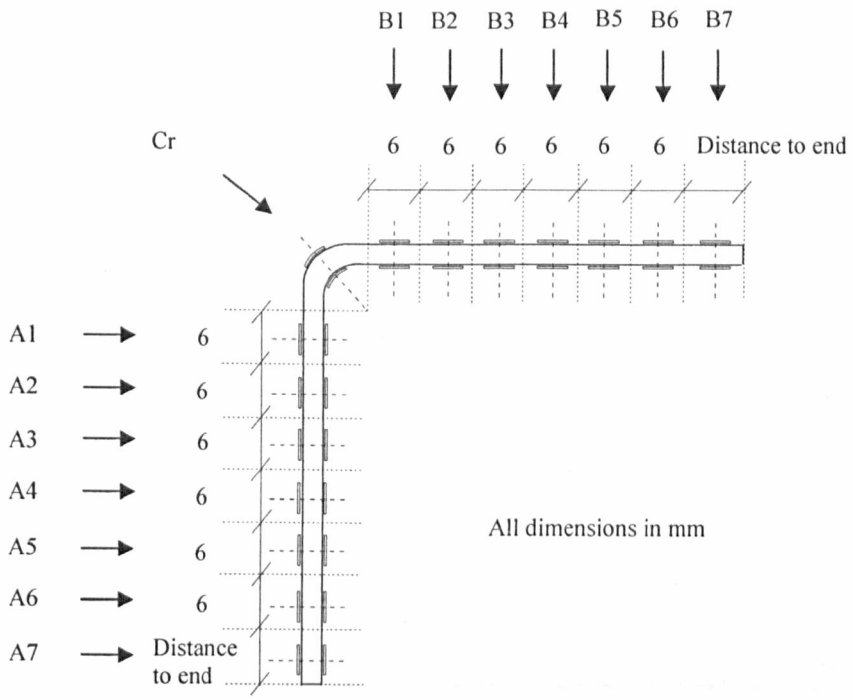

Figure A.1: *Setting out of press braked section PB2 50×50×2 (r_i=3.2)*

Table A.1: *Residual stress distribution for PB2 50×50×2 (r_i=3.2)*

PB2 50×50×2 (r_i=3.2)	*Section position (mm)*	*Width (mm)*	σ_m *(N/mm²)*	σ_b *(N/mm²)*	σ_{rc} *(N/mm²)*	$\sigma_m/\sigma_{0.2}$	$\sigma_b/\sigma_{0.2}$	$\sigma_{rc}/\sigma_{0.2}$
A7	44.0	7.39	16	1	16	0.07	0.00	0.07
A6	36.3	4.95	20	73	92	0.08	0.29	0.37
A5	30.4	4.60	37	-11	48	0.13	-0.04	0.17
A4	24.3	5.02	33	-34	67	0.13	-0.13	0.26
A3	18.4	4.40	28	5	33	0.09	0.02	0.11
A2	12.9	4.26	-	-	-	-	-	-
A1	7.2	4.66	2	-36	38	0.01	-0.10	0.11
Cr (r_i=4.5)	0.0		1	-103	104	0.00	-0.28	0.29
B1	7.6	5.29	19	-46	65	0.06	-0.15	0.21
B2	13.6	4.32	-62	-45	107	-0.20	-0.15	0.35
B3	19.1	4.28	-	-	-	-	-	-
B4	25.1	5.34	26	-1	27	0.11	0.00	0.11
B5	31.4	4.96	27	-10	37	0.08	-0.03	0.11
B6	37.6	4.96	45	3	49	0.17	0.01	0.18
B7	45.0	6.84	38	30	68	0.15	0.12	0.27

Table A.2: *Material properties distribution for PB2 50×50×2 (r_i=3.2)*

PB2 50×50×2 (r_i=3.2)	*Section position (mm)*	*Width (mm)*	*E (N/mm^2)*	*$\sigma_{0.01,exp}$ (N/mm^2)*	*$\sigma_{0.2,exp}$ (N/mm^2)*	*$\sigma_{1.0,exp}$ (N/mm^2)*	*$\sigma_{ult,exp}$ (N/mm^2)*	*$\varepsilon_{f,exp}$*
A7	44.0	7.39	189200	62	233	289	477	0.50
A6	36.3	4.95	218600	98	252	317	575	0.58
A5	30.4	4.60	198000	114	290	345	646	0.49
A4	24.3	5.02	251500	34	256	313	579	0.49
A3	18.4	4.40	196700	200	309	375	673	0.58
A2	12.9	4.26	198300	204	329	390	712	0.53
A1	7.2	4.66	202800	202	354	421	724	0.63
Cr (r_i=4.5)	0.0		181400	92	362	455	593	0.52
B1	7.6	5.29	192800	144	310	369	624	0.54
B2	13.6	4.32	210100	146	308	372	687	0.63
B3	19.1	4.28	186100	192	311	367	682	0.60
B4	25.1	5.34	189700	98	243	300	555	0.56
B5	31.4	4.96	195500	203	320	356	617	0.47
B6	37.6	4.96	194500	133	266	331	608	0.64
B7	45.0	6.84	210600	83	256	306	546	0.65

Table A.3: *Proof stress ratios and Ramberg-Osgood strain parameters for PB2 50×50×2 (r_i=3.2)*

PB2 50×50×2 (r_i=3.2)	*Section position (mm)*	*Width (mm)*	*$\sigma_{0.2,exp}$/ $\sigma_{0.2,mill}$*	*$\sigma_{0.2,exp}$/ $\sigma_{0.2,min}$*	*$n_{0.01}$*	*$n_{0.05}$*	*$n_{0.1}$*	*$n_{bestfit}$*	*n'*	*$n'_{bestfit}$*
A7	44.0	7.39	0.74	1.01	2.3	4.2	5.2	4.3	2.5	2.5
A6	36.3	4.95	0.80	1.10	3.2	4.5	4.3	4.8	3.3	3.3
A5	30.4	4.60	0.92	1.26	3.2	5.9	6.6	5.9	3.5	3.5
A4	24.3	5.02	0.81	1.11	1.5	2.0	3.5	2.4	1.7	1.7
A3	18.4	4.40	0.98	1.35	6.9	9.5	7.4	15.1	0.9	0.9
A2	12.9	4.26	1.04	1.43	6.3	7.1	5.8	8.0	2.5	2.5
A1	7.2	4.66	1.12	1.54	5.4	6.0	6.3	6.3	1.5	1.5
Cr (r_i=4.5)	0.0		1.14	1.57	2.2	4.1	5.1	4.1	3.0	3.0
B1	7.6	5.29	0.98	1.35	3.9	5.2	4.6	5.2	2.5	2.5
B2	13.6	4.32	0.97	1.34	4.0	5.8	6.0	7.1	4.4	4.4
B3	19.1	4.28	0.98	1.35	6.2	6.1	6.3	7.2	2.5	2.5
B4	25.1	5.34	0.77	1.06	3.3	8.9	8.1	6.9	2.6	2.6
B5	31.4	4.96	1.01	1.39	6.6	-	-	-	1.1	1.1
B6	37.6	4.96	0.84	1.16	4.3	5.7	7.0	5.7	2.4	2.4
B7	45.0	6.84	0.81	1.11	2.7	4.5	6.1	4.4	2.6	2.6

A.2 PB 50×50×2 (r_i=3.5)

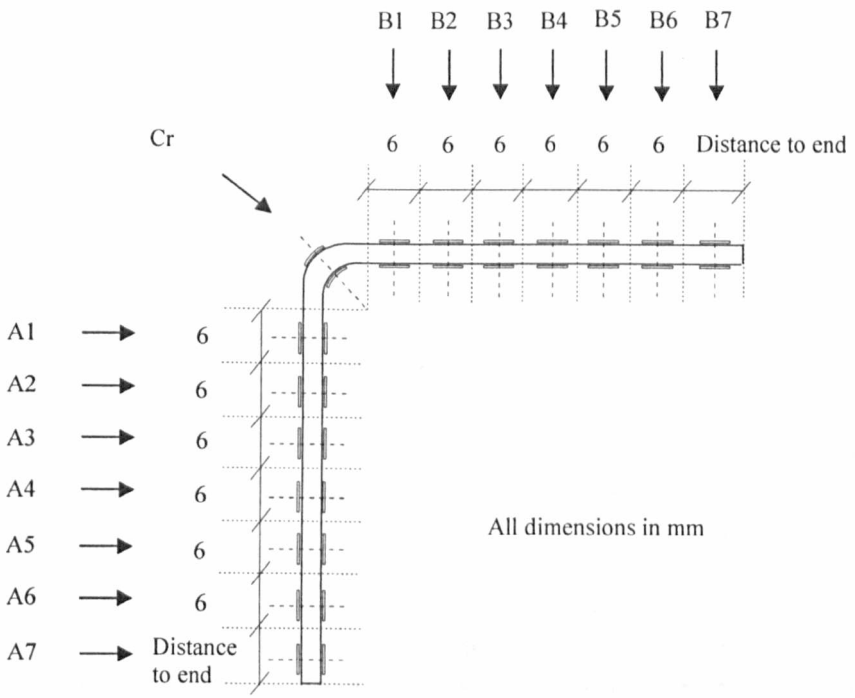

Figure A.2: *Setting out of press braked section PB 50×50×2 (r_i=3.5)*

Table A.4: *Residual stress distribution for PB 50×50×2 (r_i=3.5)*

PB 50×50×2 (r_i=3.5)	*Section position (mm)*	*Width (mm)*	σ_m *(N/mm²)*	σ_b *(N/mm²)*	σ_{rc} *(N/mm²)*	$\sigma_m/\sigma_{0.2}$	$\sigma_b/\sigma_{0.2}$	$\sigma_{rc}/\sigma_{0.2}$
A7	44.9	6.82	-3	13	16	-0.01	0.04	0.05
A6	37.4	5.20	7	-2	8	0.02	0.00	0.03
A5	31.3	4.65	8	-16	24	0.03	-0.05	0.08
A4	25.4	4.79	1	-10	12	0.00	-0.03	0.04
A3	19.4	4.80	14	-17	31	0.04	-0.05	0.10
A2	13.3	4.98	4	-6	10	0.01	-0.02	0.03
A1	7.2	4.82	4	-6	10	0.01	-0.02	0.03
Cr (r_i=4.3)	0.0		3	-60	63	0.01	-0.15	0.15
B1	7.2	4.91	4	-2	6	0.01	-0.01	0.02
B2	13.3	4.89	8	-8	16	0.02	-0.02	0.05
B3	19.4	4.81	24	-2	26	0.07	-0.01	0.08
B4	25.3	4.67	-13	31	44	-0.04	0.10	0.14
B5	31.3	4.83	2	1	4	0.01	0.00	0.01
B6	37.3	4.80	14	-15	30	0.05	-0.05	0.11
B7	44.3	6.29	-7	6	12	-0.02	0.02	0.04

Table A.5: *Material properties distribution for PB 50×50×2 (r_i=3.5)*

PB 50×50×2 (r_i=3.5)	*Section position (mm)*	*Width (mm)*	*E (N/mm^2)*	*$\sigma_{0.01,exp}$ (N/mm^2)*	*$\sigma_{0.2,exp}$ (N/mm^2)*	*$\sigma_{1.0,exp}$ (N/mm^2)*	*$\sigma_{ult,exp}$ (N/mm^2)*	*$\varepsilon_{f,exp}$*
A7	44.9	6.82	206800	169	316	378	662	0.63
A6	37.4	5.20	218400	184	331	400	730	0.61
A5	31.3	4.65	196000	152	298	365	666	0.57
A4	25.4	4.79	202000	154	315	385	678	0.57
A3	19.4	4.80	196000	192	324	388	695	0.65
A2	13.3	4.98	194900	179	313	378	665	0.54
A1	7.2	4.82	189900	190	335	411	681	0.56
Cr (r_i=4.3)	0.0		197600	185	408	500	688	0.65
B1	7.2	4.91	202700	198	360	438	674	0.53
B2	13.3	4.89	219000	169	336	419	666	0.52
B3	19.4	4.81	194500	209	334	420	664	0.51
B4	25.3	4.67	200800	143	308	373	639	0.61
B5	31.3	4.83	206500	159	269	331	635	0.65
B6	37.3	4.80	198400	146	284	346	658	0.69
B7	44.3	6.29	196600	184	355	431	663	0.57

Table A.6: *Proof stress ratios and Ramberg-Osgood strain parameters for PB 50×50×2 (r_i=3.5)*

PB 50×50×2 (r_i=3.5)	*Section position (mm)*	*Width (mm)*	*$\sigma_{0.2,exp}$/ $\sigma_{0.2,mill}$*	*$\sigma_{0.2,exp}$/ $\sigma_{0.2,min}$*	*$n_{0.01}$*	*$n_{0.05}$*	*$n_{0.1}$*	*$n_{bestfit}$*	*n'*	*$n'_{bestfit}$*
A7	44.9	6.82	1.04	1.38	4.8	5.4	5.3	5.6	2.0	2.1
A6	37.4	5.20	1.09	1.44	5.1	6.2	6.0	6.0	1.9	1.9
A5	31.3	4.65	0.98	1.30	4.5	5.4	6.3	6.5	3.7	3.7
A4	25.4	4.79	1.04	1.37	4.2	4.8	5.7	5.3	2.2	2.2
A3	19.4	4.80	1.07	1.41	5.7	5.8	5.6	6.3	2.7	2.7
A2	13.3	4.98	1.03	1.36	5.4	6.6	6.4	6.1	1.9	2.0
A1	7.2	4.82	1.10	1.46	5.3	6.4	9.1	7.7	3.0	3.1
Cr (r_i=4.3)	0.0		1.34	1.77	3.8	3.9	4.0	4.3	3.0	3.0
B1	7.2	4.91	1.18	1.57	5.0	4.9	4.6	5.5	1.9	2.0
B2	13.3	4.89	1.10	1.46	4.4	5.6	5.9	5.6	2.3	2.3
B3	19.4	4.81	1.10	1.45	6.4	6.1	7.8	7.8	3.7	3.7
B4	25.3	4.67	1.01	1.34	3.9	5.2	6.7	5.9	2.7	2.6
B5	31.3	4.83	0.88	1.17	5.7	5.0	11.3	8.7	4.3	4.3
B6	37.3	4.80	0.93	1.23	4.5	5.1	7.3	7.3	2.7	2.7
B7	44.3	6.29	1.17	1.54	4.5	5.6	6.1	5.8	4.3	4.3

Table A.7: *Hardness values HV and predicted 0.2% proof stress* $\overline{\sigma}_{0.2,exp}$ *for PB 50×50×2* (r_i=3.5)

PB 50×50×2 (r_i=3.5)	*Section position (mm)*	*HV*	$\overline{\sigma}_{0.2,exp}$ *(N/mm²)*
A7	0.92	186	375
A6	0.80	175	354
A5	0.67	181	366
A4	0.55	181	365
A3	0.42	156	315
A2	0.29	167	337
	0.22	174	351
A1	0.19	166	336
	0.16	172	347
	0.13	177	357
	0.09	194	392
Cr	0.06	227	459
	0.03	213	429
	0.00	210	424
	0.03	188	380
	0.06	180	363
	0.09	203	410
B1	0.12	178	359
	0.15	177	357
	0.18	166	336
B2	0.22	162	326
	0.28	180	364
B3	0.40	179	362
B4	0.52	178	360
B5	0.65	173	349
B6	0.77	170	344
B7	0.86	174	352

A.3 PB 50×50×2 (r_i=4.5)

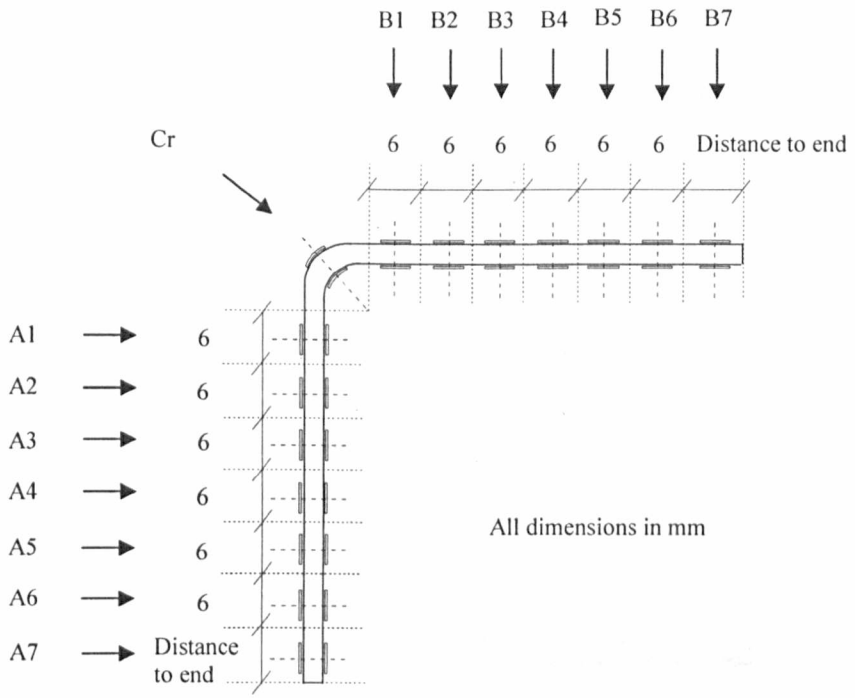

Figure A.3: *Setting out of press braked section PB 50×50×2 (r_i=4.5)*

Table A.8: *Residual stress distribution for PB 50×50×2 (r_i=4.5)*

PB 50×50×2 (r_i=4.5)	*Section position (mm)*	*Width (mm)*	σ_m (N/mm²)	σ_b (N/mm²)	σ_{rc} (N/mm²)	$\sigma_m/\sigma_{0.2}$	$\sigma_b/\sigma_{0.2}$	$\sigma_{rc}/\sigma_{0.2}$
A7	44.7	5.46	24	-10	34	0.07	-0.03	0.10
A6	38.2	4.63	8	-14	22	0.03	-0.05	0.08
A5	32.3	4.76	-8	-9	17	-0.03	-0.03	0.06
A4	26.4	4.71	-10	-11	21	-0.04	-0.04	0.07
A3	20.4	4.76	-9	-7	15	-0.03	-0.02	0.05
A2	14.5	4.76	-11	-10	21	-0.04	-0.03	0.07
A1	8.3	5.19	-4	-23	27	-0.01	-0.07	0.08
Cr (r_i=5.5)	0.0		19	-67	85	0.05	-0.19	0.25
B1	8.3	5.15	2	-29	31	0.01	-0.09	0.10
B2	14.4	4.70	12	-7	20	0.04	-0.02	0.07
B3	20.3	4.79	10	-8	18	0.04	-0.03	0.07
B4	26.3	4.72	12	-8	20	0.04	-0.03	0.07
B5	32.2	4.76	11	-10	21	0.03	-0.03	0.06
B6	38.2	4.82	2	-6	8	0.01	-0.02	0.03
B7	45.1	5.95	-11	-5	16	-0.04	-0.02	0.05

Table A.9: *Material properties distribution for PB 50×50×2 (r_i=4.5)*

PB 50×50×2 (r_i=4.5)	*Section position (mm)*	*Width (mm)*	*E (N/mm^2)*	*$\sigma_{0.01,exp}$ (N/mm^2)*	*$\sigma_{0.2,exp}$ (N/mm^2)*	*$\sigma_{1.0,exp}$ (N/mm^2)*	*$\sigma_{ult,exp}$ (N/mm^2)*	*$\varepsilon_{f,exp}$*
A7	44.7	5.46	199000	166	322	393	645	0.43
A6	38.2	4.63	218500	106	275	345	627	0.50
A5	32.3	4.76	204000	112	284	339	635	0.49
A4	26.4	4.71	191400	137	289	352	631	0.48
A3	20.4	4.76	212700	144	296	358	643	0.54
A2	14.5	4.76	180500	201	304	361	657	0.57
A1	8.3	5.19	186000	180	320	381	655	0.51
Cr (r_i=5.5)	0.0		181500	155	346	418	641	0.39
B1	8.3	5.15	192900	165	321	382	645	0.46
B2	14.4	4.70	181400	192	293	351	649	0.52
B3	20.3	4.79	187100	163	273	336	624	0.48
B4	26.3	4.72	183000	199	279	344	636	0.46
B5	32.2	4.76	200700	214	335	376	651	0.56
B6	38.2	4.82	203400	139	279	347	638	0.47
B7	45.1	5.95	214200	132	302	357	639	0.43

Table A.10: *Proof stress ratios and Ramberg-Osgood strain parameters for PB 50×50×2 (r_i=4.5)*

PB 50×50×2 (r_i=4.5)	*Section position (mm)*	*Width (mm)*	*$\sigma_{0.2,exp}$/ $\sigma_{0.2,mill}$*	*$\sigma_{0.2,exp}$/ $\sigma_{0.2,min}$*	*$n_{0.01}$*	*$n_{0.05}$*	*$n_{0.1}$*	*$n_{bestfit}$*	*n'*	*$n'_{bestfit}$*
A7	44.7	5.46	1.06	1.40	4.5	5.5	5.9	6.8	3.6	3.6
A6	38.2	4.63	0.90	1.20	3.2	5.3	4.3	5.8	3.9	3.9
A5	32.3	4.76	0.93	1.24	3.2	5.9	6.8	6.1	3.6	3.6
A4	26.4	4.71	0.95	1.25	4.0	6.0	12.2	7.6	2.4	2.4
A3	20.4	4.76	0.97	1.28	4.2	7.5	7.4	6.4	2.8	2.8
A2	14.5	4.76	1.00	1.32	7.2	7.1	6.7	8.4	2.6	2.6
A1	8.3	5.19	1.05	1.39	5.2	5.8	6.3	6.0	1.5	1.5
Cr (r_i=5.5)	0.0		1.14	1.50	3.7	4.2	4.5	4.6	2.8	2.8
B1	8.3	5.15	1.05	1.39	4.5	5.8	7.2	5.8	2.6	2.6
B2	14.4	4.70	0.96	1.27	7.1	5.9	6.0	8.9	6.7	6.7
B3	20.3	4.79	0.90	1.19	5.8	5.4	9.9	7.7	4.3	4.3
B4	26.3	4.72	0.92	1.21	8.9	10.4	13.4	9.4	4.4	4.4
B5	32.2	4.76	1.10	1.46	-	-	-	-	-	0.9
B6	38.2	4.82	0.92	1.21	4.3	5.7	7.0	5.7	2.5	2.5
B7	45.1	5.95	0.99	1.31	3.6	4.9	5.6	5.1	2.5	2.5

A.4 PB 50×50×2 (r_i=7.5)

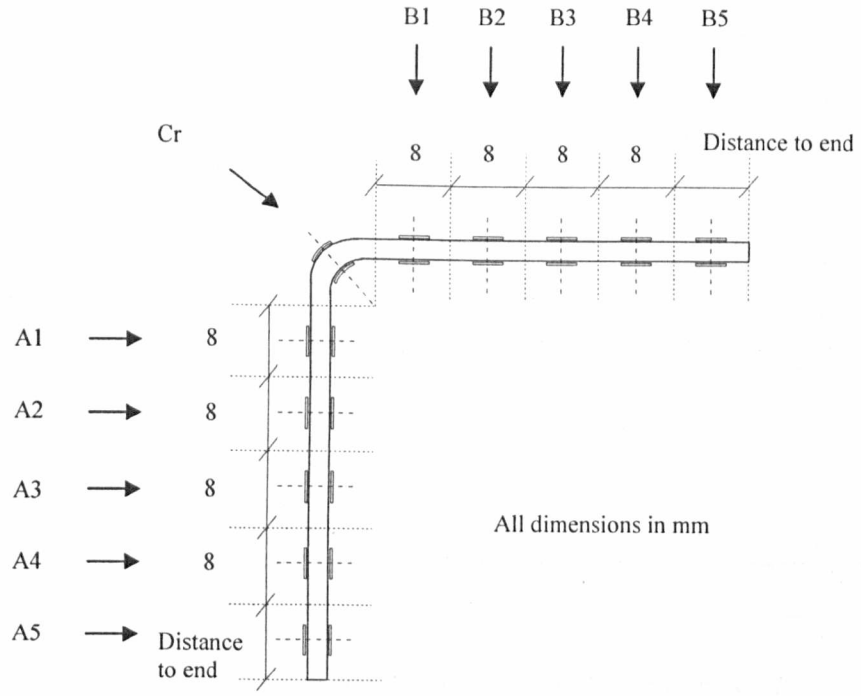

Figure A.4: *Setting out of press braked section PB 50×50×2 (r_i=7.5)*

Table A.11: *Residual stress distribution for PB 50×50×2 (r_i=7.5)*

PB 50×50×2 (r_i=7.5)	*Section position (mm)*	*Width (mm)*	σ_m *(N/mm²)*	σ_b *(N/mm²)*	σ_{rc} *(N/mm²)*	$\sigma_m/\sigma_{0.2}$	$\sigma_b/\sigma_{0.2}$	$\sigma_{rc}/\sigma_{0.2}$
A5	44.3	7.95	-12	9	21	-0.04	0.03	0.07
A4	35.4	6.73	-13	-24	37	-0.05	-0.09	0.13
A3	27.3	7.19	12	0	12	0.04	0.00	0.04
A2	19.1	6.82	13	55	68	0.05	0.20	0.24
A1	11.1	6.82	7	135	142	0.02	0.44	0.46
Cr (r_i=8.0)	0.0		-5	-58	63	-0.01	-0.17	0.19
B1	10.8	6.22	0	-27	27	0.00	-0.09	0.09
B2	18.5	6.80	8	7	14	0.03	0.02	0.05
B3	26.5	6.80	10	7	17	0.04	0.02	0.06
B4	34.5	6.85	3	4	7	0.01	0.01	0.02
B5	42.6	6.42	-8	-2	10	-0.02	-0.01	0.03

Table A.12: *Material properties distribution for PB 50×50×2 (r_i=7.5)*

PB 50×50×2 (r_i=7.5)	*Section position (mm)*	*Width (mm)*	*E (N/mm²)*	*$\sigma_{0.01,exp}$ (N/mm²)*	*$\sigma_{0.2,exp}$ (N/mm²)*	*$\sigma_{1.0,exp}$ (N/mm²)*	*$\sigma_{ult,exp}$ (N/mm²)*	*$\varepsilon_{f,exp}$*
A5	44.3	7.95	191600	195	311	365	662	0.62
A4	35.4	6.73	197500	148	278	322	652	0.68
A3	27.3	7.19	202000	171	284	327	659	0.69
A2	19.1	6.82	192900	173	278	324	662	0.70
A1	11.1	6.82	193600	182	309	365	697	0.71
Cr (r_i=8.0)	0.0		183900	186	336	400	643	0.65
B1	10.8	6.22	212500	118	298	347	640	0.61
B2	18.5	6.80	200300	145	284	328	652	0.70
B3	26.5	6.80	194600	169	285	334	654	0.71
B4	34.5	6.85	191700	173	280	325	674	0.69
B5	42.6	6.42	199700	180	314	367	668	0.58

Table A.13: *Proof stress ratios and Ramberg-Osgood strain parameters for PB 50×50×2 (r_i=7.5)*

PB 50×50×2 (r_i=7.5)	*Section position (mm)*	*Width (mm)*	*$\sigma_{0.2,exp}$/ $\sigma_{0.2,mill}$*	*$\sigma_{0.2,exp}$/ $\sigma_{0.2,min}$*	*$n_{0.01}$*	*$n_{0.05}$*	*$n_{0.1}$*	*$n_{bestfit}$*	*n'*	*$n'_{bestfit}$*
A5	44.3	7.95	1.02	1.35	6.4	8.0	7.4	8.7	2.4	2.5
A4	35.4	6.73	0.91	1.21	4.8	7.3	6.9	7.4	1.7	1.7
A3	27.3	7.19	0.93	1.23	5.9	5.3	8.5	7.0	1.6	1.6
A2	19.1	6.82	0.91	1.21	6.3	7.6	8.3	8.9	3.1	3.1
A1	11.1	6.82	1.01	1.34	5.7	7.7	8.2	8.3	2.5	2.5
Cr (r_i=8.0)	0.0		1.10	1.46	5.0	5.1	5.9	5.4	2.6	2.6
B1	10.8	6.22	0.98	1.30	3.2	4.9	5.5	4.9	2.0	2.0
B2	18.5	6.80	0.93	1.24	4.4	5.8	7.5	7.7	2.4	2.4
B3	26.5	6.80	0.94	1.24	5.7	6.9	10.1	8.6	1.5	1.5
B4	34.5	6.85	0.92	1.22	6.2	9.0	9.3	9.3	1.6	1.7
B5	42.6	6.42	1.03	1.36	5.4	7.4	7.4	6.9	1.6	1.6

A.5 PB2 50×50×3 (r_i=3.2)

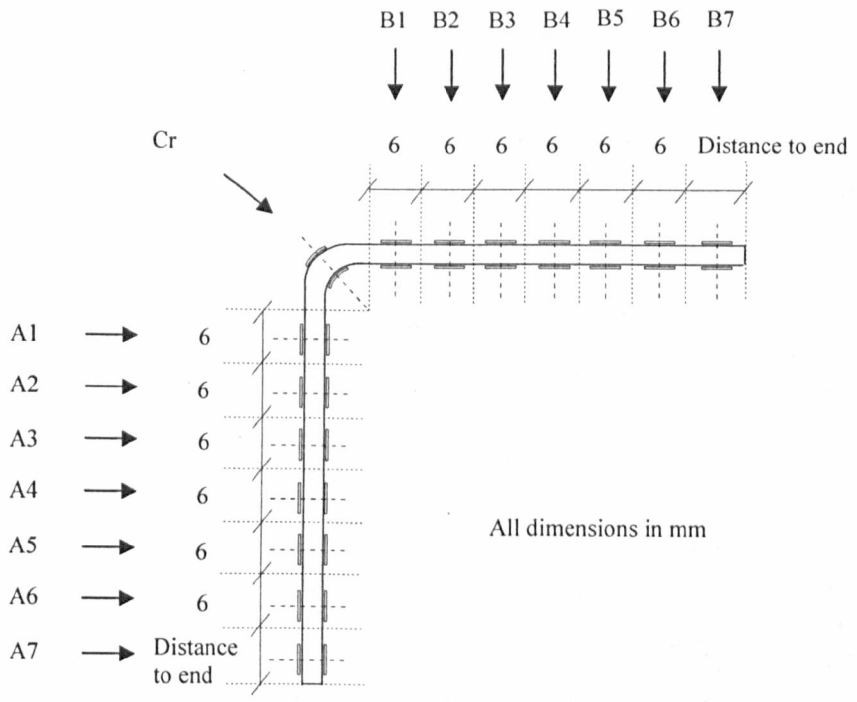

Figure A.5: *Setting out of press braked section PB2 50×50×3 (r_i=3.2)*

Table A.14: *Residual stress distribution for PB2 50×50×3 (r_i=3.2)*

PB2 50×50×3 (r_i=3.2)	*Section position (mm)*	*Width (mm)*	σ_m *(N/mm²)*	σ_b *(N/mm²)*	σ_{rc} *(N/mm²)*	$\sigma_m/\sigma_{0.2}$	$\sigma_b/\sigma_{0.2}$	$\sigma_{rc}/\sigma_{0.2}$
A7	44.9	6.64	-2	-18	20	0.00	-0.05	0.05
A6	37.7	4.74	87	42	129	0.26	0.12	0.38
A5	31.8	4.61	10	-7	17	0.03	-0.02	0.05
A4	25.9	4.76	-	-	-	-	-	-
A3	20.0	4.76	14	7	21	0.04	0.02	0.06
A2	14.0	4.84	-25	20	45	-0.08	0.06	0.14
A1	7.8	5.02	-10	-31	41	-0.03	-0.08	0.11
Cr (r_i=4.5)	0.0		7	-114	121	0.01	-0.19	0.20
B1	7.8	4.87	4	-39	43	0.01	-0.11	0.12
B2	13.7	4.68	-6	3	9	-0.02	0.01	0.03
B3	19.6	4.64	13	-14	27	0.04	-0.04	0.08
B4	25.5	4.86	1	-8	9	0.00	-0.03	0.03
B5	31.6	4.89	-15	-15	30	-0.05	-0.05	0.10
B6	37.6	4.69	-	-	-	-	-	-
B7	44.8	6.68	3	-7	10	0.01	-0.02	0.03

Table A.15: *Material properties distribution for PB2 50×50×3 (r_i=3.2)*

PB2 50×50×3 (r_i=3.2)	*Section position (mm)*	*Width (mm)*	*E (N/mm^2)*	*$\sigma_{0.01,exp}$ (N/mm^2)*	*$\sigma_{0.2,exp}$ (N/mm^2)*	*$\sigma_{1.0,exp}$ (N/mm^2)*	*$\sigma_{ult,exp}$ (N/mm^2)*	*$\varepsilon_{f,exp}$*
A7	44.9	6.64	190600	212	362	423	670	0.58
A6	37.7	4.74	209400	160	339	396	657	0.49
A5	31.8	4.61	197700	170	342	407	667	0.66
A4	25.9	4.76	203000	102	301	359	637	0.77
A3	20.0	4.76	189600	179	326	390	656	0.77
A2	14.0	4.84	190800	178	320	376	650	0.72
A1	7.8	5.02	205600	159	367	442	674	0.73
Cr (r_i=4.5)	0.0		188700	319	605	699	811	0.54
B1	7.8	4.87	205600	151	366	431	676	0.76
B2	13.7	4.68	195800	168	334	398	659	0.72
B3	19.6	4.64	210900	173	335	403	670	0.75
B4	25.5	4.86	199600	175	320	379	647	0.74
B5	31.6	4.89	198000	137	309	365	645	0.74
B6	37.6	4.69	203600	150	296	352	663	0.78
B7	44.8	6.68	203200	178	339	399	655	0.70

Table A.16: *Proof stress ratios and Ramberg-Osgood strain parameters for PB2 50×50×3 (r_i=3.2)*

PB2 50×50×3 (r_i=3.2)	*Section position (mm)*	*Width (mm)*	*$\sigma_{0.2,exp}/\sigma_{0.2,mill}$*	*$\sigma_{0.2,exp}/\sigma_{0.2,min}$*	*$n_{0.01}$*	*$n_{0.05}$*	*$n_{0.1}$*	*$n_{bestfit}$*	*n'*	*$n'_{bestfit}$*
A7	44.9	6.64	1.11	1.04	5.6	6.5	6.6	7.2	2.8	2.8
A6	37.7	4.74	1.57	1.48	4.0	5.0	5.9	5.0	2.4	2.4
A5	31.8	4.61	1.11	1.04	4.3	5.5	7.2	6.1	2.7	2.7
A4	25.9	4.76	1.57	1.48	2.8	5.2	6.3	4.7	2.0	2.0
A3	20.0	4.76	1.11	1.04	5.0	6.4	8.7	7.0	3.2	3.2
A2	14.0	4.84	1.57	1.48	5.1	5.7	5.9	5.8	2.2	2.2
A1	7.8	5.02	1.11	1.04	3.6	5.4	6.0	6.0	4.3	4.3
Cr (r_i=4.5)	0.0		1.57	1.48	4.7	7.1	6.2	7.1	4.8	4.8
B1	7.8	4.87	1.11	1.04	3.4	4.6	5.6	5.1	2.7	2.7
B2	13.7	4.68	1.57	1.48	4.4	5.7	7.3	6.1	2.0	1.9
B3	19.6	4.64	1.11	1.04	4.6	5.1	7.6	5.8	2.4	2.4
B4	25.5	4.86	1.57	1.48	5.0	6.7	5.9	6.1	2.4	2.4
B5	31.6	4.89	1.11	1.04	3.7	5.6	6.9	5.7	2.2	2.2
B6	37.6	4.69	1.57	1.48	4.4	5.1	6.0	6.0	2.6	2.6
B7	44.8	6.68	1.11	1.04	4.6	5.4	5.3	5.5	2.4	2.4

Table A.17: *Hardness values HV and predicted 0.2% proof stress* $\overline{\sigma}_{0.2,exp}$ *for PB2 50×50×3* (r_i=3.2)

PB 50×50×3 (r_i=3.2)	*Section position (mm)*	*HV*	$\overline{\sigma}_{0.2,exp}$ *(N/mm²)*
A7	1.00	186	376
	0.92	206	416
A6	0.79	189	382
A5	0.66	210	424
A4	0.54	195	394
A3	0.41	207	418
A2	0.28	193	390
	0.25	199	402
A1	0.22	197	398
	0.19	183	370
	0.16	203	410
	0.13	194	392
Cr	0.09	204	412
	0.06	259	523
	0.03	239	483
	0.00	251	507
	0.03	215	434
	0.06	201	406
	0.09	213	430
B1	0.13	188	380
	0.16	204	412
	0.19	215	434
	0.22	230	465
B2	0.25	221	446
	0.28	207	418
B3	0.41	213	430
B4	0.53	192	388
B5	0.66	239	483
B6	0.79	201	406
B7	0.91	201	406
	0.98	177	358

A.6 PB 50×50×4 (r_i=3.5)

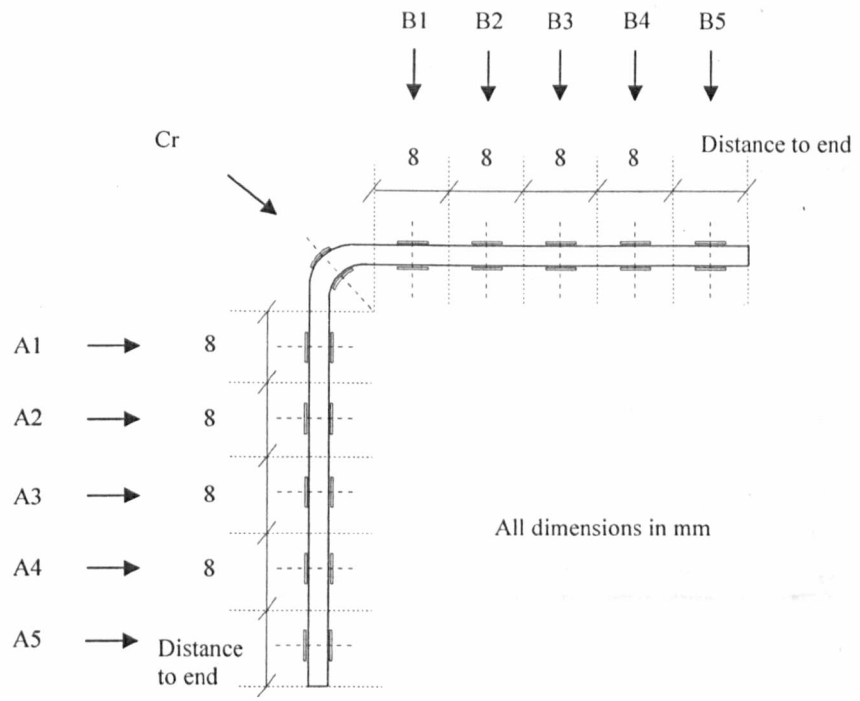

Figure A.6: *Setting out of press braked section PB 50×50×4 (r_i=3.5)*

Table A.18: *Residual stress distribution for PB 50×50×4 (r_i=3.5)*

PB 50×50×4 (r_i=3.5)	*Section position (mm)*	*Width (mm)*	σ_m *(N/mm²)*	σ_b *(N/mm²)*	σ_{rc} *(N/mm²)*	$\sigma_m/\sigma_{0.2}$	$\sigma_b/\sigma_{0.2}$	$\sigma_{rc}/\sigma_{0.2}$
A5	42.8	9.92	17	29	46	0.05	0.09	0.14
A4	32.9	6.89	5	9	14	0.01	0.02	0.04
A3	25.1	6.32	-5	-7	12	-0.01	-0.02	0.03
A2	17.4	6.70	-12	5	17	-0.04	0.02	0.06
A1	8.8	7.96	-7	-48	55	-	-	-
Cr (r_i=3.4)	0.0		65	-135	200	0.14	-0.28	0.42
B1	8.5	7.22	-73	-40	112	-0.19	-0.10	0.29
B2	16.4	6.28	1	-14	16	0.00	-0.05	0.05
B3	24.1	6.64	5	42	47	0.02	0.14	0.15
B4	32.1	7.10	3	22	25	0.01	0.07	0.08
B5	42.4	10.38	14	-3	17	0.05	-0.01	0.07

Table A.19: *Material properties distribution for PB 50×50×4 (r_i=3.5)*

PB 50×50×4 (r_i=3.5)	*Section position (mm)*	*Width (mm)*	*E (N/mm^2)*	*$\sigma_{0.01,exp}$ (N/mm^2)*	*$\sigma_{0.2,exp}$ (N/mm^2)*	*$\sigma_{1.0,exp}$ (N/mm^2)*	*$\sigma_{ult,exp}$ (N/mm^2)*	*$\varepsilon_{f,exp}$*
A5	42.8	9.92	198400	124	323	392	630	0.65
A4	32.9	6.89	190900	273	389	426	689	0.70
A3	25.1	6.32	208800	216	383	445	700	0.65
A2	17.4	6.70	189600	187	288	351	610	0.67
A1	8.8	7.96	-	-	-	-	-	-
Cr (r_i=3.4)	0.0		193400	132	479	588	657	0.50
B1	8.5	7.22	197200	238	392	467	687	0.64
B2	16.4	6.28	192000	165	310	383	634	0.59
B3	24.1	6.64	202600	148	311	380	624	0.72
B4	32.1	7.10	180100	179	294	354	610	0.70
B5	42.4	10.38	180300	165	264	308	593	0.67

Table A.20: *Proof stress ratios and Ramberg-Osgood strain parameters for PB 50×50×4 (r_i=3.5)*

PB 50×50×4 (r_i=3.5)	*Section position (mm)*	*Width (mm)*	*$\sigma_{0.2,exp}$/ $\sigma_{0.2,mill}$*	*$\sigma_{0.2,exp}$/ $\sigma_{0.2,min}$*	*$n_{0.01}$*	*$n_{0.05}$*	*$n_{0.1}$*	*$n_{bestfit}$*	*n'*	*$n'_{bestfit}$*
A5	42.8	9.92	1.02	1.54	3.1	5.2	7.2	5.6	3.4	3.4
A4	32.9	6.89	1.23	1.85	8.5	38.4	31.9	31.9	4.4	4.4
A3	25.1	6.32	1.21	1.82	5.2	5.8	6.9	7.1	2.3	2.3
A2	17.4	6.70	0.91	1.37	6.9	7.0	6.7	7.0	2.5	2.5
A1	8.8	7.96	-	-	-	-	-	-	-	-
Cr (r_i=3.4)	0.0		1.51	2.28	2.3	3.5	4.3	3.8	3.6	3.7
B1	8.5	7.22	1.24	1.87	6.0	6.5	7.0	7.2	2.9	2.9
B2	16.4	6.28	0.98	1.47	4.8	5.2	6.0	6.2	2.8	2.8
B3	24.1	6.64	0.98	1.48	4.0	5.2	4.5	5.2	2.5	2.5
B4	32.1	7.10	0.93	1.40	6.1	7.0	8.0	7.2	2.4	2.5
B5	42.4	10.38	0.83	1.26	6.3	9.4	10.2	10.3	2.0	2.0

Table A.21: *Hardness values HV and predicted 0.2% proof stress* $\overline{\sigma}_{0.2,exp}$ *for PB 50×50×4* (r_i=3.5)

PB 50×50×4 (r_i=3.5)	*Section position (mm)*	*HV*	$\overline{\sigma}_{0.2,exp}$ *(N/mm²)*
A5	0.85	202	408
A4	0.68	180	364
A3	0.51	204	412
A2	0.34	234	473
	0.31	213	430
	0.28	204	412
A1	0.25	202	408
	0.22	214	432
	0.19	205	414
	0.16	215	434
	0.13	216	436
	0.09	212	428
Cr	0.06	239	483
	0.03	235	475
	0.00	259	523
	0.03	247	499
	0.06	244	493
B1	0.10	215	434
	0.13	226	457
	0.16	212	428
	0.19	224	452
	0.23	200	404
	0.26	214	432
B2	0.29	217	438
	0.32	211	426
	0.36	206	416
B3	0.53	208	420
B4	0.70	191	386
B5	0.87	168	339

A.7 PB 50×50×5 (r_i=3.5)

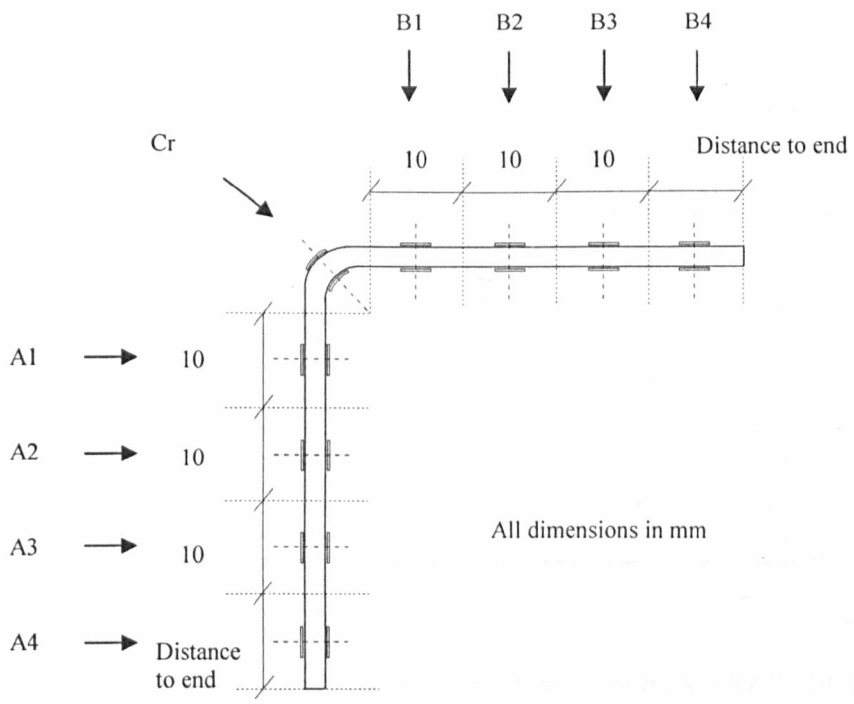

Figure A.7: *Setting out of press braked section PB 50×50×5 (r_i=3.5)*

Table A.22: *Residual stress distribution for PB 50×50×5 (r_i=3.5)*

PB 50×50×5 (r_i=3.5)	*Section position (mm)*	*Width (mm)*	σ_m *(N/mm²)*	σ_b *(N/mm²)*	σ_{rc} *(N/mm²)*	$\sigma_m/\sigma_{0.2}$	$\sigma_b/\sigma_{0.2}$	$\sigma_{rc}/\sigma_{0.2}$
A4	40.6	8.95	5	15	20	0.01	0.04	0.05
A3	30.1	9.05	-	-	-	-	-	-
A2	19.9	8.98	-8	-16	24	-0.03	-0.06	0.08
A1	9.6	9.18	-4	-42	46	-0.01	-0.12	0.14
Cr (r_i=3.2)	0.0		2	-183	185	0.00	-0.37	0.37
B1	9.4	8.79	-16	-20	36	-0.05	-0.07	0.12
B2	19.3	8.55	-13	0	14	-0.05	0.00	0.05
B3	29.1	8.74	-3	8	11	-0.01	0.03	0.04
B4	39.9	12.22	8	24	33	0.03	0.08	0.10

Table A.23: *Material properties distribution for PB 50×50×5 (r_i=3.5)*

PB 50×50×5 (r_i=3.5)	*Section position (mm)*	*Width (mm)*	*E (N/mm^2)*	*$\sigma_{0.01,exp}$ (N/mm^2)*	*$\sigma_{0.2,exp}$ (N/mm^2)*	*$\sigma_{1.0,exp}$ (N/mm^2)*	*$\sigma_{ult,exp}$ (N/mm^2)*	*$\varepsilon_{f,exp}$*
A4	40.6	8.95	204500	226	434	495	713	0.71
A3	30.1	9.05	185400	181	299	350	631	0.76
A2	19.9	8.98	199400	144	286	341	626	0.76
A1	9.6	9.18	188300	174	336	405	638	0.70
Cr (r_i=3.2)	0.0		199800	118	497	621	695	0.44
B1	9.4	8.79	191000	162	302	358	621	0.74
B2	19.3	8.55	210200	171	281	333	626	0.73
B3	29.1	8.74	185800	130	260	312	576	0.74
B4	39.9	12.22	191400	156	311	373	641	0.69

Table A.24: *Proof stress ratios and Ramberg-Osgood strain parameters for PB 50×50×5 (r_i=3.5)*

PB 50×50×5 (r_i=3.5)	*Section position (mm)*	*Width (mm)*	*$\sigma_{0.2,exp}/\sigma_{0.2,mill}$*	*$\sigma_{0.2,exp}/\sigma_{0.2,min}$*	*$n_{0.01}$*	*$n_{0.05}$*	*$n_{0.1}$*	*$n_{bestfit}$*	*n'*	*$n'_{bestfit}$*
A4	40.6	8.95	1.39	2.07	4.6	5.7	6.9	6.1	3.4	3.4
A3	30.1	9.05	0.96	1.42	6.0	6.5	7.3	7.3	2.5	2.6
A2	19.9	8.98	0.92	1.36	4.3	5.5	6.8	6.0	2.7	2.7
A1	9.6	9.18	1.08	1.60	4.6	5.0	5.7	5.2	2.9	2.9
Cr (r_i=3.2)	0.0		1.60	2.37	2.1	3.2	3.8	3.3	3.9	3.9
B1	9.4	8.79	0.97	1.44	4.8	5.6	6.2	5.7	2.4	2.4
B2	19.3	8.55	0.90	1.34	6.0	6.9	8.2	7.6	2.4	2.4
B3	29.1	8.74	0.84	1.24	4.3	5.6	6.6	6.6	2.6	2.6
B4	39.9	12.22	1.00	1.48	4.3	5.1	5.5	5.2	2.6	2.6

Table A.25: *Hardness values HV and predicted 0.2% proof stress* $\overline{\sigma}_{0.2,exp}$ *for PB 50×50×5* (r_i=3.5)

PB 50×50×5 (r_i=3.5)	*Section position (mm)*	*HV*	$\overline{\sigma}_{0.2,exp}$ *(N/mm²)*
A4	0.89	216	437
A3	0.67	197	397
A2	0.44	182	368
	0.41	185	373
	0.37	191	386
	0.34	182	368
A1	0.31	191	386
	0.27	198	400
	0.24	190	384
	0.20	192	387
	0.17	197	399
	0.14	197	399
Cr	0.10	197	397
	0.07	235	474
	0.03	254	512
	0.00	272	549
	0.03	248	501
	0.06	240	485
	0.09	206	417
B1	0.13	204	411
	0.16	192	387
	0.19	189	381
	0.22	194	392
	0.25	196	396
	0.28	207	418
B2	0.32	205	414
	0.35	202	408
	0.38	200	404
B3	0.62	217	438
B4	0.83	210	423

A.8 PB 50×50×5 (r_i=4.5)

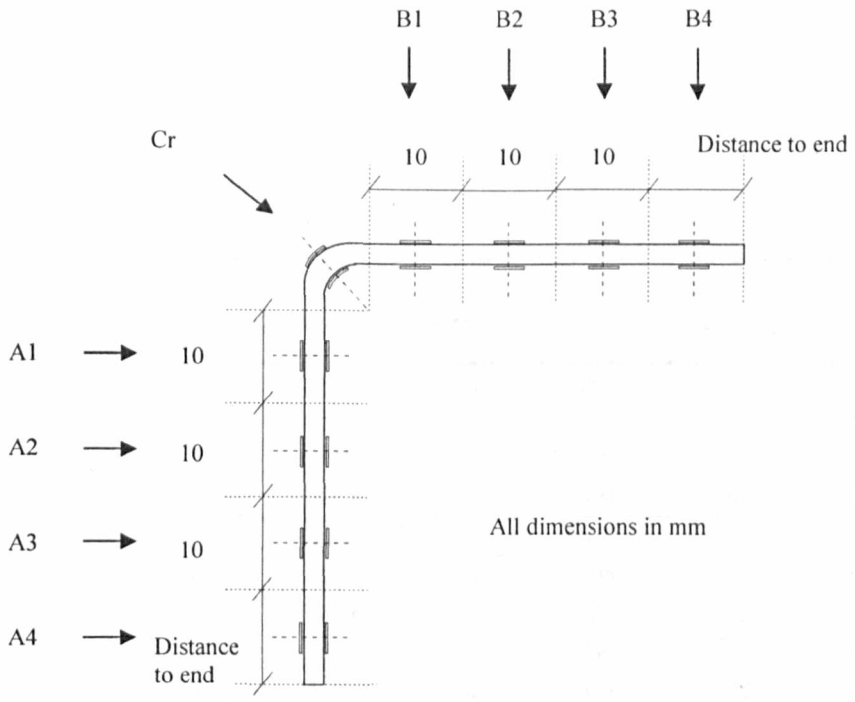

Figure A.8: *Setting out of press braked section PB 50×50×5 (r_i=4.5)*

Table A.26: *Residual stress distribution for PB 50×50×5 (r_i=4.5)*

PB 50×50×5 (r_i=4.5)	*Section position (mm)*	*Width (mm)*	σ_m *(N/mm²)*	σ_b *(N/mm²)*	σ_{rc} *(N/mm²)*	$\sigma_m/\sigma_{0.2}$	$\sigma_b/\sigma_{0.2}$	$\sigma_{rc}/\sigma_{0.2}$
A4	40.7	9.86	49	27	76	0.17	0.09	0.26
A3	29.9	8.69	-13	12	24	-0.04	0.04	0.08
A2	20.1	8.53	-27	10	37	-0.09	0.03	0.13
A1	10.3	8.68	-214	-143	357	-0.69	-0.47	1.16
Cr (r_i=4.3)	0.0		13	-159	172	0.02	-0.25	0.27
B1	10.4	8.91	-5	-19	24	-0.02	-0.06	0.08
B2	20.4	8.76	3	11	13	0.01	0.04	0.05
B3	30.3	8.69	25	8	33	0.08	0.03	0.11
B4	39.3	8.70	26	-23	49	0.07	-0.06	0.14

Table A.27: *Material properties distribution for PB 50×50×5 (r_i=4.5)*

PB 50×50×5 (r_i=4.5)	*Section position (mm)*	*Width (mm)*	*E (N/mm^2)*	*$\sigma_{0.01,exp}$ (N/mm^2)*	*$\sigma_{0.2,exp}$ (N/mm^2)*	*$\sigma_{1.0,exp}$ (N/mm^2)*	*$\sigma_{ult,exp}$ (N/mm^2)*	*$\varepsilon_{f,exp}$*
A4	40.7	9.86	180900	141	290	352	587	0.68
A3	29.9	8.69	193300	160	291	348	648	0.76
A2	20.1	8.53	199900	181	289	345	654	0.75
A1	10.3	8.68	184100	171	308	362	643	0.75
Cr (r_i=4.3 mm)	0.0		205900	274	632	745	814	0.44
B1	10.4	8.91	193100	141	306	369	633	0.71
B2	20.4	8.76	187600	154	280	336	635	0.78
B3	30.3	8.69	192200	162	290	347	633	0.73
B4	39.3	8.70	217000	162	357	438	705	0.68

Table A.28: *Proof stress ratios and Ramberg-Osgood strain parameters for PB 50×50×5 (r_i=4.5)*

PB 50×50×5 (r_i=4.5)	*Section position (mm)*	*Width (mm)*	*$\sigma_{0.2,exp}/\sigma_{0.2,mill}$*	*$\sigma_{0.2,exp}/\sigma_{0.2,min}$*	*$n_{0.01}$*	*$n_{0.05}$*	*$n_{0.1}$*	*$n_{bestfit}$*	*n'*	*$n'_{bestfit}$*
A4	40.7	9.86	0.93	1.38	4.2	4.8	5.5	5.0	2.7	2.7
A3	29.9	8.69	0.94	1.39	5.0	6.5	7.0	6.6	2.5	2.5
A2	20.1	8.53	0.93	1.38	6.4	6.6	7.6	7.7	2.5	2.5
A1	10.3	8.68	0.99	1.47	5.1	5.9	6.5	5.8	2.4	2.4
Cr (r_i=4.3 mm)	0.0		2.03	3.01	3.6	4.5	5.4	5.4	3.1	3.1
B1	10.4	8.91	0.99	1.46	3.8	5.1	5.5	5.1	2.8	2.8
B2	20.4	8.76	0.90	1.33	5.0	6.2	7.4	7.4	2.8	2.8
B3	30.3	8.69	0.93	1.38	5.1	5.9	6.6	6.2	2.4	2.4
B4	39.3	8.70	1.15	1.70	3.8	4.4	4.8	4.8	3.0	3.1

A.9 CR 100×50×2

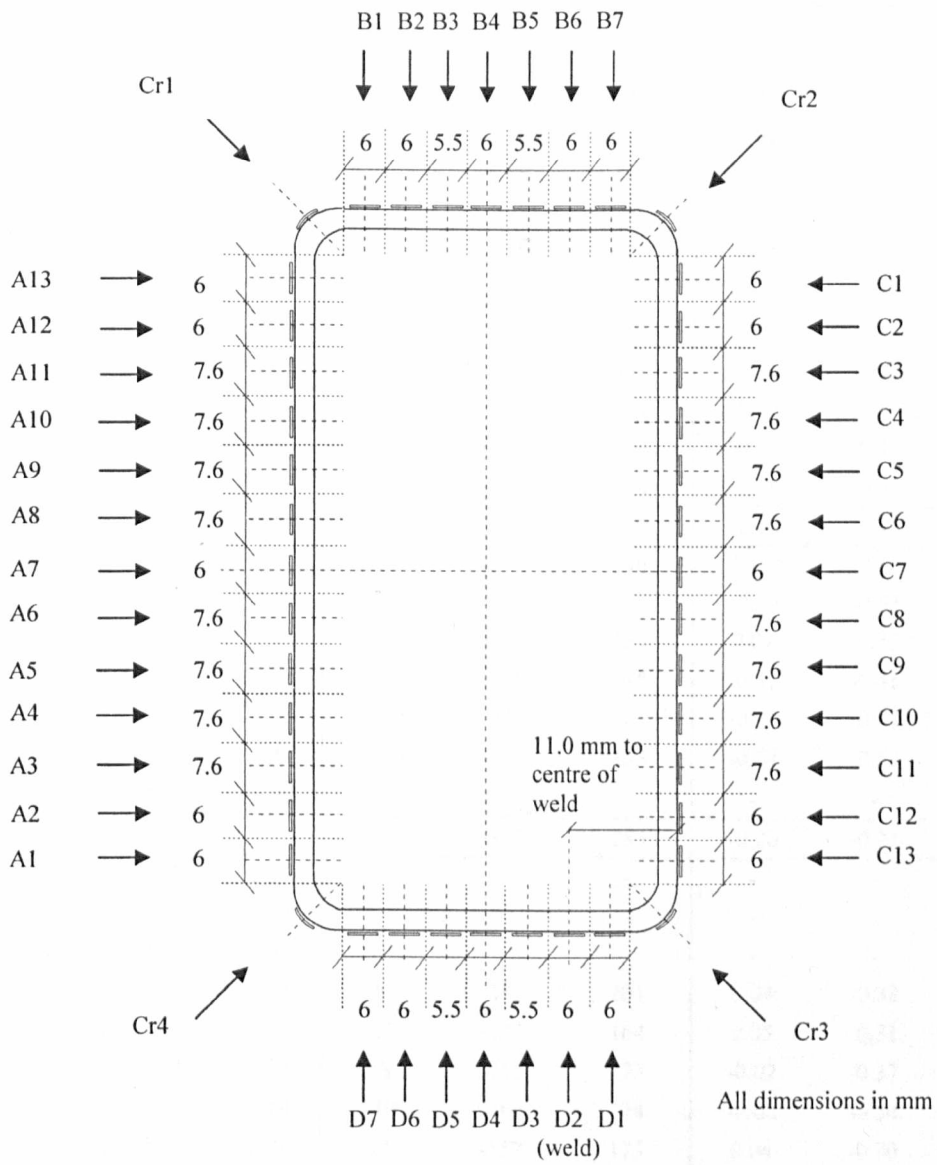

Figure A.9: *Setting out of cold rolled section CR 100×50×2*

Table A.29: *Residual stress distribution for CR 100×50×2*

CR 100×50×2	*Section position (mm)*	*Width (mm)*	σ_m *(N/mm²)*	σ_b *(N/mm²)*	σ_{rc} *(N/mm²)*	$\sigma_m/\sigma_{0.2}$	$\sigma_b/\sigma_{0.2}$	$\sigma_{rc}/\sigma_{0.2}$
A1	5.7	4.77	-82	-295	377	-0.20	-0.74	0.94
A2	11.9	5.10	-23	-187	210	-0.06	-0.49	0.55
A3	18.9	6.63	8	-211	218	0.02	-0.57	0.59
A4	26.7	6.44	5	-214	219	0.01	-0.61	0.63
A5	34.3	6.40	-9	-186	195	-0.02	-0.43	0.45
A6	41.9	6.39	-15	-185	200	-0.04	-0.45	0.49
A7	48.8	5.15	-270	-140	410	-0.57	-0.29	0.86
A8	55.8	6.42	-67	-152	219	-0.16	-0.36	0.51
A9	63.4	6.34	17	-165	182	0.04	-0.37	0.41
A10	71.0	6.35	-7	-195	202	-0.02	-0.44	0.45
A11	78.4	6.09	-27	-231	257	-0.06	-0.51	0.57
A12	85.0	4.75	-63	-261	324	-0.13	-0.54	0.67
A13	91.0	4.75	-102	-346	448	-0.18	-0.62	0.81
Cr1 (r_i=2.6)	0.0		-373	-305	678	-0.56	-0.45	1.01
B1	6.1	5.41	2	-294	296	0.00	-0.58	0.58
B2	12.5	4.86	-148	-258	406	-0.30	-0.52	0.81
B3	18.3	4.29	20	-217	237	0.04	-0.45	0.49
B4	24.0	4.78	-149	-199	348	-0.31	-0.41	0.72
B5	29.9	4.59	-190	-211	401	-0.40	-0.44	0.84
B6	35.5	4.30	-166	-286	453	-0.34	-0.58	0.91
B7	41.4	5.07	-	-	-	-	-	-
Cr2 (r_i=2.0)	0.0		-130	-155	285	-0.20	-0.24	0.45
C1	5.5	5.18	-	-	-	-	-	-
C2	12.0	5.24	-	-	-	-	-	-
C3	18.6	5.67	-	-	-	-	-	-
C4	25.5	5.78	20	-181	201	0.04	-0.38	0.42
C5	32.7	6.17	22	-143	164	0.05	-0.31	0.36
C6	40.1	6.31	-8	-165	173	-0.02	-0.37	0.39
C7	47.3	5.64	-10	-164	174	-0.02	-0.34	0.36
C8	54.0	5.30	21	-152	173	0.04	-0.30	0.34
C9	61.3	6.84	14	-188	203	0.03	-0.38	0.41
C10	69.1	6.44	33	-231	264	0.07	-0.46	0.52
C11	76.7	6.40	5	-228	232	0.01	-0.46	0.46
C12	83.7	5.22	-37	-287	325	-0.06	-0.45	0.51
C13	89.8	4.55	5	-386	391	0.01	-0.65	0.65
Cr3 (r_i=2.5)	0.0		-250	-213	463	-0.42	-0.36	0.78

Table A.29 (continued): *Residual stress distribution for CR 100×50×2*

CR 100×50×2	*Section position (mm)*	*Width (mm)*	σ_m *(N/mm²)*	σ_b *(N/mm²)*	σ_{rc} *(N/mm²)*	$\sigma_m/\sigma_{0.2}$	$\sigma_b/\sigma_{0.2}$	$\sigma_{rc}/\sigma_{0.2}$
D1	4.7	2.67	-	-	-	-	-	-
D2(weld)	9.7	5.01	-157	-297	454	-0.27	-0.51	0.78
D3	16.1	5.29	-197	-292	489	-0.39	-0.57	0.96
D4	23.0	6.18	-97	-210	307	-0.20	-0.42	0.62
D5	29.5	4.36	-153	-230	383	-0.32	-0.48	0.79
D6	35.2	4.69	-184	-245	429	-0.38	-0.51	0.89
D7	41.1	4.68	-385	-217	602	-0.65	-0.36	1.01
Cr4 (r_i=2.5)	0.0			-113			-0.20	

Table A.30: *Material properties distribution for CR 100×50×2*

CR 100×50×2	*Section position (mm)*	*Width (mm)*	*E* (N/mm^2)	$\sigma_{0.01,exp}$ (N/mm^2)	$\sigma_{0.2,exp}$ (N/mm^2)	$\sigma_{1.0,exp}$ (N/mm^2)	$\sigma_{ult,exp}$ (N/mm^2)	$\varepsilon_{f,exp}$
A1	5.7	4.77	187100	104	401	515	624	0.47
A2	11.9	5.10	194200	109	383	478	629	0.58
A3	18.9	6.63	190700	125	370	454	652	0.61
A4	26.7	6.44	207200	86	349	410	609	0.63
A5	34.3	6.40	205800	179	433	503	758	0.64
A6	41.9	6.39	194900	208	409	477	728	0.64
A7	48.8	5.15	208200	36	474	535	769	0.55
A8	55.8	6.42	181000	186	427	500	747	0.64
A9	63.4	6.34	191300	217	443	503	695	0.64
A10	71.0	6.35	196400	165	448	523	740	0.67
A11	78.4	6.09	192900	135	450	547	740	0.51
A12	85.0	4.75	181600	117	486	598	801	0.51
A13	91.0	4.75	200400	149	556	663	807	0.45
Cr1 (r_i=2.6)	0.0		188400	23	669	792	862	0.41
B1	6.1	5.41	196000	156	510	621	765	0.49
B2	12.5	4.86	201200	171	499	604	812	0.53
B3	18.3	4.29	204000	237	479	575	812	0.66
B4	24.0	4.78	204000	203	481	572	803	0.66
B5	29.9	4.59	217000	195	475	570	803	0.59
B6	35.5	4.30	195000	204	496	572	769	0.45
B7	41.4	5.07	208000	256	576	667	809	0.48
Cr2 (r_i=2.0)	0.0		195600	219	635	770	843	0.41
C1	5.5	5.18	213600	161	585	706	826	0.48
C2	12.0	5.24	199300	200	500	585	745	0.52
C3	18.6	5.67	212100	152	477	547	763	0.57
C4	25.5	5.78	206300	249	477	561	785	0.51
C5	32.7	6.17	207900	173	457	530	751	0.56
C6	40.1	6.31	211200	168	439	520	763	0.55
C7	47.3	5.64	215500	254	486	572	797	0.48
C8	54.0	5.30	210700	214	504	577	794	0.55
C9	61.3	6.84	207300	210	497	575	788	0.69
C10	69.1	6.44	215700	262	507	577	793	0.76
C11	76.7	6.40	212500	145	500	592	796	0.79
C12	83.7	5.22	209300	217	633	634	789	0.53
C13	89.8	4.55	215292	164	599	766	862	0.46
Cr3 (r_i=2.5)	0.0		187200	38	594	700	764	0.43

Table A.30 (continued): *Material properties distribution for CR 100×50×2*

CR 100×50×2	*Section position (mm)*	*Width (mm)*	*E* (N/mm^2)	$\sigma_{0.01,exp}$ (N/mm^2)	$\sigma_{0.2,exp}$ (N/mm^2)	$\sigma_{1.0,exp}$ (N/mm^2)	$\sigma_{ult,exp}$ (N/mm^2)	$\varepsilon_{f,exp}$
D1	4.7	2.67	203700	224	583	700	839	0.45
D2(weld)	9.7	5.01	198600	224	580	654	809	0.51
D3	16.1	5.29	193600	171	510	600	794	0.54
D4	23.0	6.18	212500	184	495	577	796	0.58
D5	29.5	4.36	213000	184	482	568	778	0.52
D6	35.2	4.69	203100	233	481	571	767	0.48
D7	41.1	4.68	204100	335	594	685	857	0.53
Cr4 (r_i=2.5)	0.0		202605	151	562	675	741	0.42

Table A.31: *Proof stress ratios and Ramberg-Osgood strain parameters for CR 100×50×2*

CR 100×50×2	*Section position (mm)*	*Width (mm)*	$\sigma_{0.2,exp}/\sigma_{0.2,mill}$	$\sigma_{0.2,exp}/\sigma_{0.2,min}$	$n_{0.01}$	$n_{0.05}$	$n_{0.1}$	$n_{bestfit}$	n'	$n'_{bestfit}$
A1	5.7	4.77	0.83	1.74	2.2	2.7	3.5	3.1	3.3	3.3
A2	11.9	5.10	0.79	1.66	2.4	3.1	3.2	3.3	3.4	3.4
A3	18.9	6.63	0.76	1.61	2.8	4.2	5.3	4.4	5.2	5.2
A4	26.7	6.44	0.72	1.52	2.1	3.1	3.4	3.1	2.8	2.8
A5	34.3	6.40	0.89	1.88	3.4	4.4	4.8	5.1	2.9	2.9
A6	41.9	6.39	0.84	1.78	4.4	4.4	5.0	5.0	3.4	3.4
A7	48.8	5.15	0.98	2.06	1.2	5.1	4.8	5.2	2.7	2.7
A8	55.8	6.42	0.88	1.85	3.6	6.4	6.6	6.7	8.3	8.2
A9	63.4	6.34	0.91	1.93	4.2	4.5	5.4	5.5	2.9	2.9
A10	71.0	6.35	0.92	1.95	3.0	4.6	6.6	6.6	5.0	5.0
A11	78.4	6.09	0.93	1.95	2.5	3.0	3.6	4.2	5.0	5.0
A12	85.0	4.75	1.00	2.11	2.1	3.5	5.1	3.8	3.9	3.9
A13	91.0	4.75	1.15	2.42	2.3	3.0	4.0	4.0	4.3	4.3
Cr1 (r_i=2.6)	0.0		1.38	2.91	0.9	4.5	4.0	4.8	3.6	3.6
B1	6.1	5.41	1.05	2.22	2.5	3.2	3.3	3.6	5.3	5.3
B2	12.5	4.86	1.03	2.17	2.8	3.4	7.0	5.4	5.4	5.5
B3	18.3	4.29	0.99	2.08	4.3	4.4	6.0	6.4	5.5	5.5
B4	24.0	4.78	0.99	2.09	3.5	4.8	5.3	4.9	2.7	2.7
B5	29.9	4.59	0.98	2.07	3.4	5.1	5.5	5.5	4.3	4.3
B6	35.5	4.30	1.02	2.16	3.4	4.4	5.2	5.2	5.4	5.3
B7	41.4	5.07	1.19	2.50	3.7	4.9	6.0	6.4	4.2	4.2
Cr2 (r_i=2.0)	0.0		1.31	2.76	2.8	4.1	5.8	5.8	5.6	5.6
C1	5.5	5.18	1.21	2.54	2.3	3.9	2.7	3.9	4.0	4.0
C2	12.0	5.24	1.03	2.18	3.3	3.3	6.2	6.2	3.8	3.8
C3	18.6	5.67	0.98	2.08	2.6	3.4	4.4	5.0	3.2	3.2
C4	25.5	5.78	0.98	2.07	4.6	4.6	5.1	6.4	3.6	3.6
C5	32.7	6.17	0.94	1.99	3.1	4.6	5.5	5.6	3.2	3.2
C6	40.1	6.31	0.91	1.91	3.1	4.4	6.0	5.0	2.9	2.9
C7	47.3	5.64	1.00	2.11	4.6	5.4	5.7	6.4	3.9	3.9
C8	54.0	5.30	1.04	2.19	3.5	4.7	5.7	5.7	4.4	4.4
C9	61.3	6.84	1.02	2.16	3.5	6.2	4.7	6.3	4.8	4.8
C10	69.1	6.44	1.05	2.20	4.5	5.0	5.3	7.4	4.2	4.2
C11	76.7	6.40	1.03	2.17	2.4	4.1	6.0	6.0	3.9	3.9
C12	83.7	5.22	1.30	2.75	2.8	5.8	8.6	8.8	-	-
C13	89.8	4.55	1.23	2.60	2.3	2.7	3.9	3.9	6.5	6.5
Cr3 (r_i=2.5)	0.0		1.23	2.58	1.1	4.6	4.7	5.0	4.0	4.0

Table A.31: *Proof stress ratios and Ramberg-Osgood strain parameters for CR 100×50×2*

CR 100×50×2	*Section position (mm)*	*Width (mm)*	$\sigma_{0.2,exp}/\sigma_{0.2,mill}$	$\sigma_{0.2,exp}/\sigma_{0.2,min}$	$n_{0.01}$	$n_{0.05}$	$n_{0.1}$	$n_{bestfit}$	n'	$n'_{bestfit}$
D1	4.7	2.67	1.20	2.53	3.1	3.4	4.0	3.6	3.8	3.8
D2(weld)	9.7	5.01	1.20	2.52	3.2	3.8	4.4	4.4	4.8	4.8
D3	16.1	5.29	1.05	2.22	2.7	4.3	6.4	6.5	5.0	5.0
D4	23.0	6.18	1.02	2.15	3.0	4.2	5.6	4.8	3.3	3.3
D5	29.5	4.36	0.99	2.09	3.1	4.1	4.8	5.2	3.7	3.7
D6	35.2	4.69	0.99	2.09	4.1	4.9	6.5	5.5	2.8	2.8
D7	41.1	4.68	1.22	2.58	5.2	6.4	7.7	7.7	3.9	4.0
Cr4 (r_i=2.5)	0.0		1.16	2.44	2.3	4.3	4.4	5.1	4.8	4.8

Table A.32: *Hardness values HV and predicted 0.2% proof stress $\overline{\sigma}_{0.2,exp}$ for CR 100×50×2 Face A*

CR 100×50×2	*Section position (mm)*	*HV*	$\overline{\sigma}_{0.2,exp}$ *(N/mm²)*
Cr4	0.00	253	510
	0.02	268	541
A1	0.03	280	566
	0.05	263	531
	0.06	247	499
	0.08	239	484
A2	0.09	239	482
	0.12	245	496
A3	0.19	213	429
A4	0.27	217	438
A5	0.35	219	442
A6	0.43	218	441
A7	0.50	226	456
A8	0.57	213	431
A9	0.65	222	448
A10	0.73	221	445
A11	0.81	231	467
A12	0.88	235	475
	0.91	243	490
A13	0.92	242	489
	0.94	253	510
	0.95	254	514
	0.97	284	574
Cr1	0.98	274	553
	1.00	259	523

Table A.33: *Hardness values HV and predicted 0.2% proof stress* $\bar{\sigma}_{0.2,exp}$ *for CR 100×50×2 Face B*

CR 100×50×2	*Section position (mm)*	*HV*	$\bar{\sigma}_{0.2,exp}$ *(N/mm²)*
Cr1	0.00	259	523
	0.03	256	518
B1	0.07	305	616
	0.10	272	549
	0.13	258	521
	0.16	258	521
B2	0.20	247	499
B3	0.26	263	531
B4	0.39	265	535
B5	0.51	279	564
	0.49	262	529
B6	0.61	269	543
	0.74	260	525
	0.80	251	507
B7	0.84	275	556
	0.87	281	568
	0.90	320	646
	0.93	349	705
Cr2	0.97	291	588
	1.00	292	590

Table A.34: *Hardness values HV and predicted 0.2% proof stress* $\overline{\sigma}_{0.2,exp}$ *for CR 100×50×2 Face C*

CR 100×50×2	*Section position (mm)*	*HV*	$\overline{\sigma}_{0.2,exp}$ *(N/mm²)*
Cr2	0.00	292	590
	0.02	301	608
C1	0.03	270	545
	0.05	260	525
	0.06	234	473
	0.08	253	511
	0.09	229	463
C2	0.12	232	469
C3	0.19	229	463
C4	0.27	221	446
C5	0.35	223	450
C6	0.43	220	444
C7	0.50	225	455
	0.50	238	480
C8	0.57	243	491
C9	0.65	242	489
C10	0.73	240	485
C11	0.81	241	487
C12	0.88	245	494
C13	0.91	255	516
	0.92	264	533
	0.94	254	512
	0.95	265	535
Cr3	0.97	310	626
	0.98	264	533
	1.00	244	492

Table A.35: *Hardness values HV and predicted 0.2% proof stress* $\overline{\sigma}_{0.2,exp}$ *for CR 100×50×2 Face D*

CR 100×50×2	*Section position (mm)*	*HV*	$\overline{\sigma}_{0.2,exp}$ *(N/mm²)*
Cr3	0.00	264	533
	0.03	244	492
	0.06	257	520
D1	0.10	281	568
	0.13	274	553
D2	0.16	289	583
	0.19	273	551
	0.23	263	531
D3	0.29	246	498
	0.41	267	539
D4	0.54	247	499
	0.50	253	510
	0.53	271	547
	0.56	318	641
D5	0.59	290	586
	0.62	266	537
	0.66	249	503
	0.69	256	518
D6	0.75	257	520
D7	0.88	252	508
Cr4	1.00	256	518

A.10 CR 100×100×2

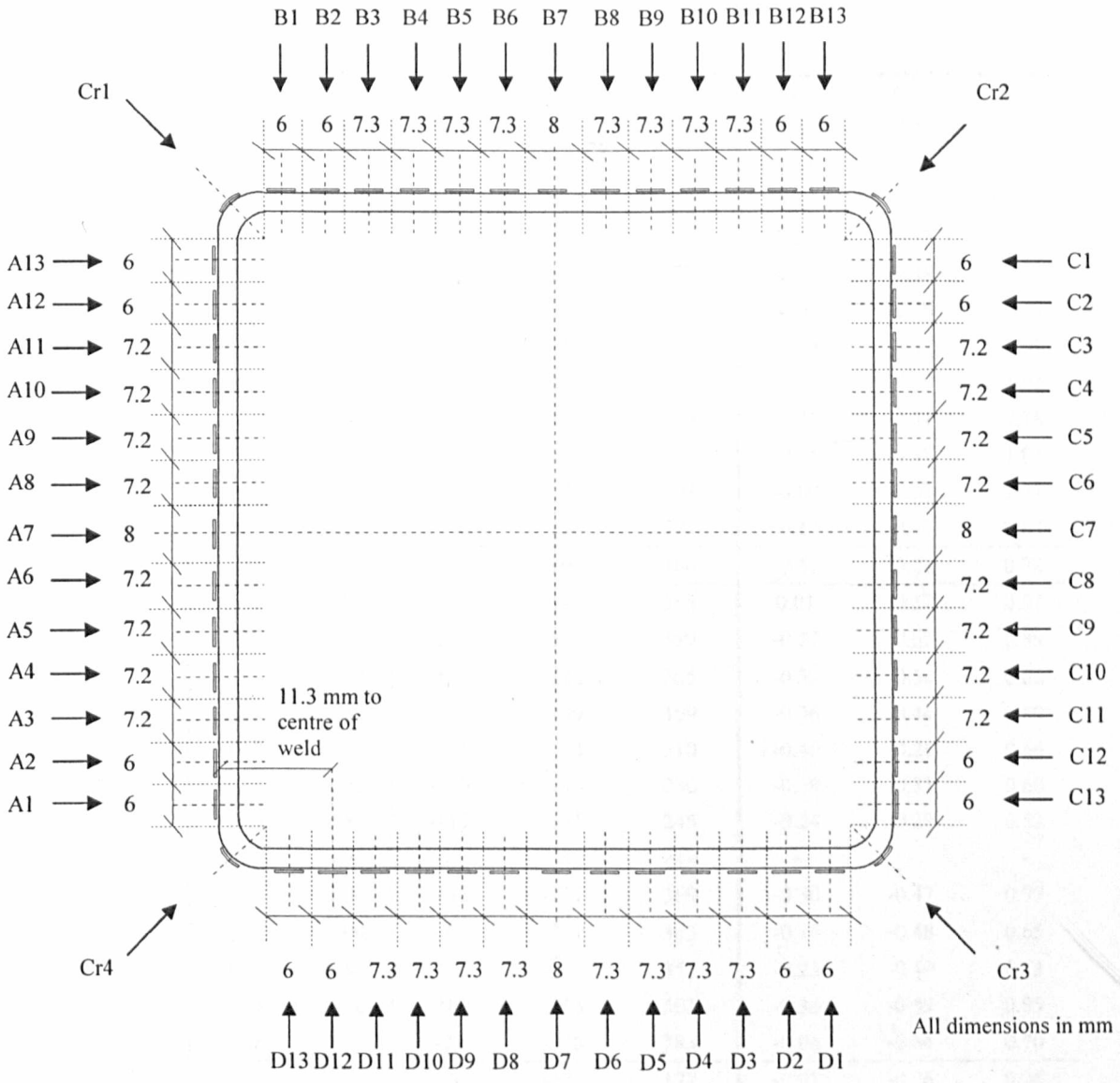

Figure A.10: *Setting out of cold rolled section CR 100×100×2*

Table A.36: *Residual stress distribution for CR 100×100×2*

CR 100×100×2	*Section position (mm)*	*Width (mm)*	σ_m *(N/mm²)*	σ_b *(N/mm²)*	σ_{rc} *(N/mm²)*	$\sigma_m/\sigma_{0.2}$	$\sigma_b/\sigma_{0.2}$	$\sigma_{rc}/\sigma_{0.2}$
A1	6.9	5.11	-	-341	-	-	-0.66	-
A2	13.6	6.00	124	-256	379	0.27	-0.57	0.84
A3	21.0	6.39	120	-230	350	0.27	-0.52	0.80
A4	28.2	5.58	39	-173	212	0.10	-0.43	0.52
A5	35.1	5.75	233	-151	385	0.55	-0.35	0.90
A6	42.1	5.87	151	-164	315	0.35	-0.38	0.73
A7	49.6	6.79	-18	-226	244	-0.04	-0.45	0.49
A8	57.2	5.93	-282	-165	447	-0.64	-0.37	1.01
A9	64.2	5.81	-298	-181	478	-0.64	-0.39	1.03
A10	72.0	7.24	-223	-149	372	-0.47	-0.31	0.78
A11	79.7	5.80	-273	-237	511	-0.55	-0.48	1.03
A12	86.2	4.79	-385	-278	663	-0.80	-0.58	1.37
A13	92.1	4.60	-99	-278	377	-0.17	-0.46	0.63
Cr1 (r_i=2.8)	0.0		-258	-109	366	-0.51	-0.21	0.72
B1	5.5	3.89	3	-312	315	0.01	-0.57	0.57
B2	11.0	4.80	-121	-278	399	-0.27	-0.62	0.89
B3	17.4	5.59	-143	-223	365	-0.32	-0.50	0.82
B4	24.3	5.78	-159	-199	359	-0.36	-0.44	0.80
B5	31.7	6.56	-186	-124	310	-0.40	-0.26	0.66
B6	39.2	6.20	-140	-146	286	-0.29	-0.31	0.60
B7	46.9	6.80	-110	-135	245	-0.24	-0.29	0.53
B8	54.5	5.96	-75	-140	214	-	-	-
B9	61.7	5.96	-142	-227	369	-0.30	-0.47	0.77
B10	68.9	6.00	-77	-227	303	-0.16	-0.48	0.65
B11	76.0	5.80	-112	-238	350	-0.23	-0.49	0.73
B12	82.5	4.78	-189	-314	503	-0.36	-0.59	0.95
B13	88.8	5.43	-35	-348	383	-0.06	-0.64	0.70
Cr2 (r_i=3.0)	0.0		-6	-172	177	-0.01	-0.26	0.26

Table A.36 (continued): *Residual stress distribution for CR 100×100×2*

CR 100×100×2	*Section position (mm)*	*Width (mm)*	σ_m *(N/mm²)*	σ_b *(N/mm²)*	σ_{rc} *(N/mm²)*	$\sigma_m/\sigma_{0.2}$	$\sigma_b/\sigma_{0.2}$	$\sigma_{rc}/\sigma_{0.2}$
C1	6.3	5.15	-82	-321	404	-0.15	-0.60	0.75
C2	12.7	5.27	-255	-249	504	-0.55	-0.54	1.09
C3	19.7	6.40	-466	-141	607	-0.98	-0.30	1.28
C4	27.2	6.19	-126	-198	324	-0.26	-0.41	0.67
C5	34.6	6.15	-90	-198	288	-0.19	-0.41	0.59
C6	41.8	5.93	-87	-137	224	-0.19	-0.30	0.49
C7	49.3	6.64	-117	-139	256	-0.28	-0.33	0.60
C8	56.8	5.98	-82	-130	212	-0.19	-0.30	0.49
C9	64.0	6.03	-131	-160	290	-0.30	-0.37	0.67
C10	71.2	5.98	-123	-203	326	-0.28	-0.46	0.74
C11	78.8	6.68	-102	-200	302	-0.23	-0.46	0.69
C12	85.9	5.15	-147	-250	397	-0.33	-0.55	0.88
C13	92.0	4.68	-136	-349	486	-0.23	-0.59	0.82
Cr3 (r_i=2.4)	0.0		-204	-40	245	-0.37	-0.07	0.44
D1	6.0	5.44	-5	-301	307	-0.01	-0.51	0.52
D2	12.3	4.82	-6	-258	264	-0.01	-0.54	0.55
D3	19.0	6.17	-8	-242	250	-0.02	-0.47	0.49
D4	26.3	6.09	0	-327	327	0.00	-0.69	0.69
D5	33.6	6.08	-1	-182	183	0.00	-0.40	0.40
D6	40.9	6.26	-2	-173	175	0.00	-0.38	0.38
D7	48.5	6.50	-2	-155	157	0.00	-0.33	0.33
D8	56.5	6.95	-1	-166	168	0.00	-0.34	0.35
D9	64.3	6.43	-1	-166	166	0.00	-0.36	0.36
D10	72.0	6.41	-1	-240	241	0.00	-0.48	0.49
D11	79.2	5.67	2	-243	245	0.00	-0.45	0.45
D12 (weld)	85.5	4.45	20	-307	327	0.04	-0.61	0.65
D13	91.7	5.65	-	-349	-	-	-0.61	-
Cr4 (r_i=3.8)	0.0		211	-160	371	0.38	-0.29	0.66

Table A.37: *Material properties distribution for CR 100×100×2*

CR 100×100×2	*Section position (mm)*	*Width (mm)*	*E* (N/mm^2)	$\sigma_{0.01,exp}$ (N/mm^2)	$\sigma_{0.2,exp}$ (N/mm^2)	$\sigma_{1.0,exp}$ (N/mm^2)	$\sigma_{ult,exp}$ (N/mm^2)	$\varepsilon_{f,exp}$
A1	6.9	5.11	204400	151	514	620	786	0.53
A2	13.6	6.00	204200	178	451	524	766	0.54
A3	21.0	6.39	193700	210	439	513	762	0.65
A4	28.2	5.58	205900	185	406	472	711	0.64
A5	35.1	5.75	215700	211	426	488	736	0.60
A6	42.1	5.87	201400	94	430	495	729	0.61
A7	49.6	6.79	199200	221	499	582	776	0.61
A8	57.2	5.93	209700	169	443	505	737	0.52
A9	64.2	5.81	207900	238	466	541	764	0.54
A10	72.0	7.24	207900	194	477	539	767	0.64
A11	79.7	5.80	206000	206	495	568	800	0.61
A12	86.2	4.79	212700	203	483	567	770	0.58
A13	92.1	4.60	189400	47	600	693	854	0.54
Cr1 (r_i=2.8)	0.0		204200	154	508	624	667	0.32
B1	5.5	3.89	207700	252	552	668	822	0.56
B2	11.0	4.80	192700	157	449	539	766	0.60
B3	17.4	5.59	192600	165	448	507	730	60.00
B4	24.3	5.78	210100	207	449	505	758	0.60
B5	31.7	6.56	209500	230	468	532	768	0.68
B6	39.2	6.20	200600	253	477	559	769	0.60
B7	46.9	6.80	209200	135	464	514	757	0.67
B8	54.5	5.96	-	-	-	-	-	-
B9	61.7	5.96	205800	252	480	544	779	0.54
B10	68.9	6.00	193200	233	468	554	776	0.58
B11	76.0	5.80	211900	156	482	564	782	0.53
B12	82.5	4.78	192500	226	528	603	793	0.56
B13	88.8	5.43	212100	174	547	676	813	0.49
Cr2 (r_i=3.0)	0.0		208100	371	671	782	885	0.38

Table A.37 (continued): *Material properties distribution for CR 100×100×2*

CR 100×100×2	*Section position (mm)*	*Width (mm)*	*E* (N/mm^2)	$\sigma_{0.01,exp}$ (N/mm^2)	$\sigma_{0.2,exp}$ (N/mm^2)	$\sigma_{1.0,exp}$ (N/mm^2)	$\sigma_{ult,exp}$ (N/mm^2)	$\varepsilon_{f,exp}$
C1	6.3	5.15	208000	105	537	683	814	0.51
C2	12.7	5.27	210800	101	465	551	746	0.56
C3	19.7	6.40	223000	187	475	545	771	0.63
C4	27.2	6.19	188600	48	484	541	766	0.58
C5	34.6	6.15	209200	158	486	560	760	0.59
C6	41.8	5.93	200500	279	453	519	751	0.59
C7	49.3	6.64	204000	157	427	501	757	0.73
C8	56.8	5.98	202900	199	432	489	761	0.63
C9	64.0	6.03	212000	204	431	499	768	0.63
C10	71.2	5.98	192800	76	443	504	770	0.62
C11	78.8	6.68	214900	208	436	519	774	0.72
C12	85.9	5.15	205800	163	451	539	757	0.61
C13	92.0	4.68	189000	137	589	711	828	0.51
Cr3 (r_i=2.4)	0.0		198000	179	551	678	757	0.47
D1	6.0	5.44	196800	181	589	715	815	0.49
D2	12.3	4.82	210800	111	478	556	786	0.60
D3	19.0	6.17	214700	225	513	588	793	0.50
D4	26.3	6.09	205300	167	475	554	769	0.56
D5	33.6	6.08	189800	97	459	525	740	0.56
D6	40.9	6.26	221800	189	455	530	758	0.58
D7	48.5	6.50	202200	81	475	544	770	0.58
D8	56.5	6.95	209500	14	484	555	775	0.60
D9	64.3	6.43	212600	172	464	549	753	0.70
D10	72.0	6.41	191900	195	497	578	766	0.59
D11	79.2	5.67	201800	168	541	628	749	0.55
D12 (weld)	85.5	4.45	192200	68	501	588	720	0.57
D13	91.7	5.65	214400	138	569	696	789	0.45
Cr4 (r_i=3.8)	0.0		185800	90	561	681	771	0.46

Table A.38: *Proof stress ratios and Ramberg-Osgood strain parameters for CR 100×100×2*

CR 100×100×2	*Section position (mm)*	*Width (mm)*	$\sigma_{0.2,exp}/\sigma_{0.2,mill}$	$\sigma_{0.2,exp}/\sigma_{0.2,min}$	$n_{0.01}$	$n_{0.05}$	$n_{0.1}$	$n_{bestfit}$	n'	$n'_{bestfit}$
A1	6.9	5.11	1.06	2.23	2.4	2.6	3.8	3.3	4.7	4.7
A2	13.6	6.00	0.93	1.96	3.2	4.7	5.9	5.9	3.0	3.0
A3	21.0	6.39	0.91	1.91	4.1	5.3	4.9	5.7	3.0	3.0
A4	28.2	5.58	0.84	1.76	3.8	4.9	5.5	5.5	4.9	4.8
A5	35.1	5.75	0.88	1.85	4.3	4.3	5.1	5.5	2.2	2.2
A6	42.1	5.87	0.89	1.87	2.0	4.5	5.1	6.0	5.2	5.2
A7	49.6	6.79	1.03	2.17	3.7	4.8	4.9	4.9	3.2	3.2
A8	57.2	5.93	0.91	1.92	3.1	5.9	6.9	5.9	3.1	3.1
A9	64.2	5.81	0.96	2.03	4.5	5.8	5.9	6.6	3.4	3.4
A10	72.0	7.24	0.98	2.07	3.3	5.4	5.3	6.2	2.2	2.2
A11	79.7	5.80	1.02	2.15	3.4	4.3	5.2	5.2	3.2	3.2
A12	86.2	4.79	1.00	2.10	3.5	4.0	4.4	4.9	3.5	3.5
A13	92.1	4.60	1.24	2.61	1.2	4.0	4.2	5.4	4.1	4.1
Cr1 (r_i=2.8)	0.0		1.05	2.21	2.5	2.5	3.9	4.3	6.4	6.4
B1	5.5	3.89	1.14	2.40	3.8	5.1	5.1	5.3	6.1	6.1
B2	11.0	4.80	0.93	1.95	2.9	3.6	4.6	4.9	4.1	4.1
B3	17.4	5.59	0.92	1.95	3.0	4.1	5.1	5.3	1.8	1.8
B4	24.3	5.78	0.93	1.95	3.9	5.1	4.9	5.1	3.0	3.0
B5	31.7	6.56	0.97	2.04	4.2	6.5	6.3	6.7	2.9	2.9
B6	39.2	6.20	0.98	2.07	4.7	5.2	5.8	6.6	2.0	2.0
B7	46.9	6.80	0.96	2.02	2.4	20.9	24.5	25.5	2.4	2.4
B8	54.5	5.96	-	-	-	-	-	-	-	-
B9	61.7	5.96	0.99	2.09	4.7	4.6	8.3	5.9	3.5	3.5
B10	68.9	6.00	0.97	2.04	4.3	5.1	6.9	7.9	5.7	5.7
B11	76.0	5.80	0.99	2.10	2.6	4.0	6.9	6.9	6.2	6.2
B12	82.5	4.78	1.09	2.30	3.5	3.5	3.9	4.8	3.0	3.0
B13	88.8	5.43	1.13	2.38	2.6	4.0	5.0	5.0	4.7	4.7
Cr2 (r_i=3.0)	0.0		1.38	2.92	5.1	5.0	5.5	6.2	3.8	3.8

Table A.38 (continued): *Proof stress ratios and Ramberg-Osgood strain parameters for CR 100×100×2*

CR 100×100×2	*Section position (mm)*	*Width (mm)*	$\sigma_{0.2,exp}/\sigma_{0.2,mill}$	$\sigma_{0.2,exp}/\sigma_{0.2,min}$	$n_{0.01}$	$n_{0.05}$	$n_{0.1}$	$n_{bestfit}$	n'	$n'_{bestfit}$
C1	6.3	5.15	1.11	2.34	1.8	3.6	4.4	5.3	6.2	6.2
C2	12.7	5.27	0.96	2.02	2.0	4.7	7.7	7.7	5.2	5.2
C3	19.7	6.40	0.98	2.06	3.2	4.2	6.0	6.0	3.0	3.0
C4	27.2	6.19	1.00	2.10	1.3	5.7	6.7	5.9	3.2	3.2
C5	34.6	6.15	1.00	2.11	2.7	4.0	6.0	6.0	2.5	2.5
C6	41.8	5.93	0.93	1.97	6.2	7.3	4.7	8.8	3.5	3.5
C7	49.3	6.64	0.88	1.86	3.0	5.4	7.2	7.2	3.5	3.6
C8	56.8	5.98	0.89	1.88	3.9	4.6	5.1	6.1	4.0	4.0
C9	64.0	6.03	0.89	1.87	4.0	5.2	5.6	6.4	2.5	2.5
C10	71.2	5.98	0.91	1.93	1.7	5.9	5.3	6.6	5.3	5.3
C11	78.8	6.68	0.90	1.90	4.1	4.2	4.8	5.2	3.5	3.5
C12	85.9	5.15	0.93	1.96	2.9	4.1	4.8	4.8	2.7	2.7
C13	92.0	4.68	1.21	2.56	2.1	3.8	3.4	4.0	3.2	3.2
Cr3 (r_i=2.4)	0.0		1.14	2.40	2.7	4.7	4.7	5.6	5.5	5.5
D1	6.0	5.44	1.21	2.56	2.5	4.3	5.0	5.7	4.3	4.3
D2	12.3	4.82	0.99	2.08	2.0	5.2	5.3	5.2	2.4	2.4
D3	19.0	6.17	1.06	2.23	3.6	4.2	4.3	5.3	3.4	3.4
D4	26.3	6.09	0.98	2.07	2.9	3.5	4.8	5.4	3.1	3.1
D5	33.6	6.08	0.95	2.00	1.9	4.4	4.0	6.5	3.7	3.7
D6	40.9	6.26	0.94	1.98	3.4	4.4	5.1	5.6	4.9	4.9
D7	48.5	6.50	0.98	2.07	1.7	5.5	5.7	7.0	3.7	3.7
D8	56.5	6.95	1.00	2.11	0.9	4.6	7.0	7.0	6.1	6.1
D9	64.3	6.43	0.96	2.02	3.0	3.6	10.1	5.8	5.9	5.9
D10	72.0	6.41	1.02	2.16	3.2	6.0	9.0	9.0	6.5	6.5
D11	79.2	5.67	1.12	2.35	2.6	3.0	5.1	5.1	5.2	5.2
D12 (weld)	85.5	4.45	1.03	2.18	1.5	3.4	3.3	3.6	2.5	2.5
D13	91.7	5.65	1.17	2.47	2.1	2.6	2.9	3.5	4.8	4.8
Cr4 (r_i=3.8)	0.0		1.16	2.44	1.6	3.2	4.7	4.7	9.1	9.1

A.11 CR 100×50×3

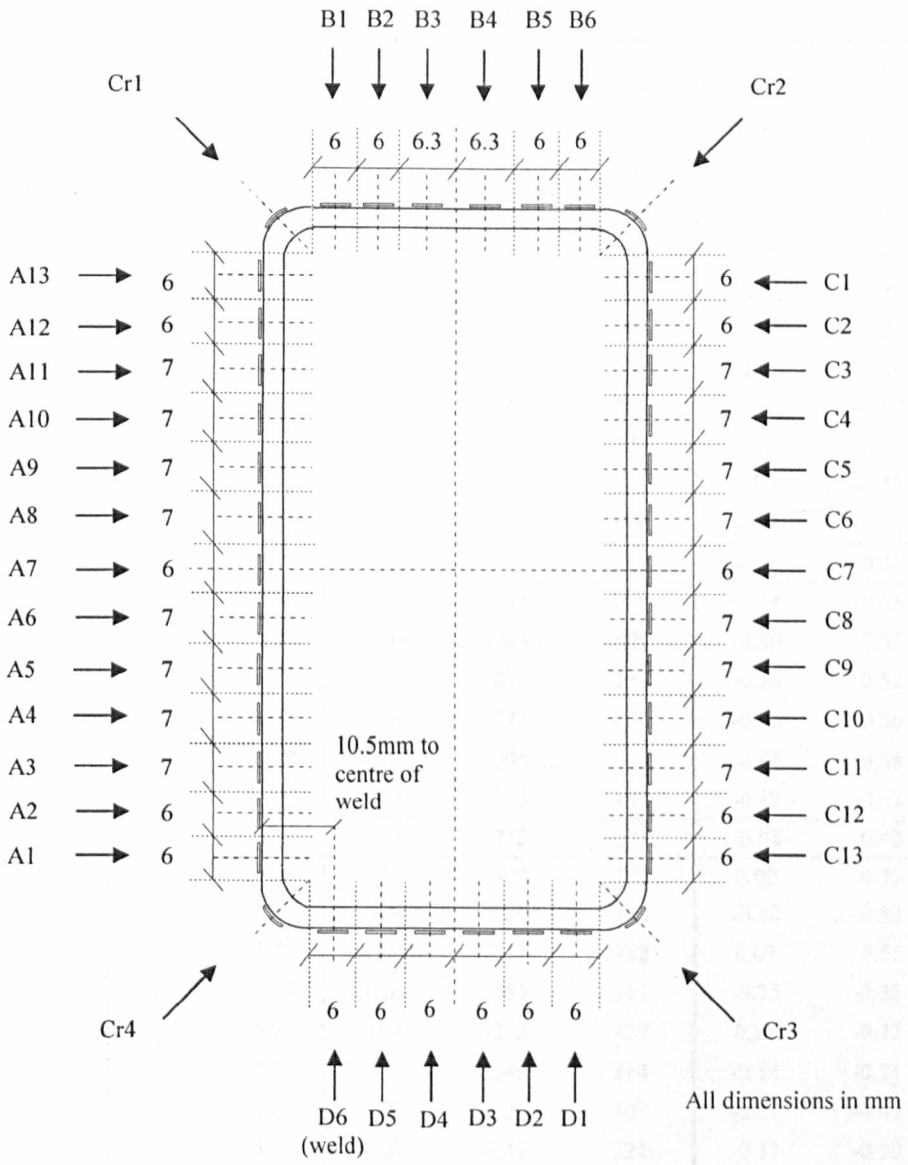

Figure A.11: *Setting out of cold rolled section CR 100×50×3*

Table A.39: *Residual stress distribution for CR 100×50×3*

CR 100×50×3	*Section position (mm)*	*Width (mm)*	σ_m *(N/mm²)*	σ_b *(N/mm²)*	σ_{rc} *(N/mm²)*	$\sigma_m/\sigma_{0.2}$	$\sigma_b/\sigma_{0.2}$	$\sigma_{rc}/\sigma_{0.2}$
A1	8.5	6.06	14	-420	434	0.02	-0.64	0.66
A2	15.8	6.20	-269	-232	502	-0.45	-0.39	0.85
A3	23.0	5.79	-5	-246	251	-0.01	-0.49	0.50
A4	29.9	5.67	-26	-249	275	-0.05	-0.51	0.57
A5	36.7	5.49	-52	-201	254	-0.10	-0.40	0.51
A6	43.3	5.27	-97	-217	314	-0.20	-0.46	0.66
A7	49.5	4.77	-48	-240	287	-0.10	-0.49	0.59
A8	56.3	6.51	-86	-260	346	-0.18	-0.56	0.74
A9	63.5	5.54	-40	-226	266	-0.08	-0.46	0.55
A10	70.5	5.93	-27	-267	294	-0.06	-0.57	0.63
A11	77.5	5.65	-22	-261	283	-0.04	-0.53	0.58
A12	83.9	4.89	0	-317	318	0.00	-0.53	0.53
A13	90.0	4.84	-70	-334	404	-0.12	-0.56	0.68
Cr1 (r_i=3.0)	0.0		66	-239	305	0.11	-0.41	0.52
B1	6.9	5.67	-72	-287	359	-0.14	-0.55	0.69
B2	13.3	4.71	-105	-284	389	-0.20	-0.55	0.75
B3	19.2	4.75	-83	-270	354	-0.16	-0.52	0.68
B4	25.3	4.98	-78	-275	353	-0.16	-0.56	0.72
B5	31.6	5.23	-127	-295	422	-0.25	-0.58	0.83
B6	38.2	5.56	-69	-363	432	-0.12	-0.63	0.75
Cr2 (r_i=4.0)	0.0		-25	-252	277	-0.04	-0.42	0.46
C1	7.2	4.76	3	-375	377	0.00	-0.59	0.60
C2	13.7	5.81	-79	-286	365	-0.14	-0.52	0.67
C3	20.2	4.72	14	-317	332	0.03	-0.55	0.58
C4	27.0	6.53	-366	-185	551	-0.75	-0.38	1.12
C5	34.4	5.80	194	-232	427	0.39	-0.47	0.86
C6	41.2	5.50	-67	-246	314	-0.14	-0.51	0.65
C7	47.6	4.89	-78	-229	307	-0.17	-0.49	0.65
C8	54.1	5.76	-80	-241	321	-0.17	-0.50	0.67
C9	61.1	5.77	-72	-228	300	-0.15	-0.49	0.64
C10	68.1	5.75	-46	-231	277	-0.10	-0.49	0.58
C11	75.0	5.69	-14	-258	272	-0.03	-0.51	0.54
C12	81.6	5.07	-49	-306	355	-0.09	-0.59	0.68
C13	87.7	4.78	-30	-343	373	-0.05	-0.61	0.66
Cr3 (r_i=3.0)	0.0		-59	-244	303	-0.10	-0.41	0.51

Table A.39 (continued): *Residual stress distribution for CR 100×50×3*

CR 100×50×3	*Section position (mm)*	*Width (mm)*	σ_m *(N/mm²)*	σ_b *(N/mm²)*	σ_{rc} *(N/mm²)*	$\sigma_m/\sigma_{0.2}$	$\sigma_b/\sigma_{0.2}$	$\sigma_{rc}/\sigma_{0.2}$
D1	7.1	6.01	-193	-288	481	-0.36	-0.53	0.89
D2	13.6	4.68	-193	-280	473	-0.39	-0.57	0.96
D3	19.5	4.66	-165	-233	398	-0.34	-0.48	0.81
D4	25.7	5.30	-107	-264	371	-0.21	-0.52	0.74
D5	32.2	5.40	-167	-320	487	-0.30	-0.58	0.88
D6 (weld)	38.4	4.52	-238	-460	698	-0.39	-0.76	1.15
Cr4 (r_i=4.8)	0.0		-41	-299	340	-0.07	-0.48	0.54

Table A.40: *Material properties distribution for CR 100×50×3*

CR 100×50×3	*Section position (mm)*	*Width (mm)*	E (N/mm^2)	$\sigma_{0.01,exp}$ (N/mm^2)	$\sigma_{0.2,exp}$ (N/mm^2)	$\sigma_{1.0,exp}$ (N/mm^2)	$\sigma_{ult,exp}$ (N/mm^2)	$\varepsilon_{f,exp}$
A1	8.5	6.06	199600	304	656	791	813	0.43
A2	15.8	6.20	200300	323	592	650	736	0.61
A3	23.0	5.79	201400	247	502	570	694	0.48
A4	29.9	5.67	202500	221	486	566	702	0.63
A5	36.7	5.49	186800	328	500	562	702	0.62
A6	43.3	5.27	201100	220	472	537	687	0.74
A7	49.5	4.77	208000	208	486	548	703	0.62
A8	56.3	6.51	208400	208	467	539	696	0.64
A9	63.5	5.54	200500	260	486	543	697	0.66
A10	70.5	5.93	216000	149	467	546	701	0.61
A11	77.5	5.65	212900	205	489	561	707	0.62
A12	83.9	4.89	209800	202	598	693	752	0.64
A13	90.0	4.84	207700	201	596	691	749	0.57
Cr1 (r_i=3.0)	0.0		205200	256	588	707	741	0.39
B1	6.9	5.67	200700	122	524	617	697	0.50
B2	13.3	4.71	204200	198	520	594	719	0.61
B3	19.2	4.75	194500	243	519	587	713	0.55
B4	25.3	4.98	194900	187	492	560	696	0.61
B5	31.6	5.23	199000	236	510	584	708	0.64
B6	38.2	5.56	208700	167	572	678	745	0.66
Cr2 (r_i=4.0)	0.0		191500	239	599	695	732	0.40
C1	7.2	4.76	204000	196	633	753	793	0.44
C2	13.7	5.81	200600	239	546	604	718	0.57
C3	20.2	4.72	203000	29	573	665	747	0.53
C4	27.0	6.53	206800	190	490	546	686	0.66
C5	34.4	5.80	206400	204	495	557	695	0.61
C6	41.2	5.50	199200	163	480	554	700	0.70
C7	47.6	4.89	205300	200	470	545	685	0.63
C8	54.1	5.76	205800	134	482	545	701	0.61
C9	61.1	5.77	205100	207	470	534	688	0.72
C10	68.1	5.75	206900	193	474	540	685	0.62
C11	75.0	5.69	200600	208	501	568	704	0.63
C12	81.6	5.07	206100	164	523	608	719	0.65
C13	87.7	4.78	204300	187	566	667	732	0.49
Cr3 (r_i=3.0)	0.0		208500	208	596	719	755	0.42

Table A.40 (continued): *Material properties distribution for CR 100×50×3*

CR 100×50×3	*Section position (mm)*	*Width (mm)*	*E* (N/mm^2)	$\sigma_{0.01,exp}$ (N/mm^2)	$\sigma_{0.2,exp}$ (N/mm^2)	$\sigma_{1.0,exp}$ (N/mm^2)	$\sigma_{ult,exp}$ (N/mm^2)	$\varepsilon_{f,exp}$
D1	7.1	6.01	193700	218	540	628	697	0.56
D2	13.6	4.68	192600	61	492	575	691	0.63
D3	19.5	4.66	207200	219	488	563	685	0.59
D4	25.7	5.30	213200	123	504	585	693	0.62
D5	32.2	5.40	185600	182	551	644	721	0.53
D6 (weld)	38.4	4.52	186100	73	606	750	774	0.35
Cr4 (r_i=4.8)	0.0		186700	183	627	703	723	0.38

Table A.41: *Proof stress ratios and Ramberg-Osgood strain parameters for CR 100×50×3*

CR 100×50×3	*Section position (mm)*	*Width (mm)*	$\sigma_{0.2,exp}/\sigma_{0.2,mill}$	$\sigma_{0.2,exp}/\sigma_{0.2,min}$	$n_{0.01}$	$n_{0.05}$	$n_{0.1}$	$n_{bestfit}$	n'	$n'_{bestfit}$
A1	8.5	6.06	1.35	2.85	3.9	3.7	3.4	4.3	4.0	4.0
A2	15.8	6.20	1.22	2.57	4.9	7.4	7.2	9.2	5.8	5.8
A3	23.0	5.79	1.03	2.18	4.2	6.0	4.0	6.0	3.9	3.9
A4	29.9	5.67	1.00	2.11	3.8	5.5	7.1	7.5	4.7	4.7
A5	36.7	5.49	1.03	2.17	7.1	8.3	9.1	9.6	4.5	4.6
A6	43.3	5.27	0.97	2.05	3.9	4.8	5.2	5.5	3.0	3.0
A7	49.5	4.77	1.00	2.11	3.5	5.1	4.9	5.8	6.0	6.0
A8	56.3	6.51	0.96	2.03	3.7	4.5	4.2	5.2	4.9	4.9
A9	63.5	5.54	1.00	2.11	4.8	6.1	5.4	6.1	2.6	2.6
A10	70.5	5.93	0.96	2.03	2.6	3.7	4.4	4.6	3.3	3.3
A11	77.5	5.65	1.01	2.13	3.5	4.7	4.6	4.6	4.4	4.4
A12	83.9	4.89	1.23	2.60	2.8	3.1	3.0	3.7	3.8	3.9
A13	90.0	4.84	1.23	2.59	2.8	3.1	3.0	3.6	3.9	3.9
Cr1 (r_i=3.0)	0.0		1.21	2.56	3.6	3.4	3.8	4.0	3.3	3.4
B1	6.9	5.67	1.08	2.28	2.1	3.3	4.3	4.3	8.1	8.1
B2	13.3	4.71	1.07	2.26	3.1	3.7	5.8	4.7	3.2	3.2
B3	19.2	4.75	1.07	2.26	3.9	4.4	6.9	6.9	5.8	5.8
B4	25.3	4.98	1.02	2.14	3.1	4.6	4.7	5.3	4.2	4.2
B5	31.6	5.23	1.05	2.22	3.9	4.9	6.2	6.2	6.6	6.5
B6	38.2	5.56	1.18	2.49	2.4	2.9	4.2	3.6	5.8	5.8
Cr2 (r_i=4.0)	0.0		1.24	2.60	3.3	4.5	5.4	5.4	3.6	3.6
C1	7.2	4.76	1.30	2.75	2.6	3.1	4.0	4.3	6.8	6.8
C2	13.7	5.81	1.13	2.37	3.6	4.9	4.6	5.1	3.5	3.5
C3	20.2	4.72	1.18	2.49	1.0	4.3	6.4	6.4	5.9	5.9
C4	27.0	6.53	1.01	2.13	3.2	5.1	5.2	6.7	4.9	4.9
C5	34.4	5.80	1.02	2.15	3.4	4.7	4.8	5.4	3.4	3.4
C6	41.2	5.50	0.99	2.08	2.8	4.5	5.0	5.6	3.9	3.9
C7	47.6	4.89	0.97	2.04	3.5	4.5	5.5	5.6	4.7	4.7
C8	54.1	5.76	0.99	2.10	2.3	4.3	4.8	5.0	6.8	6.8
C9	61.1	5.77	0.97	2.04	3.6	4.2	4.6	5.1	5.8	5.8
C10	68.1	5.75	0.98	2.06	3.3	3.9	4.1	6.2	5.1	5.1
C11	75.0	5.69	1.03	2.18	3.4	5.1	6.0	6.0	3.9	3.9
C12	81.6	5.07	1.08	2.28	2.6	4.6	4.2	4.7	3.8	3.8
C13	87.7	4.78	1.17	2.46	2.7	3.0	4.3	3.7	3.8	3.8
Cr3 (r_i=3.0)	0.0		1.23	2.59	2.8	3.2	3.9	4.1	3.3	3.3

Table A.41 (continued): *Proof stress ratios and Ramberg-Osgood strain parameters for CR 100×50×3*

CR 100×50×3	*Section position (mm)*	*Width (mm)*	$\sigma_{0.2,exp}/\sigma_{0.2,mill}$	$\sigma_{0.2,exp}/\sigma_{0.2,min}$	$n_{0.01}$	$n_{0.05}$	$n_{0.1}$	$n_{bestfit}$	n'	$n'_{bestfit}$
D1	7.1	6.01	1.11	2.35	3.3	5.0	5.2	5.6	5.0	5.0
D2	13.6	4.68	1.01	2.14	1.4	4.2	5.1	4.4	4.2	4.3
D3	19.5	4.66	1.01	2.12	3.7	3.9	5.9	5.9	3.9	3.9
D4	25.7	5.30	1.04	2.19	2.1	3.1	4.0	4.0	3.2	3.2
D5	32.2	5.40	1.14	2.39	2.7	4.0	3.8	4.6	7.3	7.3
D6 (weld)	38.4	4.52	1.25	2.63	1.4	2.5	3.3	3.6	4.7	4.7
Cr4 (r_i=4.8)	0.0		1.29	2.72	2.4	5.4	5.1	5.1	3.8	3.8

Table A.42: *Hardness values HV and predicted 0.2% proof stress* $\overline{\sigma}_{0.2,exp}$ *for CR 100×50×3 Face A*

CR 100×50×3	*Section position (mm)*	*HV*	$\overline{\sigma}_{0.2,exp}$ *(N/mm²)*
Cr4	0.00	288	581
	0.02	271	547
	0.03	261	527
	0.05	309	624
A1	0.06	232	469
	0.08	287	579
	0.09	265	535
	0.11	266	537
A2	0.13	280	566
	0.14	251	506
A3	0.21	253	510
A4	0.28	234	472
A5	0.36	248	501
A6	0.43	259	523
A7	0.50	249	503
	0.50	248	501
A8	0.57	234	472
A9	0.64	222	448
A10	0.72	225	455
A11	0.79	221	447
A12	0.86	237	479
	0.87	236	477
	0.89	245	496
	0.91	259	523
A13	0.92	274	553
	0.94	291	588
	0.95	293	592
	0.97	324	654
Cr1	0.98	286	577
	1.00	292	590

Table A.43: *Hardness values HV and predicted 0.2% proof stress* $\overline{\sigma}_{0.2,exp}$ *for CR 100×50×3 Face B*

CR 100×50×3	*Section position (mm)*	*HV*	$\overline{\sigma}_{0.2,exp}$ *(N/mm²)*
Cr1	0.00	292	590
	0.03	272	549
	0.07	287	579
B1	0.10	277	560
	0.13	256	518
	0.17	257	520
	0.20	247	499
B2	0.23	230	464
	0.27	234	472
	0.30	245	494
B3	0.44	254	512
B4	0.56	262	529
B5	0.70	245	495
	0.73	257	519
	0.77	256	517
B6	0.80	267	539
	0.83	268	541
	0.87	275	556
	0.90	290	586
	0.93	265	535
Cr2	0.97	264	533
	1.00	261	527

Table A.44: *Hardness values HV and predicted 0.2% proof stress* $\overline{\sigma}_{0.2,exp}$ *for CR 100×50×3 Face C*

CR 100×50×3	*Section position (mm)*	*HV*	$\overline{\sigma}_{0.2,exp}$ *(N/mm²)*
Cr2	0.00	261	527
	0.02	254	513
	0.03	277	560
	0.05	277	560
C1	0.06	283	572
	0.08	272	549
	0.09	260	525
C2	0.11	243	491
	0.13	245	495
	0.14	230	465
C3	0.21	234	473
C4	0.28	229	463
C5	0.36	230	465
C6	0.43	220	444
C7	0.50	222	448
	0.50	224	453
C8	0.57	214	432
C9	0.64	214	432
C10	0.72	221	447
C11	0.79	224	451
C12	0.86	226	456
	0.87	239	482
	0.89	238	480
C13	0.91	249	503
	0.92	263	531
	0.94	281	568
	0.95	308	621
Cr3	0.97	328	663
	0.98	313	631
	1.00	298	602

Table A.45: *Hardness values HV and predicted 0.2% proof stress* $\overline{\sigma}_{0.2,exp}$ *for CR 100×50×3 Face D*

CR 100×50×3	*Section position (mm)*	*HV*	$\overline{\sigma}_{0.2,exp}$ *(N/mm²)*
Cr3	0.00	298	602
	0.03	278	562
	0.07	274	553
D1	0.10	255	516
	0.13	249	503
	0.17	251	507
	0.20	255	514
	0.23	242	489
D2	0.27	267	539
	0.30	281	568
D3	0.44	283	572
D4	0.56	266	537
D5	0.70	286	577
	0.73	268	541
	0.77	283	572
D6	0.80	277	559
	0.83	298	602
	0.87	300	607
Cr4	0.90	329	665
	0.93	281	568
	0.97	290	586
	1.00	288	581

A.12 CR 100×100×3

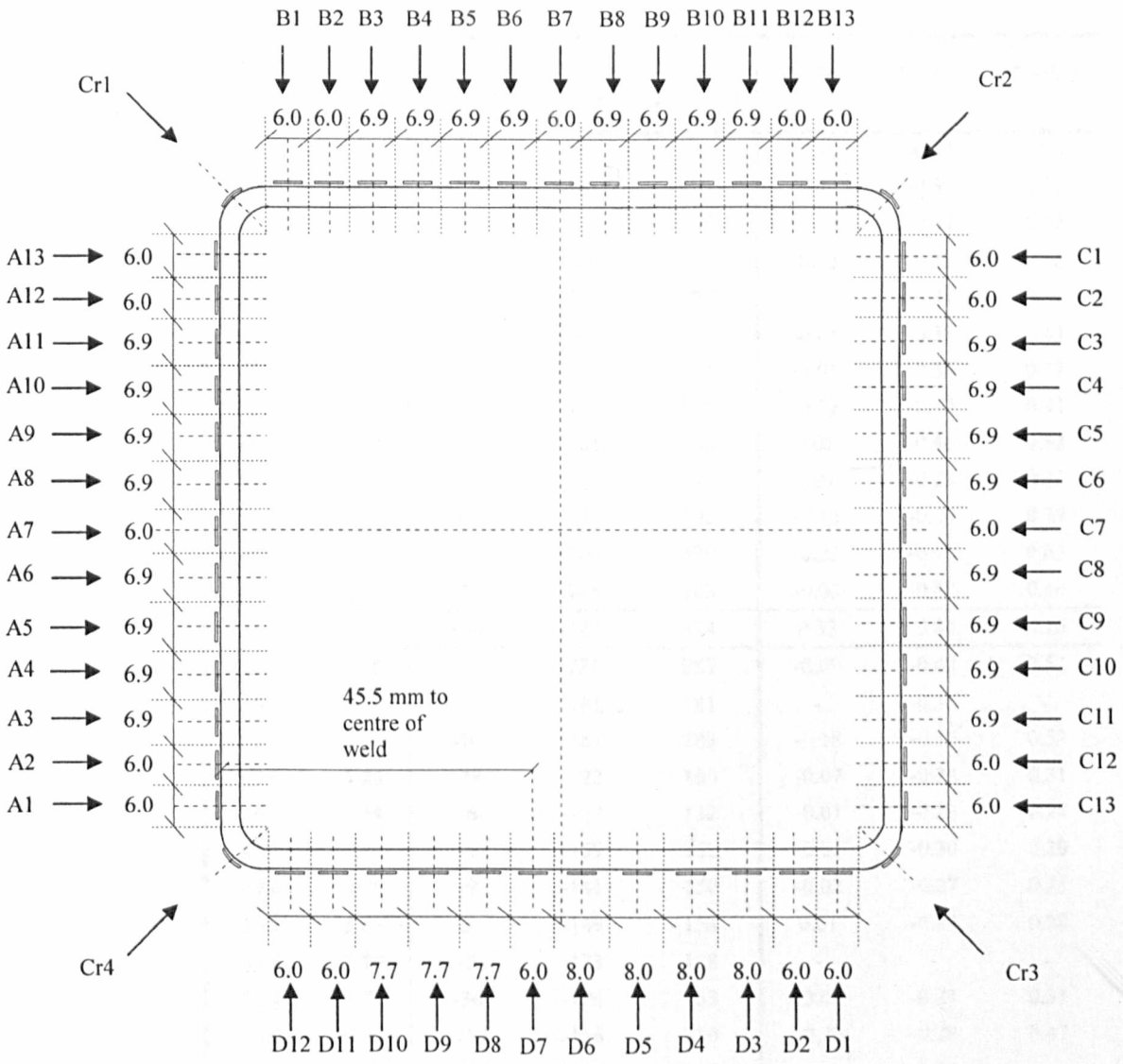

Figure A.12: *Setting out of cold rolled section CR 100×100×3*

Table A.46: *Residual stress distribution for CR 100×100×3*

CR 100×100×3	*Section position (mm)*	*Width (mm)*	σ_m *(N/mm²)*	σ_b *(N/mm²)*	σ_{rc} *(N/mm²)*	$\sigma_m/\sigma_{0.2}$	$\sigma_b/\sigma_{0.2}$	$\sigma_{rc}/\sigma_{0.2}$
A1	7.4	6.04	-202	-251	453	-0.38	-0.47	0.85
A2	14.2	5.05	-221	-183	405	-0.43	-0.36	0.79
A3	20.7	5.70	-115	-170	286	-0.25	-0.37	0.62
A4	27.7	5.78	-56	-228	284	-0.13	-0.53	0.66
A5	34.6	5.68	-28	-137	165	-0.06	-0.31	0.37
A6	41.5	5.74	-22	-168	191	-0.05	-0.38	0.43
A7	47.7	4.23	-4	-160	165	-0.01	-0.36	0.37
A8	53.8	5.59	-8	-137	145	-0.02	-0.32	0.34
A9	60.8	5.92	19	-161	180	0.05	-0.46	0.52
A10	67.9	5.93	5	-110	115	0.01	-0.23	0.25
A11	74.6	5.15	-64	-129	193	-0.13	-0.26	0.39
A12	80.9	4.97	-116	-204	320	-0.23	-0.40	0.63
A13	87.7	6.16	-17	-266	283	-0.03	-0.43	0.46
Cr1 (r_i=5.0)	0.0		160	-414	574	0.32	-0.84	1.16
B1	9.2	7.35	-51	-236	287	-0.09	-0.42	0.52
B2	16.5	4.71		-181	181	-	-0.35	-
B3	22.9	5.74	-96	-187	283	-0.18	-0.35	0.52
B4	29.6	5.26	-38	-122	160	-0.07	-0.24	0.31
B5	36.2	5.54	-6	-127	132	-0.01	-0.23	0.24
B6	43.1	5.87	-4	-159	162	-0.01	-0.30	0.30
B7	49.6	4.75	-9	-141	150	-0.02	-0.27	0.28
B8	56.1	5.83	5	-149	154	0.01	-0.27	0.28
B9	63.6	6.79	-5	-123	128	-	-	-
B10	71.1	5.76	-36	-126	163	-0.07	-0.24	0.31
B11	78.0	5.70	-104	-146	250	-0.20	-0.28	0.47
B12	84.3	4.54	-172	-181	352	-	-0.34	-
B13	90.9	6.09	-143	-195	338	-0.25	-0.34	0.58
Cr2 (r_i=4.5)	0.0		54	-216	269	0.09	-0.36	0.45

Table A.46 (continued): *Residual stress distribution for CR 100×100×3*

CR 100×100×3	*Section position (mm)*	*Width (mm)*	σ_m *(N/mm²)*	σ_b *(N/mm²)*	σ_{rc} *(N/mm²)*	$\sigma_m/\sigma_{0.2}$	$\sigma_b/\sigma_{0.2}$	$\sigma_{rc}/\sigma_{0.2}$
C1	8.4	6.45	141	-106	247	0.25	-0.19	0.43
C2	15.2	4.72	-51	-187	237	-0.09	-0.33	0.42
C3	21.2	4.98	-34	-117	151	-0.07	-0.25	0.32
C4	27.7	5.54	-99	-135	234	-0.21	-0.29	0.50
C5	34.4	5.41	-121	-119	240	-0.25	-0.25	0.50
C6	41.3	6.14	-60	-98	158	-0.13	-0.22	0.35
C7	47.9	4.64	21	-149	169	0.04	-0.32	0.37
C8	54.2	5.55	35	-150	186	0.08	-0.35	0.43
C9	61.1	5.70	72	-153	225	0.17	-0.35	0.52
C10	67.9	5.67	50	-157	207	0.11	-0.36	0.47
C11	75.0	6.11	-84	-147	230	-0.18	-0.32	0.50
C12	81.9	5.25	-171	-223	394	-0.34	-0.44	0.78
C13	88.4	5.32	-125	-219	343	-0.22	-0.38	0.60
Cr3 (r_i=4.3)	0.0		27	-217	244	0.05	-0.41	0.46
D1	7.9	5.83	-280	-213	492	-0.49	-0.38	0.87
D2	14.9	5.78	-242	-171	413	-0.46	-0.33	0.79
D3	21.8	5.63	-70	-148	218	-0.14	-0.29	0.42
D4	29.0	6.39	-40	-136	176	-0.08	-0.26	0.34
D5	36.7	6.60	-20	-133	153	-0.04	-0.25	0.29
D6	44.1	5.78	22	-182	204	0.04	-0.34	0.38
D7 (weld)	50.9	5.42	44	-173	217	0.08	-0.31	0.39
D8	58.2	6.78	19	-174	193	0.03	-0.30	0.34
D9	66.2	6.79	-9	-148	157	-0.02	-0.29	0.31
D10	74.1	6.69	-17	-185	201	-0.03	-0.37	0.40
D11	81.2	5.07	-76	-158	234	-0.14	-0.30	0.44
D12	87.6	5.32	-63	-270	333	-0.12	-0.50	0.62
Cr4 (r_i=3.5)	0.0		47	-203	251	0.09	-0.40	0.49

Table A.47: *Material properties distribution for CR 100×100×3*

CR 100×100×3	*Section position (mm)*	*Width (mm)*	E (N/mm^2)	$\sigma_{0.01,exp}$ (N/mm^2)	$\sigma_{0.2,exp}$ (N/mm^2)	$\sigma_{1.0,exp}$ (N/mm^2)	$\sigma_{ult,exp}$ (N/mm^2)	$\varepsilon_{f,exp}$
A1	7.4	6.04	199800	255	534	619	752	0.54
A2	14.2	5.05	219900	318	515	589	865	0.58
A3	20.7	5.70	211500	202	457	526	772	0.70
A4	27.7	5.78	211000	178	430	485	745	0.69
A5	34.6	5.68	209800	254	440	489	745	0.70
A6	41.5	5.74	207100	224	438	498	745	0.69
A7	47.7	4.23	206600	283	450	517	764	0.61
A8	53.8	5.59	204500	230	428	481	730	0.72
A9	60.8	5.92	200000	288	347	383	626	0.68
A10	67.9	5.93	202000	238	469	522	760	0.66
A11	74.6	5.15	211800	243	500	555	781	0.59
A12	80.9	4.97	200500	192	512	585	767	0.62
A13	87.7	6.16	203000	239	620	709	839	0.56
Cr1 (r_i=5.0)	0.0		197500	112	493	596	710	0.50
B1	9.2	7.35	198900	167	556	640	802	0.59
B2	16.5	4.71	205500	178	521	589	767	0.62
B3	22.9	5.74	201000	238	539	601	788	0.62
B4	29.6	5.26	201100	225	514	588	768	0.56
B5	36.2	5.54	209300	248	544	598	779	0.64
B6	43.1	5.87	207100	229	533	595	786	0.61
B7	49.6	4.75	204700	225	526	602	768	0.62
B8	56.1	5.83	206000	348	549	614	791	0.64
B9	63.6	6.79	-	-	-	-	-	-
B10	71.1	5.76	207500	294	527	596	787	0.64
B11	78.0	5.70	214100	247	526	589	781	0.57
B12	84.3	4.54	212000	224	532	593	779	0.64
B13	90.9	6.09	209600	332	579	652	811	0.58
Cr2 (r_i=4.5)	0.0		210200	273	595	682	801	0.52

Table A.47 (continued): *Material properties distribution for CR 100×100×3*

CR 100×100×3	*Section position (mm)*	*Width (mm)*	*E* (N/mm^2)	$\sigma_{0.01,exp}$ (N/mm^2)	$\sigma_{0.2,exp}$ (N/mm^2)	$\sigma_{1.0,exp}$ (N/mm^2)	$\sigma_{ult,exp}$ (N/mm^2)	$\varepsilon_{f,exp}$
C1	8.4	6.45	213300	274	569	669	774	0.49
C2	15.2	4.72	219700	256	564	634	801	0.50
C3	21.2	4.98	210300	280	475	544	750	0.52
C4	27.7	5.54	190800	215	471	522	716	0.57
C5	34.4	5.41	199600	254	482	544	767	0.66
C6	41.3	6.14	212400	250	451	514	715	0.61
C7	47.9	4.64	209300	212	460	524	756	0.58
C8	54.2	5.55	221000	254	436	504	754	0.70
C9	61.1	5.70	205700	243	436	484	740	0.69
C10	67.9	5.67	212800	237	438	503	754	0.67
C11	75.0	6.11	200500	150	458	504	736	0.67
C12	81.9	5.25	200100	177	505	554	753	0.60
C13	88.4	5.32	195000	249	572	644	776	0.62
Cr3 (r_i=4.3)	0.0		203200	202	532	635	754	0.46
D1	7.9	5.83	207900	323	565	632	783	0.54
D2	14.9	5.78	206300	301	523	575	783	0.62
D3	21.8	5.63	210000	268	516	566	761	0.63
D4	29.0	6.39	214000	257	522	580	787	0.60
D5	36.7	6.60	205900	186	529	593	760	0.54
D6	44.1	5.78	187900	96	531	598	699	0.54
D7 (weld)	50.9	5.42	193300	100	552	622	727	0.54
D8	58.2	6.78	214100	188	570	637	787	0.62
D9	66.2	6.79	205800	250	504	561	740	0.63
D10	74.1	6.69	208500	260	498	560	778	0.67
D11	81.2	5.07	207500	237	527	588	784	0.59
D12	87.6	5.32	203700	192	538	634	782	0.60
Cr4 (r_i=3.5)	0.0		221600	119	514	642	746	0.49

Table A.48: *Proof stress ratios and Ramberg-Osgood strain parameters for CR 100×100×3*

CR 100×100×3	*Section position (mm)*	*Width (mm)*	$\sigma_{0.2,exp}/\sigma_{0.2,mill}$	$\sigma_{0.2,exp}/\sigma_{0.2,min}$	$n_{0.01}$	$n_{0.05}$	$n_{0.1}$	$n_{bestfit}$	n'	$n'_{bestfit}$
A1	7.4	6.04	1.10	2.32	4.1	5.2	8.0	8.0	7.1	7.1
A2	14.2	5.05	1.06	2.24	6.2	6.7	10.5	10.5	3.6	3.6
A3	20.7	5.70	0.94	1.99	3.7	5.4	8.5	6.7	2.9	2.9
A4	27.7	5.78	0.89	1.87	3.4	5.1	5.3	6.3	3.6	3.6
A5	34.6	5.68	0.91	1.91	5.4	5.1	4.6	5.5	2.2	2.2
A6	41.5	5.74	0.90	1.91	4.5	6.2	6.1	7.2	4.3	4.3
A7	47.7	4.23	0.93	1.96	6.4	6.1	9.5	9.5	5.1	5.1
A8	53.8	5.59	0.88	1.86	4.8	4.9	8.5	8.5	2.6	2.7
A9	60.8	5.92	0.72	1.51	16.1	9.0	11.7	12.3	1.4	1.4
A10	67.9	5.93	0.97	2.04	4.4	5.3	6.9	7.1	2.0	2.0
A11	74.6	5.15	1.03	2.17	4.2	5.2	5.5	6.2	2.2	2.2
A12	80.9	4.97	1.06	2.22	3.1	5.0	6.5	6.6	3.5	3.5
A13	87.7	6.16	1.28	2.70	3.1	3.9	3.7	4.5	2.8	2.8
Cr1 (r_i=5.0)	0.0		1.02	2.15	2.0	3.3	3.9	3.4	3.3	3.3
B1	9.2	7.35	1.15	2.42	2.5	3.8	7.2	7.2	4.9	5.0
B2	16.5	4.71	1.07	2.26	2.8	5.8	6.0	4.9	2.1	2.1
B3	22.9	5.74	1.11	2.34	3.7	7.1	4.6	7.1	2.9	2.9
B4	29.6	5.26	1.06	2.23	3.6	7.4	6.4	10.1	5.4	5.4
B5	36.2	5.54	1.12	2.37	3.8	5.3	6.2	6.8	2.3	2.3
B6	43.1	5.87	1.10	2.32	3.5	5.9	7.7	6.6	3.1	3.1
B7	49.6	4.75	1.08	2.29	3.5	6.2	6.8	6.9	4.1	4.1
B8	56.1	5.83	1.13	2.39	6.6	6.3	9.8	9.8	4.3	4.2
B9	63.6	6.79	-	-	-	-	-	-	-	-
B10	71.1	5.76	1.09	2.29	5.1	6.9	6.6	8.0	4.4	4.4
B11	78.0	5.70	1.09	2.29	4.0	4.7	5.1	5.5	3.2	3.2
B12	84.3	4.54	1.10	2.32	3.5	5.3	7.0	5.7	4.7	4.7
B13	90.9	6.09	1.19	2.52	5.4	4.6	6.8	6.9	3.9	3.9
Cr2 (r_i=4.5)	0.0		1.23	2.59	3.9	4.6	4.9	4.8	2.8	2.8

Table A.48 (continued): *Proof stress ratios and Ramberg-Osgood strain parameters for CR 100×100×3*

CR 100×100×3	*Section position (mm)*	*Width (mm)*	$\sigma_{0.2,exp}/\sigma_{0.2,mill}$	$\sigma_{0.2,exp}/\sigma_{0.2,min}$	$n_{0.01}$	$n_{0.05}$	$n_{0.1}$	$n_{bestfit}$	n'	$n'_{bestfit}$
C1	8.4	6.45	1.17	2.48	4.1	6.4	7.3	9.5	7.1	7.1
C2	15.2	4.72	1.16	2.45	3.8	6.2	9.0	9.0	5.6	5.6
C3	21.2	4.98	0.98	2.07	5.6	5.0	8.3	8.7	6.3	6.3
C4	27.7	5.54	0.97	2.05	3.8	5.6	9.2	9.5	3.4	3.4
C5	34.4	5.41	0.99	2.10	4.7	6.9	7.5	9.4	3.5	3.5
C6	41.3	6.14	0.93	1.96	5.1	6.1	5.5	6.2	3.4	3.4
C7	47.9	4.64	0.95	2.00	3.9	6.2	6.4	7.4	3.6	3.6
C8	54.2	5.55	0.90	1.89	5.5	6.2	6.3	7.9	5.3	5.3
C9	61.1	5.70	0.90	1.90	5.1	6.8	8.6	7.5	2.4	2.5
C10	67.9	5.67	0.90	1.90	4.9	5.7	6.6	9.5	5.8	5.8
C11	75.0	6.11	0.94	1.99	2.7	5.9	9.1	9.1	3.7	3.7
C12	81.9	5.25	1.04	2.20	2.9	4.5	4.6	4.9	2.4	2.4
C13	88.4	5.32	1.18	2.49	3.6	4.5	5.8	5.8	4.0	4.0
Cr3 (r_i=4.3)	0.0		1.10	2.31	3.1	4.4	5.7	5.7	4.5	4.5
D1	7.9	5.83	1.17	2.46	5.4	6.9	6.3	7.1	4.2	4.2
D2	14.9	5.78	1.08	2.27	5.4	8.2	9.3	9.3	5.0	5.0
D3	21.8	5.63	1.06	2.24	4.6	7.0	6.7	7.8	4.2	4.2
D4	29.0	6.39	1.08	2.27	4.2	6.5	7.8	7.8	3.9	3.9
D5	36.7	6.60	1.09	2.30	2.9	5.4	6.8	7.1	4.2	4.2
D6	44.1	5.78	1.09	2.31	1.8	5.5	7.3	6.0	3.0	3.0
D7 (weld)	50.9	5.42	1.14	2.40	1.8	6.7	7.3	6.7	3.2	3.2
D8	58.2	6.78	1.18	2.48	2.7	4.9	5.2	6.1	4.2	4.2
D9	66.2	6.79	1.04	2.19	4.3	6.1	7.0	6.3	2.9	2.9
D10	74.1	6.69	1.03	2.17	4.6	5.9	6.7	6.9	4.4	4.4
D11	81.2	5.07	1.09	2.29	3.7	5.5	5.5	6.1	3.8	3.8
D12	87.6	5.32	1.11	2.34	2.9	3.6	4.0	4.5	5.3	5.3
Cr4 (r_i=3.5)	0.0		1.06	2.23	2.1	3.3	3.1	3.6	4.3	4.3

Table A.49: *Hardness values HV and predicted 0.2% proof stress* $\overline{\sigma}_{0.2,exp}$ *for CR 100×100×3 Face A*

CR 100×100×3	*Section position (mm)*	*HV*	$\overline{\sigma}_{0.2,exp}$ *(N/mm²)*
Cr4	0.00	249	503
	0.02	256	517
	0.03	280	566
A1	0.05	292	590
	0.06	257	519
	0.08	241	487
	0.09	245	495
	0.11	241	487
A2	0.13	236	477
	0.14	210	424
A3	0.21	211	426
A4	0.28	220	444
A5	0.36	237	479
A6	0.43	230	465
A7	0.50	245	495
A11	0.81	224	451
A12	0.82	211	425
	0.84	258	522
	0.85	240	484
	0.87	264	533
A13	0.88	246	496
	0.90	266	537
	0.92	276	557
	0.93	270	545
Cr1	1.00	258	521

Table A.50: *Hardness values HV and predicted 0.2% proof stress* $\overline{\sigma}_{0.2,exp}$ *for CR 100×100×3 Face B*

CR 100×100×3	*Section position (mm)*	*HV*	$\overline{\sigma}_{0.2,exp}$ *(N/mm²)*
Cr1	0.00	224	451
	0.02	230	464
	0.03	263	531
	0.05	300	607
B1	0.06	270	545
	0.08	268	541
	0.09	255	516
	0.11	238	480
	0.12	239	482
	0.14	244	492
B2	0.16	243	491
B3	0.22	236	477
B4	0.29	236	477
B5	0.37	239	482
B6	0.44	227	458
B11	0.79	225	455
B12	0.86	238	480
	0.88	250	505
	0.89	248	501
B13	0.91	234	472
	0.92	256	518
	0.94	254	514
Cr2	0.95	251	506
	0.97	229	462
	0.98	231	467
	1.00	248	501

Table A.51: *Hardness values HV and predicted 0.2% proof stress* $\overline{\sigma}_{0.2,exp}$ *for CR 100×100×3 Face C*

CR 100×100×3	*Section position (mm)*	*HV*	$\overline{\sigma}_{0.2,exp}$ *(N/mm²)*
Cr2	0.00	248	501
	0.02	234	472
	0.03	243	491
	0.05	273	551
C1	0.06	276	557
	0.08	269	543
	0.09	270	545
	0.11	257	520
	0.12	251	506
C2	0.14	244	492
C3	0.21	240	485
C4	0.28	259	523
C5	0.35	255	516
C6	0.42	284	574
C7	0.49	251	507
C11	0.81	262	529
C12	0.87	281	568
C13	0.89	257	519
	0.91	261	527
	0.92	250	505
	0.94	254	514
Cr3	0.95	271	547
	0.97	279	564
	0.98	252	508
	1.00	249	503

Table A.52: *Hardness values HV and predicted 0.2% proof stress* $\overline{\sigma}_{0.2,exp}$ *for CR 100×100×3 Face D*

CR 100×100×3	*Section position (mm)*	*HV*	$\overline{\sigma}_{0.2,exp}$ *(N/mm²)*
Cr3	0.00	249	503
	0.02	261	527
	0.03	298	602
	0.05	284	574
D1	0.06	278	562
	0.08	275	555
	0.09	246	498
	0.11	252	508
D2	0.13	249	503
	0.14	262	529
	0.16	273	551
D3	0.23	243	490
D4	0.30	251	507
D10	0.37	263	531
D11	0.84	263	531
	0.86	230	465
	0.87	228	461
D12	0.89	239	483
	0.91	239	483
	0.92	246	497
	0.94	254	513
	0.95	263	531
Cr4	0.97	268	541
	0.98	234	473
	1.00	249	503

A.13 CR 100×50×4

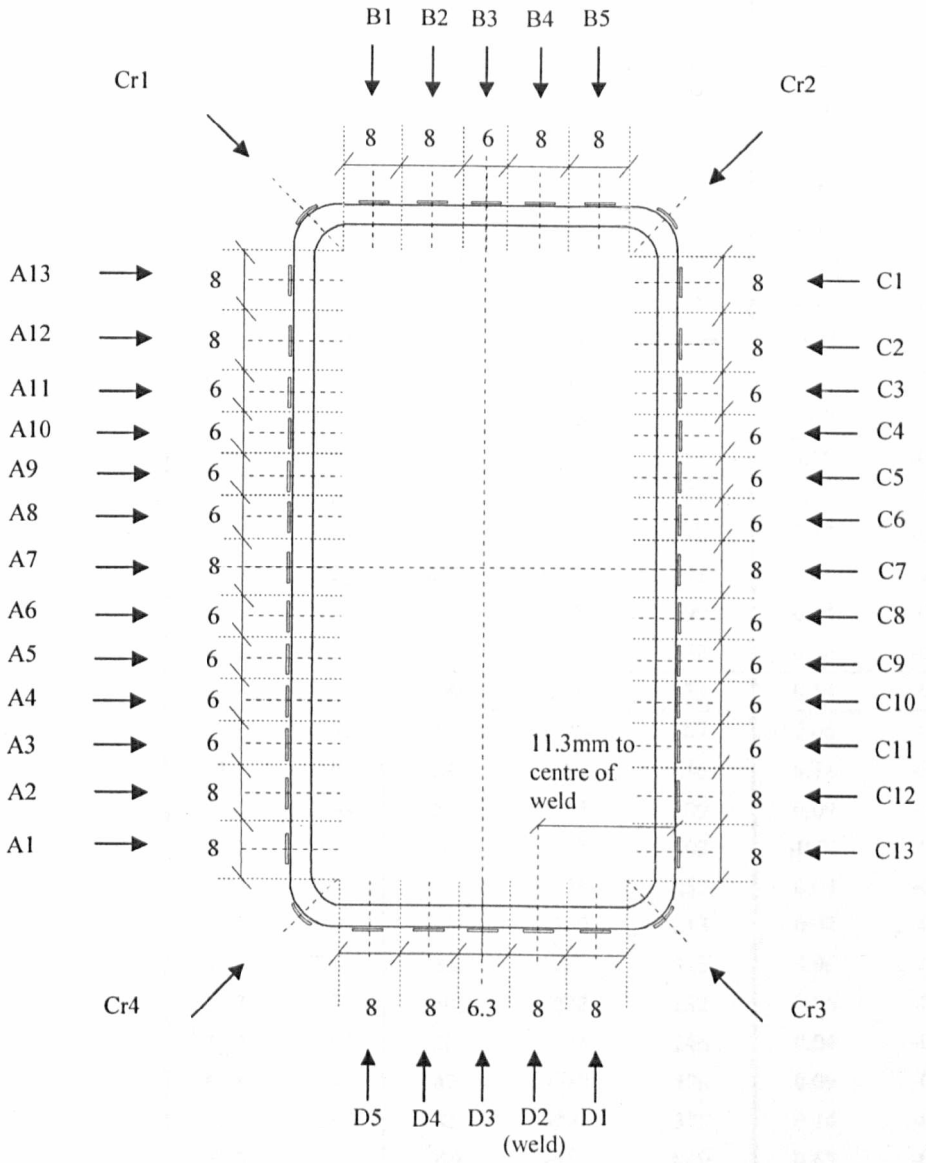

Figure A.13: *Setting out of cold rolled section CR 100×50×4*

Table A.53: *Residual stress distribution for CR 100×50×4*

CR 100×50×4	*Section position (mm)*	*Width (mm)*	σ_m *(N/mm²)*	σ_b *(N/mm²)*	σ_{rc} *(N/mm²)*	$\sigma_m/\sigma_{0.2}$	$\sigma_b/\sigma_{0.2}$	$\sigma_{rc}/\sigma_{0.2}$
A1	7.5	7.11	13	-561	574	0.02	-0.85	0.87
A2	15.5	6.60	96	-398	493	0.16	-0.68	0.85
A3	22.7	5.27	21	-239	259	0.04	-0.41	0.45
A4	28.8	4.63	-4	-187	191	-0.01	-0.35	0.35
A5	34.7	4.73	-34	-181	215	-0.06	-0.32	0.38
A6	40.8	4.93	-35	-218	253	-0.07	-0.42	0.49
A7	47.9	6.92	-54	-282	336	-0.10	-0.51	0.61
A8	55.0	4.89	-90	-237	327	-0.18	-0.46	0.64
A9	61.1	4.88	-103	-292	395	-0.19	-0.55	0.74
A10	67.1	4.69	-83	-225	308	-0.14	-0.39	0.54
A11	73.1	4.91	-6	-316	322	-0.01	-0.54	0.55
A12	80.0	6.66	89	-436	525	0.14	-0.70	0.84
A13	87.7	6.36	53	-466	519	0.07	-0.60	0.67
Cr1 (r_i=2.3)	0.0		106	-177	282	0.15	-0.25	0.40
B1	7.6	7.34	165	-428	593	0.24	-0.61	0.85
B2	15.8	6.64	233	-316	548	0.37	-0.50	0.87
B3	23.0	5.27	282	-250	532	0.46	-0.41	0.87
B4	30.3	6.92	281	-318	599	0.44	-0.49	0.93
B5	38.7	7.61	240	-419	658	0.36	-0.63	0.99
Cr2 (r_i=1.3)	0.0		100	-234	333	0.14	-0.33	0.48
C1	5.6	6.85	42	-526	567	0.06	-0.77	0.83
C2	13.8	7.07	84	-362	446	0.14	-0.60	0.74
C3	21.0	4.99	54	-255	309	0.09	-0.45	0.54
C4	27.1	4.76	-8	-195	203	-0.01	-0.36	0.38
C5	33.3	5.41	22	-231	253	0.04	-0.44	0.48
C6	40.1	5.80	13	-200	213	0.02	-0.38	0.40
C7	47.0	5.50	30	-285	315	0.06	-0.55	0.61
C8	53.3	4.73	30	-202	232	0.06	-0.39	0.45
C9	59.4	5.05	22	-224	246	0.04	-0.41	0.45
C10	65.8	5.38	47	-229	276	0.09	-0.42	0.51
C11	72.2	5.00	82	-293	375	0.14	-0.49	0.63
C12	78.9	5.93	399	-450	849	0.67	-0.75	1.42
C13	86.3	6.61	56	-585	641	0.08	-0.83	0.91
Cr3 (r_i=2.3)	0.0		59	-95	154	0.09	-0.15	0.24
D1	8.7	9.48	76	-414	490	0.11	-0.60	0.71
D2 (weld)	17.5	5.69	192	-290	481	0.32	-0.48	0.80
D3	24.1	5.22	410	-230	639	0.64	-0.36	0.99
D4	31.2	6.53	251	-322	574	0.43	-0.56	0.99
D5	39.4	7.46	223	-380	603	0.32	-0.54	0.85
Cr4 (r_i=2.3)	0.0		75	-159	234	0.09	-0.19	0.28

Table A.54: *Material properties distribution for CR 100×50×4*

CR 100×50×4	*Section position (mm)*	*Width (mm)*	*E* (N/mm^2)	$\sigma_{0.01,exp}$ (N/mm^2)	$\sigma_{0.2,exp}$ (N/mm^2)	$\sigma_{1.0,exp}$ (N/mm^2)	$\sigma_{ult,exp}$ (N/mm^2)	$\varepsilon_{f,exp}$
A1	7.5	7.11	191500	148	660	894	913	0.32
A2	15.5	6.60	199500	176	583	721	808	0.53
A3	22.7	5.27	208500	163	575	673	787	0.54
A4	28.8	4.63	189500	267	540	631	707	0.53
A5	34.7	4.73	210000	264	560	658	803	0.53
A6	40.8	4.93	203400	227	514	617	760	0.57
A7	47.9	6.92	215200	205	550	639	788	0.65
A8	55.0	4.89	202400	262	511	592	769	0.73
A9	61.1	4.88	202200	245	535	613	785	0.57
A10	67.1	4.69	190700	355	576	646	795	0.52
A11	73.1	4.91	203900	239	588	694	806	0.55
A12	80.0	6.66	211700	203	622	786	862	0.53
A13	87.7	6.36	218300	323	778	951	966	0.48
Cr1 (r_i=2.3)	0.0		214300	283	712	838	902	0.38
B1	7.6	7.34	200100	207	699	886	903	0.38
B2	15.8	6.64	207300	227	632	753	843	0.48
B3	23.0	5.27	220900	182	612	727	838	0.55
B4	30.3	6.92	210300	219	642	758	859	0.52
B5	38.7	7.61	200200	267	668	851	869	0.47
Cr2 (r_i=1.3)	0.0		216400	416	699	802	879	0.49
C1	5.6	6.85	187900	296	685	885	900	0.34
C2	13.8	7.07	2048900	224	599	726	824	0.46
C3	21.0	4.99	205800	257	567	662	774	0.51
C4	27.1	4.76	206500	249	538	652	788	0.51
C5	33.3	5.41	203100	247	528	614	755	0.53
C6	40.1	5.80	202500	320	532	606	744	0.63
C7	47.0	5.50	212800	175	515	594	758	0.59
C8	53.3	4.73	203100	250	515	610	764	0.60
C9	59.4	5.05	203400	234	552	637	793	0.58
C10	65.8	5.38	204600	200	544	626	755	0.57
C11	72.2	5.00	206600	192	600	685	795	0.51
C12	78.9	5.93	208600	110	598	737	815	0.48
C13	86.3	6.61	199400	289	707	916	934	0.35
Cr3 (r_i=2.3)	0.0		216800	302	632	727	837	0.45
D1	8.7	9.48	203800	193	694	880	891	0.36
D2 (weld)	17.5	5.69	216500	253	605	718	803	0.68
D3	24.1	5.22	212600	249	644	738	839	0.55
D4	31.2	6.53	201000	214	579	686	767	0.49
D5	39.4	7.46	209900	307	707	891	918	0.41
Cr4 (r_i=2.3)	0.0		204600	575	826	889	904	0.49

Table A.55: *Proof stress ratios and Ramberg-Osgood strain parameters for CR 100×50×4*

CR 100×50×4	*Section position (mm)*	*Width (mm)*	$\sigma_{0.2,exp}/\sigma_{0.2,mill}$	$\sigma_{0.2,exp}/\sigma_{0.2,min}$	$n_{0.01}$	$n_{0.05}$	$n_{0.1}$	$n_{bestfit}$	n'	$n'_{bestfit}$
A1	7.5	7.11	2.3	3.1	2.0	2.1	2.3	2.3	3.7	3.7
A2	15.5	6.60	2.0	2.8	2.5	3.2	3.8	3.8	4.5	4.6
A3	22.7	5.27	2.0	2.7	2.4	4.5	4.4	5.1	4.4	4.4
A4	28.8	4.63	1.9	2.6	4.3	6.3	7.3	7.3	4.6	4.6
A5	34.7	4.73	1.9	2.7	4.0	7.2	6.9	6.9	4.7	4.7
A6	40.8	4.93	1.8	2.4	3.7	4.7	5.9	6.4	4.4	4.4
A7	47.9	6.92	1.9	2.6	3.0	4.1	5.8	5.8	3.9	4.0
A8	55.0	4.89	1.8	2.4	4.5	5.5	5.4	6.1	3.8	3.8
A9	61.1	4.88	1.9	2.5	3.8	5.0	5.0	5.7	3.8	3.9
A10	67.1	4.69	2.0	2.7	6.2	4.8	5.8	7.5	4.4	4.4
A11	73.1	4.91	2.0	2.8	3.3	4.0	4.1	4.3	4.4	4.4
A12	80.0	6.66	2.2	3.0	2.7	2.8	4.0	3.5	3.9	3.9
A13	87.7	6.36	2.7	3.7	3.4	3.6	3.7	4.1	24.4	24.4
Cr1 (r_i=2.3)	0.0		2.5	3.4	3.2	4.1	5.7	6.0	3.6	3.6
B1	7.6	7.34	2.4	3.3	2.5	3.0	3.8	3.8	4.3	4.3
B2	15.8	6.64	2.2	3.0	2.9	4.1	5.7	5.7	3.9	3.9
B3	23.0	5.27	2.1	2.9	2.5	3.7	5.5	4.6	4.5	4.5
B4	30.3	6.92	2.2	3.1	2.8	4.9	4.9	4.9	3.7	3.7
B5	38.7	7.61	2.3	3.2	3.3	3.6	4.0	4.1	4.3	4.3
Cr2 (r_i=1.3)	0.0		2.4	3.3	5.8	5.1	5.2	7.2	6.0	6.0
C1	5.6	6.85	2.4	3.3	3.6	3.1	3.9	4.5	5.8	5.8
C2	13.8	7.07	2.1	2.9	3.0	3.2	3.9	3.9	4.0	4.0
C3	21.0	4.99	2.0	2.7	3.8	3.8	4.5	4.9	3.3	3.3
C4	27.1	4.76	1.9	2.6	3.9	5.2	6.0	6.7	5.3	5.3
C5	33.3	5.41	1.8	2.5	3.9	4.3	4.1	5.0	3.5	3.5
C6	40.1	5.80	1.8	2.5	5.9	4.9	7.2	7.5	3.4	3.4
C7	47.0	5.50	1.8	2.5	2.8	4.8	5.7	5.2	4.4	4.4
C8	53.3	4.73	1.8	2.5	4.1	7.4	5.8	9.5	8.7	8.7
C9	59.4	5.05	1.9	2.6	3.5	6.4	8.0	8.0	4.2	4.2
C10	65.8	5.38	1.9	2.6	3.0	3.7	3.7	4.1	2.7	2.7
C11	72.2	5.00	2.1	2.9	2.6	3.8	5.8	4.8	3.9	3.9
C12	78.9	5.93	2.1	2.8	1.8	2.6	3.2	3.2	4.2	4.2
C13	86.3	6.61	2.5	3.4	3.4	3.2	2.9	3.6	4.9	4.9
Cr3 (r_i=2.3)	0.0		2.2	3.0	4.1	5.0	5.1	6.3	5.7	5.7
D1	8.7	9.48	2.4	3.3	2.3	3.3	3.2	3.5	4.5	4.5
D2 (weld)	17.5	5.69	2.1	2.9	3.4	5.7	3.8	5.8	4.5	4.5
D3	24.1	5.22	2.2	3.1	3.1	5.0	4.8	5.2	3.5	3.6
D4	31.2	6.53	2.0	2.8	3.0	3.7	3.7	4.1	3.5	3.5
D5	39.4	7.46	2.5	3.4	3.6	3.8	3.8	4.2	4.7	4.7
Cr4 (r_i=2.3)	0.0		2.9	3.9	8.2	7.6	8.7	11.2	1.0	1.0

Table A.56: *Hardness values HV and predicted 0.2% proof stress* $\overline{\sigma}_{0.2,exp}$ *for CR 100×50×4 Face A*

CR 100×50×4	*Section position (mm)*	*HV*	$\overline{\sigma}_{0.2,exp}$ *(N/mm²)*
Cr4	0.00	255	516
	0.02	295	595
	0.03	328	663
A1	0.05	336	679
	0.06	316	639
	0.08	298	602
	0.10	296	597
	0.11	282	570
A2	0.13	275	555
	0.14	269	543
	0.16	254	512
A3	0.23	248	501
A4	0.30	253	510
A5	0.36	267	539
A6	0.43	250	505
A7	0.50	274	553
	0.50	270	545
A8	0.57	294	594
A9	0.64	265	535
A10	0.70	261	527
A11	0.77	253	511
A12	0.84	283	572
	0.86	282	570
	0.87	279	564
	0.89	299	604
A13	0.90	316	638
	0.92	321	648
	0.94	324	654
	0.95	323	652
Cr1	0.97	336	679
	0.98	314	634
	1.00	268	541

Table A.57: *Hardness values HV and predicted 0.2% proof stress* $\overline{\sigma}_{0.2,exp}$ *for CR 100×50×4 Face B*

CR 100×50×4	*Section position (mm)*	*HV*	$\overline{\sigma}_{0.2,exp}$ *(N/mm²)*
Cr1	0.00	268	541
	0.03	275	556
	0.07	321	648
B1	0.10	348	703
	0.14	316	638
	0.17	311	628
	0.20	311	628
	0.24	256	517
	0.27	287	580
B2	0.31	267	539
	0.34	298	602
B3	0.50	306	618
	0.50	308	621
B4	0.66	281	568
	0.69	306	619
	0.73	325	657
	0.76	319	644
B5	0.80	289	583
	0.83	314	634
	0.86	332	671
	0.90	318	641
	0.93	331	668
Cr2	0.97	314	634
	1.00	296	597

Table A.58: *Hardness values HV and predicted 0.2% proof stress* $\overline{\sigma}_{0.2,exp}$ *for CR 100×50×4 Face C*

CR 100×50×4	*Section position (mm)*	*HV*	$\overline{\sigma}_{0.2,exp}$ *(N/mm²)*
Cr2	0.00	296	597
	0.02	268	541
C1	0.03	327	660
	0.05	318	641
	0.06	335	676
	0.08	315	636
	0.10	309	624
C2	0.11	311	629
	0.13	280	566
	0.14	266	537
	0.16	280	566
C3	0.23	268	541
C4	0.30	277	559
C5	0.36	269	543
C6	0.42	270	545
C7	0.50	274	553
	0.50	259	523
C8	0.58	269	543
C9	0.64	267	539
C10	0.70	279	564
C11	0.77	264	533
C12	0.84	269	543
	0.86	280	566
C13	0.87	284	574
	0.89	289	583
	0.90	311	629
	0.92	318	641
	0.94	332	671
	0.95	331	668
	0.97	339	685
Cr3	0.98	315	636
	1.00	265	535

Table A.59: *Hardness values HV and predicted 0.2% proof stress* $\overline{\sigma}_{0.2,exp}$ *for CR 100×50×4 Face D*

CR 100×50×4	*Section position (mm)*	*HV*	$\overline{\sigma}_{0.2,exp}$ *(N/mm²)*
Cr3	0.00	265	535
	0.03	289	583
	0.07	319	644
D1	0.10	319	644
	0.14	306	619
	0.17	293	592
	0.20	297	600
	0.24	277	560
	0.27	279	564
	0.31	257	520
D2	0.34	269	543
D3	0.50	250	505
	0.50	247	499
D4	0.66	245	494
	0.69	263	531
	0.73	268	541
	0.76	279	564
D5	0.80	275	555
	0.83	281	568
	0.86	314	634
	0.90	289	583
	0.93	348	702
	0.97	247	499
Cr4	1.00	255	516

A.14 CR 100×100×4

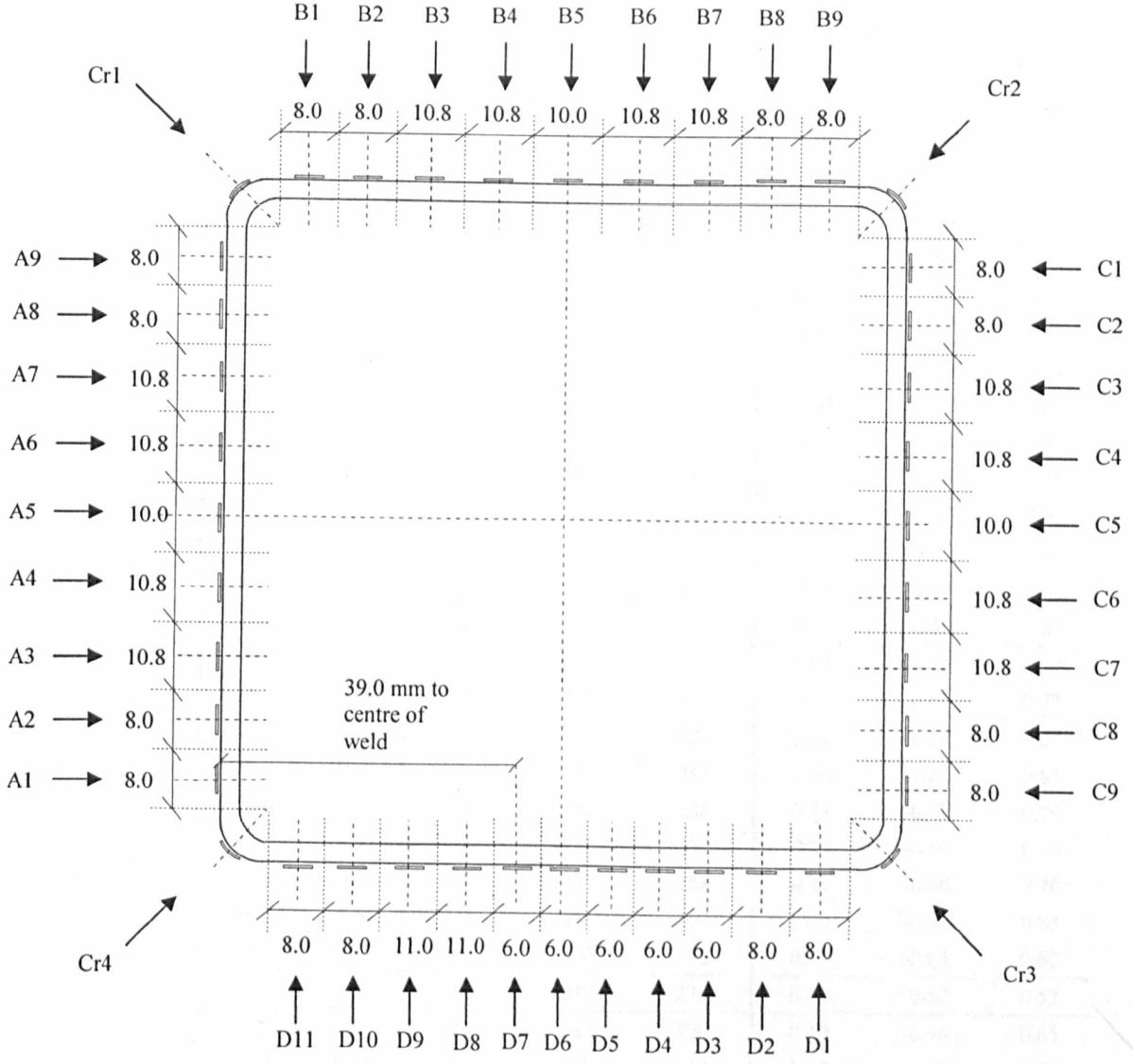

Figure A.14: *Setting out of cold rolled section CR 100×100×4*

Table A.60: *Residual stress distribution for CR 100×100×4*

CR 100×100×4	*Section position (mm)*	*Width (mm)*	σ_m *(N/mm²)*	σ_b *(N/mm²)*	σ_{rc} *(N/mm²)*	$\sigma_m/\sigma_{0.2}$	$\sigma_b/\sigma_{0.2}$	$\sigma_{rc}/\sigma_{0.2}$
A1	8.5	6.47	29	-291	321	0.05	-0.55	0.60
A2	16.2	6.65	197	-355	552	0.45	-0.81	1.26
A3	25.5	9.49	33	-263	296	0.08	-0.65	0.73
A4	36.2	9.49	12	-239	251	0.03	-0.60	0.63
A5	47.1	9.86	7	-233	240	0.02	-0.61	0.63
A6	58.0	9.50	-13	-212	225	-0.03	-0.57	0.60
A7	68.6	9.46	31	-196	227	0.08	-0.52	0.60
A8	77.9	6.72	233	-276	509	0.58	-0.69	1.27
A9	86.1	7.31	-119	-290	409	-0.24	-0.58	0.81
Cr1 (r_i=2.9)	0.0		66	-312	378	0.12	-0.55	0.67
B1	7.4	6.00	57	-260	318	0.10	-0.46	0.56
B2	15.1	7.12	124	-300	424	0.27	-0.66	0.93
B3	24.2	8.65	91	-218	309	0.21	-0.50	0.71
B4	35.1	10.68	23	-241	264	0.05	-0.52	0.57
B5	46.2	9.16	21	-280	302	0.04	-0.58	0.63
B6	56.9	9.86	-9	-283	292	-0.02	-0.58	0.60
B7	67.0	7.93	162	-301	464	0.33	-0.62	0.95
B8	75.5	6.68	129	-307	437	0.27	-0.65	0.92
B9	83.4	6.76	41	-301	342	0.08	-0.60	0.68
Cr2 (r_i=3.5)	0.0		-122	-320	442	-0.22	-0.58	0.81
C1	8.4	7.18	16	-331	347	0.04	-0.75	0.79
C2	16.4	6.38	85	-305	389	0.17	-0.61	0.78
C3	25.6	9.53	14	-215	228	0.03	-0.54	0.57
C4	36.2	9.39	-13	-230	243	-0.03	-0.61	0.65
C5	46.6	8.91	44	-242	286	0.12	-0.67	0.79
C6	56.7	8.91	38	-244	281	0.09	-0.60	0.70
C7	66.6	9.48	44	-244	288	0.11	-0.60	0.70
C8	76.4	6.64	116	-276	392	0.25	-0.60	0.85
C9	84.6	7.38	96	-336	432	0.18	-0.64	0.82
Cr3 (r_i=4.0)	0.0		-1	-277	278	0.00	-0.52	0.52
D1	8.6	6.77	97	-234	330	0.19	-0.46	0.65
D2	16.4	6.46	68	-242	310	0.15	-0.55	0.70
D3	25.2	8.57	7	-228	234	0.02	-0.53	0.55
D4	34.8	8.35	7	-241	248	0.02	-0.55	0.56
D5	43.9	7.46	3	-214	217	0.01	-0.48	0.49
D6	51.7	5.77	28	-287	315	0.06	-0.60	0.66
D7 (weld)	58.3	4.99	468	-213	682	1.04	-0.47	1.52
D8	64.5	5.04	99	-272	372	0.19	-0.53	0.73
D9	70.8	5.08	177	-249	426	0.39	-0.54	0.93
D10	77.6	6.20	45	-253	299	0.10	-0.55	0.65
D11	85.6	7.32	42	-295	337	0.08	-0.57	0.66
Cr4 (r_i=4.0)	0.0		33	-252	285	0.07	-0.51	0.57

Table A.61: *Material properties distribution for CR 100×100×4*

CR 100×100×4	*Section position (mm)*	*Width (mm)*	*E* (N/mm^2)	$\sigma_{0.01,exp}$ (N/mm^2)	$\sigma_{0.2,exp}$ (N/mm^2)	$\sigma_{1.0,exp}$ (N/mm^2)	$\sigma_{ult,exp}$ (N/mm^2)	$\varepsilon_{f,exp}$
A1	8.5	6.47	192000	150	533	661	691	0.52
A2	16.2	6.65	189600	121	438	530	629	0.62
A3	25.5	9.49	185600	154	408	468	620	0.68
A4	36.2	9.49	190000	129	401	469	620	0.69
A5	47.1	9.86	192500	145	381	448	624	0.74
A6	58.0	9.50	184200	136	374	444	611	0.78
A7	68.6	9.46	187200	132	380	444	604	0.68
A8	77.9	6.72	191000	109	399	477	612	0.70
A9	86.1	7.31	185400	125	504	608	656	0.73
Cr1 (r_i=2.9)	0.0		188900	231	567	715	746	0.43
B1	7.4	6.00	182200	258	564	639	721	0.59
B2	15.1	7.12	186200	121	458	541	646	0.72
B3	24.2	8.65	199800	50	438	527	628	0.64
B4	35.1	10.68	193000	110	465	546	644	0.59
B5	46.2	9.16	193800	89	480	568	658	0.74
B6	56.9	9.86	188100	118	485	566	640	0.56
B7	67.0	7.93	183000	149	489	568	656	0.58
B8	75.5	6.68	188700	98	477	572	650	0.72
B9	83.4	6.76	194400	98	505	610	670	0.61
Cr2 (r_i=3.5)	0.0		185100	231	547	691	727	0.41
C1	8.4	7.18	191400	81	441	533	638	0.63
C2	16.4	6.38	180600	167	499	589	639	0.60
C3	25.6	9.53	201300	168	401	466	605	0.65
C4	36.2	9.39	194800	119	375	449	625	0.67
C5	46.6	8.91	185700	137	362	435	622	0.68
C6	56.7	8.91	197800	156	403	469	678	0.69
C7	66.6	9.48	183700	156	410	488	626	0.64
C8	76.4	6.64	185400	129	461	536	664	0.64
C9	84.6	7.38	183500	188	525	623	668	0.51
Cr3 (r_i=4.0)	0.0		187100	226	531	643	716	0.46
D1	8.6	6.77	182200	217	508	584	624	0.22
D2	16.4	6.46	184800	167	442	507	617	0.27
D3	25.2	8.57	192000	145	427	495	634	0.70
D4	34.8	8.35	191200	132	440	509	631	0.68
D5	43.9	7.46	193200	157	441	515	640	0.71
D6	51.7	5.77	185400	131	476	561	637	0.75
D7 (weld)	58.3	4.99	185800	89	450	521	597	0.53
D8	64.5	5.04	189700	130	511	596	662	0.64
D9	70.8	5.08	188200	132	459	544	636	0.66
D10	77.6	6.20	180700	159	462	529	631	0.64
D11	85.6	7.32	188000	117	513	601	669	0.58
Cr4 (r_i=4.0)	0.0		184300	198	497	603	662	0.46

Table A.62: *Proof stress ratios and Ramberg-Osgood strain parameters for CR 100×100×4*

CR 100×100×4	*Section position (mm)*	*Width (mm)*	$\sigma_{0.2,exp}/\sigma_{0.2,mill}$	$\sigma_{0.2,exp}/\sigma_{0.2,min}$	$n_{0.01}$	$n_{0.05}$	$n_{0.1}$	$n_{bestfit}$	n'	$n'_{bestfit}$
A1	8.5	6.47	1.58	2.54	2.4	2.8	3.0	3.1	4.7	4.8
A2	16.2	6.65	1.30	2.09	2.3	3.2	4.1	3.3	4.6	4.6
A3	25.5	9.49	1.21	1.94	3.1	3.9	4.5	3.8	3.6	3.6
A4	36.2	9.49	1.19	1.91	2.6	3.6	4.6	3.7	4.3	4.3
A5	47.1	9.86	1.13	1.81	3.1	3.9	4.4	4.0	3.2	3.2
A6	58.0	9.50	1.11	1.78	3.0	3.9	5.2	4.2	3.4	3.4
A7	68.6	9.46	1.13	1.81	2.8	3.4	3.9	3.5	3.6	3.6
A8	77.9	6.72	1.19	1.90	2.3	3.1	3.7	3.3	4.1	4.1
A9	86.1	7.31	1.50	2.40	2.1	3.0	3.4	3.1	4.2	4.3
Cr1 (r_i=2.9)	0.0		1.68	2.70	3.3	3.5	3.7	3.7	4.0	4.0
B1	7.4	6.00	1.68	2.69	3.8	4.6	4.5	4.8	3.0	3.1
B2	15.1	7.12	1.36	2.18	2.2	3.1	3.8	3.3	4.1	4.1
B3	24.2	8.65	1.30	2.09	1.4	2.2	3.2	2.5	4.2	4.2
B4	35.1	10.68	1.38	2.21	2.1	3.4	4.5	3.6	4.1	4.1
B5	46.2	9.16	1.42	2.28	1.8	3.3	4.1	3.4	4.0	4.0
B6	56.9	9.86	1.44	2.31	2.1	3.5	4.2	3.3	3.7	3.7
B7	67.0	7.93	1.45	2.33	2.5	3.8	4.9	4.0	4.3	4.3
B8	75.5	6.68	1.42	2.27	1.9	2.7	4.0	3.0	3.8	3.9
B9	83.4	6.76	1.50	2.40	1.8	2.8	3.1	2.8	4.7	4.7
Cr2 (r_i=3.5)	0.0		1.62	2.60	3.5	3.8	4.4	4.0	4.2	4.2
C1	8.4	7.18	1.31	2.10	1.8	2.7	3.2	2.9	4.3	4.3
C2	16.4	6.38	1.48	2.38	2.7	3.4	3.9	3.5	4.0	4.1
C3	25.6	9.53	1.19	1.91	3.4	4.1	4.9	4.9	3.6	3.6
C4	36.2	9.39	1.11	1.79	2.6	3.6	4.3	3.7	3.4	3.4
C5	46.6	8.91	1.08	1.73	3.1	4.1	4.7	4.4	3.9	3.9
C6	56.7	8.91	1.20	1.92	3.2	3.9	4.5	4.0	3.1	3.1
C7	66.6	9.48	1.22	1.95	3.1	3.8	4.1	4.1	2.5	2.5
C8	76.4	6.64	1.37	2.20	2.4	3.1	3.6	3.2	3.4	3.5
C9	84.6	7.38	1.56	2.50	2.9	3.4	3.6	3.8	5.8	5.7
Cr3 (r_i=4.0)	0.0		1.58	2.53	3.5	4.0	4.5	4.2	3.9	3.9
D1	8.6	6.77	1.51	2.42	3.5	4.2	4.6	4.6	4.2	4.2
D2	16.4	6.46	1.31	2.10	3.1	3.8	4.9	4.0	3.8	3.8
D3	25.2	8.57	1.27	2.04	2.8	4.0	4.7	4.1	3.6	3.7
D4	34.8	8.35	1.31	2.10	2.5	3.5	4.4	3.9	3.4	3.4
D5	43.9	7.46	1.31	2.10	2.9	4.0	4.7	4.1	3.5	3.5
D6	51.7	5.77	1.41	2.27	2.3	3.7	4.3	3.8	4.2	4.2
D7 (weld)	58.3	4.99	1.34	2.14	1.9	3.1	3.7	3.1	3.6	3.6
D8	64.5	5.04	1.52	2.44	2.2	3.6	4.0	3.7	3.5	3.5
D9	70.8	5.08	1.36	2.19	2.4	3.9	5.7	4.6	4.0	4.0
D10	77.6	6.20	1.37	2.20	2.8	3.8	4.8	4.8	4.1	4.2
D11	85.6	7.32	1.52	2.44	2.0	3.0	3.9	3.3	4.4	4.4
Cr4 (r_i=4.0)	0.0		1.48	2.37	3.2	3.8	4.2	3.8	4.0	4.0

Table A.63: *Hardness values HV and predicted 0.2% proof stress* $\overline{\sigma}_{0.2,exp}$ *for CR 100×100×4 Face A*

CR 100×100×4	*Section position (mm)*	*HV*	$\overline{\sigma}_{0.2,exp}$ *(N/mm²)*
Cr4	0.00	253	511
	0.02	239	483
	0.03	263	531
	0.05	325	657
A1	0.06	287	580
	0.08	282	570
	0.10	258	521
	0.11	262	529
A2	0.13	237	479
	0.14	239	483
	0.16	223	450
	0.18	223	450
A3	0.28	223	450
A4	0.39	209	422
A5	0.50	201	406
A8	0.82	250	505
	0.84	243	491
	0.86	257	520
	0.87	239	482
A9	0.89	258	521
	0.90	246	498
	0.92	252	508
	0.94	267	539
	0.95	277	559
Cr1	0.97	316	639
	0.98	275	555
	1.00	274	553

Table A.64: *Hardness values HV and predicted 0.2% proof stress $\overline{\sigma}_{0.2,exp}$ for CR 100×100×4 Face B*

CR 100×100×4	*Section position (mm)*	*HV*	$\overline{\sigma}_{0.2,exp}$ *(N/mm²)*
Cr1	0.00	274	553
	0.02	287	579
	0.03	319	644
B1	0.05	302	609
	0.06	303	611
	0.08	281	568
	0.10	279	564
	0.11	263	531
B2	0.13	256	518
	0.14	240	485
	0.16	231	466
	0.18	224	453
B3	0.28	220	444
B4	0.39	216	437
B5	0.50	205	414
B8	0.82	257	520
B9	0.84	246	498
	0.86	252	508
	0.87	254	514
	0.89	252	508
	0.90	256	518
	0.92	265	535
	0.94	284	574
Cr2	0.95	289	583
	0.97	257	520
	0.98	245	494
	1.00	250	505

Table A.65: *Hardness values HV and predicted 0.2% proof stress* $\overline{\sigma}_{0.2,exp}$ *for CR 100×100×4 Face C*

CR 100×100×4	*Section position (mm)*	*HV*	$\overline{\sigma}_{0.2,exp}$ *(N/mm²)*
Cr2	0.00	250	505
	0.02	269	543
	0.03	335	676
C1	0.05	298	602
	0.06	304	614
	0.08	292	590
	0.10	291	588
	0.11	275	555
	0.13	254	514
C2	0.14	237	479
	0.16	216	437
	0.18	229	462
C3	0.28	219	442
C4	0.39	224	453
C5	0.50	231	467
C8	0.82	231	466
	0.84	238	480
	0.86	238	480
C9	0.87	247	499
	0.89	249	503
	0.90	259	523
	0.92	266	537
	0.94	265	535
Cr3	0.95	274	553
	0.97	241	487
	0.98	226	456
	1.00	213	429

Table A.66: *Hardness values HV and predicted 0.2% proof stress* $\overline{\sigma}_{0.2,exp}$ *for CR 100×100×4 Face D*

CR 100×100×4	*Section position (mm)*	*HV*	$\overline{\sigma}_{0.2,exp}$ *(N/mm²)*
Cr3	0.00	213	429
	0.02	239	482
	0.03	262	529
	0.05	309	624
D1	0.06	304	614
	0.08	277	560
	0.10	274	553
	0.11	263	531
	0.13	251	506
D2	0.14	247	499
	0.16	255	516
	0.18	249	503
D3	0.28	251	507
D4	0.39	227	459
D5	0.50	222	448
D10	0.82	246	497
	0.84	231	467
	0.86	240	485
D11	0.87	230	465
	0.89	246	497
	0.90	259	523
	0.92	261	527
	0.94	271	547
	0.95	293	592
Cr4	0.97	225	455
	0.98	210	424
	1.00	253	511

A.15 CR 150×150×4

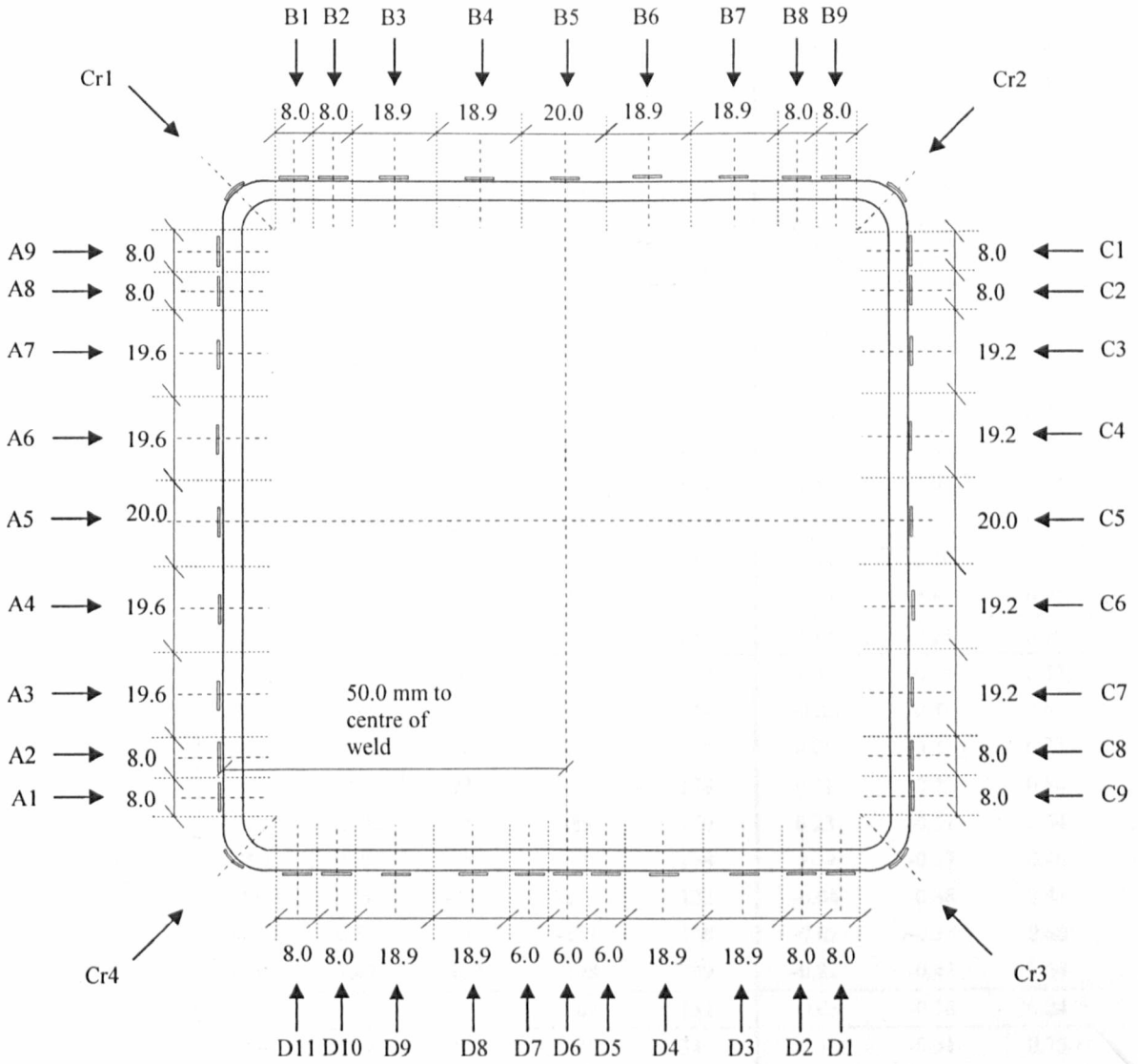

Figure A.15: *Setting out of cold rolled section CR 150×150×4*

Table A.67: *Residual stress distribution for CR 150×150×4*

CR 150×150×4	*Section position (mm)*	*Width (mm)*	σ_m *(N/mm²)*	σ_b *(N/mm²)*	σ_{rc} *(N/mm²)*	$\sigma_m/\sigma_{0.2}$	$\sigma_b/\sigma_{0.2}$	$\sigma_{rc}/\sigma_{0.2}$
A1	10.6	7.67	-101	-248	349	-0.22	-0.53	0.74
A2	19.6	7.99	-52	-180	233	-	-	-
A3	34.9	20.10	-20	-139	158	-0.07	-0.48	0.55
A4	56.1	19.99	46	-129	176	0.16	-0.46	0.62
A5	77.3	20.02	201	-33	235	0.70	-0.12	0.82
A6	98.6	20.16	57	-114	171	0.19	-0.38	0.57
A7	120.1	20.38	5	-124	128	0.02	-0.40	0.42
A8	135.3	7.59	-58	-166	224	-0.16	-0.45	0.60
A9	143.5	6.55	28	-304	333	0.06	-0.60	0.65
Cr1 (r_i=5.6)	0.0		-16	-178	194	-0.03	-0.32	0.35
B1	10.3	7.69	241	-243	484	-	-	-
B2	18.7	6.66	86	-126	211	0.22	-0.32	0.54
B3	33.2	19.96	18	-164	183	0.05	-0.47	0.52
B4	53.6	18.52	-58	-208	267	-0.19	-0.67	0.85
B5	73.3	18.50	6	-149	155	0.02	-0.48	0.50
B6	93.9	20.17	3	-181	184	0.01	-0.61	0.62
B7	115.0	19.72	35	-143	178	0.10	-0.42	0.52
B8	129.8	7.42	13	-155	168	0.03	-0.39	0.42
B9	138.3	7.22	-61	-338	399	-0.11	-0.61	0.72
Cr2 (r_i=9.0)	0.0		-44	-111	155	-0.08	-0.21	0.29
C1	13.2	8.10	-53	-216	269	-0.11	-0.44	0.55
C2	22.4	7.81	-84	-160	244	-0.23	-0.44	0.67
C3	36.7	18.39	16	-101	118	0.05	-0.33	0.38
C4	55.9	17.68	93	-85	178	0.31	-0.29	0.60
C5	75.0	18.02	65	-85	150	0.23	-0.31	0.54
C6	95.1	19.85	25	-103	128	0.09	-0.37	0.46
C7	115.0	17.53	-11	-112	122	-0.04	-0.38	0.41
C8	128.2	6.59	-7	-131	138	-0.02	-0.38	0.40
C9	136.4	7.42	-102	-198	299	-0.22	-0.42	0.64
Cr3 (r_i=4.4)	0.0		-30	-102	131	-0.05	-0.18	0.24
D1	9.6	8.18	-202	-139	341	-0.44	-0.31	0.75
D2	18.9	8.04	-52	-221	273	-	-	-
D3	31.7	15.02	-8	-174	182	-0.02	-0.54	0.57
D4	48.3	15.86	-22	-132	154	-0.06	-0.38	0.44
D5	61.5	8.06	9	-200	209	0.02	-0.54	0.56
D6 (weld)	70.7	8.03	-42	-269	311	-0.11	-0.71	0.82
D7	79.9	7.99	96	-147	243	0.25	-0.39	0.64
D8	94.1	17.99	-3	-119	121	-0.01	-0.36	0.37
D9	113.1	17.54	-19	-163	182	-	-	-
D10	127.1	8.07	-34	-172	207	-0.09	-0.47	0.56
D11	136.4	8.15	-109	-224	333	-0.25	-0.51	0.76
Cr4 (r_i=6.0)	0.0		54	-162	216	-	-	-

Table A.68: *Material properties distribution for CR 150×150×4*

CR 150×150×4	*Section position (mm)*	*Width (mm)*	*E* (N/mm^2)	$\sigma_{0.01,exp}$ (N/mm^2)	$\sigma_{0.2,exp}$ (N/mm^2)	$\sigma_{1.0,exp}$ (N/mm^2)	$\sigma_{ult,exp}$ (N/mm^2)	$\varepsilon_{f,exp}$
A1	10.6	7.67	195000	246	469	526	664	-
A2	19.6	7.99	-	-	-	-	-	-
A3	34.9	20.10	188700	154	290	341	612	-
A4	56.1	19.99	186400	160	282	328	604	-
A5	77.3	20.02	186300	179	287	343	678	-
A6	98.6	20.16	199400	188	300	345	633	-
A7	120.1	20.38	206800	177	308	353	621	-
A8	135.3	7.59	186200	180	372	427	642	-
A9	143.5	6.55	182700	183	509	597	688	-
Cr1 (r_i=5.6)	0.0		188200	268	556	651	714	-
B1	10.3	7.69	-	-	-	-	-	-
B2	18.7	6.66	188200	225	392	444	650	-
B3	33.2	19.96	184300	215	353	405	655	-
B4	53.6	18.52	198500	170	313	367	633	-
B5	73.3	18.50	193200	171	309	361	647	-
B6	93.9	20.17	204900	157	297	356	622	-
B7	115.0	19.72	198300	192	344	394	643	-
B8	129.8	7.42	189200	209	397	451	646	-
B9	138.3	7.22	195200	267	555	638	749	-
Cr2 (r_i=9.0)	0.0		191000	280	537	619	700	-
C1	13.2	8.10	186100	242	494	565	673	-
C2	22.4	7.81	182400	176	362	421	604	-
C3	36.7	18.39	192000	183	310	358	650	-
C4	55.9	17.68	158700	215	297	343	629	-
C5	75.0	18.02	200400	189	278	323	611	-
C6	95.1	19.85	361500	69	280	335	640	-
C7	115.0	17.53	196800	174	296	344	631	-
C8	128.2	6.59	213800	88	347	418	611	-
C9	136.4	7.42	207100	389	469	508	642	-
Cr3 (r_i=4.4)	0.0		215000	329	556	641	781	-
D1	9.6	8.18	189300	254	455	522	667	-
D2	18.9	8.04	-	-	-	-	-	-
D3	31.7	15.02	187600	170	320	369	635	-
D4	48.3	15.86	189500	189	346	392	645	-
D5	61.5	8.06	179300	209	372	429	610	-
D6 (weld)	70.7	8.03	182800	183	381	432	576	-
D7	79.9	7.99	191300	204	382	430	642	-
D8	94.1	17.99	184600	185	328	374	639	-
D9	113.1	17.54	-	-	-	-	-	-
D10	127.1	8.07	183100	209	366	422	624	-
D11	136.4	8.15	199500	240	439	489	642	-
Cr4 (r_i=6.0)	0.0		-	-	-	-	-	-

Table A.69: *Proof stress ratios and Ramberg-Osgood strain parameters for CR 150×150×4*

CR 150×150×4	*Section position (mm)*	*Width (mm)*	$\sigma_{0.2,exp}/\sigma_{0.2,mill}$	$\sigma_{0.2,exp}/\sigma_{0.2,min}$	$n_{0.01}$	$n_{0.05}$	$n_{0.1}$	$n_{bestfit}$	n'	$n'_{bestfit}$
A1	10.6	7.67	1.54	2.24	4.6	5.9	6.5	6.6	3.2	3.2
A2	19.6	7.99	-	-	-	-	-	-	-	-
A3	34.9	20.10	0.95	1.38	4.7	5.5	6.2	6.2	3.2	3.2
A4	56.1	19.99	0.93	1.34	5.3	5.9	7.1	6.3	2.4	2.4
A5	77.3	20.02	0.95	1.37	6.3	6.8	7.8	7.2	1.9	1.8
A6	98.6	20.16	0.99	1.43	6.4	7.8	9.6	8.2	2.1	2.1
A7	120.1	20.38	1.01	1.47	5.4	5.9	7.3	7.3	2.2	2.2
A8	135.3	7.59	1.22	1.77	4.1	5.0	5.9	5.3	3.1	3.1
A9	143.5	6.55	1.67	2.42	2.9	3.7	4.4	3.8	3.9	3.9
Cr1 (r_i=5.6)	0.0		1.83	2.65	4.1	4.5	5.2	5.4	3.6	3.6
B1	10.3	7.69	-	-	-	-	-	-	-	-
B2	18.7	6.66	1.29	1.86	5.4	5.7	6.5	6.1	2.8	2.8
B3	33.2	19.96	1.16	1.68	6.1	6.4	7.2	6.8	2.7	2.7
B4	53.6	18.52	1.03	1.49	4.9	5.3	5.7	5.7	2.8	2.8
B5	73.3	18.50	1.02	1.47	5.1	5.4	6.0	5.6	2.6	2.6
B6	93.9	20.17	0.98	1.41	4.7	4.8	5.1	5.0	3.3	3.3
B7	115.0	19.72	1.13	1.64	5.2	5.9	6.6	6.0	2.7	2.7
B8	129.8	7.42	1.31	1.89	4.7	5.2	6.1	5.4	2.7	2.7
B9	138.3	7.22	1.83	2.64	4.1	4.4	4.9	4.6	4.4	4.4
Cr2 (r_i=9.0)	0.0		1.77	2.56	4.6	5.3	6.0	6.0	3.2	3.2
C1	13.2	8.10	1.63	2.35	4.2	5.0	5.8	5.2	3.4	3.4
C2	22.4	7.81	1.19	1.72	4.2	5.0	5.6	5.2	3.4	3.4
C3	36.7	18.39	1.02	1.48	5.7	6.0	6.8	6.4	2.3	2.3
C4	55.9	17.68	0.98	1.42	9.3	7.3	12.5	12.5	1.2	1.2
C5	75.0	18.02	0.91	1.32	7.8	8.9	10.2	9.2	1.7	1.7
C6	95.1	19.85	0.92	1.33	2.1	3.9	4.9	3.7	2.2	2.2
C7	115.0	17.53	0.97	1.41	5.6	5.9	7.1	7.1	2.3	2.3
C8	128.2	6.59	1.14	1.65	2.2	4.4	5.0	4.6	3.0	3.0
C9	136.4	7.42	1.54	2.23	16.0	14.6	18.3	19.1	3.1	3.1
Cr3 (r_i=4.4)	0.0		1.83	2.65	5.7	5.8	6.2	6.4	3.2	3.2
D1	9.6	8.18	1.50	2.17	5.1	5.0	5.5	5.5	3.5	3.5
D2	18.9	8.04	-	-	-	-	-	-	-	-
D3	31.7	15.02	1.05	1.52	4.8	4.6	5.3	5.0	2.8	2.8
D4	48.3	15.86	1.14	1.65	4.9	5.9	7.0	6.2	2.4	2.4
D5	61.5	8.06	1.22	1.77	5.2	5.5	6.0	5.8	3.2	3.2
D6 (weld)	70.7	8.03	1.25	1.82	4.1	5.3	6.5	5.5	2.6	2.6
D7	79.9	7.99	1.26	1.82	4.8	6.0	6.6	6.0	2.8	2.7
D8	94.1	17.99	1.08	1.56	5.2	5.7	6.4	6.0	2.3	2.3
D9	113.1	17.54	-	-	-	-	-	-	-	-
D10	127.1	8.07	1.20	1.74	5.4	5.8	6.9	6.2	1.8	1.8
D11	136.4	8.15	1.44	2.09	5.0	5.8	6.9	6.1	3.1	3.1
Cr4 (r_i=6.0)	0.0		1.54	2.24	4.6	5.9	6.5	6.6	3.2	3.2

A.16 HR 50×50×3

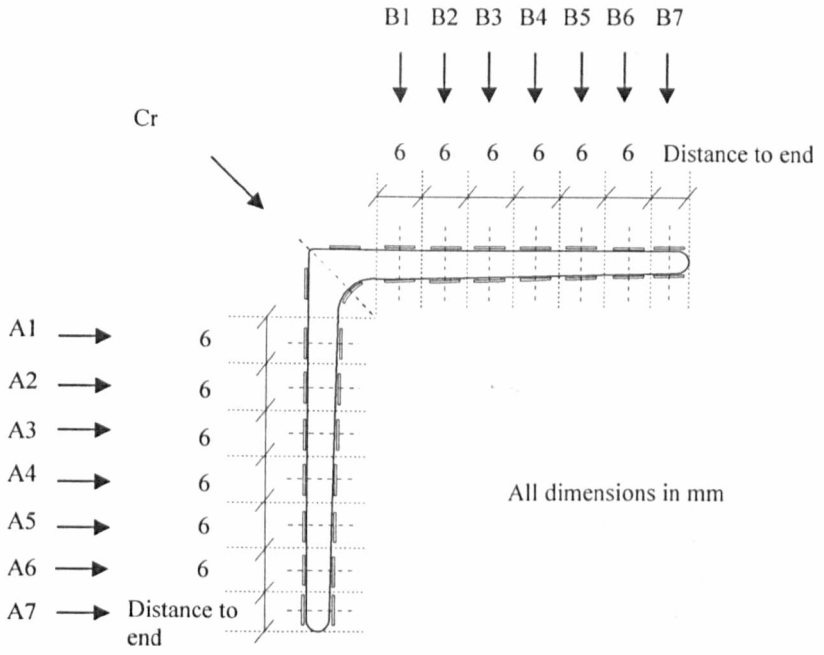

Figure A.16: *Setting out of hot rolled section HR 50×50×3*

Table A.70: *Residual stress distribution for HR 50×50×3*

HR 50×50×3	*Section position (mm)*	*Width (mm)*	σ_m *(N/mm²)*	σ_b *(N/mm²)*	σ_{rc} *(N/mm²)*	$\sigma_m/\sigma_{0.2}$	$\sigma_b/\sigma_{0.2}$	$\sigma_{rc}/\sigma_{0.2}$
A7	38.4	3.36	-32	-36	68	-0.08	-0.09	0.16
A6	33.2	3.36	-27	4	31	-0.07	0.01	0.08
A5	28.3	3.44	-21	-26	47	-0.06	-0.07	0.13
A4	23.3	3.51	-26	-42	68	-0.07	-0.12	0.19
A3	18.3	3.52	-1	-67	68	0.00	-0.20	0.20
A2	13.3	3.50	24	-18	42	0.07	-0.05	0.13
A1	8.3	3.49	-5	-50	55	-0.01	-0.14	0.15
Cr (r_i=5.0)	0.0		-31	-107	138	-0.11	-0.37	0.48
B1	8.4	3.56	-29	-60	89	-0.08	-0.17	0.25
B2	13.4	3.60	17	-22	39	0.05	-0.07	0.12
B3	18.5	3.62	7	-34	41	0.02	-0.10	0.12
B4	23.7	3.60	-19	-28	46	-0.05	-0.08	0.13
B5	28.7	3.54	92	119	211	0.27	0.34	0.61
B6	33.8	3.56	2	22	23	0.00	0.06	0.07
B7	39.2	3.58	-20	-4	24	-0.05	-0.01	0.06

Table A.71: *Material properties distribution for HR 50×50×3*

HR 50×50×3	Section position (mm)	Width (mm)	E (N/mm^2)	$\sigma_{0.01,exp}$ (N/mm^2)	$\sigma_{0.2,exp}$ (N/mm^2)	$\sigma_{1.0,exp}$ (N/mm^2)	$\sigma_{ult,exp}$ (N/mm^2)	$\varepsilon_{f,exp}$
A7	38.4	3.36	199100	181	419	494	794	0.64
A6	33.2	3.36	183800	164	381	450	725	0.70
A5	28.3	3.44	189900	202	366	428	709	0.88
A4	23.3	3.51	190700	217	356	422	707	0.73
A3	18.3	3.52	187900	221	340	408	691	0.80
A2	13.3	3.50	194300	200	334	402	690	0.77
A1	8.3	3.49	206100	166	371	439	713	0.68
Cr (r_i=5.0)	0.0		180400	150	289	338	588	0.70
B1	8.4	3.56	204200	157	353	415	702	0.89
B2	13.4	3.60	186800	227	339	400	694	0.82
B3	18.5	3.62	187600	234	335	395	697	0.82
B4	23.7	3.60	186100	245	348	407	702	0.82
B5	28.7	3.54	185200	237	346	401	698	0.82
B6	33.8	3.56	195100	171	346	402	675	0.82
B7	39.2	3.58	205300	235	427	495	826	0.64

Table A.72: *Proof stress ratios and Ramberg-Osgood strain parameters for HR 50×50×3*

HR 50×50×3	Section position (mm)	Width (mm)	$\sigma_{0.2,exp}/\sigma_{0.2,mill}$	$\sigma_{0.2,exp}/\sigma_{0.2,min}$	$n_{0.01}$	$n_{0.05}$	$n_{0.1}$	$n_{bestfit}$	n'	$n'_{bestfit}$
A7	38.4	3.36	1.0	2.2	3.6	3.8	4.5	3.9	2.7	2.7
A6	33.2	3.36	0.9	2.0	3.6	3.7	4.4	3.9	2.7	2.7
A5	28.3	3.44	0.8	1.9	5.0	7.8	9.4	7.8	2.2	2.2
A4	23.3	3.51	0.8	1.9	6.1	7.7	8.6	7.8	2.3	2.3
A3	18.3	3.52	0.8	1.8	6.9	7.8	8.1	7.6	2.4	2.4
A2	13.3	3.50	0.8	1.8	5.9	7.5	8.2	7.3	2.4	2.4
A1	8.3	3.49	0.8	2.0	3.7	6.2	7.3	5.7	2.3	2.3
Cr (r_i=5.0)	0.0		0.7	1.5	4.6	6.7	8.0	6.7	2.0	2.0
B1	8.4	3.56	0.8	1.9	3.7	6.3	7.6	6.0	2.1	2.1
B2	13.4	3.60	0.8	1.8	7.4	9.3	10.0	9.1	2.3	2.3
B3	18.5	3.62	0.8	1.8	8.3	9.2	9.4	9.2	2.8	2.8
B4	23.7	3.60	0.8	1.8	8.5	9.3	10.0	10.0	2.3	2.3
B5	28.7	3.54	0.8	1.8	7.9	9.0	9.1	9.2	2.2	2.2
B6	33.8	3.56	0.8	1.8	4.3	6.5	10.8	6.6	1.7	1.7
B7	39.2	3.58	1.0	2.2	5.0	6.0	6.7	6.3	2.0	2.0

A.17 HR 50×50×5

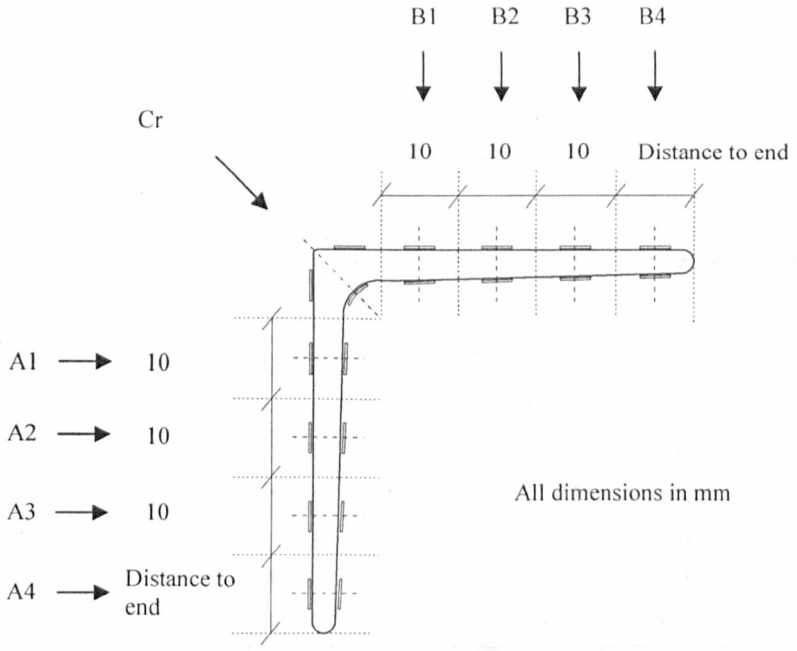

Figure A.17: *Setting out of hot rolled section HR 50×50×5*

Table A.73: *Residual stress distribution for HR 50×50×5*

HR 50×50×5	*Section position (mm)*	*Width (mm)*	σ_m *(N/mm²)*	σ_b *(N/mm²)*	σ_{rc} *(N/mm²)*	$\sigma_m/\sigma_{0.2}$	$\sigma_b/\sigma_{0.2}$	$\sigma_{rc}/\sigma_{0.2}$
A4	41.3	4.93	92	-22	113	0.15	-0.04	0.19
A3	30.8	4.96	50	5	-	-	-	-
A2	20.8	4.91	-4	74	78	-0.01	0.15	0.16
A1	11.1	4.89	9	-73	82	0.02	-0.14	0.16
Cr (r_i=4.5)	0.0		31	169	200	0.06	0.32	0.38
B1	10.7	5.06	-15	72	87	-0.03	0.15	0.18
B2	21.2	5.08	5	53	59	0.01	0.11	0.12
B3	31.2	5.07	-54	-91	144	-0.11	-0.18	0.29
B4	40.9	5.02	47	-91	138	0.10	-0.19	0.28

Table A.74: *Material properties distribution for HR 50×50×5*

HR 50×50×5	*Section position (mm)*	*Width (mm)*	*E* (N/mm^2)	$\sigma_{0.01,exp}$ (N/mm^2)	$\sigma_{0.2,exp}$ (N/mm^2)	$\sigma_{1.0,exp}$ (N/mm^2)	$\sigma_{ult,exp}$ (N/mm^2)	$\varepsilon_{f,exp}$
A4	41.3	4.93	212300	354	605	665	813	0.48
A3	30.8	4.96	-	-	-	-	-	-
A2	20.8	4.91	192900	343	491	542	676	0.56
A1	11.1	4.89	204200	284	506	555	670	0.57
Cr (r_i=4.5)	0.0		193300	252	528	604	692	0.44
B1	10.7	5.06	195000	300	492	541	673	0.60
B2	21.2	5.08	184200	372	485	524	661	0.58
B3	31.2	5.07	188100	358	503	544	677	0.53
B4	40.9	5.02	189500	235	490	538	666	0.52

Table A.75: *Proof stress ratios and Ramberg-Osgood strain parameters for HR 50×50×5*

HR 50×50×5	*Section position (mm)*	*Width (mm)*	$\sigma_{0.2,exp}/\sigma_{0.2,mill}$	$\sigma_{0.2,exp}/\sigma_{0.2,min}$	$n_{0.01}$	$n_{0.05}$	$n_{0.1}$	$n_{bestfit}$	n'	$n'_{bestfit}$
A4	41.3	4.93	1.98	3.18	5.6	6.8	7.7	7.1	3.2	3.2
A3	30.8	4.96	-	-	-	-	-	-	-	-
A2	20.8	4.91	1.60	2.58	8.4	9.5	10.1	9.7	2.7	2.8
A1	11.1	4.89	1.65	2.66	5.2	8.0	9.3	7.7	3.0	3.0
Cr (r_i=4.5)	0.0		1.73	2.78	4.1	4.6	5.2	5.2	4.2	4.2
B1	10.7	5.06	1.61	2.59	6.0	8.3	9.9	9.9	3.6	3.7
B2	21.2	5.08	1.59	2.55	11.3	11.3	13.2	13.4	2.5	2.5
B3	31.2	5.07	1.64	2.65	8.8	10.8	13.6	12.1	2.5	2.6
B4	40.9	5.02	1.60	2.58	4.1	7.2	8.1	6.8	3.5	3.5

A.18 HR 50×50×6

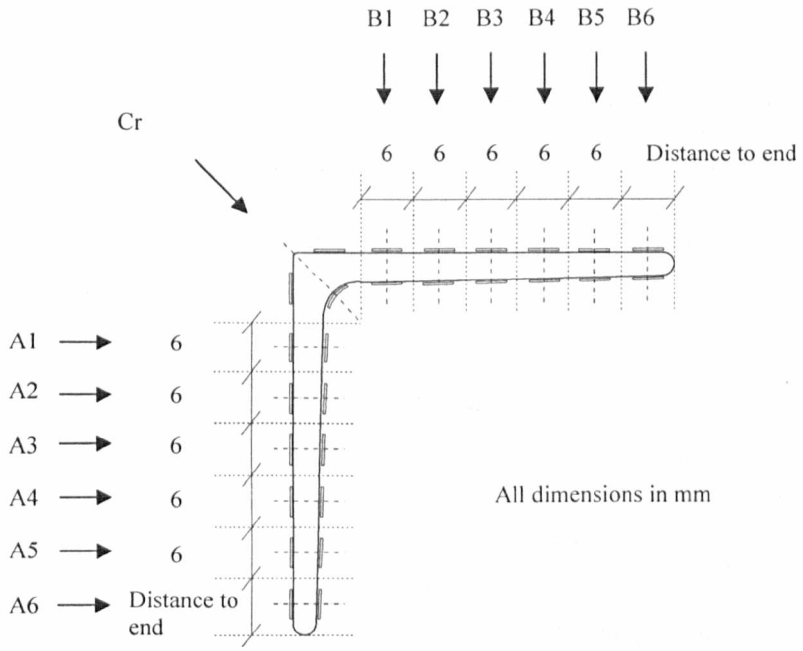

Figure A.18: *Setting out of hot rolled section HR 50×50×6*

Table A.76: *Material properties distribution for HR 50×50×6*

HR 50×50×6	*Section position (mm)*	*Width (mm)*	*E* (N/mm^2)	$\sigma_{0.01,exp}$ (N/mm^2)	$\sigma_{0.2,exp}$ (N/mm^2)	$\sigma_{1.0,exp}$ (N/mm^2)	$\sigma_{ult,exp}$ (N/mm^2)	$\varepsilon_{f,exp}$
A6	41.5	7.67	207100	337	587	667	833	0.39
A5	33.9	5.31	186300	162	380	453	661	0.59
A4	27.5	5.10	185600	217	356	425	649	0.55
A3	21.6	4.26	191600	197	336	398	637	0.61
A2	15.9	4.72	180200	211	325	388	635	0.64
A1	9.6	5.52	185900	185	345	412	655	0.61
Cr (r_i=4.8)	0.0		205700	223	399	466	727	0.48
B1	9.3	4.99	188700	190	339	422	659	0.59
B2	15.6	5.27	203100	118	325	402	615	0.59
B3	21.8	4.76	193700	227	365	445	678	0.63
B4	27.9	5.03	208600	217	353	432	664	0.61
B5	34.3	5.25	190500	170	371	449	675	0.61
B6	42.5	8.73	179000	249	488	550	706	0.43

Table A.77: *Proof stress ratios and Ramberg-Osgood strain parameters for HR 50×50×6*

HR 50×50×6	*Section position (mm)*	*Width (mm)*	$\sigma_{0.2,exp}/\sigma_{0.2,mill}$	$\sigma_{0.2,exp}/\sigma_{0.2,min}$	$n_{0.01}$	$n_{0.05}$	$n_{0.1}$	$n_{bestfit}$	n'	$n'_{bestfit}$
A6	41.5	7.67	1.34	3.09	5.4	6.0	10.2	7.2	3.3	3.3
A5	33.9	5.31	0.86	1.99	3.5	5.6	6.4	5.6	2.3	2.3
A4	27.5	5.10	0.81	1.85	6.0	7.8	7.8	7.8	2.8	2.8
A3	21.6	4.26	0.77	1.74	5.6	8.6	8.5	7.7	2.5	2.5
A2	15.9	4.72	0.74	1.68	6.9	8.5	8.5	8.5	2.6	2.6
A1	9.6	5.52	0.78	1.77	4.8	6.6	7.1	6.6	2.6	2.6
Cr (r_i=4.8)	0.0		0.91	2.03	5.1	7.5	6.6	6.4	2.1	2.1
B1	9.3	4.99	0.77	1.72	5.2	5.9	6.2	6.2	3.4	3.4
B2	15.6	5.27	0.74	1.64	3.0	5.3	5.9	4.8	2.6	2.6
B3	21.8	4.76	0.83	1.83	6.3	6.8	6.9	6.9	2.5	2.5
B4	27.9	5.03	0.80	1.76	6.2	7.2	7.4	7.7	3.7	3.7
B5	34.3	5.25	0.84	1.84	3.8	5.2	6.0	5.3	2.5	2.5
B6	42.5	8.73	1.11	2.42	4.4	5.5	6.0	6.0	2.9	2.9

A.19 HR 50×50×10

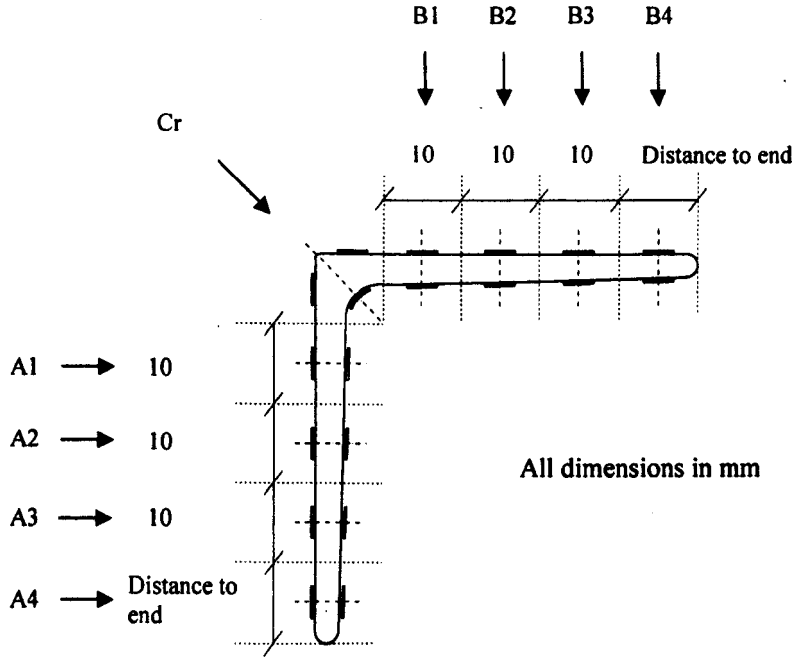

Figure A.19: *Setting out of hot rolled section HR 50×50×10*

Table A.78: *Residual stress distribution for HR 50×50×10*

HR 50×50×10	*Section position (mm)*	*Width (mm)*	σ_m *(N/mm²)*	σ_b *(N/mm²)*	σ_{rc} *(N/mm²)*	$\sigma_m/\sigma_{0.2}$	$\sigma_b/\sigma_{0.2}$	$\sigma_{rc}/\sigma_{0.2}$
A4	42.3	6.93	16	21	37	0.03	0.04	0.07
A3	33.2	7.48	-8	19	28	-0.02	0.06	0.08
A2	23.1	9.64	-15	26	41	-0.04	0.07	0.12
A1	12.5	8.71	-16	81	98	-0.05	0.25	0.30
Cr (r_i =4.5)	0.0		-14	63	77	-0.04	0.18	0.22
B1	12.7	9.10	19	8	26	0.05	0.02	0.07
B2	23.0	8.51	1	6	7	0.00	0.02	0.02
B3	32.7	7.93	-19	17	37	-0.06	0.05	0.11
B4	40.5	6.91	-23	60	83	-0.04	0.11	0.16

Table A.79: *Material properties distribution for HR 50×50×10*

HR 50×50×10	*Section position (mm)*	*Width (mm)*	*E (N/mm²)*	$\sigma_{0.01,exp}$ *(N/mm²)*	$\sigma_{0.2,exp}$ *(N/mm²)*	$\sigma_{1.0,exp}$ *(N/mm²)*	$\sigma_{ult,exp}$ *(N/mm²)*	$\varepsilon_{f,exp}$
A4	42.3	6.93	197500	235	535	602	764	0.43
A3	33.2	7.48	188500	198	347	399	653	0.56
A2	23.1	9.64	204500	281	356	408	686	0.58
A1	12.5	8.71	189800	260	330	379	639	0.62
Cr (r_i =4.5)	0.0		211400	254	353	404	682	0.47
B1	12.7	9.10	190500	193	399	404	632	0.57
B2	23.0	8.51	185100	246	318	368	617	0.58
B3	32.7	7.93	187100	215	345	398	630	0.56
B4	40.5	6.91	200800	201	536	590	727	0.39

Table A.80: *Proof stress ratios and Ramberg-Osgood strain parameters for HR 50×50×10*

HR 50×50×10	*Section position (mm)*	*Width (mm)*	$\sigma_{0.2,exp}/\sigma_{0.2,mill}$	$\sigma_{0.2,exp}/\sigma_{0.2,min}$	$n_{0.01}$	$n_{0.05}$	$n_{0.1}$	$n_{bestfit}$	n'	$n'_{bestfit}$
A4	42.3	6.93	1.12	2.82	3.6	5.9	7.7	6.4	3.1	3.1
A3	33.2	7.48	0.73	1.82	5.3	10.1	11.6	9.0	2.0	2.0
A2	23.1	9.64	0.75	1.85	12.6	16.0	15.8	14.8	2.5	2.5
A1	12.5	8.71	0.69	1.71	12.5	14.7	16.1	15.0	2.5	2.5
Cr (r_i=4.5)	0.0		0.74	1.82	9.2	11.1	12.0	11.4	1.7	1.7
B1	12.7	9.10	0.84	2.05	4.1	8.0	21.8	11.3	-	-
B2	23.0	8.51	0.66	1.62	11.8	13.6	12.8	13.1	2.3	2.3
B3	32.7	7.93	0.72	1.75	6.3	11.1	12.0	10.1	2.1	2.1
B4	40.5	6.91	1.12	2.71	3.0	5.9	6.6	5.4	2.3	2.3